

DYNAMIC PROPERTIES OF ICE AND FROZEN CLAY UNDER
CYCLIC TRIAXIAL LOADING CONDITIONS

by

Ted S. Vinson and Thira Chaichanavong
Department of Civil Engineering

Volume I of II
Final Report of Research Conducted Under Research Grant ENG74-13506
SHEAR MODULI AND DAMPING FACTORS IN FROZEN SOILS
for the Period October 1, 1974 to September 30, 1976

sponsored by the
NATIONAL SCIENCE FOUNDATION
Washington, D.C. 20550

Report No. MSU-CE-76-4

October 1976

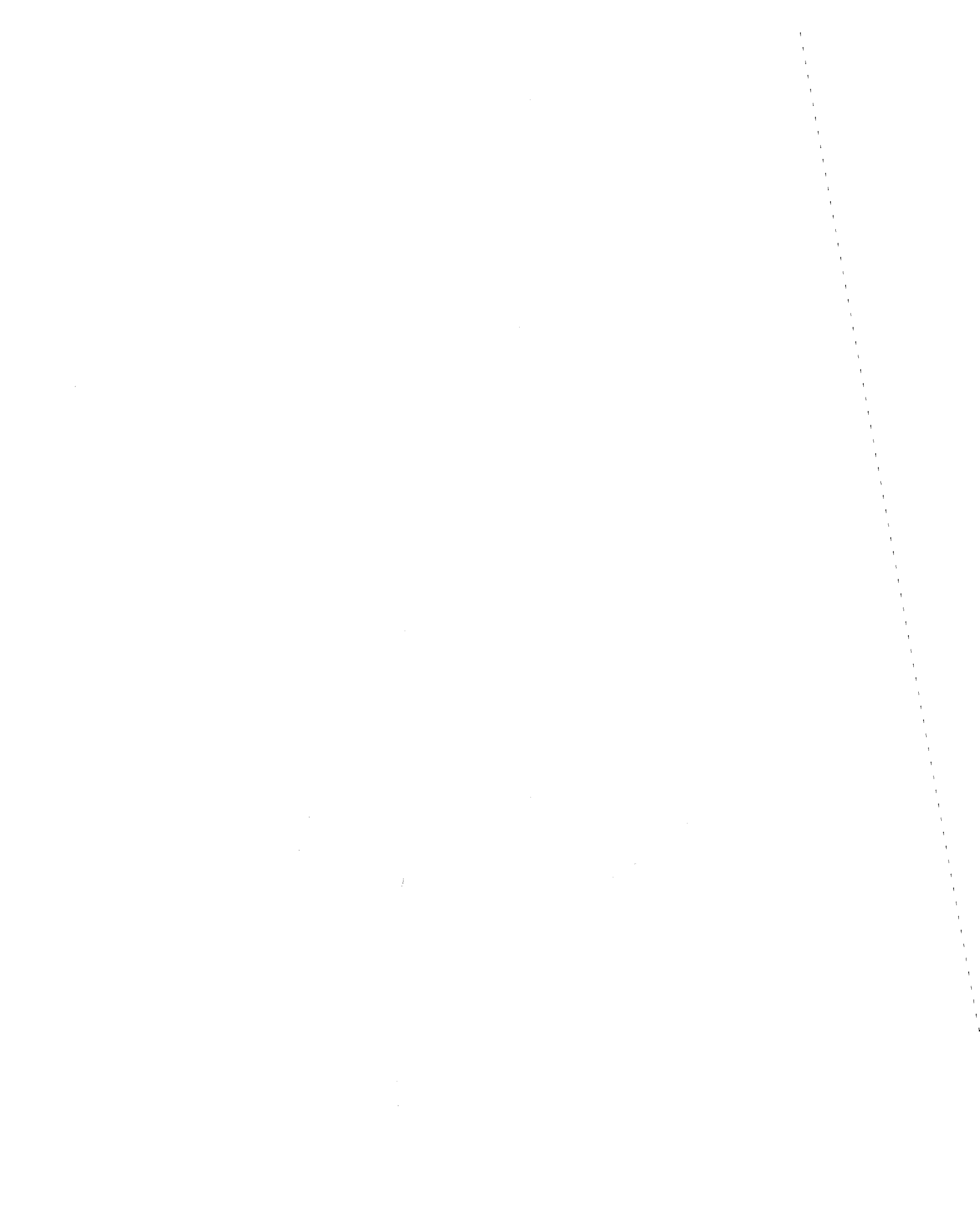
Division of Engineering Research
MICHIGAN STATE UNIVERSITY
East Lansing, Michigan 48824

BIBLIOGRAPHIC DATA SHEET	1. Report No. MSU-CE-76-4	2.	3. Recipient's Accession No. 1288951
	4. Title and Subtitle DYNAMIC PROPERTIES OF ICE AND FROZEN CLAY UNDER CYCLIC TRIAXIAL LOADING CONDITIONS		5. Report Date October 1976
7. Author(s) Ted S. Vinson (Oregon State University) & Thira Chaichanavong		8. Performing Organization Rept. No.	
9. Performing Organization Name and Address Division of Engineering Research Michigan State University East Lansing, Michigan 48824		10. Project/Task/Work Unit No.	11. Contract/Grant No. ENG74-13506
12. Sponsoring Organization Name and Address National Science Foundation Washington, D.C. 20550		13. Type of Report & Period Covered Final Oct. 1, 1974 to Sept. 30, 1976	
14.			
15. Supplementary Notes Volume I of II; Final Report of research conducted under project entitled "Shear Moduli and Damping Factors in Frozen Soils"			
16. Abstracts As part of a long-term study to evaluate dynamic properties of frozen soils under simulated earthquake and low frequency loading conditions, cyclic triaxial tests were performed on laboratory prepared samples of ice and frozen clay. The cylindrical polycrystalline ice samples used in the research program were prepared using natural snow and distilled water. The samples were tested at strain amplitudes from 3×10^{-3} to $2 \times 10^{-2}\%$, temperatures from -1 to -10°C , frequencies from 0.05 to 5 cps and confining pressures from 0 to 200 psi. The values of dynamic Young's modulus over the range of material and test conditions were from 260×10^3 to 900×10^3 psi; the values of damping ratio were from 0.001 to 0.14. Two types of frozen clay samples were used in the research program: (1) Ontonagon clay and (2) a mixture of Ontonagon and sodium montmorillonite clay (fifty percent each by weight). The samples were tested at strain amplitudes from 3×10^{-3} to $1 \times 10^{-1}\%$, temperatures from -1 to -10°C , frequencies from 0.05 to 5 cps, and confining pressures from 0 to 200 psi. The values of dynamic Young's modulus over the range of test conditions were from 90×10^3 to 880×10^3 psi; the values			
17. Key Words and Document Analysis. 17a. Descriptors of damping ratio were from 0.02 to 0.30. * Geotechnical Engineering * Dynamics * Earthquakes * Permafrost * Ice * Clay Cyclic Loading Damping Young's Modulus Triaxial tests Frozen soils 17b. Identifiers/Open-Ended Terms			
17c. COSATI Field/Group 8/13; 8/12; 8/11			
18. Availability Statement No restriction on distribution.		19. Security Class (This Report) UNCLASSIFIED	20. Security Class (This Page) UNCLASSIFIED
NSF Approved COB 10/14/78		22. Price PC A14/A31	

FORWARD

This report presents the results from a research project entitled "Shear Moduli and Damping Factors in Frozen Soils" sponsored by the National Science Foundation under Grant ENG74-13506. The Principal Investigator for the research project was Dr. Ted S. Vinson, Associate Professor of Civil Engineering, Michigan State University. Mr. Thira Chaichanavong, Mr. Ronald L. Czajkowski, and Mr. John C. Li, Graduate Research Assistants in the Division of Engineering Research, conducted the laboratory tests associated with the study. Ms. Charlene Burns, Ms. Sheila Eddington, and Ms. Geraldine Wright, Undergraduate Research Aides in the Division of Engineering Research, assisted in the data reduction and presentation. Mr. Dave Aditays and Mr. Elbert Mills, Undergraduate Research Aides in the Division of Engineering Research, assisted in the development and fabrication of the electronic instrumentation associated with the test system. Mr. Don Childs, Shop Supervisor in the Division of Engineering Research, assisted in the design and construction of the mechanical and hydraulic components associated with the test system. Ms. Charlene Burns typed the final draft of the report. Finally, Dr. O.B. Andersland offered many helpful suggestions during the course of the study. His contribution is sincerely appreciated.

The results of the research project are presented in two volumes entitled: "Dynamic Properties of Ice and Frozen Clay Under Cyclic Triaxial Loading Conditions" and "Dynamic Properties of Frozen Cohesionless Soils Under Cyclic Triaxial Loading Conditions." The work presented in this volume is associated with the development of the cyclic triaxial test system and experimental techniques employed to evaluate dynamic properties of ice and frozen clay, a discussion of the experimental results, and a comparison of the experimental results of the present study to those of previous studies.

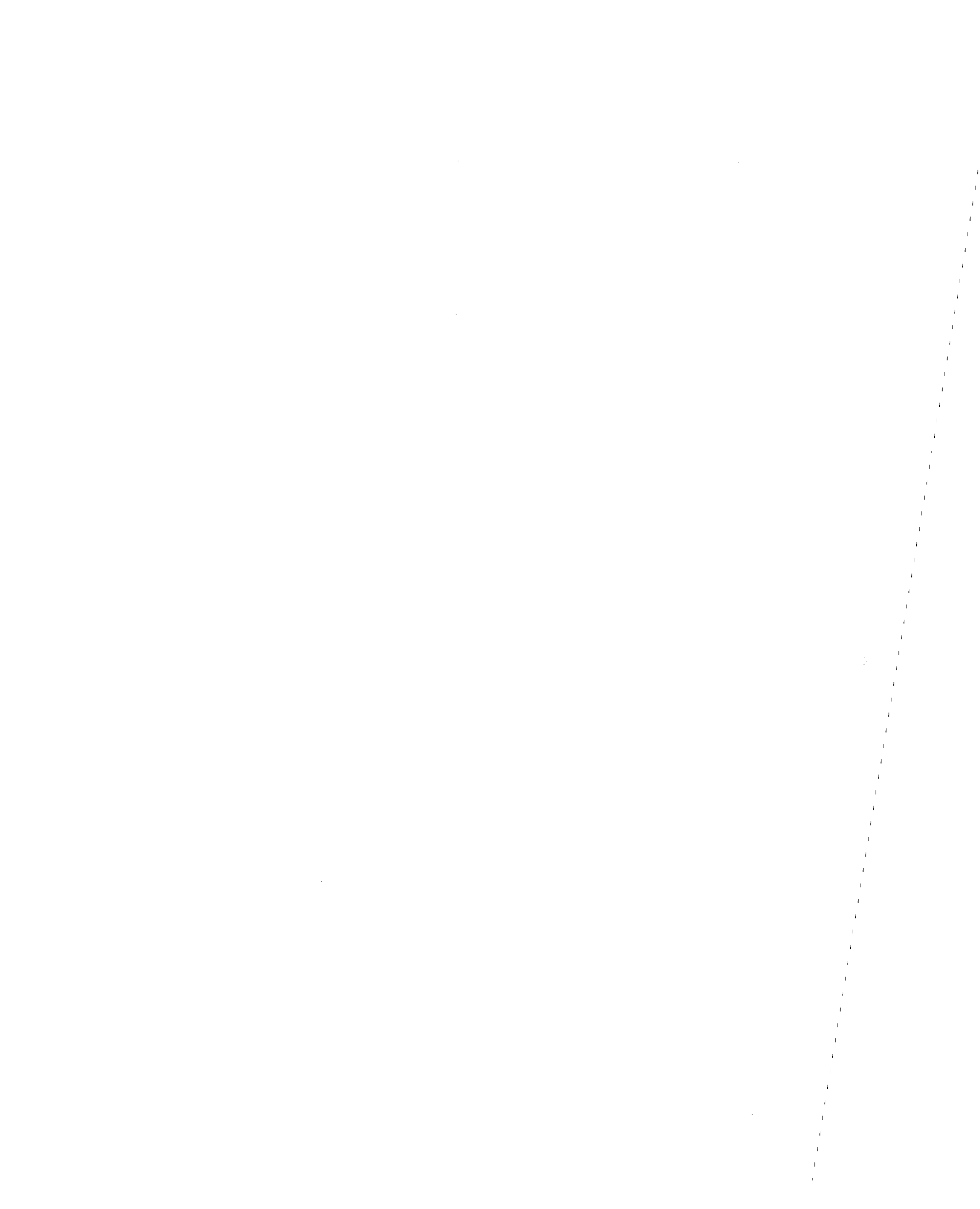


ABSTRACT

As part of a long-term study to evaluate dynamic properties of frozen soils under simulated earthquake and low frequency loading conditions, cyclic triaxial tests were performed on laboratory prepared samples of ice and frozen clay. The cyclic triaxial test setup consists of four basic components: (1) an MTS electrohydraulic closed loop test system which applies a cyclic deviator stress to the sample, (2) a triaxial cell which contains the sample and noncirculating coolant, (3) a refrigeration unit and cold bath which circulates the coolant around the triaxial cell, (4) output recording devices to monitor the load (stress) and displacement (strain) of the sample during the test.

The cylindrical polycrystalline ice samples used in the research program were prepared using natural snow and distilled water for high density samples (about 0.904 g/cc) or natural snow and carbonated water for low density samples (about 0.77 g/cc). The samples were tested at strain amplitudes from 3×10^{-3} to $2 \times 10^{-2}\%$, temperatures from -1 to -10°C, frequencies from 0.05 to 5 cps and confining pressures from 0 to 200 psi. The values of dynamic Young's modulus over the range of material and test conditions were from 260×10^3 to 900×10^3 psi; the values of damping ratio were from 0.001 to 0.14. The test results indicate that the dynamic Young's modulus of ice increases, in general, with increasing confining pressure, density, and frequency. The dynamic Young's modulus of ice decreases with ascending temperature and increasing strain amplitude. The test results indicate that, in general, damping ratio of ice decreases as frequency increases from 0.05 to 1.0 cps and increases as frequency increases from 1.0 to 5.0 cps. The damping ratio tends to decrease with descending temperature and increases with increasing strain amplitude for high density ice. It is apparently not affected by strain amplitude for low density ice. There appears to be no well-defined relationship between damping ratio of ice and confining pressure or density.

Two types of frozen clay samples were used in the research program: (1) Ontonagon clay, termed "O-clay," and (2) a mixture of Ontonagon and sodium montmorillonite clay (fifty percent each by weight), termed "M + O-clay." The O-clay was prepared at different water contents to assess the influence of water (ice) content on dynamic properties. The M + O-



clay was used to investigate the influence of specific surface area (related to unfrozen water content). The samples were tested at strain amplitudes from 3×10^{-3} to $1 \times 10^{-1}\%$, temperatures from -1 to -10°C , frequencies from 0.05 to 5 cps, and confining pressures from 0 to 200 psi. The values of dynamic Young's modulus over the range of test conditions were from 90×10^3 to 880×10^3 psi; the values of damping ratio were from 0.02 to 0.3. The test results indicate that the dynamic Young's modulus of frozen clay decreases with increasing strain amplitude and specific surface area. The dynamic Young's modulus of frozen clay increases with descending temperature and increasing water content and frequency. It is apparently not affected by confining pressure. The test results indicate that the damping ratio of frozen clay increases with increasing strain amplitude and ascending temperature. The damping ratio, in general, decreases for an increase in frequency from 0.05 to 5 cps; for frequencies greater than 5 cps, damping ratio increases as frequency increases. There appears to be no well-defined relationship between the damping ratio and water content or specific surface area. The damping ratio is apparently not affected by confining pressure.

The dynamic properties of ice and frozen clay obtained in the present study at the lowest strain amplitude were compared to those obtained in previous studies. The values of longitudinal and compressional wave velocities of ice determined in the present study are lower than comparable wave velocities determined in previous laboratory & field studies. This may be a consequence of the fact that the strain amplitude of testing in the present study is greater than those associated with previous studies and the test frequencies in the present study are much lower than those associated with previous studies. The values of damping ratio of ice determined in the present are close to the values obtained in previous studies. The values of longitudinal wave velocities of frozen clay obtained in the present study compare favorably with the results from previous studies. It appears any differences in longitudinal wave velocities can be explained by differences in the test techniques and material types employed between the present and previous studies. The values of damping ratio of frozen clay obtained in the present study are close to values obtained in one previous laboratory study.

TABLE OF CONTENTS

	Page
FORWARD	i
ABSTRACT.	ii
LIST OF TABLES.	vii
LIST OF FIGURES	viii
LIST OF SYMBOLS	xvii
 Chapter	
1. INTRODUCTION.	1
1.1. Statement of the Problem.	1
1.2. Purpose and Scope of Studies.	2
1.3. Background.	3
1.3.1. Mechanical Properties of Frozen Soils, Thermal Characteristics of Frozen Soil Deposits and Dynamic Properties of Unfrozen Soils.	3
1.3.2. Fundamentals of Cyclic Triaxial Testing	4
2. DYNAMIC PROPERTIES OF ICE AND FROZEN CLAY	7
2.1. General	7
2.2. Previous Methods to Evaluate Dynamic Properties of Ice and Frozen Clay	7
2.3. Dynamic Elastic Properties of Ice	17
2.3.1. Effect of Temperature	17
2.3.2. Effect of Density	21
2.3.3. Effect of Frequency	23
2.3.4. Effect of Confining Pressure.	26
2.4. Damping of Ice.	26
2.5. Dynamic Elastic Properties of Frozen Clay	29
2.5.1. Effect of Void Ratio.	29
2.5.2. Effect of Ice Saturation.	29
2.5.3. Effect of Temperature	29
2.5.4. Effect of Frequency	32
2.5.5. Effect of Unfrozen Water Content.	32
2.5.6. Effect of Dynamic Stress (or Strain)	36
2.6. Damping of Frozen Clay.	36
2.7. Poisson's Ratio of Ice and Frozen Clay.	36
2.7.1. Poisson's Ratio of Ice.	38
2.7.2. Poisson's Ratio of Frozen Clay.	38
3. SAMPLE PREPARATION, SAMPLE INSTALLATION, TRIAXIAL CELL ASSEMBLY, AND TEST PROCEDURE.	43
3.1. General	43
3.2. Preparation of Ice Sample	43
3.3. Preparation of Frozen Clay Sample	45
3.4. Sample Installation and Triaxial Cell Assembly.	50
3.5. Test Procedure.	52

Chapter	Page
4. DYNAMIC PROPERTIES OF ICE UNDER CYCLIC TRIAXIAL LOADING CONDITIONS	55
4.1. General	55
4.2. Test History Effects on Dynamic Properties.	55
4.3. Influence of Number of Cycles on Evaluation of Dynamic Properties.	59
4.4. Dynamic Young's Modulus of Ice.	59
4.4.1. Effect of Strain Amplitude.	63
4.4.2. Effect of Confining Pressure.	64
4.4.3. Effect of Frequency	76
4.4.4. Effect of Temperature	79
4.4.5. Effect of Density	82
4.5. Damping Ratio of Ice.	82
4.5.1. Effect of Strain Amplitude.	85
4.5.2. Effect of Frequency	85
4.5.3. Effect of Temperature	90
4.5.4. Effect of Density	91
4.5.5. Effect of Confining Pressure.	91
5. DYNAMIC PROPERTIES OF FROZEN CLAY UNDER CYCLIC TRIAXIAL LOADING CONDITIONS.	93
5.1. General	93
5.2. Test History.	93
5.3. Influence of Number of Cycles on Evaluation of Dynamic Properties.	95
5.4. Dynamic Young's Modulus of Frozen Clay.	100
5.4.1. Effect of Strain Amplitude.	100
5.4.2. Effect of Frequency	107
5.4.3. Effect of Temperature	109
5.4.4. Effect of Water Content	109
5.4.5. Effect of Specific Surface Area	114
5.5. Damping Ratio of Frozen Clay.	114
5.5.1. Effect of Strain Amplitude.	114
5.5.2. Effect of Frequency	117
5.5.3. Effect of Temperature	124
5.5.4. Effect of Water Content	124
5.5.5. Effect of Specific Surface Area	129
6. COMPARISONS OF DYNAMIC PROPERTIES OF ICE AND FROZEN CLAY	131
6.1. General	131
6.2. Comparison of Dynamic Properties of Ice	132
6.2.1. Longitudinal and Compression Wave Velocity.	132
6.2.2. Damping Ratio	134
6.3. Comparison of Dynamic Properties of Frozen Clay.	137
6.3.1. Longitudinal and Compression Wave Velocity.	137
6.3.2. Damping Ratio	140

1

1

Chapter	Page
7. SUMMARY AND CONCLUSIONS	143
LIST OF REFERENCES.	151
APPENDIX	
A. DESCRIPTION OF CYCLIC TRIAXIAL TEST EQUIPMENT	156
A.1. The MTS Electrohydraulic Closed Loop Test System	156
A.1.1. MTS 406.11 Controller	160
A.1.2. MTS 436.11 Controller	165
A.2. Triaxial Cell	167
A.3. Cooling System.	172
A.4. Output Recording System	175
B. DESCRIPTION OF SAMPLE COUPLING DEVICE	181
C. CYCLIC TRIAXIAL TEST RESULTS - DYNAMIC YOUNG'S MODULUS OF ICE.	185
D. CYCLIC TRIAXIAL TEST RESULTS - DAMPING RATIO OF ICE.	223
E. CYCLIC TRIAXIAL TEST RESULTS - DYNAMIC YOUNG'S MODULUS OF FROZEN CLAY.	239
F. CYCLIC TRIAXIAL TEST RESULTS - DAMPING RATIO OF FROZEN CLAY.	264

LIST OF TABLES

Table		Page
2.1	Conversion Equations Between Terms to Characterize Dynamic Properties.	8
3.1	Index and Mineralogical Properties of O-Clay and M + O-Clay.	46
3.2	Water Content and Density of Clay Samples	49
4.1	Variation of Dynamic Young's Modulus of High Density Ice with Number of Cycles	60
4.2	Variation of Damping Ratio of High Density Ice with Number of Cycles	61
5.1	Variation of Dynamic Young's Modulus of Frozen Clay with Number of Cycles.	96
5.2	Variation of Damping Ratio of Frozen Clay with Number of Cycles.	97



LIST OF FIGURES

Figure		Page
1.1	Stress State in Triaxial Tests with Cyclic Axial Stress . . .	5
1.2	Deviator Stress Versus Axial Strain for One Load Cycle. . .	5
2.1	Electromagnetic Three-Mode Beam Vibrator (after Kaplar, 1969)	10
2.2	Schematic of Forced Vibration Dynamic Test Equipment (after Smith, 1969).	11
2.3	Ultrasonic Pulsing Method (after Bennett, 1972)	13
2.4	Critical Angle Method	14
2.5	Schematic of Forced Vibration Dynamic Test Equipment (after Stevens, 1973).	16
2.6	P-Wave Velocity of Ice Versus Temperature (after Roethlisberger, 1972)	18
2.7	S-Wave Velocity of Ice Versus Temperature (after Roethlisberger, 1972)	19
2.8	P-Wave Velocity in the Principal Directions of Single-Crystal Ice Versus Temperature (after Brockamp and Querfurth from Roethlisberger, 1972).	19
2.9	Sound Velocity in Synthetic Ice Cores Versus Temperature (after Müller, 1961, from Roethlisberger, 1972).	20
2.10	Summary of Longitudinal or P-Wave Velocities in Ice Measured by Various Investigators (after Kaplar, 1969). . .	20
2.11	P-Wave Velocity of Ice Versus Density (after Roethlisberger, 1972)	22
2.12	P-Wave Velocity Versus Ice Density From Seismic and Ultrasonic Measurements (after Bennett, 1972).	24
2.13	S-Wave Velocity Versus Ice Density From Seismic and Ultrasonic Measurements (after Bennett, 1972).	24
2.14	P-Wave Velocity of Ice Versus Depth at Camp Century (after Clarke, 1966)	25
2.15	Complex Dynamic Moduli of Ice Versus Frequency (after Smith, 1969)	25
2.16	Loss Factor of Ice Versus Frequency (after Smith, 1969) . .	27
2.17	Loss Factor of Ice Versus Driving Force (after Smith, 1969)	27
2.18	Loss Factor of Ice Versus Density (after Smith, 1969) . . .	28
2.19	Effect of Temperature on $\tan \delta$ of Ice (after Stevens, 1975)	28
2.20	Sound Velocity in Synthetic Frozen Cores at Two Porosities Versus Temperature (after Müller, 1961, from Roethlisberger, 1972)	30



Figure	Page	
2.21	Effect of Ice Saturation on Complex Shear Modulus for Frozen Suffield Clay (after Stevens, 1973)	31
2.22	S-Wave Velocity Versus Temperature for Frozen Goodrich Clay (after Nakano and Froula, 1973)	31
2.23	Longitudinal Wave Velocity Versus Temperature for Frozen Boston Blue Clay and Fargo Clay (after Kaplar, 1969)	33
2.24	Effect of Temperature on Complex Moduli of Frozen Goodrich Clay (modified after Stevens, 1975)	33
2.25	Dilational Velocity and Unfrozen Water Content Versus Temperature (after Nakano and Froula, 1973)	35
2.26	Effect of Temperature on Tan δ of Frozen Goodrich Clay (modified after Stevens, 1975)	37
2.27	Poisson's Ratio of Ice Versus Temperature (after Kaplar, 1969)	39
2.28	Poisson's Ratio for Dry Snow Versus Density (after Mellor from Roethlisberger, 1972)	40
2.29	Poisson's Ratio of Ice Versus Density (after Smith, 1969)	40
2.30	Poisson's Ratio of Frozen Clay Versus Temperature (after Kaplar, 1969)	41
3.1	Hollow Cylindrical Teflon Mold and Sample Caps with Couplings	44
3.2	Typical Cylindrical Ice Sample.	44
3.3	Typical Cylindrical Frozen Clay Sample.	48
3.4	Observed Hysteresis Loop for LVDT Core in Contact with Housing	51
4.1	Diagram of Acceptable Test History for Ice.	57
4.2	Typical Records Obtained During Cyclic Triaxial Testing of Ice	62
4.3	Least Squares Best Fit Line for Dynamic Young's Modulus of High Density Ice Versus Axial Strain.	65
4.4	Least Squares Best Fit Line for Dynamic Young's Modulus of Low Density Ice Versus Axial Strain	65
4.5	Dynamic Young's Modulus Versus Axial Strain for High Density Ice at -1°C and 0.05 cps	66
4.6	Dynamic Young's Modulus Versus Axial Strain for High Density Ice at -1°C and 0.3 cps.	66
4.7	Dynamic Young's Modulus Versus Axial Strain for High Density Ice at -1°C and 1.0 cps.	66
4.8	Dynamic Young's Modulus Versus Axial Strain for High Density Ice at -1°C and 5.0 cps.	66
4.9	Dynamic Young's Modulus Versus Axial Strain for High Density Ice at -2°C and 0.05 cps	67

Figure		Page
4.10	Dynamic Young's Modulus Versus Axial Strain for High Density Ice at -2°C and 0.3 cps.	67
4.11	Dynamic Young's Modulus Versus Axial Strain for High Density Ice at -2°C and 1.0 cps.	67
4.12	Dynamic Young's Modulus Versus Axial Strain for High Density Ice at -2°C and 5.0 cps.	67
4.13	Dynamic Young's Modulus Versus Axial Strain for High Density Ice at -4°C and 0.05 cps	68
4.14	Dynamic Young's Modulus Versus Axial Strain for High Density Ice at -4°C and 0.3 cps.	68
4.15	Dynamic Young's Modulus Versus Axial Strain for High Density Ice at -4°C and 1.0 cps.	68
4.16	Dynamic Young's Modulus Versus Axial Strain for High Density Ice at -4°C and 5.0 cps.	68
4.17	Dynamic Young's Modulus Versus Axial Strain for High Density Ice at -6°C and 0.3 cps.	69
4.18	Dynamic Young's Modulus Versus Axial Strain for High Density Ice at -6°C and 1.0 cps.	69
4.19	Dynamic Young's Modulus Versus Axial Strain for High Density Ice at -6°C and 5.0 cps.	69
4.20	Dynamic Young's Modulus Versus Axial Strain for High Density Ice at -10°C and 0.05 cps.	70
4.21	Dynamic Young's Modulus Versus Axial Strain for High Density Ice at -10°C and 0.3 cps	70
4.22	Dynamic Young's Modulus Versus Axial Strain for High Density Ice at -10°C and 1.0 cps	70
4.23	Dynamic Young's Modulus Versus Axial Strain for High Density Ice at -10°C and 5.0 cps	70
4.24	Dynamic Young's Modulus Versus Axial Strain for Low Density Ice at -1°C and 0.3 cps	71
4.25	Dynamic Young's Modulus Versus Axial Strain for Low Density Ice at -1°C and 1.0 cps	71
4.26	Dynamic Young's Modulus Versus Axial Strain for Low Density Ice at -1°C and 5.0 cps	71
4.27	Dynamic Young's Modulus Versus Axial Strain for Low Density Ice at -4°C and 0.3 cps	72
4.28	Dynamic Young's Modulus Versus Axial Strain for Low Density Ice at -4°C and 1.0 cps	72
4.29	Dynamic Young's Modulus Versus Axial Strain for Low Density Ice at -4°C and 5.0 cps	72
4.30	Dynamic Young's Modulus Versus Axial Strain for Low Density Ice at -10°C and 0.3 cps.	73



Figure		Page
4.31	Dynamic Young's Modulus Versus Axial Strain for Low Density Ice at -10°C and 1.0 cps.	73
4.32	Dynamic Young's Modulus Versus Axial Strain for Low Density Ice at -10°C and 5.0 cps.	73
4.33	Dynamic Young's Modulus Versus Confining Pressure for High Density Ice at -1°C	74
4.34	Dynamic Young's Modulus Versus Confining Pressure for High Density Ice at -2°C	74
4.35	Dynamic Young's Modulus Versus Confining Pressure for High Density Ice at -4°C	74
4.36	Dynamic Young's Modulus Versus Confining Pressure for High Density Ice at -6°C	74
4.37	Dynamic Young's Modulus Versus Confining Pressure for High Density Ice at -10°C	75
4.38	Dynamic Young's Modulus Versus Confining Pressure for Low Density Ice at -1°C	75
4.39	Dynamic Young's Modulus Versus Confining Pressure for Low Density Ice at -4°C	75
4.40	Dynamic Young's Modulus Versus Confining Pressure for Low Density Ice at -10°C	75
4.41	Dynamic Young's Modulus Versus Frequency for High Density Ice at -1°C	77
4.42	Dynamic Young's Modulus Versus Frequency for High Density Ice at -2°C	77
4.43	Dynamic Young's Modulus Versus Frequency for High Density Ice at -4°C	77
4.44	Dynamic Young's Modulus Versus Frequency for High Density Ice at -6°C	77
4.45	Dynamic Young's Modulus Versus Frequency for High Density Ice at -10°C	78
4.46	Dynamic Young's Modulus Versus Frequency for Low Density Ice at -1°C	78
4.47	Dynamic Young's Modulus Versus Frequency for Low Density Ice at -4°C	78
4.48	Dynamic Young's Modulus Versus Frequency for Low Density Ice at -10°C	78
4.49	Dynamic Young's Modulus Versus Temperature for High Density Ice at a Confining Pressure of 25 psi	80
4.50	Dynamic Young's Modulus Versus Temperature for High Density Ice at a Confining Pressure of 50 psi	80
4.51	Dynamic Young's Modulus Versus Temperature for High Density Ice at a Confining Pressure of 100 psi.	80

Figure		Page
4.52	Dynamic Young's Modulus Versus Temperature for High Density Ice at a Confining Pressure of 200 psi.	80
4.53	Dynamic Young's Modulus Versus Temperature for Low Density Ice at a Confining Pressure of 0 psi.	81
4.54	Dynamic Young's Modulus Versus Temperature for Low Density Ice at a Confining Pressure of 25 psi	81
4.55	Dynamic Young's Modulus Versus Temperature for Low Density Ice at a Confining Pressure of 50 psi	81
4.56	Dynamic Young's Modulus Versus Temperature for Low Density Ice at a Confining Pressure of 100 psi.	81
4.57	Dynamic Young's Modulus Versus Density of Ice at -1°C for Three Frequencies	83
4.58	Dynamic Young's Modulus Versus Density of Ice at -4°C for Three Frequencies	83
4.59	Dynamic Young's Modulus Versus Density of Ice at -10°C for Three Frequencies	83
4.60	Dynamic Young's Modulus Versus Density of Ice at -1°C for Three Confining Pressures	84
4.61	Dynamic Young's Modulus Versus Density of Ice at -4°C for Four Confining Pressures.	84
4.62	Dynamic Young's Modulus Versus Density of Ice at -10°C for Four Confining Pressures.	84
4.63	Least Squares Best Fit Line for Damping Ratio of High Density Ice Versus Axial Strain.	86
4.64	Least Squares Best Fit Line for Damping Ratio of Low Density Ice Versus Axial Strain.	86
4.65	Damping Ratio Versus Axial Strain for High Density Ice at 0.05 cps.	87
4.66	Damping Ratio Versus Axial Strain for High Density Ice at 0.3 cps	87
4.67	Damping Ratio Versus Axial Strain for High Density Ice at 1.0 cps	87
4.68	Damping Ratio Versus Axial Strain for High Density Ice at 5.0 cps	87
4.69	Damping Ratio Versus Axial Strain for Low Density Ice at 0.3 cps	88
4.70	Damping Ratio Versus Axial Strain for Low Density Ice at 1.0 cps	88
4.71	Damping Ratio Versus Axial Strain for Low Density Ice at 5.0 cps	88
4.72	Damping Ratio Versus Frequency for High Density Ice	89



Figure		Page
4.73	Damping Ratio Versus Frequency for Low Density Ice.	89
4.74	Damping Ratio Versus Temperature for High Density Ice	89
4.75	Damping Ratio Versus Temperature for Low Density Ice.	89
4.76	Damping Ratio Versus Frequency for Ice at Two Densities . . .	92
4.77	Damping Ratio Versus Temperature for Ice at Two Densities . .	92
4.78	Typical Variation of Damping Ratio with Confining Pressure.	92
5.1	Diagram of Acceptable Test History for Frozen Clay.	94
5.2	Typical Record of Load and Displacement Obtained During Cyclic Triaxial Testing of Frozen Clay.	98
5.3	Typical Hysteresis Loops (non-dimensional) Obtained During Cyclic Triaxial Testing of Frozen Clay.	99
5.4	Dynamic Young's Modulus Versus Confining Pressure for 0- Clay at an Axial Strain of $1.1 \times 10^{-2}\%$	101
5.5	Dynamic Young's Modulus Versus Axial Strain for 0-Clay at 0.3 cps and 29.2% Water Content	102
5.6	Dynamic Young's Modulus Versus Axial Strain for 0-Clay at 1.0 cps and 29.2% Water Content	102
5.7	Dynamic Young's Modulus Versus Axial Strain for 0-Clay at 5.0 cps and 29.2% Water Content	102
5.8	Dynamic Young's Modulus Versus Axial Strain for 0-Clay at 0.05 cps and 36.0% Water Content.	103
5.9	Dynamic Young's Modulus Versus Axial Strain for 0-Clay at 0.3 cps and 36.0% Water Content	103
5.10	Dynamic Young's Modulus Versus Axial Strain for 0-Clay at 1.0 cps and 36.0% Water Content	103
5.11	Dynamic Young's Modulus Versus Axial Strain for 0-Clay at 5.0 cps and 36.0% Water Content	103
5.12	Dynamic Young's Modulus Versus Axial Strain for 0-Clay at 0.3 cps and 46.3% Water Content	104
5.13	Dynamic Young's Modulus Versus Axial Strain for 0-Clay at 1.0 cps and 46.3% Water Content	104
5.14	Dynamic Young's Modulus Versus Axial Strain for 0-Clay at 5.0 cps and 46.3% Water Content	104
5.15	Dynamic Young's Modulus Versus Axial Strain for 0-Clay at 0.3 cps and 55.1% Water Content	105
5.16	Dynamic Young's Modulus Versus Axial Strain for 0-Clay at 1.0 cps and 55.1% Water Content	105
5.17	Dynamic Young's Modulus Versus Axial Strain for 0-Clay at 5.0 cps and 55.1% Water Content	105
5.18	Dynamic Young's Modulus Versus Axial Strain for M + 0- Clay at 0.3 cps and 57.2% Water Content	106

Figure		Page
5.19	Dynamic Young's Modulus Versus Axial Strain for M + 0-Clay at 1.0 cps and 57.2% Water Content	106
5.20	Dynamic Young's Modulus Versus Axial Strain for M + 0-Clay at 5.0 cps and 57.2% Water Content	106
5.21	Dynamic Young's Modulus Versus Frequency for 0-Clay at an Axial Strain of $3.16 \times 10^{-3}\%$	108
5.22	Dynamic Young's Modulus Versus Frequency for 0-Clay at an Axial Strain of $1.0 \times 10^{-1}\%$	108
5.23	Dynamic Young's Modulus Versus Frequency for 0-Clay Tested to 50.0 cps	108
5.24	Dynamic Young's Modulus Versus Temperature for 0-Clay at an Axial Strain of $3.16 \times 10^{-3}\%$	110
5.25	Dynamic Young's Modulus Versus Temperature for 0-Clay at an Axial Strain of $1.0 \times 10^{-1}\%$	110
5.26	Dynamic Young's Modulus Versus Water Content for 0-Clay at -1°C and an Axial Strain of $3.16 \times 10^{-3}\%$	111
5.27	Dynamic Young's Modulus Versus Water Content for 0-Clay at -1°C and an Axial Strain of $1.0 \times 10^{-1}\%$	111
5.28	Dynamic Young's Modulus Versus Water Content for 0-Clay at -4°C and an Axial Strain of $3.16 \times 10^{-3}\%$	112
5.29	Dynamic Young's Modulus Versus Water Content for 0-Clay at -4°C and an Axial Strain of $1.0 \times 10^{-1}\%$	112
5.30	Dynamic Young's Modulus Versus Water Content for 0-Clay at -10°C and an Axial Strain of $3.16 \times 10^{-3}\%$	113
5.31	Dynamic Young's Modulus Versus Water Content for 0-Clay at -10°C and an Axial Strain of $1.0 \times 10^{-1}\%$	113
5.32	Dynamic Young's Modulus Versus Temperature for 0-Clay and M + 0-Clay at an Axial Strain of $3.16 \times 10^{-3}\%$	115
5.33	Dynamic Young's Modulus Versus Temperature for 0-Clay and M + 0-Clay at an Axial Strain of $1.0 \times 10^{-1}\%$	115
5.34	Damping Ratio Versus Confining Pressure for 0-Clay at an Axial Strain of $1.0 \times 10^{-2}\%$	116
5.35	Damping Ratio Versus Axial Strain for 0-Clay at -1°C and 29.2% Water Content	118
5.36	Damping Ratio Versus Axial Strain for 0-Clay at -4°C and 29.2% Water Content	118
5.37	Damping Ratio Versus Axial Strain for 0-Clay at -10°C and 29.2% Water Content	118
5.38	Damping Ratio Versus Axial Strain for 0-Clay at -1°C and 36.0% Water Content	119
5.39	Damping Ratio Versus Axial Strain for 0-Clay at -4°C and 36.0% Water Content	119

Figure		Page
5.40	Damping Ratio Versus Axial Strain for 0-Clay at -10°C and 36.0% Water Content	119
5.41	Damping Ratio Versus Axial Strain for 0-Clay at -1°C and 46.3% Water Content	120
5.42	Damping Ratio Versus Axial Strain for 0-Clay at -4°C and 46.3% Water Content	120
5.43	Damping Ratio Versus Axial Strain for 0-Clay at -10°C and 46.3% Water Content	120
5.44	Damping Ratio Versus Axial Strain for 0-Clay at -1°C and 55.1% Water Content	121
5.45	Damping Ratio Versus Axial Strain for 0-Clay at -4°C and 55.1% Water Content	121
5.46	Damping Ratio Versus Axial Strain for 0-Clay at -10°C and 55.1% Water Content	121
5.47	Damping Ratio Versus Axial Strain for M + 0-Clay at -1°C and 57.2% Water Content	122
5.48	Damping Ratio Versus Axial Strain for M + 0-Clay at -4°C and 57.2% Water Content	122
5.49	Damping Ratio Versus Axial Strain for M + 0-Clay at -10°C and 57.2% Water Content	122
5.50	Damping Ratio Versus Frequency for 0-Clay at an Axial Strain of $3.16 \times 10^{-3}\%$	123
5.51	Damping Ratio Versus Frequency for 0-Clay at an Axial Strain of $1.0 \times 10^{-1}\%$	123
5.52	Damping Ratio Versus Frequency for 0-Clay Tested to 50.0 cps	123
5.53	Damping Ratio Versus Temperature for 0-Clay at an Axial Strain of $3.16 \times 10^{-3}\%$	125
5.54	Damping Ratio Versus Temperature for 0-Clay at an Axial Strain of $1.0 \times 10^{-1}\%$	125
5.55	Damping Ratio Versus Water Content for 0-Clay at -1°C and an Axial Strain of $3.16 \times 10^{-3}\%$	126
5.56	Damping Ratio Versus Water Content for 0-Clay at -1°C and an Axial Strain of $1.0 \times 10^{-1}\%$	126
5.57	Damping Ratio Versus Water Content for 0-Clay at -4°C and an Axial Strain of $3.16 \times 10^{-3}\%$	127
5.58	Damping Ratio Versus Water Content for 0-Clay at -4°C and an Axial Strain of $1.0 \times 10^{-1}\%$	127
5.59	Damping Ratio Versus Water Content for 0-Clay at -10°C and an Axial Strain of $3.16 \times 10^{-3}\%$	128
5.60	Damping Ratio Versus Water Content for 0-Clay at -10°C and an Axial Strain of $1.0 \times 10^{-1}\%$	128

Figure		Page
5.61	Damping Ratio Versus Temperature for O-Clay and M + O-Clay at an Axial Strain of $3.16 \times 10^{-3}\%$	130
5.62	Damping Ratio Versus Temperature for O-Clay and M + O-Clay at an Axial Strain of $1.0 \times 10^{-1}\%$	130
6.1	Wave Velocity Versus Temperature of Ice	133
6.2	Wave Velocity Versus Density of Ice	135
6.3	Damping Ratio Versus Temperature of Ice	136
6.4	Wave Velocity Versus Temperature of Frozen Clay	138
6.5	Damping Ratio Versus Temperature of Frozen Clay	141

LIST OF SYMBOLS

A_L	area of hysteresis loop
A_T	area of triangle
\bar{B}	pore pressure parameter
c_p	confining pressure
D	damping ratio
E_d	dynamic Young's modulus
E_f	Young's modulus (flexural vibration)
E_L	Young's modulus (longitudinal vibration)
E^*	complex Young's modulus
F, f	frequency
G	(dynamic) shear modulus or dynamic modulus of rigidity
G^*	complex shear modulus
S	specific surface area
T	temperature
$\tan \delta/2$	loss factor
V_L	longitudinal wave velocity
V_{lq}	velocity of incident wave in bath liquid
V_p , P-wave	compression wave velocity
V_s , S-wave	shear wave velocity
w_u	unfrozen water content
α	angle of incidence between wave train and sample face
δ	lag angle between stress vector and strain vector
ϵ_A	axial strain
ϵ_L	lateral strain
θ	temperature
θ_d	angle of refraction for longitudinal wave

θ_s	angle of refraction for shear wave
λ	damping ratio
μ	Poisson's ratio
μ^*	complex Poisson's ratio
ρ	density
σ'_m	mean principal effective stress
$\sigma_1, \sigma_2, \sigma_3$	major, intermediate, and minor principal stress

CHAPTER 1

INTRODUCTION

1.1 Statement of the Problem

In the past decade considerable attention has been focused on Alaska owing to its abundance of natural resources, particularly those related to our increasing demand for energy. The Alaskan pipeline, presently under construction, represents a monumental engineering undertaking to recover an estimated 25 to 30 billion barrels of petroleum beneath Alaska's North Slope; plans have recently been announced by El Paso Natural Gas Company to develop and bring into production the gas fields beneath Prudhoe Bay, which contain an estimated 25 trillion cubic feet of natural gas; undoubtedly, many other projects will follow.

With the recovery of natural resources, significant development of transporting facilities, transportation systems, utility networks, and general civil and industrial works must occur. Engineers concerned with this development will be faced with many challenging problems associated with the fact that 85 percent of Alaska lies within a permafrost region, i.e., a region of perennially or permanently frozen ground (Brown and Pewe, 1973). Clearly, knowledge of the behavior of frozen soils is essential to the solution of permafrost related problems.

Further, Alaska is located in one of the world's most active seismic zones. This was exemplified by the 1964 "Good Friday" earthquake and more than sixty other earthquakes that have equaled or exceeded a Richter magnitude of 7 since the 1800's (Davis and Echols, 1962).

It is now generally accepted that the ground surface motions which occur during an earthquake are influenced to a large extent by the characteristics of the underlying soil deposit under dynamic loading conditions (Idriss and Seed, 1968; Seed and Idriss, 1969). The importance of soil conditions and ground motions to the response of structures has been recognized for over half a century (Wood, 1908) and demonstrated conclusively in several recent earthquakes (Seed and Idriss, 1971; Seed, et al, 1972). Several analytic techniques are presently available to predict ground surface motions during earthquakes (Idriss and Seed, 1968;

Lysmer, et al, 1974; Schnabel, Lysmer, and Seed, 1972; Streeter, Wylie, and Richart, 1974). To employ these techniques two soil properties are required: (1) the dynamic shear modulus, and (2) the damping ratio. (These properties are also required to determine the response of foundations subjected to vibratory loads.) For unfrozen soils these properties have been determined by several investigators, using field and laboratory techniques, and design equations and curves to establish the properties for representative soil types have been developed (Hardin and Drnevich, 1972; Seed and Idriss, 1970). For frozen soils these properties (or equivalent properties) have been evaluated from seismic field studies and from ultrasonic, forced vibration, and resonant column tests in the laboratory. In general, however, it appears that the majority of these studies may be associated with test ranges that would not be useful in earthquake response analyses. Thus, an engineer confronted with a seismic design problem involving frozen soils cannot use existing analytic techniques to predict ground surface motions because the necessary properties of frozen soils have not been determined.

1.2 Purpose and Scope of Studies

As part of a long-term study to evaluate dynamic properties of frozen soils under simulated earthquake and low frequency loading conditions, dynamic Young's moduli and damping ratios of several types of artificially frozen soils and ice at two densities have been evaluated using cyclic triaxial test equipment. The scope of studies associated with the research program includes the development of the cyclic triaxial test system and experimental techniques employed to evaluate dynamic properties of frozen soils and ice, a discussion of the experimental results, and a comparison of the experimental results obtained in the present study to those obtained by previous investigators.

The results of the research work are presented in two volumes entitled: "Dynamic Properties of Ice and Frozen Clay Under Cyclic Triaxial Loading Conditions" and "Dynamic Properties of Frozen Cohesionless Soils Under Cyclic Triaxial Loading Conditions." The work presented in this volume is associated with the development of the cyclic triaxial test system and experimental techniques employed to evaluate dynamic properties of ice and frozen clay, a discussion of the experimental results, and a comparison of the experimental results of the present study to

those obtained by previous investigators. Specifically, in Chapter 2 a thorough review of previous studies to evaluate dynamic properties of ice and frozen clay is presented. All of the information given in Chapter 2 is associated with field or laboratory experimental methods which are significantly different from the method employed in the research program. Chapter 3 provides information on the laboratory preparation of samples of ice and frozen clay, installation of the samples in a triaxial cell, and the procedure used to test the samples. (Appendix A gives a detailed description of the components of the cyclic triaxial test system.) Chapter 4 presents the experimental results on the dynamic properties of ice. The influence on dynamic properties caused by variations in density, temperature, confining pressure, frequency, strain amplitude, and number of cycles of loading is included. In Chapter 5 the experimental results on the dynamic properties of frozen clay are presented. The influence on dynamic properties caused by variations in water content, specific surface area of the clay mineral, temperature, confining pressure, frequency, strain amplitude, and number of cycles of loading is included. Chapter 6 presents a comparison of the dynamic properties of ice and frozen clay obtained in the research program to those obtained by previous investigators. Chapter 7 summarizes the results of the research program and presents conclusions that can be reached.

1.3 Background

An understanding of the research work is enhanced by a knowledge of the mechanical properties of frozen soils and thermal characteristics of frozen soil deposits, the dynamic properties of unfrozen soils, and fundamentals of cyclic triaxial testing. This is presented in the next two sections of this chapter.

1.3.1 Mechanical Properties of Frozen Soils, Thermal Characteristics of Frozen Soil Deposits, and Dynamic Properties of Unfrozen Soils

In a previous research report (Vinson, 1975) a background knowledge of (1) the mechanical properties of frozen soils and the thermal characteristics of frozen soil deposits, and (2) the dynamic properties of unfrozen soils has been presented. This material may be summarized as follows:

(1) Frozen soils are a multiphase system of soil mineral particles,

polycrystalline ice, unfrozen pore water, and entrapped air. The relative proportions of these components influence their behavior.

- (2) The behavior of frozen soils are strongly dependent on time, strain rate, and temperature.
- (3) The unfrozen water content of frozen soils at a given sub-freezing temperature is a function of the specific surface area. Nearly all available water in sands is frozen at temperatures slightly below freezing, whereas unfrozen water can exist in clays at temperatures below -30°C .
- (4) The temperature in permafrost increases from close to the mean annual ground surface temperature to 0°C at some depth below the surface, at an average thermal gradient of $0.033 (^{\circ}\text{C})\text{m}^{-1}$. The ground temperatures over a significant portion of Alaska are in the range 0° to -6°C .
- (5) The dynamic properties of unfrozen soils are strain dependent. For cohesionless soils, dynamic properties are also dependent on confining pressure and relative density. The dynamic properties of cohesive soils are related to the shear strength.

1.3.2 Fundamentals of Cyclic Triaxial Testing

The stress states that a sample is subjected to during a cyclic triaxial test are shown in Figure 1.1. A cylindrical sample is placed in a cell and confined to an initial isotropic stress state. The axial load on the sample is then cycled causing a reversal of shear stresses in the sample which are a maximum on 45 degree planes. The principal stress directions rotate through 90 degrees every half cycle of loading.

During the test the cyclic axial load and sample deformation are recorded. The axial stress and strain in the sample are determined with a knowledge of the cross-sectional area and length of the sample. The axial stress when the sample is confined is the deviator stress, (i.e., the major principal stress minus minor principal stress, $\sigma_1 - \sigma_3$). Typical test results expressed in these terms for one cycle of loading are shown in Figure 1.2. From this record dynamic Young's modulus, E_d , and

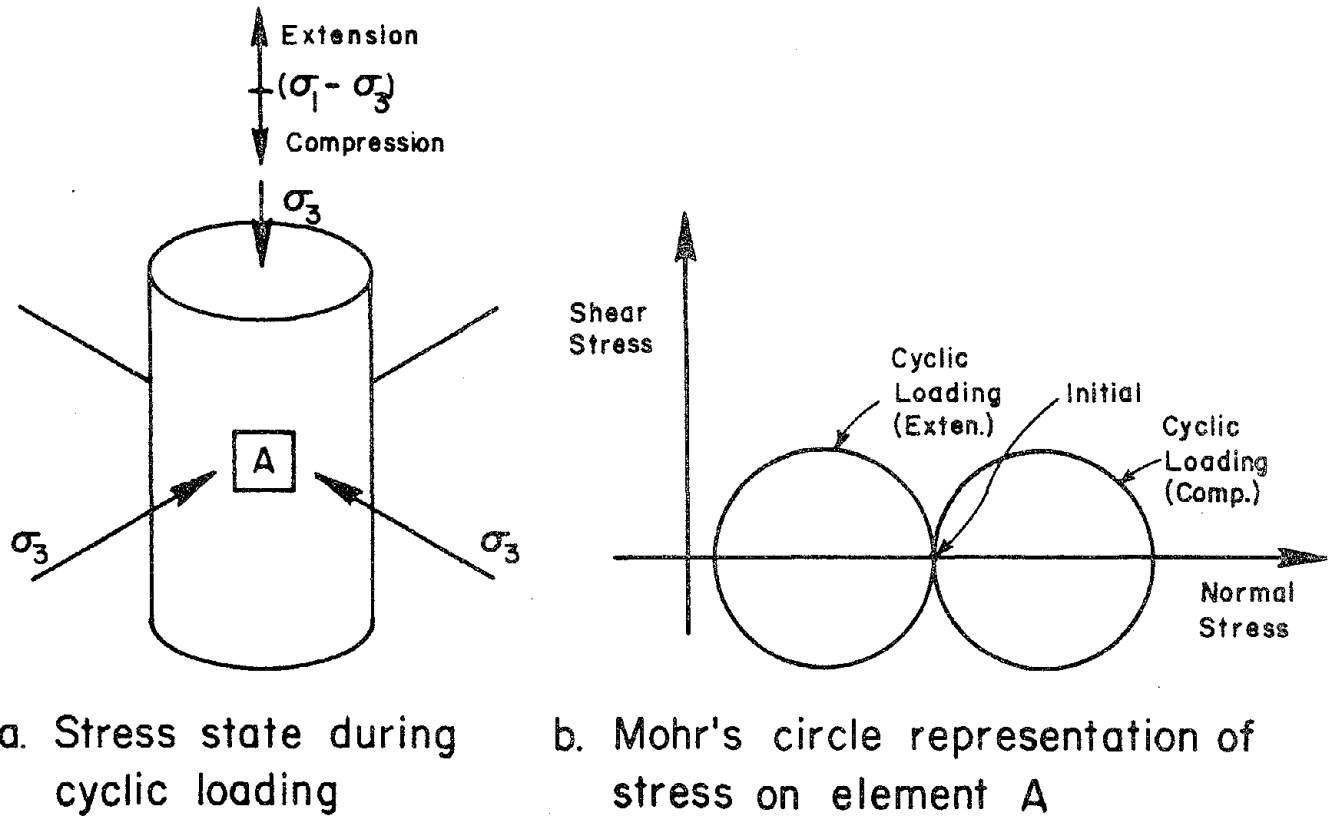


Figure 1.1 STRESS STATE IN TRIAXIAL TESTS WITH CYCLIC AXIAL STRESS

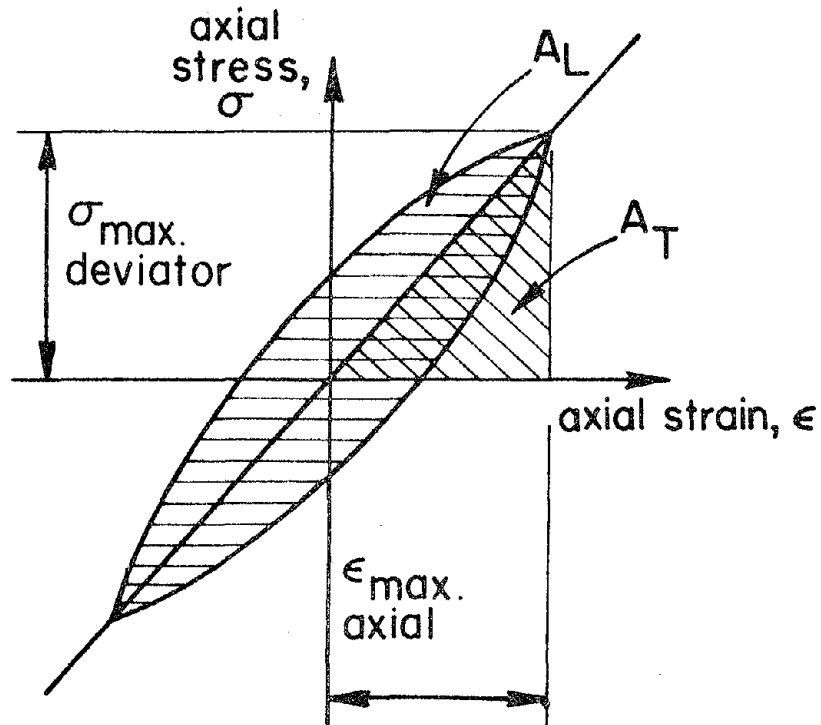


Figure 1.2 DEVIATOR STRESS VERSUS AXIAL STRAIN FOR ONE LOAD CYCLE

damping ratio, D , are determined as follows

$$E_d = \frac{\sigma \text{ max. deviator}}{\epsilon \text{ max. axial}} \quad (1.1)$$

and

$$D = \frac{A_L}{4\pi A_T} \quad (1.2)$$

with the terms as defined in Figure 1.2. A_L represents the total dissipated energy per cycle and A_T represents the work capacity per cycle.

The shear modulus may be calculated from the dynamic Young's modulus by employing:

$$G = \frac{E_d}{2(1 + \mu)} \quad (1.3)$$

in which,

μ = Poisson's ratio

Poisson's ratio may be determined experimentally by observing the lateral strain of the sample during cyclic loading and employing:

$$\mu = \frac{\epsilon_L}{\epsilon_A} \quad (1.4)$$

in which,

ϵ_L = lateral strain

ϵ_A = axial strain

CHAPTER 2

DYNAMIC PROPERTIES OF ICE AND FROZEN CLAY

2.1 General

The dynamic properties of ice and frozen clay have been determined by many investigators. Both field and laboratory research programs have been conducted and several parameters influencing the dynamic properties have been identified. As a consequence of the different test methods employed, dynamic properties have been expressed using many different terms. These fall into two major groups. The first group, "dynamic stress-strain" properties, includes terms such as compression, dilatational, longitudinal, irrotational, primary, bulk, or "P" and shear, transverse, secondary, rotational, or "S" wave velocity, sound velocity, complex Young's and shear (rigidity) moduli, and dynamic Young's and shear (rigidity) moduli. The second group, "energy absorbing" properties, includes terms such as angle of phase lag, attenuation coefficient, damping coefficient, loss factor, quality factor, log decrement, and damping ratio. Several of these terms are identified in Table 2.1 and conversion equations between them are given.

In this research program, dynamic Young's modulus was obtained from the cyclic triaxial tests performed. The shear modulus can be evaluated from dynamic Young's modulus for an isotropic material using the relationship:

$$G = \frac{E_d}{2(1 + \mu)} \quad (1.3)$$

in which,

E_d = dynamic Young's modulus

μ = Poisson's ratio

To allow this conversion to be made, Poisson ratio values for ice and frozen clay obtained from other investigator's work are also presented in this chapter. Poisson's ratio was not determined for the ice and clay samples tested in this research program.

2.2 Previous Methods to Evaluate Dynamic Properties of Ice and Frozen Soils

Seismic methods have been the most widely used field technique to determine the dynamic properties of ice and frozen soils. Specifically,

Table 2.1 CONVERSION EQUATIONS BETWEEN TERMS TO CHARACTERIZE DYNAMIC PROPERTIES

(a) Dynamic Stress Strain Properties

To Calculate	Dynamic or Complex Young's Modulus	Dynamic or Complex Shear Modulus	Poisson's Ratio	Compression Wave Velocity	Shear Wave Velocity	Longitudinal Wave Velocity
Given	E or E^{*1}	G or G^{*1}	μ or μ^{*1}	V_p	V_s	V_L
E, ρ, μ	E	$\frac{E}{2(1+\mu)}$	μ	$\left(\frac{E}{\rho} \frac{1-\mu}{(1+\mu)(1-2\mu)}\right)^{\frac{1}{2}}$		$\left(\frac{E}{\rho}\right)^{\frac{1}{2}}$
G, μ, ρ	$2(1+\mu)G$	G	μ	$\left(\frac{(1-\mu)2G}{(1-2\mu)\rho}\right)^{\frac{1}{2}}$	$\left(\frac{G}{\rho}\right)^{\frac{1}{2}}$	
E, G	E	G	$\frac{E}{2G} - 1$		$\left(\frac{G}{\rho}\right)^{\frac{1}{2}}$	$\left(\frac{E}{\rho}\right)^{\frac{1}{2}}$
ρ, μ, V_p	$\frac{V_p^2 \rho (1-2\mu)(1+\mu)}{(1-\mu)}$	$\frac{(1-2\mu)\rho V_p^2}{2(1-\mu)}$	μ	V_p	$V_p \left(\frac{1-2\mu}{2(1-\mu)}\right)^{\frac{1}{2}}$	$V_p \left(\frac{(1+\mu)(1-2\mu)}{(1-\mu)}\right)^{\frac{1}{2}}$
ρ, μ, V_s	$2\rho(1+\mu)V_s^2$	ρV_s^2	μ		V_s	$V_s (2(1+\mu))^{\frac{1}{2}}$
ρ, V_p, V_s	$\frac{V_s^2 (3V_p^2 - 4V_s^2)\rho}{V_p^2 - V_s^2}$	ρV_s^2	$\frac{1}{2} \frac{V_p^2 - 2V_s^2}{V_p^2 - V_s^2}$	V_p	V_s	

¹Complex moduli are not significantly different from elastic moduli for materials with low damping, such as frozen ground.

(b) Energy Absorbing Properties

To Calculate	Damping Ratio	Loss Factor	Quality Factor
Given	D	$\tan \delta$	Q
Phase Lag δ	$\sin \frac{\delta}{2}$	$\tan \delta$	$\frac{1}{\tan \delta}$
Attenuation Coefficient, Wavelength a, λ	$\sin\left(\frac{\tan^{-1} \frac{a\lambda}{2\pi}}{2}\right)$	$\frac{\lambda}{2\pi}$	$\frac{\pi}{a\lambda}$
Damping Coefficient, Angular Frequency β, ω	$\sin\left(\frac{\tan^{-1} \frac{2\beta}{\omega}}{2}\right)$	$\frac{2\beta}{\omega}$	$\frac{\omega}{2\beta}$
Log Decrement Δ	$\frac{-2\pi \pm (4\pi^2 + 4\Delta^2)^{\frac{1}{2}}}{2\Delta}$	$\tan 2 \sin^{-1} \left(\frac{-2\pi \pm (4\pi^2 + 4\Delta^2)^{\frac{1}{2}}}{2\Delta} \right)$	$\frac{\pi}{\Delta}$

the compression and shear wave velocities can be determined. In the seismic method, elastic waves are produced by a source at a known location and the waves are detected at various distances from the source by vibration sensitive detectors called seismographs or geophones. (The source of the waves is usually an explosive charge for measurements over great distances, but for a short distance the impact of a hammer can be used.) The waves are produced at a known instant of time so that the travel time of propagation can be observed. Knowledge of the travel time and distance from the source allows the wave velocity to be computed. If the seismic wave velocities for given materials are known, then information on the geometry of the substrata of the earth's surface at a location can be determined by an interpretation technique from the travel time observations. A complete treatment of seismic methods is given by Dobrin (1960) and Roethlisberger (1972).

In 1969, Kaplar determined dynamic properties of ice and frozen soil samples in the laboratory by vibrating beams of frozen specimens with electromagnets. A schematic diagram of the test apparatus is shown in Figure 2.1. The beams were approximately 3.81 x 3.81 x 27.94 cm. Permanent bar magnets, 0.476 x 0.476 x 5.08 cm, were frozen at each end of the specimens. The specimens were vibrated by the electromagnet mounted at one end. The waves that propagated through the specimens were detected by the electromagnet which was mounted at the other end of the specimens. The orientation of the two electromagnets was the same. The specimens were vibrated in the longitudinal, flexural and torsional modes and the dynamic properties could be evaluated at the resonant frequency of the specimens. [The equations used for the calculation of the dynamic properties are given by Kaplar (1969).] The dynamic Young's modulus from flexural vibration (E_f), the dynamic Young's modulus from longitudinal vibration (E_L), the dynamic modulus of rigidity (G), and Poisson's ratio (μ) were obtained from the experiments.

In 1969, Smith performed forced vibration tests in the laboratory and measured the dynamic properties of ice core samples. A schematic of his test equipment is shown in Figure 2.2. The samples were 7.5 cm in diameter and had a minimum length to diameter ratio of 4:1. One end of the sample was fixed to the drive assembly vibration table by freezing. A thin aluminum plate was frozen to the other end of the sample (free

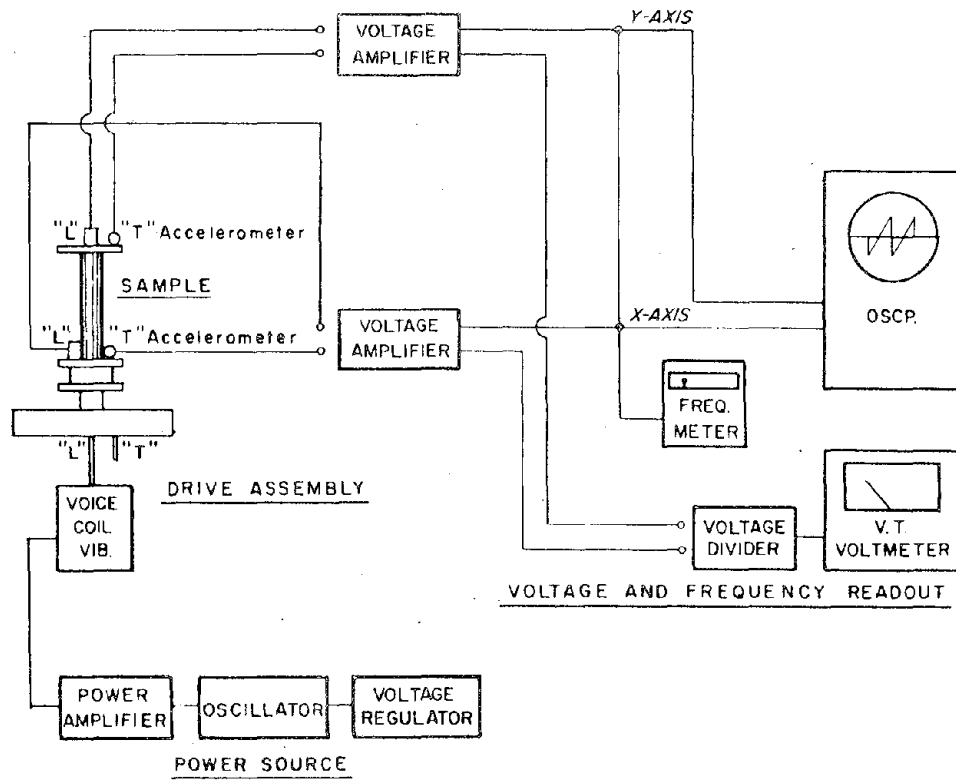
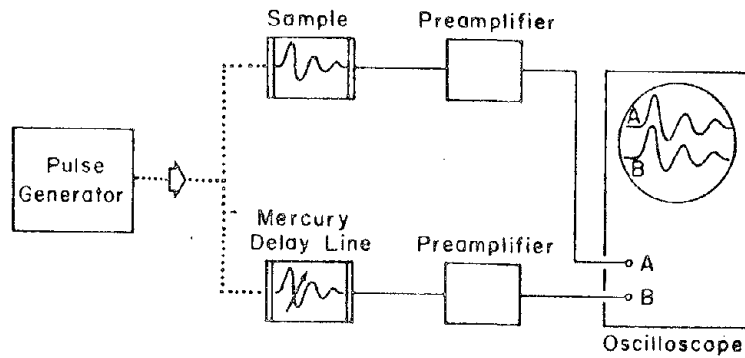


Figure 2.2 SCHEMATIC OF FORCED VIBRATION DYNAMIC TEST EQUIPMENT (after Smith, 1969)

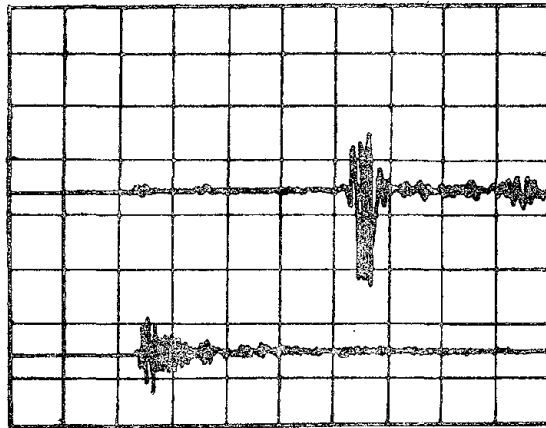
end). Two accelerometers were attached to the bottom of the sample to monitor longitudinal and torsional excitation (one for each mode) and two were attached to the aluminum top plate to monitor the sample response to the excitation. As the excitation frequency was varied the accelerometer signals were displayed on an oscilloscope to determine when the sample was at resonance. At resonance the dynamic properties could be calculated (Lee, 1963). The range of test frequencies was 600 to 2200 cps. The complex dynamic Young's modulus (E^*), complex dynamic shear modulus (G^*), loss factor ($\tan \delta/2$), and complex Poisson's ratio (μ^*) were determined from the tests.

In 1972, Bennett measured the compression and shear wave velocities of ice cores from Greenland and Antarctica by an ultrasonic pulsing method. A schematic diagram of the time measurement system is shown in Figure 2.3a. This method requires the simultaneous production of mechanical waves at one end of a frozen specimen and at one end of a mercury delay line. The mechanical waves received at the opposite end of the samples and the mercury delay line were transformed to electrical signals by transducers. The signals were amplified and displayed on an oscilloscope. The signal from the mercury delay line was adjusted to match the signal from the sample as shown in Figure 2.3b. Knowledge of the travel time and sample length allowed the wave velocity to be calculated. The compression and shear wave velocities were obtained from the test program.

Nakano and his co-workers (Nakano and Arnold, 1973; Nakano and Froula, 1973; Nakano, Martin, and Smith, 1972) used an ultrasonic pulse transmission method similar to that used by Bennett (1972) and the critical angle method to evaluate dynamic properties of frozen soils. The critical angle method is based upon the variation in intensity of transmitted wave energy with the angle of incidence, α , between a wave train and sample face. In a typical test system, as shown in Figure 2.4a, the oscillator excites the piezoelectric crystal which produces a mechanical wave in the fluid at one end of the liquid filled bath. The wave impinges on one side of the disc sample. The sample is in a holder which is free to rotate about an axis perpendicular to the wave train. As shown in Figure 2.4b, when the incident wave is not normal to the sample both longitudinal and shear waves are induced in the sample. Since the wave velocity in the solid is greater than in the liquid, the waves in the solid

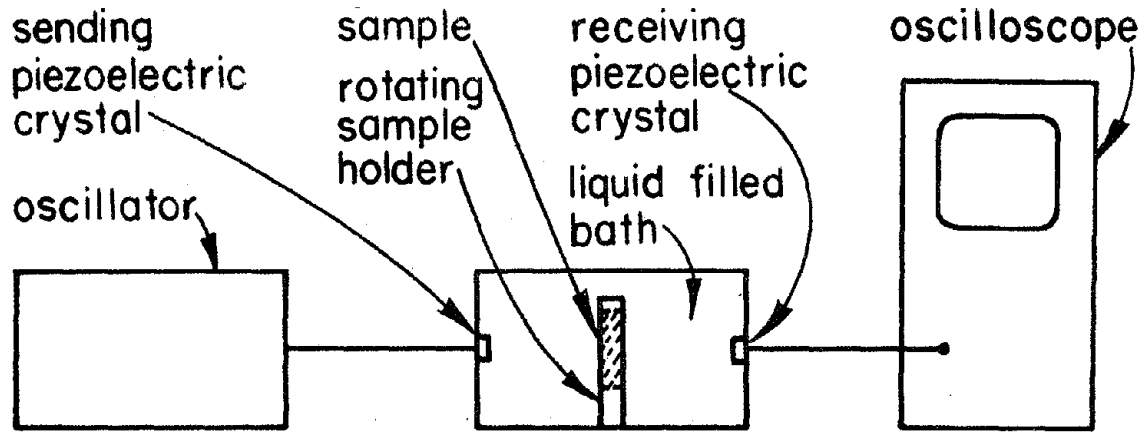


(a) Schematic Diagram of Time Measurement System Used in Ultrasonic Pulsing Method

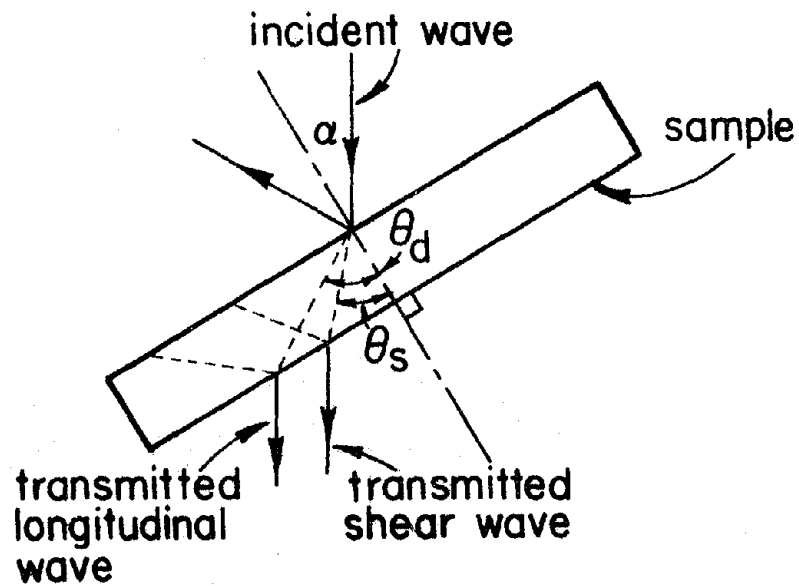


(b) P-Wave Arrival Through Mercury Delay Line (bottom trace) and Ice Sample (top trace)

Figure 2.3 ULTRASONIC PULSING METHOD (after Bennett, 1972)



(a) Schematic of Critical Angle Test System



(b) Wave Transmission Through Parallel Plate

Figure 2.4 CRITICAL ANGLE METHOD

are refracted away from the normal. From Snell's law the following relations hold:

$$\frac{\sin\alpha}{\sin\theta_d} = \frac{V_{lq}}{V_d} \quad (2.1)$$

$$\frac{\sin\alpha}{\sin\theta_s} = \frac{V_{lq}}{V_s} \quad (2.2)$$

in which,

θ_d = angle of refraction for longitudinal wave

θ_s = angle of refraction for shear wave

V_{lq} = velocity of incident wave in the bath liquid

It is apparent from these relationships that the two types of waves are refracted at different angles in the sample because of the difference in their velocities. As the sample is rotated away from the normal there will be two critical angles of incidence, α_1 critical and α_2 critical, at which θ_d and θ_s , respectively, equal 90° . At these critical angles the longitudinal or shear waves will be totally reflected and only the shear waves or longitudinal waves, respectively, will be transmitted. The determination of wave velocities in the sample involves monitoring the wave transmitted through the sample with the receiving piezoelectric crystal and noting when it is at a minimum amplitude. The first minimum allows V_d to be calculated from equation (2.1) upon substitution of 90° for θ_d and α_1 critical for α . The second minimum allows V_s to be calculated from equation (2.2) upon substitution of 90° for θ_s and α_2 critical for α .

In 1973, with forced vibration equipment similar to Smith (1969), Stevens tested ice and frozen soil samples by applying steady-state sinusoidal vibrations to the samples. A schematic diagram of the test equipment is shown in Figure 2.5. The specimens were 7.6 cm in diameter and the lengths were equal to or greater than 15.2 cm. The bottom of the sample was frozen to the base plate of the drive assembly and a light steel plate was frozen to the top. Three accelerometers were attached to the top plate, one on the longitudinal axis to measure the longitudinal response and two on the circumference to measure the torsional response. At the base plate two accelerometers were attached for measuring the longitudinal or torsional sinusoidal driving motion. The driving

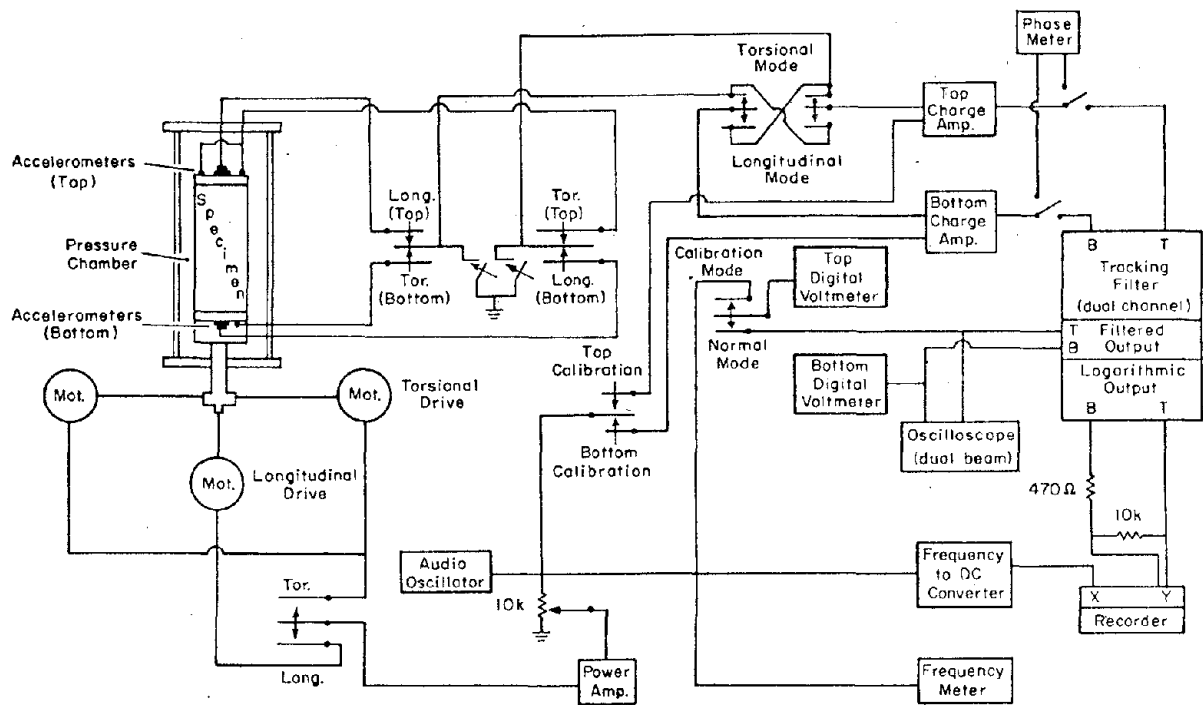


Figure 2.5 SCHEMATIC OF FORCED VIBRATION DYNAMIC TEST EQUIPMENT (after Stevens, 1973)

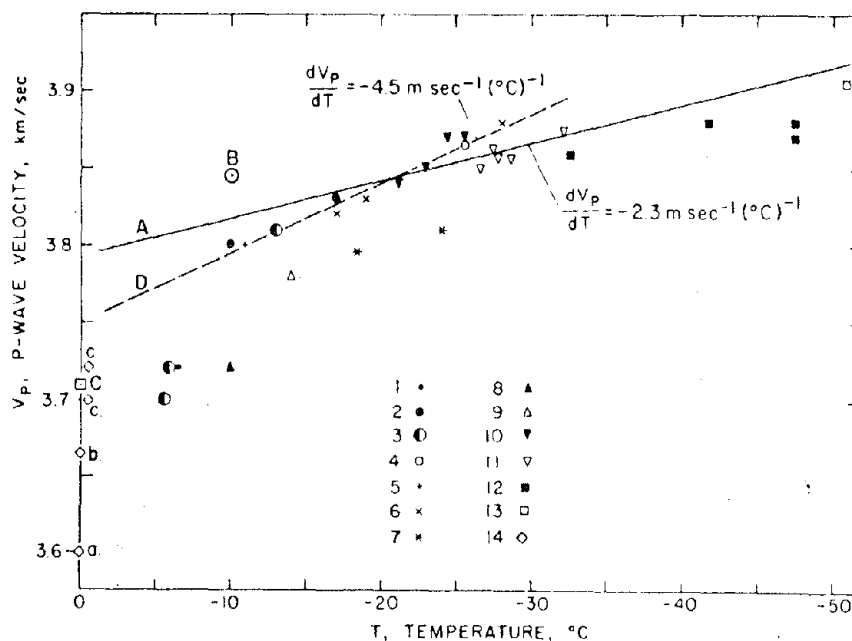
motion frequency was varied until the sample was at resonance. Alternatively, an "off-resonance" technique can also be employed (Stevens, 1975). The complex dynamic Young's modulus (E^*), complex dynamic shear modulus (G^*), damping expressed as ($\tan \delta$), and complex Poisson's ratio (μ^*) were obtained from the test program.

2.3 Dynamic Elastic Properties of Ice

Considerable progress has been made in recent years to determine the dynamic elastic properties of ice and a substantial effort has been made to compare the dynamic elastic properties from field and laboratory tests. Most of the field work has been done on the Greenland ice sheets. The laboratory work has been conducted on artificially frozen samples and ice cores from Greenland. Several parameters influencing the dynamic elastic properties have been identified and investigated. The most important appear to be temperature, density and frequency. The influence of strain amplitude and confining pressure apparently has not been investigated.

2.3.1 Effect of Temperature

The influence of temperature on dynamic elastic moduli has been reported by several investigators and summarized by Roethlisberger (1972), as shown in Figures 2.6, 2.7, 2.8, and 2.9. The figures illustrate that as the temperature approaches the freezing point shear and compression wave velocities decrease. In Figure 2.6, compression wave velocities from many investigations are plotted as a function of temperature. At a temperature of -50°C the velocity is about 3.88 km/sec, but it decreases to about 3.85 km/sec at a temperature of -20°C . The velocity drops rapidly from 3.85 km/sec at -20°C to about 3.68 km/sec at the melting point. For the lower temperature range -20 to -50°C , the compression wave velocity appears to decrease linearly with temperature and the rate of decrease is smaller than for the temperature range -20 to 0°C . Figure 2.7 shows the influence of temperature on the shear wave velocity. The shear wave velocity is about 1.94 km/sec at -20°C and about 1.68 km/sec at the melting point (for samples taken from various Mountain Glaciers). As the melting point is approached, the velocity drops sharply as shown in Figure 2.8. As shown in Figure 2.9, the sound velocity in synthetic ice cores is almost constant at about 3.5 km/sec in the range of temperature -20 to -4°C .



Seismic measurements:

1. Greenland ice sheet, Brockamp et al., 1933; after Thyssen, 1967.
2. Greenland ice sheet, Joset and Holtzscherer, 1954.
3. Baffin Island, Roethlisberger, 1955.
4. Greenland ice sheet, Bentley et al., 1957.
5. Novaya Zemlya, Wöloken; after Thyssen, 1967.
6. Greenland ice sheet, Brockamp and Kohnen, 1965; after Thyssen, 1967.
7. Ellesmere Island, Hattersley-Smith, 1959; Weber and Sandstrom, 1960.
8. Edge of Greenland ice sheet, Roethlisberger, 1961.
9. Edge of Greenland ice sheet, Bentley et al., 1957, Goldthwait, 1960.
10. Antarctic Peninsula Plateau, Bentley, 1964.
11. Byrd Plateau, Bentley, 1964.
12. Victoria Plateau, Bentley, 1964.
13. Polar Plateau, Bentley, 1964.
14. Various Mountain glaciers: a) Thyssen, 1967; b) Vallon, 1967; c) Clarke, 1967.

Ultrasonic measurements: Line A Robin, 1958; Point B Bennett, 1972; Point C Thyssen, 1967; Line D Thyssen's empirical relationship.

Figure 2.6 P-WAVE VELOCITY OF ICE VERSUS TEMPERATURE (after Roethlisberger, 1972)

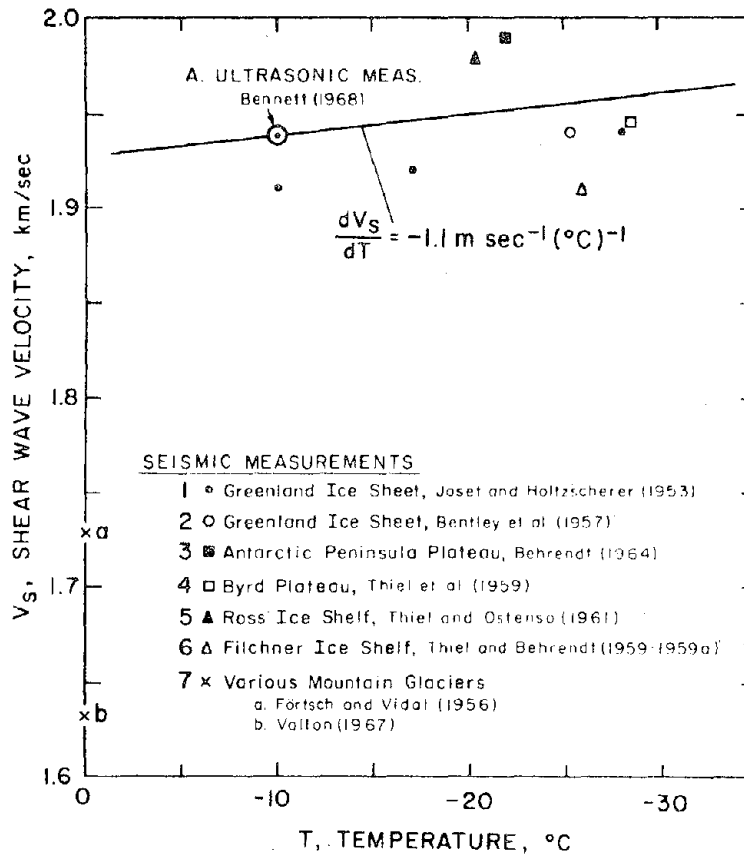


Figure 2.7 S-WAVE VELOCITY OF ICE VERSUS TEMPERATURE (after Roethlisberger, 1972)

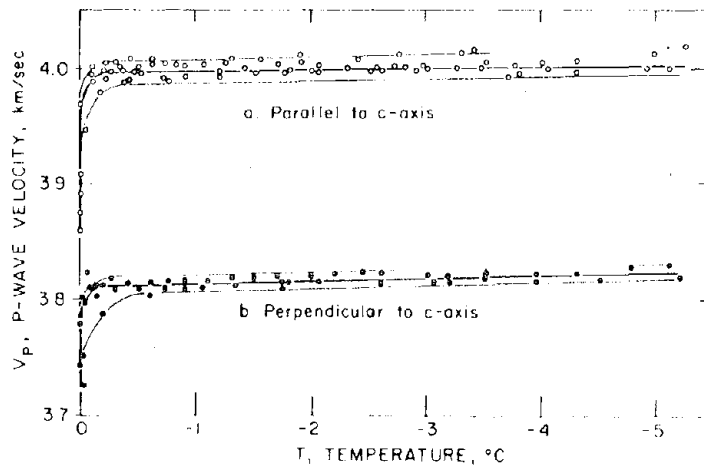


Figure 2.8 P-WAVE VELOCITY IN THE PRINCIPAL DIRECTIONS OF SINGLE-CRYSTAL ICE VERSUS TEMPERATURE (after Brockamp and Querfurth from Roethlisberger, 1972)

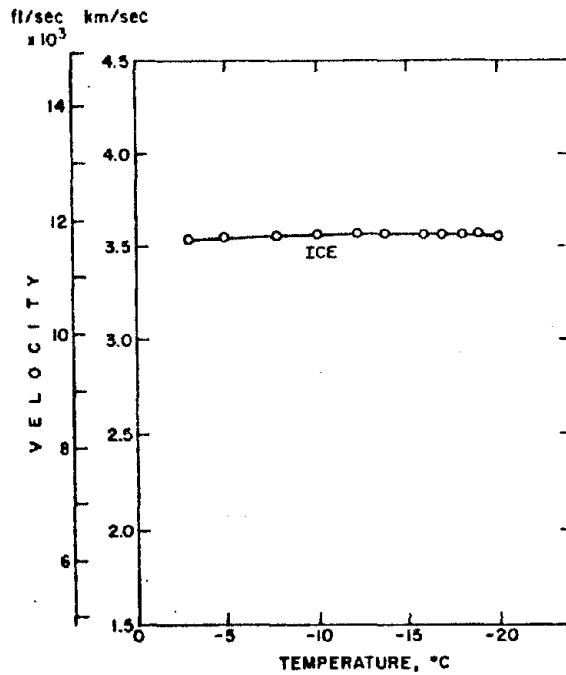


Figure 2.9 SOUND VELOCITY IN SYNTHETIC ICE CORES VERSUS TEMPERATURE (after Müller, 1961, from Roethlisberger, 1972)

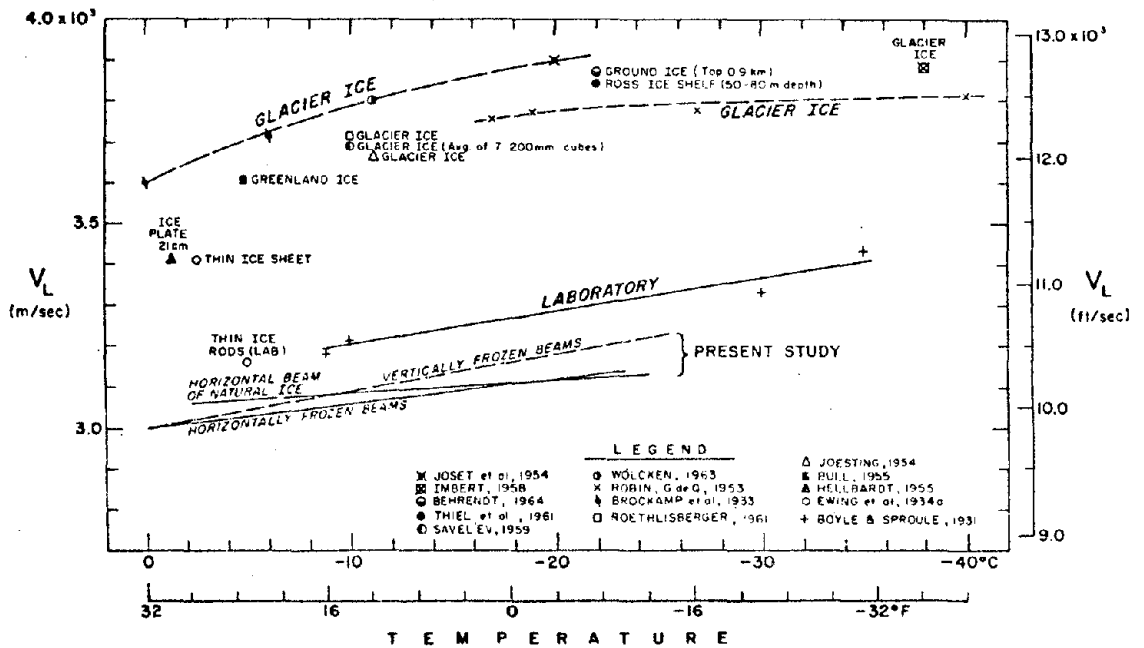


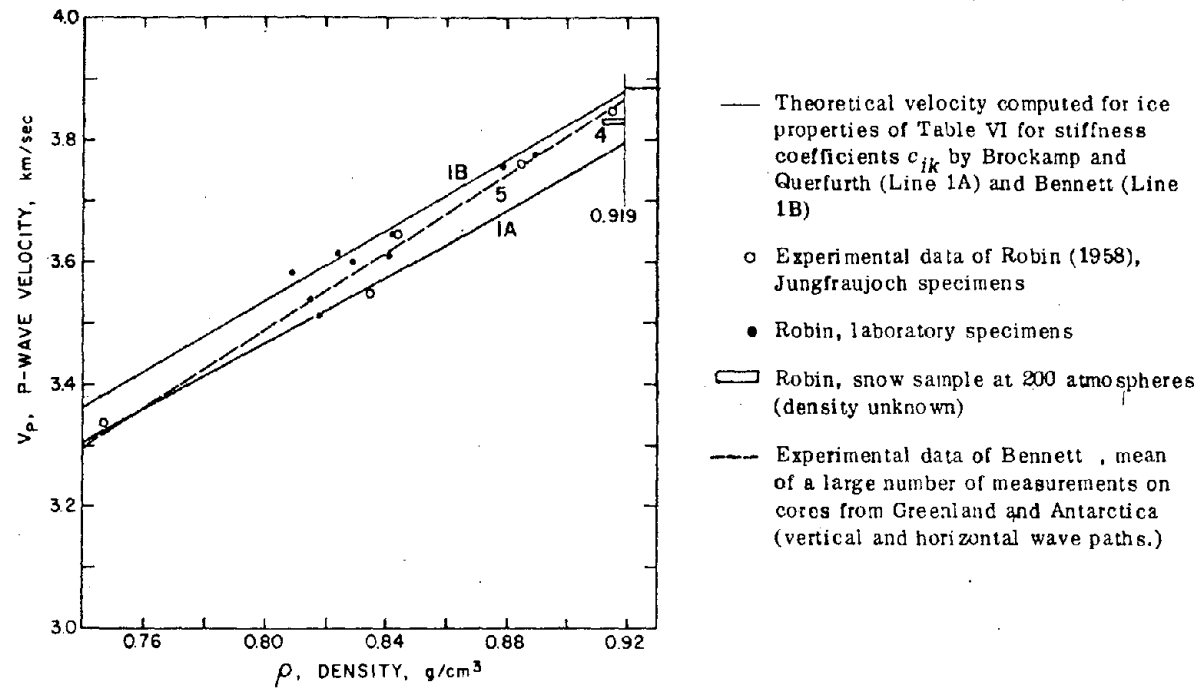
Figure 2.10 SUMMARY OF LONGITUDINAL OR P-WAVE VELOCITIES IN ICE MEASURED BY VARIOUS INVESTIGATORS (after Kaplar, 1969)

The influence of temperature on wave velocity may be expressed by a "temperature coefficient" with units (meters/second)/°C. Robin (1958) reports a temperature coefficient of -2.3 (meters/second)/°C for compression wave velocity. Roethlisberger (1972) indicates that the temperature coefficient of the compression wave velocity decreases in its absolute value with decreasing temperature and he also suggests that a temperature coefficient of -1.1 (meters/second)/°C is appropriate for the shear wave velocity. Kaplar (1969) determined the dynamic elastic moduli of artificial samples of frozen ice and natural ice cores. Kaplar summarized the influence of temperature using his tests and those of others as shown in Figure 2.10. The data presented indicates that the field velocities of ice sheets and ground ice are higher than the velocities determined in the laboratories by about 20%. Kaplar states "This is due to the fact that velocities of longitudinal waves in thin bars or rods, in thin plates, and in infinitely extended solids are all different. Available formulas (Ewing, et al, 1934) show that longitudinal velocities in a thin ice plate may be 5 to 10% higher than in thin ice rods, and in extended ice masses the velocities may be 20-25% higher depending upon the value of Poisson's ratio μ used in the formulas. This is borne out by the experimental data presented in Figure 2.10." Kaplar concluded that the dynamic elastic properties of ice, whether laboratory frozen or natural, appear little affected by temperature.

2.3.2 Effect of Density

Considerable work has been reported on the influence of ice density on dynamic elastic properties. Roethlisberger (1972) compiled field and laboratory data from many investigators and corrected these data to -16°C based on a temperature coefficient of -2.3 (meters/second)/°C. The results are shown in Figure 2.11. The results fall within a relatively narrow band. The compression wave velocity of the band varies linearly with the density of ice. The velocity decreases from about 3.83 km/sec at 0.92 g/cm^3 to about 3.38 km/sec at 0.76 g/cm^3 . This band indicates that the compression wave velocity of ice is significantly influenced by the ice density.

In a study conducted by Bennett (1972), the velocity of ice cores from Greenland and Antarctica were determined by ultrasonic methods and, in addition, refraction seismic surveys were conducted at the locations



Note: All data corrected to -16°C based on a temperature coefficient of -2.3 (meters/second)/ $^{\circ}\text{C}$.

Figure 2.11 P-WAVE VELOCITY OF ICE VERSUS DENSITY (after Roethlisberger, 1972)

in the field where the cores were taken. The results employing these two test methods are presented in Figure 2.12 and 2.13. The figures show the variation of compression and shear wave velocities with density. The compression wave velocity varies from about 3800 m/sec at 0.90 g/cc to about 1100 m/sec at 0.40 g/cc. The shear wave velocity varies from about 1800 m/sec at 0.90 g/cc to about 520 m/sec at 0.40 g/cc. The compression and shear wave velocities decrease almost linearly from 0.90 to 0.6 g/cc. At densities lower than 0.6 g/cc, the velocities drop rapidly. The rate of decrease is greater for densities lower than 0.6 g/cc than for densities above this value.

Robin (1958) obtained an empirical relationship between compression wave velocity, temperature, and density of ice as follows:

$$V_p = \frac{\rho - 0.059 (1 - 0.00061 T) 10^4}{2.21} \quad (2.3)$$

in which,

V_p = compression wave velocity in m/sec

ρ = ice density in g/cc

T = temperature in °C

Clarke (1966) studied the velocity of ice by seismic methods and compared his results with Robin's empirical formula as shown in Figure 2.14. The compression wave velocity was plotted against depth from the ground surface. The velocity increases with depth from 600 m/sec at the surface to about 3800 m/sec at a depth of 100 m. The rate of increase in velocity decreases with depth and when the depth is greater than 100 m the rate of increase is almost negligible. Clarke commented that Robin's formula gives good results up to a density of 0.892 g/cc. For ice above this density Robin's formula apparently overestimates the compression wave velocity.

2.3.3 Effect of Frequency

Only limited work has been reported on the influence of frequency on the dynamic elastic properties of ice. Smith (1969) states that dynamic moduli increase slightly with increasing frequency as shown in Figure 2.15. The complex dynamic Young's and shear moduli were plotted against frequency over a range 800 to 2800 cps. The rate of increase of the complex Young's modulus and complex shear modulus are nearly identical.

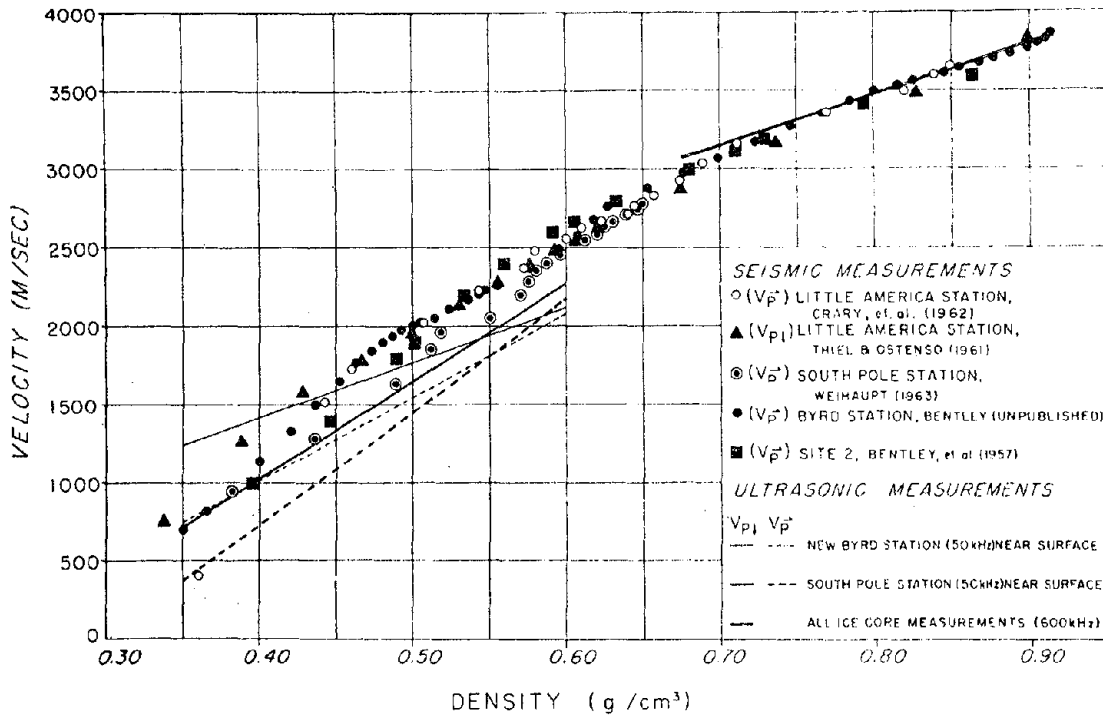


Figure 2.12 P-WAVE VELOCITY VERSUS ICE DENSITY FROM SEISMIC AND ULTRASONIC MEASUREMENTS (after Bennett, 1972)

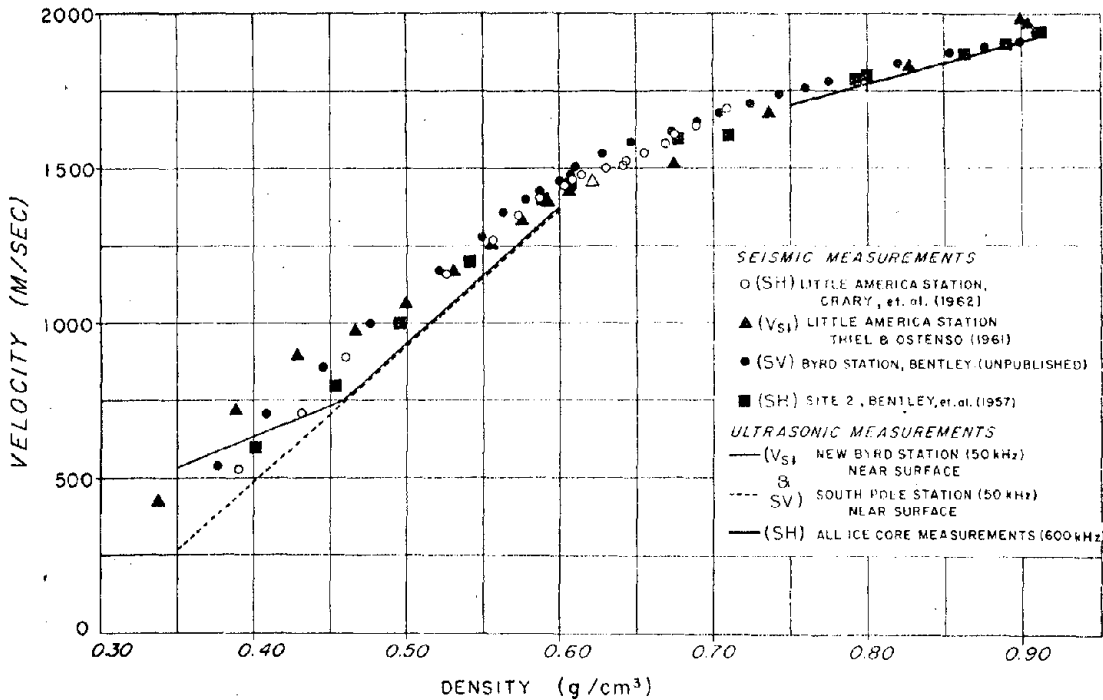


Figure 2.13 S-WAVE VELOCITY VERSUS ICE DENSITY FROM SEISMIC AND ULTRASONIC MEASUREMENTS (after Bennett, 1972)

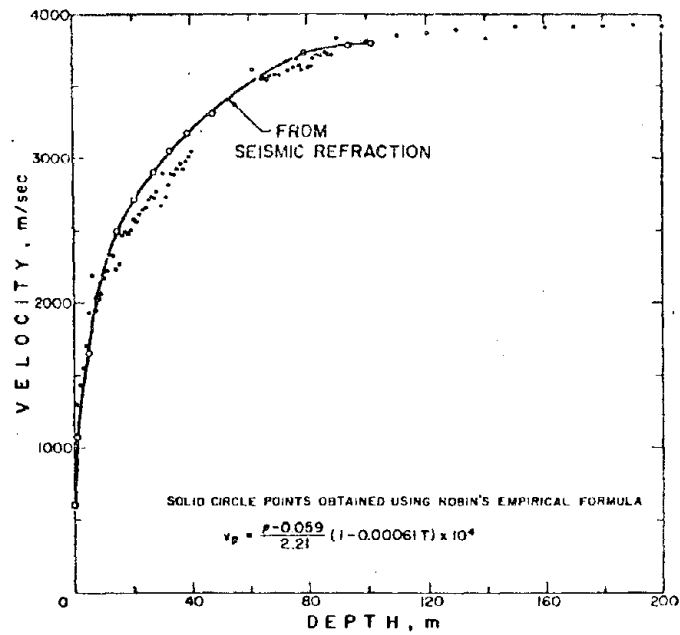


Figure 2.14 P-WAVE VELOCITY OF ICE VERSUS DEPTH AT CAMP CENTURY (after Clarke, 1966)

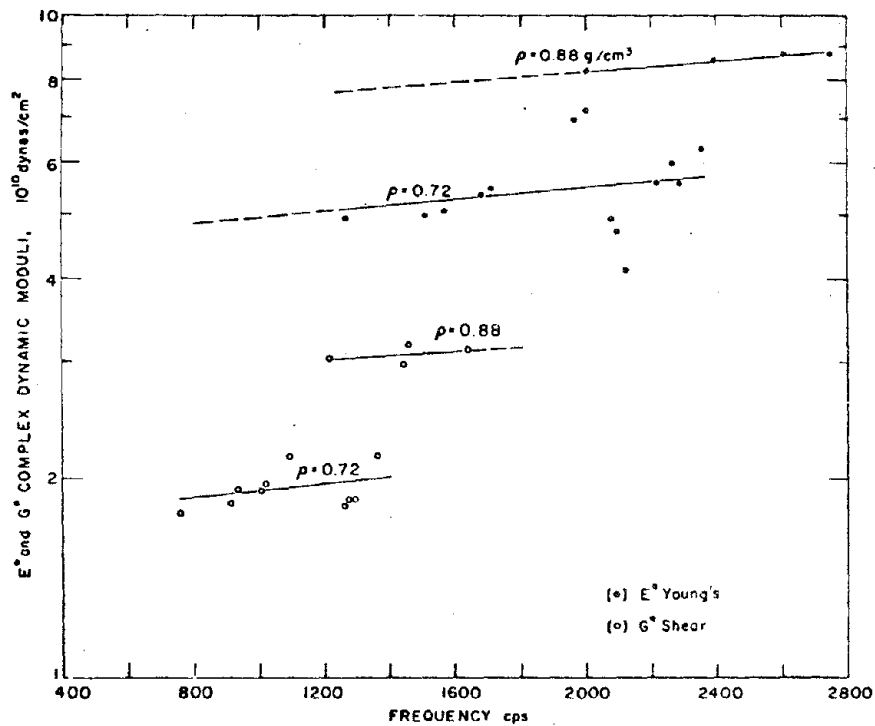


Figure 2.15 COMPLEX DYNAMIC MODULI OF ICE VERSUS FREQUENCY (after Smith, 1969)

2.3.4 Effect of Confining Pressure

Information on the effect of confining pressure on dynamic elastic properties is very limited. Bennett (1972) conducted ultrasonic tests on unconfined ice cores and seismic surveys were performed in the field at locations where the cores were taken. As shown in Figures 2.12 and 2.13, the results from the ultrasonic tests on the unconfined core samples are not significantly different from the seismic survey results where the ice was subjected to the in situ confining pressure. Roethlisberger (1972) reports that the effect of pressure is to reduce porosity and, hence, increase the density of bubbly ice. With increasing density the shear and compression wave velocities should increase. He states that a slight increase in velocity should be expected with increasing pressure, but provides no justification for this statement.

2.4 Damping of Ice

Smith (1969) studied the parameters influencing the damping properties of snow and ice core samples and presented the test results in terms of a loss factor ($\tan \delta/2$). His work indicates:

- (1) The loss factor appears to decrease with an increase in frequency but the trend is not well established because considerable scatter exists in the data as shown in Figure 2.16. The density of the ice sample was 0.72 g/cm^3 . The loss factor varied between 0.01 and 0.07 when the frequency increased from 800 to 2400 cps.
- (2) With increasing driving force, the loss factor tends to increase, but again the trend is not well established owing to the scatter of the data as shown in Figure 2.17. The density of the ice sample was 0.72 g/cc . The driving force was expressed in acceleration voltage output (RMS) at the sample base. When the acceleration voltage was increased from 0.01 RMS to 0.05 RMS the loss factor varied between 0.01 and 0.07.
- (3) The most significant influence on the loss factor is density. As shown in Figure 2.18, the loss factor is 0.04 at 0.4 g/cc but drops to 0.005 at a density of 0.9 g/cc .

Stevens (1973) studied the influence of temperature on damping of ice. His work indicates that as the temperature increases the damping ($\tan \delta$) increases as shown in Figure 2.19. $\tan \delta$ is 0.045 at 0°F and increases to 0.06 at 25°F for longitudinal vibration whereas $\tan \delta$

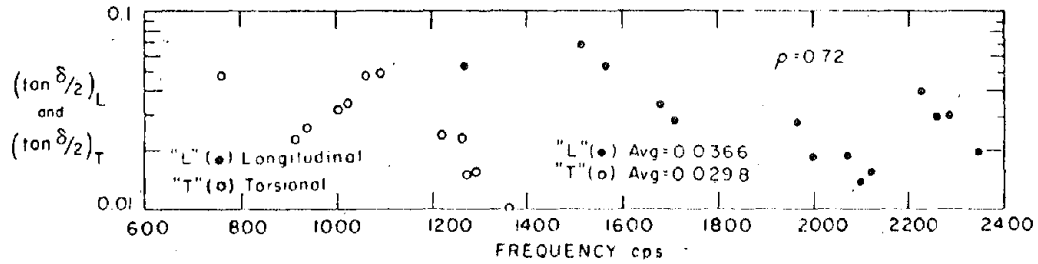


Figure 2.16 LOSS FACTOR OF ICE VERSUS FREQUENCY (after Smith, 1969)

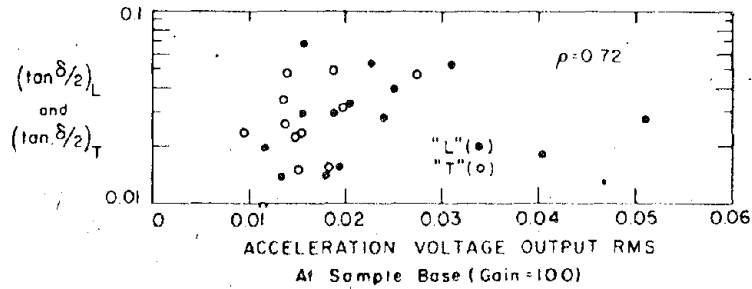


Figure 2.17 LOSS FACTOR OF ICE VERSUS DRIVING FORCE (after Smith, 1969)

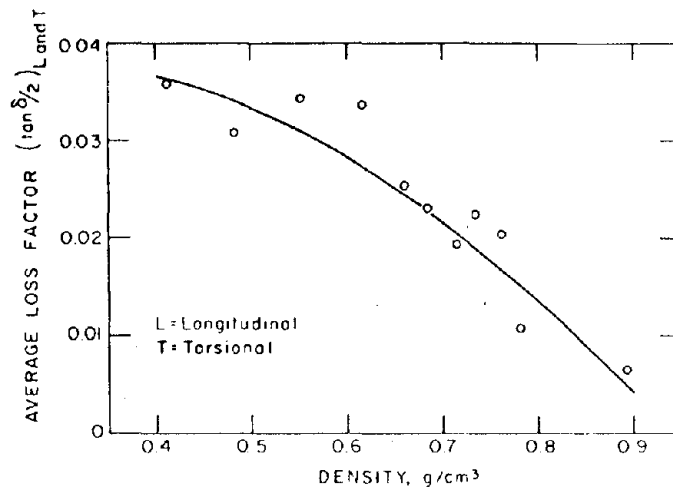


Figure 2.18 LOSS FACTOR OF ICE VERSUS DENSITY (after Smith, 1969)

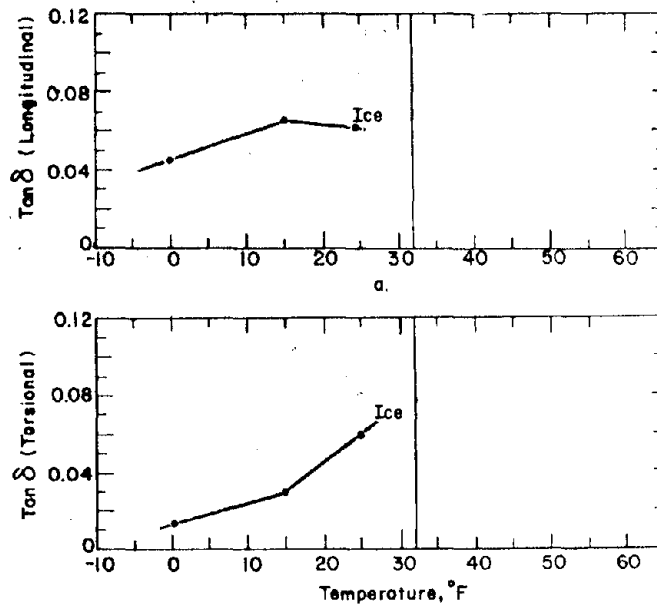


Figure 2.19 EFFECT OF TEMPERATURE ON TAN δ OF ICE (after Stevens, 1975)

is 0.013 at 0°F and increases to 0.06 at 25°F for torsional vibration.

2.5 Dynamic Elastic Properties of Frozen Clay

Most of the work to evaluate the dynamic elastic properties of frozen clays has been in the laboratory. Apparently, the only in situ measurements were reported by Barnes (1963); the shear wave velocity of alluvial clay at Northway, Alaska, at -2°C was 7.8 kilo ft/sec.

2.5.1 Effect of Void Ratio

The effect of void ratio has been studied by Stevens (1975). He indicates that as the void ratio of frozen clay increases beyond 1.0 (i.e., the volume of ice becomes significantly greater than the volume of frozen clay) the dynamic elastic modulus tends to approach that of ice. Similar results were obtained by Müller (1961) as shown in Figure 2.20. At a temperature of -10°C, the sound wave velocity of frozen clay cores increases about 20% for an increase in porosity from 67% to 96%.

2.5.2 Effect of Ice Saturation

It is generally believed that the dynamic elastic properties of frozen clay at a constant void ratio should be dependent on the volume of ice in the voids available to cement the soil grains together. This can be expressed in terms of the degree of ice saturation which is the ratio of the volume of the ice to the volume of the voids in a soil mass. As shown in Figure 2.21, Stevens (1973) found that the increase in modulus with increasing ice saturation for Suffield clay is nearly constant on a semi-logarithmic plot. The ice saturation is plotted against the log of dynamic complex shear modulus of Suffield clay. The modulus increases from about 0.075 GN/m² at 0% ice saturation to 1.14 GN/m² at 100% ice saturation.

2.5.3 Effect of Temperature

The dynamic elastic properties of frozen clay tend to decrease with ascending temperature. At temperatures near 0°C, the decrease with increasing temperature is fairly rapid. Nakano and Froula (1973) determined the shear wave velocity of Goodrich clay as a function of temperature using ultrasonic techniques. The results are presented in Figure 2.22. The shear wave velocity is 2.0 km/sec at -16°C but drops to 1.7 km/sec at -1°C.

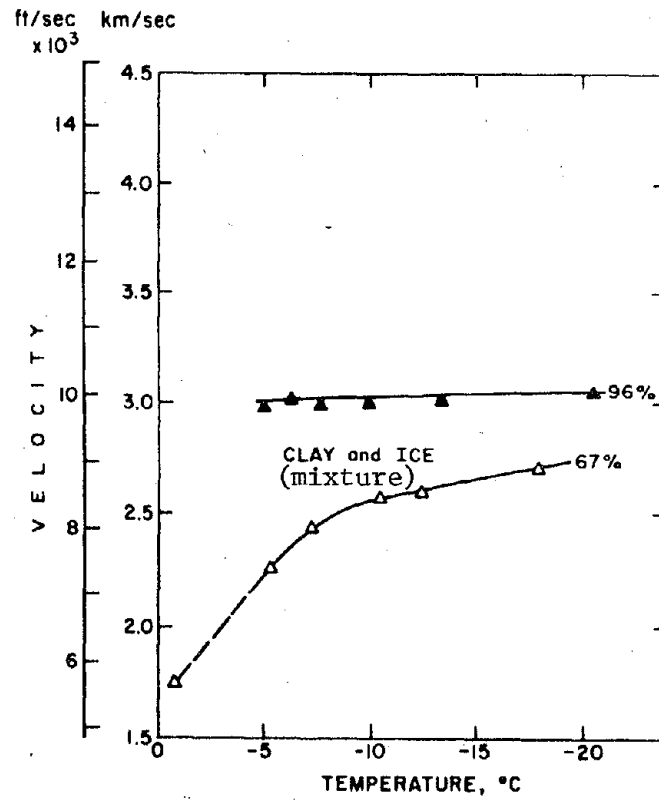


Figure 2.20 SOUND VELOCITY IN SYNTHETIC FROZEN CORES AT TWO POROSITIES VERSUS TEMPERATURE (after Müller, 1961, from Roethlisberger, 1972)

Point Design.	Non-frozen Soils	W.C. %
G	Suffield Clay	12.7

Point Design.	Frozen Soils	f kHz	Temp °C
G	Suffield Clay	1	-9.4

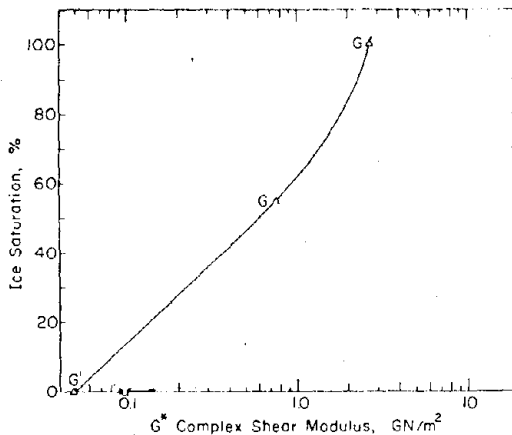


Figure 2.21 EFFECT OF ICE SATURATION ON COMPLEX SHEAR MODULUS FOR FROZEN SUFFIELD CLAY (after Stevens, 1973)

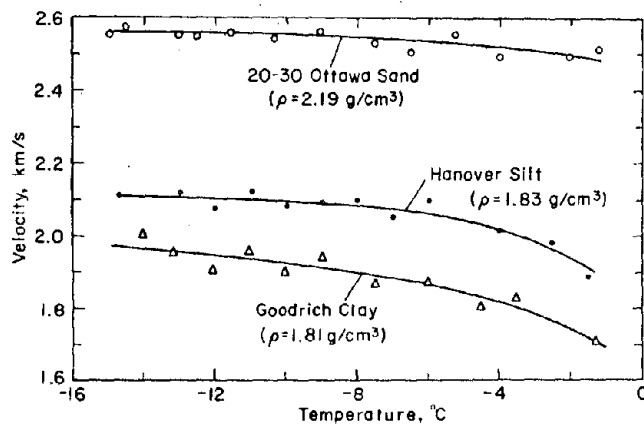


Figure 2.22 S-WAVE VELOCITY VERSUS TEMPERATURE FOR FROZEN GOODRICH CLAY (after Nakano and Froula, 1973)

Kaplar (1969), using resonant frequency techniques, tested beams of frozen Boston blue clay and frozen Fargo clay. The results are presented in Figure 2.23. The longitudinal wave velocity of frozen Fargo clay drops from 6.5×10^3 ft/sec at -10°F to 3.2×10^3 ft/sec at 30°F whereas the longitudinal wave velocity of frozen Boston blue clay drops from 10.3×10^3 ft/sec at -10°F to 6.4×10^3 ft/sec at 30°F .

Stevens (1975), using forced vibration resonant column tests, studied the influence of temperature on Goodrich and Suffield clay. The results are shown in Figure 2.24. The dynamic complex Young's modulus of Goodrich clay drops from 1.7×10^7 psi at 0°F to 5.5×10^6 psi at 30°F . The dynamic complex shear modulus drops from 6×10^6 psi at 0°F to 1.8×10^6 psi at 30°F . Similar results are noted for Suffield clay. Stevens indicates that temperature has a greater effect on fine-grained soil (clay) than on coarse-grained soil (sand).

Müller (1961) determined the sound velocity of frozen clay cores as a function of temperature as shown in Figure 2.20. At a porosity of 67%, the velocity drops from about 2.7 km/sec at -20°C to about 2.6 km/sec at -10°C . For the temperature range -10 to -1°C , the velocity drops significantly from 2.6 km/sec at -10°C to 1.75 km/sec at -1°C . At a porosity of 96%, the velocity decreases only slightly in the temperature range -4 to -20°C .

2.5.4 Effect of Frequency

Information on the influence of frequency on the dynamic elastic properties of frozen clay is given by Stevens (1975). His results indicate that the dynamic elastic properties of Goodrich and Suffield clay increase slightly with an increase in frequency from 1 to 10 kHz.

2.5.5 Effect of Unfrozen Water Content

Nakano and Froula (1973) suggest that a strong correlation exists between the dilatational wave velocity and the unfrozen water content. Figure 2.25 presents the results of an experiment in which the dilatational wave velocity and unfrozen water content of a Kaolinite clay were measured simultaneously. As the unfrozen water content decreases the dilatational wave velocity increases. The observed hysteresis in the velocity during a freeze-thaw (cooling-heating) cycle is believed to be caused by the hysteresis of unfrozen water content. Based on the results

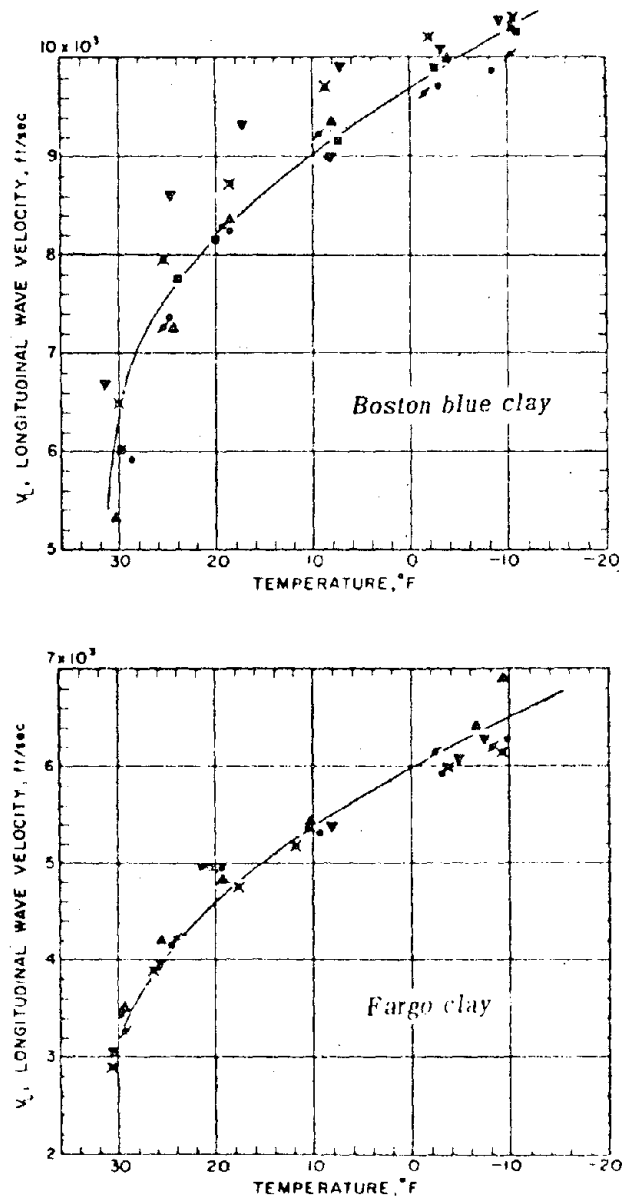


Figure 2.23 LONGITUDINAL WAVE VELOCITY VERSUS TEMPERATURE FOR FROZEN BOSTON BLUE CLAY AND FARGO CLAY (after Kaplar, 1969)

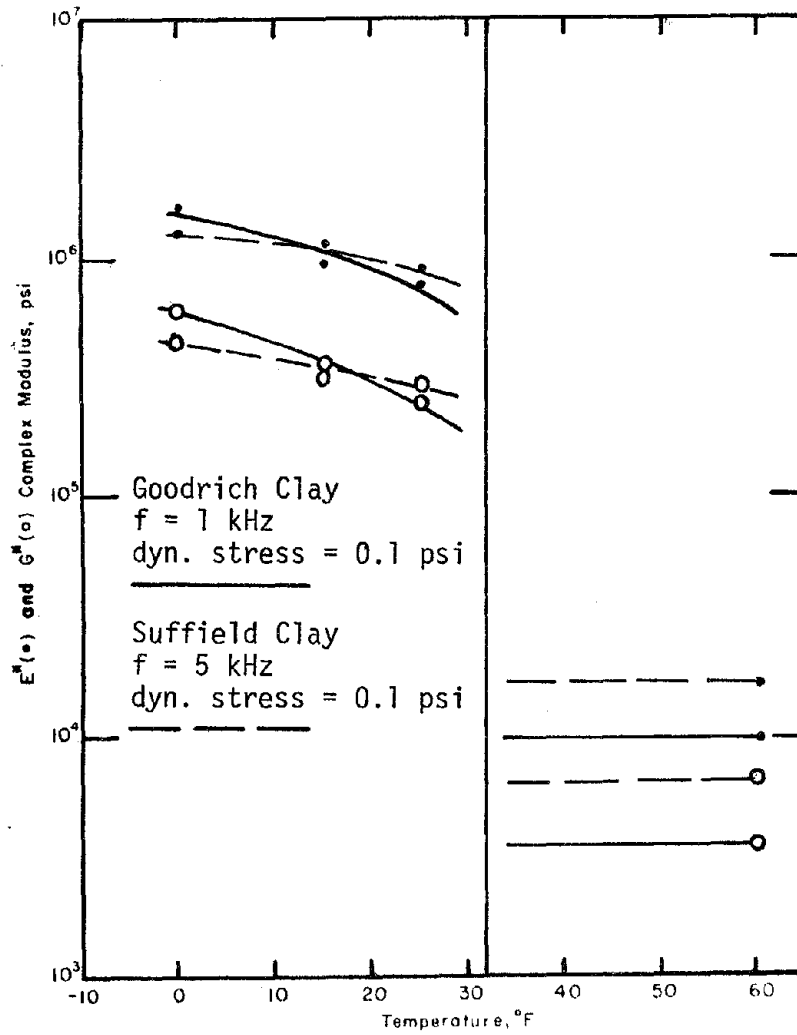


Figure 2.24 EFFECT OF TEMPERATURE ON COMPLEX MODULI OF FROZEN GOODRICH CLAY (modified after Stevens, 1975)

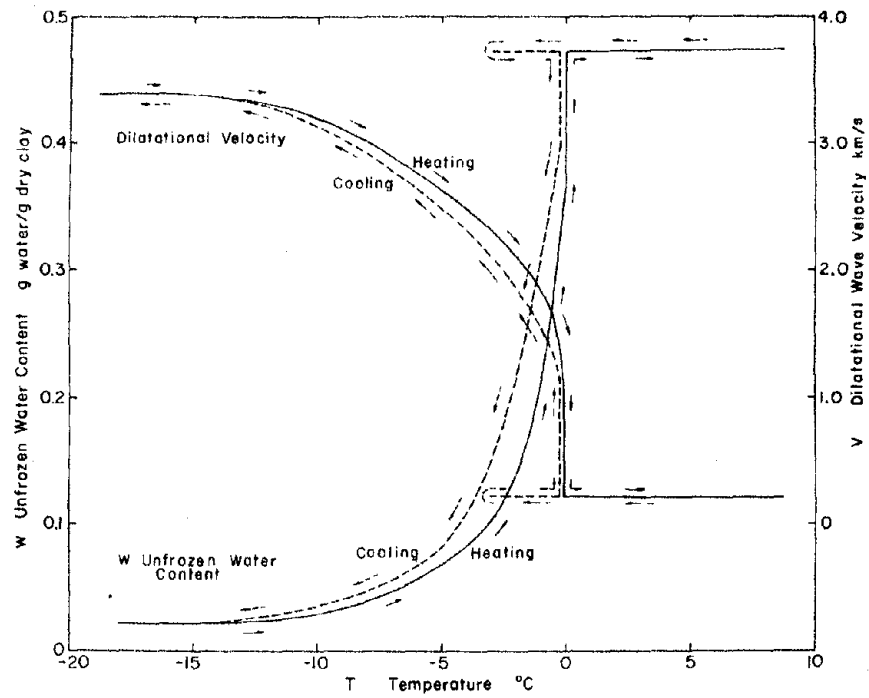


Figure 2.25 DILATIONAL VELOCITY AND UNFROZEN WATER CONTENT VERSUS TEMPERATURE (after Nakano and Froula, 1973)

of this experiment, Nakano and Froula state, "there is very little doubt that the unfrozen water content is a major factor contributing to a variation of the dilatational wave velocity with temperature."

2.5.6 Effect of Dynamic Stress (or Strain)

The effect of dynamic stress (or strain) on the dynamic elastic properties of frozen clay has been investigated by Stevens (1975). His results indicate that dynamic elastic properties of Goodrich and Suffield clay do not change, for all practical purposes, with a dynamic (loading) stress increase from 0.1 to 5.0 psi.

2.6 Damping of Frozen Clay

Damping of frozen clay in terms of $\tan \delta$ has been reported by Stevens (1975). Stevens' work, as shown in Figure 2.26, indicates the effect of temperature on $\tan \delta$. At 1 kHz and a dynamic stress of 0.1 psi, $\tan \delta$ of Goodrich clay increases from 0.07 at 0°F to 0.10 at 25°F for longitudinal vibrations. $\tan \delta$ of the same frozen clay increases from 0.06 at 0°F to 0.11 at 25°F for torsional vibrations. Similar results are shown for the Suffield clay. $\tan \delta$ appears to be approximately the same for the frozen state and the unfrozen state.

The influence of frequency on damping of frozen clay has been investigated by Stevens (1975). His results indicate damping of frozen Goodrich clay decreases with an increase in frequency from 1 to 10 kHz. Damping of frozen Suffield clay does not change appreciably for an increase in frequency from 1 to 10 kHz.

Stevens (1975) investigated the effect of dynamic stress (or strain) on damping of frozen clay. His results indicate that damping properties of frozen Goodrich and Suffield clay do not change, for all practical purposes, with a dynamic (loading) stress increase from 0.1 to 5.0 psi.

Stevens (1973) found that $\tan \delta$ is not significantly affected by void ratio. There is only a slight decrease in $\tan \delta$ as void ratio increases. Generally, damping of frozen clay is greater than that of ice.

2.7 Poisson's Ratio of Ice and Frozen Clay

Poisson's ratio is defined as the ratio of unit lateral strain to unit longitudinal strain, under the condition of uniform and uniaxial longitudinal stress within the proportional limit.

Goodrich Clay
f = 1 kHz
dyn. stress = 0.1 psi

Suffield Clay
f = 5 kHz
dyn. stress = 0.1 psi

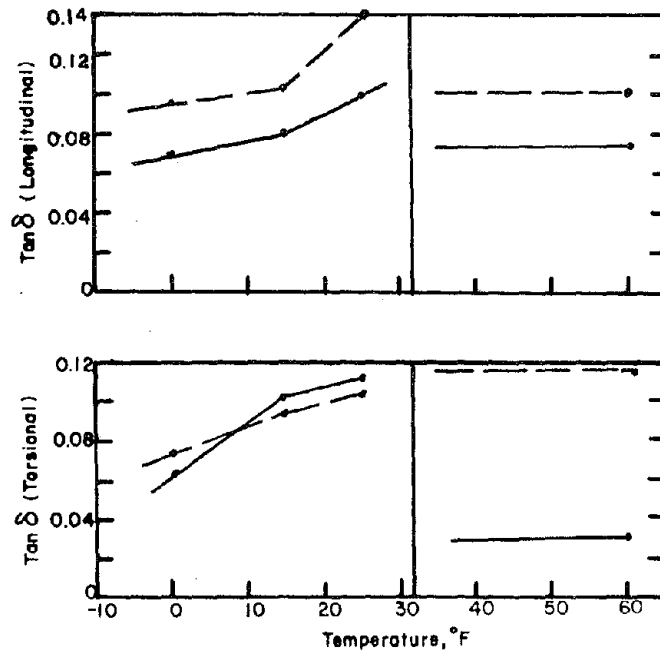


Figure 2.26 EFFECT OF TEMPERATURE ON TAN δ OF FROZEN GOODRICH CLAY (modified after Stevens, 1975)

2.7.1 Poisson's Ratio of Ice

Kaplar (1969) computed Poisson's ratio of ice from the relation:

$$\mu = \frac{E_d}{2G} - 1 \quad (2.4)$$

in which,

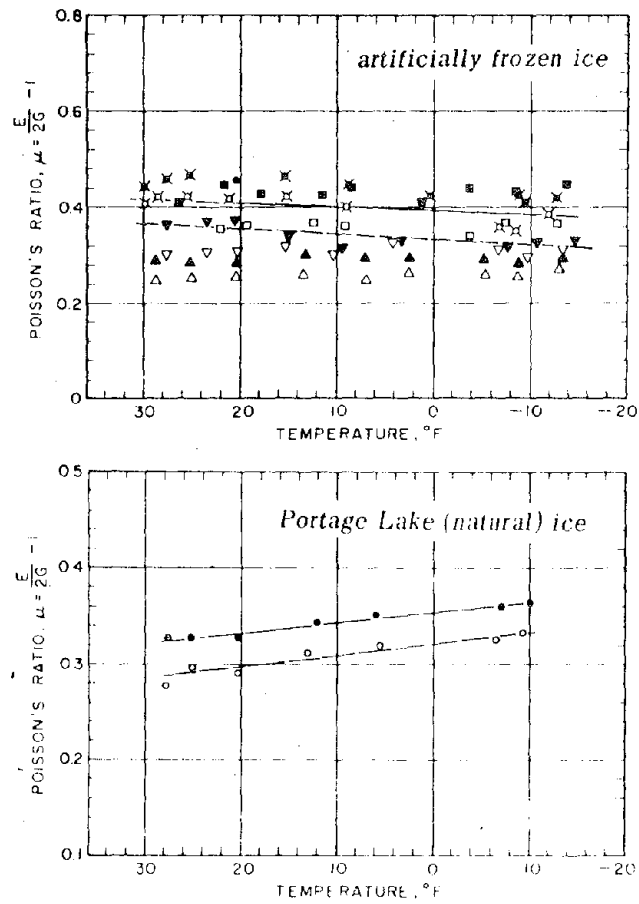
E_d = dynamic Young's modulus

G = dynamic shear modulus.

His results indicate Poisson's ratio for artificially frozen ice varies with temperature from about 0.33 to about 0.41 whereas Poisson's ratio for Portage Lake (natural) ice varies with temperature from about 0.28 to about 0.36 as shown in Figure 2.27. Roethlisberger (1972) suggests that Poisson's ratio of bubbly ice and snow is approximately 0.33. The influence of density on Poisson's ratio, deduced from seismic, in situ measurements and ultrasonic laboratory studies, were summarized by Mellor (1964) and were presented by Roethlisberger, as shown in Figure 2.28. The summary of results indicates that Poisson's ratio is between 0.25 and 0.30 and is apparently not influenced by density. In contrast to this, Smith (1969) reports the results from forced vibration tests which indicated a dependency of Poisson's ratio on density. This is shown in Figure 2.29. Smith comments, however, that the values appear to be unreasonable. Gold (1976) gives a range of Poisson's ratio of 0.31 to 0.55 for ice depending on ice structure and temperature.

2.7.2 Poisson's Ratio of Frozen Clay

Based on longitudinal and flexural vibration tests, Poisson's ratio for frozen Boston blue clay and frozen Fargo clay has been reported as a function of temperature by Kaplar (1969). The results are shown in Figure 2.30. Poisson's ratio for both clays is about 0.4 for longitudinal vibration and 0.2 for flexural vibration and is apparently not influenced by temperature. Kaplar comments that the values computed using longitudinal vibrations are believed to be more reliable. In another study conducted by Stevens (1975), Poisson's ratio of Goodrich clay was generally found to be between 0.32 and 0.59. (One value of 0.72 was reported for Goodrich clay; Poisson's ratio for Suffield clay appeared to be unrealistically high.) Stevens indicated the values of Poisson's ratio cannot be considered as accurate because their determination is wholly dependent



Note: Open symbols indicate flexural vibration and closed symbols indicate longitudinal vibration.

Figure 2.27 POISSON'S RATIO OF ICE VERSUS TEMPERATURE (after Kaplar, 1969)

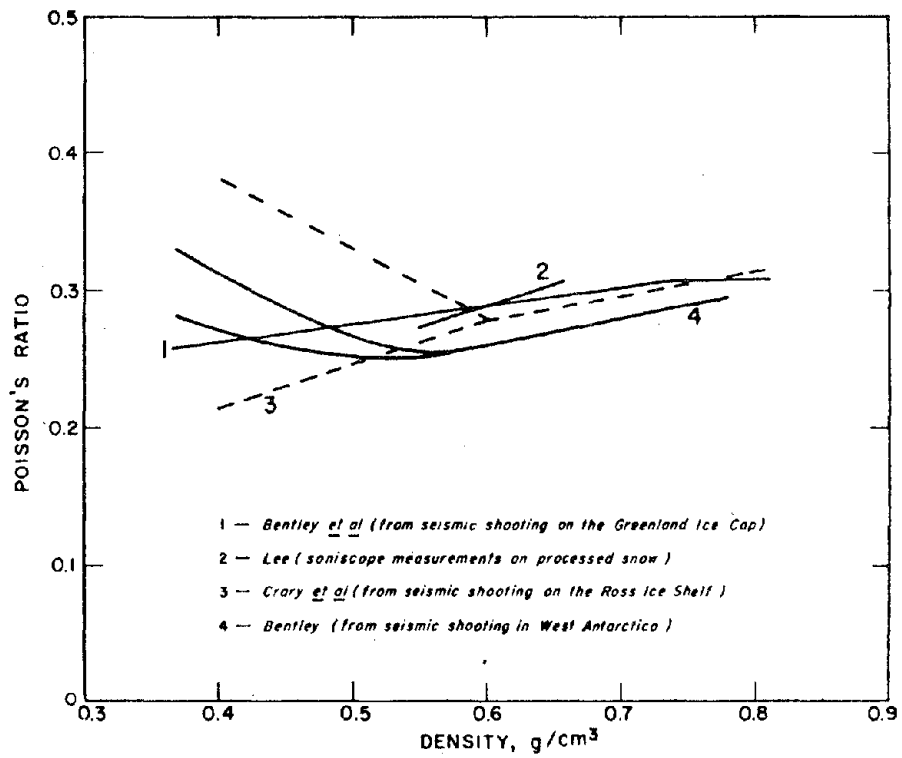


Figure 2.28 POISSON'S RATIO FOR DRY SNOW VERSUS DENSITY (after Mellor from Roethlisberger, 1972)

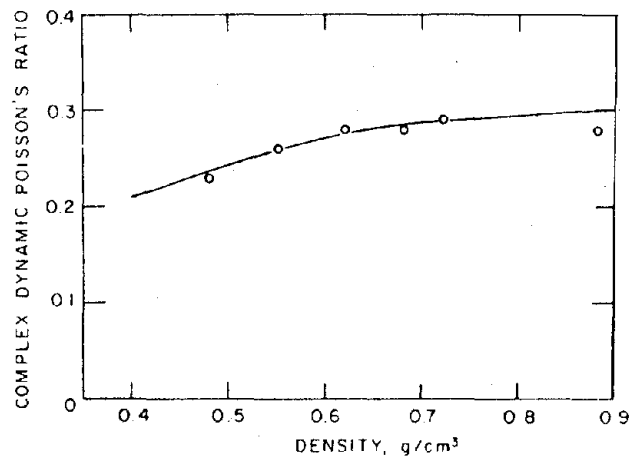
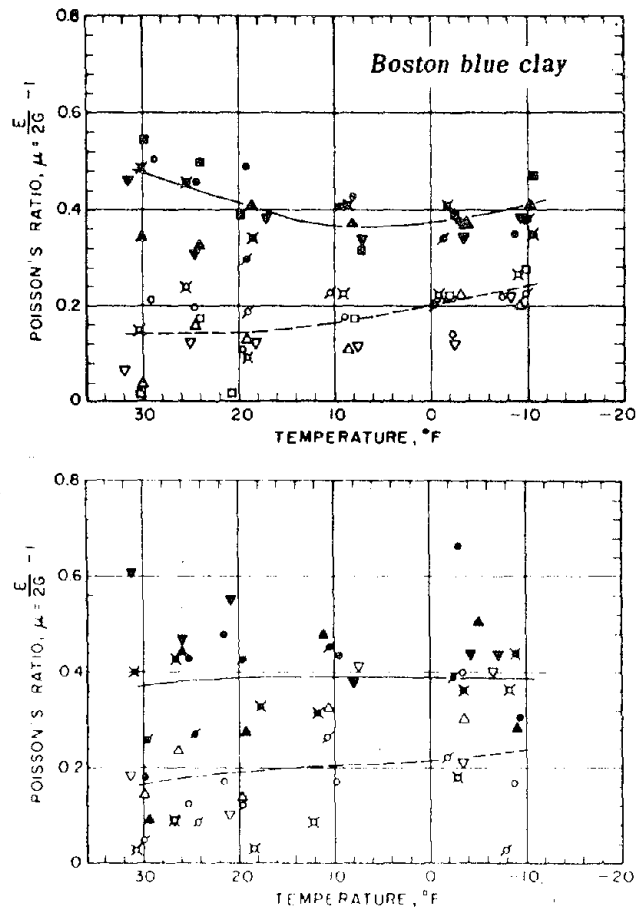


Figure 2.29 POISSON'S RATIO OF ICE VERSUS DENSITY (after Smith, 1969)



Note: Open symbols indicate flexural vibration and closed symbols indicate longitudinal vibration.

Figure 2.30 POISSON'S RATIO OF FROZEN CLAY VERSUS TEMPERATURE (after Kaplar, 1969)

on the accuracy of the modulus values, and small errors in either complex Young's or shear modulus results in a very sizeable error in Poisson's ratio. For Goodrich clay, Poisson's ratio decreases with decreasing temperature, increasing dynamic stress, and increasing frequency. Stevens states that, however, that it is not certain that these trends are reliable.

CHAPTER 3
SAMPLE PREPARATION, SAMPLE INSTALLATION,
TRIAXIAL CELL ASSEMBLY, AND
TEST PROCEDURE

3.1 General

This chapter provides information on the laboratory preparation of samples of ice and frozen clay, installation of the samples in a triaxial cell, assembly of the triaxial cell and the procedure used to test the samples. A basic understanding of the cyclic triaxial test system used in the research program to evaluate the dynamic properties of ice and frozen clay is assumed. A detailed description of the components of the test system, specifically the MTS electrohydraulic closed loop test system, a triaxial cell, a cooling system and output recording and monitoring devices, is given in Appendix A.

3.2 Preparation of Ice Sample

The cylindrical polycrystalline ice samples used in the research program were prepared using natural snow and distilled water for high density samples (about 0.904 g/cc) or natural snow and carbonated water for low density samples (about 0.77 g/cc). Hollow cylindrical teflon molds, 7.1 cm inside diameter, 30.5 cm high and 1.3 cm thick were used to form the ice samples (see Figure 3.1). The frozen ice samples were prepared as follows:

- (1) The mold, with the bottom cap inserted at one end, and the top cap, were placed in a large freezer box maintained at a temperature of $-20 \pm 1^{\circ}\text{C}$.
- (2) The mold and caps were chilled for approximately one hour and the mold was filled with loose, dry clean snow (passing the no. 4 sieve) up to about two inches from the top.
- (3) Precooled water (close to 0°C) or carbonated water was poured into the snow from the top and the top cap was inserted. A hole, 0.3 cm, drilled at the side of the mold (5.0 cm from one end), was used to release air which was trapped in the mold during the insertion of the top cap.
- (4) The sample was placed in the freezer box and left for approximately 24 hours. The samples were then extruded outside the

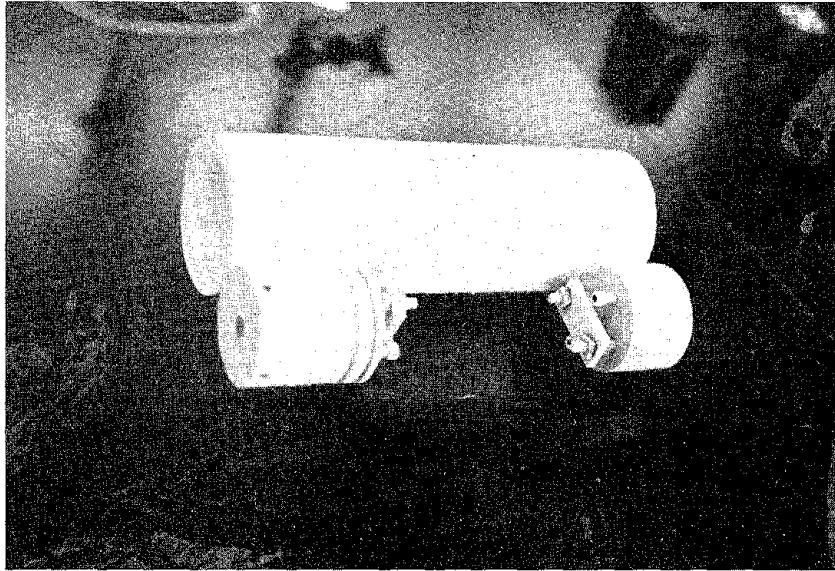


Figure 3.1 HOLLOW CYLINDRICAL TEFLON MOLD AND
SAMPLE CAPS WITH COUPLINGS

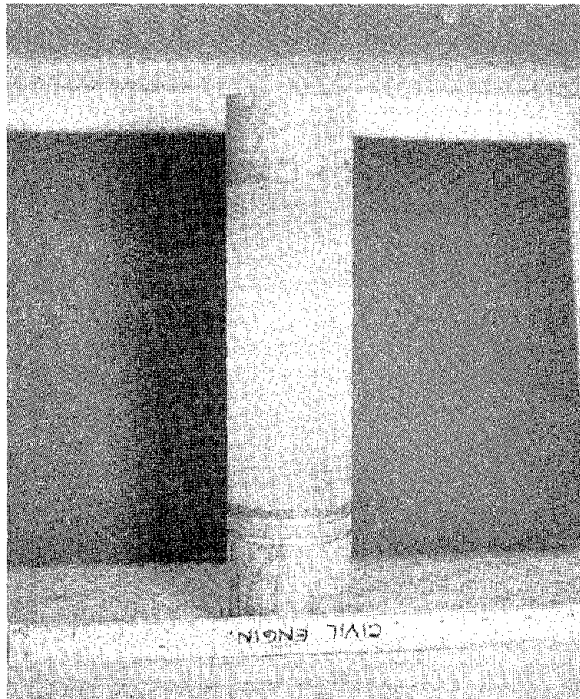


Figure 3.2 TYPICAL CYLINDRICAL ICE SAMPLE

freezer with a hydraulic jack as fast as possible. (It was found that if a sample was left in the mold outside the freezer for approximately 5 minutes or longer tension cracks occurred, presumably due to shrinkage of the samples caused by a temperature increase.)

The resulting polycrystalline ice samples were cloudy and bubbly in appearance. A typical ice sample is shown in Figure 3.2. The grains were usually a regular shape and ranged in size from 1 to 2 mm. They had a random crystallographic orientation. Measured densities ranged from 0.900 to 0.908 g/cc for the high density samples and 0.767 to 0.782 g/cc for the low density samples. Approximately one out of three samples contained excessive bubbles, cracks, or voids, or appeared to have large variations in density and were rejected. The samples used in the test were, therefore, quite homogenous for the two ranges of ice density. There was a slight radial pattern of ice crystals visible in some samples when they were broken apart and examined in cross-section.

3.3 Preparation of Frozen Clay Sample

Two types of frozen clay samples were used in the research program: (1) Ontonagon clay, termed "O-clay," and (2) a mixture of Ontonagon and sodium montmorillonite clay (50 percent each by weight), termed "M + O-clay." The O-clay was prepared at different water contents to assess the influence of water (ice) content on dynamic properties. The M + O-clay was used to investigate the influence of specific surface area (related to unfrozen water content) on dynamic properties. The physical properties of both clays are given in Table 3.1. The air-dried clays, previously crushed and screened through the no. 40 sieve, were thoroughly mixed with distilled water to a water content slightly greater than their liquid limit. The resultant slurry was stored in a humidity room for about one month prior to sample preparation. The frozen clay samples were prepared as follows:

- (1) The clay slurry was taken from the humidity room and isotropically consolidated in a triaxial cell in a cylindrical shape approximately 10 cm in diameter and 20 cm high. To facilitate drainage, porous stones were placed on the top and bottom of the sample and four vertical paper drainage strips were placed around the sample. Differences in water content of the clay samples

Table 3.1 INDEX AND MINERALOGICAL PROPERTIES OF O-CLAY AND M + O-CLAY

 a. O-clay (after Warder and Andersland, 1971)

Plastic limit	24%
Liquid limit	61%
Plasticity index	37%
Gradation (% finer by wt.)	
2 mm	100
0.06 mm	90
0.002 mm	70
Clay mineral content of clay fraction	
Illite	45%
Vermiculite	20%
Kaolinite	15%
Chlorite	10%
Montmorillonite, quartz, feldspar, and amorphous material	10%
Surface area	215 m ² /g

b. M+O-clay

Plastic limit	37%
Liquid limit	98%
Plasticity index	61%
Clay mineral content of clay fraction	
Illite	22%
Vermiculite	10%
Kaolinite	7%
Chlorite	5%
Montmorillonite, quartz, feldspar, and amorphous material + Sodium Montmor- illonite	56%
Surface area	475 m ² /g

obtained by consolidating the clay slurry in the triaxial cell to different confining pressures.

- (2) The consolidated sample was taken from the cell and trimmed to a diameter which was slightly smaller than the diameter of the teflon mold. The void space between the caps and the coupling assembly was filled with residual soil from the trimming.
- (3) The sample was put in a mold and the two caps were forced into the two ends of the molds with a hydraulic jack. The mold was placed in a freezer maintained at a temperature of $-30 \pm 1^\circ\text{C}$ for approximately 24 hours. The sample was then extruded outside the freezer box with a hydraulic jack. The sample was not subjected to a surcharge load during freezing.

The degree of saturation of a few samples was determined after isotropic consolidation by measuring the pore pressure parameter \bar{B} . The values of \bar{B} of the consolidated samples were greater than 0.98, indicating that the samples were, for all practical purposes, fully saturated.

Four of the highest moisture content O-clay samples were prepared by pouring the unconsolidated clay slurry directly into the teflon molds. The molds were then vibrated to insure that no air was trapped in the samples before they were put in the freezer box.

The frozen clay samples prepared had a random orientation of ice lenses whose thicknesses varied from 0.8 mm for the lowest water content samples to 2.0 mm for the highest. The frozen clay samples were classified as CH, Vr (Linell and Kaplar, 1966). Photographs of typical frozen clay samples are shown in Figure 3.3. There was a thin film of ice surrounding the specimens caused by water being expelled from the samples during the freezing process. Thus, the water content of the frozen samples was slightly lower than that of the material placed in the molds. This is exemplified by the data given in Table 3.2. (The film was removed before the water content of the frozen samples was determined.) The frozen samples were weighed, their lengths measured, and their densities obtained, as given in Table 3.2.

Three samples were frozen at a temperature of $-5 \pm 1^\circ\text{C}$ and it was found that they were not different from the samples frozen at -30°C in terms of the orientation of ice lenses, water content, and their dynamic properties. A vertical load equivalent to 15 psi was applied to several

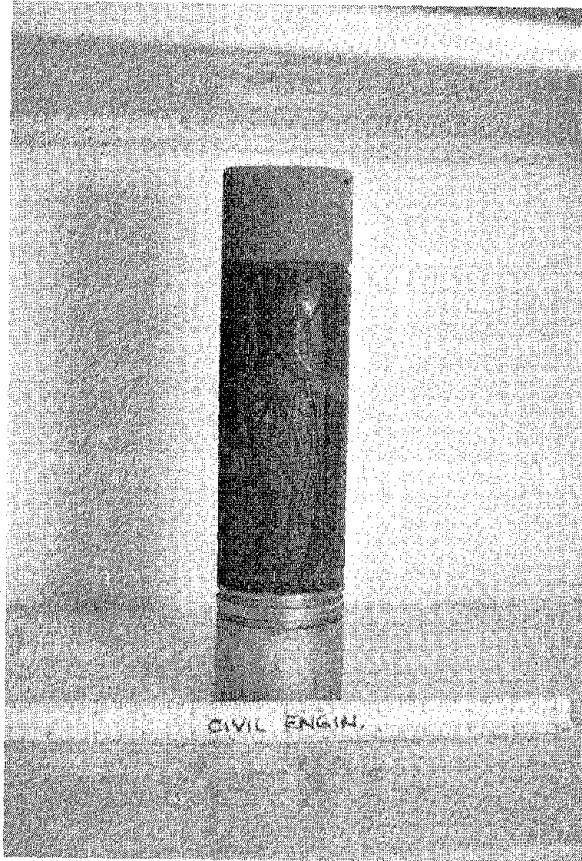


Figure 3.3 TYPICAL CYLINDRICAL FROZEN CLAY SAMPLE

Table 3.2 WATER CONTENT AND DENSITY OF CLAY SAMPLES

Sample Number	Water content before freezing (%)	Average water content before freezing (%)	Water content after freezing (%)	Average water content after freezing (%)	Density of frozen samples (g/cc)
CL-1	29.8		28.5		1.96
CL-2	29.9	29.8	29.6	29.2	1.92
CL-3	30.3		29.8		1.98
CL-4	29.1		29.0		2.00
C-30-1	39.5		36.8		1.78
C-30-2	38.7	38.6	35.5	36.0	1.80
C-30-3	38.4		36.1		1.82
C-30-4	37.9		35.3		1.82
C-30-5	38.3		36.4		1.82
C-30-6	37.6		34.9		1.81
C-5-1	37.5		34.5		1.86
C-5-2	38.7	36.1	1.84		
C-5-3	41.0	38.3	1.82		
C-30-7	50.5	50.5	46.3	46.3	1.73
CH-1	61.0	61.0	55.2	55.1	1.60
CH-2	61.0		55.4		1.61
CH-3	61.0		54.7		1.64
CH-4	61.0		54.9		1.60
MC-30-1	58.5	58.8	56.4	57.2	1.65
MC-30-2	57.9		56.9		1.68
MC-30-3	61.1		59.0		1.59
MC-30-4	57.8		56.6		1.70

samples during the freezing process and it was found that these samples were not different (considering the parameters mentioned above) from the others. These results apparently indicate there was significant constraint between the mold and the sample during the freezing process. The constraint was sufficient to counteract the frost heave force and the associated development of ice lenses. In an attempt to produce thicker ice lenses, many samples were frozen at $-5 \pm 1^\circ\text{C}$ without horizontal or vertical constraint. It was possible to produce ice lenses up to 5 mm, however, the samples could not be used in the test program because the sample and the caps were not in alignment. A high degree of alignment is necessary to perform the cyclic triaxial tests on the frozen samples.

3.4 Sample Installation and Triaxial Cell Assembly

The frozen ice and clay samples were stored in a freezer at $-20 \pm 1^\circ\text{C}$ after they were jacketed with two rubber membranes, each with a wall thickness of 0.05 cm. Prior to testing, the base clamp of the anti-tilt device (see Appendix A, Section A.2) was connected to the sample base. The sample was immersed in the cold bath and the base was connected to the load cell (see Figure A.7). The anti-tilt device was assembled as follows:

- (1) The LVDT body was attached to the standard of the anti-tilt device fixed to the base clamp.
- (2) The anti-tilt ring with the core of the LVDT attached was clamped to the top cap.
- (3) The anti-tilt ring (opposite to the core of the LVDT) was connected to the spring steel extending from the base clamp in a position such that the voltage output from the LVDT was close to zero.
- (4) The position of the LVDT body was adjusted so that the core of the LVDT was at the center (horizontal plane) of the LVDT housing. This insured that the core would not come into contact with the housing when conducting a test. This adjustment is very important. If any contact between the core and the LVDT occurs, the damping ratio obtained at low strain amplitudes is significantly larger than the correct value. Core contact with the housing could be observed from the hysteresis loops as shown in Figure 3.4. If the line of the loops squared off at the end points it indicated that the load was changing with no change in displace-

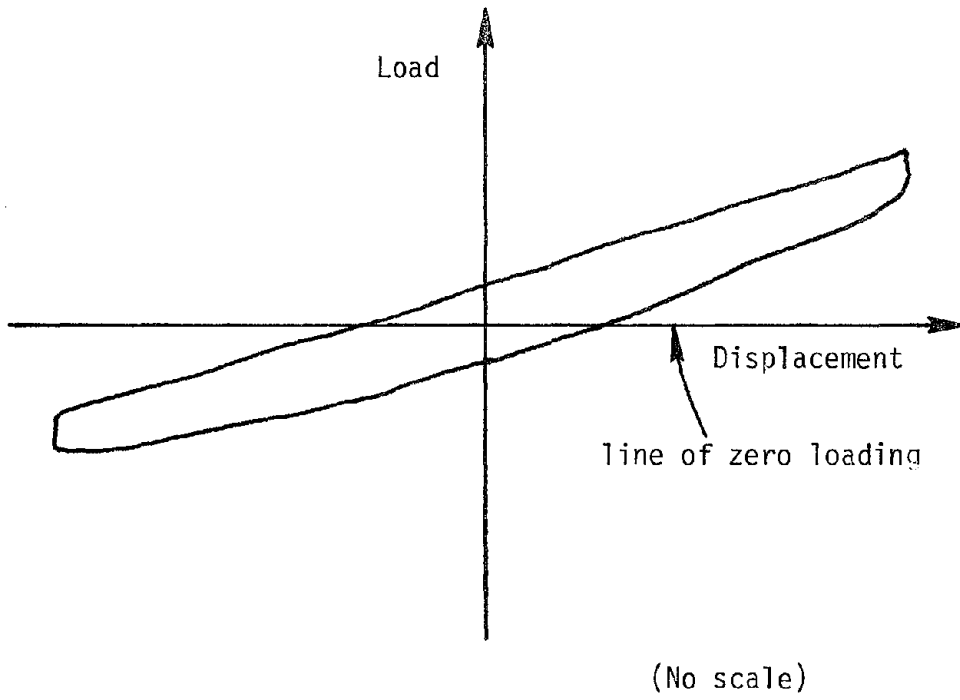


Figure 3.4 OBSERVED HYSTERESIS LOOP FOR LVDT CORE IN CONTACT WITH HOUSING

ment. However, since the load was changing there must be a corresponding displacement. Therefore, the core must be "sticking" to the housing of the LVDT. The significance of this error obviously decreases with increasing strain amplitude.

After the anti-tilt device was attached to the sample the triaxial cell cylinder was placed on the base plate of the cell and the thermistor collar was placed around the sample. Finally, the top plate was tightened down on the cell cylinder and the piston loading rod was connected to the top cap by inserting it through a ball bushing loading collar. Care must be taken when attaching the piston rod. If the torque applied in tightening the piston rod is too great the sample will fail.

Since the LVDT attached to the anti-tilt device was used for the feedback signal to the MTS controller, any deformations associated with loose connections or elastic deformations of the piston rod were eliminated. After the piston rod was attached, the center positioning of the LVDT core could be checked by applying a cyclic vertical force manually to the connecting rod and observing the hysteresis loop. If the loop exhibited the shape shown in Figure 3.4 the LVDT body had to be reset until a satisfactory loop was obtained. This required removing the top plate and piston loading rod.

When a satisfactory loop was obtained the cold bath was covered with styrofoam and an auxiliary coolant line was placed on the top plate of the triaxial cell. A small increase in temperature was usually experienced during the installation of the sample. Therefore, the samples were left in the cell for at least two hours to insure temperature equilibrium in the triaxial cell and sample before a dynamic test was conducted. The temperature of the sample was controlled by the mercury thermometer thermostat in the refrigeration unit. The two thermistors attached to the side of the sample were monitored to obtain the temperature to within $\pm 0.1^{\circ}\text{C}$. If the temperature was not correct, the thermostat was readjusted and the test was delayed two hours to insure that a temperature equilibrium condition was reached.

3.5 Test Procedure

An electrohydraulic closed loop system was used to apply a cyclic deviator stress to the samples for cyclic triaxial testing. The test procedure used in the research is as follows:

- (1) The LVDT in the actuator was used as the feedback signal to move the actuator ram in contact with the triaxial cell piston loading rod. (The sample was subjected to a slight load during this operation.) The hydraulic power supply was turned off and a valve at the supply port of the hydraulic manifold of the actuator was closed to prevent fluid movement.
- (2) The feedback connection was changed from the LVDT in the actuator to the LVDT on the anti-tilt device. The actuator and the piston loading rod were connected, and a confining pressure of approximately 50 psi was applied to the sample to prevent disturbance caused by the movement of the actuator during the application of hydraulic pressure to the actuator. Gain and Rate adjustments were strongly dependent on the strength of the samples and "snugness" of the connection. For practical purposes, they were readjusted whenever the movement of the actuator, observed on the strip-chart recorder, deviated from a sine wave.
- (3) The Cal Factor and the Zero control of the LVDT were readjusted to correspond to the LVDT on the anti-tilt device. Set Point was adjusted to eliminate any difference between the feedback and the command signal. The hydraulic pressure was then applied and the valve at the supply port of the hydraulic manifold was opened. The actuator was now controlled by the LVDT on the anti-tilt device.
- (4) In general, it was not possible to set the LVDT exactly at its null point. Therefore, there was an initial voltage from the LVDT that would cause the strip-chart and x-y recorder to go "off scale" when they were set at high sensitivity. To achieve a voltage output close to zero the Set Point and the Zero control of XCDRI were gradually adjusted one after the other. During this adjustment the load on the sample was monitored to insure that an excessive load was not applied.
- (5) The sensitivities of the recording devices were set for the range of frequencies and voltage outputs anticipated during testing. The setting for the load cell could be made from experience after testing a number of samples. When the frequency of testing was less than or equal to 0.3 cps, the hysteresis loops

were recorded directly on the x-y recorder. For higher frequencies, the hysteresis loops were recorded by playing back the signal stored in the transient recorder. The results from these two techniques were compared and they were found to give, for all practical purposes, equal values of damping ratio. The strip-chart recorder monitored peak-to-peak displacement and load signals. From this record the dynamic elastic modulus could be determined.

- (6) A confining pressure was applied to the cell and the Zero control of XCDRI (feedback) was adjusted to obtain zero load on the sample (with this procedure there was no change in voltage output from the LVDT). The Span control was set to achieve the desired strain and the frequency of the sinusoidal command waveform was selected. The test was then conducted by engaging the Run control.

CHAPTER 4

DYNAMIC PROPERTIES OF ICE UNDER CYCLIC TRIAXIAL LOADING CONDITIONS

4.1 General

Cyclic triaxial tests were carried out on two groups of laboratory prepared samples of ice. In the first group the density ranged from 0.900 to 0.908 g/cc; in the second group the density ranged from 0.767 to 0.782 g/cc. It was felt that several parameters might influence the dynamic properties of ice. Hence, in addition to density the effects on dynamic properties caused by variations in temperature, confining pressure, strain amplitude, frequency, and number of cycles of loading were investigated.

4.2 Test History Effects on Dynamic Properties

At the onset of the research program it was felt that the "test history" a sample experienced might influence the dynamic properties measured. By test history is meant (1) the sequence in which the various physical parameters considered in the test program (temperature, confining pressure, frequency, strain amplitude, and number of cycles) were applied to the sample, and (2) the magnitude of the parameters considered following a given sequence. The results of the many tests conducted to establish an acceptable test history for a sample may be summarized as follows:

- (1) Temperature - individual samples were tested through a range of temperatures. It was found that the dynamic properties were comparable to those of samples tested at a single temperature if the samples were tested from high (-1°C) to low (-10°C) temperature. It was observed that if the sample temperature was decreased and it was allowed to readjust to the new temperature for a 24-hour period it would "erase" any disturbance effects that might have occurred at the higher temperature. When the tests were performed from low (-10°C) to high (-1°C) temperature, the samples were disturbed, apparently at the coupling, even if they were left in the cell at a new test temperature for 24 hours prior to testing. The disturbance could be observed from the hysteresis loop. Melting between the samples

and the caps was found when the samples were taken out of the cell.

- (2) Strain amplitude - the laboratory tests were conducted from low to high strain amplitude at a given confining pressure. If the sample was retested at the lowest strain amplitude it was observed that the damping ratio of the later test was greater than the damping ratio of the former by about 50 percent. The dynamic Young's modulus appeared to be equal in magnitude.
- (3) Confining pressure - when the samples were subjected to a high confining pressure (greater than 100 psi) they deformed rapidly. The rate of deformation decreased with time and the volume of the samples appeared to decrease which would cause the density to increase. This effect was demonstrated by testing a sample at a low confining pressure, subjecting it to a high confining pressure, then retesting at the low confining pressure. The dynamic Young's modulus of the sample after it was subjected to a high confining pressure was slightly greater than the dynamic Young's modulus of the sample before experiencing the high confining pressure. To avoid this problem the samples were subjected to the highest confining pressure (200 psi) used in the test sequence for approximately 20 minutes before a test was performed. The rate of deformation of the samples was very small for subsequent applications of confining pressure after employing this procedure.
- (4) Frequency - variations in the frequencies of testing (0.3, 1.0, and 5.0 cps) did not appear to cause sample disturbance.
- (5) Number of cycles - the dynamic properties of the ice samples did not appear to be influenced by the number of cycles a sample was subjected to provided the number of cycles of loading did not exceed approximately 20 per one test. One sample was found to be disturbed when it was subjected to more than 100 cycles per one test. A sample subjected to about 150 cycles per one test melted at the couplings and the dynamic Young's modulus was found to be very low.

An acceptable test history and the one used in the research program is shown in Figure 4.1. The range of test conditions was chosen to include the field conditions and loadings anticipated for frozen soil de-

Constant temperature

(sample subjected to an initial confining pressure of 200 psi prior to testing)

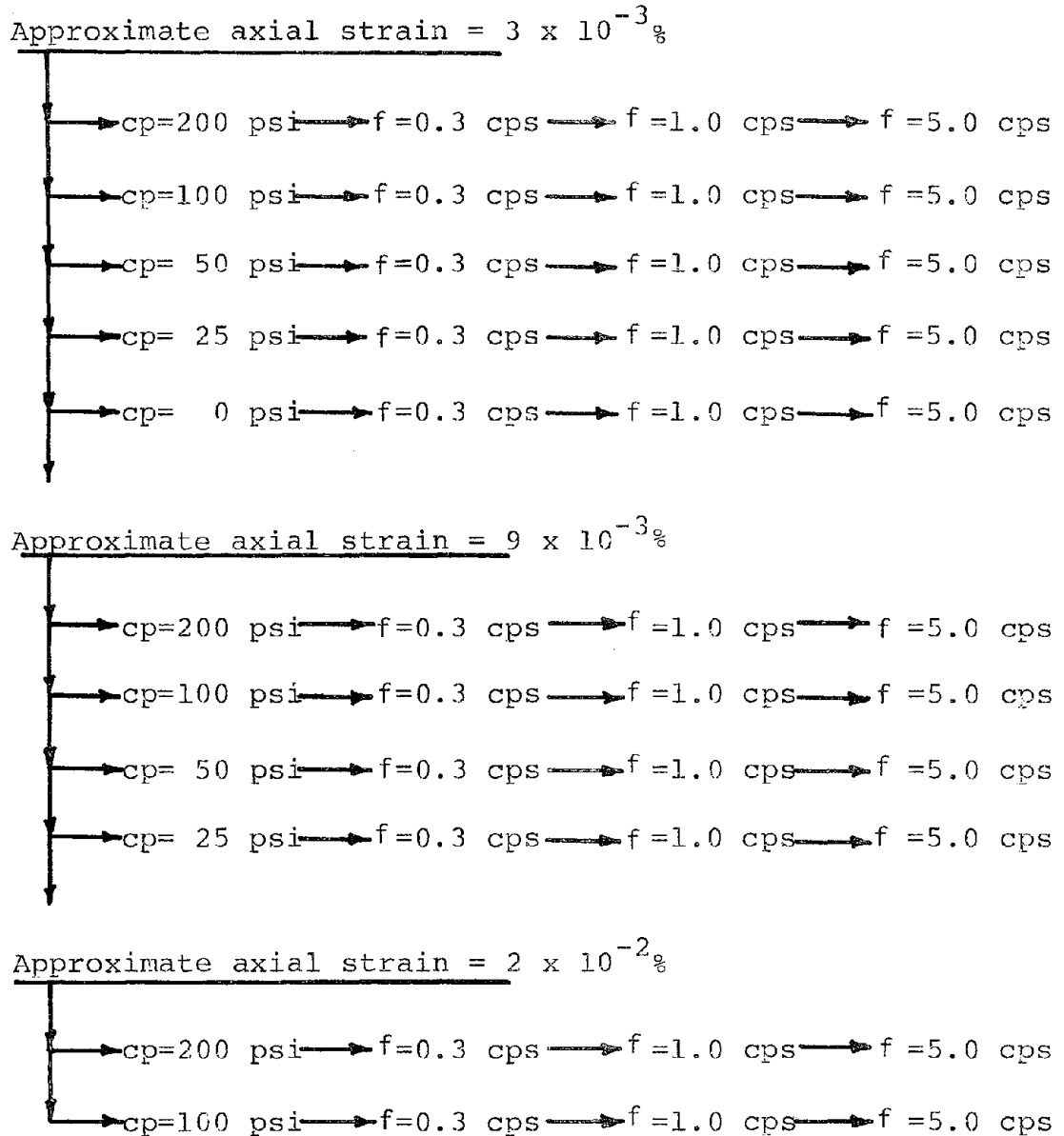


Figure 4.1 DIAGRAM OF ACCEPTABLE TEST HISTORY FOR ICE

posits subjected to strong motion earthquakes (Vinson, 1975). The range of specific test parameters are as follows:

- (1) Temperature - the high density samples were tested at five temperatures (-1, -2, -4, -6 and -10°C); the low density samples were tested at three temperatures (-1, -4, and -10°C). A given sample was tested at one temperature only.
- (2) Strain amplitude - the range of strain amplitude was approximately 3×10^{-3} to $2 \times 10^{-2}\%$ axial strain. The maximum strain amplitude of testing at $cp = 0$ was limited to about $5 \times 10^{-3}\%$; at $cp = 25$ and 50 psi it was limited to about $9 \times 10^{-3}\%$; at $cp = 100$ and 200 psi it was limited to about $2 \times 10^{-2}\%$. The maximum strain amplitudes were associated (approximately) with a tensile failure of the sample. (It was found that ice samples with the coupling described in Appendix B could be subjected to a tensile stress of about 80 psi.)
- (3) Confining pressure - the high density samples were tested at five confining pressures (0, 25, 50, 100 and 200 psi). At a confining pressure of 0 psi, only a limited number of tests were performed at low strain amplitudes (2×10^{-3} to $5 \times 10^{-3}\%$). The low density samples were tested at four confining pressures (0, 25, 50 and 100 psi). The low density samples were not tested at $cp = 200$ psi because the deformations associated with the application of this confining pressure were quite large. (The deformation of the low density samples under 200 psi confining pressure was greater than the range of the LVDT, ± 0.254 cm.) At a temperature equal to -1°C, the maximum confining pressure was limited to 50 psi, because of excessive deformations at 100 psi. A limited number of tests were performed at $cp = 0$ psi at low strain amplitudes, 3×10^{-3} and $5 \times 10^{-3}\%$.
- (4) Frequency - in general only three frequencies of loading were used in the test program: 0.3, 1.0 and 5.0 cps. A limited number of samples were tested at a very low frequency, 0.05 cps.
- (5) Number of cycles - for each test condition a sample was subjected to 20 cycles of loading.

Before a sample was subjected to the acceptable test history the cell pressure was increased to 200 psi for approximately 20 minutes. The

dynamic Young's modulus was evaluated at a strain amplitude of $9 \times 10^{-3}\%$ and a frequency of 0.3 cps. The value obtained from this test was compared to that obtained during the course of the test history as another check on the disturbance of the sample. If they were found to be in good agreement, the test was presumed to be acceptable. (For all the test results reported herein the comparison was quite good.)

4.3 Influence of Number of Cycles on Evaluation of Dynamic Properties

It is generally felt by researchers conducting cyclic triaxial tests on unfrozen soils that the dynamic properties associated with the 5th or 10th cycle are the most appropriate for predicting ground response during earthquakes. To assess the influence of the choice of the cycle number on dynamic properties the variation of the ratio (E at Nth cycle/ E at 10th cycle) and (λ at Nth cycle/ λ at 10th cycle) with number of cycles at different frequencies, confining pressures, strain amplitudes, and temperature was determined. These ratios are shown for high density ice at 1, 5, 10 and 20 cycles in Tables 4.1 and 4.2, respectively. There appears to be no significant variation in dynamic Young's modulus with number of cycles for different frequencies, confining pressures, strain amplitudes, and temperatures. At the greatest, the dynamic Young's modulus at the Nth cycle is approximately 3.0% different from the modulus at the 10th cycle. Further, the damping ratio does not appear to vary with the number of cycles for different frequencies, confining pressures, strain amplitudes, and temperatures. The damping ratio at the Nth cycle is at most about 10% different from the damping ratio at the 10th cycle.

The dynamic Young's modulus was evaluated from the load and displacement channels of the strip-chart recorder at the 10th cycle by measuring the peak-to-peak amplitude of the recorded waveform. The damping ratio was evaluated from the hysteresis loop for the 10th cycle obtained from the x-y recorder. Typical strip-chart and x-y recorder records are shown in Figure 4.2. The area of the hysteresis loop was determined with a planimeter. The error associated with this determination was estimated to be approximately 5%.

4.4 Dynamic Young's Modulus of Ice

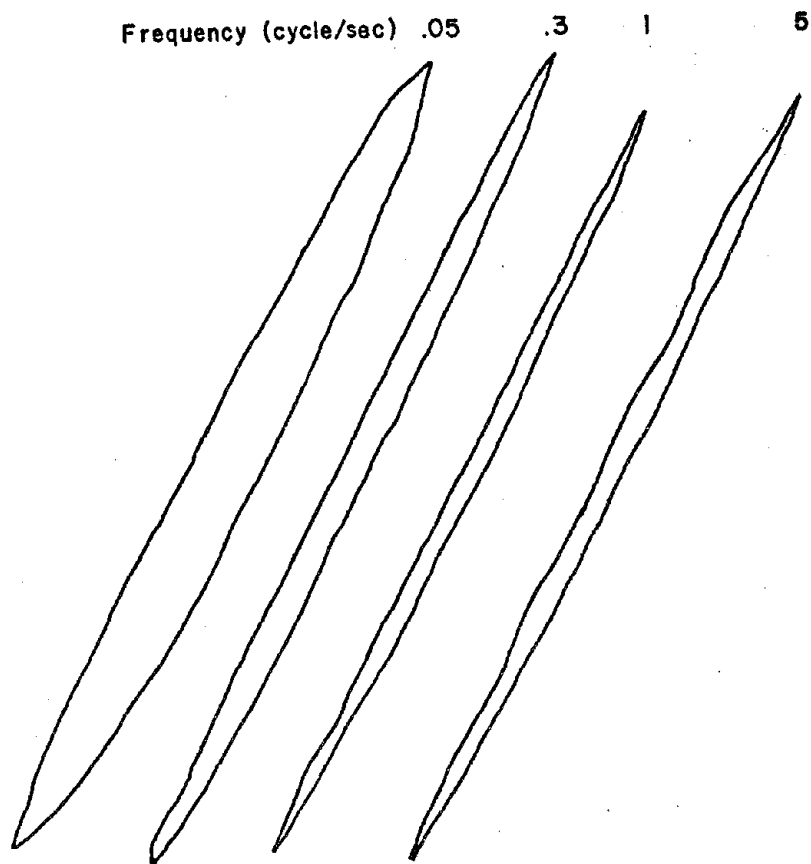
The dynamic Young's modulus from the laboratory test program was plotted against the log of axial strain amplitude expressed as a percent.

Table 4.1 VARIATION OF DYNAMIC YOUNG'S MODULUS OF HIGH DENSITY ICE WITH NUMBER OF CYCLES

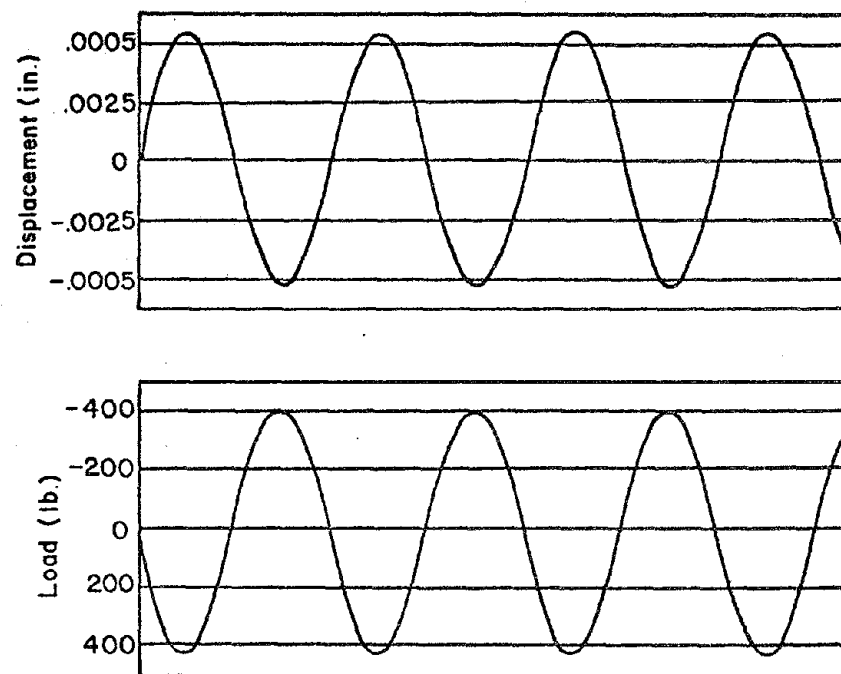
Temperature (°C)	Axial strain amplitude (%)	Confining pressure (psi)	Frequency (cps)	$\frac{E \text{ at Nth cycle}}{E \text{ at 10th cycle}}$			
				1	5	10	20
-4	0.00287	50	0.05	0.988	1.003	1	0.995
-4	0.00287	50	0.3	1.035	1.014	1	1.020
-4	0.00287	50	1.0	0.981	1.012	1	1.024
-4	0.00287	50	5.0	1.002	1.008	1	0.989
-4	0.00287	200	0.3	0.992	1.014	1	1.015
-4	0.00287	50	0.3	1.035	1.014	1	1.020
-4	0.00287	0	0.3	1.033	1.001	1	0.987
-4	0.00127	200	0.3	1.015	1.038	1	1.063
-4	0.00287	200	0.3	0.992	1.015	1	1.014
-4	0.0093	200	0.3	1.005	1.003	1	1.005
-4	0.0192	200	0.3	0.996	0.995	1	0.984
-1	0.00287	50	0.3	1.000	1.008	1	1.013
-4	0.00287	50	0.3	0.992	1.015	1	1.014
-10	0.00287	50	0.3	1.034	1.011	1	1.019

Table 4.2 VARIATION OF DAMPING RATIO OF HIGH DENSITY ICE WITH NUMBER OF CYCLES

Temperature (°C)	Axial strain amplitude (%)	Confining pressure (psi)	Frequency (cps)	$\frac{\lambda \text{ at Nth cycle}}{\lambda \text{ at 10th cycle}}$			
				1	5	10	20
-4	0.00287	50	0.05	0.909	0.860	1	0.871
-4	0.00287	50	0.3	1.029	1.035	1	0.994
-4	0.00287	200	0.3	0.944	0.958	1	1.007
-4	0.00287	50	0.3	1.029	1.035	1	0.994
-4	0.00287	0	0.3	0.970	0.965	1	0.970
-4	0.00127	200	0.3	0.990	0.962	1	0.942
-4	0.00287	200	0.3	0.944	0.958	1	1.007
-4	0.0093	200	0.3	0.973	0.965	1	1.013
-4	0.0192	200	0.3	0.996	1.021	1	1
-1	0.00287	50	0.3	0.955	0.977	1	1.008
-4	0.00287	50	0.3	1.029	1.035	1	0.994
-10	0.00287	50	0.3	1.103	1.000	1	1.046



a. Typical hysteresis loops
(non-dimensional)



b. Typical load and displacement records

Figure 4.2 TYPICAL RECORDS OBTAINED DURING CYCLIC TRIAXIAL TESTING OF ICE

The plots are shown in Appendix C, Figures C.1 to C.93 for the high density samples and Figures C.94 to C.126 for the low density samples. Each plot represents a test condition associated with a specific frequency, temperature, and confining pressure. In general, the data from three (or more) tests are available for each test condition.

For any given test condition there is "scatter" in the data points. It is believed that this was caused by:

- (1) Slight variations of density of the samples which ranged from 0.900 to 0.908 g/cc for the high density samples and 0.767 to 0.782 g/cc for the low density samples.
- (2) Slight differences in the structural composition of the samples, particularly near the coupling.
- (3) Slight temperature differences between tests.
- (4) Loosening of the coupling between the samples and the cap and base.
- (5) At the lower strain amplitudes of testing the test system approached its limit of capability both electronically and mechanically. Some variations in test results at this extreme of testing are to be expected.

Overall, however, it is felt that the data is reliable and provides a good basis for the interpretation of material properties.

4.4.1 Effect of Strain Amplitude

The data presented in Figures C.1 to C.126 in Appendix C suggests that the dynamic Young's modulus of ice varies linearly with the log of percent axial strain amplitude, as least over the range of strain amplitude associated with the experimental program. The dashed lines in the figures represent the least squares best fit line of the data. The slopes of the least squares best fit lines vary slightly from one another but do not appear to be influenced by frequency, confining pressure, or temperature. The slopes of a few of the lines vary significantly from the majority of the lines because they are associated with only a limited number of data points. This is exemplified by Figures C.1, C.16, C.21, C.41, C.61, C.66 and C.77 at a confining pressure of 0 psi and at a frequency of 0.05 cps.

Since the relationship between dynamic Young's modulus and the log of percent axial strain is not significantly influenced by other test

parameters it was assumed to be independent of the parameters. To establish the average least squares best fit line the dynamic Young's modulus for all the experimental data was plotted against log of percent axial strain amplitude, as shown in Figure 4.3 for the high density samples, and Figure 4.4 for the low density samples. The average slope is -0.0934 (psi/log %) for the high density samples and 0.0067 (psi/log %) for the low density samples. The average slopes indicate that the influence of strain amplitude for the high density samples is greater than for the low density samples.

To assess the influence of frequency, temperature, and confining pressure on the dynamic Young's modulus the average best fit least squares line was plotted through the data points for a given test condition. These are shown as solid lines in Figures C.1 to C.126. These lines were drawn intersecting the dashed lines at the "center" of the data set for a given test condition. Obviously, personal judgment was involved in this construction. The best fit least squares line through the center of the data set for given test conditions are summarized in Figures 4.5 to 4.23 for the high density samples and Figures 4.24 to 4.32 for the low density samples. The figures show the influence of confining pressure on dynamic Young's modulus at a specified temperature and frequency. Dynamic Young's modulus varies from 340×10^3 to 900×10^3 psi for the high density samples and 260×10^3 to 600×10^3 psi for the low density samples.

The relationship between dynamic Young's modulus and confining pressure, frequency, and temperature can be established by interpolation of the results presented in Figures 4.5 to 4.32 at a specified strain amplitude. In this chapter a strain amplitude of $4.4 \times 10^{-3}\%$ ($\log_{10} = -2.36$) was selected for this purpose. Another strain amplitude could be selected without changing the conclusions reached in Sections 4.4.2, 4.4.3, and 4.4.4 owing to the fact that the variation between dynamic Young's modulus and log percent axial strain was assumed to be linear and independent of confining pressure, frequency, and temperature.

4.4.2 Effect of Confining Pressure

The relationship between dynamic Young's modulus and confining pressure at an axial strain of $4.4 \times 10^{-3}\%$ is shown in Figures 4.33 to 4.37 for the high density ice and Figures 4.38 to 4.40 for the low density ice.

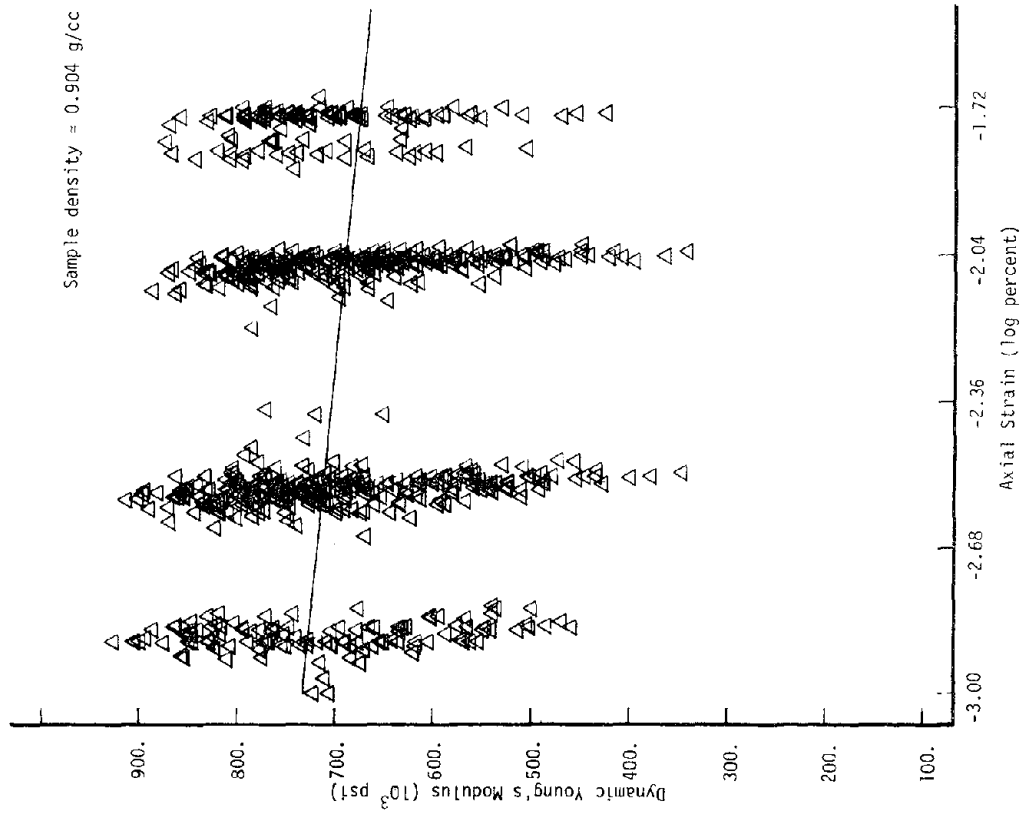


Figure 4.3 LEAST SQUARES BEST FIT LINE FOR DYNAMIC YOUNG'S MODULUS OF HIGH DENSITY ICE VERSUS AXIAL STRAIN

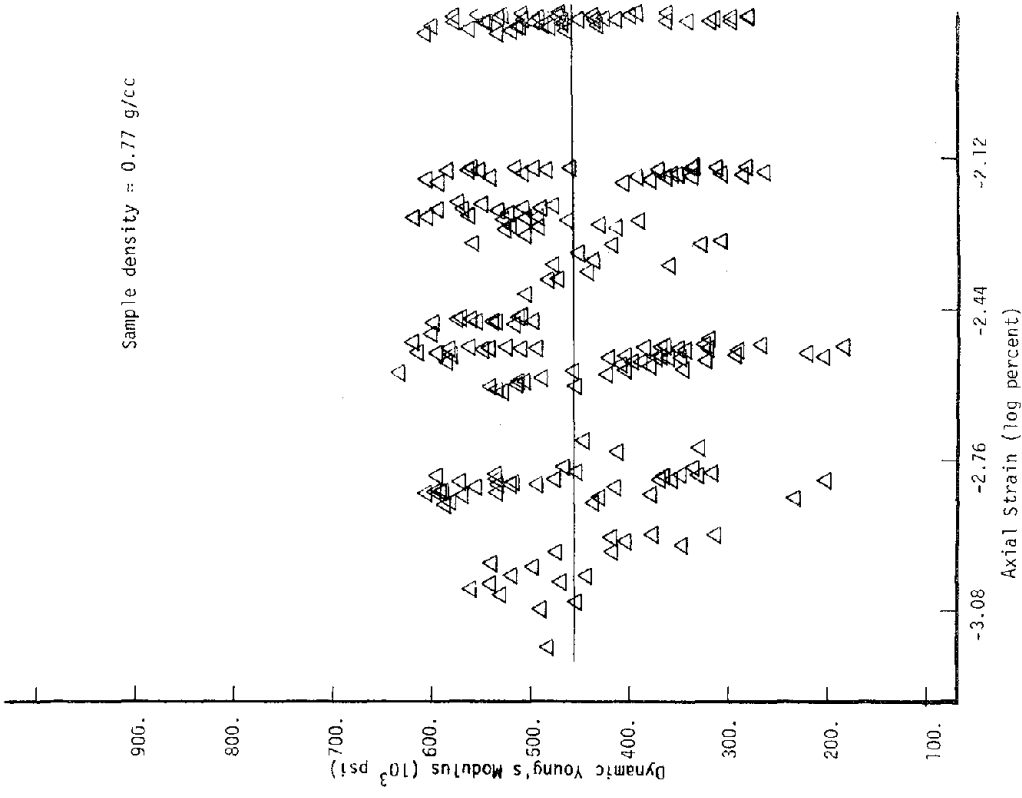


Figure 4.4 LEAST SQUARES BEST FIT LINE FOR DYNAMIC YOUNG'S MODULUS OF LOW DENSITY ICE VERSUS AXIAL STRAIN

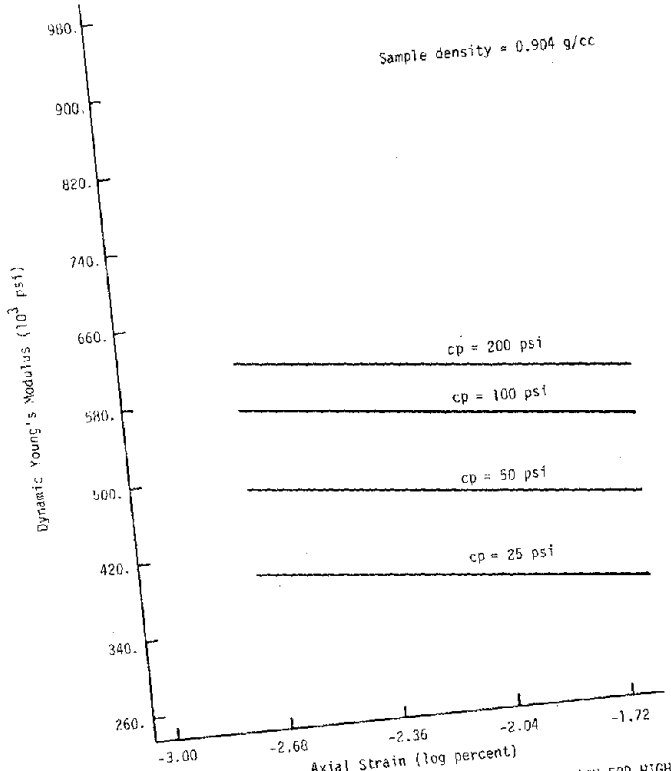


Figure 4.5 DYNAMIC YOUNG'S MODULUS VERSUS AXIAL STRAIN FOR HIGH DENSITY ICE AT -1°C AND 0.05 CPS

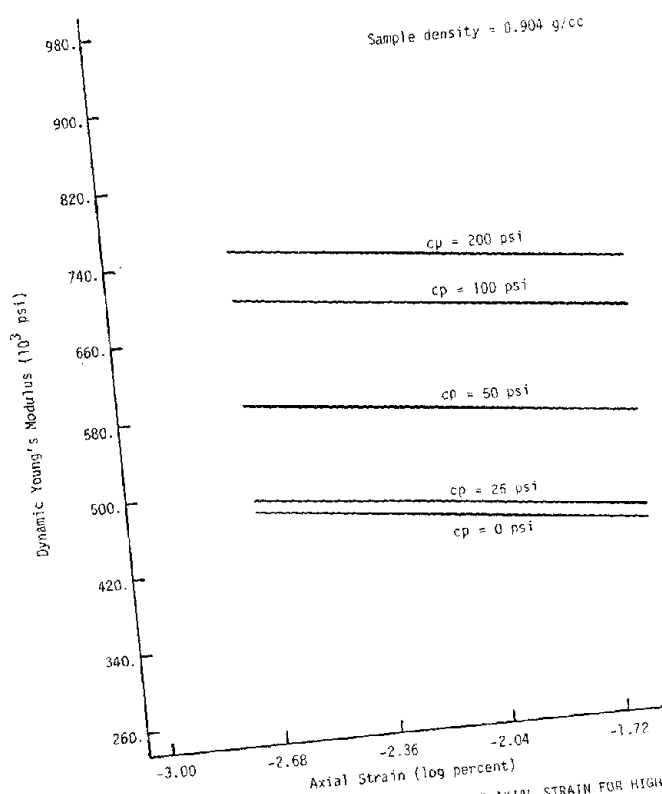


Figure 4.6 DYNAMIC YOUNG'S MODULUS VERSUS AXIAL STRAIN FOR HIGH DENSITY ICE AT -1°C AND 0.3 CPS

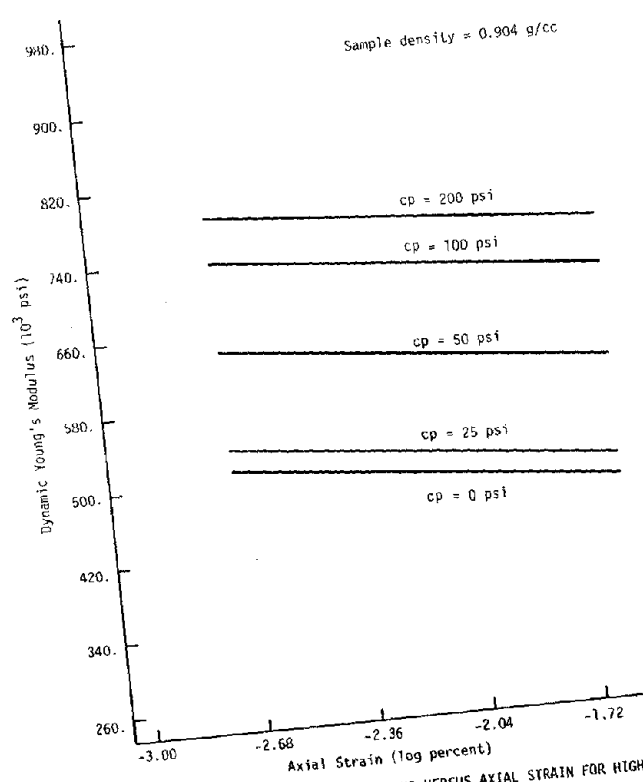


Figure 4.7 DYNAMIC YOUNG'S MODULUS VERSUS AXIAL STRAIN FOR HIGH DENSITY ICE AT -1°C AND 1.0 CPS

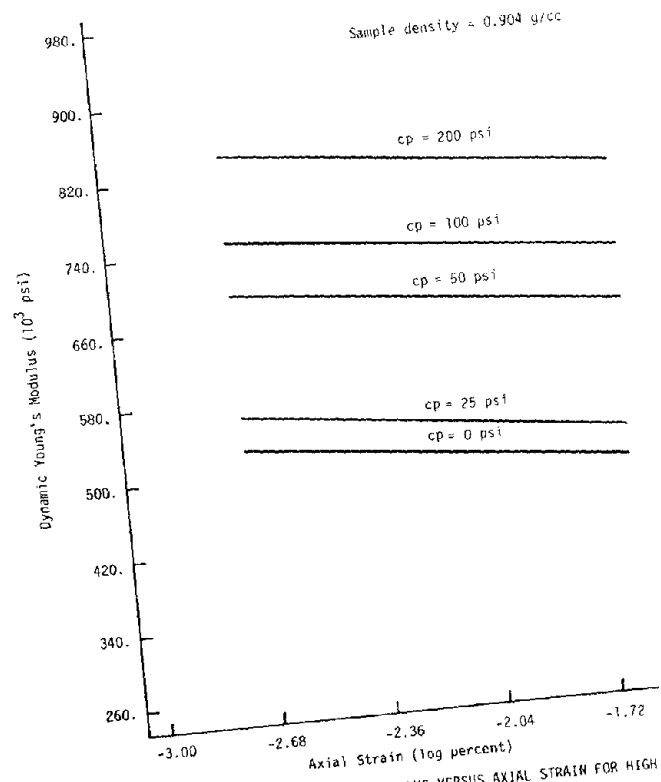


Figure 4.8 DYNAMIC YOUNG'S MODULUS VERSUS AXIAL STRAIN FOR HIGH DENSITY ICE AT -1°C AND 5.0 CPS

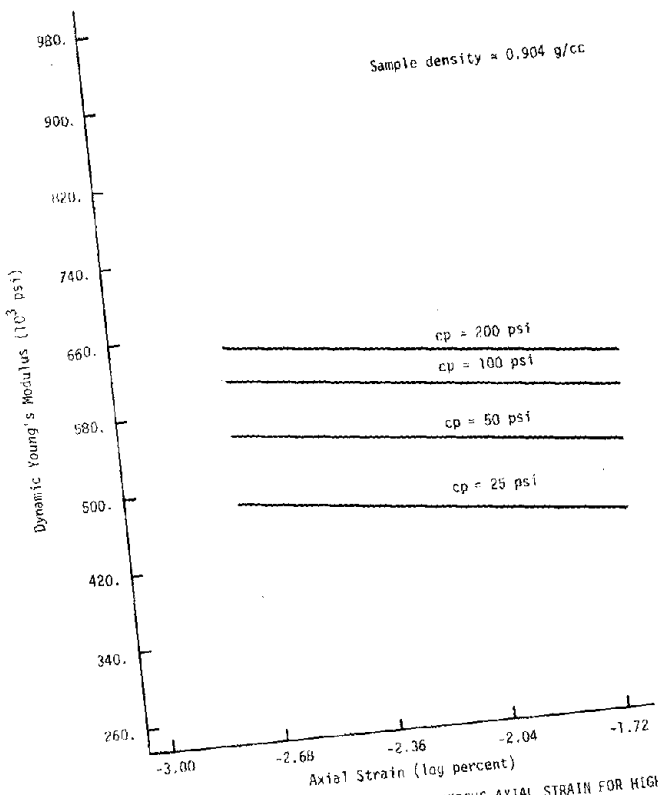


Figure 4.9 DYNAMIC YOUNG'S MODULUS VERSUS AXIAL STRAIN FOR HIGH DENSITY ICE AT -2°C AND 0.05 CPS

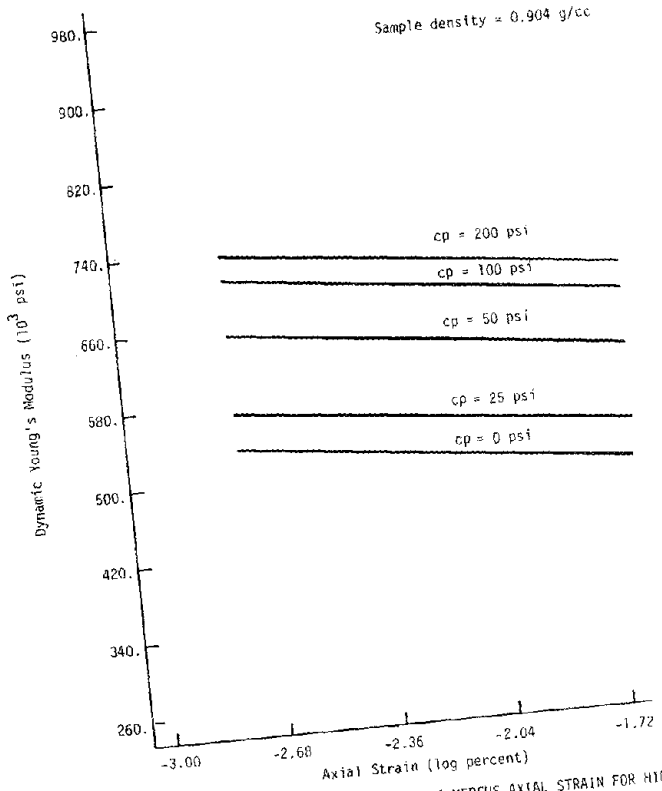


Figure 4.10 DYNAMIC YOUNG'S MODULUS VERSUS AXIAL STRAIN FOR HIGH DENSITY ICE AT -2°C AND 0.3 CPS

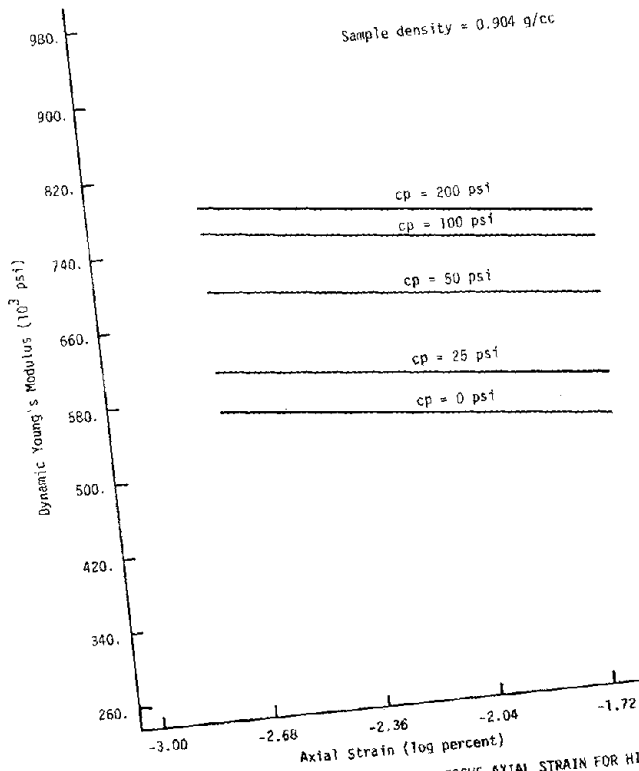


Figure 4.11 DYNAMIC YOUNG'S MODULUS VERSUS AXIAL STRAIN FOR HIGH DENSITY ICE AT -2°C AND 1.0 CPS

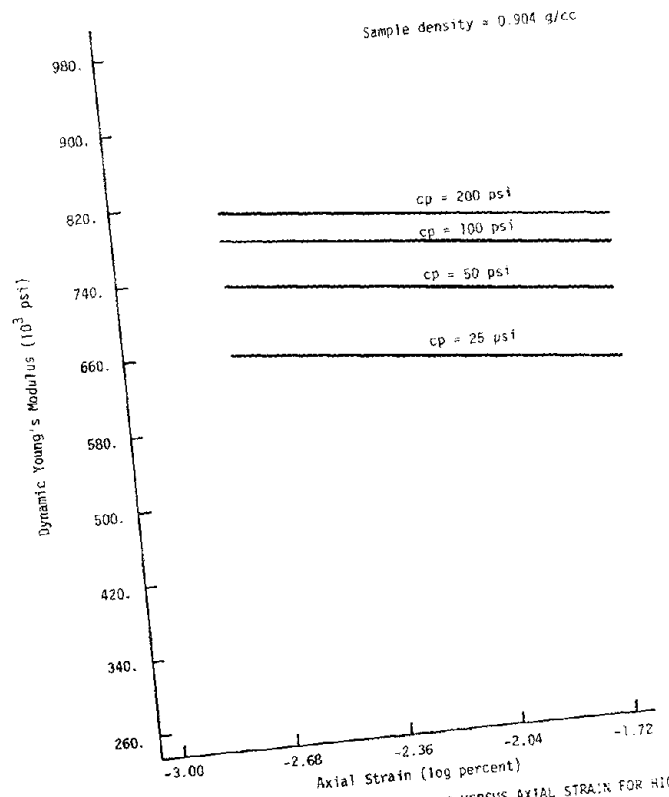


Figure 4.12 DYNAMIC YOUNG'S MODULUS VERSUS AXIAL STRAIN FOR HIGH DENSITY ICE AT -2°C AND 5.0 CPS

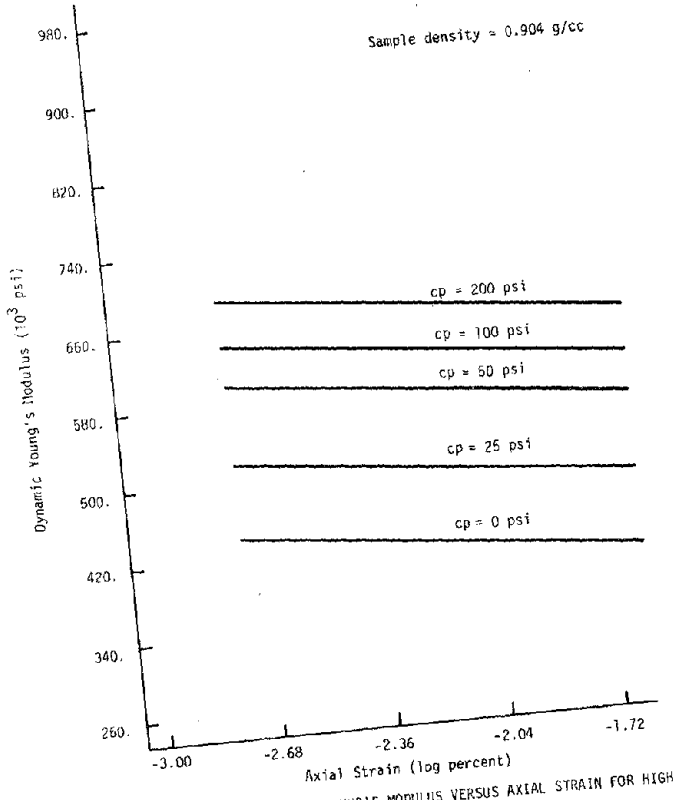


Figure 4.13 DYNAMIC YOUNG'S MODULUS VERSUS AXIAL STRAIN FOR HIGH DENSITY ICE AT -4°C AND 0.05 CPS

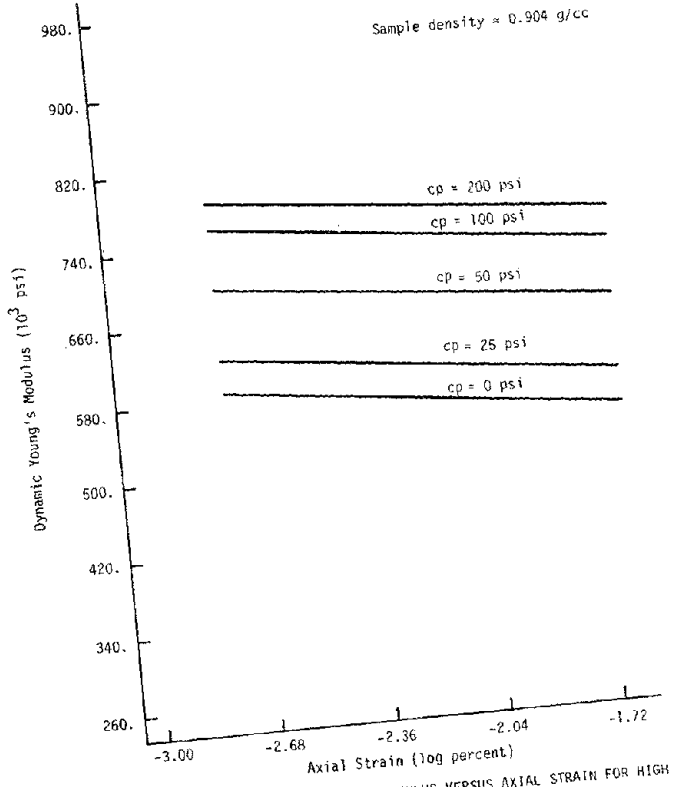


Figure 4.14 DYNAMIC YOUNG'S MODULUS VERSUS AXIAL STRAIN FOR HIGH DENSITY ICE AT -4°C AND 0.3 CPS

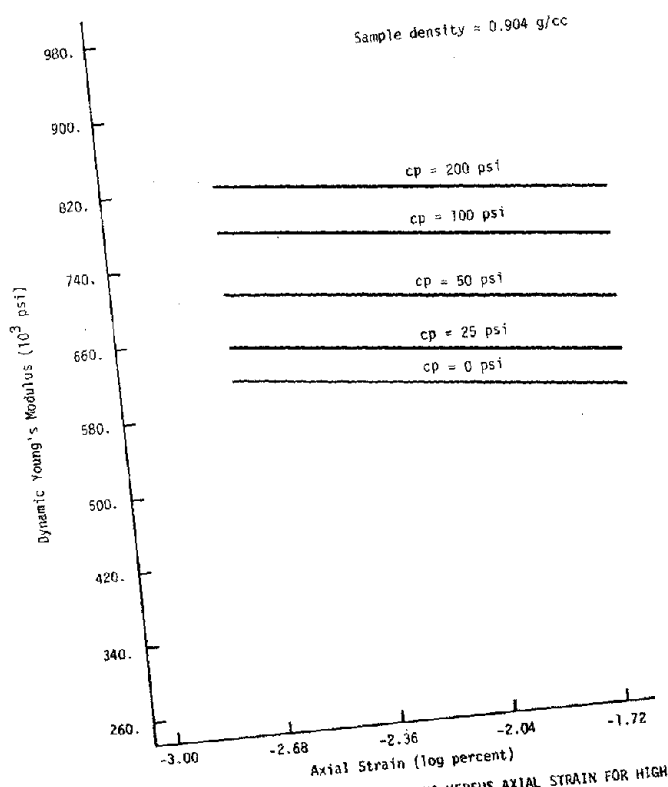


Figure 4.15 DYNAMIC YOUNG'S MODULUS VERSUS AXIAL STRAIN FOR HIGH DENSITY ICE AT -4°C AND 1.0 CPS

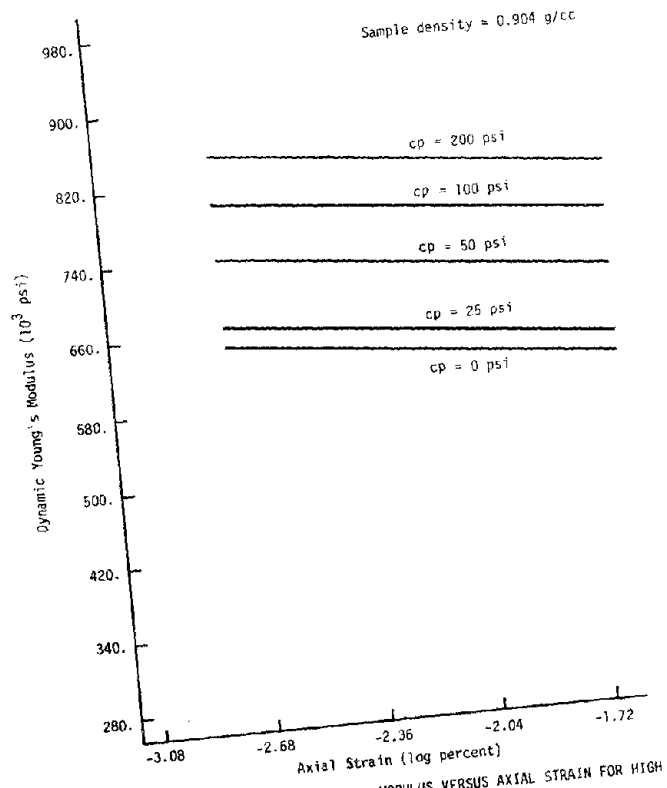


Figure 4.16 DYNAMIC YOUNG'S MODULUS VERSUS AXIAL STRAIN FOR HIGH DENSITY ICE AT -4°C AND 5.0 CPS

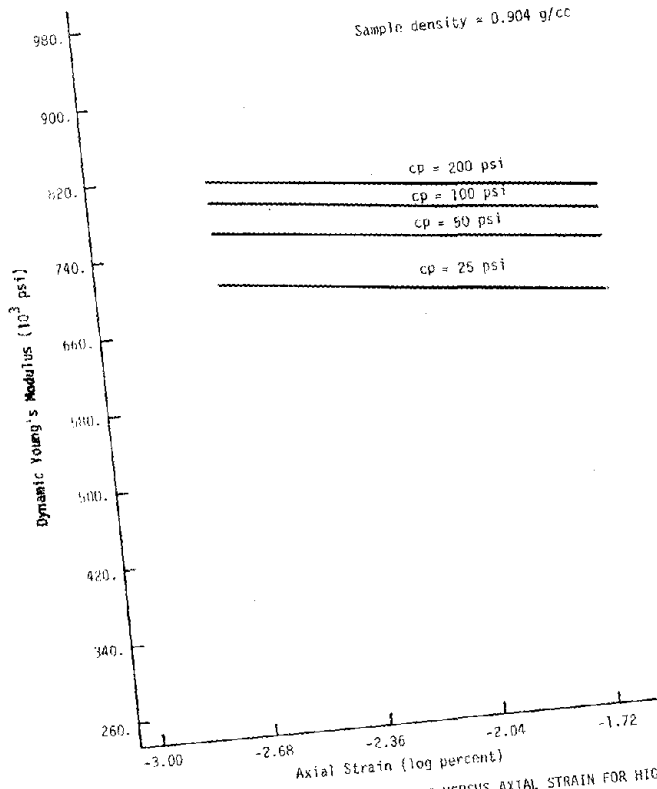


Figure 4.17 DYNAMIC YOUNG'S MODULUS VERSUS AXIAL STRAIN FOR HIGH DENSITY ICE AT -6°C AND 0.3 CPS

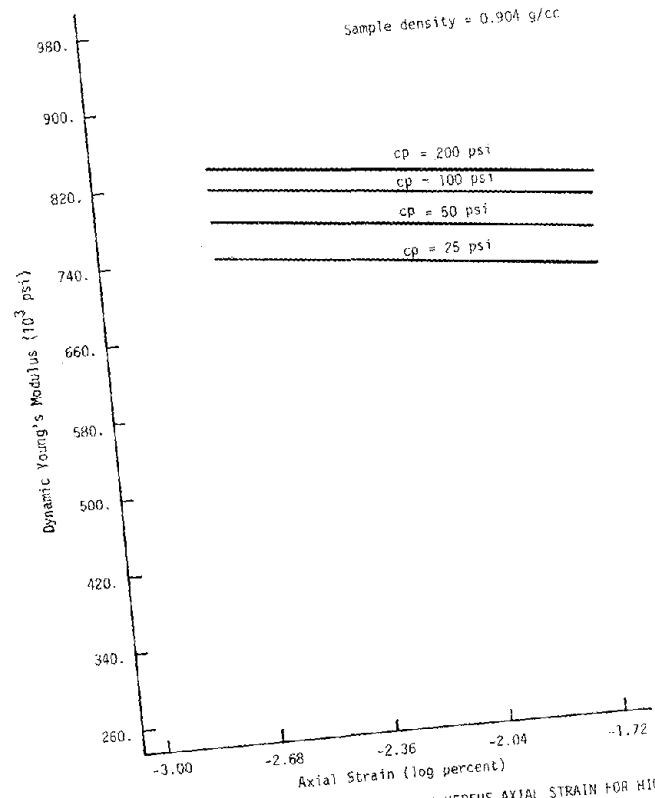


Figure 4.18 DYNAMIC YOUNG'S MODULUS VERSUS AXIAL STRAIN FOR HIGH DENSITY ICE AT -6°C AND 1.0 CPS

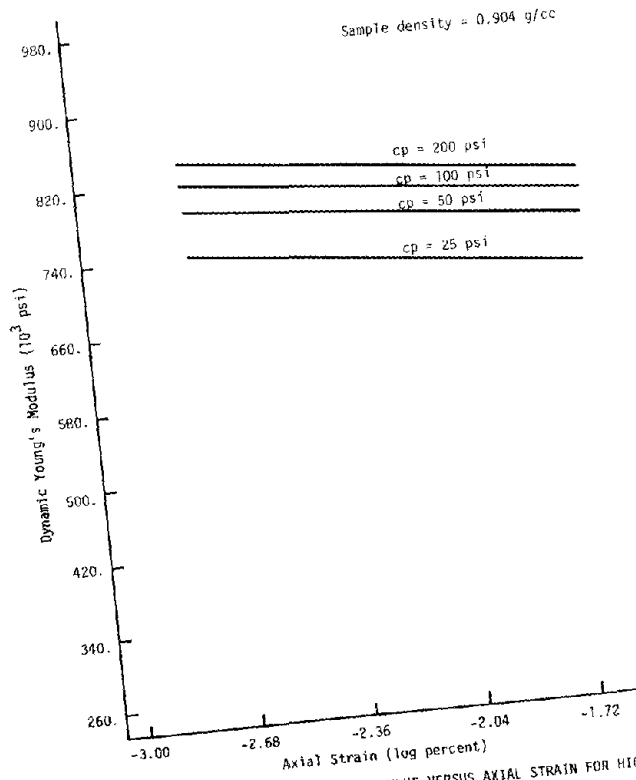


Figure 4.19 DYNAMIC YOUNG'S MODULUS VERSUS AXIAL STRAIN FOR HIGH DENSITY ICE AT -6°C AND 5.0 CPS

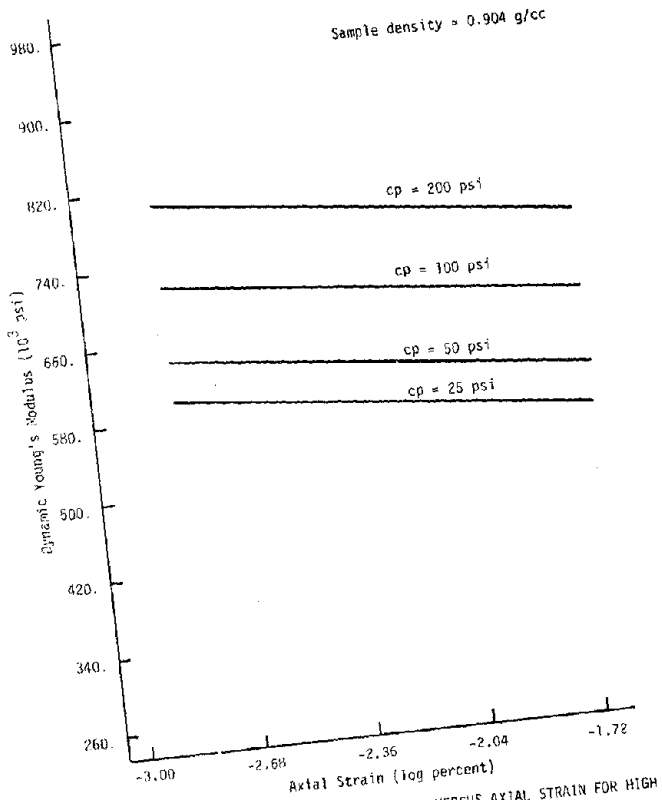


Figure 4.20 DYNAMIC YOUNG'S MODULUS VERSUS AXIAL STRAIN FOR HIGH DENSITY ICE AT -10°C AND 0.05 CPS

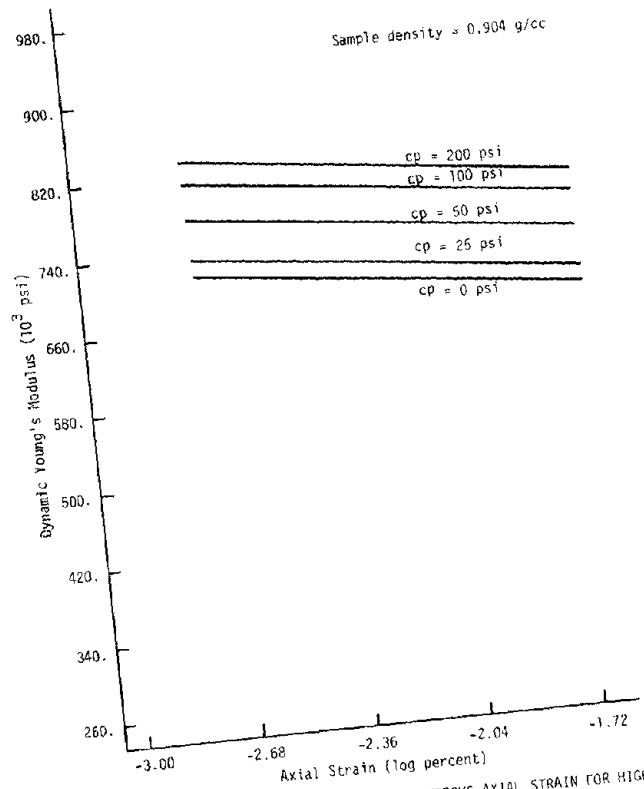


Figure 4.21 DYNAMIC YOUNG'S MODULUS VERSUS AXIAL STRAIN FOR HIGH DENSITY ICE AT -10°C AND 0.3 CPS

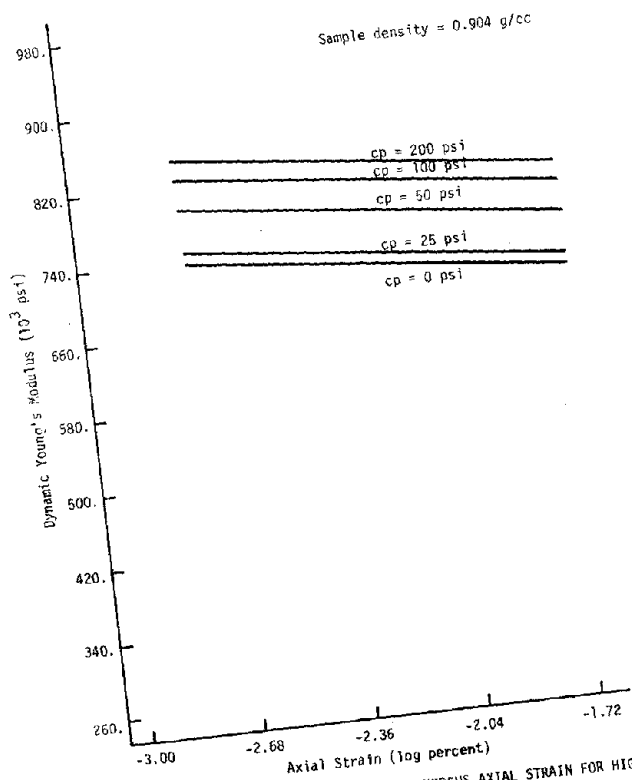


Figure 4.22 DYNAMIC YOUNG'S MODULUS VERSUS AXIAL STRAIN FOR HIGH DENSITY ICE AT -10°C AND 1.0 CPS

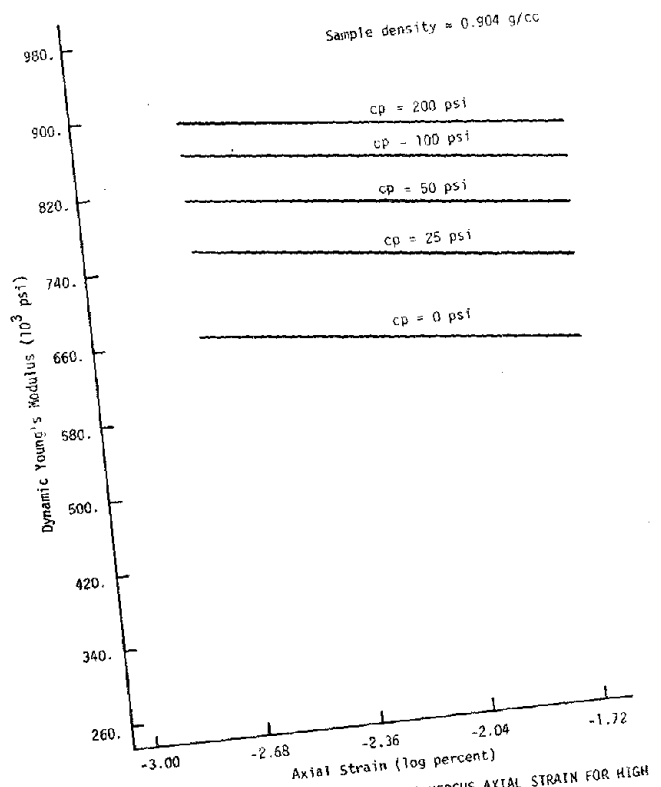


Figure 4.23 DYNAMIC YOUNG'S MODULUS VERSUS AXIAL STRAIN FOR HIGH DENSITY ICE AT -10°C AND 5.0 CPS

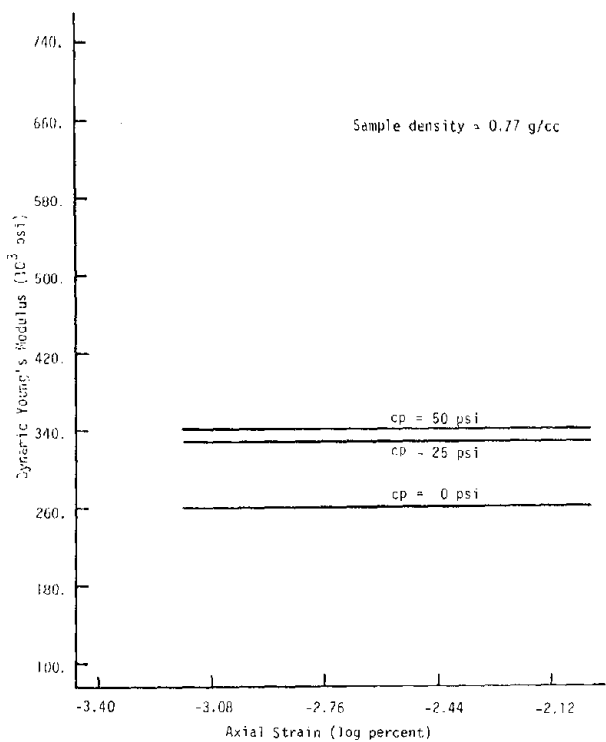


Figure 4.24 DYNAMIC YOUNG'S MODULUS VERSUS AXIAL STRAIN FOR LOW DENSITY ICE AT -1°C AND 0.3 CPS

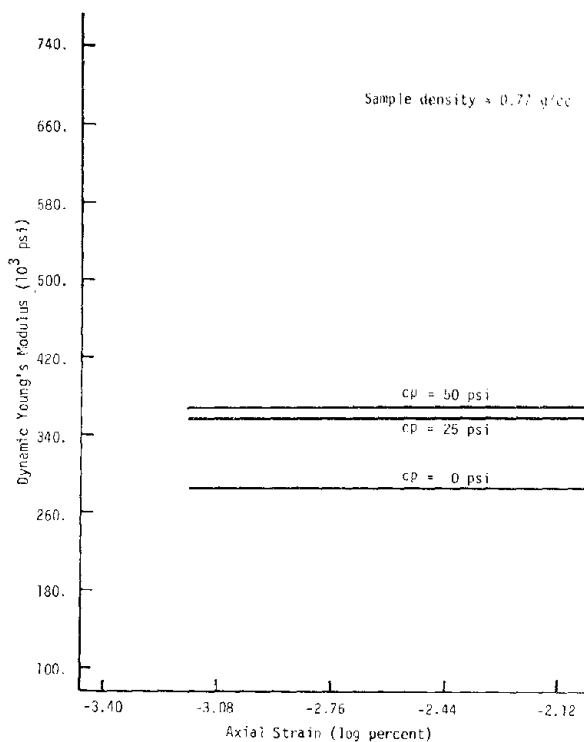


Figure 4.25 DYNAMIC YOUNG'S MODULUS VERSUS AXIAL STRAIN FOR LOW DENSITY ICE AT -1°C AND 1.0 CPS

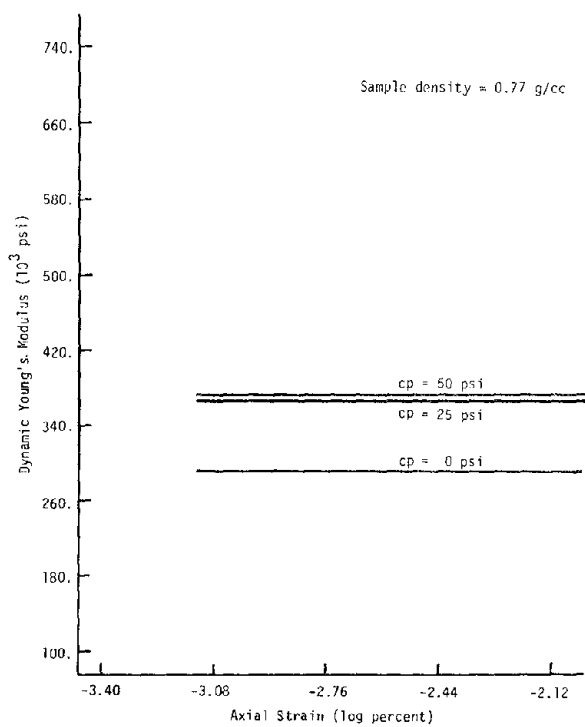


Figure 4.26 DYNAMIC YOUNG'S MODULUS VERSUS AXIAL STRAIN FOR LOW DENSITY ICE AT -1°C AND 5.0 CPS

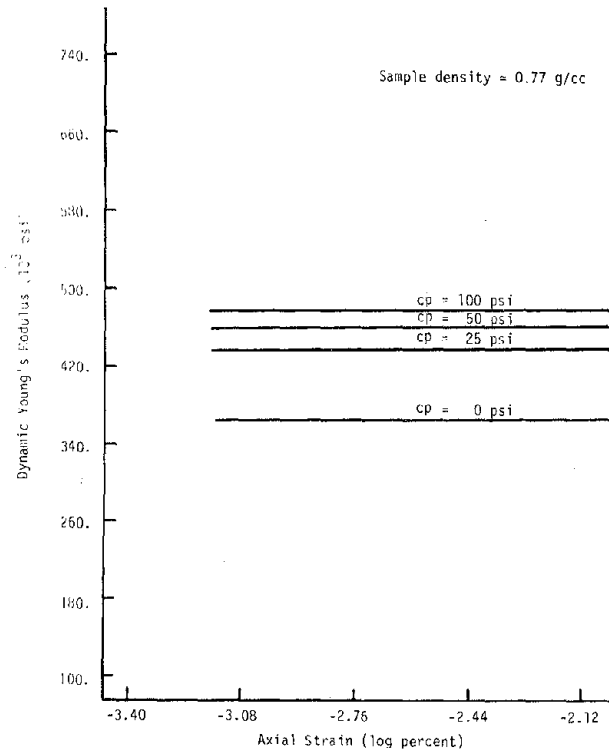


Figure 4.27 DYNAMIC YOUNG'S MODULUS VERSUS AXIAL STRAIN FOR LOW DENSITY ICE AT -4°C AND 0.3 CPS

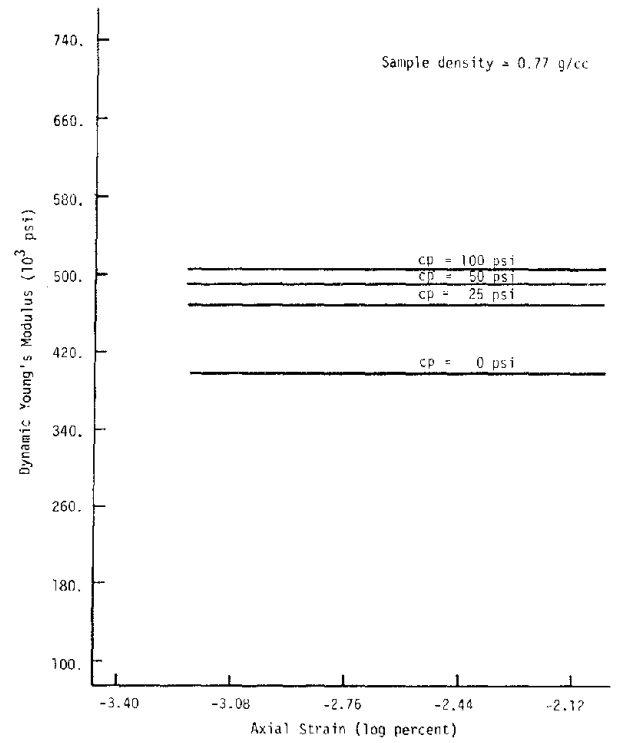


Figure 4.28 DYNAMIC YOUNG'S MODULUS VERSUS AXIAL STRAIN FOR LOW DENSITY ICE AT -4°C AND 1.0 CPS

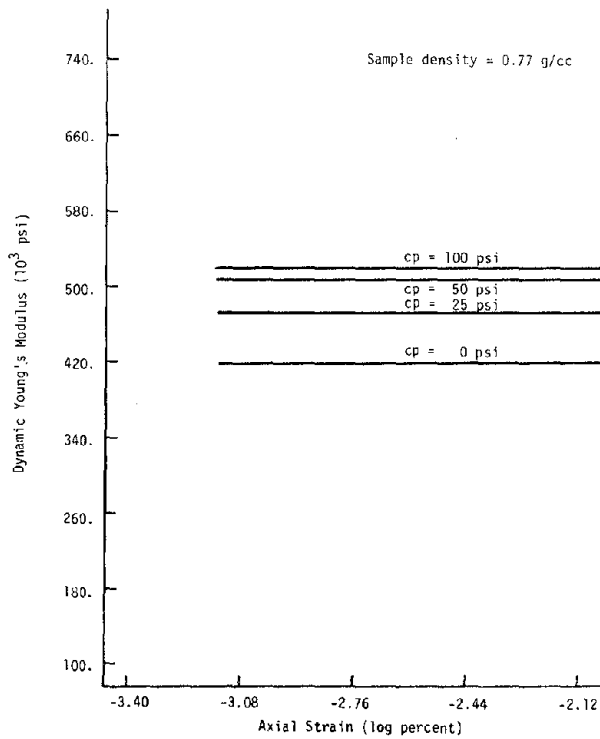


Figure 4.29 DYNAMIC YOUNG'S MODULUS VERSUS AXIAL STRAIN FOR LOW DENSITY ICE AT -4°C AND 5.0 CPS

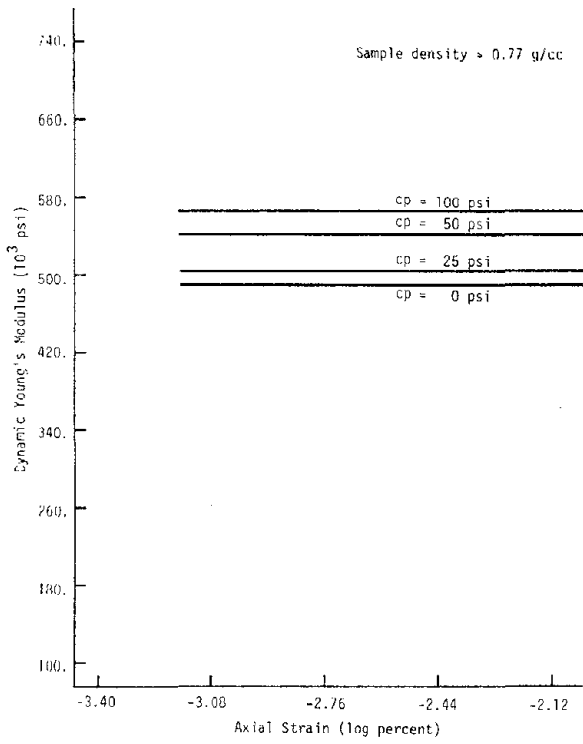


Figure 4.30 DYNAMIC YOUNG'S MODULUS VERSUS AXIAL STRAIN FOR LOW DENSITY ICE AT -10°C AND 0.3 CPS

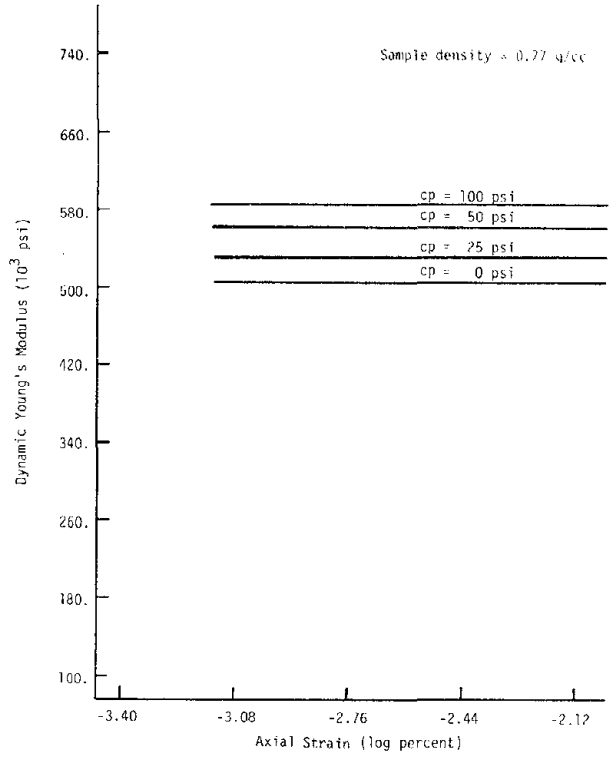


Figure 4.31 DYNAMIC YOUNG'S MODULUS VERSUS AXIAL STRAIN FOR LOW DENSITY ICE AT -10°C AND 1.0 CPS

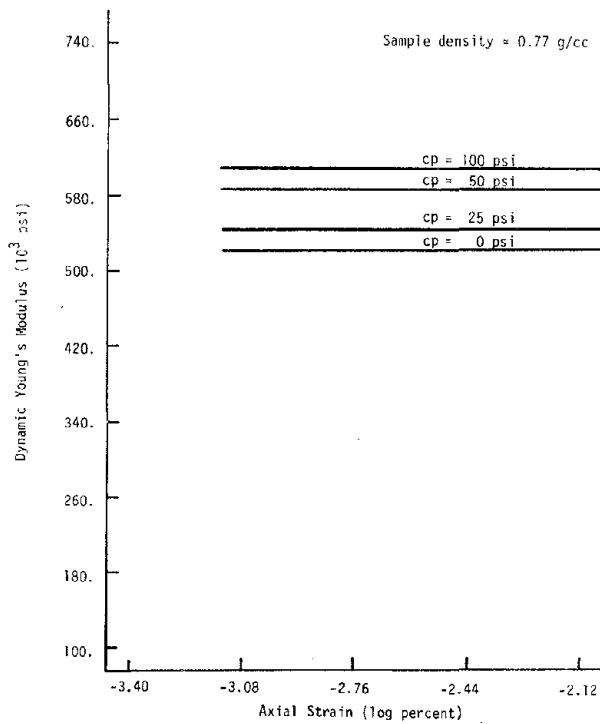


Figure 4.32 DYNAMIC YOUNG'S MODULUS VERSUS AXIAL STRAIN FOR LOW DENSITY ICE AT -10°C AND 5.0 CPS

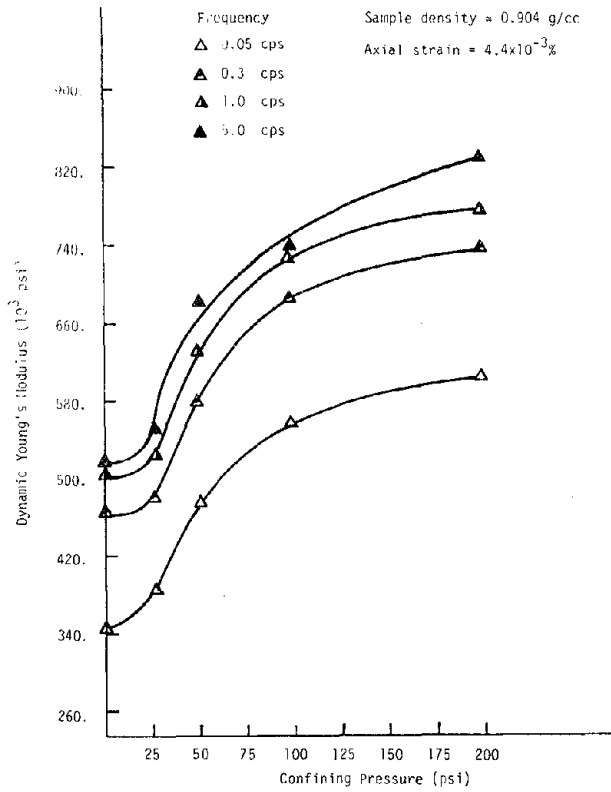


Figure 4.33 DYNAMIC YOUNG'S MODULUS VERSUS CONFINING PRESSURE FOR HIGH DENSITY ICE AT -1°C

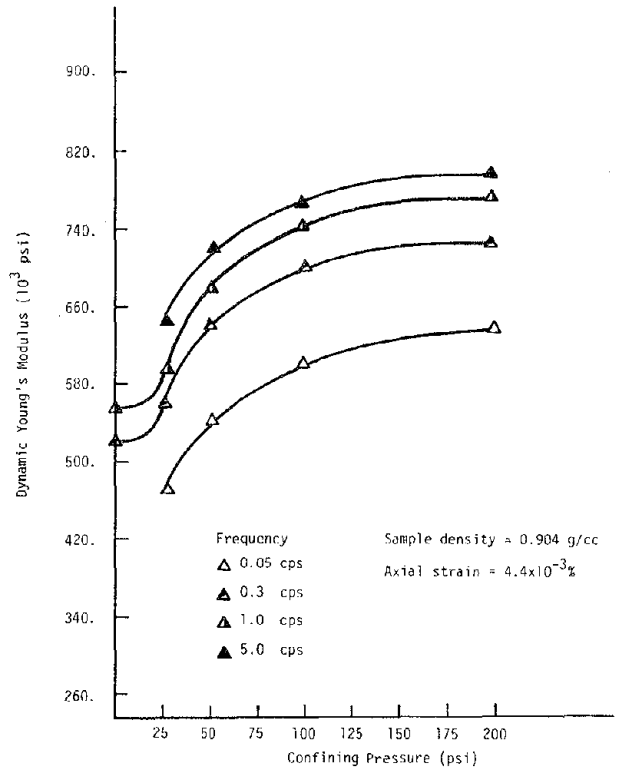


Figure 4.34 DYNAMIC YOUNG'S MODULUS VERSUS CONFINING PRESSURE FOR HIGH DENSITY ICE AT -2°C

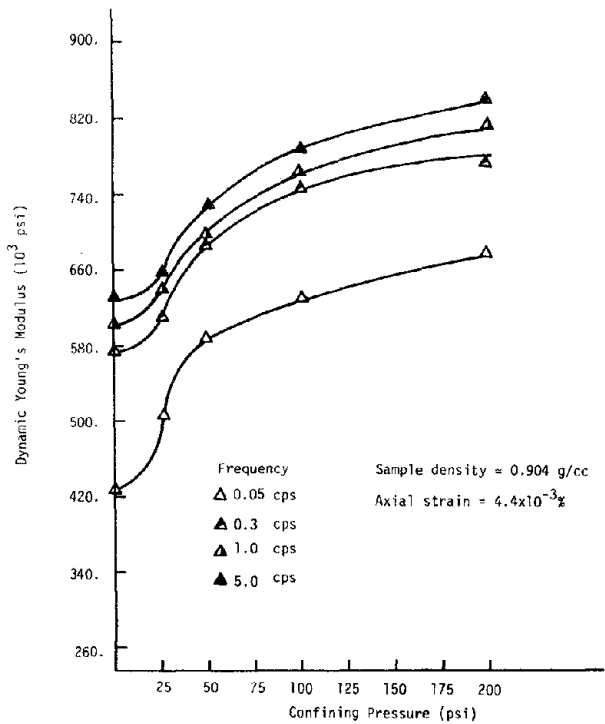


Figure 4.35 DYNAMIC YOUNG'S MODULUS VERSUS CONFINING PRESSURE FOR HIGH DENSITY ICE AT -4°C

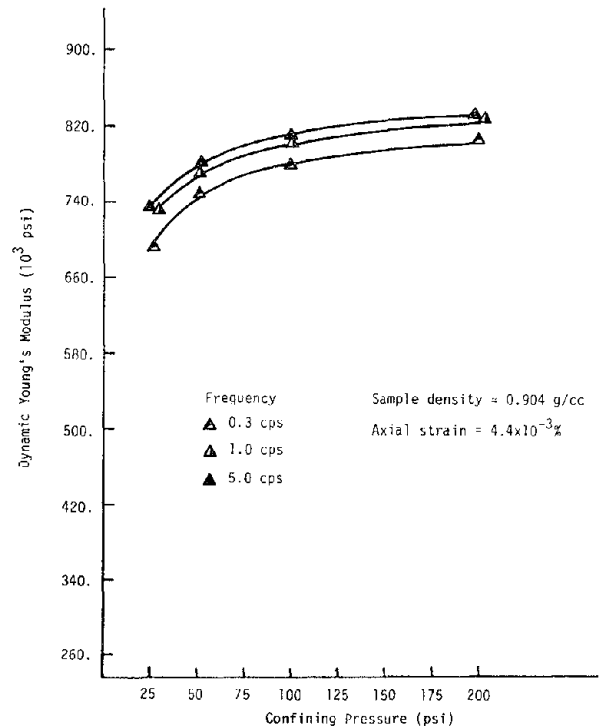


Figure 4.36 DYNAMIC YOUNG'S MODULUS VERSUS CONFINING PRESSURE FOR HIGH DENSITY ICE AT -6°C

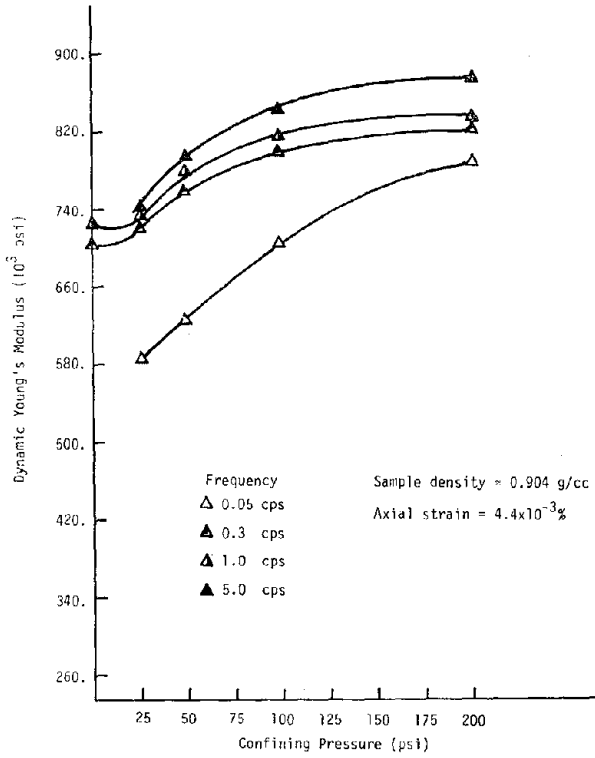


Figure 4.37 DYNAMIC YOUNG'S MODULUS VERSUS CONFINING PRESSURE FOR HIGH DENSITY ICE AT -10°C

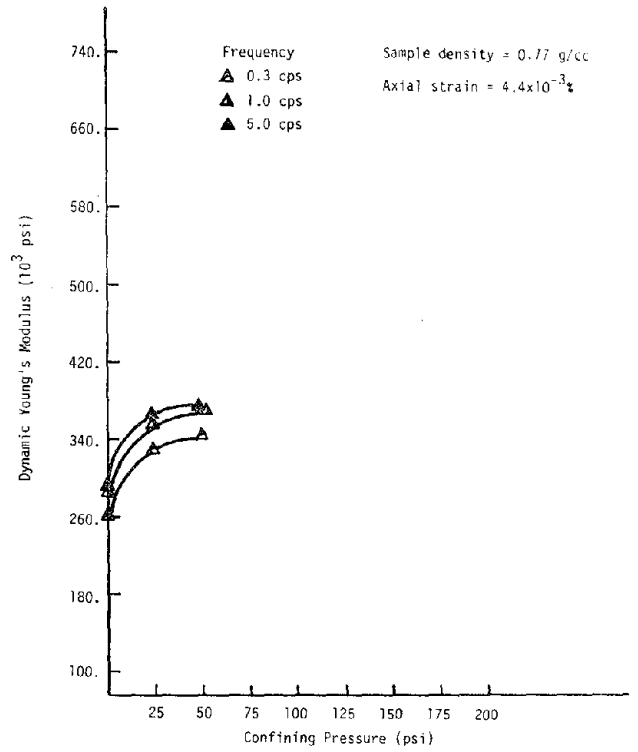


Figure 4.38 DYNAMIC YOUNG'S MODULUS VERSUS CONFINING PRESSURE FOR LOW DENSITY ICE AT -1°C

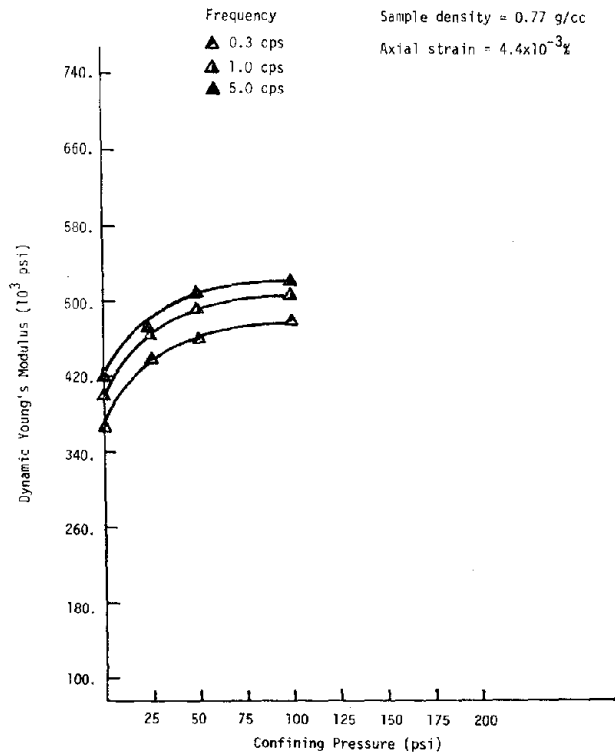


Figure 4.39 DYNAMIC YOUNG'S MODULUS VERSUS CONFINING PRESSURE FOR LOW DENSITY ICE AT -4°C

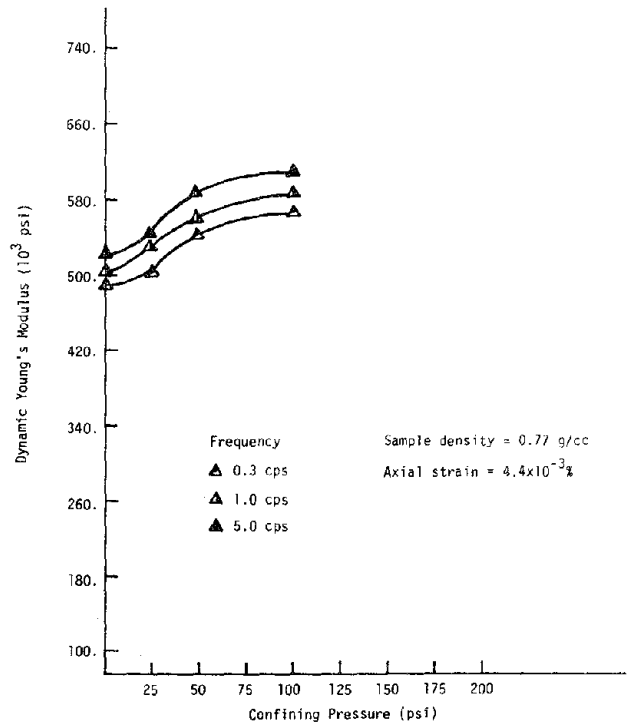


Figure 4.40 DYNAMIC YOUNG'S MODULUS VERSUS CONFINING PRESSURE FOR LOW DENSITY ICE AT -10°C

The relationship is, in general, plotted at four frequencies for a given temperature. The data at five temperatures (-1, -2, -4, -6 and -10°C) was available for the high density ice, and at three temperatures (-1, -4 and -10°C) for the low density ice.

The results shown in Figures 4.33 to 4.37 indicate the dynamic Young's modulus of high density ice increases with increasing confining pressure (1) gradually from 0 to 25 psi (approximately 8%), (2) steeply from 25 psi to 50 psi (approximately 20%), (3) gradually from 50 psi to 100 psi (approximately 8%), and only slightly from 100 psi to 200 psi. Temperature and frequency do not appear to have a significant influence on the relationship between dynamic Young's modulus and confining pressure.

The dynamic Young's modulus of low density ice at temperatures of -1 and -4°C increases rapidly with increasing confining pressure from 0 to 25 psi (approximately 14%). At a temperature of -10°C, the rate of increase in this range of confining pressure is gradual and comparable to high density ice. The dynamic Young's modulus increases gradually for all test temperatures with increasing confining pressure from 25 psi to 50 psi; it is almost constant with increasing confining pressure from 50 psi to 100 psi. Frequency does not appear to have an influence on the relationship between dynamic Young's modulus and confining pressure.

The relationship between dynamic Young's modulus of ice and confining pressure might be caused by changes in the microstructure of the ice under various confining pressures. Microfissures might close when a sample is subjected to a high confining pressure. This would lead to a sample with a higher dynamic modulus. Conversely, they might open when a sample is subjected to a lower confining pressure which would lead to a lower dynamic modulus. This tendency was exemplified by the fact that when the confining pressure was released from the triaxial cell and the sample was not allowed to deform there was a gradual increase of load on the sample. This load might be associated with the elastic rebound characteristics of the microfissures.

4.4.3 Effect of Frequency

The relationship between dynamic Young's modulus and frequency at an axial strain of $4.4 \times 10^{-3}\%$ is shown in Figures 4.41 to 4.45 for high density ice and Figures 4.46 to 4.48 for low density ice. The relation-

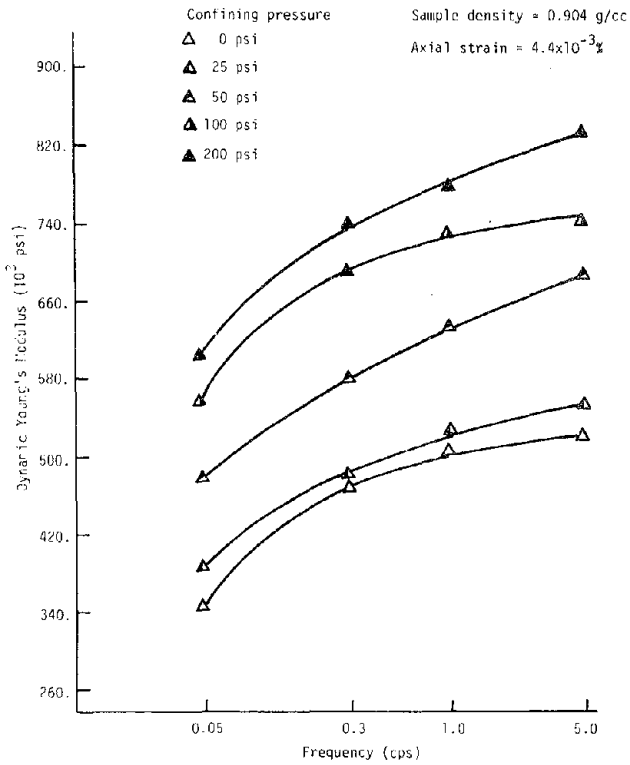


Figure 4.41 DYNAMIC YOUNG'S MODULUS VERSUS FREQUENCY FOR HIGH DENSITY ICE AT -1°C

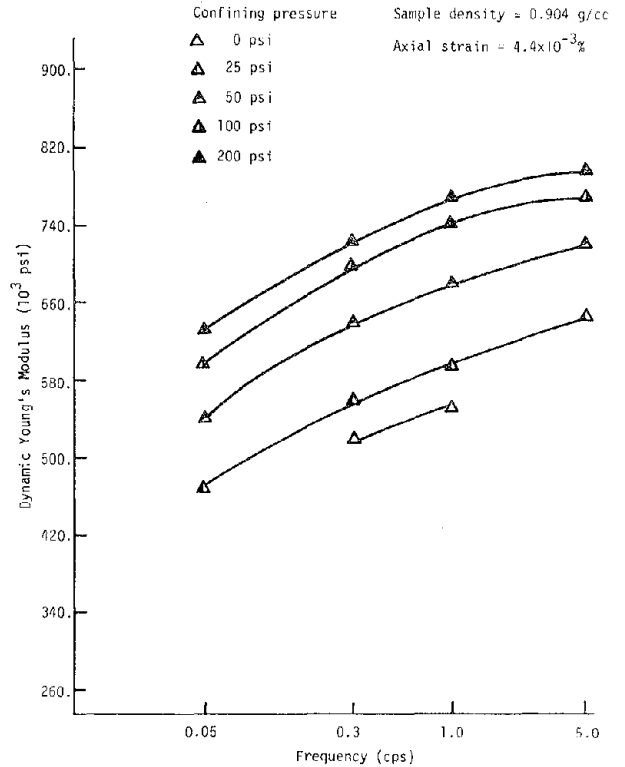


Figure 4.42 DYNAMIC YOUNG'S MODULUS VERSUS FREQUENCY FOR HIGH DENSITY ICE AT -2°C

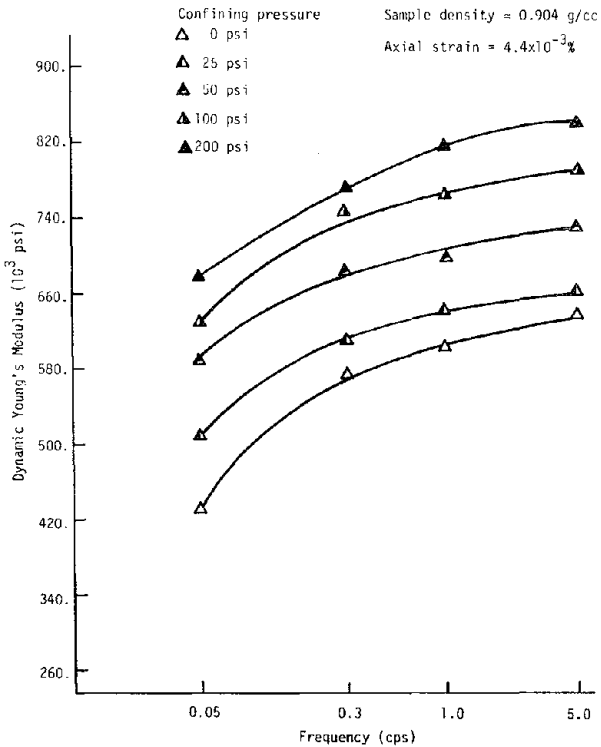


Figure 4.43 DYNAMIC YOUNG'S MODULUS VERSUS FREQUENCY FOR HIGH DENSITY ICE AT -4°C

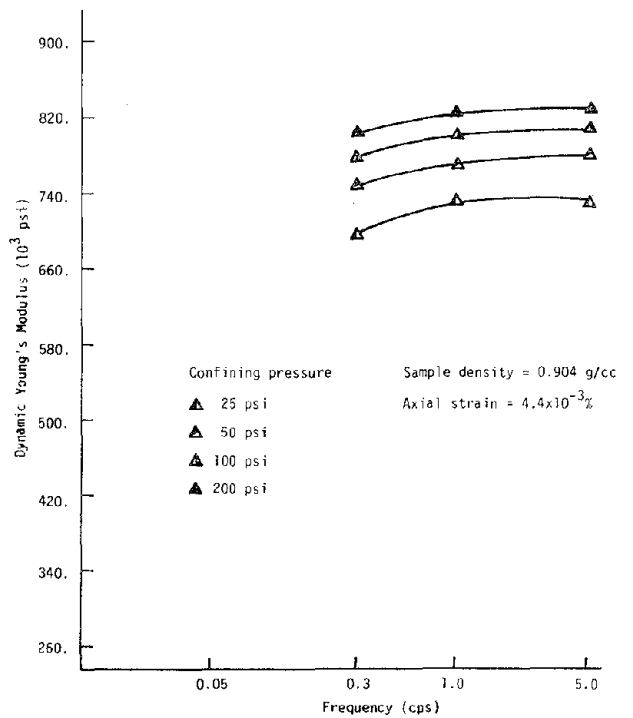


Figure 4.44 DYNAMIC YOUNG'S MODULUS VERSUS FREQUENCY FOR HIGH DENSITY ICE AT -6°C

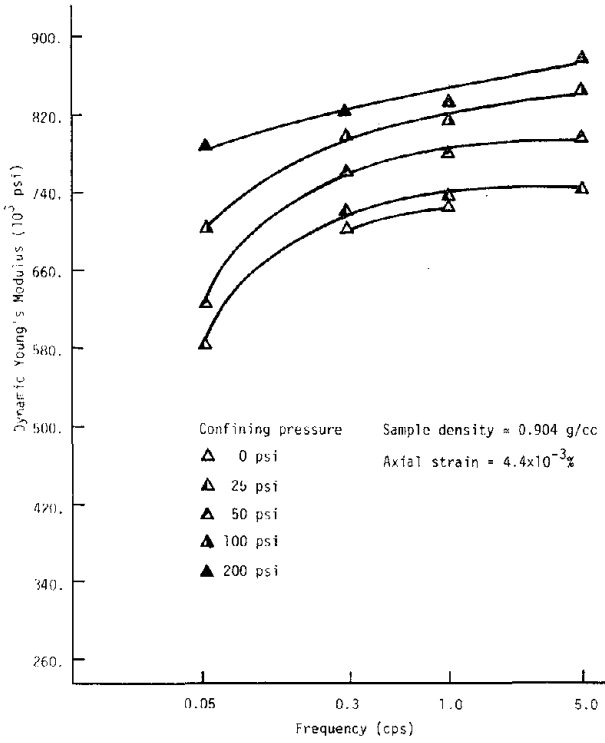


Figure 4.45 DYNAMIC YOUNG'S MODULUS VERSUS FREQUENCY FOR HIGH DENSITY ICE AT -10°C

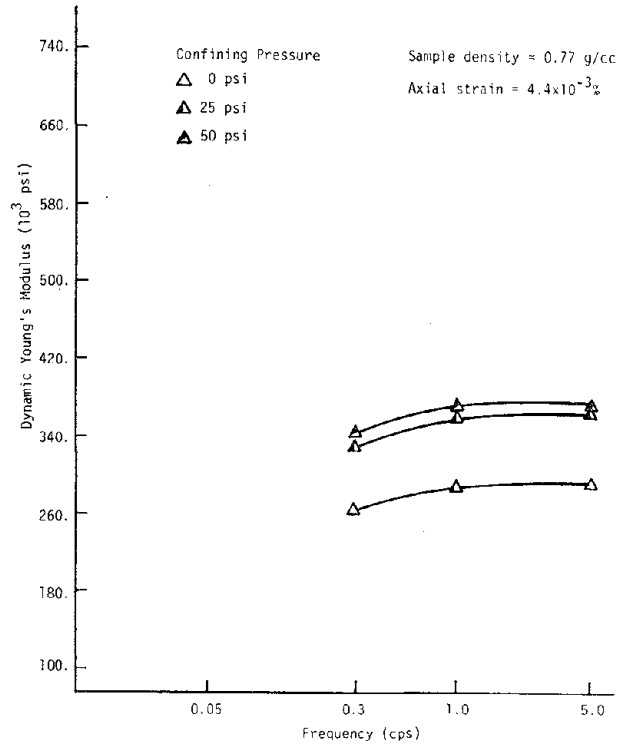


Figure 4.46 DYNAMIC YOUNG'S MODULUS VERSUS FREQUENCY FOR LOW DENSITY ICE AT -1°C

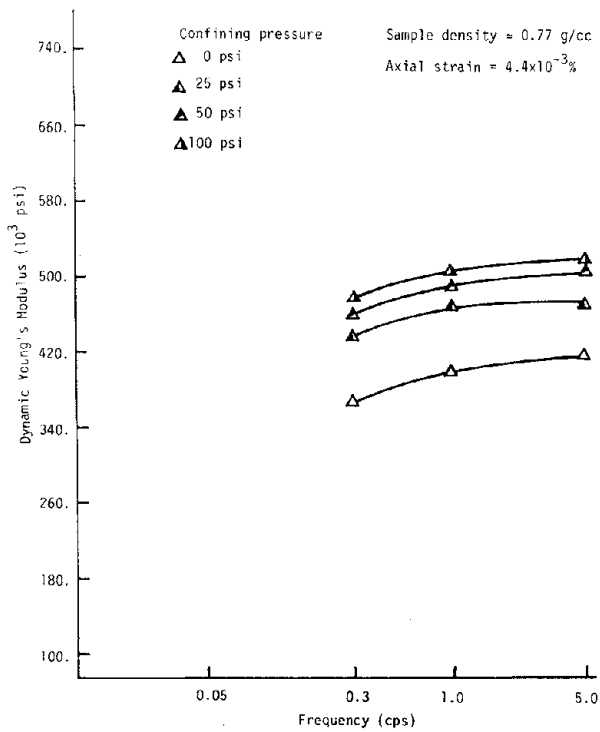


Figure 4.47 DYNAMIC YOUNG'S MODULUS VERSUS FREQUENCY FOR LOW DENSITY ICE AT -4°C

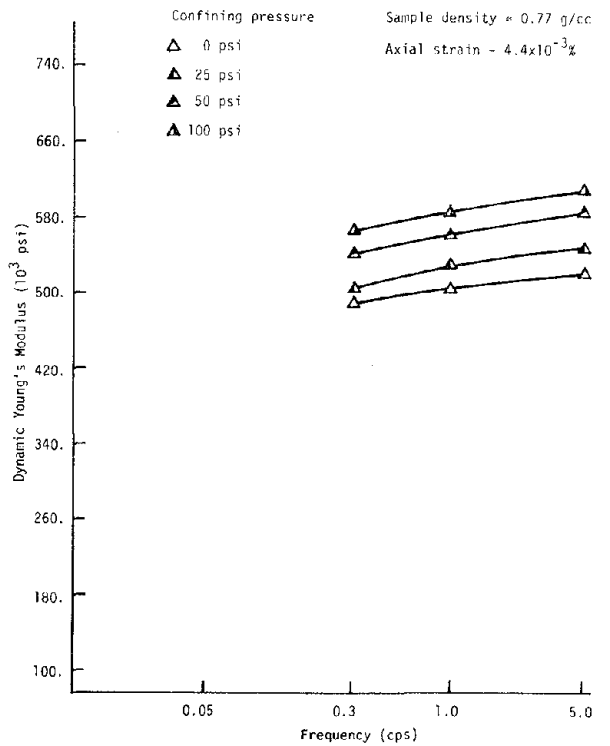


Figure 4.48 DYNAMIC YOUNG'S MODULUS VERSUS FREQUENCY FOR LOW DENSITY ICE AT -10°C

ship is, in general, plotted at five confining pressures for a given temperature.

The dynamic Young's modulus of high density ice increases rapidly (approximately 20%) for an increase in frequency from 0.05 to 0.3 cps. Between 0.3 and 5.0 cps the rate of increase is, in general, not as rapid. The increase of dynamic Young's modulus with frequency appears to be greater for higher temperatures (-1°C) than for lower temperatures (-10°C). Confining pressure does not appear to have an influence on the relationship between dynamic Young's modulus and frequency.

No tests were performed at a frequency of 0.05 cps on the low density ice samples. The dynamic Young's modulus of low density ice increases approximately 4% for an increase in frequency from 0.3 to 5 cps. For samples at a temperature of -1 and -4°C the rate of increase is greater in the frequency range 0.3 to 1.0 cps than in the range 1.0 to 5.0 cps. For samples at a temperature of -10°C , the relationship between dynamic Young's modulus and frequency is almost linear in the range 0.3 to 5.0 cps. Confining pressure does not appear to have an influence on the relationship between dynamic Young's modulus and frequency.

4.4.4 Effect of Temperature

The relationship between dynamic Young's modulus and temperature is shown in Figures 4.49 to 4.52 for high density ice and Figures 4.53 to 4.56 for low density ice. The relationship is, in general, plotted at four frequencies for a given confining pressure.

The dynamic Young's modulus of the high density ice increases with decreasing temperatures. At a confining pressure of 25 psi the modulus increases approximately 20% for a temperature decrease from -1 to -4°C . It also increases approximately 20% for a temperature decrease from -4 to -10°C . The modulus increases more rapidly in the temperature range -1 to -4°C than in the temperature range -4 to -10°C . For the temperature range -4 to -10°C , the rate of increase is almost constant. At low confining pressures, the rate of increase is slightly greater than at high confining pressures. The frequency of testing appears to have no significant influence on the relationship between dynamic Young's modulus and temperature.

The dynamic Young's modulus of low density ice increases approximately 35% for an increase in temperature from -1 to -4°C and approxi-

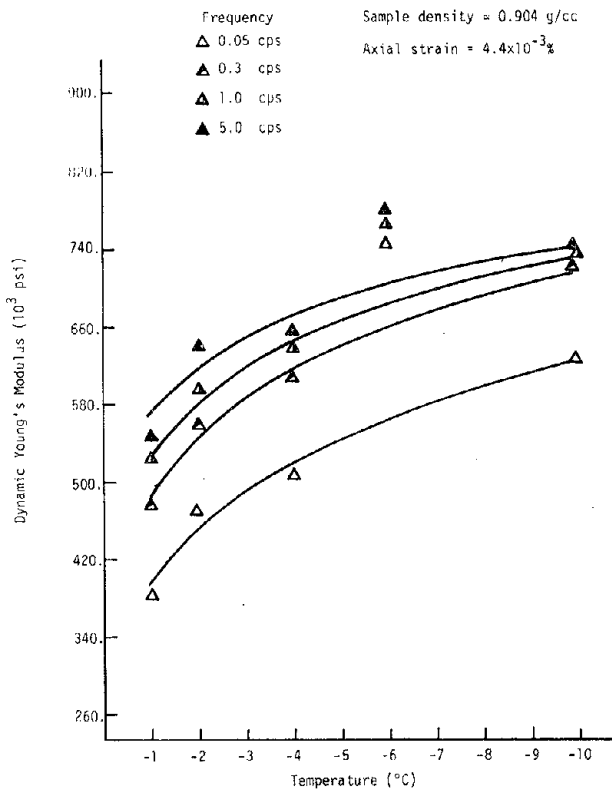


Figure 4.49 DYNAMIC YOUNG'S MODULUS VERSUS TEMPERATURE FOR HIGH DENSITY ICE AT A CONFINING PRESSURE OF 25 PSI

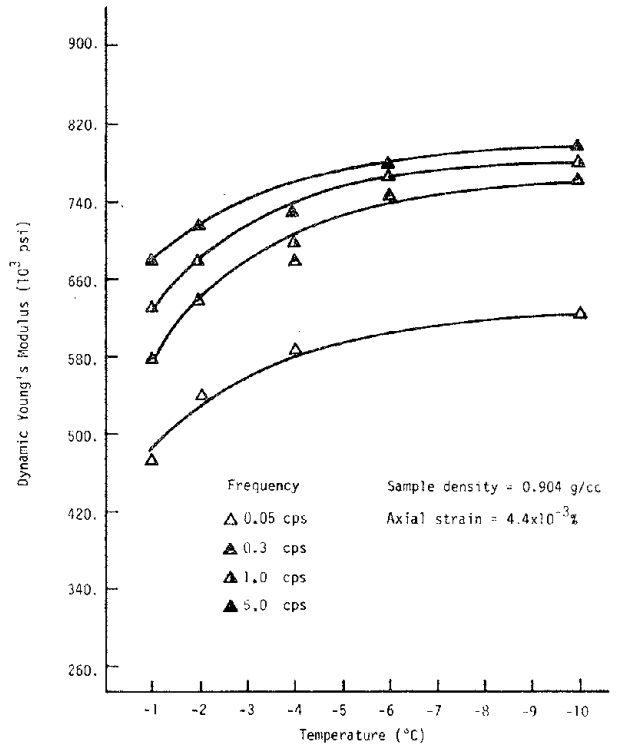


Figure 4.50 DYNAMIC YOUNG'S MODULUS VERSUS TEMPERATURE FOR HIGH DENSITY ICE AT A CONFINING PRESSURE OF 50 PSI

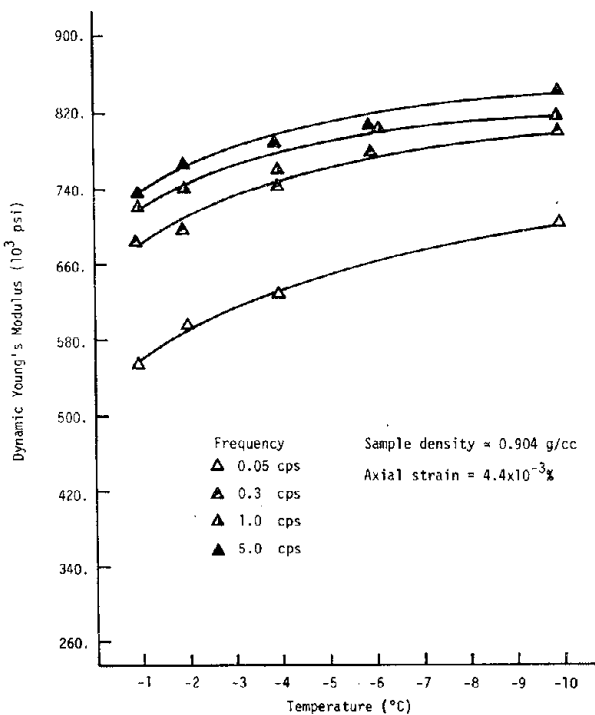


Figure 4.51 DYNAMIC YOUNG'S MODULUS VERSUS TEMPERATURE FOR HIGH DENSITY ICE AT A CONFINING PRESSURE OF 100 PSI

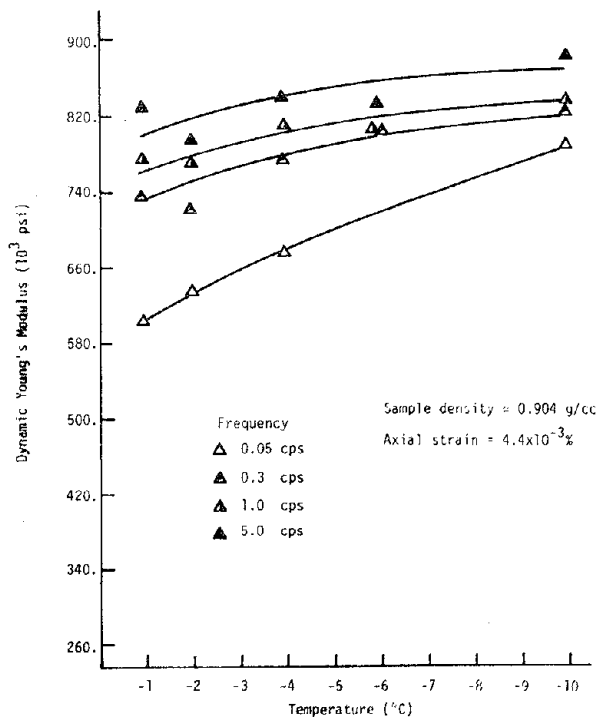


Figure 4.52 DYNAMIC YOUNG'S MODULUS VERSUS TEMPERATURE FOR HIGH DENSITY ICE AT A CONFINING PRESSURE OF 200 PSI

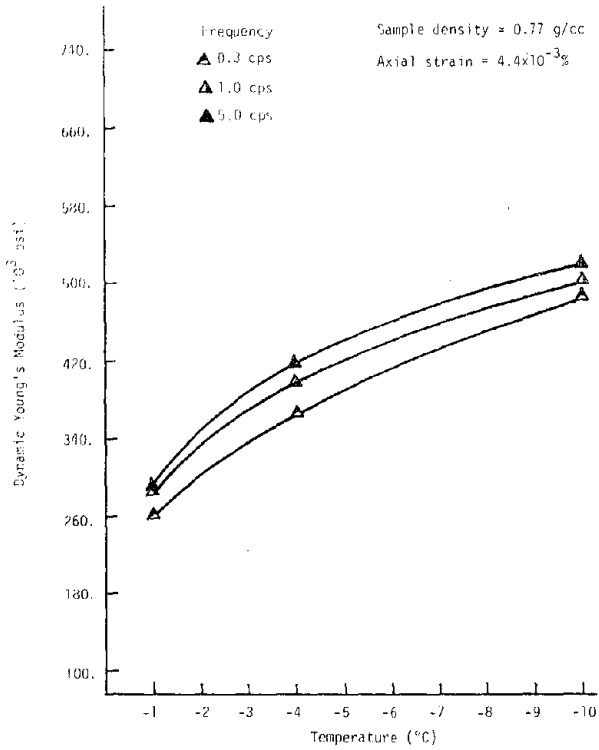


Figure 4.53 DYNAMIC YOUNG'S MODULUS VERSUS TEMPERATURE FOR LOW DENSITY ICE AT A CONFINING PRESSURE OF 0 PSI

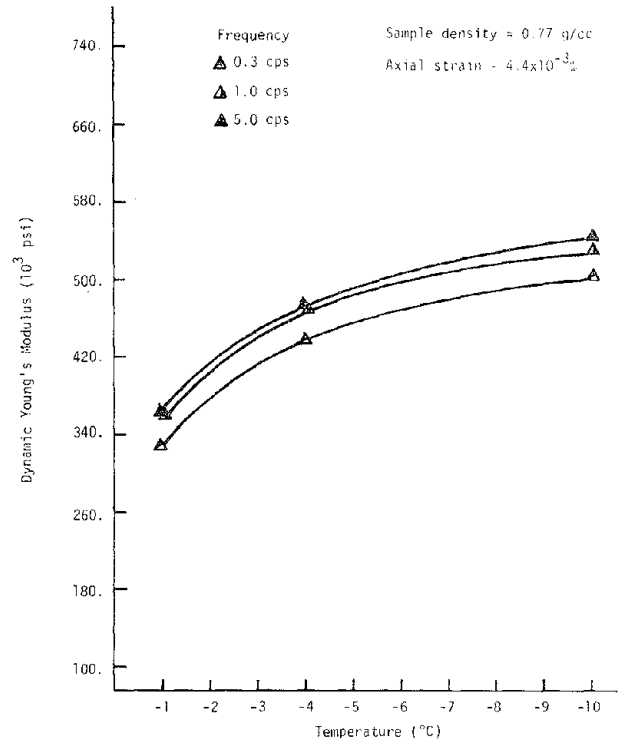


Figure 4.54 DYNAMIC YOUNG'S MODULUS VERSUS TEMPERATURE FOR LOW DENSITY ICE AT A CONFINING PRESSURE OF 25 PSI

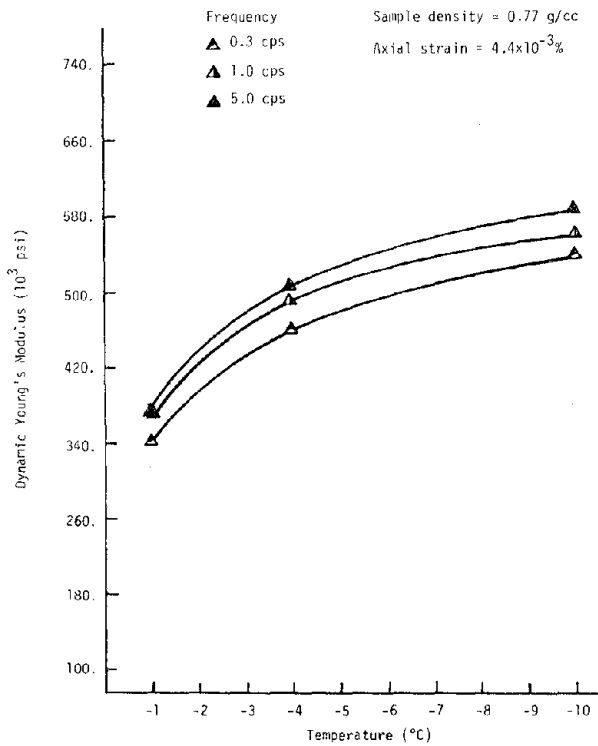


Figure 4.55 DYNAMIC YOUNG'S MODULUS VERSUS TEMPERATURE FOR LOW DENSITY ICE AT A CONFINING PRESSURE OF 50 PSI

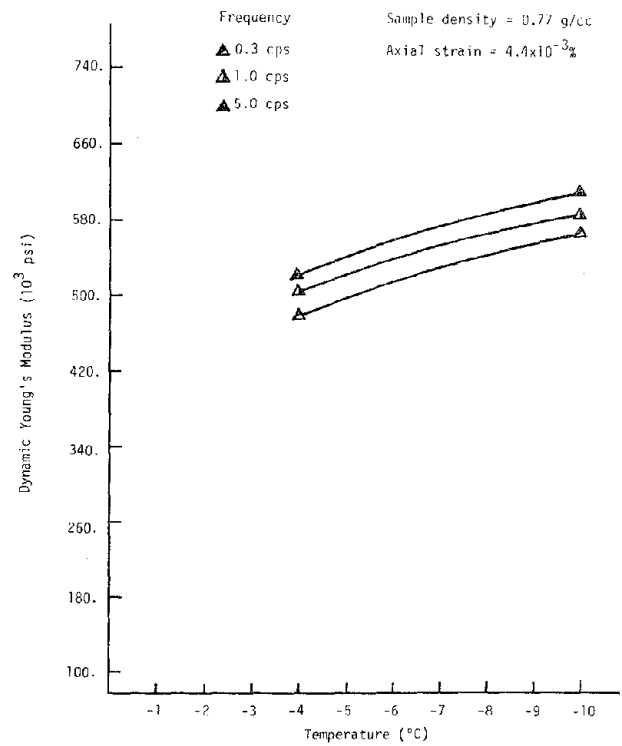


Figure 4.56 DYNAMIC YOUNG'S MODULUS VERSUS TEMPERATURE FOR LOW DENSITY ICE AT A CONFINING PRESSURE OF 100 PSI

mately 20% for an increase in temperature from -4 to -10°C. The modulus increases almost linearly in the temperature range -4 to -10°C. The rate of increase is smaller than for the temperature range -1 to -4°C. Frequency and confining pressure appear to have no significant influence on the relationship between dynamic Young's modulus and temperature.

4.4.5 Effect of Density

The results presented by Roethlisberger (1972) and Bennett (1972) indicate that the dynamic elastic properties of ice vary linearly with density in the range 0.7 to 0.919 g/cc (refer to Figures 2.11, 2.12, and 2.13, Section 2.3.2). In the research program the dynamic Young's modulus was evaluated at two densities: 0.77 and 0.904 g/cc. The relationship between dynamic Young's modulus and density was assumed to be linear. The relationship is shown in Figures 4.57 to 4.59 for three frequencies at a confining pressure of 50 psi, axial strain of $4.4 \times 10^{-3}\%$, and a given temperature. In Figures 4.60 to 4.62 the relationship between dynamic Young's modulus and density is shown for three confining pressures at a frequency of 1.0 cps, axial strain of $4.4 \times 10^{-3}\%$, and a given temperature.

The dynamic Young's modulus increases approximately 60% as density increases from 0.77 to 0.904 g/cc. Temperature, frequency, and confining pressure do not appear to have a significant influence on the relationship.

4.5 Damping Ratio of Ice

Damping ratio was plotted against the log of axial strain expressed as a percent as shown in Appendix D, Figures D.1 to D.19, for the high density ice samples and Figures D.20 to D.28 for the low density ice. The range of damping ratio is from 0.001 to 0.14 for the high density ice and from 0.001 to 0.10 for the low density ice.

For a given test condition considerable "scatter" exists in the data. Several reasons for this scatter are given in Section 4.4. In addition to these reasons it is also felt that "scatter" occurred in measurements of damping ratio owing to personal error in the measurement of the area of the hysteresis loop.

As a consequence of the "scatter" in the data there appears to be no identifiable relationship between damping ratio and confining pressure

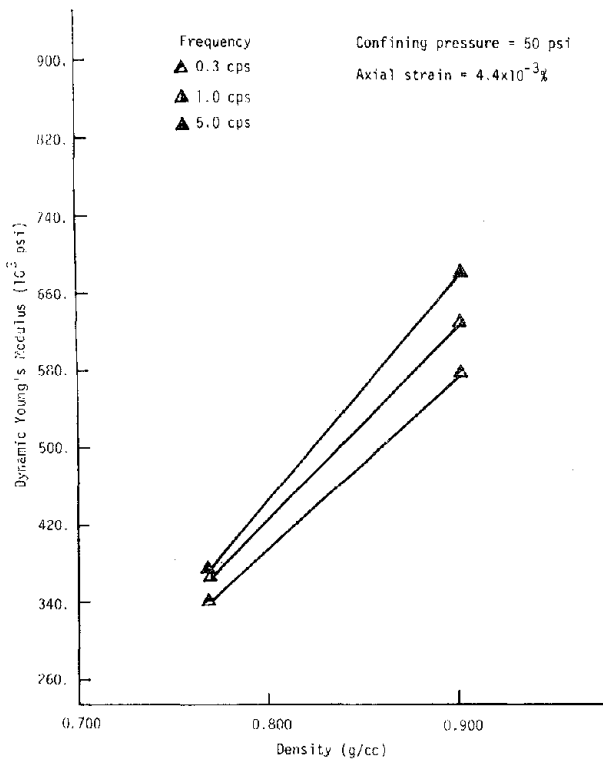


Figure 4.57 DYNAMIC YOUNG'S MODULUS VERSUS DENSITY OF ICE AT -1°C FOR THREE FREQUENCIES

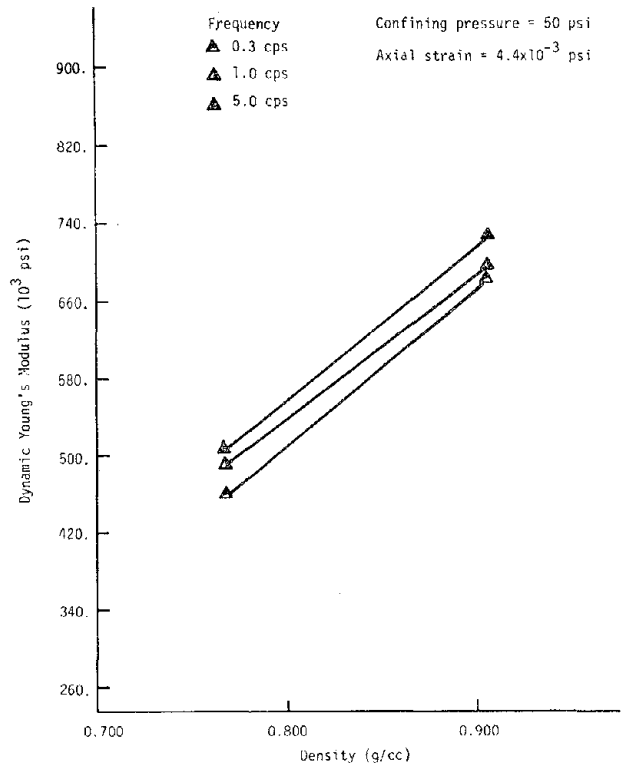


Figure 4.58 DYNAMIC YOUNG'S MODULUS VERSUS DENSITY OF ICE AT -4°C FOR THREE FREQUENCIES

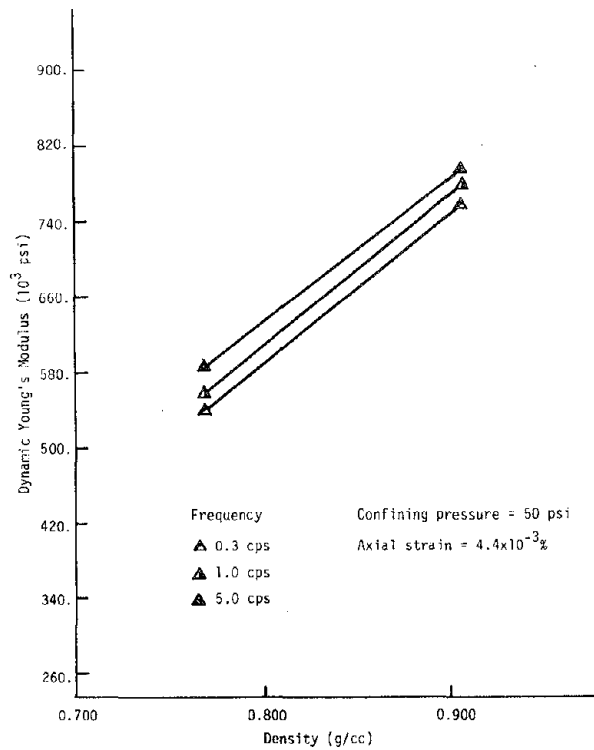


Figure 4.59 DYNAMIC YOUNG'S MODULUS VERSUS DENSITY OF ICE AT -10°C FOR THREE FREQUENCIES

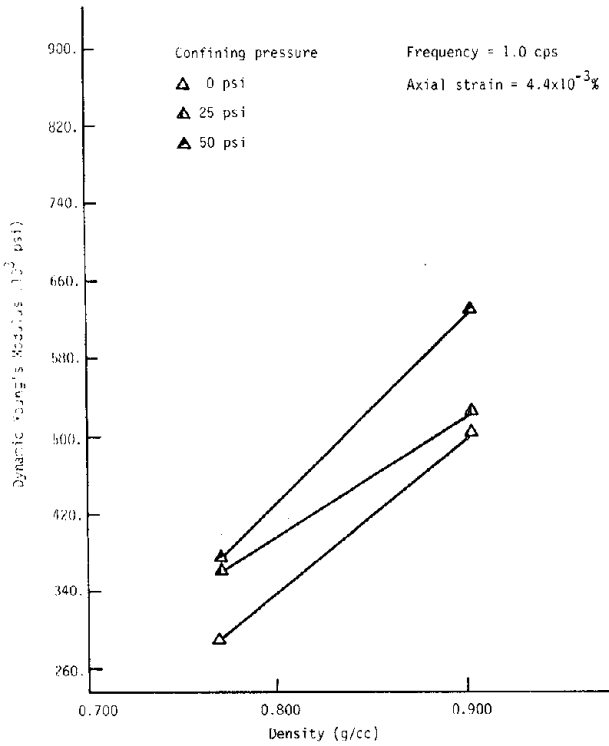


Figure 4.60 DYNAMIC YOUNG'S MODULUS VERSUS DENSITY OF ICE AT -1°C FOR THREE CONFINING PRESSURES

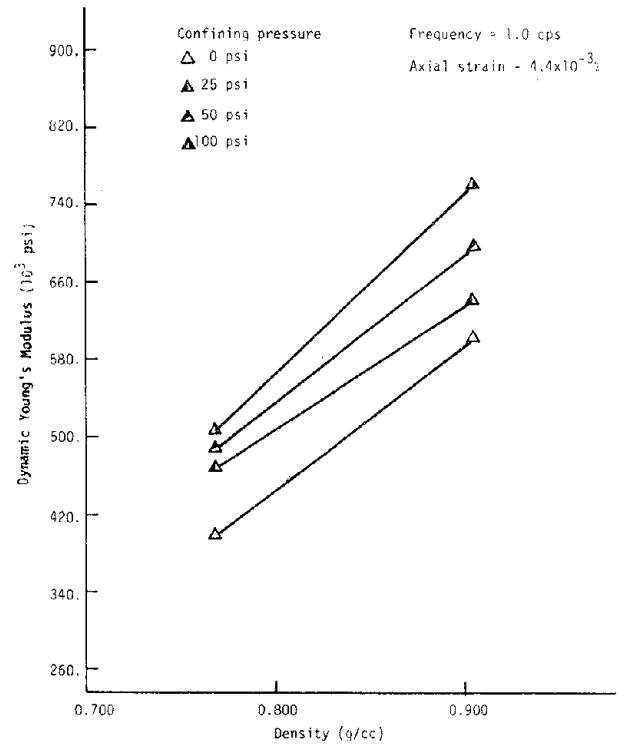


Figure 4.61 DYNAMIC YOUNG'S MODULUS VERSUS DENSITY OF ICE AT -4°C FOR FOUR CONFINING PRESSURES

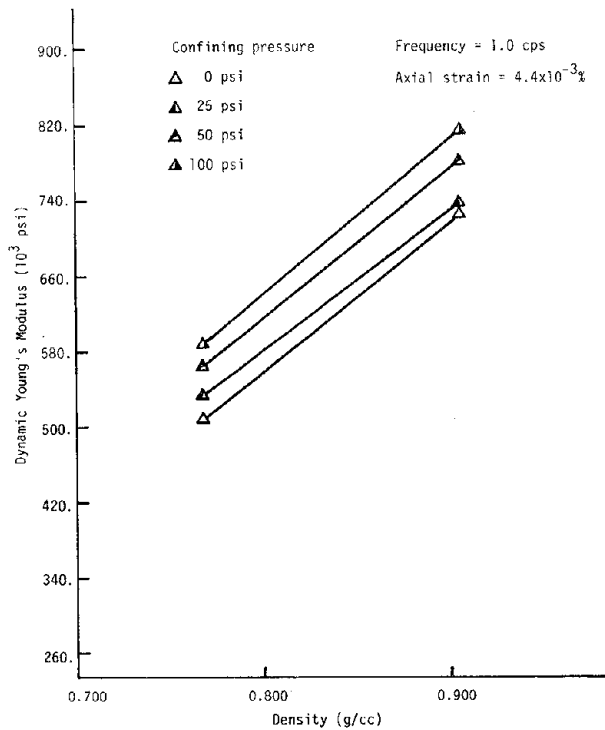


Figure 4.62 DYNAMIC YOUNG'S MODULUS VERSUS DENSITY OF ICE AT -10°C FOR FOUR CONFINING PRESSURES

for the majority of the samples. Therefore, the data presented reflect only the influence of two variables: frequency and temperature. At a given frequency and temperature the damping ratios for all confining pressures are presented on the same figure.

4.5.1 Effect of Strain Amplitude

Referring to Figures D.1 to D.28, it can be seen that there is no pronounced relationship between damping ratio and log percent axial strain. Consequently, it was assumed that the relationship between these quantities was linear. An assumption of a functional relationship is necessary to assess the influence of frequency and temperature on damping ratio. The slope of the "average" straight line of all the data points was established by obtaining the least squares best fit line through the data set associated with all test conditions. This is shown in Figure 4.63 for the high density ice samples and Figure 4.64 for the low density ice samples. The slope of the line is 0.1134 for the high density ice and 0.00 for the low density ice. The average slopes indicate that the damping ratio of high density ice is affected slightly by the strain amplitude whereas the damping ratio of low density ice is apparently not affected by the strain amplitude. The dashed lines in Figures D.1 to D.28 represent the least squares best fit line for the data set shown. The solid lines in the figures were drawn at the average slope through the center of the data set for a given test condition. The least squares best fit line through the center of the data sets for given test conditions are summarized in Figures 4.65 to 4.68 for the high density samples and Figures 4.69 to 4.71 for the low density samples. The relationships are plotted at four test temperatures for a given frequency. The variation of damping ratio ranges from 0.02 to 0.15 for high density ice and from 0.016 to 0.08 for low density ice.

4.5.2 Effect of Frequency

The relationship between frequency and damping ratio is shown in Figure 4.72 for high density ice and Figure 4.73 for low density ice at an axial strain amplitude of $6.35 \times 10^{-3}\%$ ($\log_{10} = -2.2$). The relationship is shown at five temperatures (-1, -2, -4, -6 and -10°C) for high density ice and three temperatures (-1, -4 and -10°C) for low density ice.

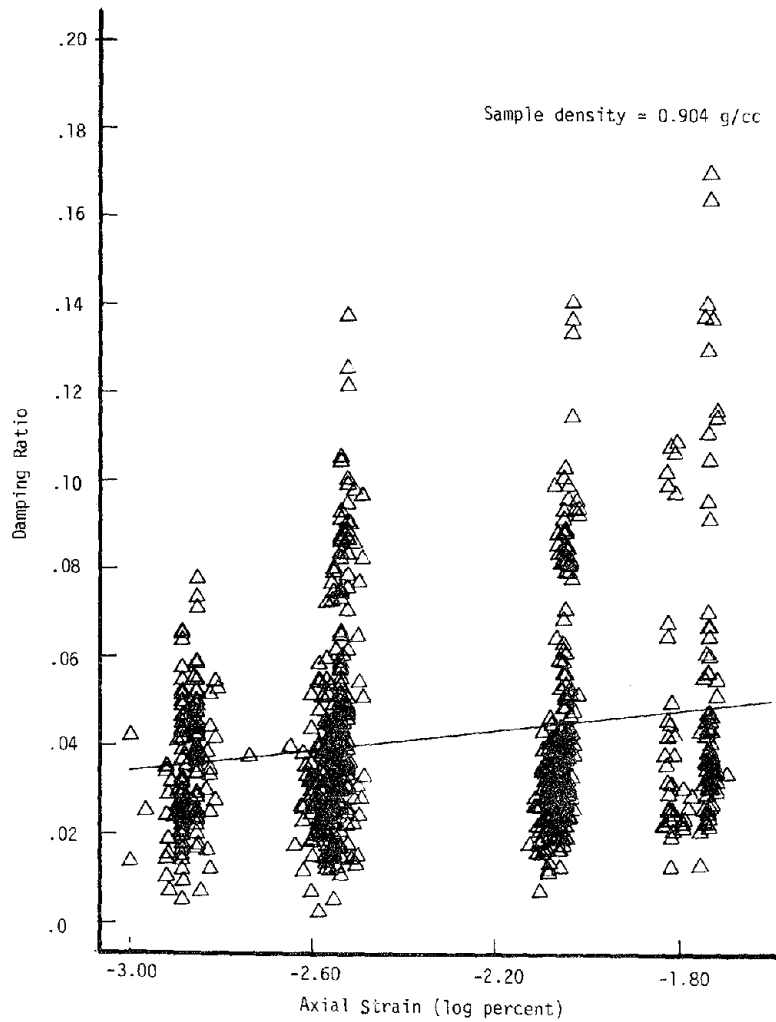


Figure 4.63 LEAST SQUARES BEST FIT LINE FOR DAMPING RATIO OF HIGH DENSITY ICE VERSUS AXIAL STRAIN

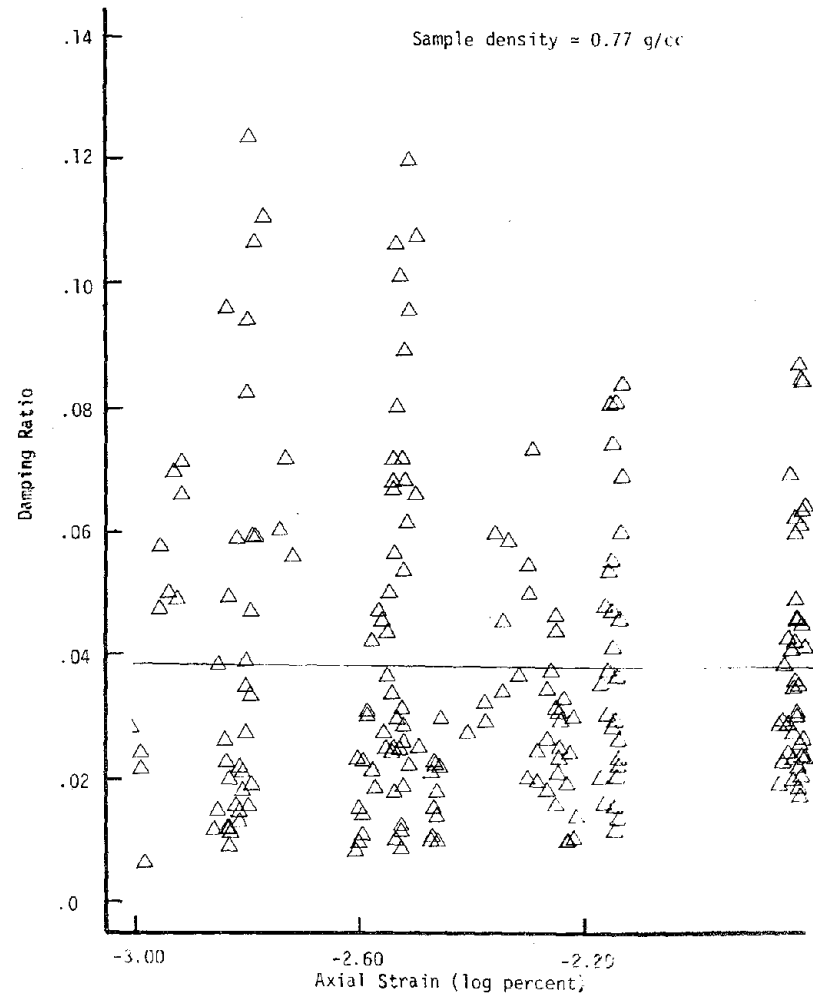


Figure 4.64 LEAST SQUARES BEST FIT LINE FOR DAMPING RATIO OF LOW DENSITY ICE VERSUS AXIAL STRAIN

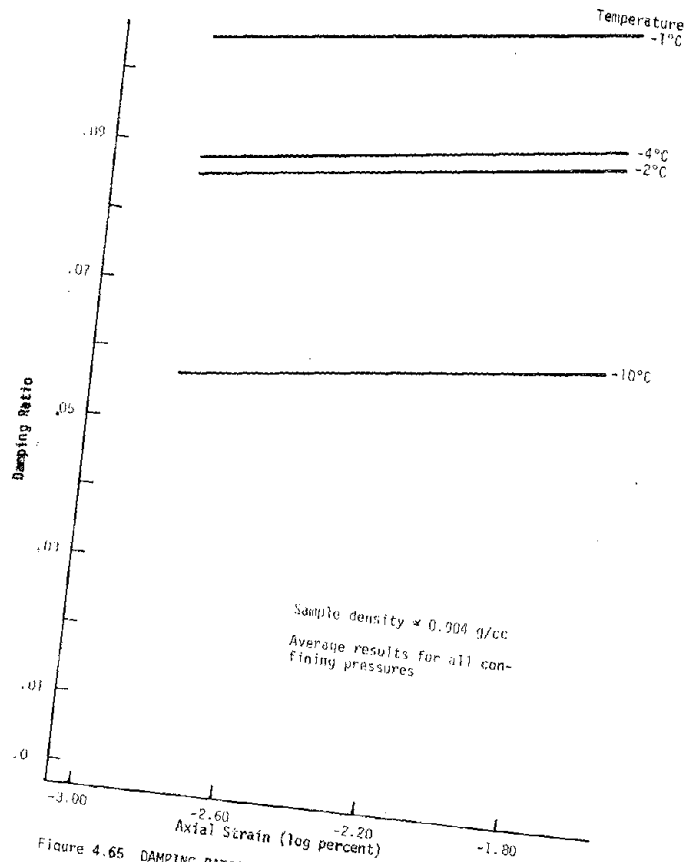


Figure 4.65 DAMPING RATIO VERSUS AXIAL STRAIN FOR HIGH DENSITY ICE AT 0.05 CPS

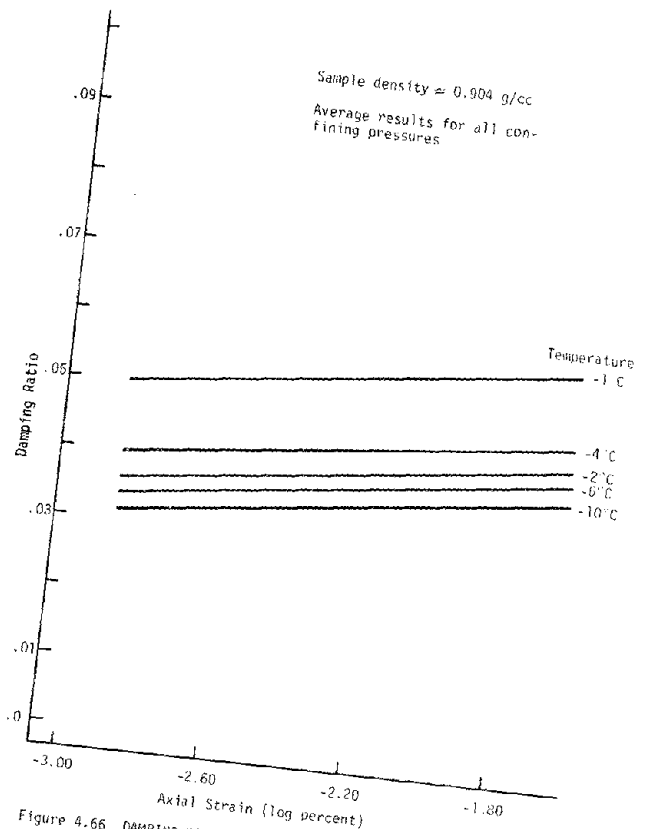


Figure 4.66 DAMPING RATIO VERSUS AXIAL STRAIN FOR HIGH DENSITY ICE AT 0.3 CPS

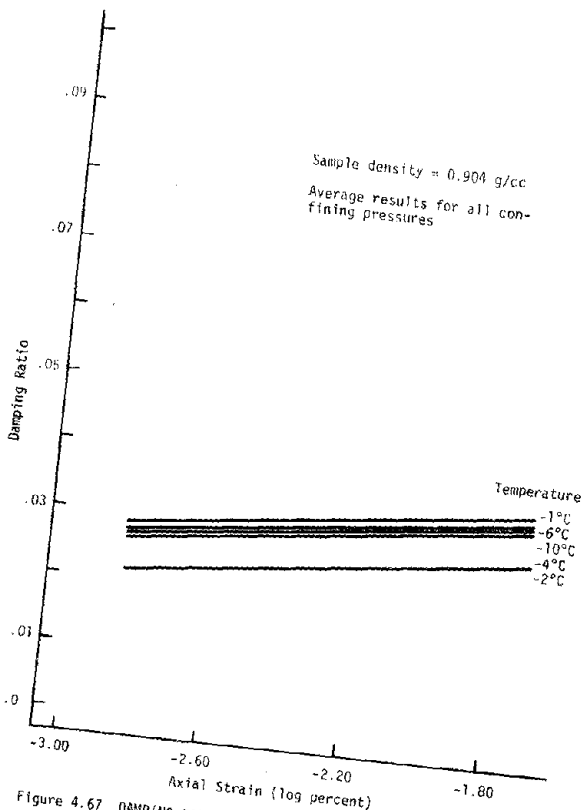


Figure 4.67 DAMPING RATIO VERSUS AXIAL STRAIN FOR HIGH DENSITY ICE AT 1.0 CPS

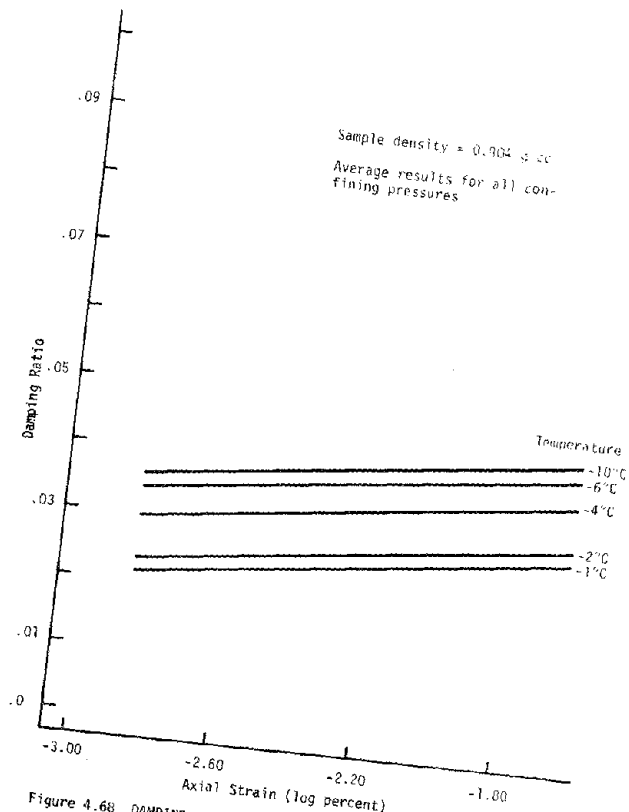


Figure 4.68 DAMPING RATIO VERSUS AXIAL STRAIN FOR HIGH DENSITY ICE AT 5.0 CPS

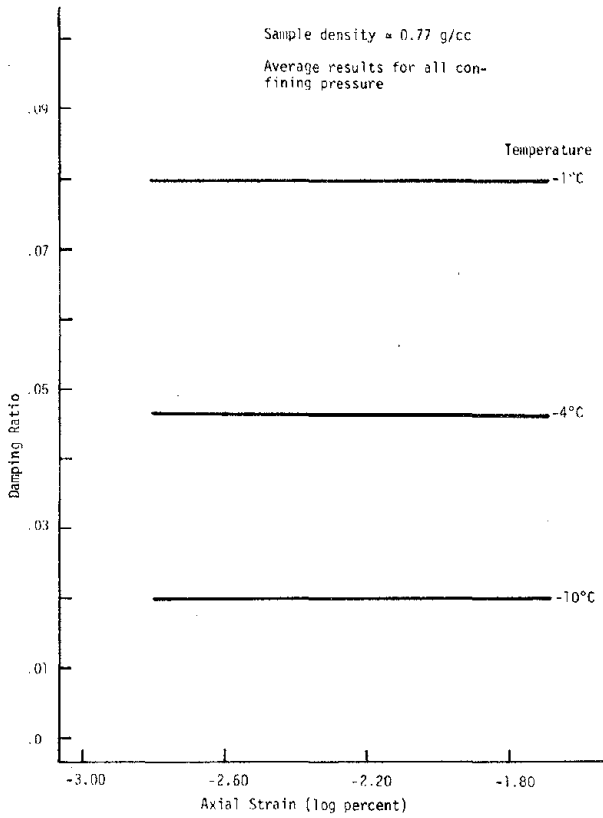


Figure 4.69 DAMPING RATIO VERSUS AXIAL STRAIN FOR LOW DENSITY ICE AT 0.3 CPS

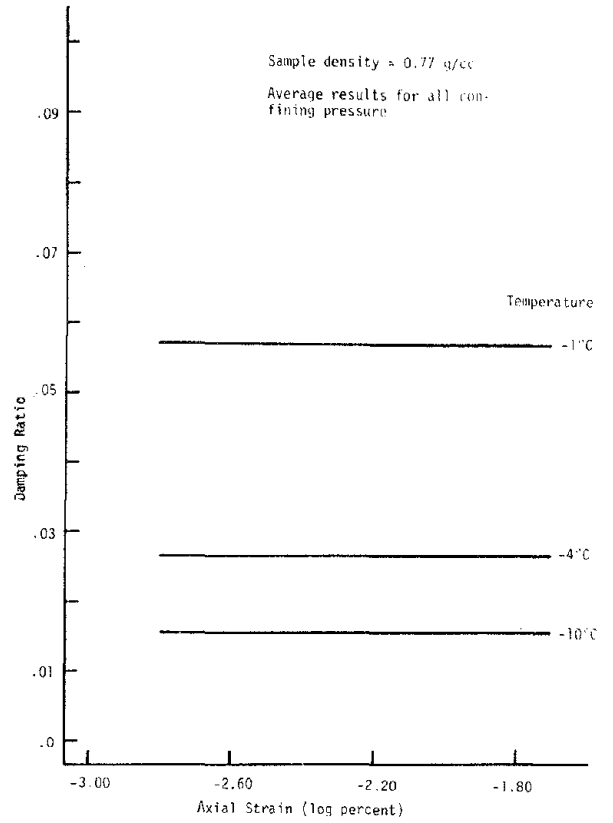


Figure 4.70 DAMPING RATIO VERSUS AXIAL STRAIN FOR LOW DENSITY ICE AT 1.0 CPS

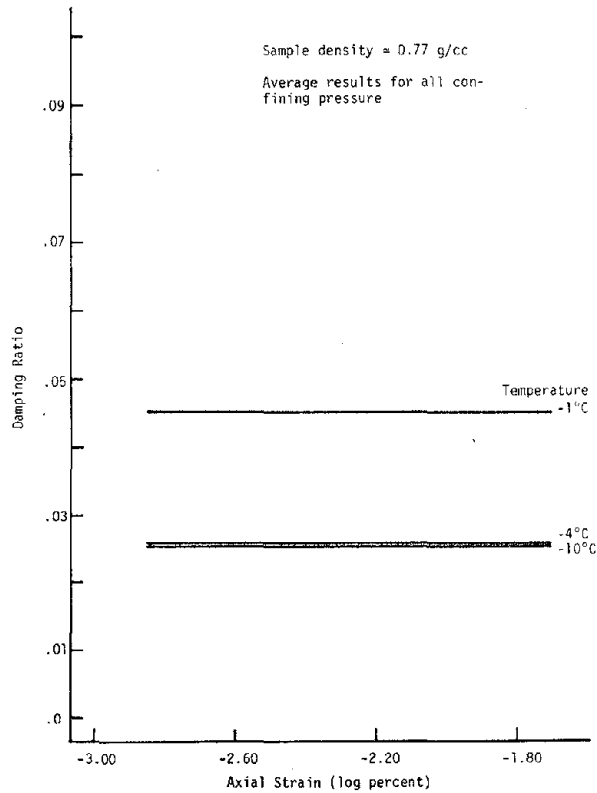


Figure 4.71 DAMPING RATIO VERSUS AXIAL STRAIN FOR LOW DENSITY ICE AT 5.0 CPS

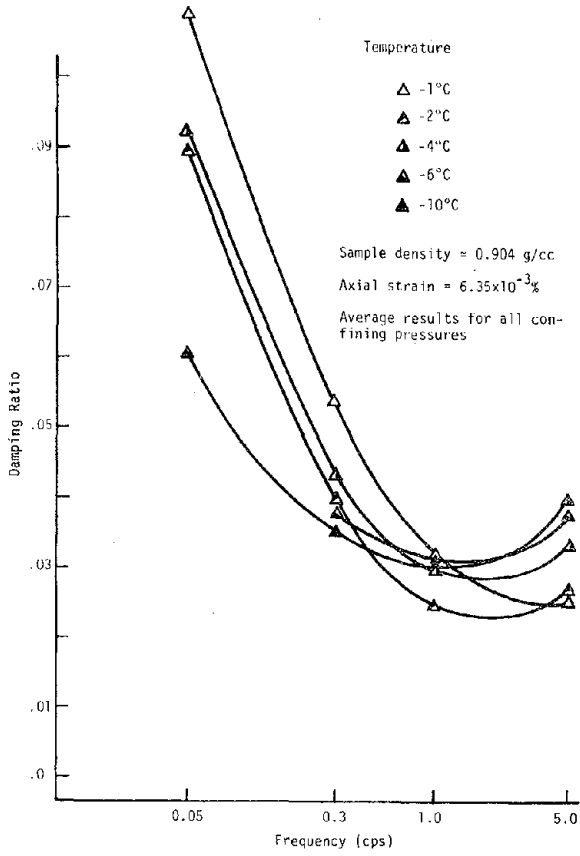


Figure 4.72 DAMPING RATIO VERSUS FREQUENCY FOR HIGH DENSITY ICE

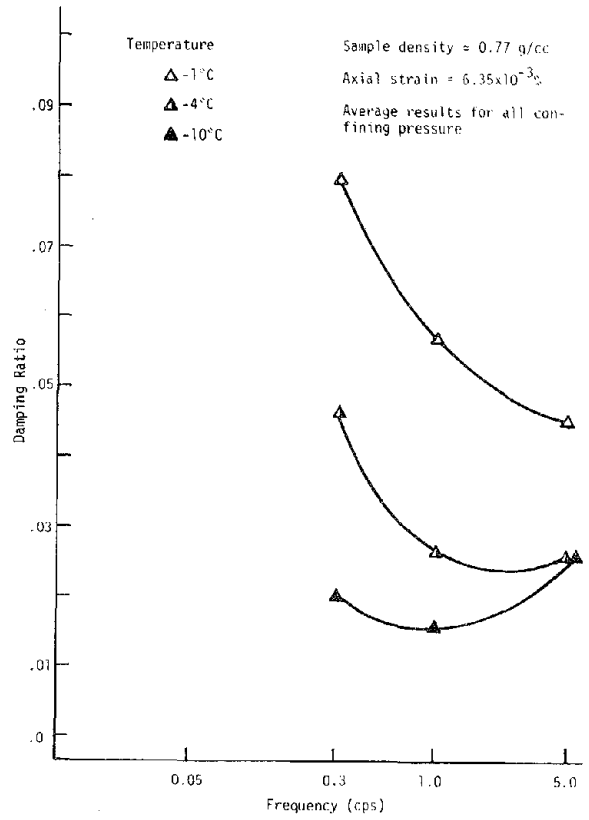


Figure 4.73 DAMPING RATIO VERSUS FREQUENCY FOR LOW DENSITY ICE

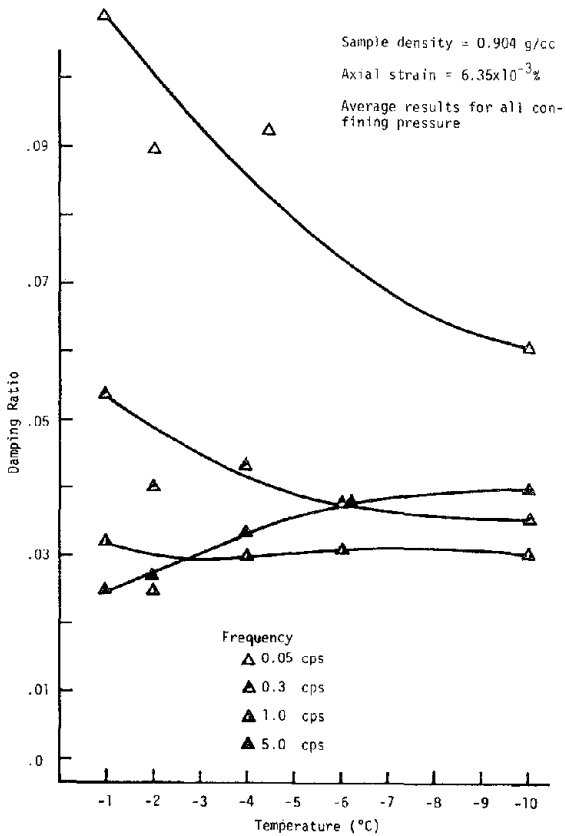


Figure 4.74 DAMPING RATIO VERSUS TEMPERATURE FOR HIGH DENSITY ICE

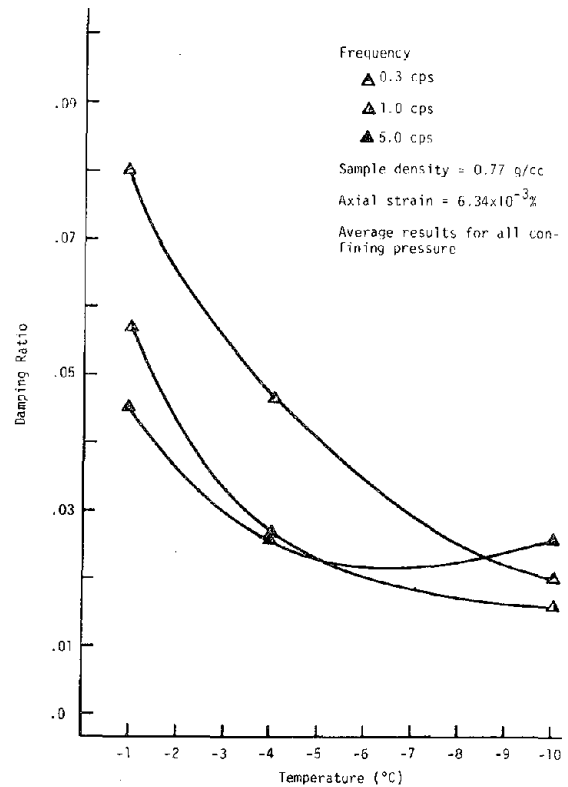


Figure 4.75 DAMPING RATIO VERSUS TEMPERATURE FOR LOW DENSITY ICE

In general, for the high density ice, damping ratio decreases as frequency increases from 0.05 to 1.0 cps and increases as frequency increases from 1.0 to 5.0 cps. The degree to which the damping ratio follows these trends, however, appears to be dependent on temperature. The greatest decrease in damping ratio in the frequency range 0.05 to 1.0 cps occurs at high test temperatures (-1, -2°C); the greatest increase in the frequency range 1.0 to 5.0 cps occurs at low test temperatures (-6, -10°C).

For the low density ice the damping ratio decreases as frequency increases from 0.3 to 5.0 cps at a test temperature of -1°C. Damping ratio decreases as frequency increases from 0.3 to 1.0 cps and increases as frequency increases from 1.0 to 5.0 cps for test temperatures of -4 and -10°C.

4.5.3 Effect of Temperature

The relationship between temperature and damping ratio is shown in Figure 4.74 for high density ice and Figure 4.75 for low density ice. The relationship is shown at four frequencies (0.05, 0.3, 1.0 and 5.0 cps) for high density ice and three frequencies (0.3, 1.0 and 5.0 cps) for low density ice.

The damping ratio of high density ice tends to decrease with decreasing temperature. At a frequency of 0.05 cps, the rate of increase is most pronounced; the damping ratio decreases from 0.11 to 0.06 as temperature decreases from -1 to -10°C. The influence of temperature is small for the frequency range 0.3 to 5.0 cps. The difference between damping ratios for temperatures in the range -1 to -4°C is greater than for temperatures in the range -4 to -10°C. At a frequency of 5.0 cps, the damping ratio appears to increase as the temperature decreases.

As shown in Figure 4.75, the influence of temperature on the damping ratio of low density ice is more pronounced than for the high density ice for the frequency range 0.3 to 5.0 cps. For a frequency of 1.0 cps, the damping ratio decreases from 0.058 to 0.018 as temperature decreases from -1 to -10°C. The effect of temperature tends to decrease with increasing frequency. The influence of temperature is most significant in the range -1 to -5°C. At a frequency of 5.0 cps and temperature in the range of -5 to -10°C, the damping ratio appears to increase as temperature decreases.

4.5.4 Effect of Density

A comparison of the damping ratio for the high density ice samples and the low density ice samples is shown in Figures 4.76 and 4.77. The damping ratio of the high and low density samples is presented as a function of frequency in Figure 4.76 and as a function of temperature in Figure 4.77. There appears to be no well-defined relationship between density and damping ratio. The damping ratio of low density ice at -1°C is greater than that of high density ice, but at -4 and -10°C , the damping ratio of high density ice is, in general, greater than low density ice. At higher temperatures (-1 to -3°C), the damping ratio of low density ice is greater than high density ice whereas for lower temperatures (-7 to -10°C) it is less than high density ice.

4.5.5 Effect of Confining Pressure

For the majority of the samples tested, there was not a well-defined relationship between confining pressure and damping ratio. However, the test results for a few samples were exceptions to this statement. Figure 4.78 shows the relationship between confining pressure and damping ratio for sample I-46 at a strain amplitude of $9.0 \times 10^{-3}\%$. There appears to be a decrease in damping ratio of approximately 25% for an increase in confining pressure from 25 to 200 psi. This relationship does not appear to be influenced by frequency over the range 0.05 to 5.0 cps.

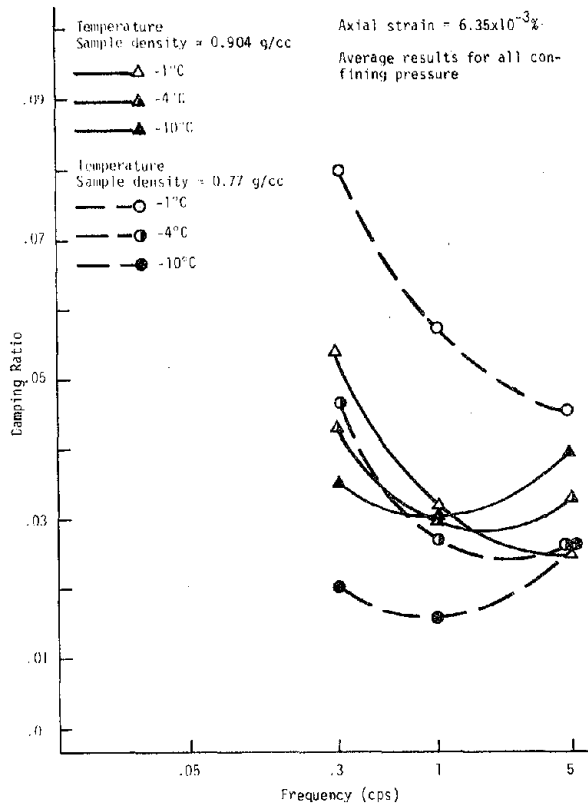


Figure 4.76 DAMPING RATIO VERSUS FREQUENCY FOR ICE AT TWO DENSITIES

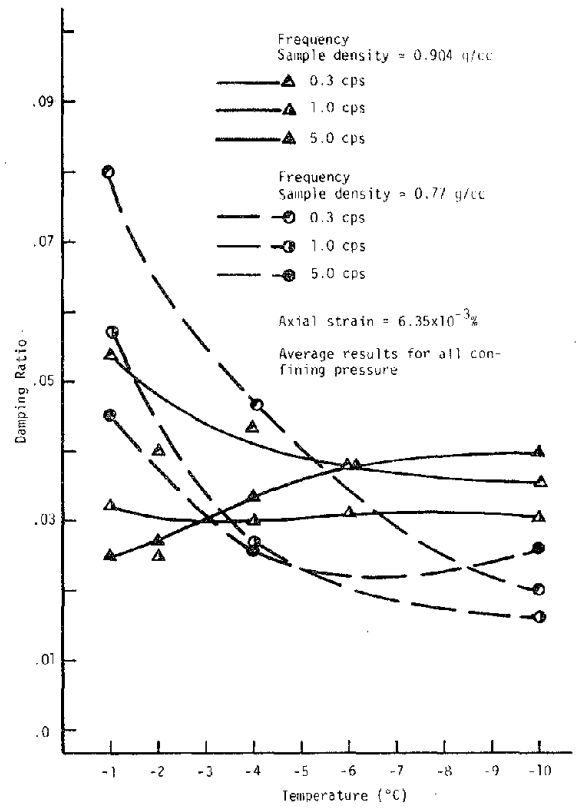


Figure 4.77 DAMPING RATIO VERSUS TEMPERATURE FOR ICE AT TWO DENSITIES

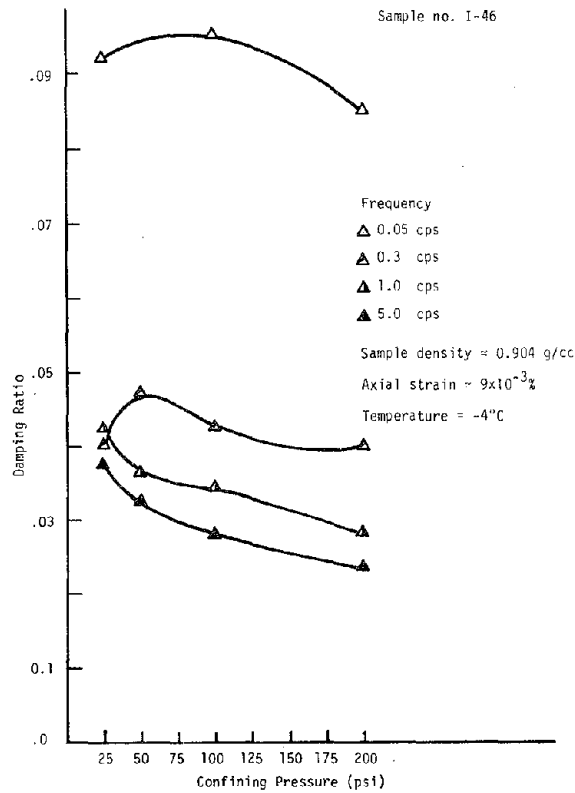


Figure 4.78 TYPICAL VARIATION OF DAMPING RATIO WITH CONFINING PRESSURE

CHAPTER 5

DYNAMIC PROPERTIES OF FROZEN CLAY UNDER CYCLIC TRIAXIAL LOADING CONDITIONS

5.1 General

Cyclic triaxial tests were performed on laboratory prepared samples of frozen Ontonagon clay (O-clay) and a mixture of Ontonagon and sodium montmorillonite clay (M + O-clay), 50 percent each by weight. (Details of the preparation technique are given in Section 3.3.) The influence of water (ice) content on dynamic properties was investigated using the frozen Ontonagon clay. Comparing the dynamic properties of the Ontonagon clay to the mixture of Ontonagon and sodium montmorillonite clay allowed an evaluation of the influence of specific surface area (unfrozen water content) to be made. In addition to these parameters, the effects on dynamic properties caused by variations in temperature, confining pressure, strain amplitude, frequency, and number of cycles of loading were considered.

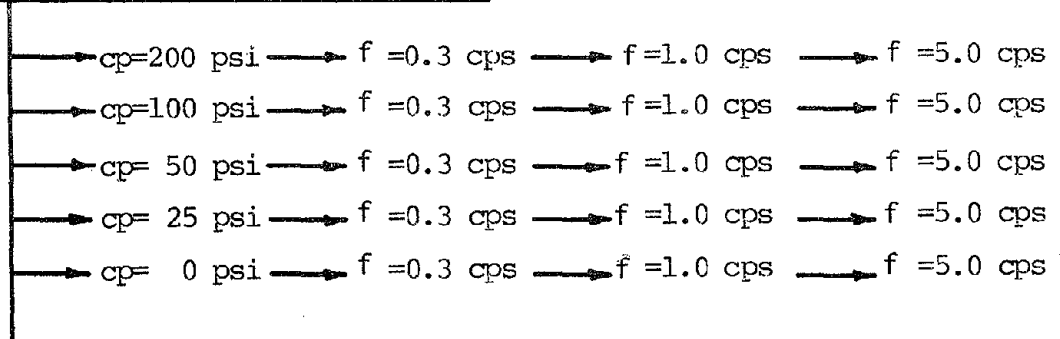
5.2 Test History

The test history used in the research program to evaluate the dynamic properties of clay is shown in Figure 5.1. This test history is, for all practical purposes, equivalent to that for ice. Tests to evaluate various test history effects on the dynamic properties of clay were not performed. The ranges of the various test parameters are as follows:

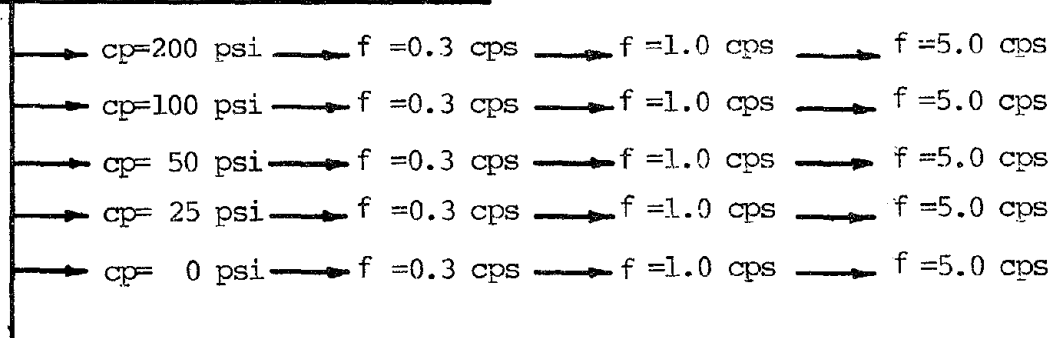
- (1) Temperature - the samples were tested at three temperatures (-1, -4 and -10°C). The majority of the samples were tested at one temperature only. Seven samples, however, were tested at all three temperatures.
- (2) Strain amplitude - the range of strain amplitude was approximately 3.2×10^{-3} to $1 \times 10^{-1}\%$ axial strain. The higher strain amplitudes were dependent on the confining pressure. The maximum strain amplitudes of testing were limited to $1 \times 10^{-2}\%$ for $c_p = 0$ psi and 25 psi, $5.6 \times 10^{-2}\%$ for $c_p = 50$ psi, and $1 \times 10^{-1}\%$ for $c_p = 100$ psi and 200 psi. The maximum strain amplitudes are associated (approximately) with a tensile failure of the sample or significant sample disturbance.
- (3) Confining pressure - the samples were tested at five confining

Constant temperature

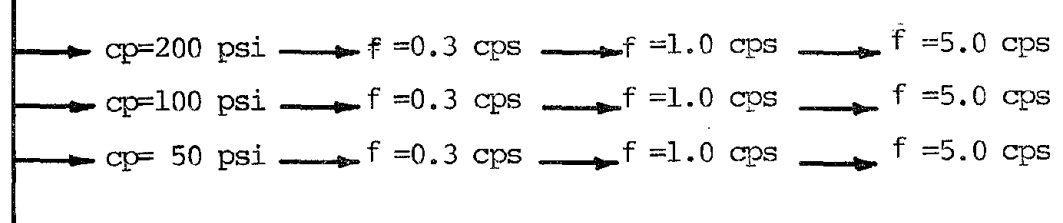
Approximate axial strain $3.2 \times 10^{-3}\%$



Approximate axial strain $1.0 \times 10^{-2}\%$



Approximate axial strain $5.6 \times 10^{-2}\%$



Approximate axial strain $1.0 \times 10^{-1}\%$

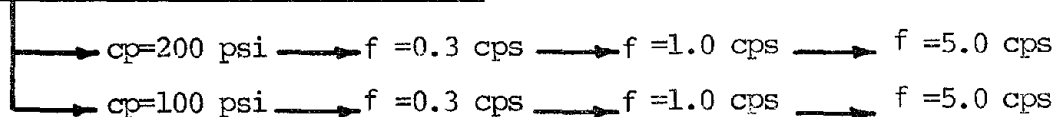


Figure 5.1 DIAGRAM OF ACCEPTABLE TEST HISTORY FOR FROZEN CLAY

pressures (0, 25, 50, 100 and 200 psi).

- (4) Frequency - in general, only three frequencies of loading were used in the test program (0.3, 1.0 and 5.0 cps). The O-clay samples at a water content of 36 percent were tested at a very low frequency, 0.05 cps. To investigate the effect of frequencies greater than 5 cps, an O-clay sample at a water content of 29.2%, temperature of -4°C , confining pressures of 25, 50 and 100 psi, and strain amplitude of $1 \times 10^{-2}\%$ was tested at 0.3, 1.0, 5.0, 10.0, 20.0 and 50.0 cps.
- (5) Number of cycles - for each test condition a sample was subjected to 20 cycles of loading.
- (6) Water content - O-clay samples were prepared at four water contents (29.2, 36.0, 46.3 and 55.1%). The M + O-clay was prepared at one water content (57.2%).

5.3 Influence of Number of Cycles on Evaluation of Dynamic Properties

To assess the influence of the choice of the cycle number used to evaluate dynamic properties, the variation of the ratio (E at Nth cycle/ E at 10th cycle) and (λ at Nth cycle/ λ at 10th cycle) with number of cycles at different frequencies, confining pressures, strain amplitudes, and temperatures was determined for the O-clay samples. These ratios are shown at 1, 5, 10 and 20 cycles in Tables 5.1 and 5.2. There appears to be no significant variation in the dynamic Young's modulus with number of cycles for different frequencies, confining pressures, strain amplitudes and temperature. At the greatest, the dynamic Young's modulus at the Nth cycle is approximately 3.0% different from the modulus at the 10th cycle. Further, the damping ratio does not appear to vary with the number of cycles for different frequencies, confining pressures, strain amplitudes, and temperatures. The damping ratio at the Nth cycle is at most 12% different from the damping ratio at the 10th cycle.

The dynamic Young's modulus was evaluated from the load and displacement channels of the strip-chart recorder at the 10th cycle by measuring the peak-to-peak amplitude of the recorded waveform. A typical record for frozen clay is shown in Figure 5.2. Hysteresis loops obtained from the x-y recorder at the 10th cycle of loading were used to evaluate the damping ratio. Typical hysteresis loops are shown in Figure 5.3.

Table 5.1 VARIATION OF DYNAMIC YOUNG'S MODULUS OF FROZEN CLAY WITH NUMBER OF CYCLES

Temperature (°C)	Axial strain amplitude (%)	Confining pressure (psi)	Frequency (cps)	$\frac{E \text{ at Nth cycle}}{E \text{ at 10th cycle}}$			
				1	5	10	20
-4	0.01	50	0.05	0.987	1.0	1.0	0.996
-4	0.01	50	0.3	1.004	1.019	1.0	0.989
-4	0.01	50	1.0	1.009	1.005	1.0	1.019
-4	0.01	50	5.0	0.987	0.996	1.0	1.0
-4	0.01	0	0.3	1.009	1.005	1.0	1.001
-4	0.01	25	0.3	1.004	0.995	1.0	0.995
-4	0.01	50	0.3	1.004	1.019	1.0	0.989
-4	0.01	100	0.3	1.019	0.995	1.0	0.987
-4	0.01	200	0.3	1.012	1.0	1.0	1.0
-4	0.00316	50	0.3	0.993	0.993	1.0	0.980
-4	0.01	50	0.3	1.004	1.019	1.0	0.989
-4	0.056	50	0.3	1.025	1.0	1.0	0.994
-1	0.01	50	0.3	1.018	1.009	1.0	0.999
-4	0.01	50	0.3	1.004	1.019	1.0	0.989
-10	0.01	50	0.3	1.010	1.012	1.0	0.995

Table 5.2 VARIATION OF DAMPING RATIO OF FROZEN CLAY WITH NUMBER OF CYCLES

Temperature (°C)	Axial strain amplitude (%)	Confining pressure (psi)	Frequency (cps)	$\frac{\lambda \text{ at Nth cycle}}{\lambda \text{ at 10th cycle}}$			
				1	5	10	20
-4	0.01	50	0.05	1.075	0.987	1.0	0.965
-4	0.01	50	0.3	0.953	0.985	1.0	1.031
-4	0.01	25	0.3	0.992	0.969	1.0	1.016
-4	0.01	50	0.3	0.953	0.985	1.0	1.031
-4	0.01	100	0.3	1.022	1.0	1.0	1.029
-4	0.01	200	0.3	1.028	0.986	1.0	0.979
-4	0.00316	100	0.3	1.022	1.022	1.0	1.055
-4	0.01	100	0.3	1.022	1.0	1.0	1.029
-4	0.056	100	0.3	1.0	1.0	1.0	1.0
-4	0.10	100	0.3	1.122	1.0	1.0	0.977
-1	0.01	50	0.3	0.957	1.0	1.0	1.0
-4	0.01	50	0.3	0.953	0.985	1.0	1.031
-10	0.01	50	0.3	1.114	1.0	1.0	1.029

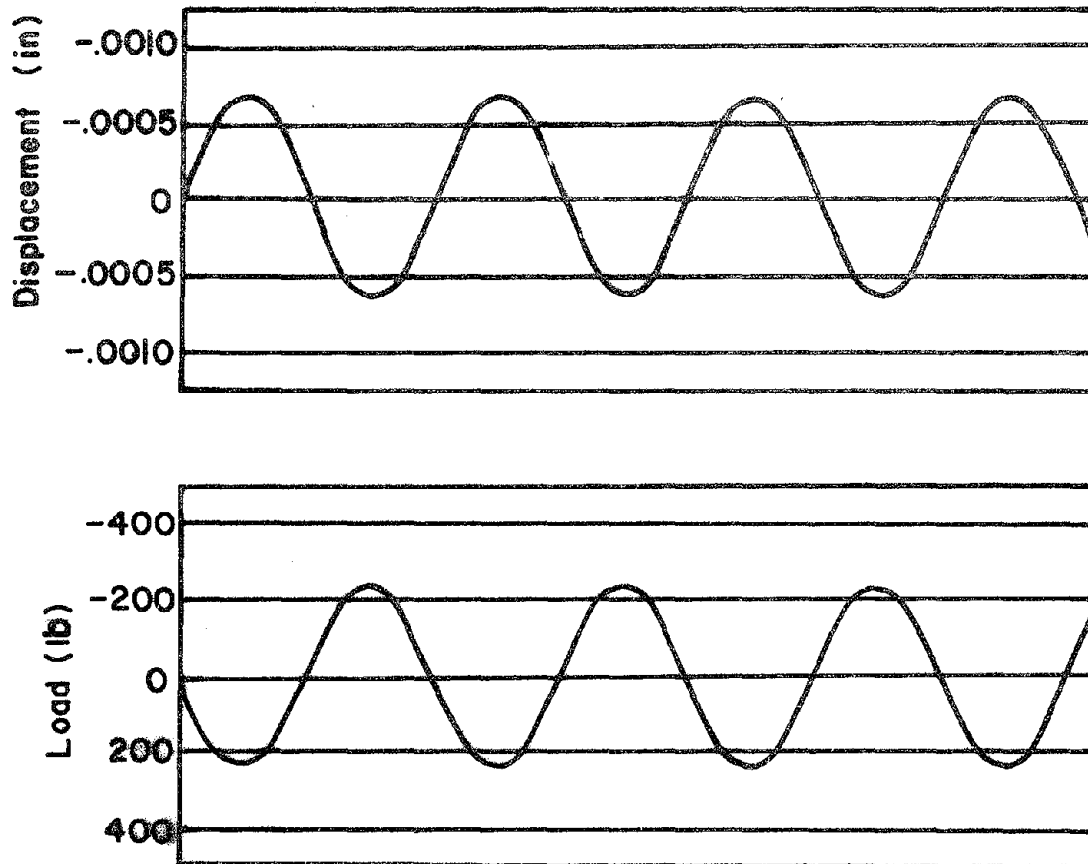


Figure 5.2 TYPICAL RECORD OF LOAD AND DISPLACEMENT OBTAINED DURING CYCLIC TRIAXIAL TESTING OF FROZEN CLAY

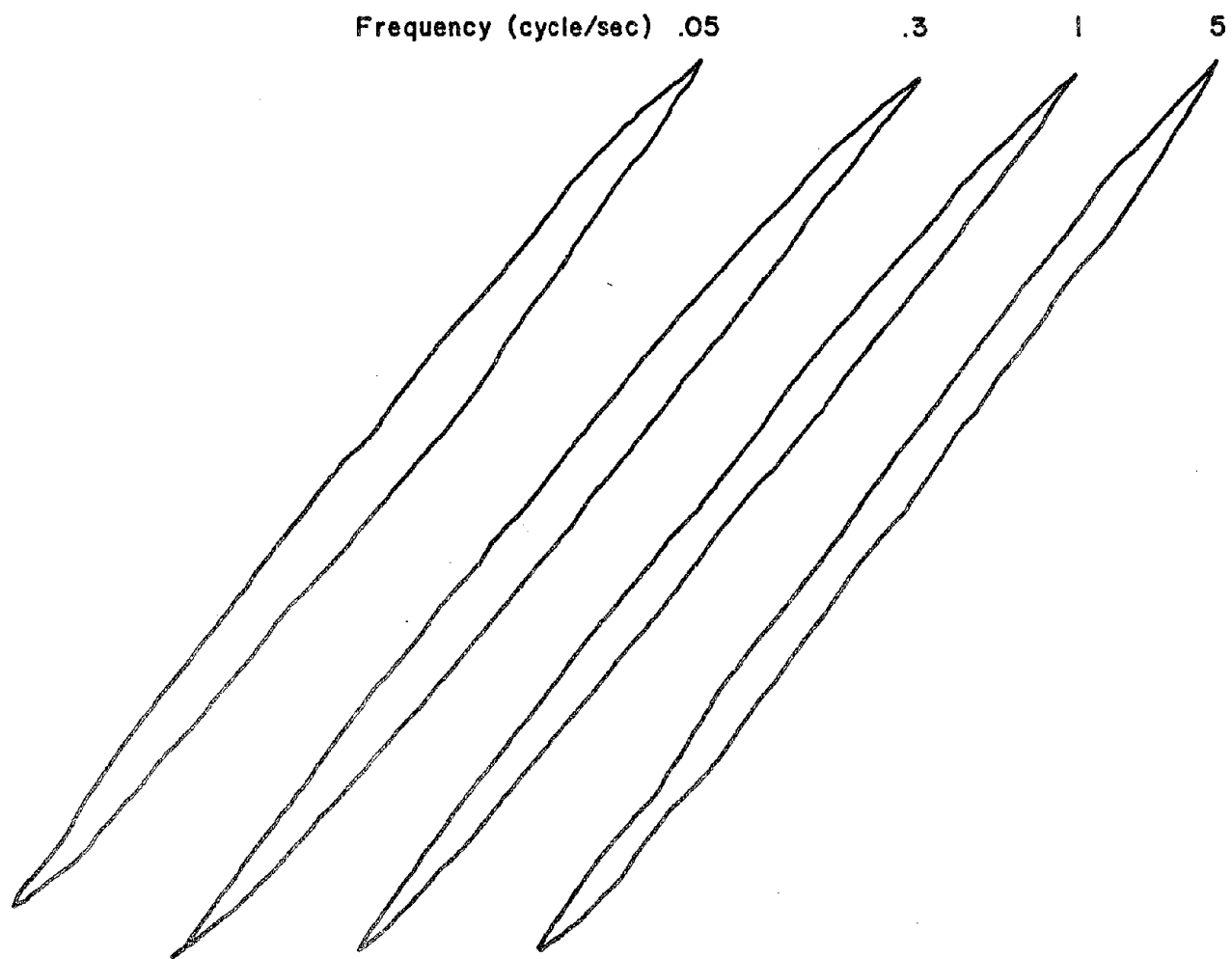


Figure 5.3 TYPICAL HYSTERESIS LOOPS (non-dimensional) OBTAINED DURING CYCLIC TRIAXIAL TESTING OF FROZEN CLAY

5.4 Dynamic Young's Modulus of Frozen Clay

The dynamic Young's modulus of frozen clay was plotted against the log of axial strain amplitude expressed as a percent. The plots are shown in Appendix E. Upon close examination of the test data it was determined that there is no pronounced relationship between Young's modulus and confining pressure. A typical test result which exemplifies this is shown in Figure 5.4. The dynamic Young's modulus of an O-clay sample at a water content of 36.0% was plotted against confining pressure at frequencies of 0.05, 0.3, 1.0 and 5.0 cps, and at a temperature of -4°C . It can be seen in the figure that the influence of confining pressure is almost negligible. Therefore, the data presented in Appendix E represent test results at all confining pressures for a specific frequency and temperature. In general, the data from two or more samples are available for each test condition.

For any given test condition, the data appears to be very consistent. The data is felt to be very reliable and provides a good basis for the interpretation of material properties.

5.4.1 Effect of Strain Amplitude

To assess the effect of strain amplitude, frequency, temperature, and water (ice) content on dynamic Young's modulus, an average "best fit" line was drawn through the data set for a given test condition. These lines are shown in Figures E.1 to E.48. Obviously, personal judgment was involved in this construction. The average "best fit" lines for given test conditions are summarized in Figures 5.5 to 5.20. The relationships between dynamic Young's modulus and log percent axial strain are shown at a given frequency (0.05, 0.3, 1.0 or 5.0 cps) and sample water content (29.2, 36.0, 46.3, 55.1 or 57.2%) at three temperatures (-1 , -4 and -10°C). The dynamic Young's modulus varies from 9×10^3 to 880×10^3 psi.

Dynamic Young's modulus decreases with increasing strain amplitude. The influence of strain amplitude at the lowest temperature (-10°C) is greater than at the highest temperature (-1°C). At the lowest temperature (-10°C) the modulus decreases sharply (approximately 55%) for an increase in strain amplitude from 2×10^{-2} to $6 \times 10^{-2}\%$. For strain amplitudes in the range of 3.16×10^{-3} to $2 \times 10^{-2}\%$ and 6×10^{-2} to $1.0 \times 10^{-1}\%$ the rate of decrease is, in general, small. For higher tem-

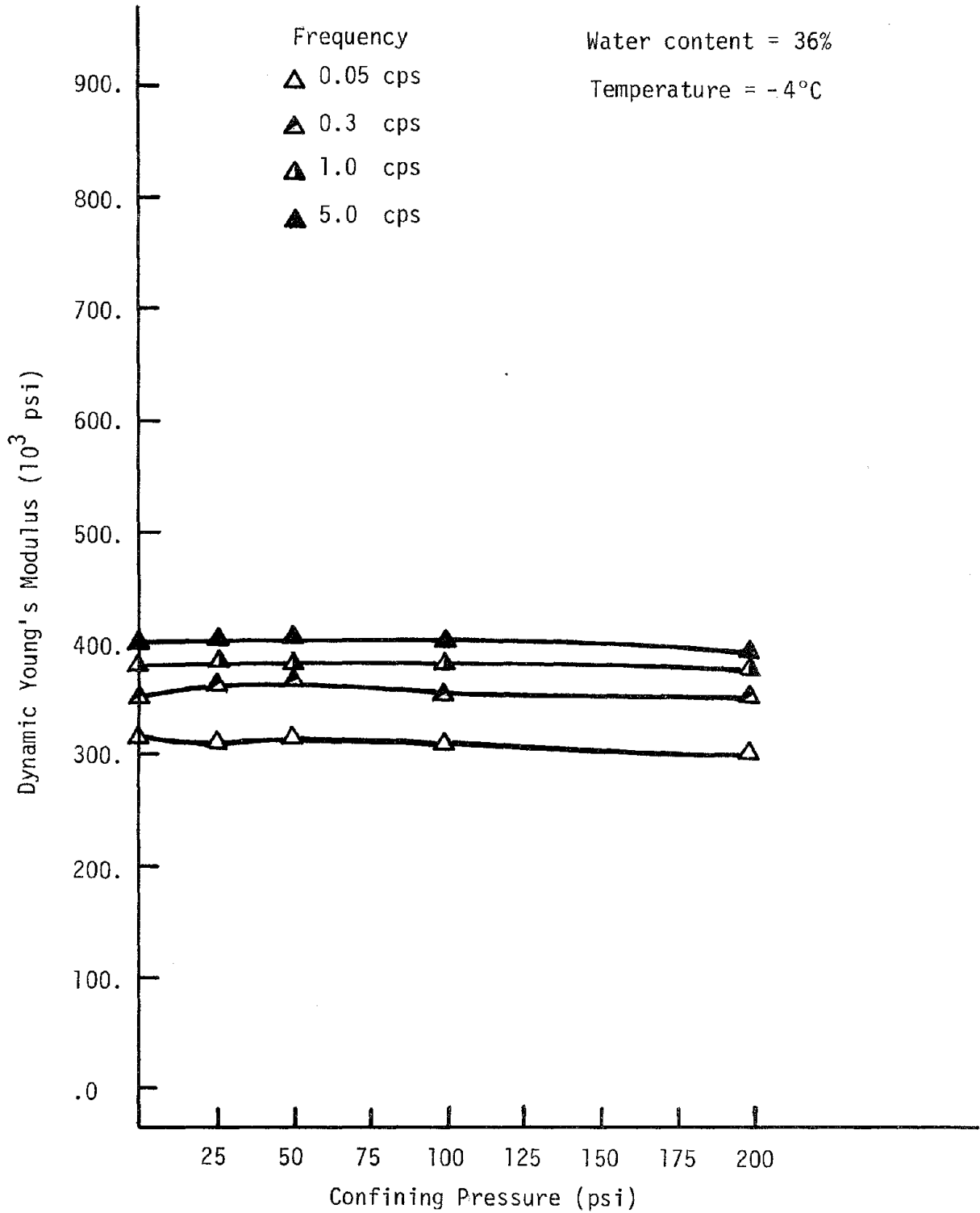


Figure 5.4 DYNAMIC YOUNG'S MODULUS VERSUS CONFINING PRESSURE FOR O-CLAY AT AN AXIAL STRAIN OF $1.1 \times 10^{-2}\%$

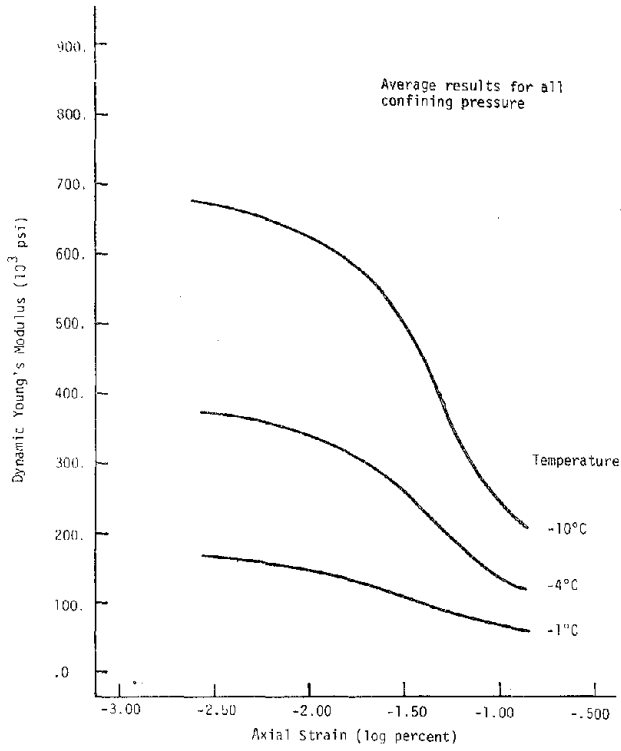


Figure 5.5 DYNAMIC YOUNG'S MODULUS VERSUS AXIAL STRAIN FOR O-CLAY AT 0.3 CPS AND 29.2% WATER CONTENT

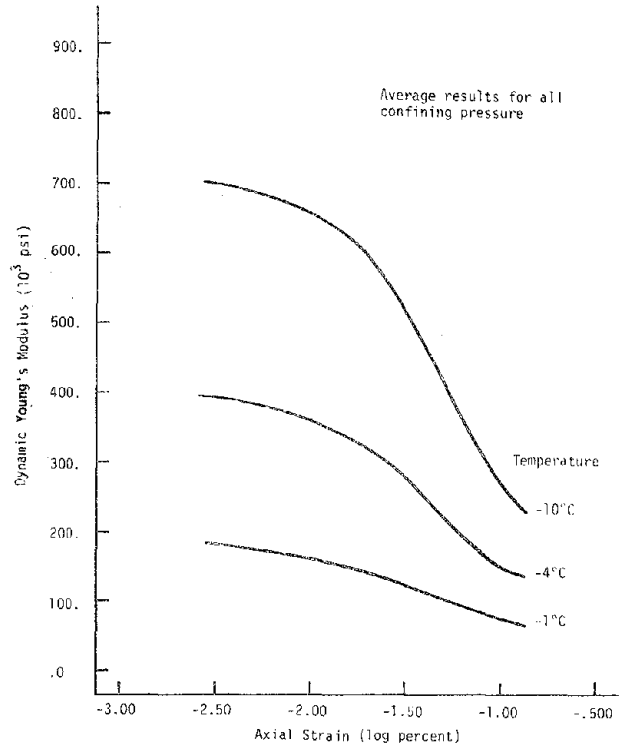


Figure 5.6 DYNAMIC YOUNG'S MODULUS VERSUS AXIAL STRAIN FOR O-CLAY AT 1.0 CPS AND 29.2% WATER CONTENT

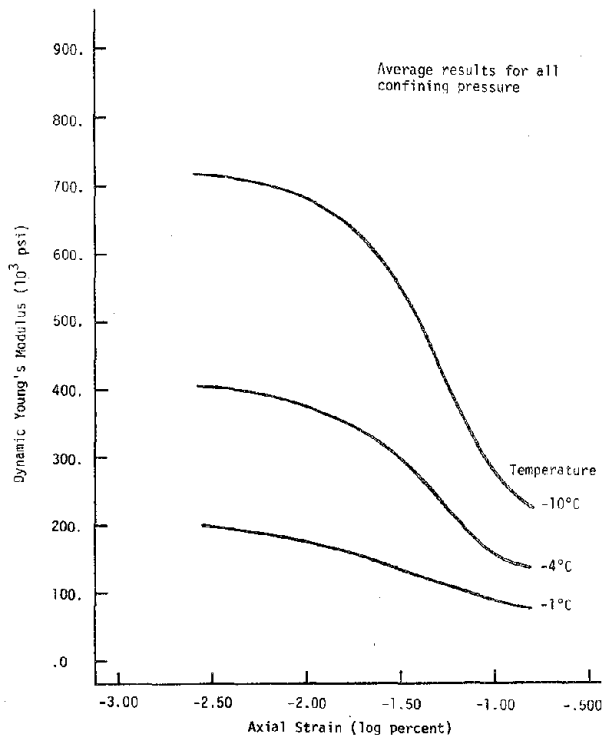


Figure 5.7 DYNAMIC YOUNG'S MODULUS VERSUS AXIAL STRAIN FOR O-CLAY AT 5.0 CPS AND 29.2% WATER CONTENT

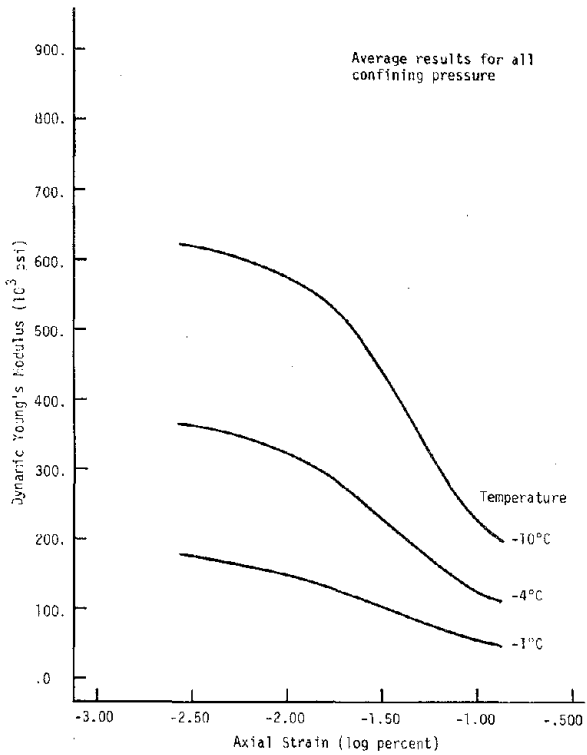


Figure 5.8 DYNAMIC YOUNG'S MODULUS VERSUS AXIAL STRAIN FOR 0-CLAY AT 0.05 CPS AND 36.0% WATER CONTENT

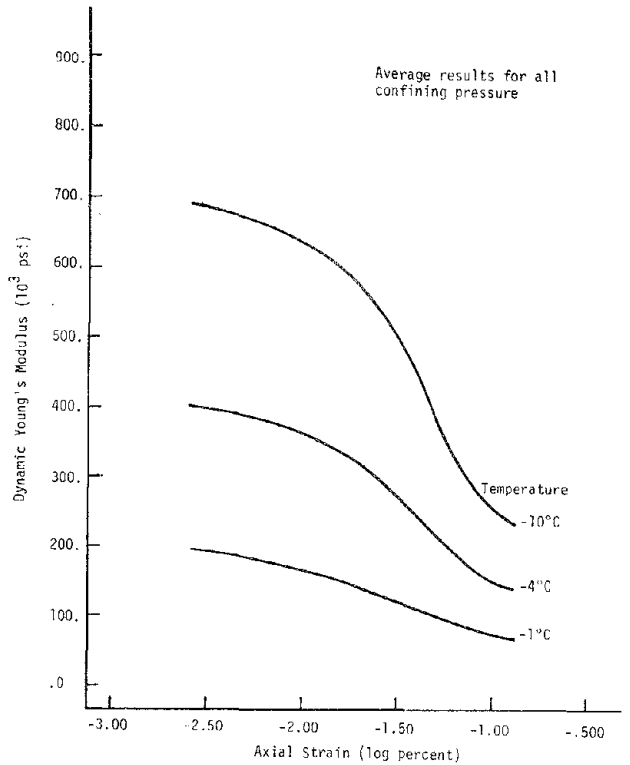


Figure 5.9 DYNAMIC YOUNG'S MODULUS VERSUS AXIAL STRAIN FOR 0-CLAY AT 0.3 CPS AND 36.0% WATER CONTENT

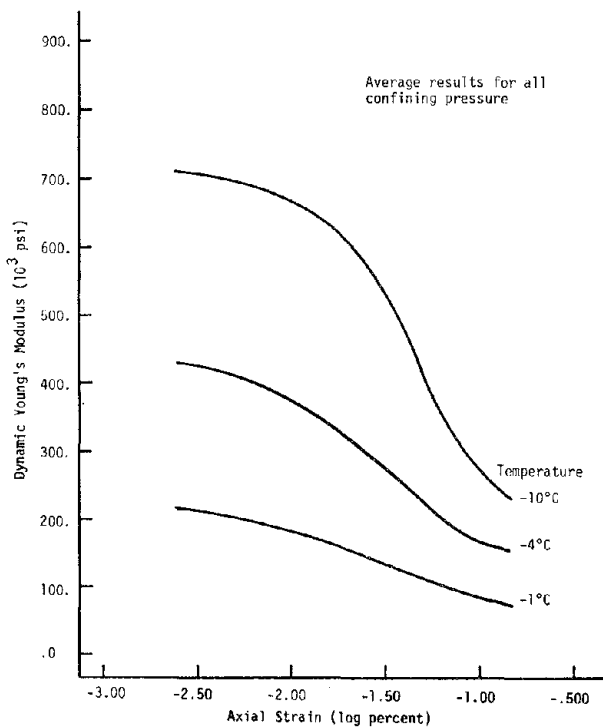


Figure 5.10 DYNAMIC YOUNG'S MODULUS VERSUS AXIAL STRAIN FOR 0-CLAY AT 1.0 CPS AND 36.0% WATER CONTENT

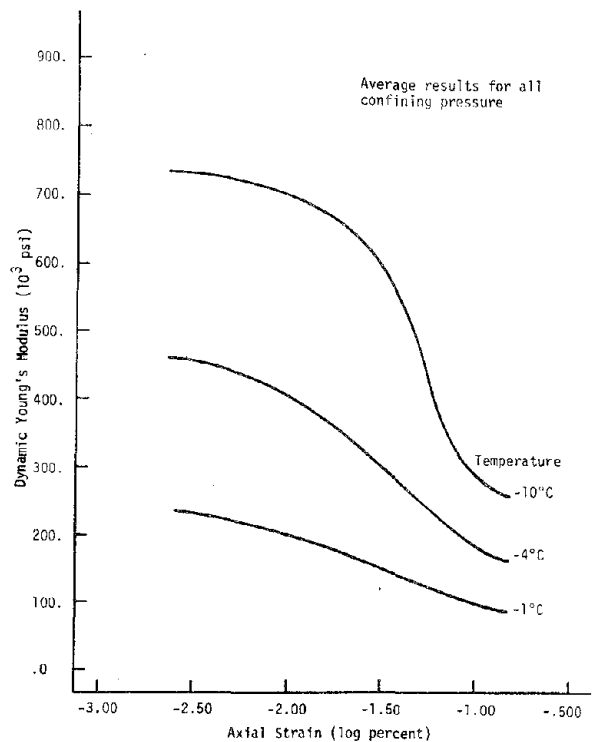


Figure 5.11 DYNAMIC YOUNG'S MODULUS VERSUS AXIAL STRAIN FOR 0-CLAY AT 5.0 CPS AND 36.0% WATER CONTENT

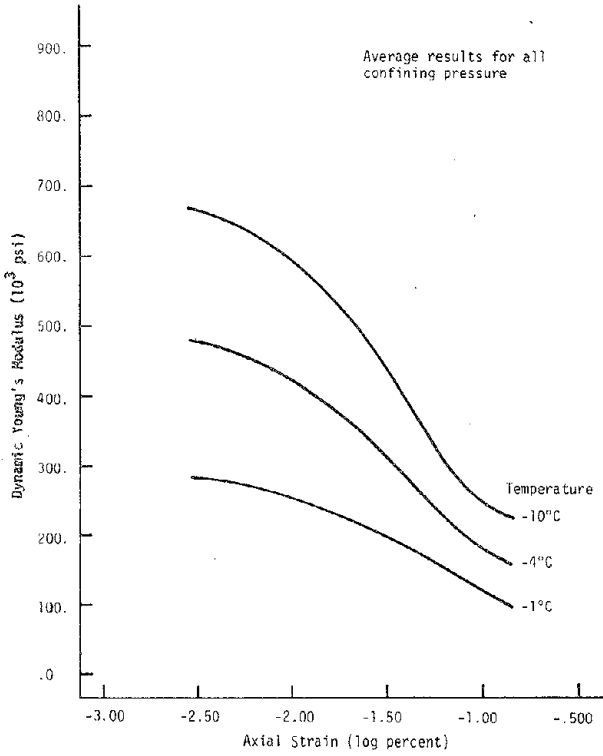


Figure 5.12 DYNAMIC YOUNG'S MODULUS VERSUS AXIAL STRAIN FOR O-CLAY AT 0.3 CPS AND 46.3% WATER CONTENT

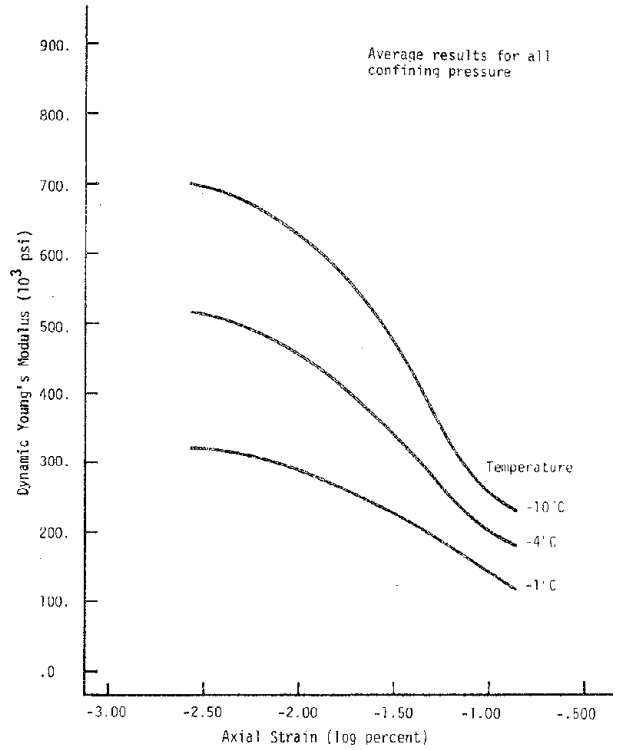


Figure 5.13 DYNAMIC YOUNG'S MODULUS VERSUS AXIAL STRAIN FOR O-CLAY AT 1.0 CPS AND 46.3% WATER CONTENT

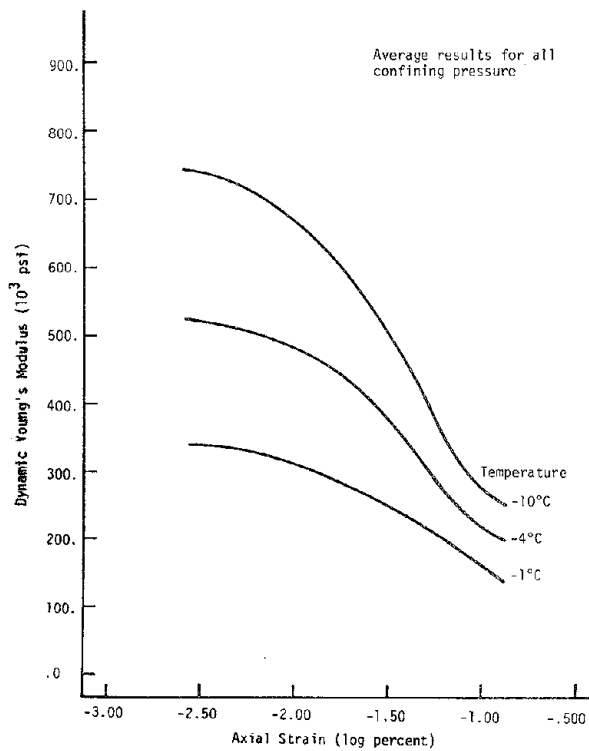


Figure 5.14 DYNAMIC YOUNG'S MODULUS VERSUS AXIAL STRAIN FOR O-CLAY AT 5.0 CPS AND 46.3% WATER CONTENT

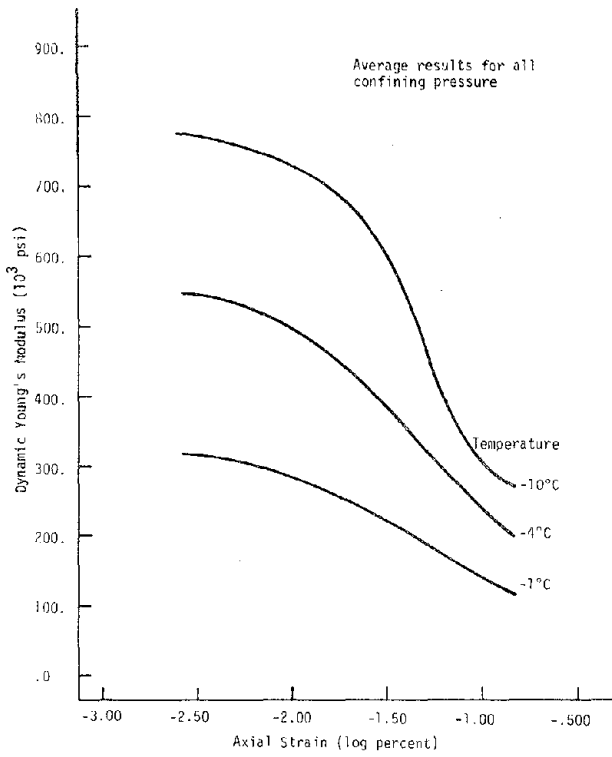


Figure 5.15 DYNAMIC YOUNG'S MODULUS VERSUS AXIAL STRAIN FOR O-CLAY AT 0.3 CPS AND 55.1% WATER CONTENT

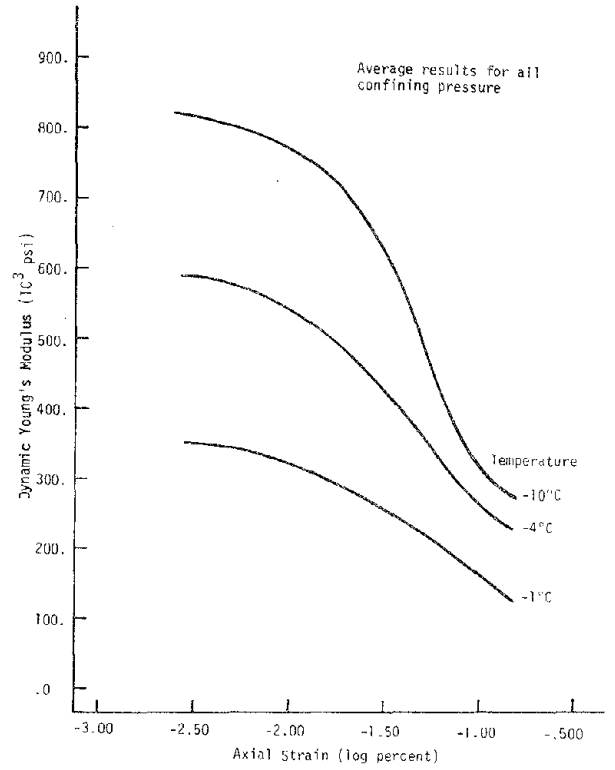


Figure 5.16 DYNAMIC YOUNG'S MODULUS VERSUS AXIAL STRAIN FOR O-CLAY AT 1.0 CPS AND 55.1% WATER CONTENT

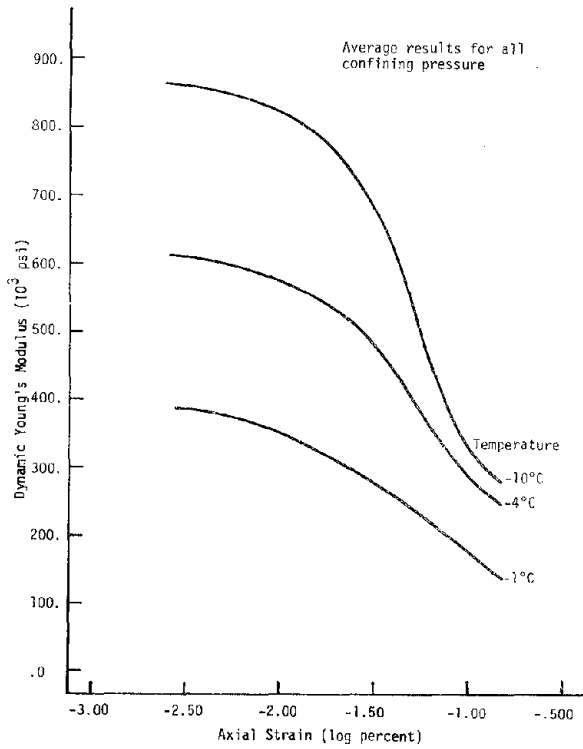


Figure 5.17 DYNAMIC YOUNG'S MODULUS VERSUS AXIAL STRAIN FOR O-CLAY AT 5.0 CPS AND 55.1% WATER CONTENT

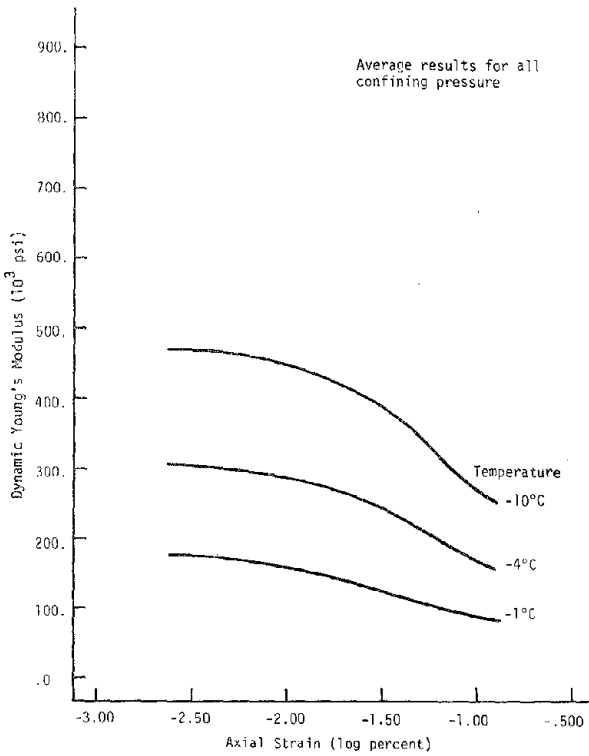


Figure 5.18 DYNAMIC YOUNG'S MODULUS VERSUS AXIAL STRAIN FOR M+O-CLAY AT 0.3 CPS AND 57.2% WATER CONTENT

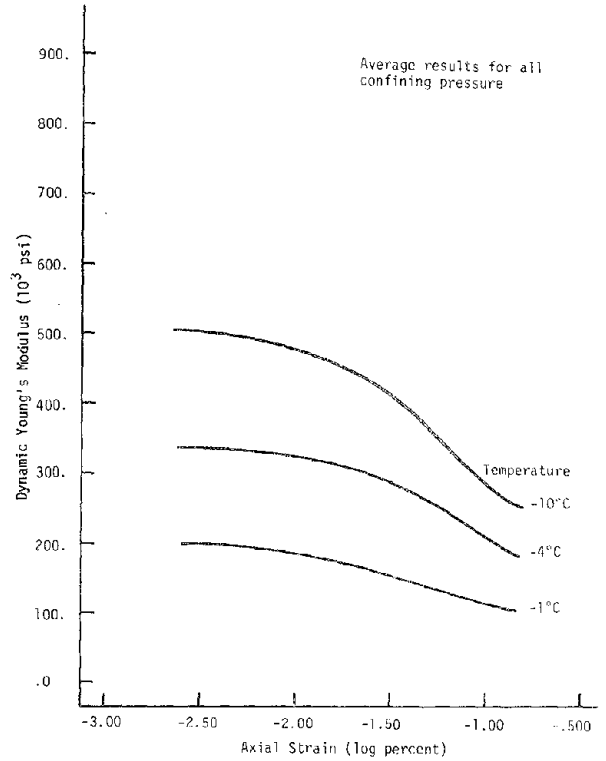


Figure 5.19 DYNAMIC YOUNG'S MODULUS VERSUS AXIAL STRAIN FOR M+O-CLAY AT 1.0 CPS AND 57.2% WATER CONTENT

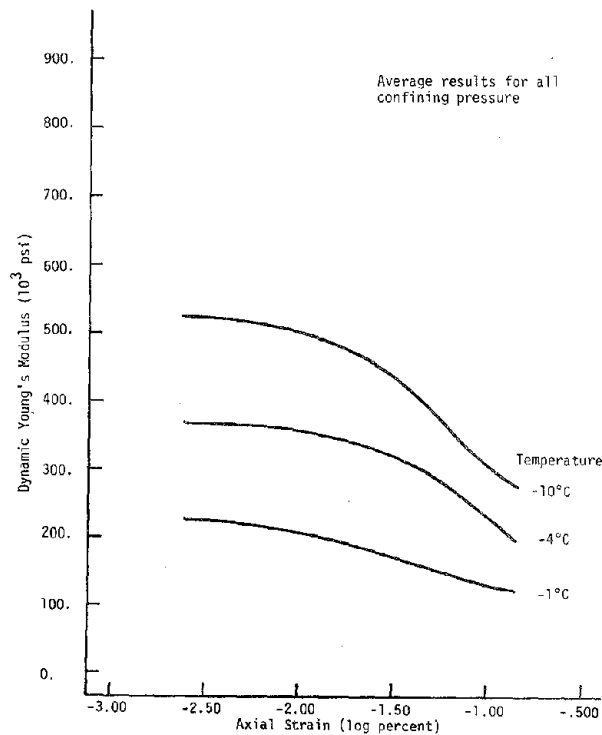


Figure 5.20 DYNAMIC YOUNG'S MODULUS VERSUS AXIAL STRAIN FOR M+O-CLAY AT 5.0 CPS AND 57.2% WATER CONTENT

peratures (-1°C) there is a gradual decrease in modulus over the entire range of strain amplitudes. The relationship for -4°C is intermediate between -10 and -1°C .

The relationship between dynamic Young's modulus and frequency or temperature at a specific water content can be established by interpolating the results presented in Figures 5.5 to 5.20. Owing to the fact that the relationship between dynamic Young's modulus and log percent axial strain is not linear, the relationship between Young's modulus and frequency or temperature will be strain dependent. Therefore, axial strain amplitudes of $3.16 \times 10^{-3}\%$ ($\log_{10} = -2.5$) and $1.0 \times 10^{-1}\%$ ($\log_{10} = -1.00$) were selected for the purpose of establishing the relationship between dynamic Young's modulus and frequency or temperature. Referring to Figures 5.5 to 5.20 it would appear that the relationship would be affected only slightly by differences in water content for the 0-clay samples. (The dynamic properties of M + 0-clay were evaluated at only one water content.) Hence, the relationship between dynamic Young's modulus and frequency or temperature was evaluated at one water content for 0-clay, 36%.

5.4.2 Effect of Frequency

The relationship between dynamic Young's modulus and the log of frequency of 0-clay at a water content of 36.0% is shown in Figures 5.21 and 5.22. The relationship is plotted at three temperatures (-1 , -4 and -10°C) at a strain amplitude of $3.16 \times 10^{-3}\%$ in Figure 5.21 and $1 \times 10^{-1}\%$ in Figure 5.22. The dynamic Young's modulus, in general, increases slightly for an increase in frequency from 0.05 to 5.0 cps. The rate of increase is almost constant over the range of frequency. Temperature and strain amplitude do not appear to have an influence on the relationship.

One frozen 0-clay sample at a water content of 29.2% was tested at six frequencies (0.3, 1.0, 5.0, 10.0, 20.0 and 50.0 cps). The results are shown in Figure 5.23. The relationship is plotted from test results at three confining pressures (25, 50 and 100 psi) for a temperature of -4°C . It appears from the results shown in Figure 5.23 that the relationships shown in Figures 5.21 and 5.22 would be valid up to at least 50 cps.

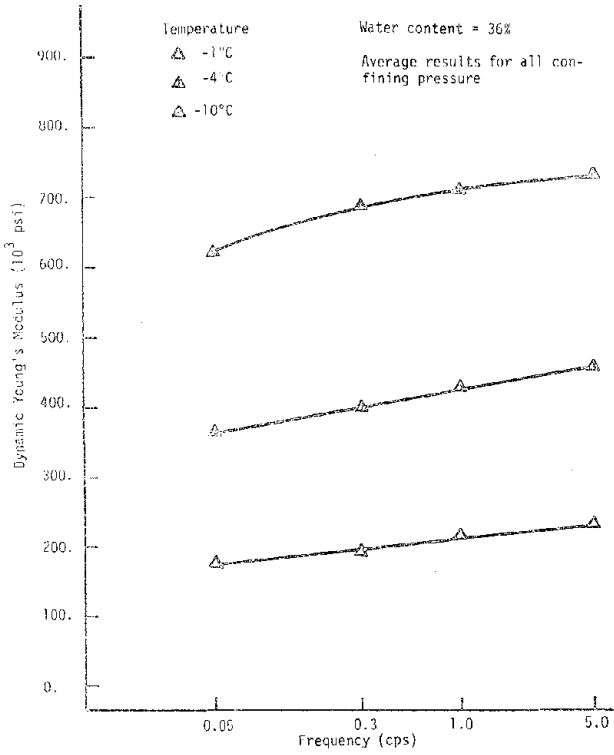


Figure 5.21 DYNAMIC YOUNG'S MODULUS VERSUS FREQUENCY FOR 0-CLAY AT AN AXIAL STRAIN OF $3.16 \times 10^{-3}\%$

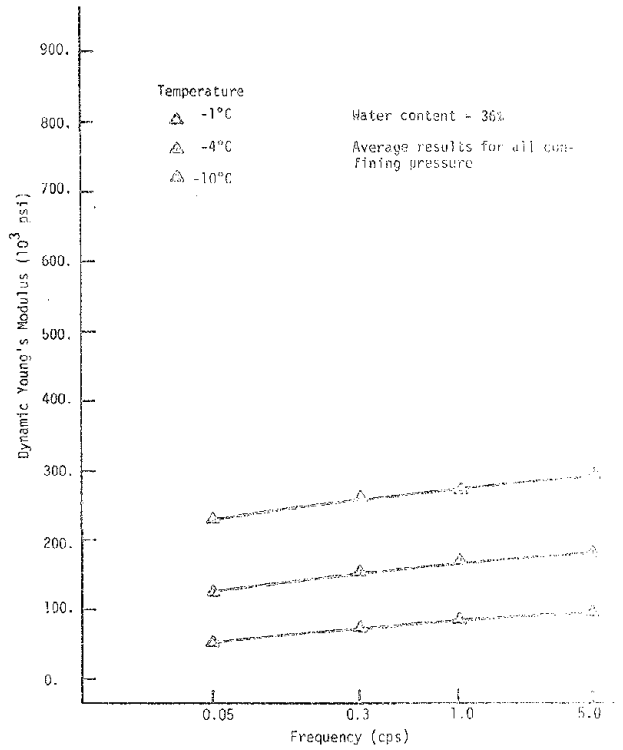


Figure 5.22 DYNAMIC YOUNG'S MODULUS VERSUS FREQUENCY FOR 0-CLAY AT AN AXIAL STRAIN OF $1.0 \times 10^{-1}\%$

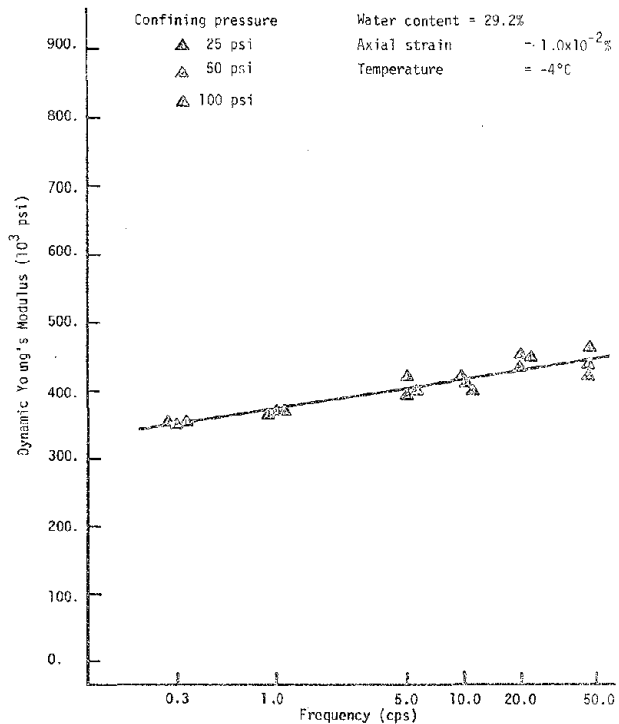


Figure 5.23 DYNAMIC YOUNG'S MODULUS VERSUS FREQUENCY FOR 0-CLAY TESTED TO 50.0 CPS

5.4.3 Effect of Temperature

The relationship between dynamic Young's modulus and temperature for 0-clay at a water content of 36.0% is shown in Figures 5.24 and 5.25. The relationship is plotted at four frequencies (0.05, 0.3, 1.0 and 5.0 cps) at a strain amplitude of $3.16 \times 10^{-3}\%$ in Figure 5.24 and $1.0 \times 10^{-1}\%$ in Figure 5.25.

The dynamic Young's modulus increases significantly with decreasing temperature. The rate of increase is greater for lower strain amplitude ($3.6 \times 10^{-3}\%$) than for higher strain amplitude ($1.0 \times 10^{-1}\%$). At a strain amplitude of $3.6 \times 10^{-3}\%$, the dynamic Young's modulus increases sharply from approximately 200×10^3 psi to 700×10^3 psi for a temperature decrease from -1 to -10°C . At a strain amplitude of $1.0 \times 10^{-1}\%$, the dynamic Young's modulus increases gradually from approximately 80×10^3 to 250×10^3 psi for a temperature decrease from -1 to -10°C . The frequency of testing does not appear to influence the relationship between dynamic Young's modulus and temperature.

5.4.4 Effect of Water Content

The relationship between dynamic Young's modulus and water content of 0-clay samples is shown in Figures 5.26 to 5.31. The relationship is plotted at three frequencies (0.3, 1.0, 5.0 cps) for strain amplitudes of 3.16×10^{-2} and $1.0 \times 10^{-1}\%$ and temperatures of -1 , -4 and -10°C .

The dynamic Young's modulus increases with increasing water content. The rate of increase is greater for a strain amplitude of $3.16 \times 10^{-3}\%$ than for a strain amplitude of $1.0 \times 10^{-1}\%$ at all test temperatures. Frequency does not appear to influence the relationship between dynamic Young's modulus and water content.

At a water content of 46.3% and a temperature of -10°C , the data points appear to deviate from the trend. The dynamic Young's modulus appears to be smaller than the relationship constructed through the data points for the other three water contents. It is believed that this was associated with melting at the coupling between the sample and the cap and base. Melting of the sample associated with these data points at the cap and base was observed when the sample was taken out of the triaxial cell. This was presumably caused by a leak in the rubber membranes surrounding the sample.

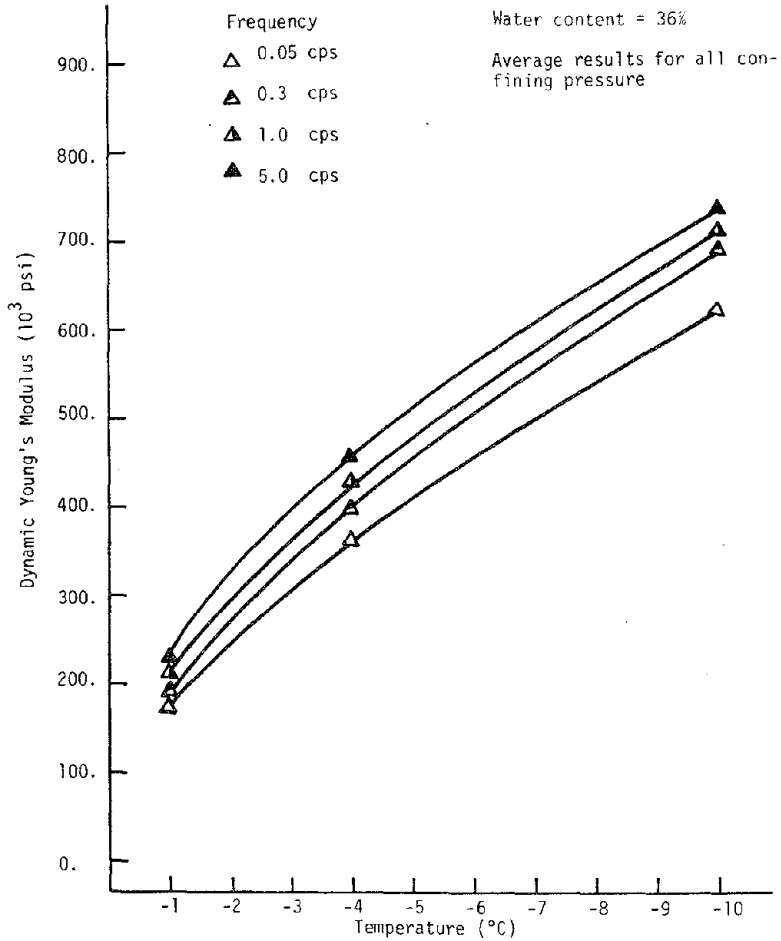


Figure 5.24 DYNAMIC YOUNG'S MODULUS VERSUS TEMPERATURE FOR 0-CLAY AT AN AXIAL STRAIN OF 3.16×10^{-3} .

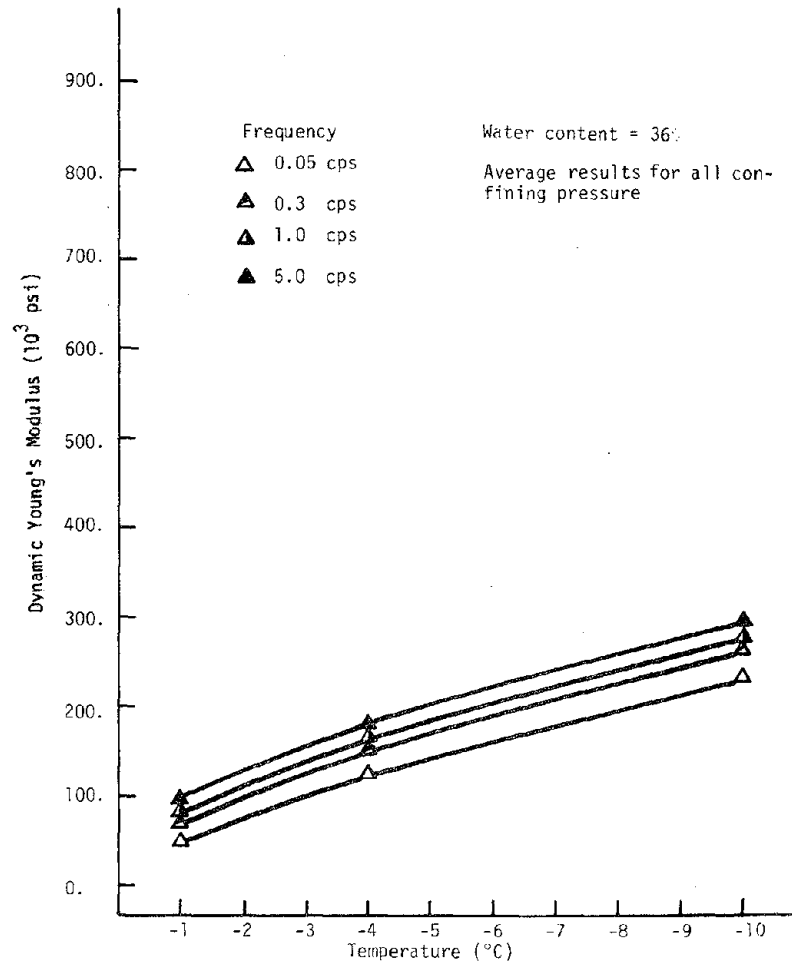


Figure 5.25 DYNAMIC YOUNG'S MODULUS VERSUS TEMPERATURE FOR 0-CLAY AT AN AXIAL STRAIN OF 1.0×10^{-1} .

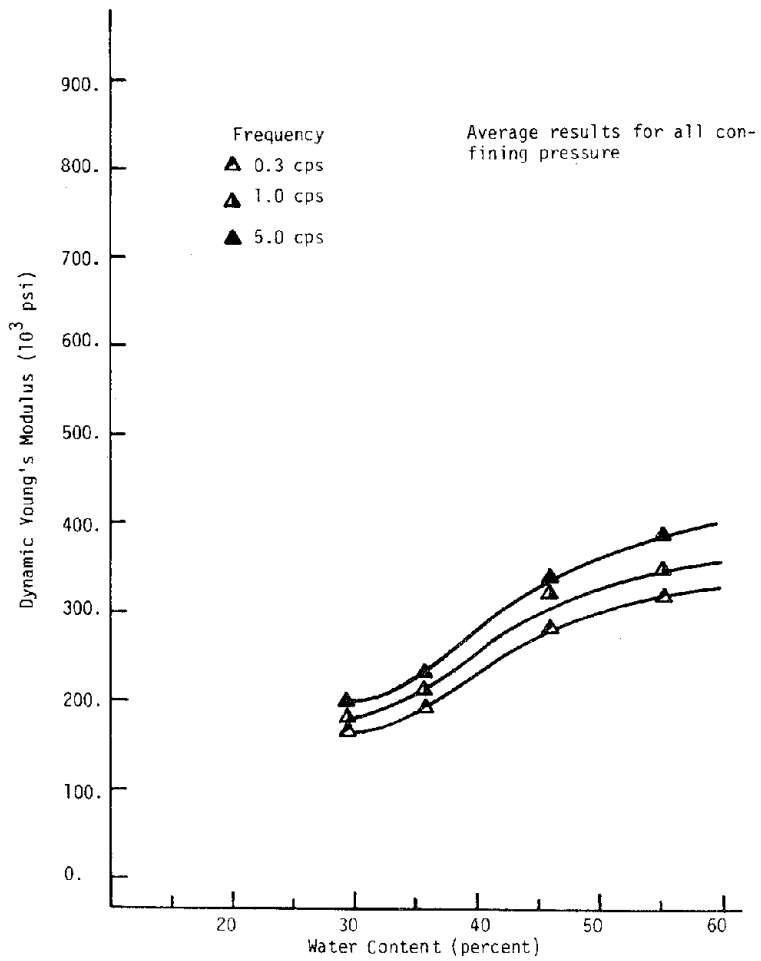


Figure 5.26 DYNAMIC YOUNG'S MODULUS VERSUS WATER CONTENT FOR 0-CLAY AT -1°C AND AN AXIAL STRAIN OF $3.16 \times 10^{-3}\%$

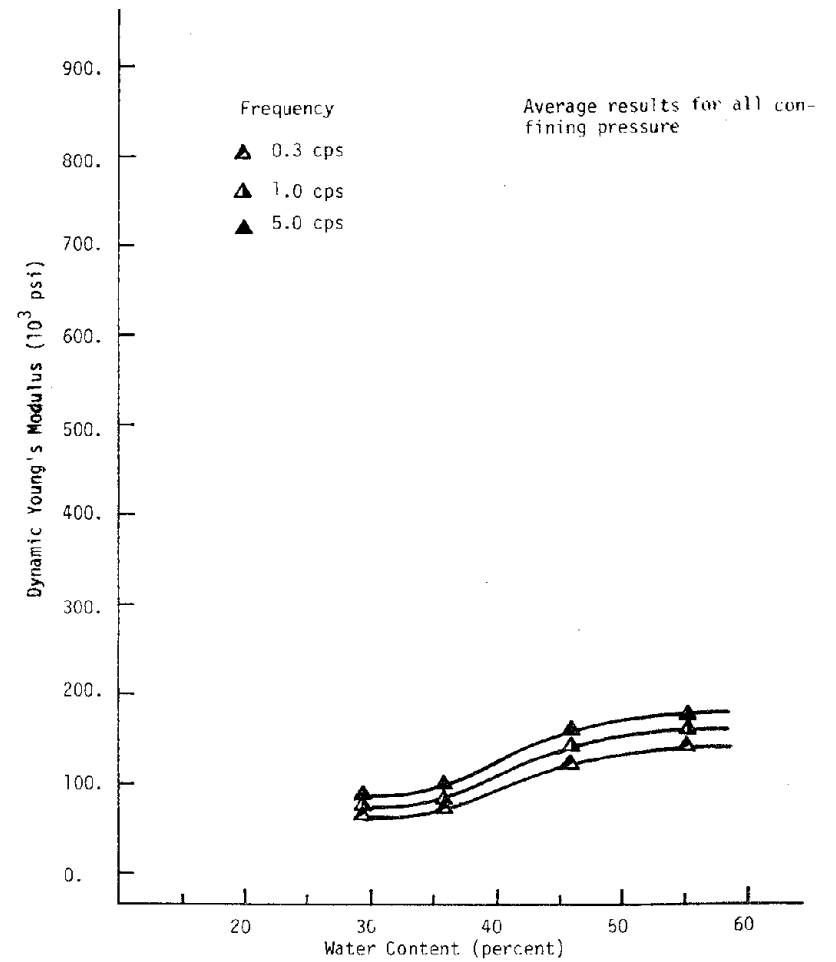


Figure 5.27 DYNAMIC YOUNG'S MODULUS VERSUS WATER CONTENT FOR 0-CLAY AT -1°C AND AN AXIAL STRAIN OF $1.0 \times 10^{-1}\%$

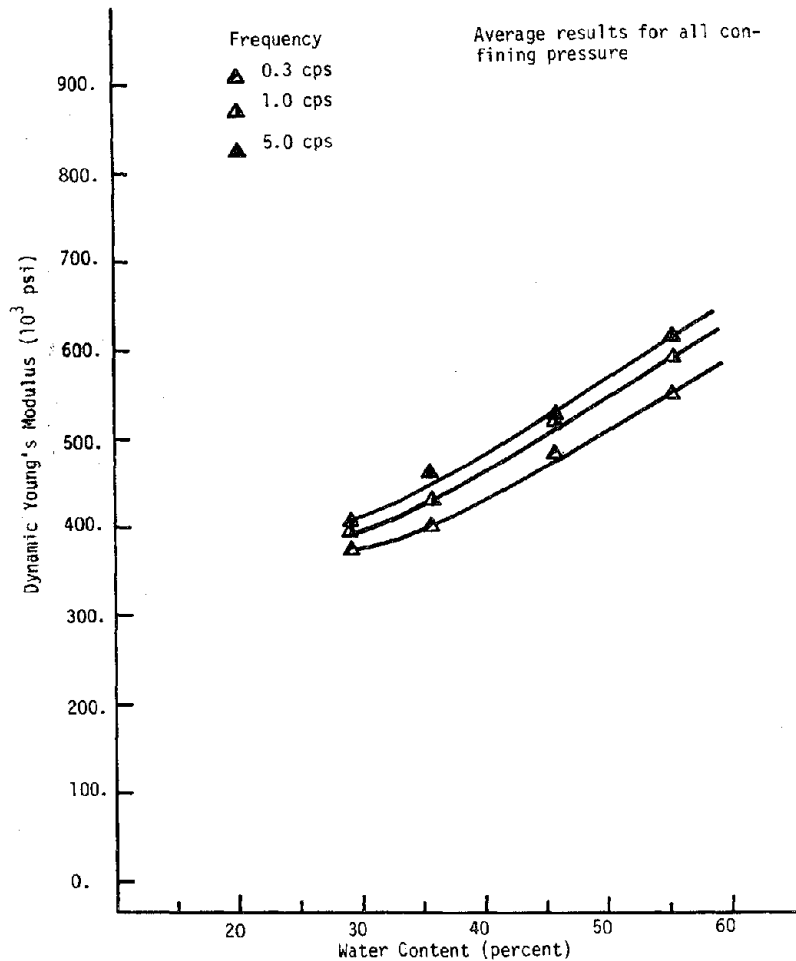


Figure 5.28 DYNAMIC YOUNG'S MODULUS VERSUS WATER CONTENT FOR 0-CLAY AT -4°C AND AN AXIAL STRAIN OF $3.16 \times 10^{-3}\%$

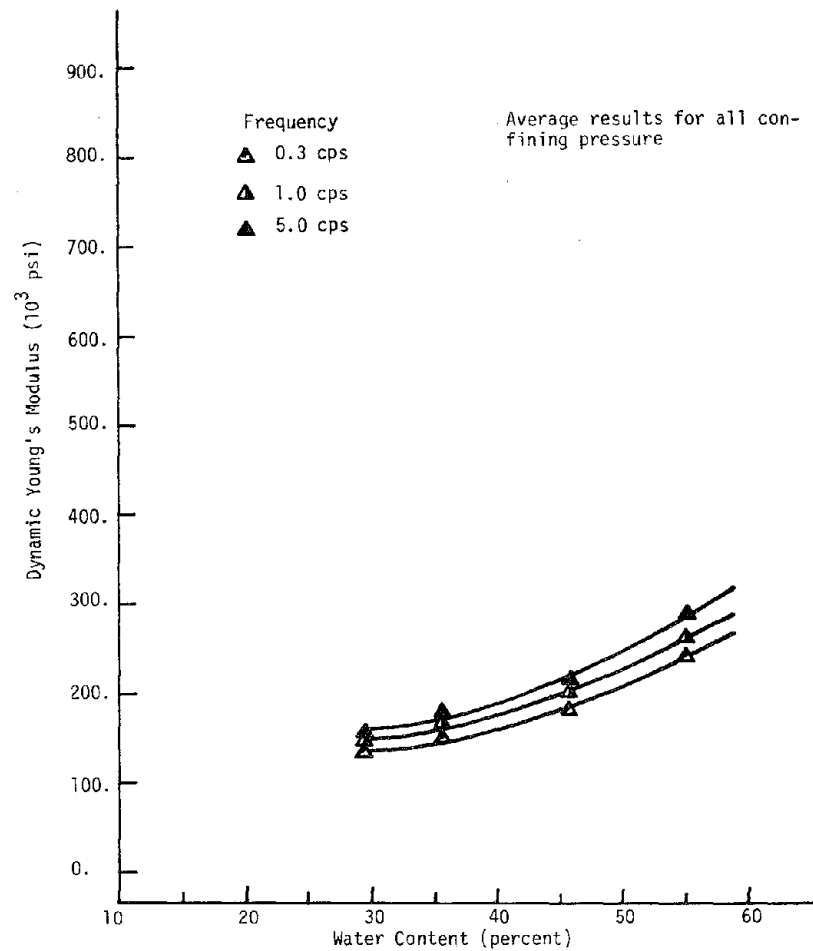


Figure 5.29 DYNAMIC YOUNG'S MODULUS VERSUS WATER CONTENT FOR 0-CLAY AT -4°C AND AN AXIAL STRAIN OF $1.0 \times 10^{-3}\%$

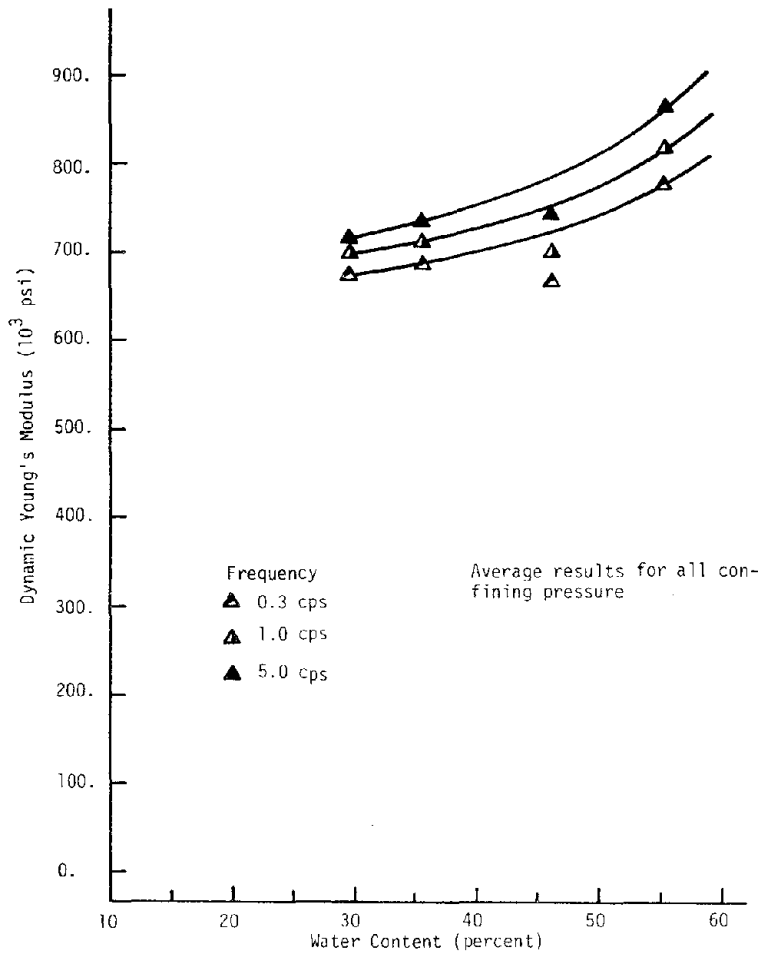


Figure 5.30 DYNAMIC YOUNG'S MODULUS VERSUS WATER CONTENT FOR 0-CLAY AT -10°C AND AN AXIAL STRAIN OF 3.16×10^{-3}

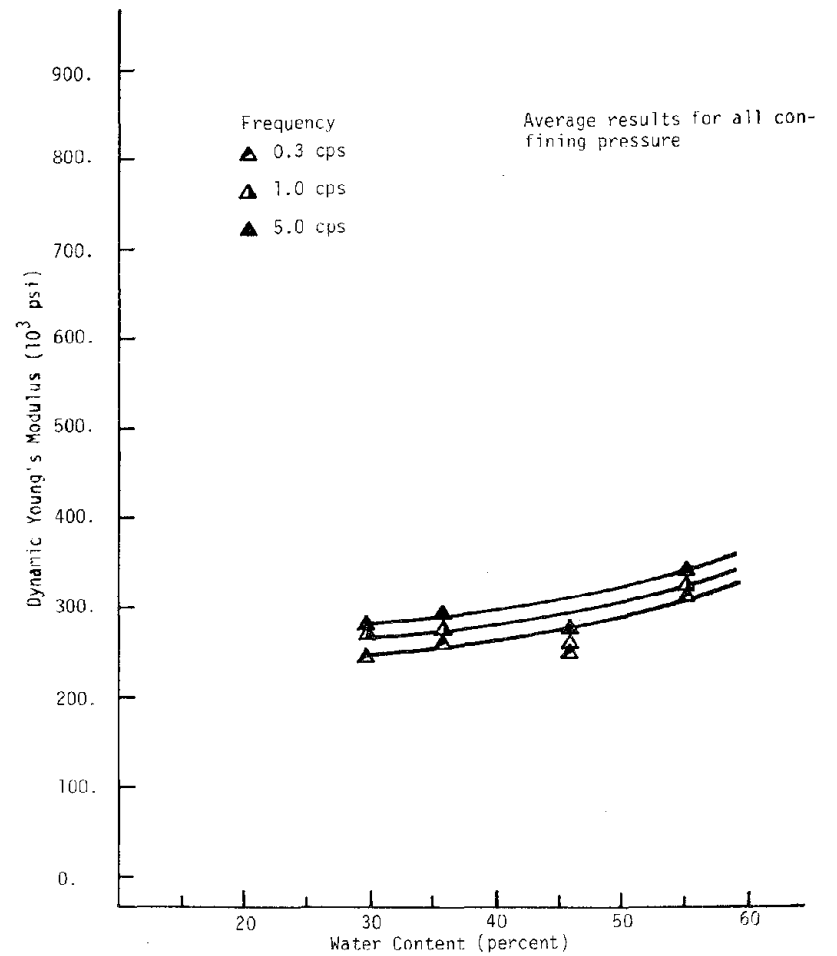


Figure 5.31 DYNAMIC YOUNG'S MODULUS VERSUS WATER CONTENT FOR 0-CLAY AT -10°C AND AN AXIAL STRAIN OF 1.0×10^{-1}

5.4.5 Effect of Specific Surface Area

Two types of clay with significantly different specific surface areas were evaluated in the research program. The 0-clay samples had an estimated specific surface area of $215 \text{ m}^2/\text{g}$ while the M + 0-clay samples had an estimated specific surface area of $475 \text{ m}^2/\text{g}$. The relationship between dynamic Young's modulus and temperature for the two clays is shown in Figures 5.32 and 5.33. The relationship is plotted at two strain amplitudes, 3.2×10^{-3} and $1.0 \times 10^{-1}\%$, at three frequencies (0.3, 1.0 and 5.0 cps) and a water content of 57.2%. (The results for the 0-clay samples at a water content of 57.2% were interpolated from Figures 5.26 to 5.31.)

The results shown in Figures 5.32 and 5.33 indicate 0-clay, with the lower specific surface area, has the higher dynamic modulus. This may be attributed to the higher ice content in the frozen 0-clay at a given test temperature. The difference between the modulus for the 0-clay and M + 0-clay is greater for the high strain amplitude than for the low strain amplitude.

5.5 Damping Ratio of Frozen Clay

The damping ratio of frozen clay from the laboratory test program was plotted against the log of axial strain amplitude expressed as a percent. The plots are shown in Appendix F. An examination of the test results suggests that no pronounced relationship between damping ratio and confining pressure exists. This is exemplified by the relationship between damping ratio and confining pressure for an 0-clay sample at a water content of 36.0% shown in Figure 5.34. The relationship is plotted at four frequencies (0.05, 0.3, 1.0 and 5.0 cps) at a strain amplitude of $1.0 \times 10^{-2}\%$ and a temperature of -4°C . It can be seen that damping ratio of frozen clay does not appear to be affected by confining pressure. Therefore, the data presented represent test results associated with all confining pressures at a specific frequency and temperature. In general, the data from two or more samples are available for each test condition.

5.5.1 Effect of Strain Amplitude

Referring to Figures F.1 to F.48 in Appendix F, the lines in the figures represent the "best fit" lines of the data set for a given test condition. The average "best fit" lines for given test conditions are

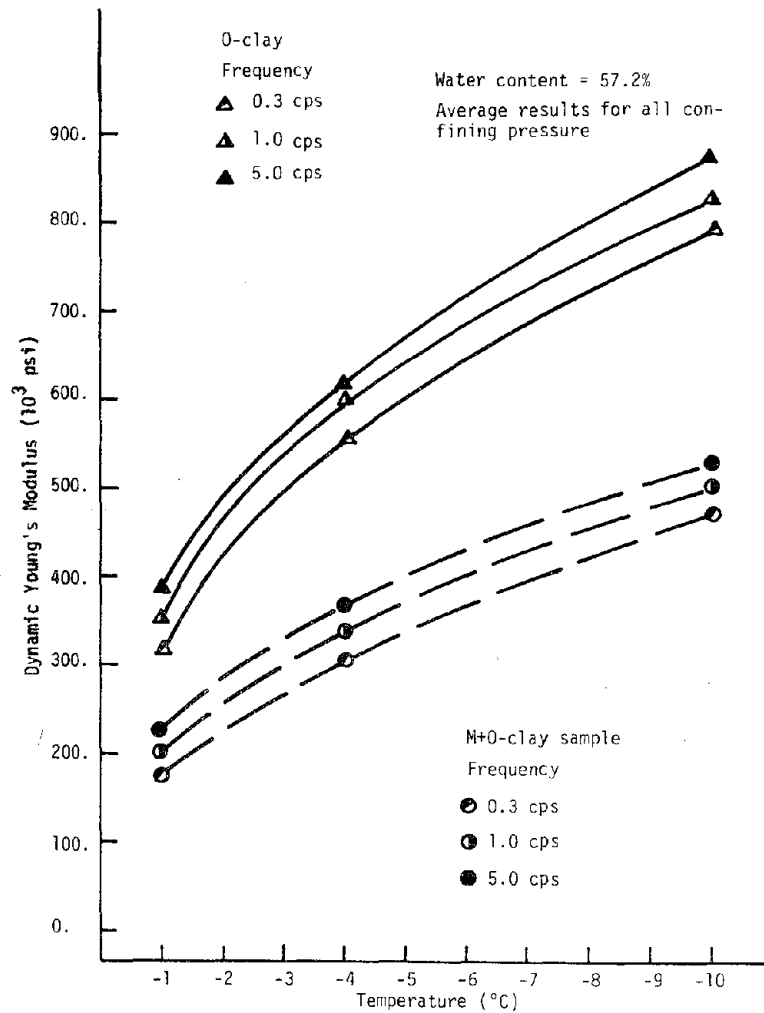


Figure 5.32 DYNAMIC YOUNG'S MODULUS VERSUS TEMPERATURE FOR 0-CLAY AND M+0-CLAY AT AN AXIAL STRAIN OF $3.16 \times 10^{-3}\%$

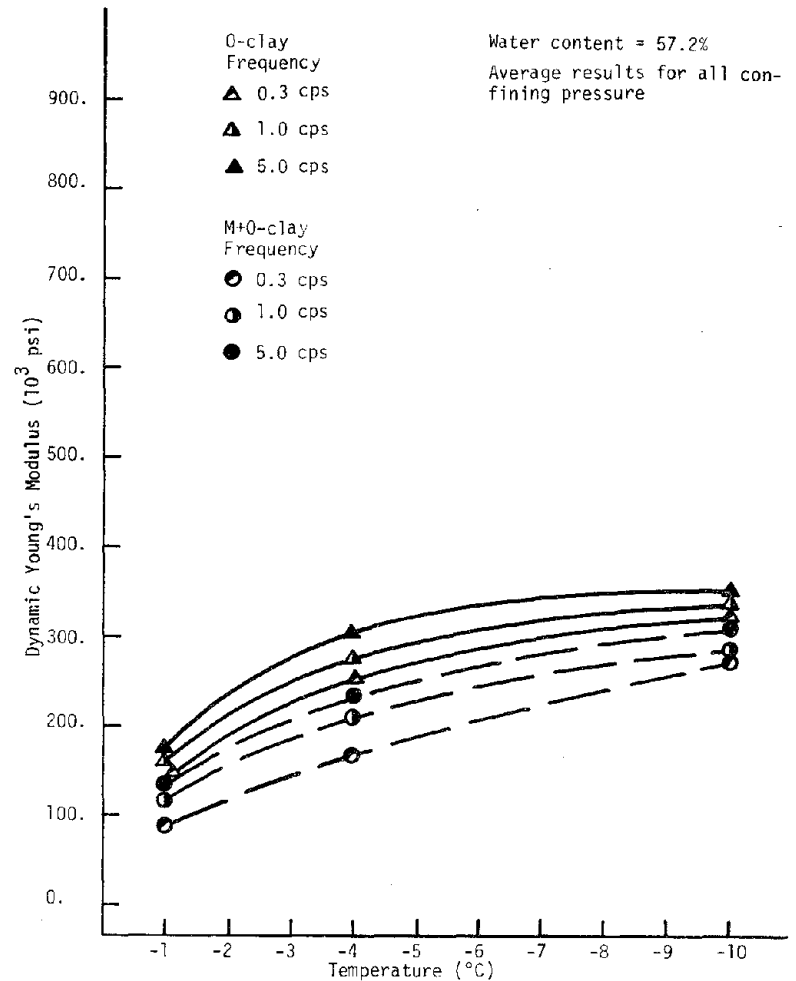


Figure 5.33 DYNAMIC YOUNG'S MODULUS VERSUS TEMPERATURE FOR 0-CLAY AND M+0-CLAY AT AN AXIAL STRAIN OF $1.0 \times 10^{-1}\%$

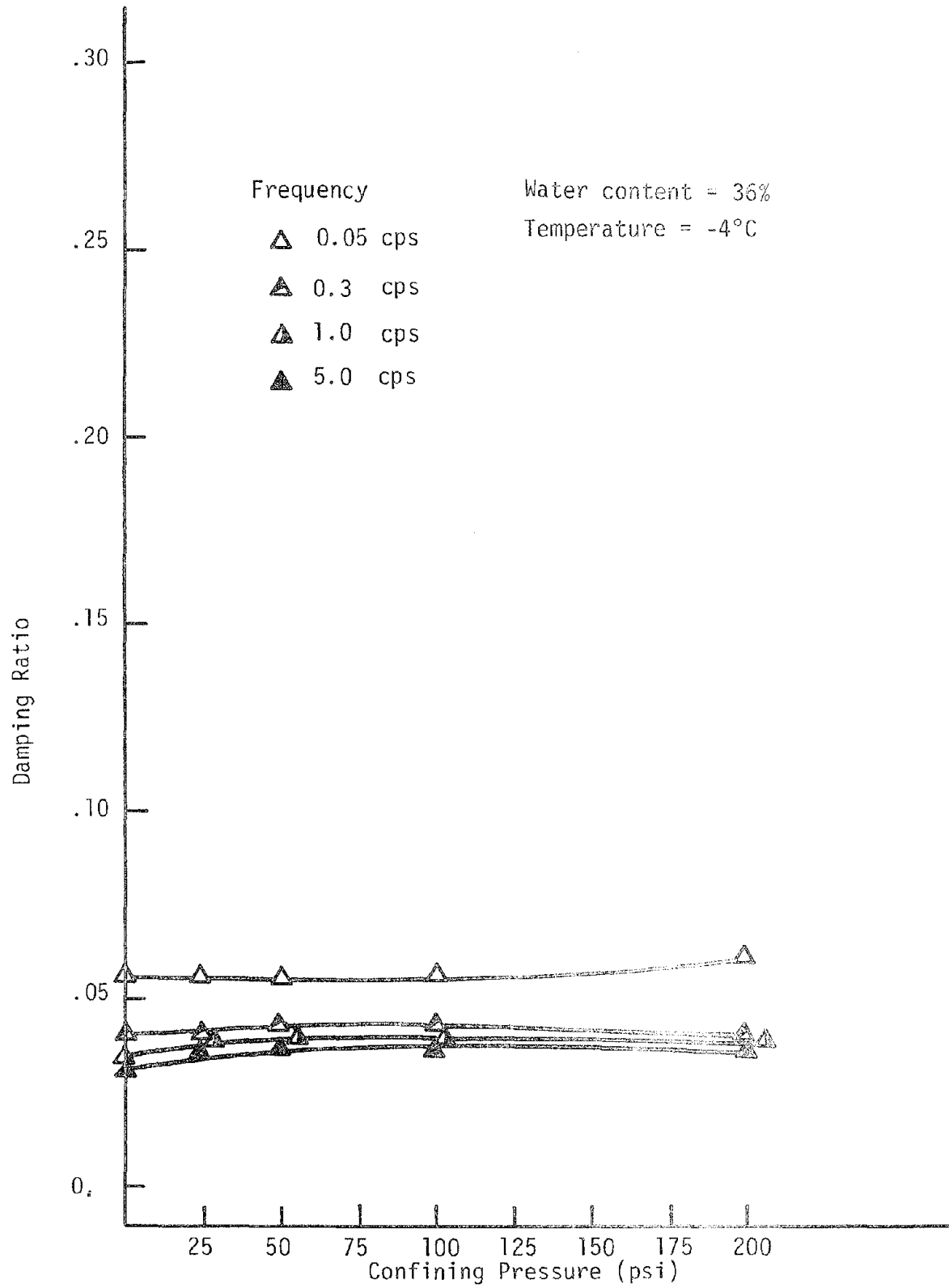


Figure 5.34 DAMPING RATIO VERSUS CONFINING PRESSURE FOR O-CLAY
AT AN AXIAL STRAIN OF $1.0 \times 10^{-2}\%$

summarized in Figures 5.35 to 5.49. The relationships between damping ratio and log percent axial strain are shown at a given temperature (-1, -4 and -10°C) and sample water content (29.2, 36.0, 46.3, 55.1 and 57.2%) at three or four test frequencies.

The results shown in Figures 5.35 to 5.49 indicate the damping ratio of frozen clay increases with increasing strain amplitude. The rate of increase of the damping ratio increases with increasing strain amplitude. At a strain amplitude of $3.16 \times 10^{-3}\%$, the rate of increase is small; at a strain amplitude of $1.0 \times 10^{-1}\%$, the rate of increase is great. The damping ratio increases from about 0.02 to 0.3 as strain amplitude increases from 3.16×10^{-3} to $1.0 \times 10^{-1}\%$.

The relationship between damping ratio and frequency, temperature, and water content can be established by interpolating the results presented in Figures 5.35 to 5.49 at a specified strain amplitude. Strain amplitudes of $3.16 \times 10^{-3}\%$ ($\log_{10} = -2.5$) and $1.0 \times 10^{-1}\%$ ($\log_{10} = -1.0$) were selected for this purpose. The relationships between damping ratio and frequency and temperature were interpolated at a water content of 36.0% only owing to the fact that they would be affected only slightly by differences in water content.

5.5.2 Effect of Frequency

The relationship between damping ratio and frequency is shown in Figures 5.50 to 5.52. The relationship in Figures 5.50 and 5.51 is plotted at three temperatures (-1, -4 and -10°C) and a strain amplitude of $3.16 \times 10^{-3}\%$ in Figure 5.50 and $1.0 \times 10^{-1}\%$ in Figure 5.51. A frozen clay sample at a water content of 29.2% was tested at six frequencies (0.3, 1.0, 5.0, 10.0, 20.0 and 50.0 cps), as shown in Figure 5.52. The relationship is plotted at three confining pressures (25, 50 and 100 psi) at a temperature of -4°C.

Referring to Figure 5.50 and 5.51, the damping ratio of frozen clay, in general, decreases for an increase in frequency from 0.05 to 5.0 cps; for frequencies greater than 5.0 cps, damping ratio increases as frequency increases, as shown in Figure 5.52. The rate of decrease of damping ratio for an increase in frequency from 0.05 to 0.3 cps appears to be slightly greater than for an increase in frequency from 0.3 to 5.0 cps. The damping ratio gradually increases for an increase in frequency from 5.0 to 10.0 cps. In the frequency range 20.0 to 50.0 cps, the rate of

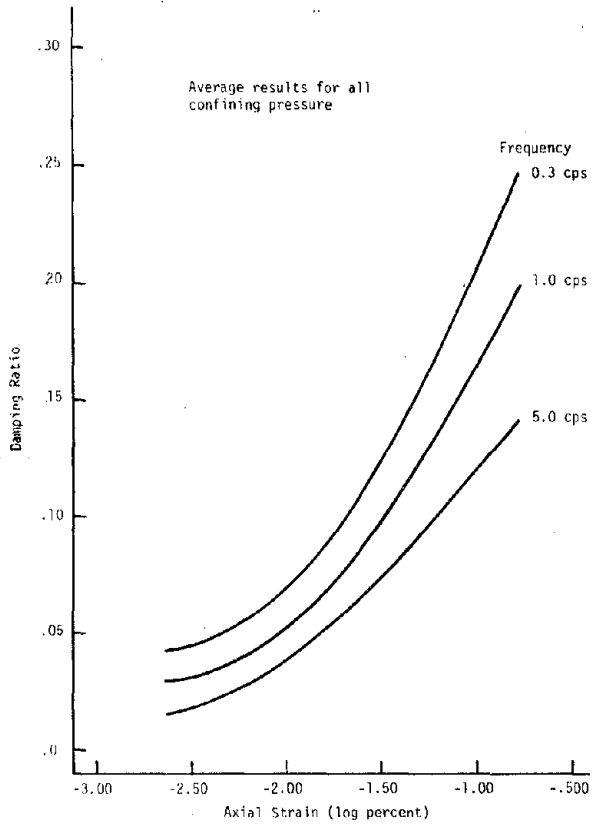


Figure 5.35 DAMPING RATIO VERSUS AXIAL STRAIN FOR 0-CLAY AT -1°C AND 29.2% WATER CONTENT

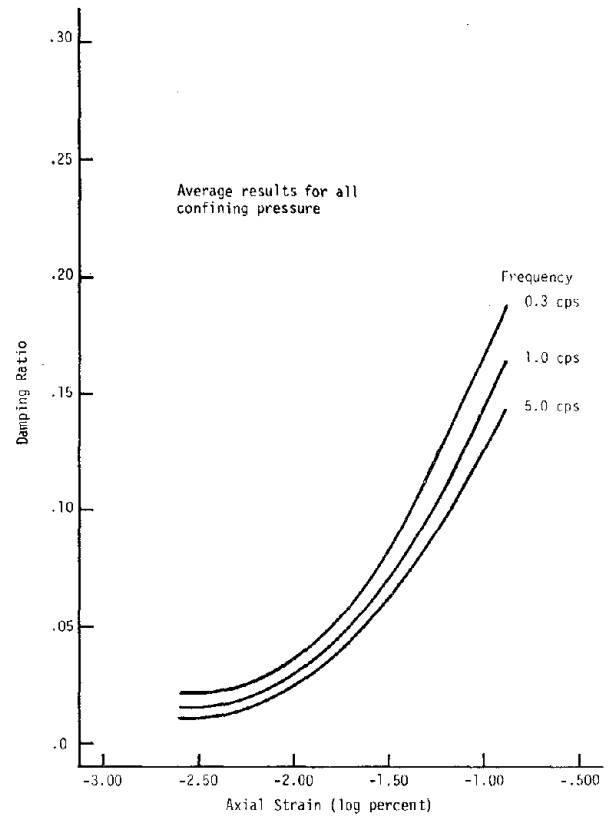


Figure 5.36 DAMPING RATIO VERSUS AXIAL STRAIN FOR 0-CLAY AT -4°C AND 29.2% WATER CONTENT

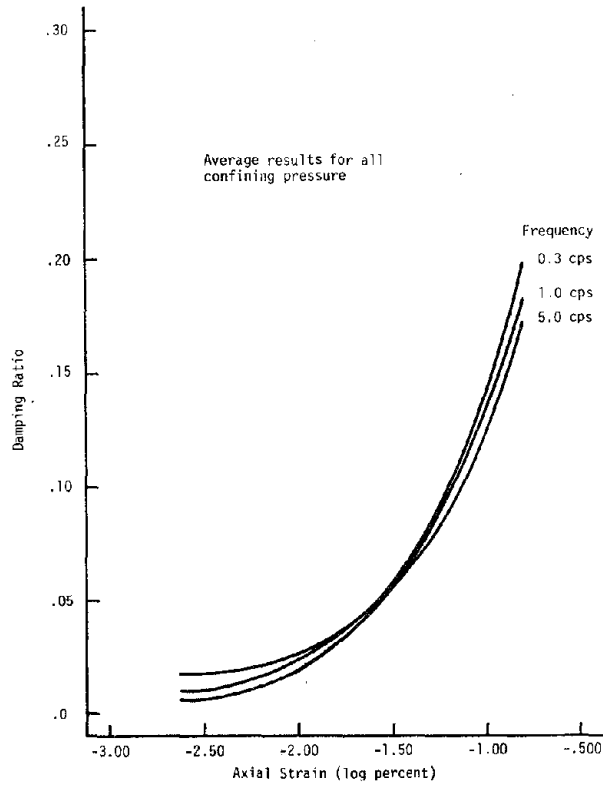


Figure 5.37 DAMPING RATIO VERSUS AXIAL STRAIN FOR 0-CLAY AT -10°C AND 29.2% WATER CONTENT

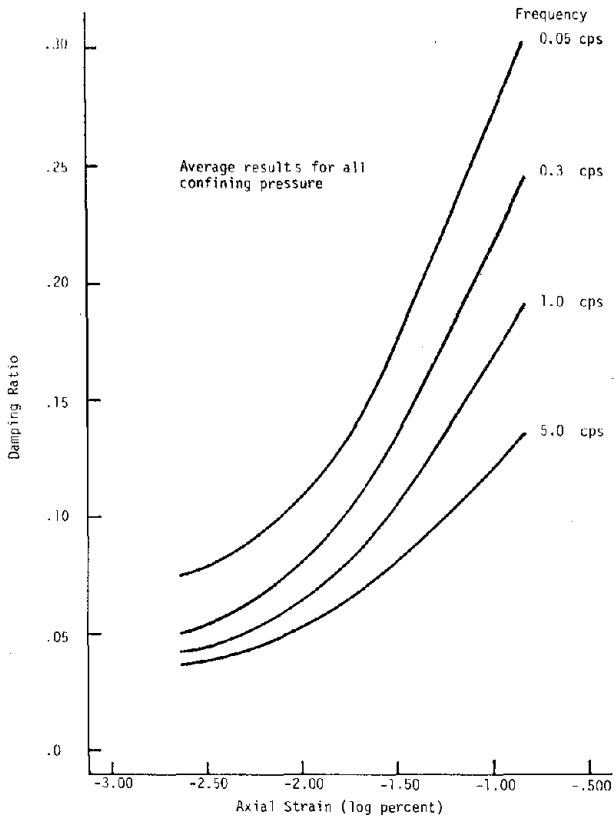


Figure 5.38 DAMPING RATIO VERSUS AXIAL STRAIN FOR 0-CLAY AT -1°C AND 36.0% WATER CONTENT

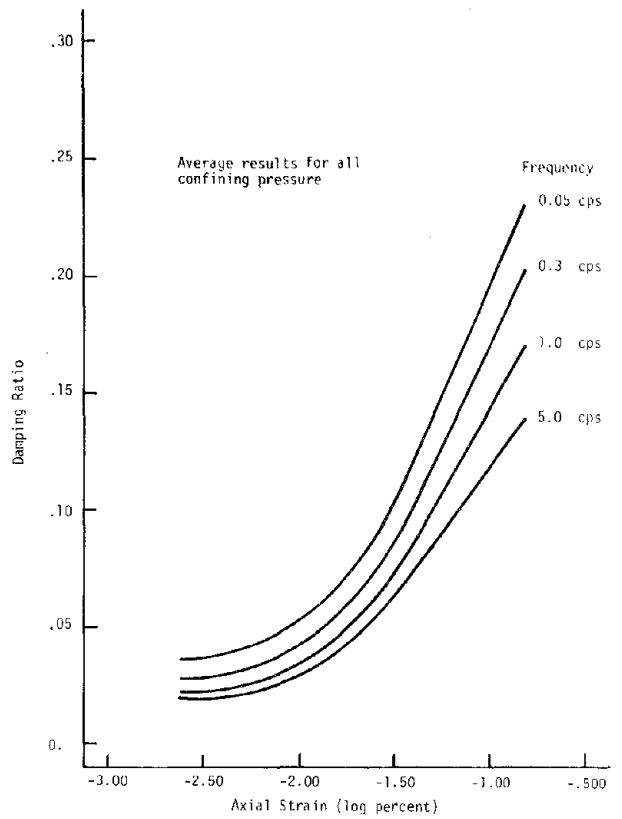


Figure 5.39 DAMPING RATIO VERSUS AXIAL STRAIN FOR 0-CLAY AT -4°C AND 36.0% WATER CONTENT

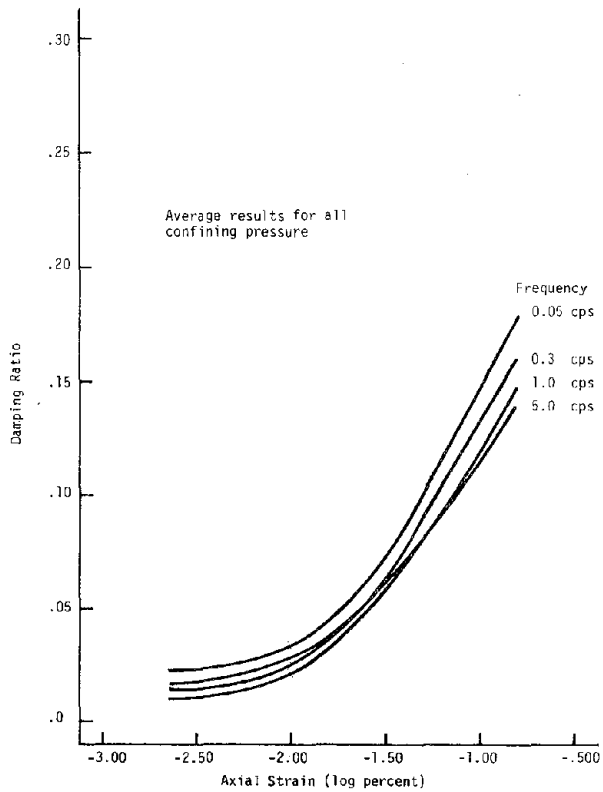


Figure 5.40 DAMPING RATIO VERSUS AXIAL STRAIN FOR 0-CLAY AT -10°C AND 36.0% WATER CONTENT

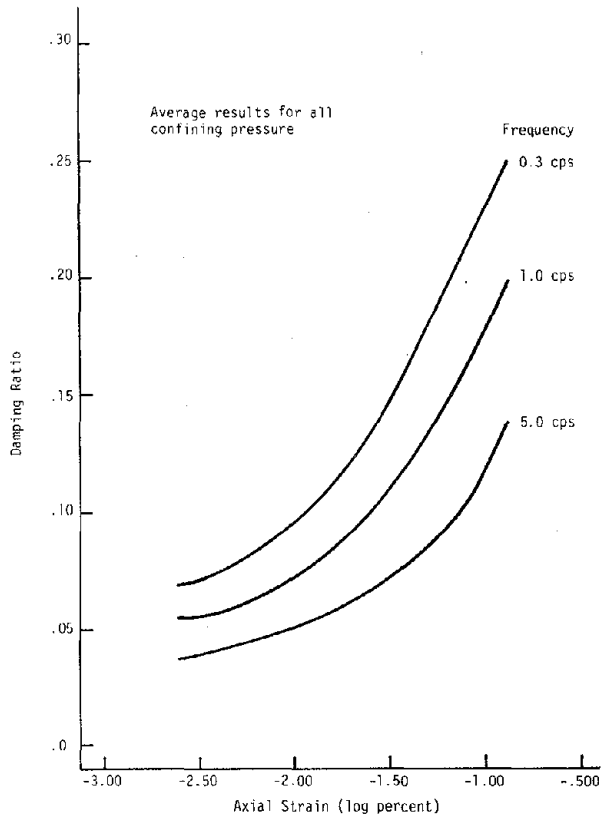


Figure 5.41 DAMPING RATIO VERSUS AXIAL STRAIN FOR 0-CLAY AT -1°C AND 46.3% WATER CONTENT

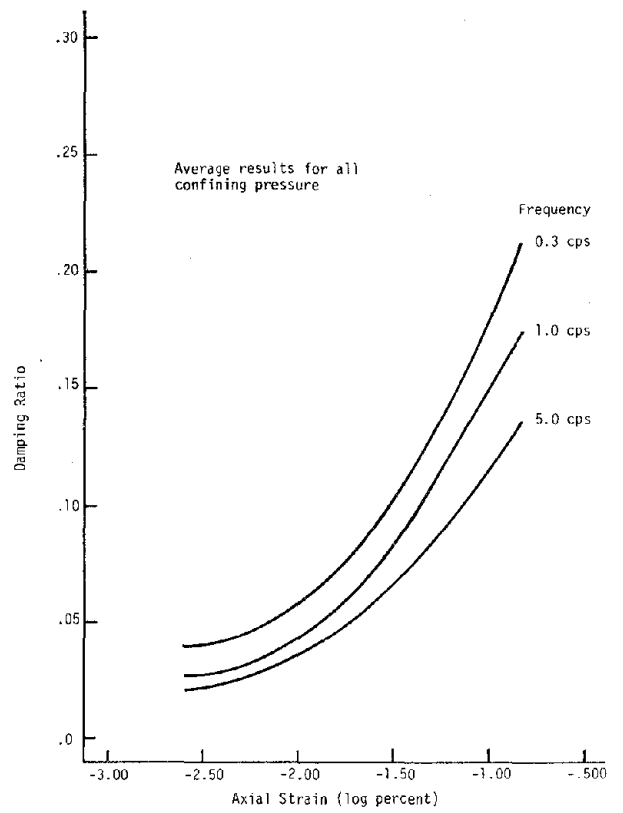


Figure 5.42 DAMPING RATIO VERSUS AXIAL STRAIN FOR 0-CLAY AT -4°C AND 46.3% WATER CONTENT

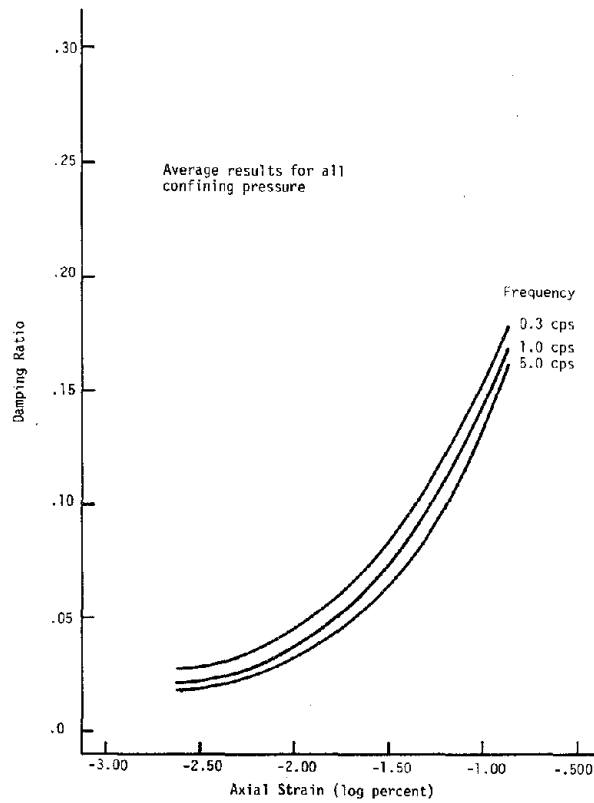


Figure 5.43 DAMPING RATIO VERSUS AXIAL STRAIN FOR 0-CLAY AT -10°C AND 46.3% WATER CONTENT

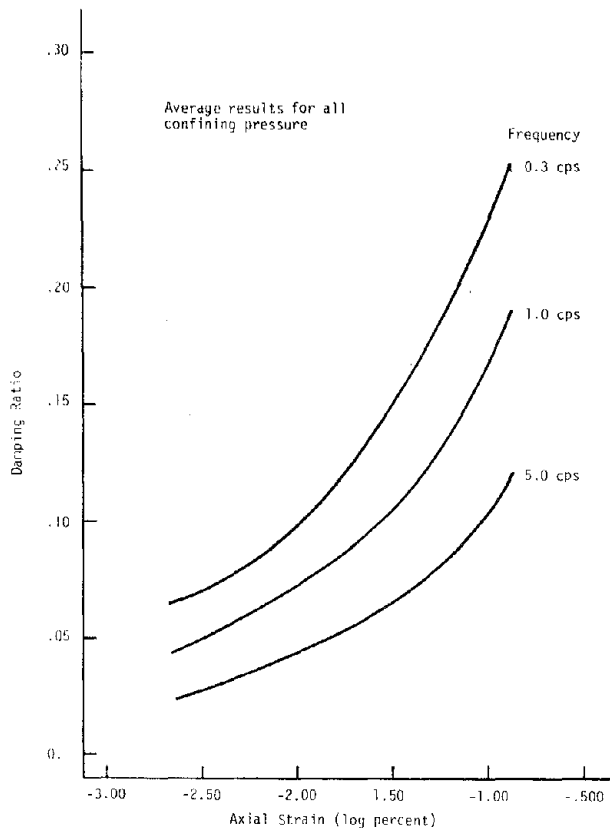


Figure 5.44 DAMPING RATIO VERSUS AXIAL STRAIN FOR O-CLAY AT -1°C AND 55.1% WATER CONTENT

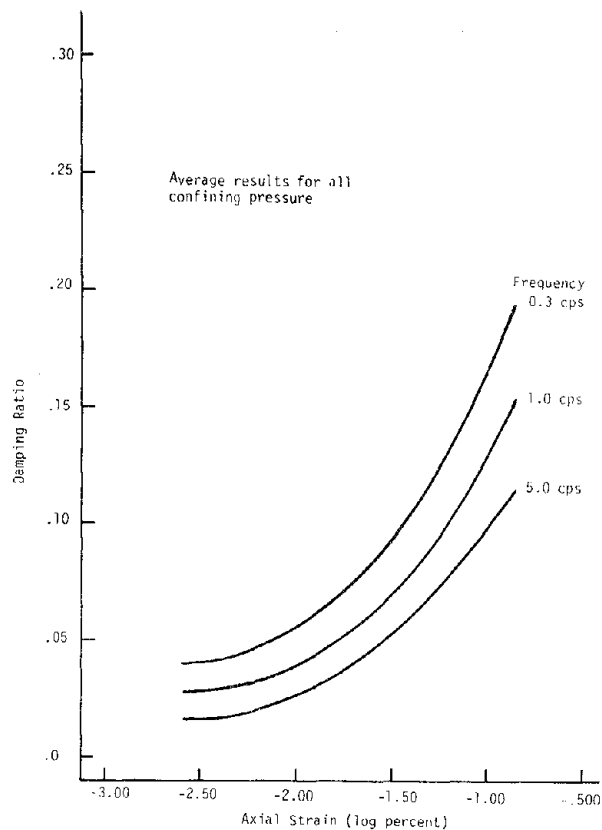


Figure 5.45 DAMPING RATIO VERSUS AXIAL STRAIN FOR O-CLAY AT -4°C AND 55.1% WATER CONTENT

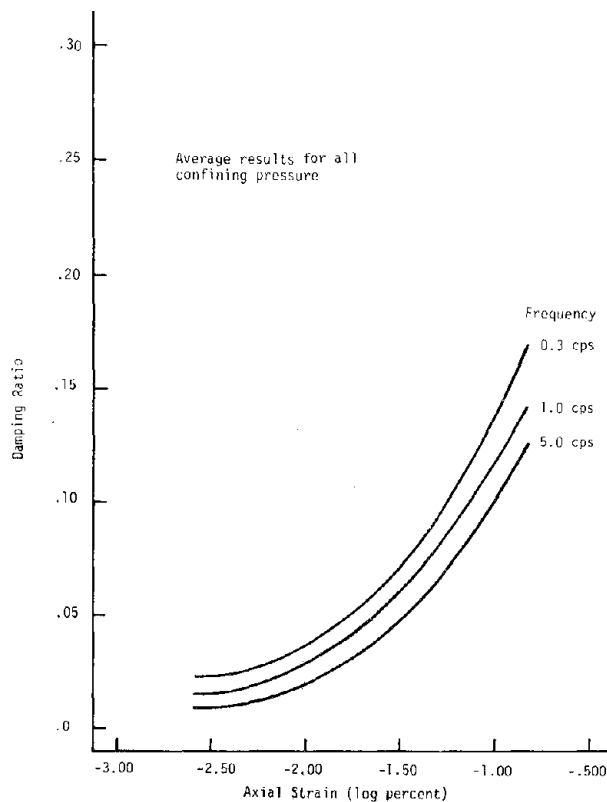


Figure 5.46 DAMPING RATIO VERSUS AXIAL STRAIN FOR O-CLAY AT -10°C AND 55.1% WATER CONTENT

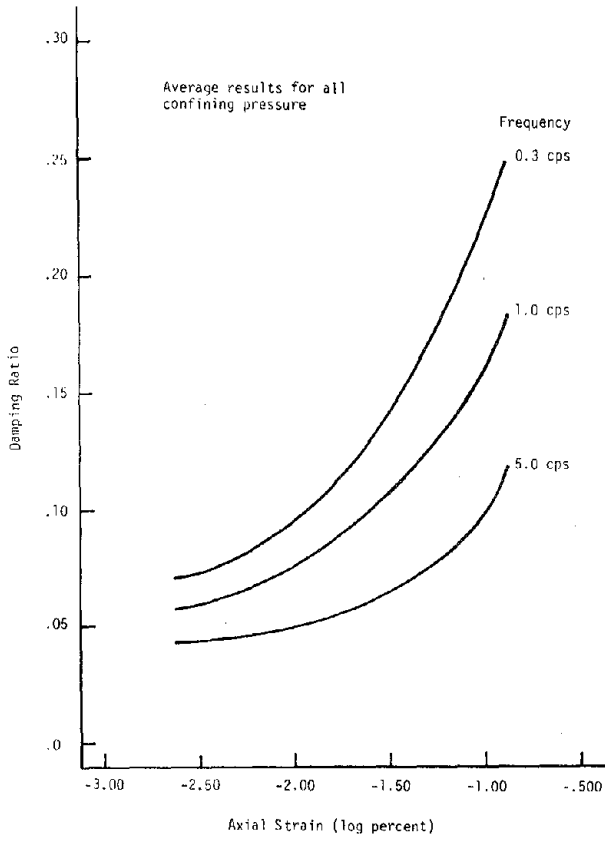


Figure 5.47 DAMPING RATIO VERSUS AXIAL STRAIN FOR M+O-CLAY AT -1°C AND 57.2% WATER CONTENT

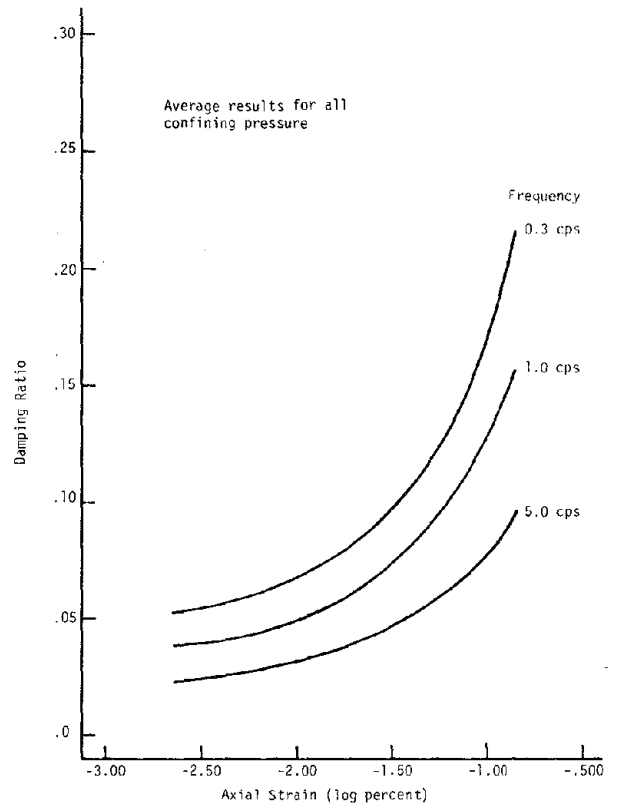


Figure 5.48 DAMPING RATIO VERSUS AXIAL STRAIN FOR M+O-CLAY AT -4°C AND 57.2% WATER CONTENT

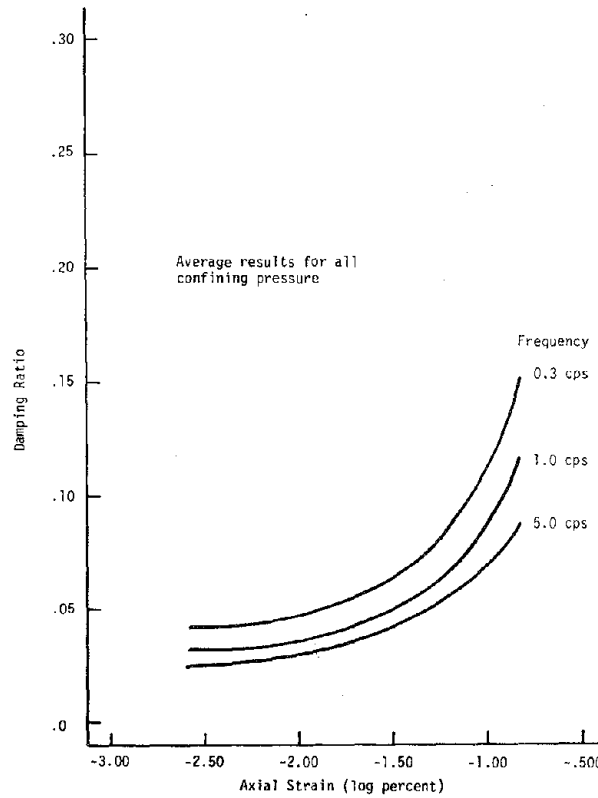


Figure 5.49 DAMPING RATIO VERSUS AXIAL STRAIN FOR M+O-CLAY AT -10°C AND 57.2% WATER CONTENT

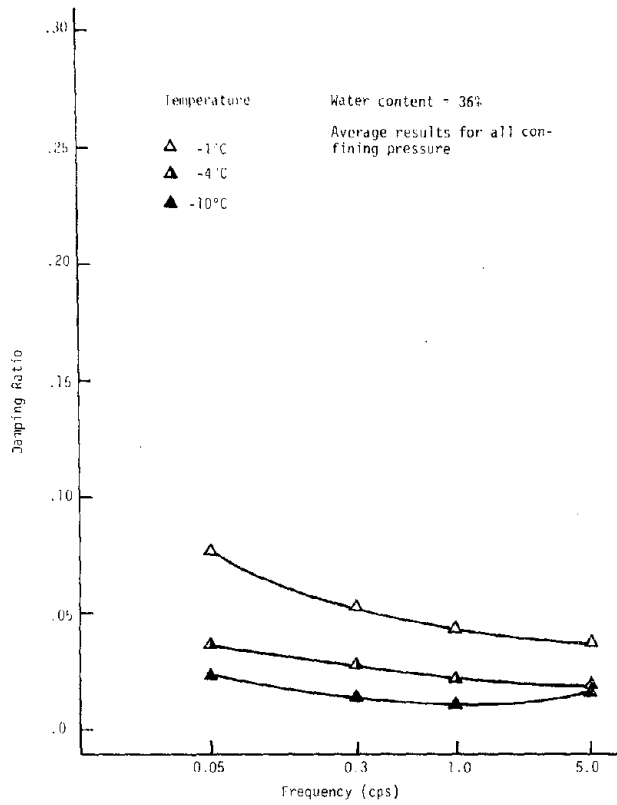


Figure 5.50 DAMPING RATIO VERSUS FREQUENCY FOR 0-CLAY AT AN AXIAL STRAIN OF $3.16 \times 10^{-3}\%$

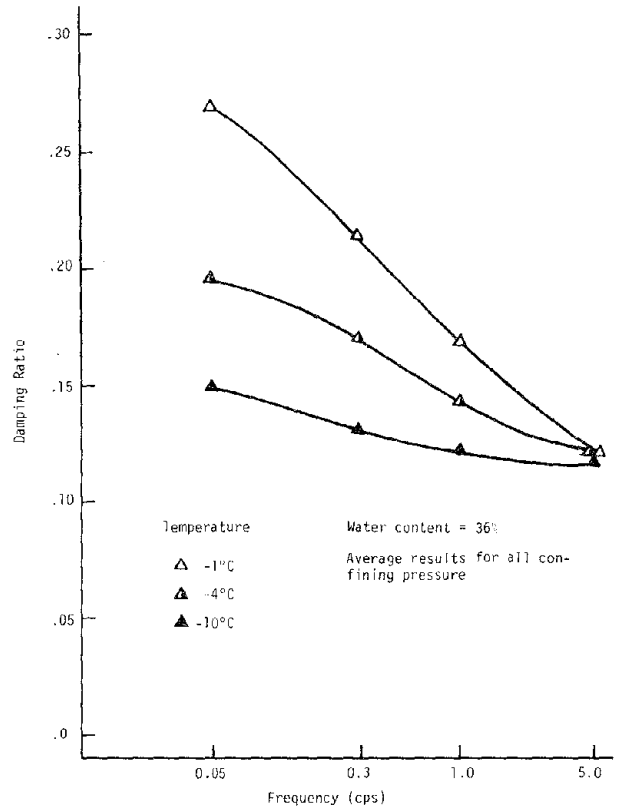


Figure 5.51 DAMPING RATIO VERSUS FREQUENCY FOR 0-CLAY AT AN AXIAL STRAIN OF $1.0 \times 10^{-1}\%$

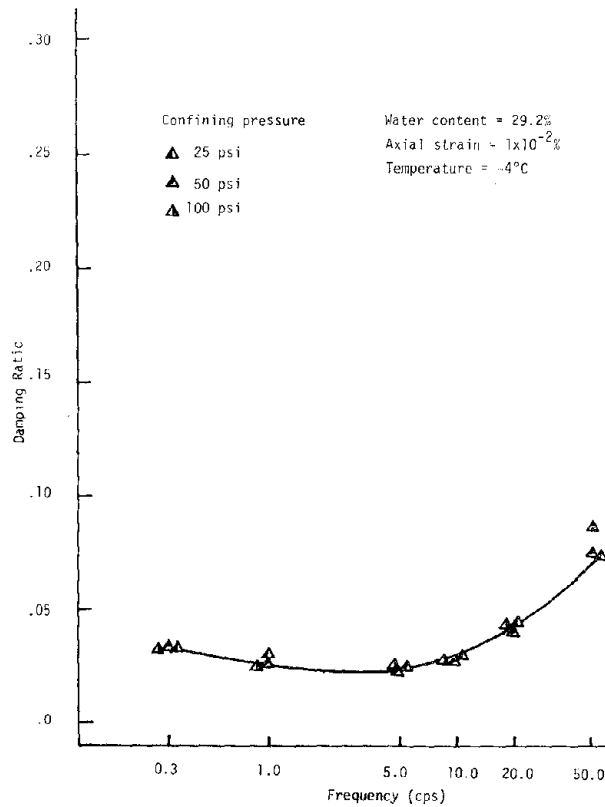


Figure 5.52 DAMPING RATIO VERSUS FREQUENCY FOR 0-CLAY TESTED TO 50.0 CPS

increase is significant. The influence of frequency on damping ratio of frozen clay is greater for higher temperatures (-1°C) than for lower temperatures (-10°C); and is greater for higher strain amplitudes ($1.0 \times 10^{-1}\%$) than for lower ($3.16 \times 10^{-3}\%$).

5.5.3 Effect of Temperature

The relationship between damping ratio of frozen clay and temperature is shown in Figures 5.53 and 5.54. The relationship is plotted at four frequencies for a given strain amplitude.

The damping ratio of frozen clay decreases sharply for an increase in temperature from -1 to -4°C . Between -4 and -10°C the rate of decrease is, in general, not as sharp. The decrease of damping ratio is greater for lower frequencies (0.05 cps) than for higher frequencies (5.0 cps). At a frequency of 5.0 cps, the influence of temperature on damping ratio appears to be small.

5.5.4 Effect of Water Content

The relationship between damping ratio and water content of the frozen clay samples is shown in Figures 5.55 to 5.60. The relationship is plotted at three frequencies (0.3, 1.0, 5.0 cps) for a given temperature and strain amplitude.

There appears to be no well-defined relationship between damping ratio and water content of frozen clay. It is believed, however, that frequency, temperature, and strain amplitude may have an influence. The relationship between damping ratio and water content may be stated as follows:

- (1) At a temperature of -1°C and a strain amplitude of $3.16 \times 10^{-3}\%$, damping ratio increases slightly for an increase in water content from 29.2 to 55.1% for frequencies of 0.3 and 1.0 cps; but for a frequency of 5.0 cps, damping ratio increases for an increase in water content from 29.2 to 40% and decreases for an increase in water content from 40 to 55.1%.
- (2) At a temperature of -1°C and a strain amplitude of $1.0 \times 10^{-1}\%$, damping ratio increases slightly for an increase in water content from 29.2 to 55.1% for frequencies of 0.3 and 1.0 cps, whereas for a frequency of 5.0 cps damping ratio decreases slightly over the entire range of water contents.

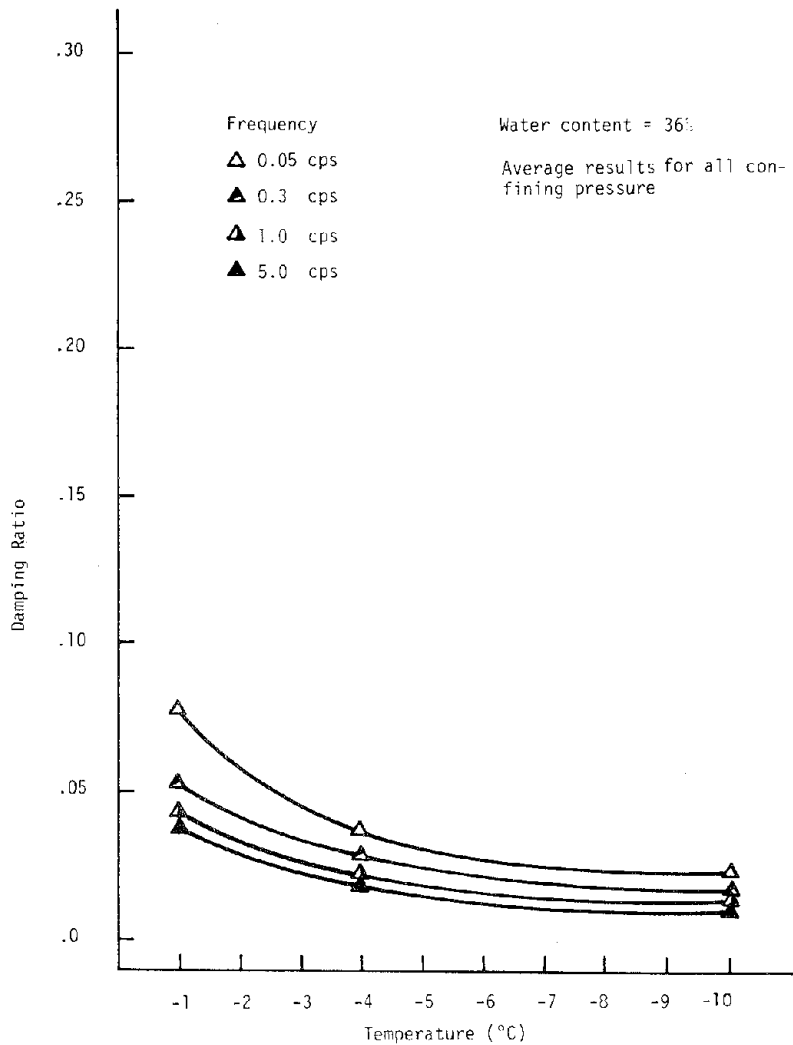


Figure 5.53 DAMPING RATIO VERSUS TEMPERATURE FOR 0-CLAY AT AN AXIAL STRAIN OF 3.16×10^{-3} .

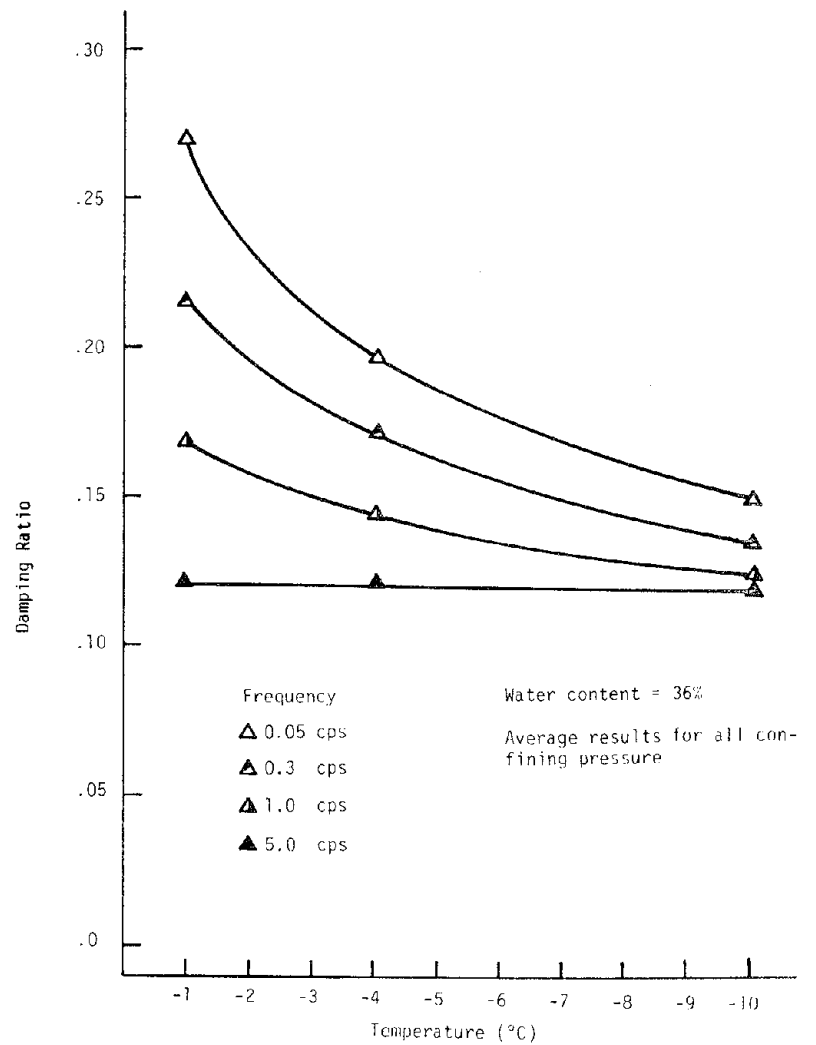


Figure 5.54 DAMPING RATIO VERSUS TEMPERATURE FOR 0-CLAY AT AN AXIAL STRAIN OF 1.0×10^{-1} .

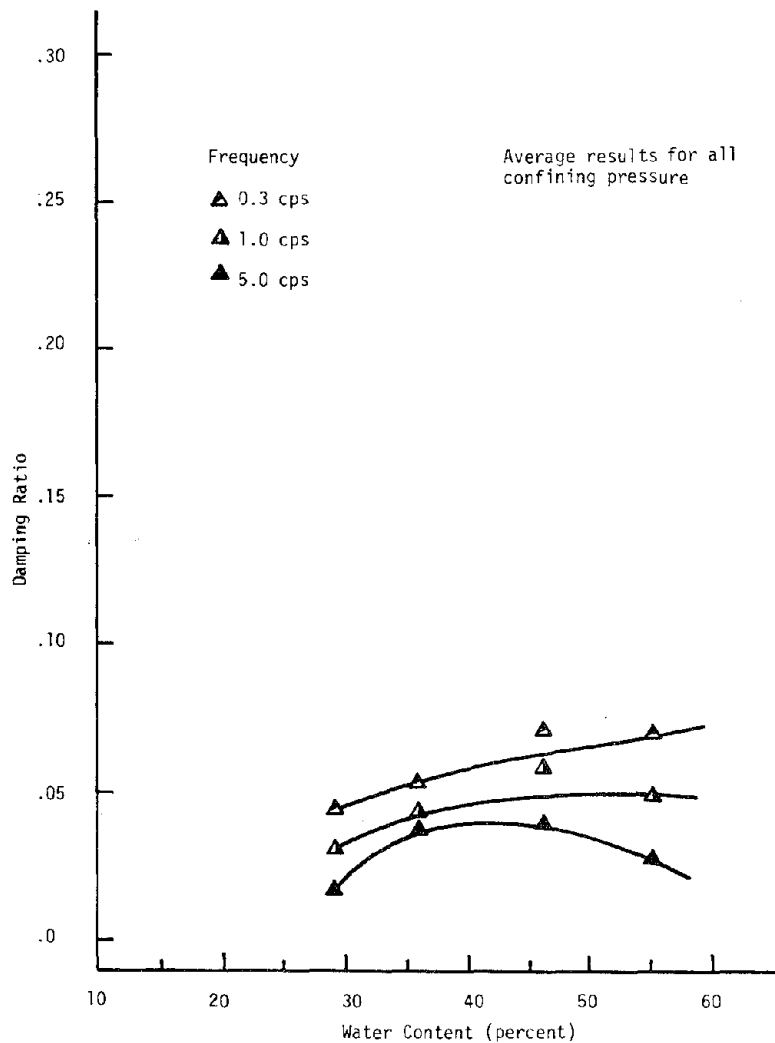


Figure 5.55 DAMPING RATIO VERSUS WATER CONTENT FOR 0-CLAY AT -1°C AND AN AXIAL STRAIN OF $3.16 \times 10^{-3}\%$

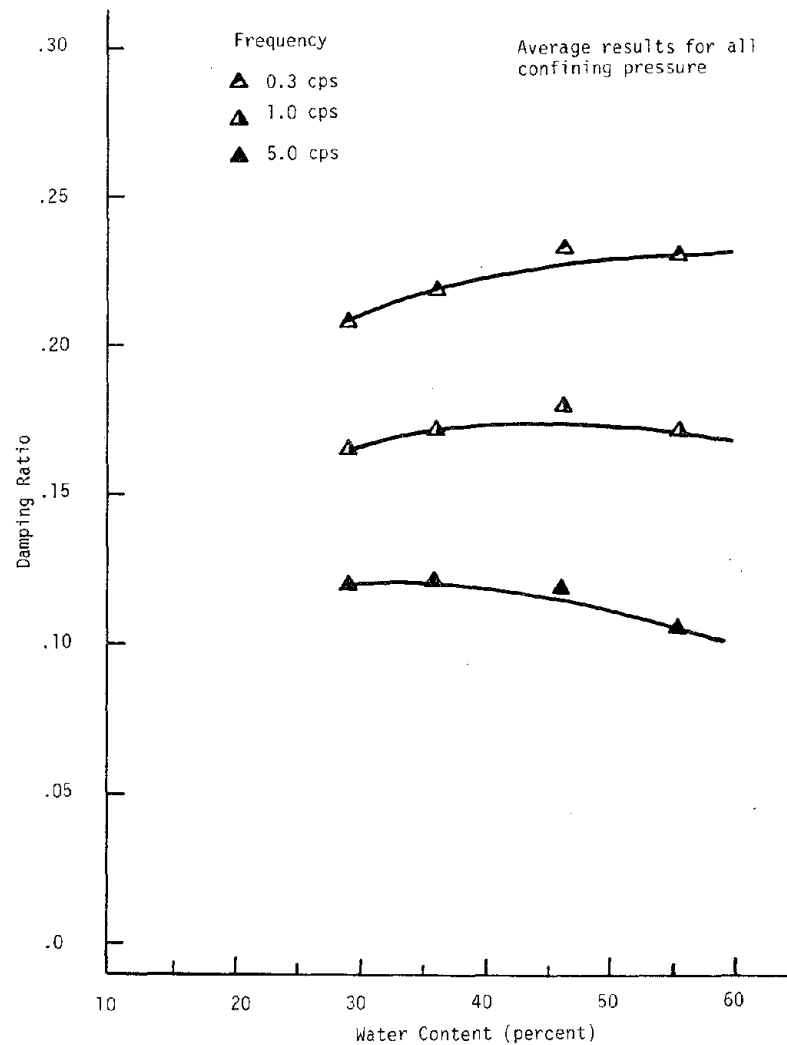


Figure 5.56 DAMPING RATIO VERSUS WATER CONTENT FOR 0-CLAY AT -1°C AND AN AXIAL STRAIN OF $1.0 \times 10^{-1}\%$

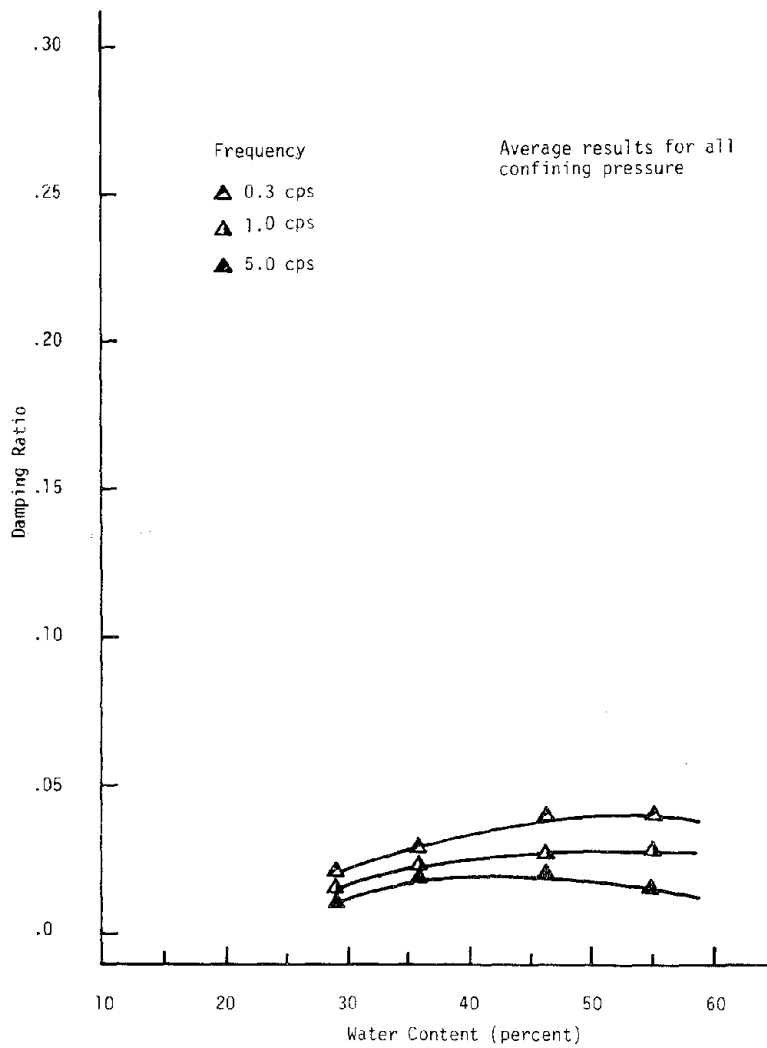


Figure 5.57 DAMPING RATIO VERSUS WATER CONTENT FOR O-CLAY AT -4°C AND AN AXIAL STRAIN OF 3.16×10^{-3} .

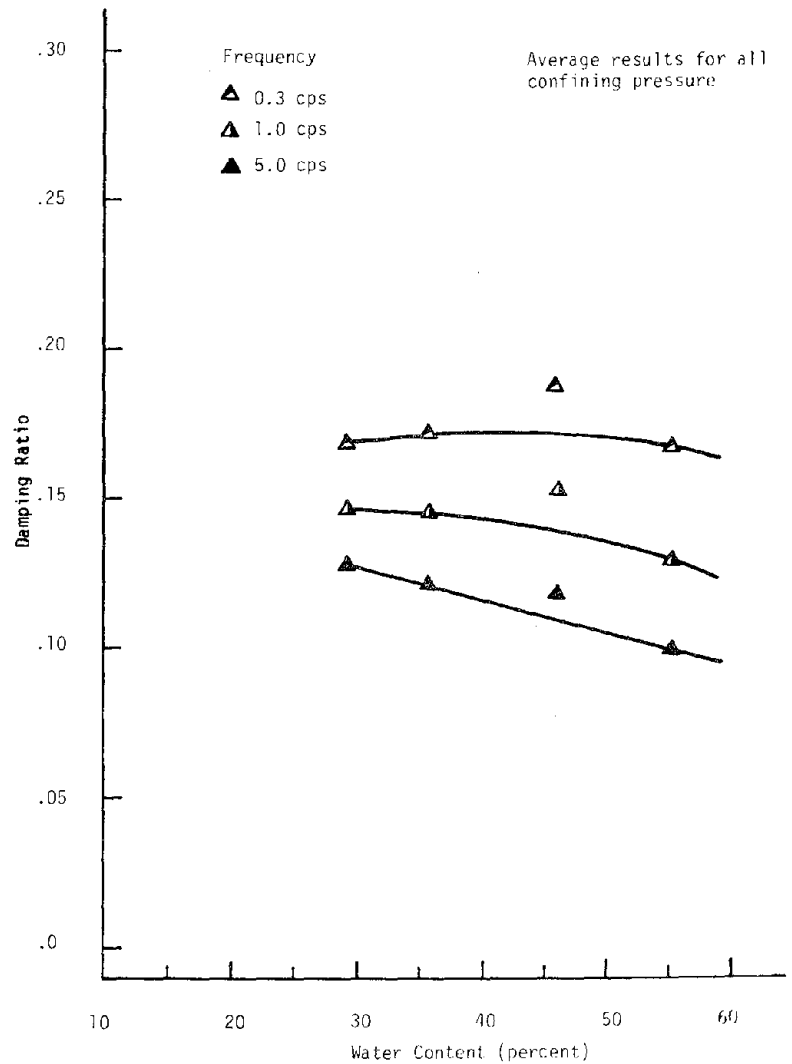


Figure 5.58 DAMPING RATIO VERSUS WATER CONTENT FOR O-CLAY AT -4°C AND AN AXIAL STRAIN OF 1.0×10^{-1} .

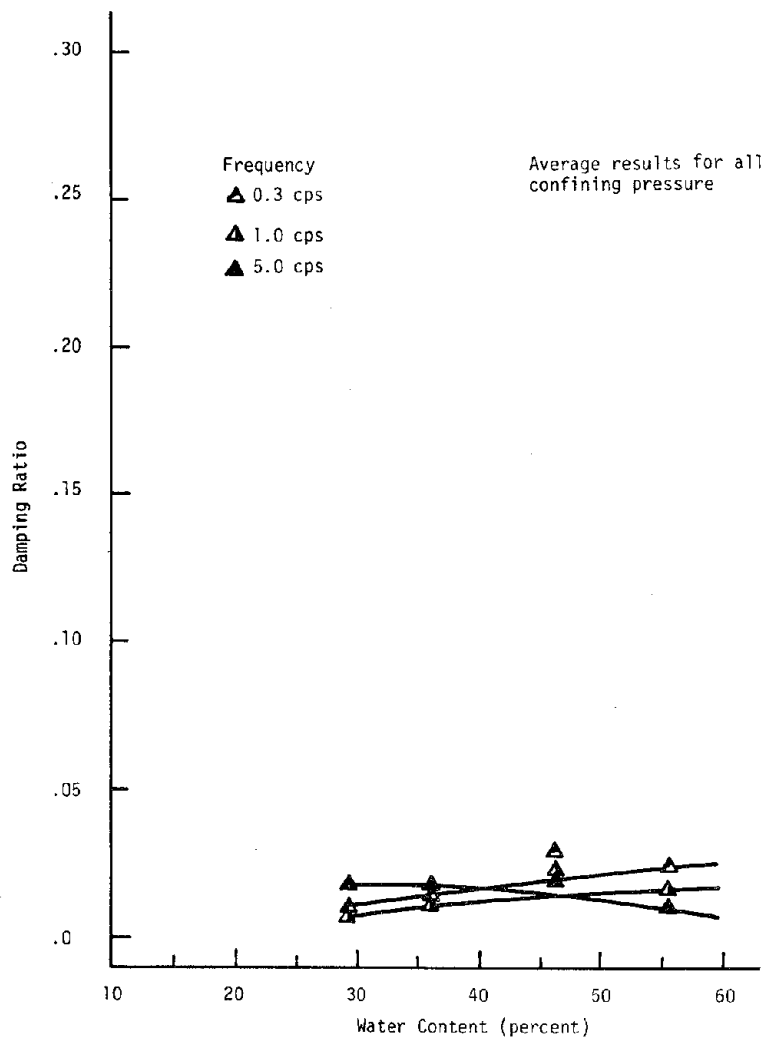


Figure 5.59 DAMPING RATIO VERSUS WATER CONTENT FOR O-CLAY AT -10°C AND AN AXIAL STRAIN OF $3.16 \times 10^{-3}\%$

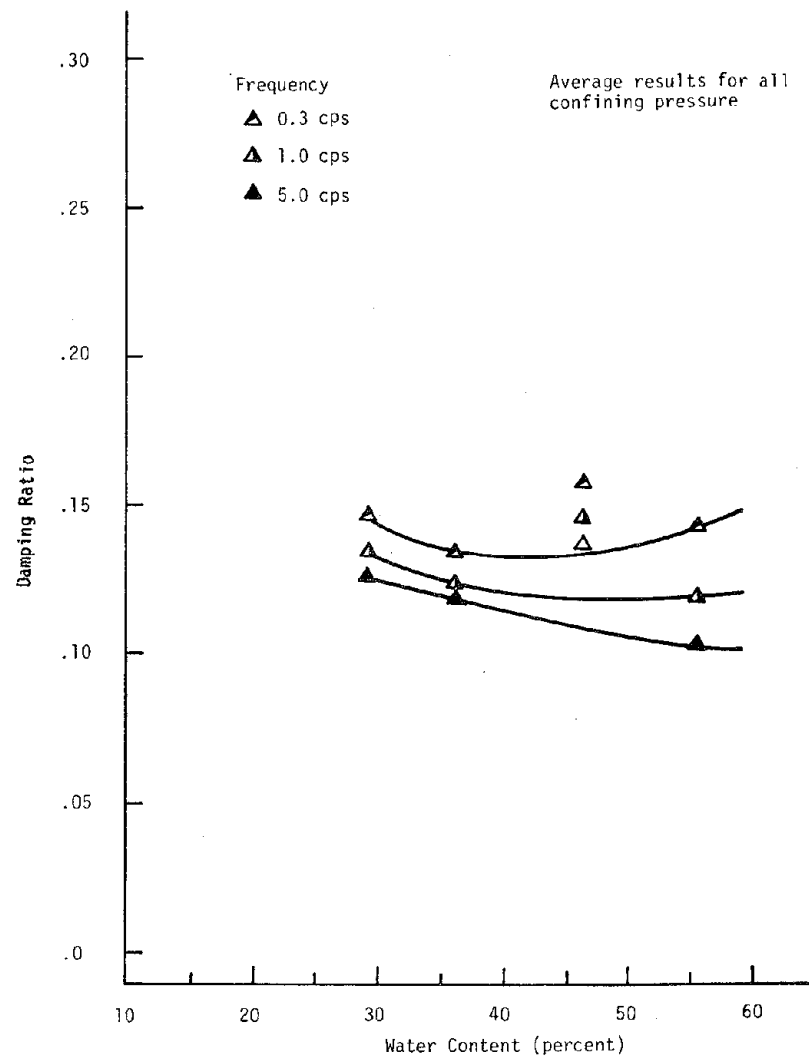


Figure 5.60 DAMPING RATIO VERSUS WATER CONTENT FOR O-CLAY AT -10°C AND AN AXIAL STRAIN OF $1.0 \times 10^{-1}\%$

- (3) At a temperature of -4°C and a strain amplitude of $3.16 \times 10^{-3}\%$, damping ratio increases slightly for an increase in water content from 29.2 to 55.1% for all test frequencies.
- (4) At a temperature of -4°C and a strain amplitude of $1.0 \times 10^{-1}\%$, damping ratio appears to decrease for an increase in water content from 29.2 to 55.1% for all test frequencies.
- (5) At a temperature of -10°C and a strain amplitude of $3.16 \times 10^{-3}\%$, damping ratio increases slightly for an increase in water content from 29.2 to 55.1% for frequencies of 0.3 and 1.0; but for a frequency of 5.0 cps, damping ratio decreases slightly with increasing water content.
- (6) At a temperature of -10°C and a strain amplitude of $1.0 \times 10^{-1}\%$, damping ratio decreases slightly for an increase in water content from 29.2 to 55.1% for frequencies of 1.0 and 5.0 cps; but for a frequency of 0.3 cps, damping ratio decreases for an increase in water content from 29.2 to 40% and increases for an increase in water content from 40 to 55.1%.

At a temperature of -10°C , the data points at a water content of 46.3% deviate from the others. The sample associated with these results was disturbed, as described in Section 5.4.4.

5.5.5 Effect of Specific Surface Area

The relationship between damping ratio and temperature for 0-clay and M + 0-clay at a water content of 57.2% is shown in Figure 5.61 for a strain amplitude of $3.16 \times 10^{-3}\%$ and Figure 5.62 for a strain amplitude of $1.0 \times 10^{-1}\%$. The relationship is plotted at three frequencies (0.3, 1.0 and 5.0 cps).

At a strain amplitude of $3.16 \times 10^{-3}\%$, the damping ratio of M + 0-clay is greater than that of 0-clay by approximately 0.015. The magnitude of the difference between damping ratio of the two clays does not appear to be affected by temperature.

At a strain amplitude of $1.0 \times 10^{-1}\%$, and frequencies of 0.3 and 1.0 cps, damping ratio of M + 0-clay is greater than that of 0-clay for the temperature range -1 to -5°C ; for the temperature range -5 to -10°C , the damping ratio of M + 0-clay is smaller than that of 0-clay. At a frequency of 5.0 cps, the damping ratio of M + 0-clay is smaller than that of 0-clay for all test temperatures.

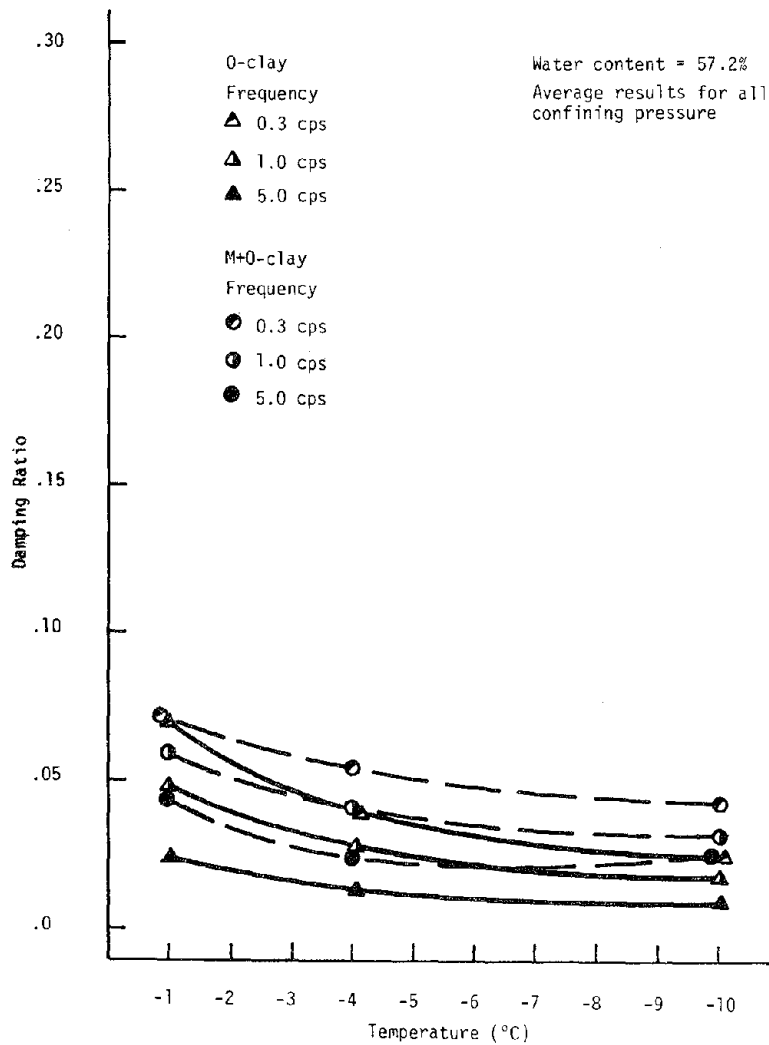


Figure 5.61 DAMPING RATIO VERSUS TEMPERATURE FOR O-CLAY AND M+O-CLAY AT AN AXIAL STRAIN OF $3.16 \times 10^{-3}\%$

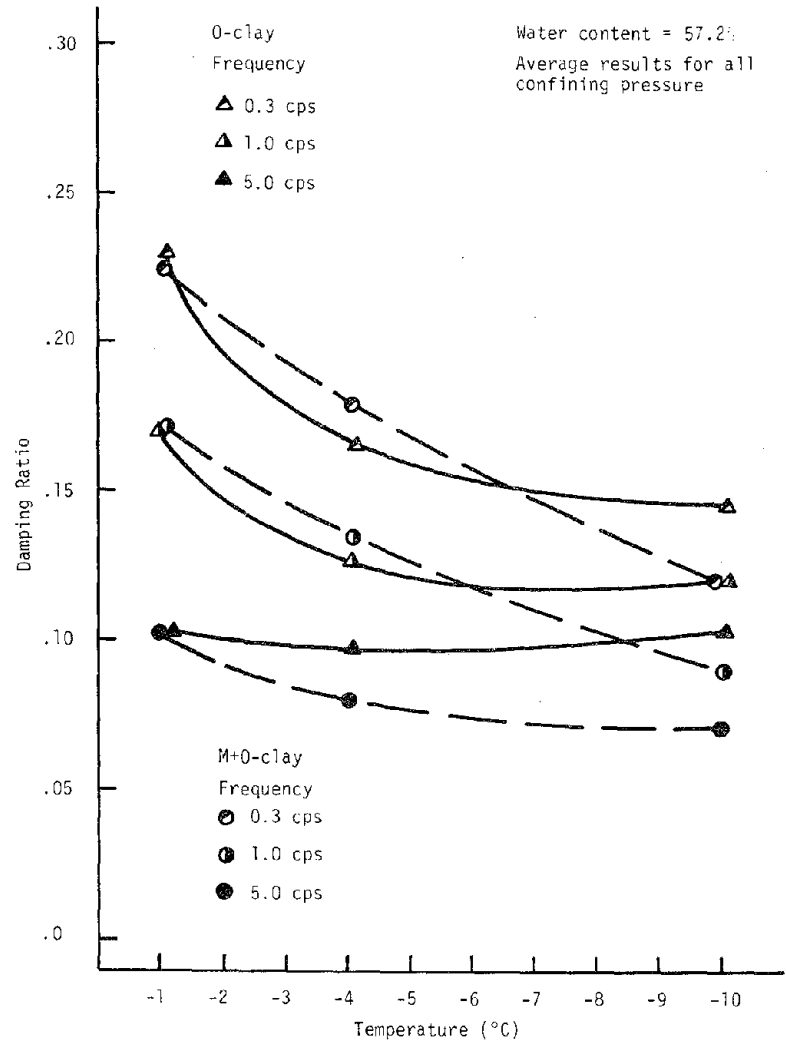


Figure 5.62 DAMPING RATIO VERSUS TEMPERATURE FOR O-CLAY AND M+O-CLAY AT AN AXIAL STRAIN OF $1.0 \times 10^{-1}\%$

CHAPTER 6
COMPARISONS OF DYNAMIC PROPERTIES
OF ICE AND FROZEN CLAY

6.1 General

This chapter presents a comparison of the dynamic properties of ice and frozen clay obtained in previous studies to those of the present study. The longitudinal and compression wave velocity and damping ratio appear to be the most convenient terms to use as a basis for comparison of the results from previous studies to those of the present study. This is a consequence of the fact that:

- (1) Longitudinal and compression wave velocities have generally been reported in previous studies.
- (2) The physical and geometrical characteristics of the test specimens are known in the present study that allow a conversion to longitudinal wave velocity to be made whereas they are unknown in several of the previous studies and, hence, would not allow a conversion of the results to dynamic Young's modulus. (The compression wave velocity can be calculated from the longitudinal wave velocity after assuming a value of Poisson's ratio.)
- (3) The damping ratio is easily calculated from the results reported in previous studies. (Conversion equations between damping terms are given in Table 2.1.)

The longitudinal wave velocity, V_L , was calculated from the results of the present study using:

$$V_L = \sqrt{\frac{E_d}{\rho}} \quad (6.1)$$

in which

E_d = dynamic Young's modulus

ρ = material density

This equation was employed to calculate the longitudinal wave velocity in the cylindrical specimens of the present study because the length of the specimen is much shorter than the wavelength of the compression wave which propagated from the top cap to the bottom cap during cyclic loading.

Poisson's ratio was not determined for the ice and frozen clay samples tested in the research program. However, based on the values reported in Section 2.7.1 and 2.7.2, reasonable values of Poisson's ratio

for the materials tested in the research program are as follows:

$$\mu_{\text{ice}} = 0.35$$

$$\mu_{\text{frozen clay}} = 0.40$$

The compression wave velocity, V_p , may be computed from the longitudinal wave velocity using:

$$V_p = V_L \sqrt{\frac{(1 - \mu)}{(1 + \mu)(1 - 2\mu)}} \quad (6.2)$$

Then, given the values of Poisson's ratio assumed above, the relationship between longitudinal and compression wave velocity is

$$V_{\text{ice}} = (1.27) V_{L \text{ ice}} \quad (6.3)$$

$$V_{\text{clay}} = (1.46) V_{L \text{ frozen clay}} \quad (6.4)$$

6.2 Comparison of Dynamic Properties of Ice

6.2.1 Longitudinal and Compression Wave Velocity

Figure 6.1 presents the results of the present study at two confining pressures and two frequencies as a function of temperature, together with the results from previous studies. It can be seen in this figure that the longitudinal wave velocity of the present study is between 2.0 to 2.5 km/sec (depending on confining pressure and frequency); and the compression wave velocity is between 2.5 to 3.2 km/sec. The longitudinal wave velocity from previous laboratory studies [see Figure 2.10, after Kaplar (1969)] is approximately 3.1 km/sec; the compression wave velocity from seismic and ultrasonic methods [see Figure 2.6, after Roethlisberger (1972)] is approximately 3.7 km/sec. Overall it appears there is a favorable comparison. The difference between the results shown may be attributed to differences in the test techniques used to measure the dynamic properties. The differences in the test techniques and their influence on the comparison of wave velocities are as follows:

- (1) Strain amplitude - the strain amplitude of the present study ($4.4 \times 10^{-3}\%$) is greater than for the resonant frequency procedure (approximately 10^{-6} to $10^{-3}\%$) or the geophysical and ultrasonic procedures (approximately 10^{-7} to $10^{-4}\%$). It was found in the present study that the elastic modulus of ice decreases slightly with increasing strain amplitude. Therefore, the wave velocities of the present study should be lower than the results asso-

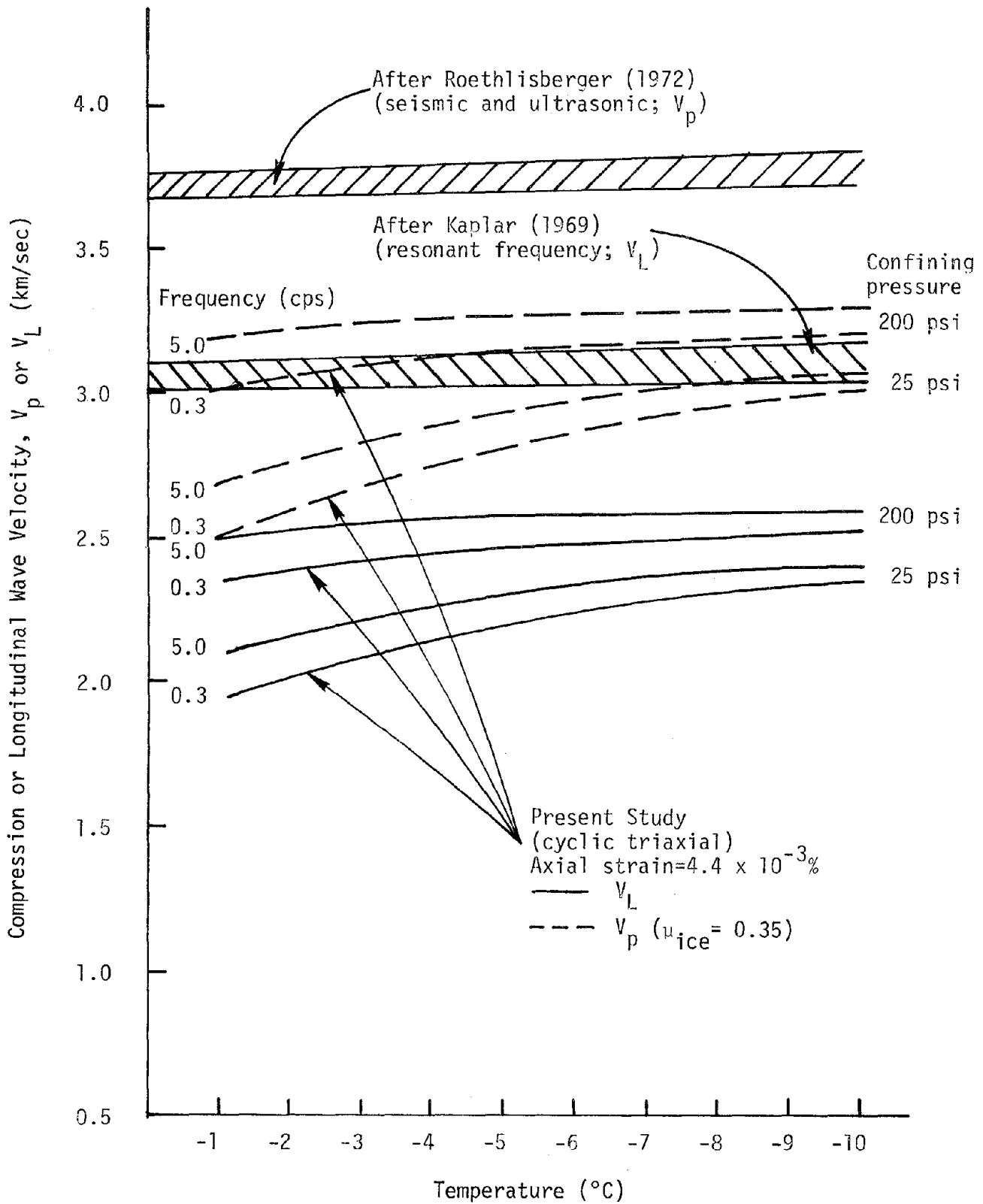


Figure 6.1 WAVE VELOCITY VERSUS TEMPERATURE OF ICE

ciated with resonant frequency, geophysical or ultrasonic procedures.

- (2) Frequency - the test frequencies in the present study (0.05, 0.3, 1.0, 5.0 Hz) are much lower than for the resonant frequency procedure (approximately 1 to 10 kHz), seismic procedure (approximately 150 Hz), or ultrasonic procedure (approximately 50 to 1000 kHz). The present study indicates that the dynamic Young's modulus of ice increases with increasing frequency in the range of frequency from 0.05 to 5 Hz. Smith (1969) reports that the modulus increases with frequency in a very high range of frequency, 800 to 2800 Hz (see Figure 2.15). Therefore, the lower values of wave velocities obtained in the present study compared to those obtained by previous researchers seem reasonable owing to the lower frequency of testing in the present study.

It can be seen from Figure 6.1 that the influence of temperature on the longitudinal or compression wave velocity was found to be greater in the present study than in previous studies particularly near the melting point. This may be a consequence of the fact that the influence of temperature decreases with increasing frequency (based on results of the present study) and all of the previous studies are at much higher frequencies than the present study.

Figure 6.2 shows the relationship between wave velocity at -10°C and density obtained in the present study compared to the results obtained by Bennett (1972; see Figure 2.12) and Roethlisberger (1972; see Figure 2.11) at -16°C . The results of the present study are lower than those from previous researchers owing to the reasons given above and, in addition, to the difference in the test temperature of the relationships shown. All of the results indicate an increase in compression wave velocity with density. The rate of increase from the present study is not as steep as the rate of increase obtained in previous studies.

6.2.2 Damping Ratio

Figure 6.3 shows the relationship between damping ratio and temperature obtained in the present study and the relationship obtained by Stevens (1975; see Figure 2.19). Ignoring the relationship at 0.05 cps obtained in the present study, the comparison appears to be extremely favorable. The damping ratios from the present study, at frequencies of

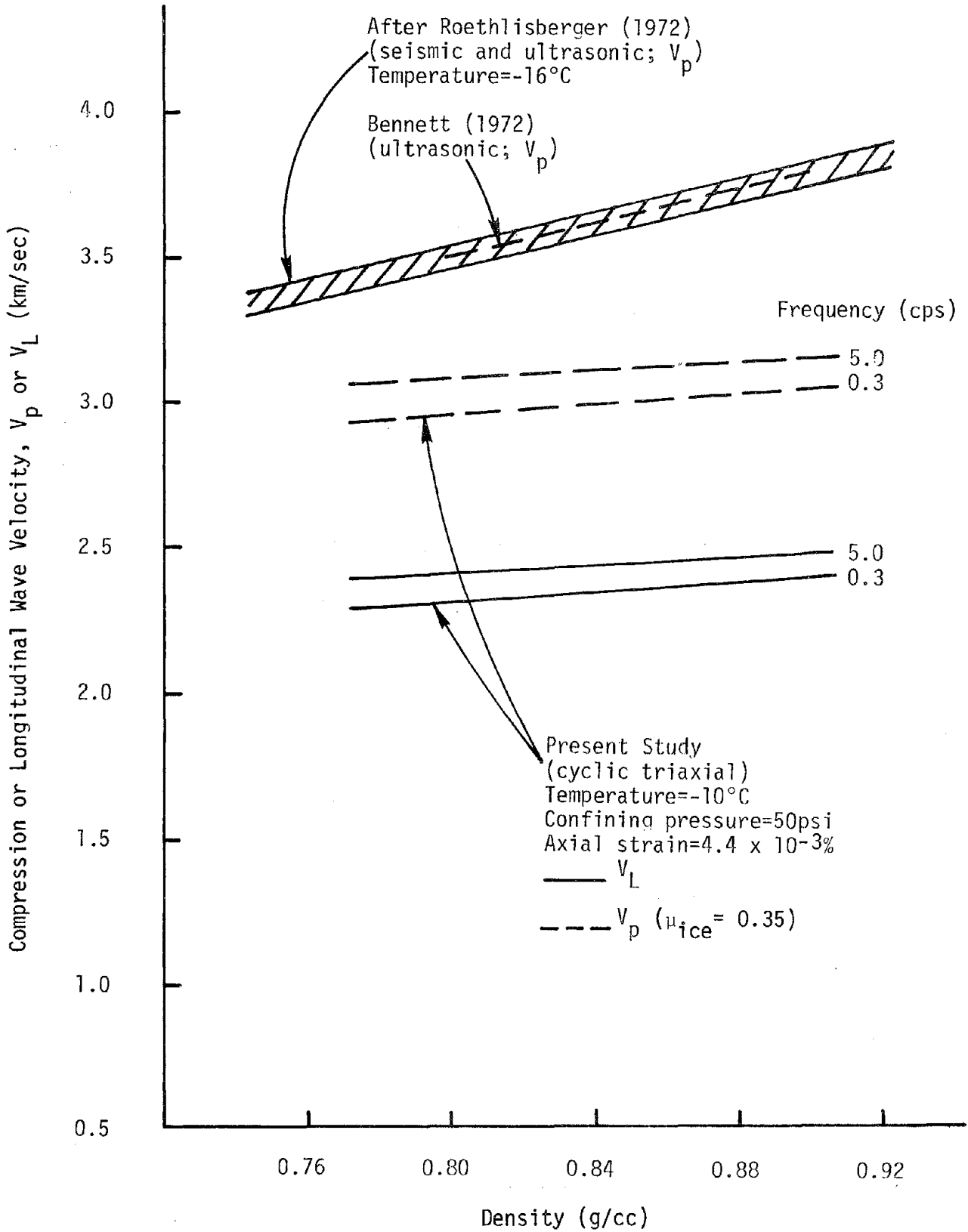


Figure 6.2 WAVE VELOCITY VERSUS DENSITY OF ICE

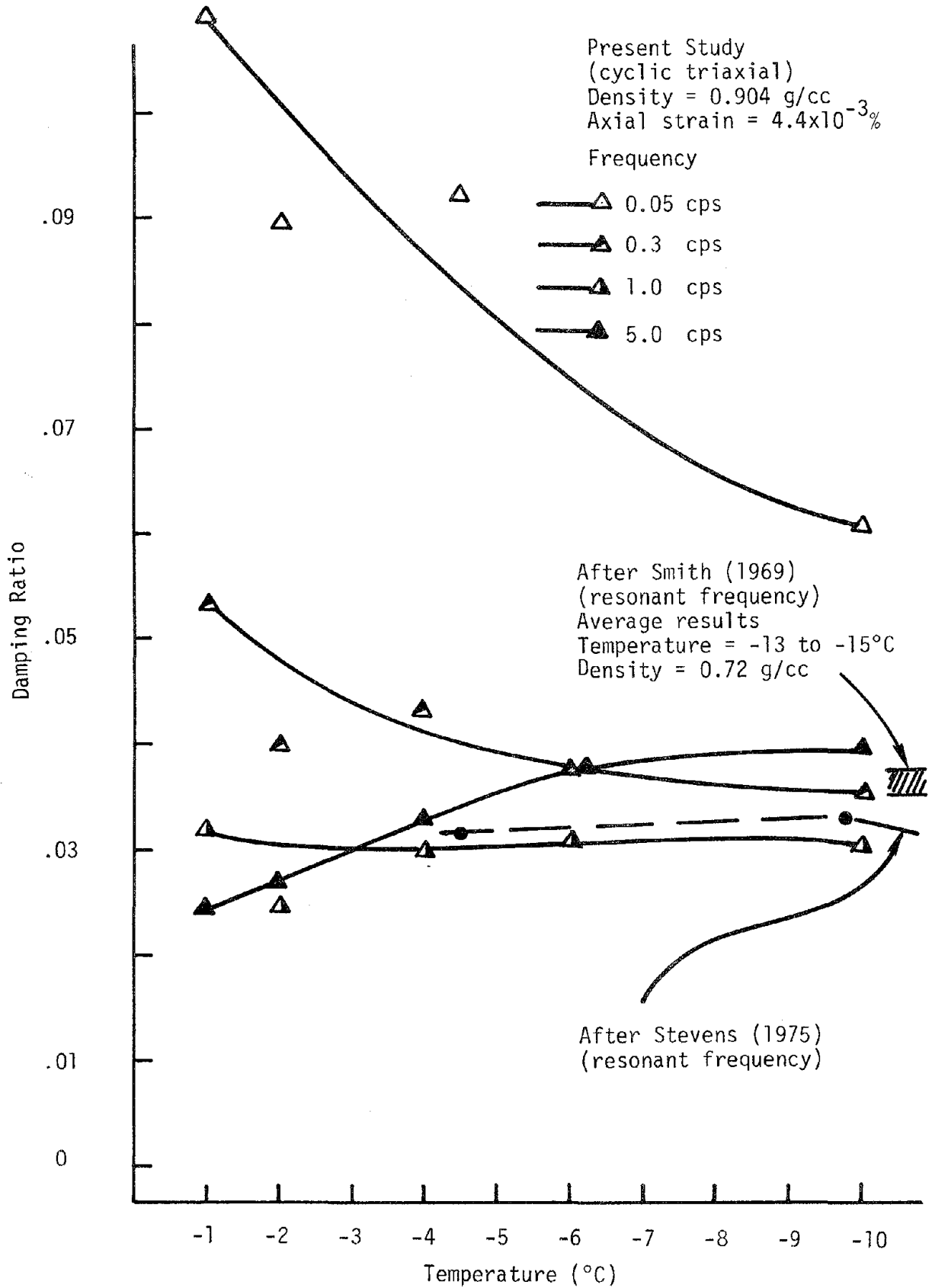


Figure 6.3 DAMPING RATIO VERSUS TEMPERATURE OF ICE

0.3, 1.0 and 5.0 cps, are in the range 0.023 to 0.045 (with the exception of one point at 0.3 cps and -1°C). The damping ratios obtained by Stevens are approximately 0.033. The average of the damping ratios obtained from resonant frequency tests by Smith (1969; see Figure 2.17) for ice at temperatures from -13 to -15°C is approximately 0.036. The damping ratio of the present study in the frequency range 0.3 to 5.0 cps is close to the values obtained from both of the resonant frequency studies. The close comparison may be explained by a consideration of the strain amplitudes and frequencies of the different test procedures as follows:

- (1) Strain amplitude - the strain amplitude of the present study ($4.4 \times 10^{-3}\%$) is greater than that associated with resonant frequency procedures. It was found in the present study that the damping ratio of ice decreases slightly with decreasing strain amplitude. Therefore, the damping ratios obtained in the resonant frequency studies should be smaller than those for the present study.
- (2) Frequency - the frequencies associated with resonant frequency tests are much greater than for the present study. The present study indicates that the damping ratio of ice increases with increasing frequency in the range 1.0 to 5.0 cps. If the increase in damping ratio with increasing frequency is valid up to frequencies of the resonant frequency tests, the damping ratio obtained from the resonant frequency tests should be greater than those of the present study.

Therefore, the combination of the decrease of damping ratio with decreasing strain amplitude and the increase of damping ratio with increasing frequency has apparently caused the damping ratios from the present study to be close to those of previous studies, i.e., the effects of strain amplitude and frequency tend to cancel each other.

6.3 Comparison of Dynamic Properties of Frozen Clay

6.3.1 Longitudinal and Compression Wave Velocity

Figure 6.4 shows the relationship between the longitudinal wave velocity of frozen O and M + O-clay and temperature obtained in the present study and the results from previous studies. The differences in the test techniques and material types and their influence on the comparison

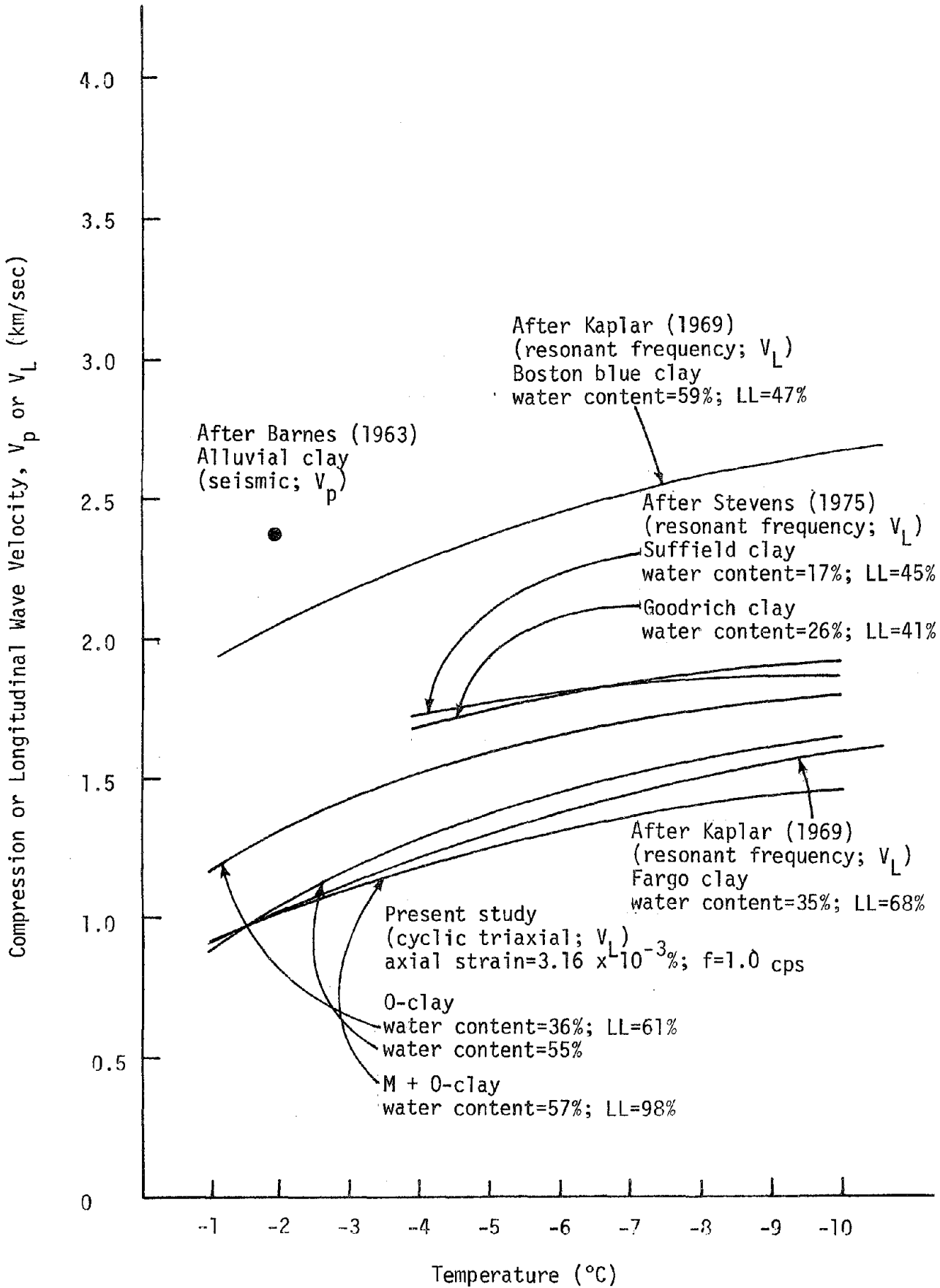


Figure 6.4 WAVE VELOCITY VERSUS TEMPERATURE OF FROZEN CLAY

of wave velocities are as follows:

- (1) Strain amplitude - the strain amplitude for the present study is greater than for the resonant frequency tests. It was found in the present study that the dynamic elastic modulus of frozen clay decreases with increasing strain amplitude for strain amplitudes greater than $3.16 \times 10^{-3}\%$. For strain amplitudes less than $3.16 \times 10^{-3}\%$ it is felt that there is no change in dynamic elastic properties with strain amplitude. Since the results of the present study presented in Figure 6.4 are for a strain amplitude of $3.16 \times 10^{-3}\%$ the difference in the wave velocity associated with differences in the strain amplitudes of testing should be negligible.
- (2) Frequency - the frequencies associated with resonant frequency tests are much greater than for the present study. The results of the present study indicate that the dynamic elastic modulus of frozen clay increases with increasing frequency. Therefore, the wave velocities obtained in the present study should be lower than those presented in previous studies.
- (3) Specific surface area - in the present study it was found that the dynamic elastic properties decreased with increasing specific surface area. Specific surface areas of the clays from the previous studies are not reported, however, liquid limits of the clays are available. The liquid limit is associated with specific surface area; the higher the liquid limit the higher the specific surface area. The liquid limits of the Boston blue clay (47%), Suffield clay (45%), and Goodrich clay (41%) are lower than the liquid limits of the O-clay (61%) or M + O-clay (98%) of the present study. The liquid limit of the Fargo clay (68%) is greater than the liquid limit of the O-clay but less than the liquid limit of the M + O-clay. Based on the liquid limits (and inferred specific surface areas) the relative position of the wave velocity versus temperature relationships from previous studies to those of the present study appear to be reasonable, i.e., at a given temperature the Boston blue clay, Suffield clay, and Goodrich clay should have higher wave velocities than the O-clay and M + O-clay owing to their lower (inferred)

specific surface areas; the Fargo clay should be intermediate to the O-clay and M + O-clay owing to its intermediate (inferred) specific surface area.

- (4) Water content - the results of the present study indicate the dynamic elastic properties increase with increasing water content. The water content of the Boston blue clay (59%), O-clay (55%), and M + O-clay (57%) are close and, therefore, should not influence their relative positions. The water content of the Suffield clay (17%) and the Goodrich clay (26%) are lower than the water contents of the O-clay (36%, 55%) and M + O-clay (57%) tested in the present study. Based on this they should have lower wave velocities than those associated with the O-clay. However, as mentioned above, their (inferred) specific surface areas are also lower and, therefore, their wave velocities should be greater. Apparently, the specific surface area has the greatest influence.

The compression wave velocity for the alluvial clay at -2°C reported by Barnes (1963) is higher than the longitudinal wave velocities found in the present study and the longitudinal wave velocities found by Kaplar (1969) and Stevens (1975). As shown in Section 6.1 the compression wave velocity should be higher than the longitudinal wave velocity. There is not sufficient information available on the alluvial clay to explain the difference shown in Figure 6.1 to any greater degree.

Overall, the values of wave velocities obtained in the present study compared to those obtained in previous studies appear to be very reasonable.

6.3.2 Damping Ratio

Figure 6.5 shows the relationships between damping ratio and temperature obtained in the present study and the relationships from resonant frequency tests conducted by Stevens (1975). The damping ratios obtained by Stevens at a frequency of 5 kHz in the temperature range -4 to -10°C are approximately 0.06 for the Suffield clay and 0.05 for the Goodrich clay. Those obtained in the present study in the same temperature range at a frequency of 1.0 cps are approximately 0.025. The difference in the test techniques and material types and their influence on the comparison

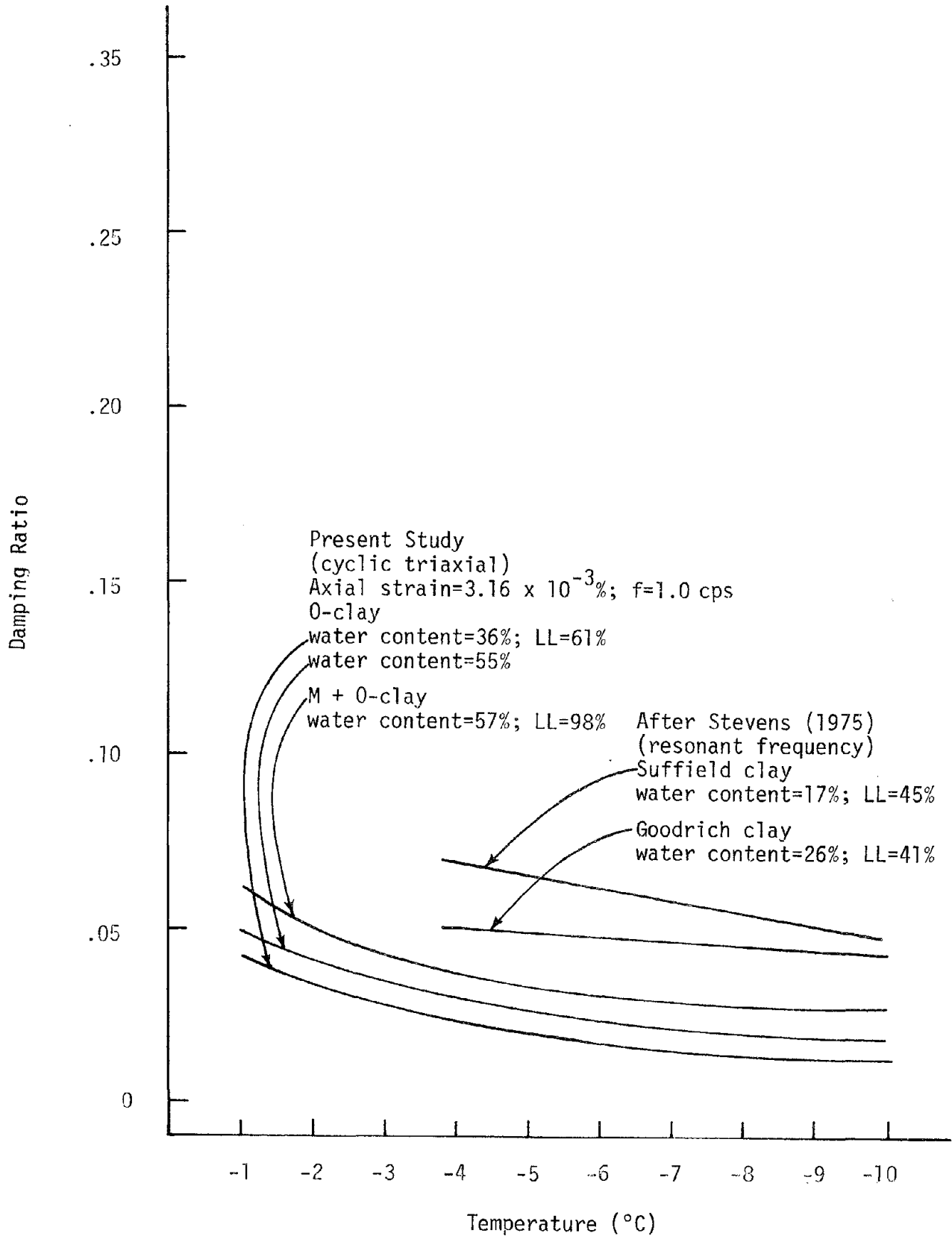


Figure 6.5 DAMPING RATIO VERSUS TEMPERATURE OF FROZEN CLAY

of damping ratio is as follows:

- (1) Strain amplitude - the strain amplitude for the present study is greater than for the resonant frequency test. It was found in the present study that the damping ratio of frozen clay increases with increasing strain amplitude for strain amplitudes greater than $3.16 \times 10^{-3}\%$. For strain amplitudes less than $3.16 \times 10^{-3}\%$ it is felt that there is no change in damping ratio with strain amplitude. Since the results of the present study presented in Figure 6.5 are for a strain amplitude of $3.16 \times 10^{-3}\%$ the difference in damping ratio associated with differences in the strain amplitudes of testing should be negligible.
- (2) Frequency - the frequencies associated with resonant frequency tests are much greater than for the present study. It was found in the present study that the damping ratio decreases with increasing frequency in the range 0.05 to 5.0 cps and increases for frequencies greater than 5.0 cps (based on limited test results). Stevens (1975) has found that the damping ratio of Goodrich clay decreases slightly with increasing frequency in the 1 to 10 kHz range whereas the damping ratio of Suffield clay does not change appreciably. The results from the present study and Steven's study appear to be somewhat contradictory and do not clarify the relative position of the relationship shown in Figure 6.5.
- (3) Specific surface area - based on the results from the present study, at a strain amplitude of $3.16 \times 10^{-3}\%$, the higher the specific surface area the higher the value of damping ratio. Suffield and Goodrich clay both have lower liquid limits (and inferred specific surface areas) than the clays tested in the present study. Consequently, they should have lower values of damping ratio than the clays tested in the present study.
- (4) Water content - based on the results from the present study there appears to be no well-defined relationship between damping ratio and water content of frozen clay.

Overall, it is felt that a complete explanation of the relative position of the relationships shown in Figure 6.5 is not possible at this time. It should be noted however, that the values of damping ratio obtained in the present study appear to be very reasonable when compared to results from Stevens' work.

CHAPTER 7

SUMMARY AND CONCLUSIONS

Cyclic triaxial tests were performed on laboratory prepared samples of ice and frozen clay and dynamic Young's moduli and damping ratios were determined. The test results may be summarized as follows:

1. Values of dynamic Young's modulus of ice for the densities of ice considered (0.77 and 0.904 g/cc) and range of strain amplitude (3×10^{-3} to $2 \times 10^{-2}\%$), temperature (-1 to -10°C), frequency (0.05 to 5 cps) and confining pressure (0 to 200 psi) associated with the test program were from 260×10^3 to 900×10^3 psi; values of damping ratio were from 0.001 to 0.14.
2. In the order of their importance the influences of the various parameters on the dynamic Young's modulus of ice are:
 - a. Confining pressure - the dynamic Young's modulus of ice increases with increasing confining pressure (1) gradually from 0 to 25 psi (approximately 8%) for high density ice and steeply (approximately 14%) for low density ice, (2) steeply from 25 to 50 psi (approximately 20%) for high density ice and slightly for low density ice, (3) gradually from 50 to 100 psi for both ice densities, and (4) only slightly from 100 to 200 psi for high density ice. (Note: no test was conducted at 200 psi for low density ice.) Temperature, frequency and strain amplitude do not appear to have a significant influence on the relationship between dynamic Young's modulus and confining pressure.
 - b. Density - the dynamic Young's modulus increases approximately 60% as density increases from 0.77 to 0.904 g/cc. Temperature, frequency, strain amplitude and confining pressure do not appear to have a significant influence on the relationship.
 - c. Frequency - the dynamic Young's modulus of ice increases steeply for an increase in frequency from 0.05 to 0.3 cps. Between 0.3 and 5.0 cps the rate of increase is, in general, not as steep. The increase of dynamic Young's modulus with frequency appears to be greater for higher temperatures (-1°C) than for low temperatures (-10°C). Confining pres-

- sure, strain amplitude and density do not appear to have an influence on the relationship between dynamic Young's modulus and frequency.
- d. Temperature - the dynamic Young's modulus of high density ice increases with decreasing temperature. At a confining pressure of 25 psi the modulus increases approximately 20% for a temperature decrease from -1 to -4°C. It also increases approximately 20% for a temperature decrease from -4 to -10°C. The rate of increase at low confining pressures is slightly greater than at high confining pressures. The influence of temperature for low density ice appears to be greater than for high density ice. The dynamic Young's modulus increases approximately 35% for an increase in temperature from -1 to -4°C and approximately 20% for an increase in temperature from -4 to -10°C. The frequency of testing and strain amplitude appear to have no significant influence on the relationship between dynamic Young's modulus and temperature.
 - e. Strain amplitude - the dynamic Young's modulus of ice decreases only slightly with increasing strain amplitude over the strain range 3×10^{-3} to 2×10^{-2} %. Strain amplitude apparently has no influence on the dynamic Young's modulus of low density ice. The relationship is apparently not influenced by frequency, temperature, or confining pressure.
3. There appears to be no well-defined relationship between damping ratio of ice and confining pressure or density. The influence of other parameters on the damping ratio of ice is, in the order of their importance:
 - a. Frequency - in general, damping ratio decreases as frequency increases from 0.05 to 1.0 cps and increases as frequency increases from 1.0 to 5.0 cps. The degree to which the damping ratio follows these trends, however, appears to be dependent on temperature.
 - b. Temperature - the damping ratio of ice tends to decrease with decreasing temperature. At a frequency of 0.05 cps, the rate of decrease is most pronounced; the damping ratio decreases from 0.11 to 0.06 as temperature decreases from -1 to -10°C. The influence of temperature is small for

the frequency range 0.3 to 5.0 cps. The difference between damping ratios for temperatures in the range -1 to -4°C is greater than for temperatures in the range -4 to -10°C .

- c. Strain amplitude - the damping ratio of high density ice increases approximately 20% over the strain range 3×10^{-3} to $2 \times 10^{-2}\%$. Strain amplitude apparently has no influence on the damping ratio of low density ice. The relationship is apparently not influenced by other parameters.
4. Values of dynamic Young's modulus of frozen clay for the two clays considered (specific surface areas of 215 and $475 \text{ m}^2/\text{g}$), and range of water content (29.2 to 57.2%), strain amplitude (3×10^{-3} to $1 \times 10^{-1}\%$), temperature (-1 to -10°C), frequency (0.05 to 5 cps), and confining pressure (0 to 200 psi) associated with the test program were from 90×10^3 to 880×10^3 psi; values of damping ratio were from 0.02 to 0.30.
 5. In the order of their importance the influences of the various parameters on the dynamic Young's modulus of frozen clay are:
 - a. Strain amplitude - the dynamic Young's modulus of frozen clay decreases with increasing strain amplitude. The influence of strain amplitude at the lowest temperature (-10°C) is greater than at the highest temperature (-1°C). At the lowest temperature (-10°C) the modulus decreases steeply (approximately 55%) for an increase in strain amplitude from 2×10^{-2} to $6 \times 10^{-2}\%$. For strain amplitudes in the range 3.16×10^{-3} to $2 \times 10^{-2}\%$ and 6×10^{-2} to $1.0 \times 10^{-1}\%$ the rate of decrease is, in general, small. At the highest temperature (-1°C) there is a gradual decrease in modulus over the entire range of strain amplitudes. The influence of strain amplitude for O-clay appears to be greater than for M + O-clay. The relationship is apparently not influenced by frequency and water content.
 - b. Temperature - the dynamic Young's modulus increases significantly with decreasing temperature. The rate of increase is greater for a low strain amplitude ($3.16 \times 10^{-3}\%$) than for a high strain amplitude ($1.0 \times 10^{-1}\%$).

At a strain amplitude of $3.16 \times 10^{-3}\%$, the dynamic Young's modulus increases steeply from approximately 200×10^3 to 700×10^3 psi for a temperature decrease from -1 to -10°C . At a strain amplitude of $1.0 \times 10^{-1}\%$, the dynamic Young's modulus increases gradually from approximately 80×10^3 to 250×10^3 psi for a temperature decrease from -1 to -10°C . At a low strain amplitude ($3.16 \times 10^{-3}\%$), the influence of temperature for clay at a high specific surface area ($475 \text{ m}^2/\text{g}$) is smaller than for clay at a low specific surface area ($215 \text{ m}^2/\text{g}$); at a high strain amplitude ($1.0 \times 10^{-2}\%$), the relationship is apparently not influenced by specific surface area. Frequency appears to have no influence on the relationship. The influence of water content on the relationship has not been investigated.

- c. Water content - the dynamic Young's modulus increases with increasing water content. The rate of increase is greater at lower strain amplitudes than at higher strain amplitudes. Temperature and frequency do not appear to have a significant influence on the relationship.
- d. Specific surface area - the lower the specific surface area the higher the dynamic Young's modulus. The difference between the dynamic Young's modulus for O-clay and M + O-clay with different specific surface areas is greater for high strain amplitudes than for low strain amplitudes. At a low strain amplitude ($3.16 \times 10^{-3}\%$), the influence of specific surface area at a low temperature (-10°C) is greater than at a high temperature (-1°C); at a high strain amplitude ($1.0 \times 10^{-2}\%$), temperature does not appear to have a significant influence on the relationship. The relationship is apparently not influenced by frequency.
- e. Frequency - the dynamic Young's modulus of frozen clay, in general, increases slightly for an increase in frequency from 0.05 to 5.0 cps. The rate of increase is almost constant over the range of frequency. (The results from one test indicate the modulus continues to increase only

slightly up to 50 cps.) Strain amplitude, temperature, water content and specific surface area do not appear to have a significant influence on the relationship.

- f. Confining pressure - confining pressure does not appear to affect the dynamic Young's modulus of frozen clay. This conclusion was reached for all test conditions considered.
6. In the order of their importance the influences of the various parameters on the damping ratio of frozen clay are:
 - a. Strain amplitude - the damping ratio of frozen clay increases with increasing strain amplitude. At a strain amplitude of $3.16 \times 10^{-3}\%$, the rate of increase is small; at a strain amplitude of $1.0 \times 10^{-1}\%$, the rate of increase is great. The damping ratio varies from about 0.02 to 0.3 as strain amplitude increases from 3.16×10^{-3} to $1.0 \times 10^{-1}\%$. The relationship is apparently not influenced by frequency, temperature, water content, or specific surface area.
 - b. Temperature - the damping ratio of frozen clay decreases sharply for an increase in temperature from -1 to -4°C . Between -4 and -10°C the rate of decrease is, in general, not as sharp. The decrease of damping ratio is greater for lower frequencies (0.05 cps) than for higher frequencies (5.0 cps). Specific surface area does not appear to have a significant influence on the relationship. The influence of water content on the relationship has not been investigated.
 - c. Frequency - the damping ratio of frozen clay, in general, decreases for an increase in frequency from 0.05 to 5.0 cps; for frequencies greater than 5.0 cps, damping ratio increases as frequency increases. At a low temperature (-10°C), the influence of frequency on damping ratio is small; at a high temperature (-1°C), the influence of frequency is great. The influence of frequency at a low strain amplitude ($3.16 \times 10^{-3}\%$) is smaller than at a high strain amplitude ($1.0 \times 10^{-1}\%$). Water content and specific surface area apparently do not have a significant

influence on the relationship.

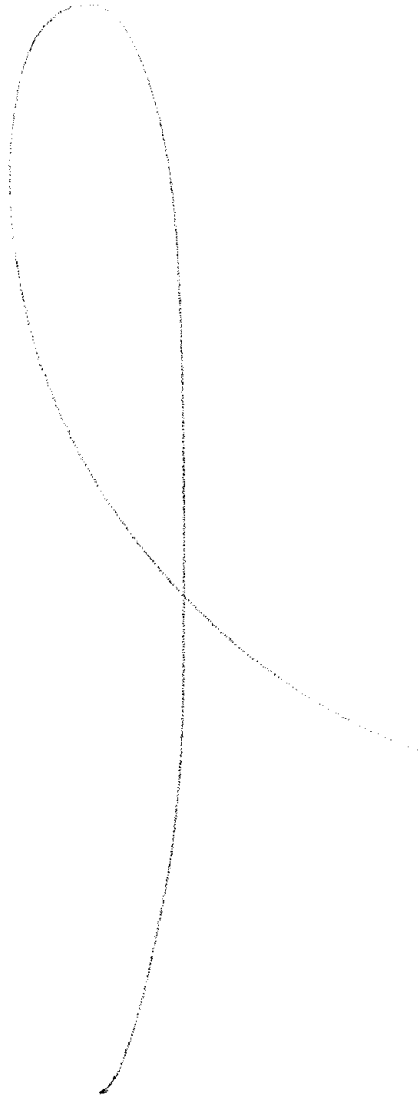
- d. Water content - there appears to be no well-defined relationship between damping ratio and water content of frozen clay.
- e. Specific surface area - at a low strain amplitude ($3.16 \times 10^{-3}\%$), the damping ratio is greater for a clay with a high specific surface area than for a clay with a low specific surface area. At a high strain amplitude ($1.0 \times 10^{-1}\%$), the influence of specific surface area appears to vary with temperature and frequency.
- f. Confining pressure - confining pressure does not appear to affect the damping ratio of frozen clay. This conclusion was reached for all test conditions considered.

A comparison of dynamic properties of ice and frozen clay obtained in the present study to those obtained in previous studies indicates:

1. The values of longitudinal and compressional wave velocities of ice determined in the present study are lower than comparable wave velocities determined in previous laboratory field studies. This may be a consequence of the fact that the strain amplitude of testing in the present study is greater than those associated with previous studies and the test frequencies in the present study are much lower than those associated with previous studies. (It was found in the present study that the wave velocity of ice decreases with increasing strain amplitude and decreasing frequency.)
2. The values of damping ratio of ice determined in the present study are close to the values obtained in previous studies. The combination of a decrease of damping ratio with decreasing strain amplitude and an increase of damping ratio with increasing frequency (as found in the present study) has apparently contributed to the close agreement, i.e., the effects of strain amplitude and frequency tend to cancel each other.
3. The values of longitudinal wave velocities of frozen clay obtained in the present study compare favorably with the results from previous studies. It appears any differences in longitudinal wave velocities can be explained by differences

in the test techniques and material types employed between the present and previous studies.

4. The values of damping ratio of frozen clay obtained in the present study are close to values obtained in one previous laboratory study.



LIST OF REFERENCES

1. Barnes, D.F. "Geophysical Methods for Delineating Permafrost," Proceedings of the Permafrost International Conference, National Academy of Sciences, National Research Council Publication No. 1287, 1963.
2. Behrendt, J.C. "Antarctic Peninsula Traverse Geophysical Results Relating to Glaciological and Geological Studies," Geophysical Polar Research Center, Research Report Ser. 64-1, Wisconsin University, Department of Geology, 1964.
3. Bennett, H.F. "Measurements of Ultrasonic Wave Velocities in Ice Cores from Greenland and Antarctica," USACRREL Research Report 237, June, 1972.
4. Bentley, C.R., P.W. Pomeroy and H.J. Dorman. "Seismic Measurements on the Greenland Icecap," Part I: Studies at 76°59'N 56°05'W; Part II: Reflection Studies, Annales de Geophysique, Vol. 13, 1957, pp. 253-275, 276-285.
5. Bentley, C.R. "The Structure of Antarctica and Its Ice Cover," In Research in Geophysics, Vol. 2, Solid Earth and Interface Phenomena (H. Odishaw, Ed.), Cambridge, Mass., MIT Press, 1964.
6. Boyle, R.W. and D.O. Sproule. "Velocity of Longitudinal Vibration in Solid Rods (Ultrasonic Method) with Special Reference to the Elasticity of Ice," Canadian Journal of Research, Vol. 5, 1931
7. Brockamp, B. and Kohnen. "Ein Beitrag zu den Seismischen Untersuchungen auf dem Grönländischen Inlandeis (Seismic Investigations on the Greenland Ice Sheet)," Polarforschung, Vol. 6, No. 35, 1965.
8. Brockamp, B. and H. Querfurth. "Untersuchungen über die Elastizitätskonstanten von See und Kunsteis (Investigations of the Elastic Constants of Lake and Artificial Ice)," Polarforschung, Vol. 5, No. 34, 1/2, 1964.
9. Brockamp, B., E. Sorge and K.K. Wölcken. "Wissenschaftlich Ergebnisse der Deutschen Grönland - Expedition Alfred Wegener 1929 und 1930/31, Band II., Seismik (Scientific Results of the German Greenland Expedition Alfred Wegener 1929 and 1930/31, Vol. II, Seismic Investigations)," Brockhaus, Leipzig, 1933.
10. Brown, R.J.E. and T.L. Pewe. "Distribution of Permafrost in North America and Its Relationship to the Environment: A Review, 1963-1973," North American contribution to the Second International Conference on Permafrost, National Academy of Science, 1973.
11. Bull, C. "Seismic Investigations on the Northern Part of the Greenland Expedition 1952-54, IV., Geographical Journal, Vol. 122, 1956.
12. Clarke, G.K.C. "Seismic Survey Northwest Greenland, 1964," USACRREL Research Report 191, 1966.
13. Clarke, G.K.C. "Geophysical Measurements on the Kaskawulsh and Hubbard Glaciers, Yukon Territory," Arctic Institute of North America Technical Paper 20, 1967.
14. Crary, A.P., et al. "Glaciological Studies of the Ross Ice Shelf, Antarctica, 1957-1960," IGY Glaciological Report 6, IGY World Data Center A, Glaciology, American Geographical Society, New York, pp. 1-144, 1962.
15. Davis, T.N. and C. Echols. "A Table of Alaska Earthquakes 1788-1961," Alaska University Geophysics Institute, Research Report 8, 1962.

16. Dobrin, M.B. Introduction to Geophysical Prospecting, 2nd Ed., McGraw Hill, New York, 1960.
17. Ewing, M., Crary and A.M. Thorn, Jr. "Propagation of Elastic Waves in Ice," Part I, Physics, Vol. 5, 1934.
18. Förtsch, O. and H. Vidal. "Die Ergebnisse der seismischen Messungen auf dem Hintereisferner in den Oetztaler Alpen 1954 (Results of Seismic Measurements of Hintereis Glacier in the Oetztaler Alps in 1964)," Gerlands Beitr., Geophysics, Vol. 65, 1956.
19. Gold, L.W. "Ice Pressures and Bearing Capacity," Chapter 10, Geo-Technical Engineering in Cold Regions, O.B. Andersland and D.M. Anderson, Editors, McGraw-Hill Book Company (manuscript submitted for publication), 1976.
20. Goldthwait, R.P. "Study of Ice Cliff in Nunatarssuag, Greenland," USASIPRE Technical Report 39, 1960.
21. Hardin, B.O. and V.P. Drnevich. "Shear Modulus and Damping in Soils: I. Measurement and Parameter Effects, II. Design Equations and Curves," Technical Reports UKY 27-70-CE2 and 3, College of Engineering, University of Kentucky, July, 1970.
22. Hattersley-Smith, G. "Operation Hazen, Narrative and Preliminary Reports 1957-58," Operation Hazen, D, Phys. R (G), Hazen, Vol. 4, Defence Research Board, Ottawa, 1959.
23. Hellbardt, G. "Seismische Versuche auf einer Eisplatte (Seismic Investigations on an Ice Plate)," Zeitschrift für Geophysik, Vol. 21, No. 1, 1955.
24. Idriss, I.M. and H.B. Seed. "Seismic Response of Horizontal Soil Layers," Journal of the Soil Mechanics and Foundations Division, ASCE, Vol. 94, No. SM4, July, 1968.
25. Imbert, B. "Ice Cover and Glacial Relief," Symposium on Antarctic Research, Wellington, New Zealand (unpublished), 1958.
26. Joesting, H.R. "Geophysical Exploration in Alaska," Arctic, Vol. 7, No. 3 and 4, 1954.
27. Johnson, H.C. "Application of Electro-hydraulic Servo Control to Physical Testing," Proceedings of the National Conference on Fluid Power, XVIII, Chicago, October, 1964.
28. Joset, A. and J.J. Holtzscherer. "Etude des Vitesses de Propagation des Ondes Seismiques sur l'Inlandsis du Groenland (Study of the Propagation Velocity of Seismic Waves on the Greenland Inland Ice)," Annales de Geophysique, Vol. 9, 1953.
29. Joset, A. and J.J. Holtzscherer. "Determination des Epaisseurs de l'Inlandsis du Groenland (Determination of the Thickness of the Greenland Ice Cap)," Annales de Geophysique, Vol. 10, 1954.
30. Kaplar, C.W. "Laboratory Determination of Dynamic Moduli of Frozen Soils and of Ice," USACCREL Research Report 163, January, 1969.
31. Lee, T.M. "Method of Determining Dynamic Properties of Visco-Elastic Solids Employing Forced Vibration," Journal of Applied Physics, Vol. 34, No. 5, 1963.
32. Linell, K.A. and C.W. Kaplar. "Description and Classification of Frozen Soils," Technical Report 150, USACRREL, Hanover, New Hampshire, January, 1969.
33. Lysmer, J., et al. "LUSH - A Computer Program for Complex Response Analysis of Soil-Structure Systems," Report No. EERC 74-4, Earthquake Engineering Research Center, University of California, Berkeley, California, April, 1974.

34. Mellor, M. "Properties of Snow," Cold Regions Science and Engineering (F.J. Sanger, Ed.), USACRREL Monograph III-AI, AD611023, 1964.
35. Müller, G. "Geschwindigkeitsbestimmungen Elastischer wellen in gefrorenen Gesteinen und die Anwendung akustischer Messungen auf Untersuchungen des Frostmantels an Gefrierschächten (Velocity Determinations for Elastic Waves in Frozen Rocks and the Application of Acoustic Surveys for Investigation of the Frozen Zone Around a Freezing Shaft)," Geophysical Prospecting, Vol. 9, No. 2, 1961.
36. Nakano, Y. and Arnold, R. "Acoustic Properties of Frozen Ottawa Sand," Journal of Water Resources Research, Vol. 9, No. 1, February, 1973, pp. 178-184.
37. Nakano, Y. and Froula, N.H. "Sound and Shock Transmission in Frozen Soils," North American Contribution to the Second International Conference on Permafrost, National Academy of Science, 1973.
38. Nakano, Y., R.J. Martin, and M. Smith. "Ultrasonic Velocities of the Dilatational and Shear Waves in Frozen Soils," Journal of Water Resources Research, Vol. 8, No. 4, August, 1972, pp. 1024-1030.
39. Robin, G. de Q. "Measurements of Ice Thickness in Dronning Maud Land, Antarctica," Nature, Vol. 171, 1953.
40. Robin, G. de Q. "Seismic Shooting and Related Investigations," Glaciology III, Norwegian-British-Swedish Antarctic Expedition 1949-52, Scientific Results, Vol. 5, 1958.
41. Roethlisberger, H. "Studies in Glacier Physics on the Penney Ice Cap, Baffin Island, 1953," Part III, Seismic Sounding, Journal of Glaciology, Vol. 2, No. 18, 1955.
42. Roethlisberger, H. "The Applicability of Seismic Refraction Soundings in Permafrost near Thule, Greenland," USACRREL Technical Report 81, 1961.
43. Roethlisberger, H. "Seismic Exploration in Cold Regions," USACRREL Monograph 11-A2a, October, 1972.
44. Savel'ev, B.A. "Gliatsiologicheskije issledovania Chetvertoi Antarkticheskoi Ekspenditsii [1959] (Glaciological Investigations of the Fourth Antarctic Expedition [1959])," in Materials of Glaciological Investigations: Chronicle and Discussions, Institute Geografii AN SSSR, Issue 4, text in Russian, 1962.
45. Schnabel, P.B., J. Lysmer, and H.B. Seed. "SHAKE - A Computer Program for Earthquake Response Analysis of Horizontally Layered Sites," Research Report EERC 72-12, Earthquake Engineering Research Center, University of California, Berkeley, California, 1972.
46. Seed, H.B. and I.M. Idriss. "Influence of Soil Conditions on Ground Motions During Earthquakes," Journal of the Soil Mechanics and Foundations Division, ASCE, Vol. 95, No. SM1, January, 1969.
47. Seed, H.B. and I.M. Idriss. "Soil Moduli and Damping Factors for Dynamic Response Analyses," Report No. EERC 70-10, University of California, Berkeley, 1970.
48. Seed, H.B. and I.M. Idriss. "Influence of Local Soil Conditions on Building Damage Potential During Earthquakes," Journal of the Structural Division, ASCE, Vol. 97, No. ST2, February, 1971.
49. Seed, H.B., et al. "Soil Conditions and Building Damage in 1967 Caracas Earthquake," Journal of the Soil Mechanics and Foundation Division, ASCE, Vol. 98, No. SM8, Proc. Paper 9108, August, 1972, pp. 787-806.

50. Smith, N. "Determining the Dynamic Properties of Snow and Ice by Forced Vibration," USACRREL Technical Report 216, June, 1969.
51. Stevens, H.W. "Viscoelastic Properties of Frozen Soil Under Vibratory Loads," North American Contribution to the Second International Conference on Permafrost, National Academy of Sciences, 1973.
52. Stevens, H.W. "The Response of Frozen Soils to Vibratory Loads," USACRREL Technical Report 265, June, 1975.
53. Streeter, V.L., E.B. Wylie, and F.E. Richart, Jr. "Soil Motion Computations by Characteristics Method," Journal of the Geotechnical Engineering Division, ASCE, Vol. 100, No. GT3, Proc. Paper 10410, March, 1974, pp. 247-263.
54. Thiel, E., et al. "Oversnow Traverse Programs, Byrd and Ellsworth Stations, Antarctica, 1957-1958," Seismology, Gravity and Magnetism, IGY Glaciological Report Ser. 2, IGY World Data Center A, Glaciology, American Geographical Society, 1959.
55. Thiel, E. and J. Behrendt. "Seismic Studies on the Filchner Ice Shelf, Antarctica, 1957-1958," See Thiel, et al, 1959; 1959.
56. Thiel, E. and N.A. Ostenso. "Seismic Studies on Antarctic Ice Shelves," Geophysics, Vol. 26, No. 6, 1961.
57. Thyssen, F. "Die Temperaturabhängigkeit der P-Wellen geschwindigkeit in Gletschern und Inlandeisen (Temperature Dependency of the P-Wave Velocity in Glaciers and Continental Ice Sheets)," Zeitschrift für Geophysik, Vol. 33, 1967.
58. Vallon, M. "Etude de la Mer de Glace, 4: Le Glacier du Tacul (Investigations of Mer de Glace, 4: Glacier du Tacul)," Rapport. Sci. Laboratoire Geophys. et Glaciol. Grenoble, Vol. 102, 1967.
59. Vinson, T.S. "Cyclic Triaxial Test Equipment to Evaluate Dynamic Properties of Frozen Soils," Report No. MSU-CE-75-1, Division of Engineering Research, Michigan State University, March, 1975.
60. Warder, D.L. and O.B. Andersland. "Soil-ice Behavior in a Model Retaining Structure," Canadian Geotechnical Journal, Vol. 8, No. 1, 1971.
61. Weber, J.R. and H. Sandstrom. "Geophysical Methods in Glaciology," Part II: Seismic Measurements on Operation Hazen in 1958, Operation Hazen, D Phys. R (G), Hazen, Vol. 6, Defence Research Board, Ottawa, 1960.
62. Weihaupt, J.G. "Seismic and Gravity Studies at the South Pole," Geophysics, Vol. 28, No. 4, 1963, pp. 582-592.
63. Wolcken, K. "Seismic Ice-thickness Measurements on Novaya Zemlya, 1932-33," Polarforschung, Vol. 5, (1/2), 1961.
64. Wood, H.O. "Distribution of Apparent Intensity in San Francisco, in: The California Earthquake of April 18, 1906," Report to the State Earthquake Investigation Commission, Carnegie Institute of Washington, Washington, D.C., 1908, pp. 220-245.

APPENDICES

APPENDIX A
DESCRIPTION OF CYCLIC TRIAXIAL
TEST EQUIPMENT

Figure A.1 shows the cyclic triaxial test equipment developed for the research program. A schematic is shown in Figure A.2. The test setup consists of four basic components:

- (1) An MTS electrohydraulic closed loop test system consisting of the actuator, servovalve, hydraulic power supply, servo controller, and hydraulic controller. (This applies a cyclic deviator stress to the sample.)
- (2) A triaxial cell which contains the sample and non-circulating coolant.
- (3) A refrigeration unit and cold bath which circulates the coolant around the triaxial cell.
- (4) Output recording devices to monitor the load (stress) and displacement (strain) of the sample during the test.

A.1 The MTS Electrohydraulic Closed Loop Test System

The heart of the test setup is the MTS electrohydraulic closed loop test system. As shown in Figure A.3, it consists of an MTS Model 500.10, 2.8 gpm (0.010 m³/min)/3000 psi (20,700 kN/m²), hydraulic power supply; a Model 436.11 hydraulic control unit with a function generator; a Model 406.11 controller (servovalve controller with AC and DC feedback signal conditioning); and a Model 204.61 11 kip (5000 Kg) actuator with a 252.25, 15 gpm (0.057 m³/min) servovalve and an internal linear variable differential transformer (LVDT). The system operates as follows:

- (1) A command signal (voltage) from the function generator in the 436.11 or other external source is input to the 406.11 where it is compared to the feedback signal (voltage) from a transducer (e.g., a load cell or LVDT) monitoring the response of the specimen in the closed loop.
- (2) The difference (error) between the two signals is amplified and applied to the torque motor in the servovalve coupled to the actuator.

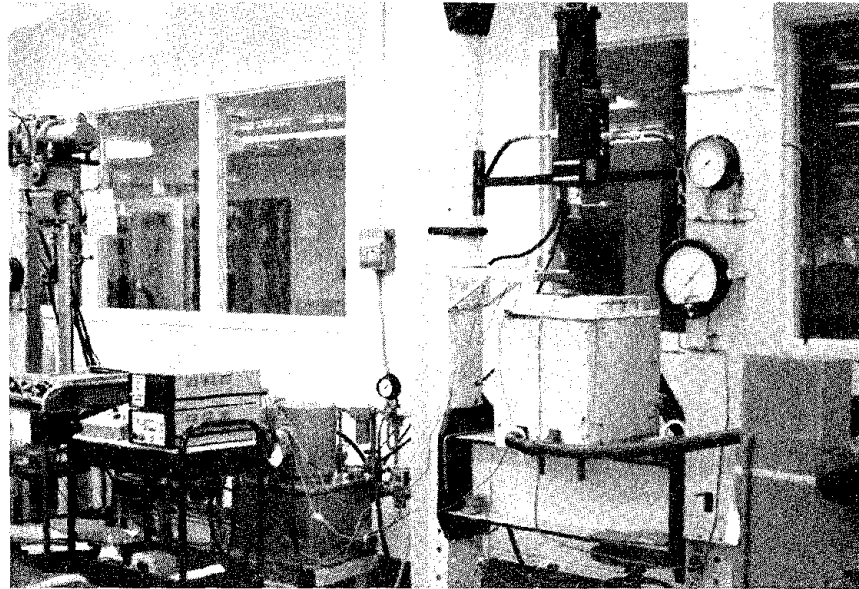


Figure A.1 CYCLIC TRIAXIAL TEST EQUIPMENT

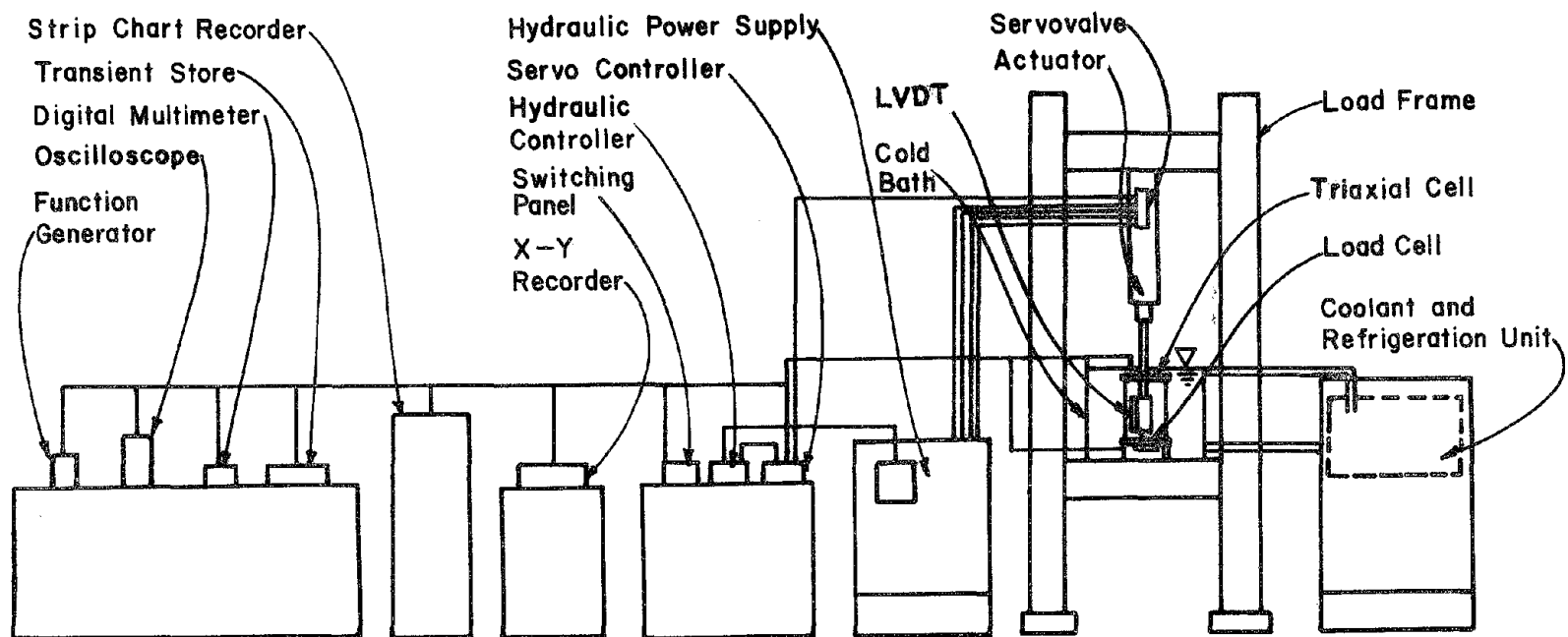


Figure A.2 SCHEMATIC OF CYCLIC TRIAXIAL TEST EQUIPMENT

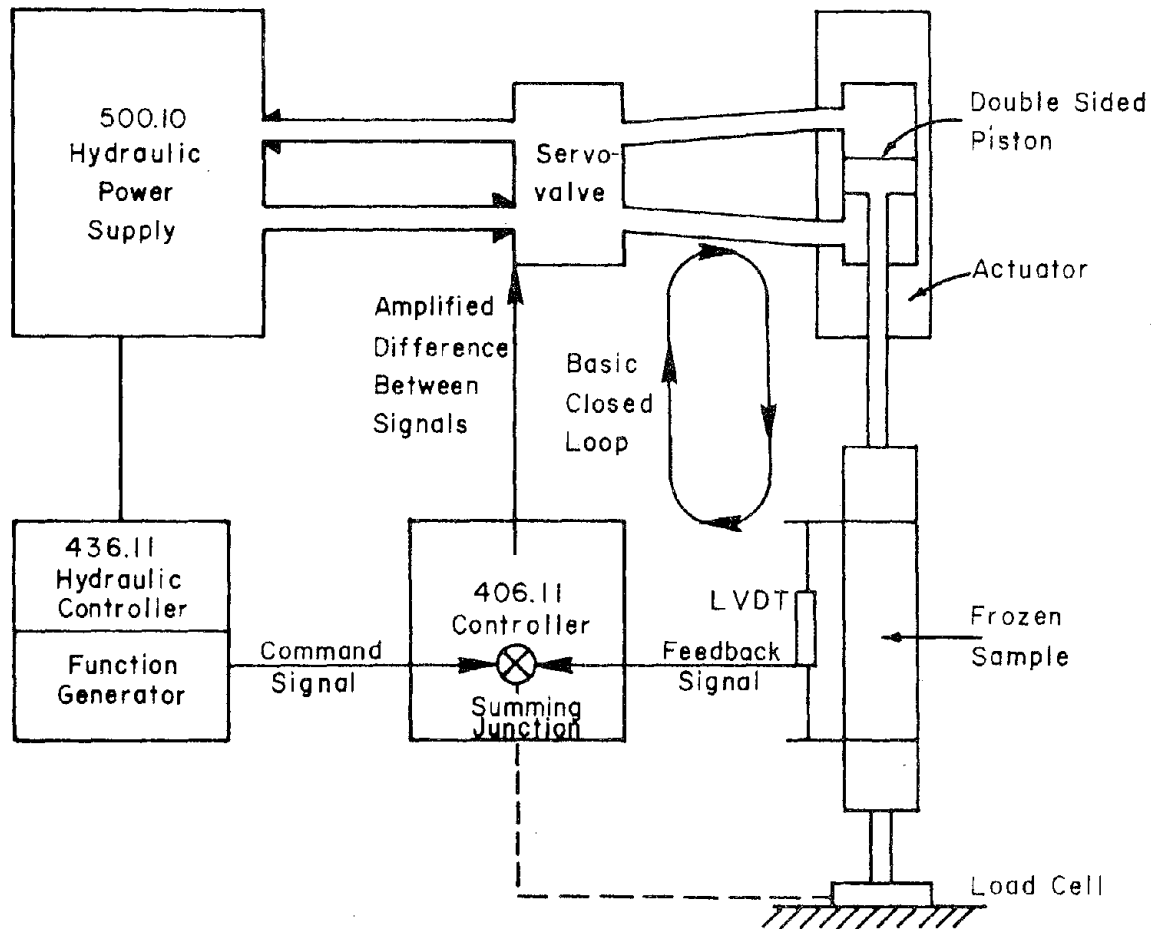


Figure A.3 SCHEMATIC OF MTS ELECTROHYDRAULIC CLOSED LOOP TEST SYSTEM

- (3) The torque motor drives a pilot stage which in turn drives a power stage of the servovalve which directs hydraulic fluid under pressure to one side or the other of the double-sided actuator piston to cause the actuator to move.
- (4) The movement of the actuator causes the specimen to respond in such a way that the transducer monitoring the specimen "feeds back" a signal which is equal to the command signal.

The speed at which these steps are executed causes the sample, for all practical purposes, to be subjected to a loading equal to the command signal. A more complete treatment of closed loop testing theory is given by Johnson (1964).

A.1.1 MTS 406.11 Controller

The front panel of the 406.11 controller is shown in Figure A.4. The controls indicated by the circled numbers are discussed in order below.

- (1) The panel voltmeter has two functions. First, it can be used to indicate the error between the command signal and the feedback transducer. Second, it can be used to indicate the voltage output of feedback transducer XDCR1, XDCR2, or the servovalve drive. (The servovalve regulates the flow of hydraulic pressure between the hydraulic power supply and the actuator.) For the cyclic triaxial tests a negative error means compression and positive error means tension to the specimen. The panel voltmeter was most often used to monitor the error between the command signal and the feedback transducer before applying the hydraulic pressure. To insure that the actuator does not move when hydraulic pressure was applied, the error signal must be zero.
- (2) The Set Point control provides a static command signal (voltage). There are 1000 divisions on the Set Point dial. Each division is equivalent to 20 mv. A positive command signal (Set Point between 500 and 1000) produces actuator piston compression; a negative command signal (Set Point between 500 and 000) produces actuator piston extension. When the feedback signal is from the LVDT in the actuator, Set Point is used to move the actuator up or down even with no specimen in

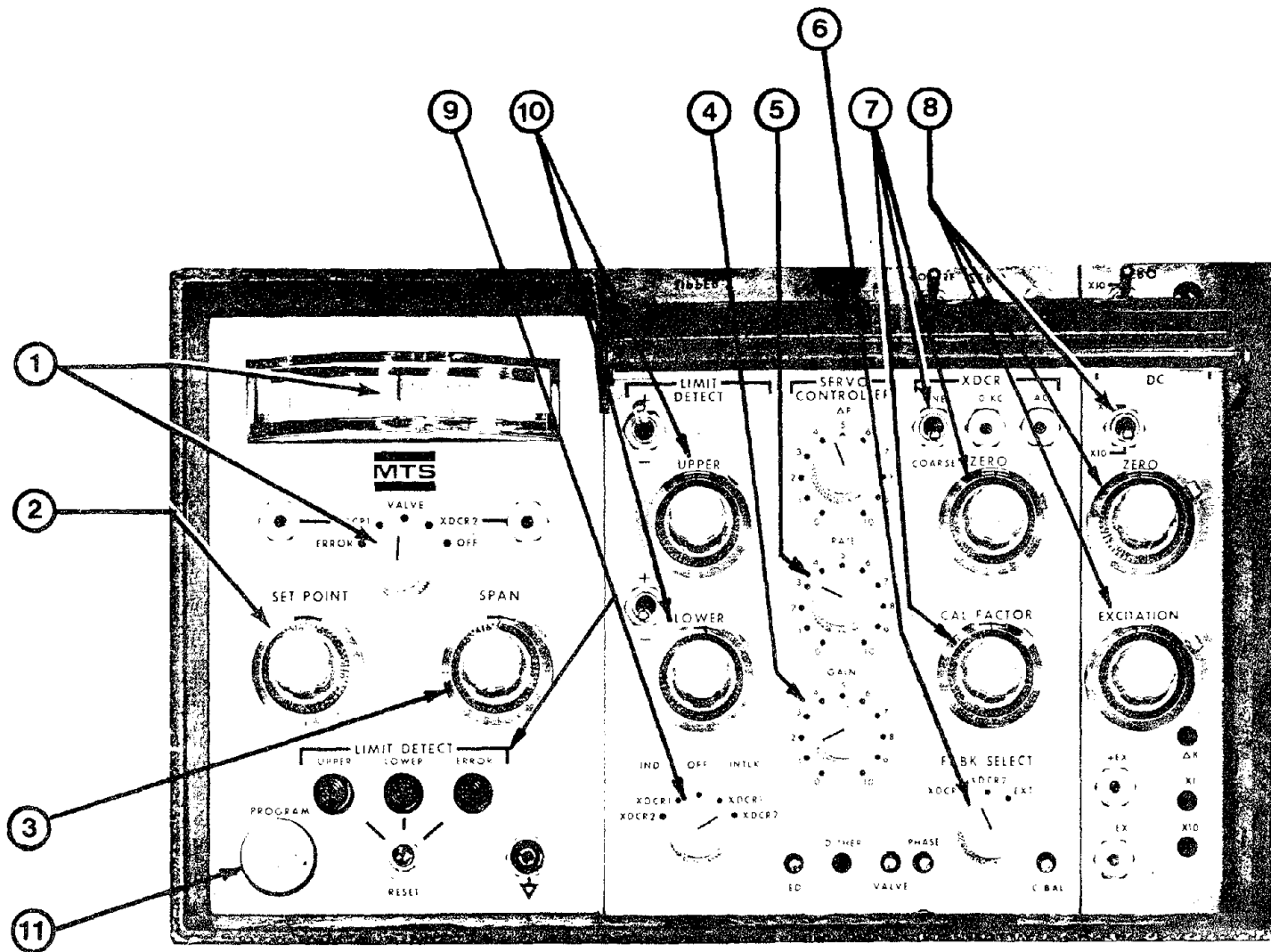
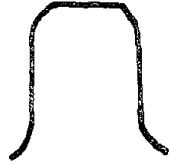


Figure A.4 CONTROLS AND INDICATORS ON 406.11 FRONT PANEL

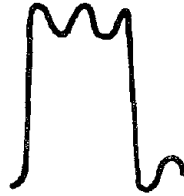
the loop. When the feedback is from any other transducer the Set Point control establishes a static level of response of the specimen. When feedback was from the LVDT mounted across the sample, Set Point could be used to obtain zero loading on the sample.

- (3) The Span control establishes the amplitude of a command signal waveform during cyclic loading. The amplitude is about the Set Point level. There are 1000 divisions on the Span control dial. Each division is equivalent to an amplitude of 10 mv. The Span was used to vary the strain amplitude during cyclic triaxial testing.
- (4) The Gain control establishes the rate and accuracy of response of the actuator ram to the command signal. The Gain control is therefore used to improve the response of the closed loop system which includes the specimen. To set the system at optimum Gain, the sample was subjected to a low frequency, low amplitude square wave loading. The feedback signal was monitored with an oscilloscope. The Gain control was turned clockwise until small oscillations were observed at the peak of the square wave, as shown in Figure A.5b. At this point the Gain was reduced until the oscillations stopped, as shown in Figure A.5c. The Rate (described below) was adjusted to eliminate "overshoot" at the corner of the peak of the square wave as shown in Figure A.5c.
- (5) The Rate control helps prevent "overshoot" at high Gain settings. The Rate was adjusted after the Gain had been set as described above.
- (6) The Feedback Select position determines which feedback signal will be used in the closed loop test circuit. This may be the signal from Transducer Conditioner 1 (XDCR1), Transducer Conditioner 2 (XDCR2), or from an external transducer conditioner (EXT).
- (7) The Cal Factor, Zero, and Fine/Coarse controls provide adjustment of the signal from the transducer used with XDCR1.

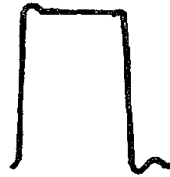
Cal Factor was used to adjust the voltage output from the LVDT. The Cal Factor was adjusted to obtain ± 10 volts



a. Over-damped, Gain too low



b. Under-damped, Gain too high



c. Optimum Gain

Figure A.5 GAIN AND STABILITY ADJUSTMENT

when the core of the LVDT moved 0.254 cm.

The Zero control introduces an electrical offset to the signal from the LVDT. It has 1000 divisions on the dial. A Zero control setting of 500 corresponds to zero voltage offset. The Zero control provides negative electrical offset when it is between 500 and 000 and positive offset when it is between 500 and 1000.

The Fine/Coarse switch determines the operating range for the Zero control. When it is selected to Fine, the electrical offset from the Zero control per division is lower than when it is selected to Coarse. In this experiment, high electrical offset is necessary, therefore, the switch was selected to Coarse.

- (8) The Excitation, Zero, and x1/x10 switch provide adjustment of the signal from transducer XDCR2. In general a load cell was the transducer used with XDCR2.

The Excitation was used to adjust the voltage output from the load cell. It has 1000 divisions on the dial. The Excitation was adjusted to obtain 25 mv per 10 lbs of loading using a 5 kip load cell with a sensitivity of 2 mv/volt.

The Zero control introduces an electrical offset to the signal from the load cell. It has 1000 divisions on the dial. A zero control setting of 500 corresponds to zero voltage offset. It provides positive electrical offset when it is between 500 and 000 and negative offset when it is between 500 and 1000.

The x1/x10 switch determines the operating range for the signal from the load cell. When in the x10 position the signal from the load cell is amplified 10 times that of the x1 position. The x1 position was, in general, used in the research program.

- (9) The Limit Detector determines which transducer conditioner (XDCR1 or XDCR2) signal will be monitored in the "failsafe" circuit. If the switch is set on INTLK the failsafe interlock circuit will turn off the hydraulic power supply when the signal voltage is greater or lower than a selected range

of voltage.

The Reset is used to extinguish the indicator light when the signal voltage level is within the selected range of voltage. If the light for the Limit Detector is still lit with the failsafe interlock circuit in operation, the hydraulic power supply cannot be engaged. Therefore, before applying the hydraulic power supply the light has to be extinguished with the Reset button. If the switch is in the off position the failsafe circuit is inoperative.

- (10) The Upper and Lower limit controls are used to select the range of acceptable voltage. The Upper limit is set at the most positive or least negative limit. The Lower limit is set at the most negative or least positive limit. Each limit dial has 1000 divisions corresponding to 10 volts.
- (11) Program is used to input an external source of command signal.

A.1.2 MTS 436.11 Controller

The front panel of the 436.11 is shown in Figure A.6. The controls indicated by the circled number are discussed in order below.

- (1) The Power control applies AC operating voltage to the control unit.
- (2) The Hyd Pressure Low or High or Hydraulic Off control is used to turn the hydraulic power supply on and off. (The 500.10 hydraulic power supply has no low pressure option.)
- (3) The Program Stop or Run control is used to start or stop generation of a command signal waveform.
- (4) Emergency Stop is used to stop the hydraulic power supply and generation of the command signal waveform. Emergency Stop and Hyd Off have the same effect.
- (5) The Wave Form control of the Function Generator module is used to select the type of command waveform to be generated. Square, triangular, and harmonic waveforms are available.
- (6) The Frequency vernier and range selector are used to obtain the desired frequency characteristic of the command waveform. Frequencies between 0.01 and 1100 cps are available.

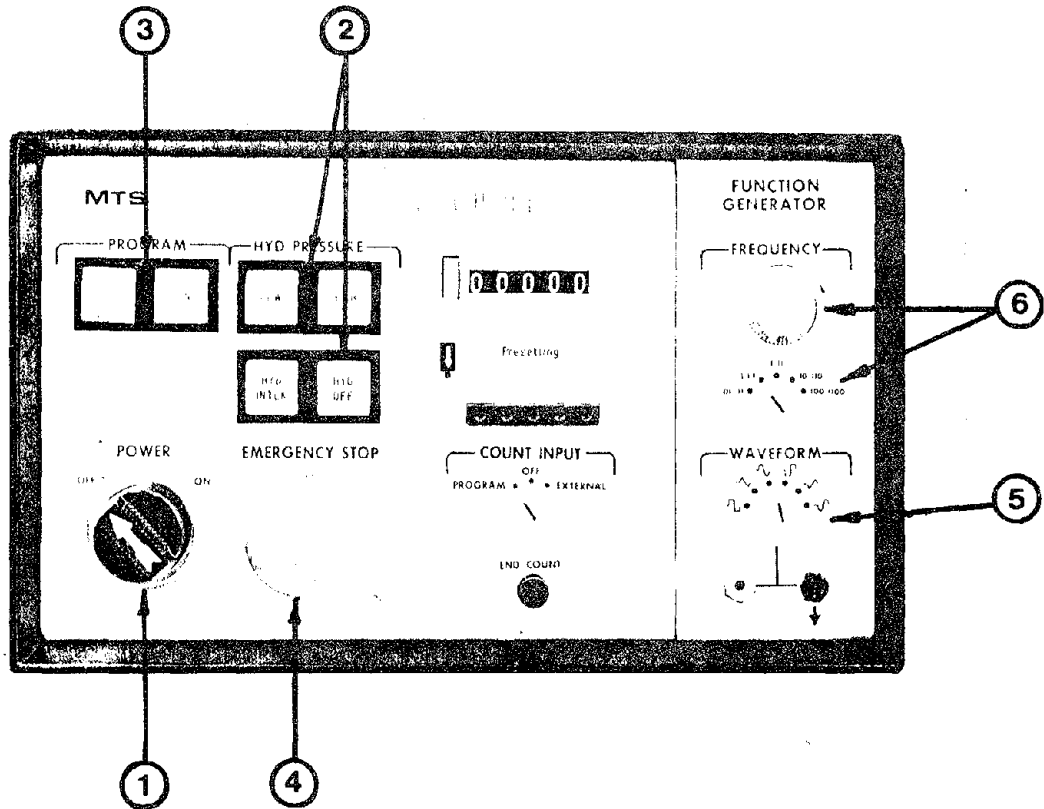


Figure A.6 CONTROLS AND INDICATORS ON 436.11 FRONT PANEL

A.2 Triaxial Cell

A schematic of the triaxial cell inside the cold bath is shown in Figure A.7. The cell is 18 cm in diameter and 35 cm high. An aluminum cell was chosen over steel or lucite for three reasons:

- (1) It has sufficient strength to allow testing at high confining pressure (compared to lucite).
- (2) It was lightweight for ease of handling (compared to steel).
- (3) It has a higher thermal conductivity (compared to steel and particularly to lucite) to insure the noncirculating coolant inside the bath remains at a temperature approximately equal to the coolant circulating outside the bath.

Two thermistors were attached to the 7.1 cm diameter, and 17.5 cm high sample to monitor its temperature during the test. An LVDT was attached across the sample to the cap and base to monitor displacement. The output of this LVDT was also the feedback signal in the closed loop discussed in Section A.1. A load cell attached to the base plate of the cell monitors the load. Two copper tubes were connected to the cell at the base plate to apply and monitor pressure in the cell. Pressure to the cell was supplied by a nitrogen pressure tank. As a precaution against pressure fluctuations which might be introduced by movement of the loading rod during cyclic loading, an air reservoir was connected to the pressure line. When applying pressure, coolant which was left in the pressure line could be forced into the cell if air was trapped in the cell. The coolant which would be introduced into the cell would be at a higher temperature than the cell fluid. This could cause variations of temperature during pressure application. To eliminate this problem, a pressure line made of copper (high thermal conductivity) was rolled inside the bath to cool the coolant which was trapped in the line. With this system it was found that there was no temperature change during application of pressure.

When the LVDT is mounted at the side of the sample, care must be taken to insure that tilt of the sample cap does not influence the displacement reading. A device developed in this research program to eliminate tilt is shown in Figures A.8a and A.8b. It consists of three basic components:

- (1) A base clamp with a fixed standard for the LVDT body and a

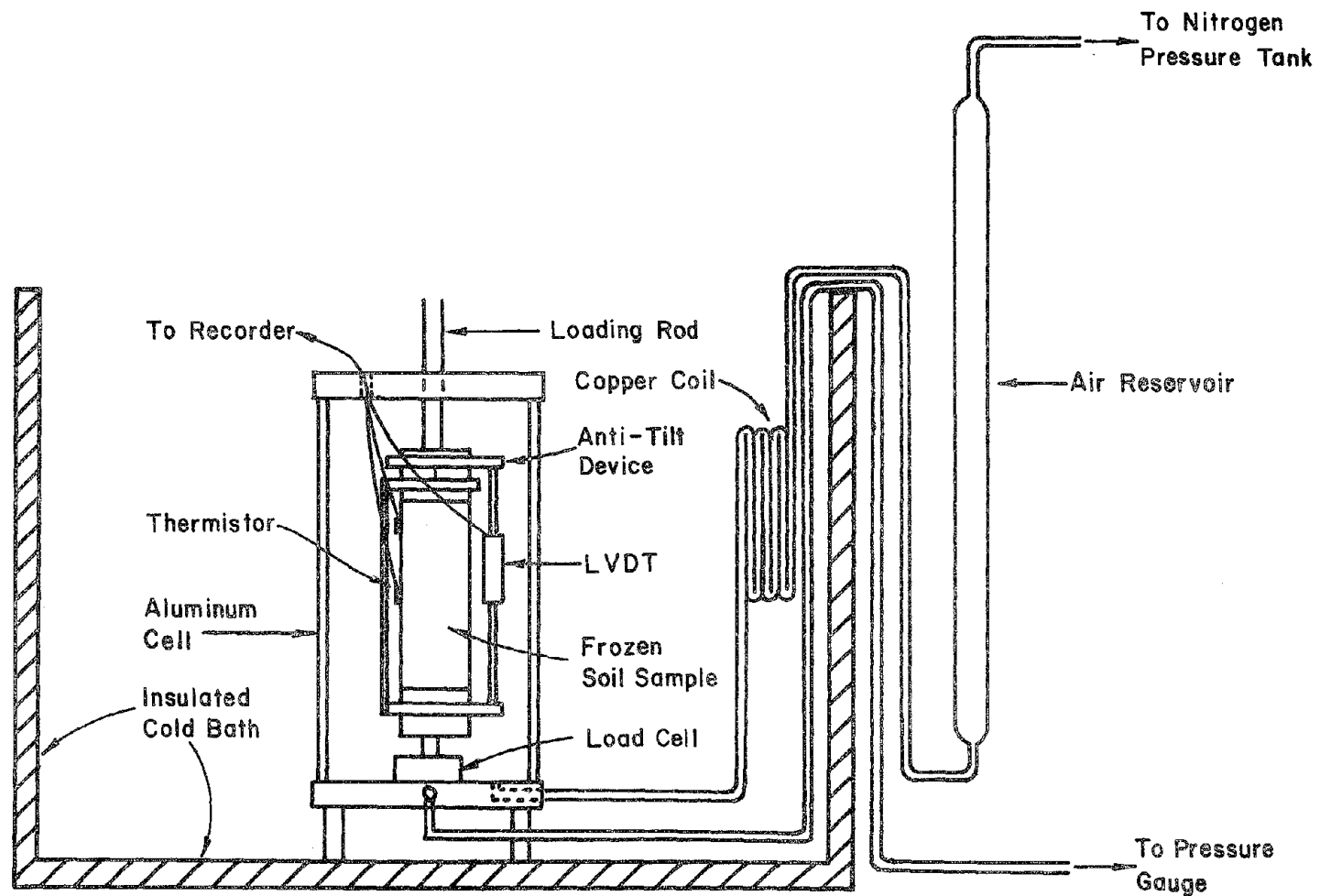
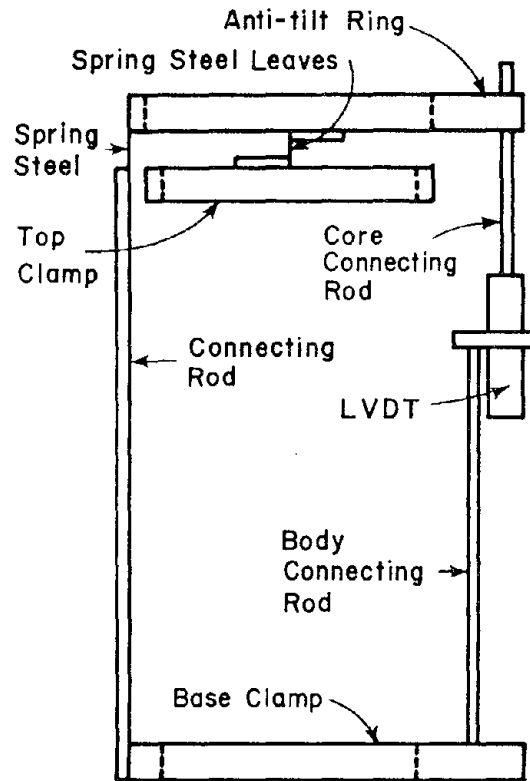
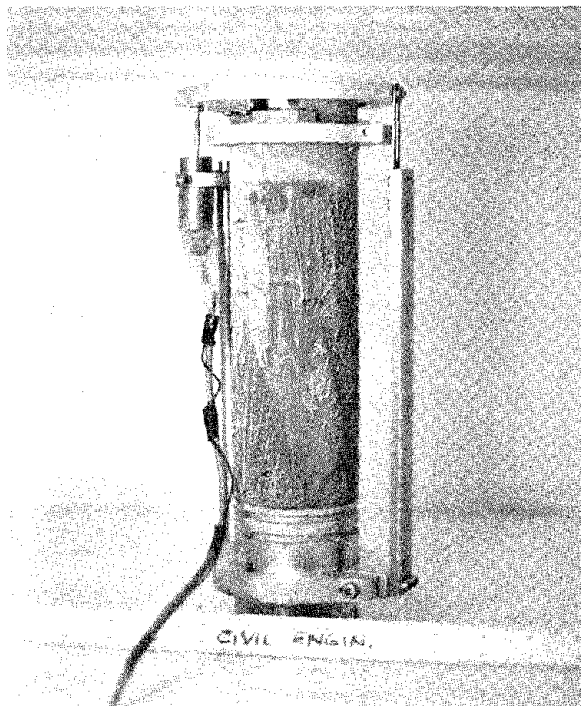


Figure A.7 SCHEMATIC OF TRIAXIAL CELL INSIDE COLD BATH



a. Schematic of anti-tilt device



b. Anti-tilt device

Figure A.8 ANTI-TILT DEVICE FOR LVDT SIDE MOUNTING

connecting rod to the sample cap assembly.

- (2) An anti-tilt ring connected to the base clamp connecting rod with a piece of spring steel and with a connecting rod for the movable LVDT core. The anti-tilt ring has a diameter 0.63 cm greater than the sample cap to allow free movement about the cap.
- (3) A top clamp attached to the anti-tilt ring with two spring steel leaves.

The spring steel leaves between the anti-tilt ring and the top clamp act as a pivot point. Any (slight) tilt of the sample cap will not be transmitted to the anti-tilt ring through the spring steel. As the sample cap moves, the LVDT core is forced to move because the anti-tilt ring is fixed to the base clamp by the connecting rod. The movement at the pivot point causes the displacement measured at the LVDT to be twice that of the sample at the centerline. (This is another advantage of the anti-tilt assembly since it effectively doubles the output of the LVDT for a given sample displacement.)

The vertical displacement of the cap with respect to the base at the two spring steel leaves will cause the anti-tilt ring to rotate such that the spring steel at the middle of the ring acts as a pivot point. The movement of the anti-tilt ring about the pivot point causes the core of the LVDT to move in both the vertical and horizontal directions. The horizontal component of movement causes an error in measuring the strain of the specimen. To determine the magnitude of the error consider the representation shown in Figure A.9. In the figure, when the two steel leaves move from point C to point D the core will move from point F to point G. Without restraint the core should move vertically for a distance FI. With restraint it moves a vertical distance FH which is shorter than the true vertical movement by an amount HI. To determine the error HI note that for small θ ,

$$\theta_A = \frac{\Delta L}{AC} = 2 \frac{\Delta L}{AB} \quad (A.1)$$

Since

$$\theta_A = \theta_E = \theta_G,$$

$$GH = EG \cdot \theta_E = BF \cdot \theta_E = BF \cdot \theta_G \quad (A.2)$$

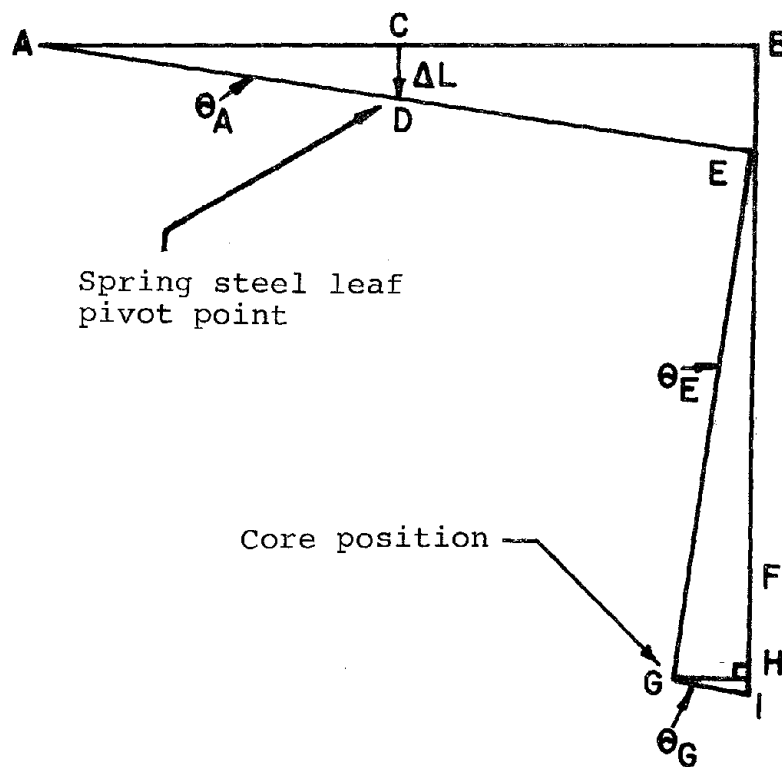


Figure A.9 ANTI-TILT DEVICE MOVEMENT DURING CYCLIC LOADING

Then

$$HI = GH \cdot \theta_G \quad (A.3)$$

Substituting (A.2) into (A.3)

$$HI = BF \cdot \theta_G^2 \quad (A.4)$$

Substituting (A.1) into (A.4)

$$HI = \frac{4 (\Delta L)^2 \cdot BF}{(AB)^2} \quad (A.5)$$

in which

HI = the error of the anti-tilt device

L = the displacement of the sample

AB = the diameter of the anti-tilt ring

BF = the distance between the edge of the anti-tilt ring
and the center of the LVDT core

For the anti-tilt ring used in the research program, AB = 12.22 cm and BF = 3.89 cm. Substituting these values into Equation (A.5) the error associated with the anti-tilt device has been calculated and is shown in Figure A.10. The maximum strain of testing was about 2×10^{-4} cm/cm for ice and 1×10^{-3} cm/cm for clay. Thus, the maximum error expressed as a percentage of displacement was 0.05 and 0.25%, respectively. [Note: when the displacement was approximately 0.07 cm (0.4 percent strain) the core would come into contact with the housing of the LVDT.] Since this error was relatively small no attempt was made to correct for it in the research program.

The two thermistors used to monitor temperature of the sample were calibrated with a laboratory thermometer with a scale division of 0.1°C. The thermistors were capable of reading to the nearest 0.1°C. The temperature of the samples was obtained by averaging the readings of the two thermistors.

A.3 Cooling System

The cold bath is approximately 0.35 m x 0.35 m x 0.46 m and contains 0.048 m³ of circulating coolant, excluding the volume of the triaxial cell. The bath was constructed so that the coolant entered at the bottom and returned to the refrigeration unit from a line at the top of the bath. This is shown in Figure A.11. It is important to insulate the top of the

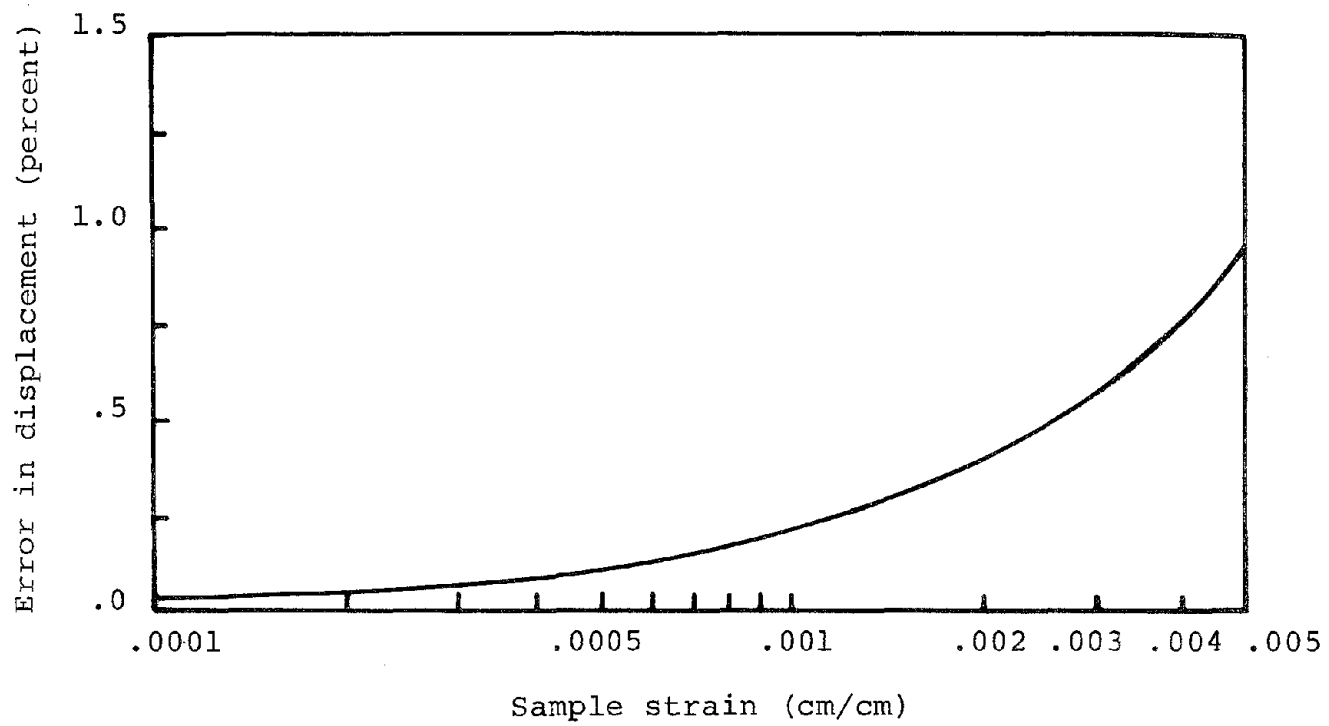


Figure A.10 ERROR IN DISPLACEMENT MEASUREMENT VERSUS SAMPLE STRAIN FOR THE ANTI-TILT DEVICE

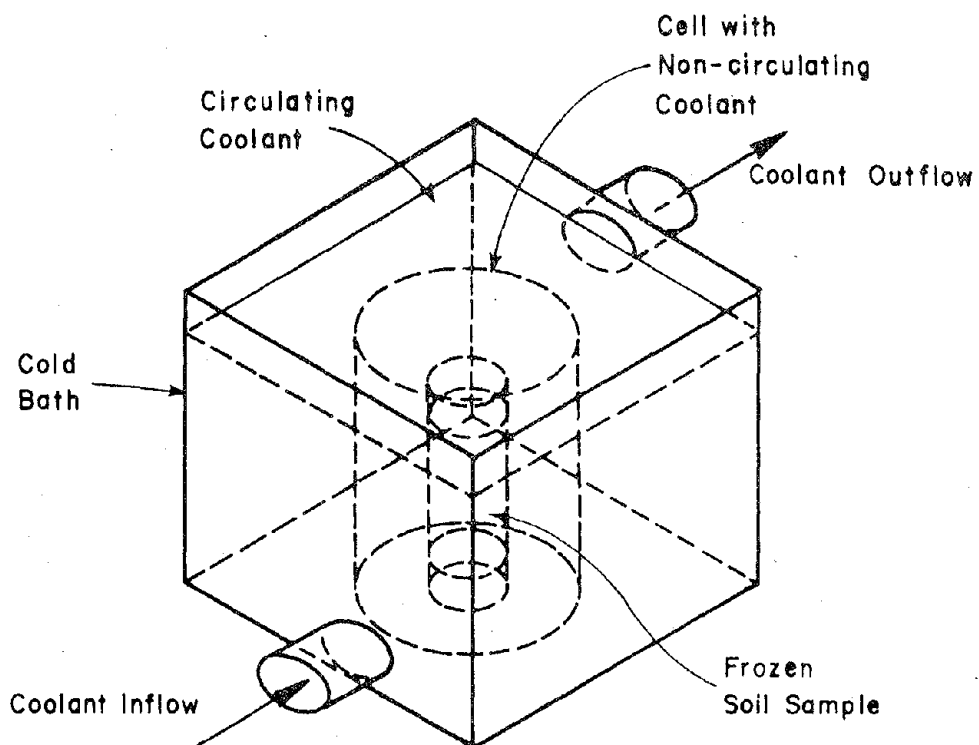


Figure A.11 SCHEMATIC OF COLD BATH

cold bath as this represents a potential source of heat loss in the cell (and sample through the cell top plate). Two 1-inch thick sheets of styrofoam were used for this purpose. In addition, coolant was "washed" across the top plate of the cell through an auxiliary circulating line. With these precautions it was found that the temperature inside the cell adjacent to the sample did not vary by more than 0.2°C along the length of the sample.

To insure that thermal equilibrium had been reached in the specimen and the coolant surrounding it in the cell, temperature measurements were made at the center of several ice and frozen clay samples and adjacent to the sample, as shown in Figure A.12. The figure illustrates the variation of temperature as a function of time for three test conditions. In one test (Figure A.12a), an ice sample and aluminum caps were at an initial temperature of -12.7°C , the coolant inside the cell was at a temperature of -12.2°C . After approximately one hour, the temperature of the sample (measured with a thermistor frozen in the center of the sample) and the coolant inside the cell were equal and remained constant. Similar results were obtained when a stainless steel cap and base was used with an ice sample (Figure A.12b) and when an aluminum cap and base was used with a clay sample (Figure A.12c).

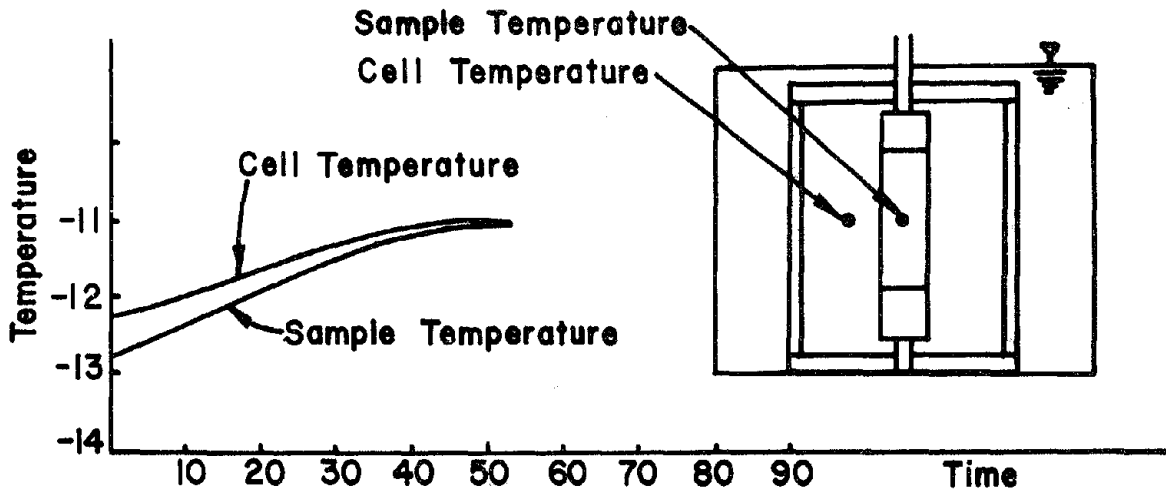
The temperature of the coolant in the refrigeration unit was controlled by a mercury thermometer thermostat submerged in the coolant. The temperature difference between the cold bath and refrigeration unit was approximately 0.5°C . Therefore it was possible to set the thermostat in the refrigeration unit and obtain any test temperature desired with reasonable accuracy.

A.4 Output Recording Devices

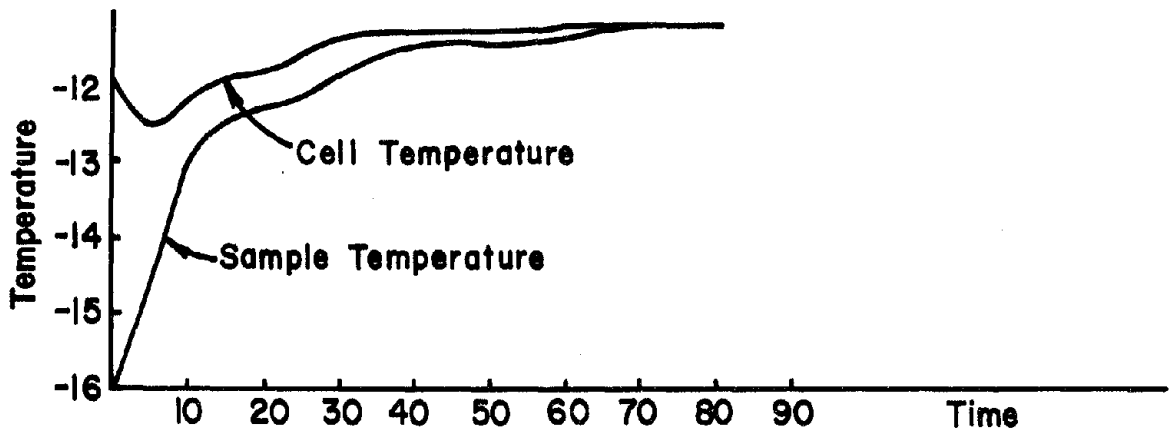
The following devices were used to monitor the load cell, LVDT, and thermistors employed in the test program:

- (1) Transient Recorder (Physical data Model 512 A).
- (2) x-y Recorder (Varian Associates Model F-80).
- (3) Strip-Chart Recorder (Sanborn Model 150).
- (4) 3-1/2 Digit-Digital Multimeter.
- (5) Oscilloscope.

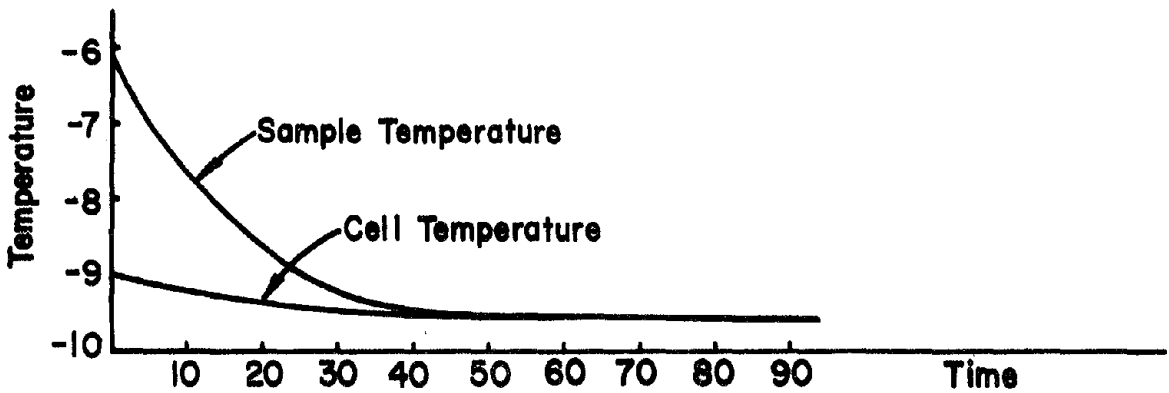
In order to minimize the amount of time required for calibration and monitoring, these devices were connected to a switching panel which, in



a. Variation of temperature of ice using aluminum cap and base



b. Variation of temperature of ice using steel cap and base



c. Variation of temperature of clay using aluminum cap and base

Figure A.12 SAMPLE TEMPERATURE VERSUS TIME FOR DIFFERENT TEST CELLS

turn, received the output signals from the load cell, LVDT, and thermistors. The switching panel is shown schematically in Figure A.13.

The transient recorder is an electronic instrument which accepts and stores analog electrical signals. The signals can be played back repetitively at a selected timebase which may be different from the recording timebase. This allows storage of a high speed event and playback at a low speed. Two channels are provided to permit storage of two parallel events. The storage is in a digital form in a solid-state, microcircuit memory. The duration of recording time can be varied from 100 to 0.01 seconds. The signals are stored in such a manner that all words of storage (2048 words for one event and 1024 words for two parallel events) are stored totally within a recording time of the selected timebase. The transient recorder was used to record load and displacement signals taken during high frequency tests (greater than 0.3 cps) and to play them back at slower frequencies on the x-y recorder.

It was observed that high frequency, low amplitude sine waves were superimposed on the output signals of load and displacement from the MTS 406.11 controller. This is shown in Figure A.14a for the output signal displayed on an oscilloscope. The "noise" was approximately 1 to 2 kHz with an amplitude of 80 mv for the displacement signal and 5 mv for the load signal. The noise was produced by the AC Transducer Conditioner in the 406.11 controller which excited the LVDT and the load cell. The x-y recorder and strip-chart recorder could not respond to this high frequency noise, but it was picked up by the transient recorder as shown in Figure A.14a. When this signal was played back to the x-y recorder it caused a "shaking," irregular movement of the pen. This movement could also be seen when the signals were displayed on the oscilloscope as shown in Figure A.14b. The effect was more pronounced when the output voltage signals were small compared to the noise. To eliminate this problem, a low pass filter was used on the displacement signal at the input to the transient recorder. The noise on the load signal was low enough to be ignored.

The x-y recorder was used to obtain a plot of load versus displacement during cyclic testing. The load cell output was displayed on the y-axis and the LVDT output was displayed on the x-axis. The damping characteristics of the sample could be determined from this plot as explained in Section 4.3. It was found that the x-y recorder itself created a hysteresis loop when two duplicate sine wave signals from a function

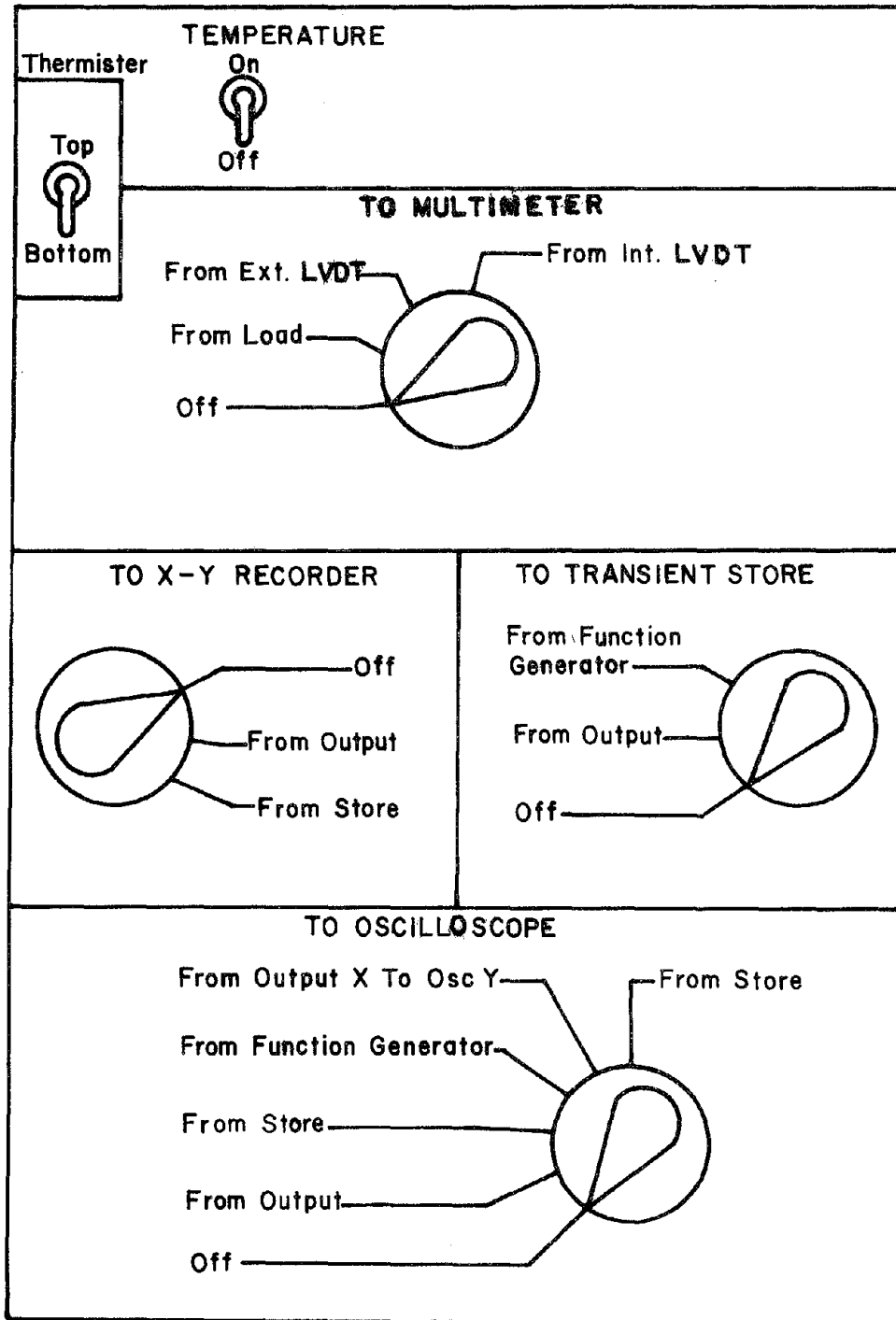
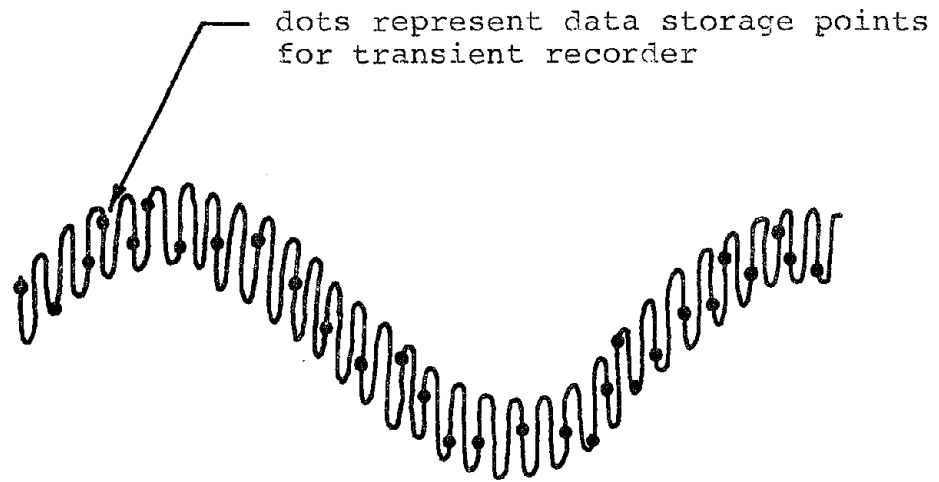
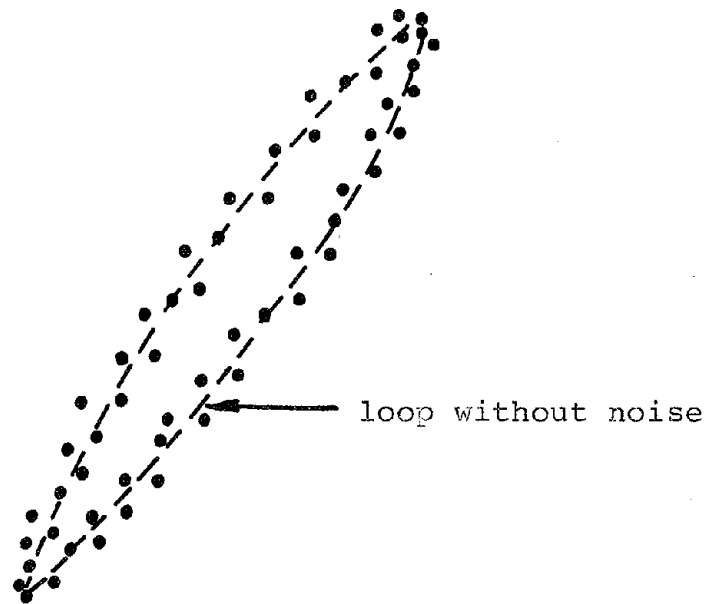


Figure A.13 SCHEMATIC OF CONTROL SWITCHING PANEL



a. Typical signal from LVDT at low voltage level.



b. Typical hysteresis loop from transient store at low strain amplitude of testing.

Figure A.14 INFLUENCE OF "NOISE" ON SIGNALS FROM TRANSIENT RECORDER

generator were monitored on the x-y recorder. This error could be eliminated by adjusting the tension in the wire cable of the slewing system of the recorder. The maximum frequency which could be plotted by the x-y recorder without significant hysteresis was approximately 0.3 cps. For higher frequencies of testing, the signals were stored in the transient recorder and played back at frequencies lower than 0.3 cps. Some amplification of the input signals occurred when the transient recorder was used. The amplification appeared to be dependent on frequency. To avoid many calibrations, only damping ratio was determined from x-y recordings. This could be done because damping ratio is a non-dimensional parameter.

The load and deformation at all frequencies of testing were recorded directly on a strip-chart recorder. The frequency response of the strip-chart recorder was checked and it was determined that there was no variation in the amplitude of the input signal when the frequency was varied from 0.05 to 50 cps. The dynamic Young's modulus was determined from the amplitude of load and displacement recorded on the strip-chart.

APPENDIX B

DESCRIPTION OF SAMPLE COUPLING DEVICE

A cohesive unfrozen soil can only be subjected to a very small tensile stress and a cohesionless soil cannot be subjected to any tensile stress. Consequently, no consideration must be made to insure that an unfrozen sample can be subjected to tension during cyclic triaxial testing since this state of stress cannot exist. Cyclic triaxial tests are, therefore, performed on unfrozen soils with the sample always in a compressive state of stress. In contrast to this, ice and frozen soils can be subjected to tensile stresses.

Two possible devices to couple the sample to the cap and base to achieve a tensile state of stress were considered in the research program as shown in Figure B.1. The "screw" coupling shown in Figure B.1a consists of four screws, 0.64 cm in diameter, in the top and bottom caps. The "screw and metal plate" coupling shown in Figure B.1b is essentially the same as the "screw" coupling except an aluminum plate, 5.4 cm long, 2.54 cm wide and 0.64 cm thick was attached to two of the screws in the top and bottom caps. The clearance between the cap and the aluminum plate was set at 1.27 cm.

Figure B.2 shows a comparison of the hysteresis loops obtained for an ice sample without a coupling and for ice samples with the "screw" and "screw and metal plate" couplings. The hysteresis loop for the sample without a coupling is highly non-symmetric. This is reasonable since the sample can only be subjected to compressive stresses. The minimum deviator stress is equal to 12.8 psi; it is not equal to the confining pressure, 25 psi. There are two possible explanations for this discrepancy:

- (1) The sample did not separate from the caps because the sample elongated owing to the confining pressure acting on the side of the sample. As a result of the sample elongation there was an axial stress in the sample which would be measured as the deviator stress, 12.8 psi.
- (2) The sample separated from the cap but the membrane did not penetrate into the gap. Consequently, there was an air pressure in the gap less than the confining pressure. (If the membrane penetrated through the gap between the sample and the cap the minimum deviator stress would be zero.) The minimum deviator

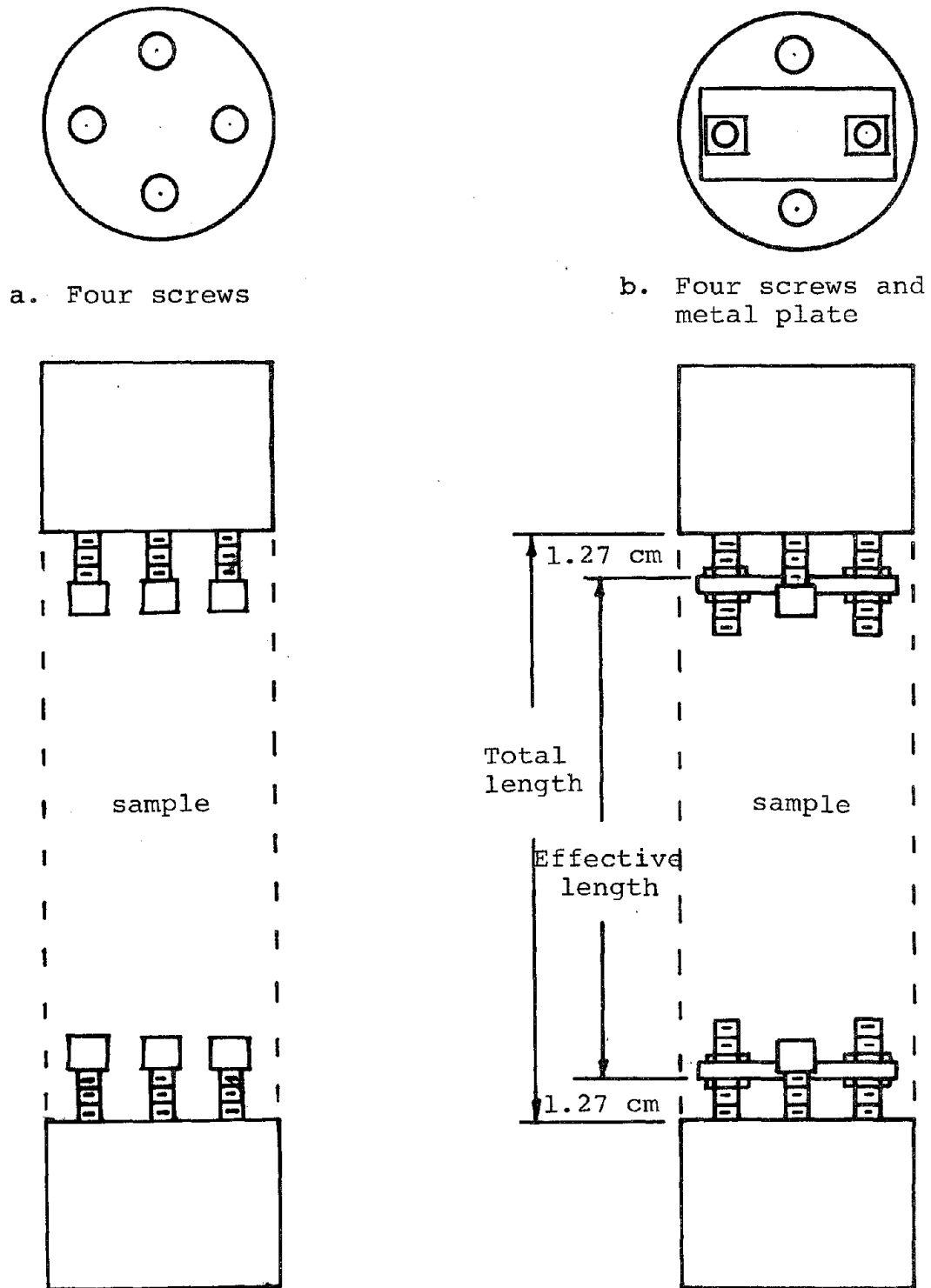
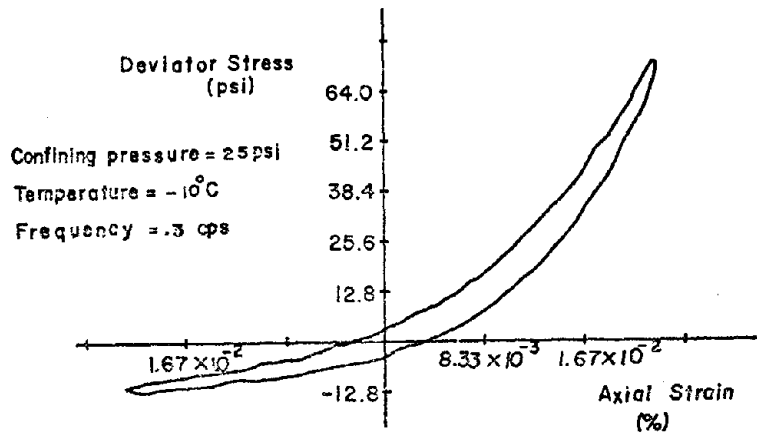
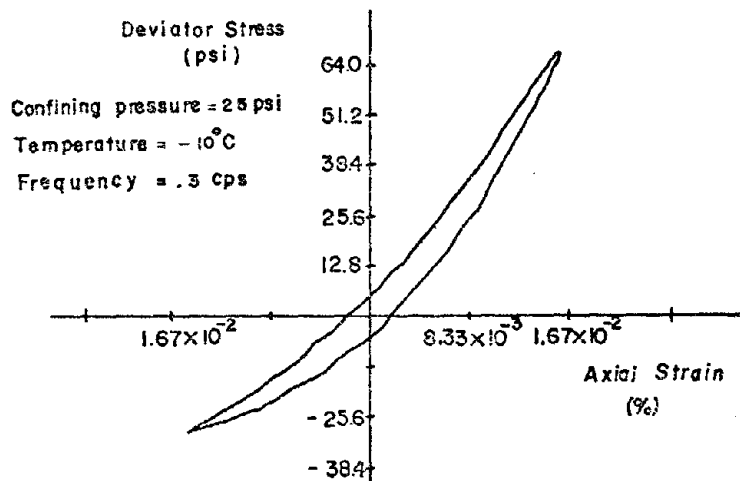


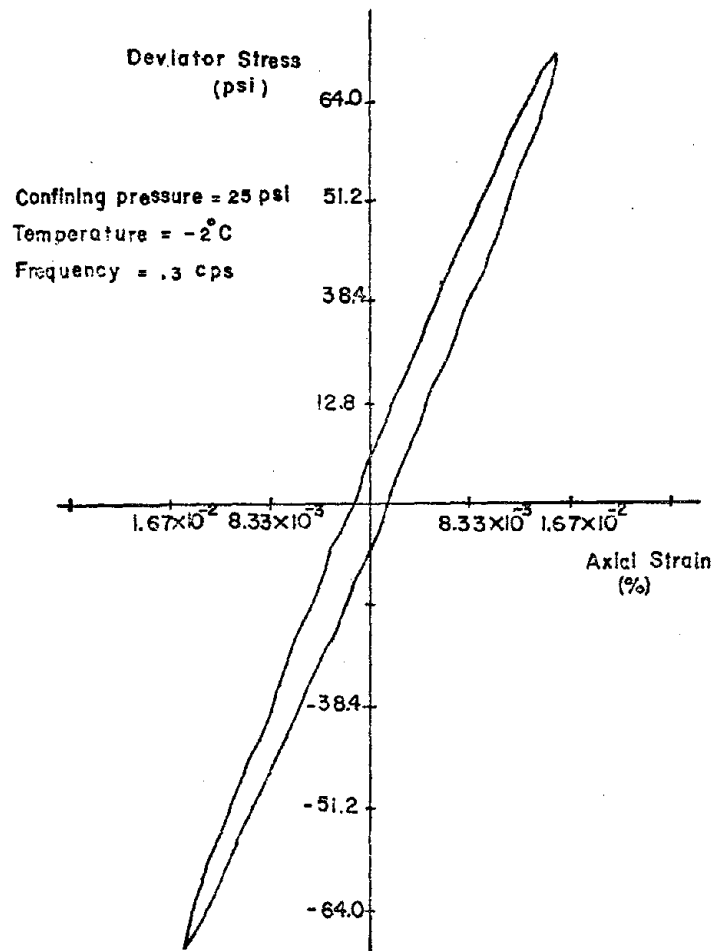
Figure B.1 COUPLING DEVICE USED IN CYCLIC TRIAXIAL TESTING OF ICE AND FROZEN CLAY



(a) Ice sample without coupling



(b) Ice sample coupled with four screws



(c) Ice sample coupled with four screws and metal plate

Figure B.2 TYPICAL HYSTERESIS LOOPS OF ICE SAMPLE FOR DIFFERENT COUPLING DEVICES

stress, 12.8 psi, would be equal to a reduction of the confining pressure, 25 psi, by a pressure of 12.2 psi in the gap.

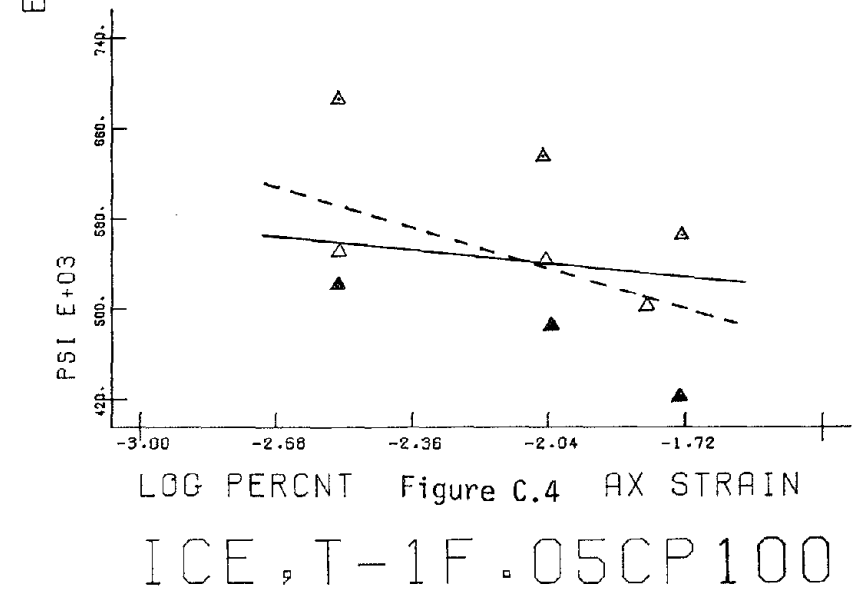
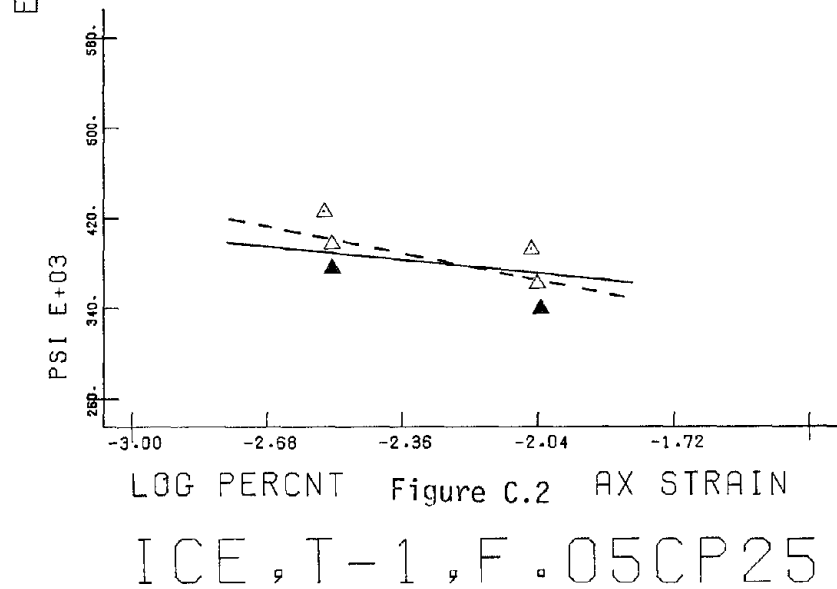
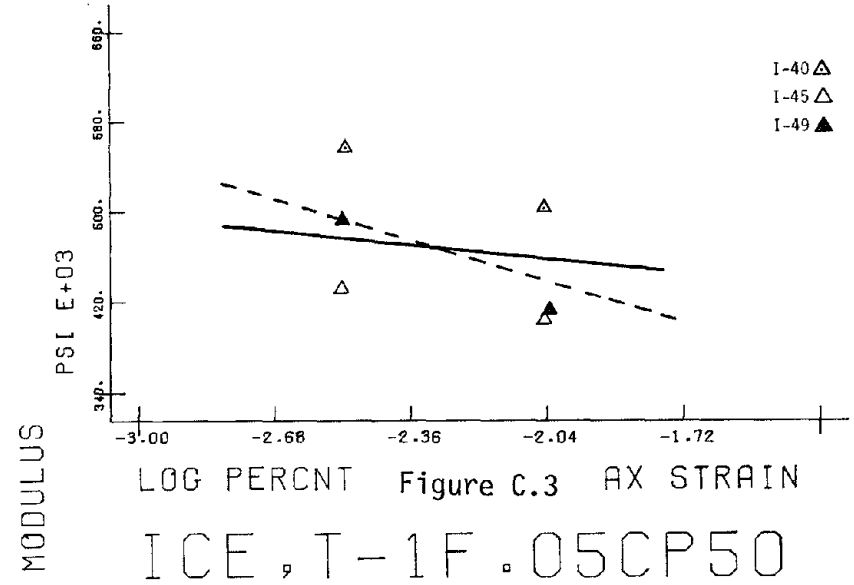
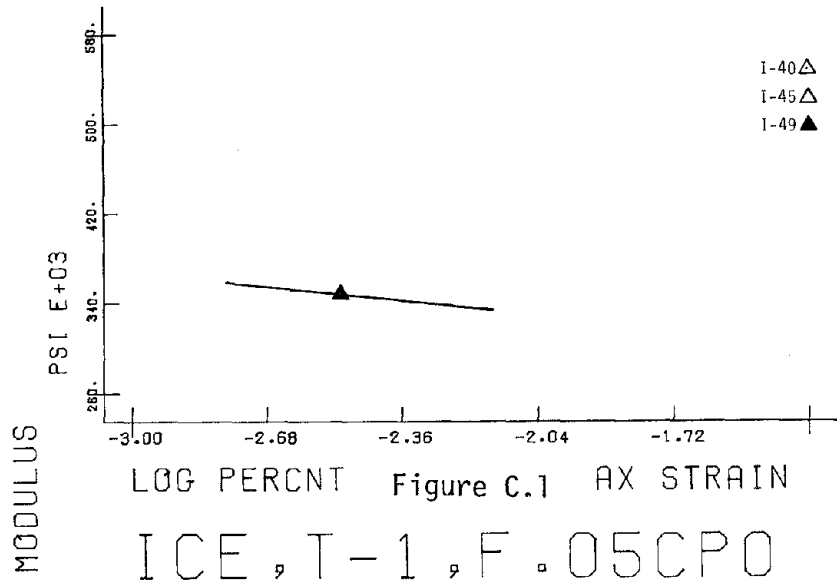
The hysteresis loop for the sample with the "screw" coupling is also highly non-symmetric. This indicates (1) the sample failed, (2) the dynamic modulus in compression is much greater than that in tension, or (3) the coupling was not sufficient to resist the tensile force applied. Inspection of the samples from the tests with this coupling indicated they had not failed. There is no reason to believe the modulus in tension for ice is significantly different than the modulus in compression. Thus, the hysteresis loop could not be explained on this basis. Therefore, it was concluded the coupling did not provide sufficient resistance to the tensile force. The screw coupling was rejected for this reason.

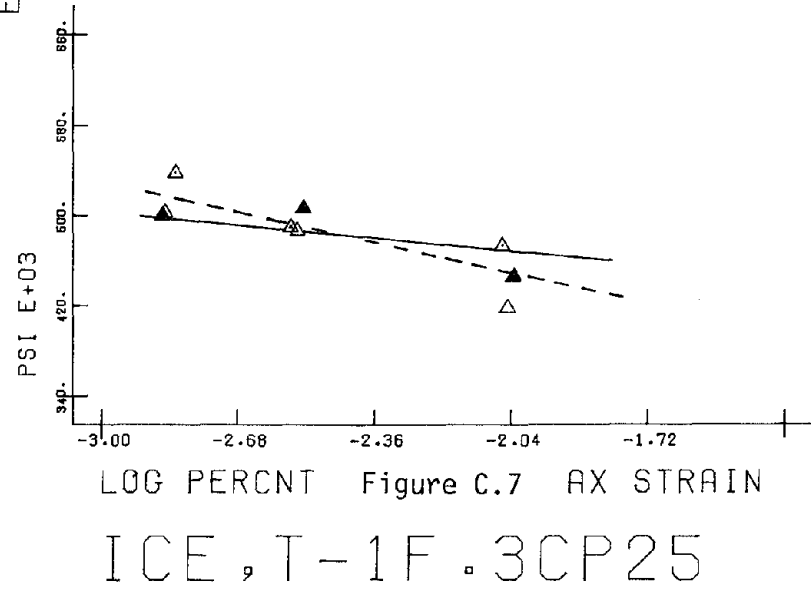
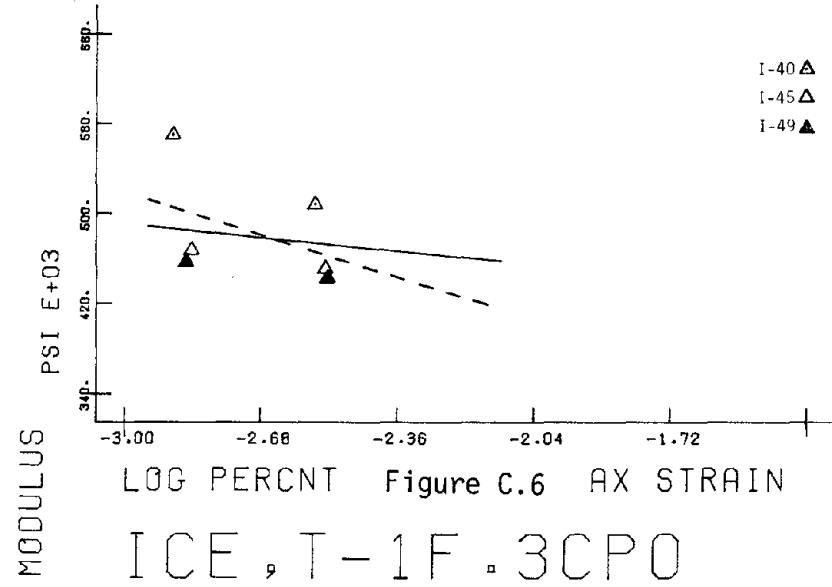
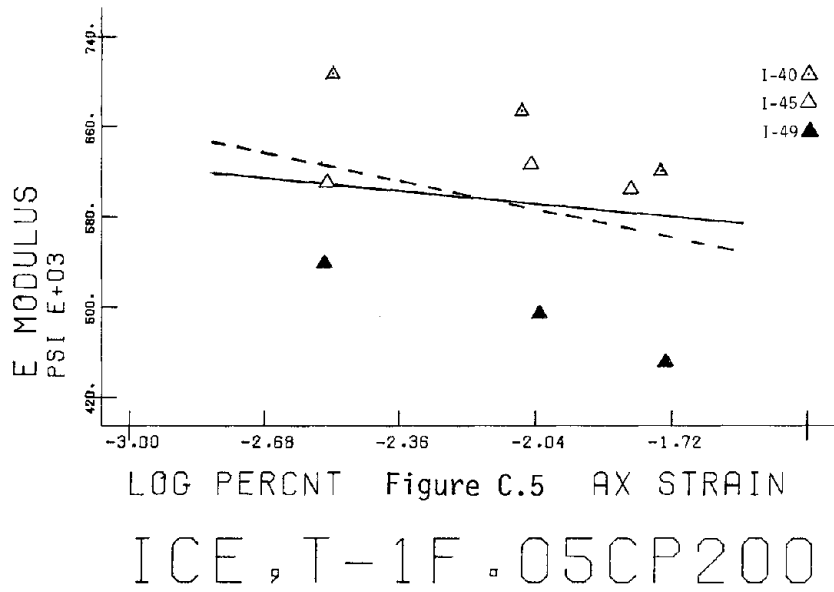
The hysteresis loop for the sample with the four screws and metal plate is symmetric and indicates that a resistance to the tensile force was developed which allowed the sample to be subjected to a tensile stress. This coupling was selected for use in the research program.

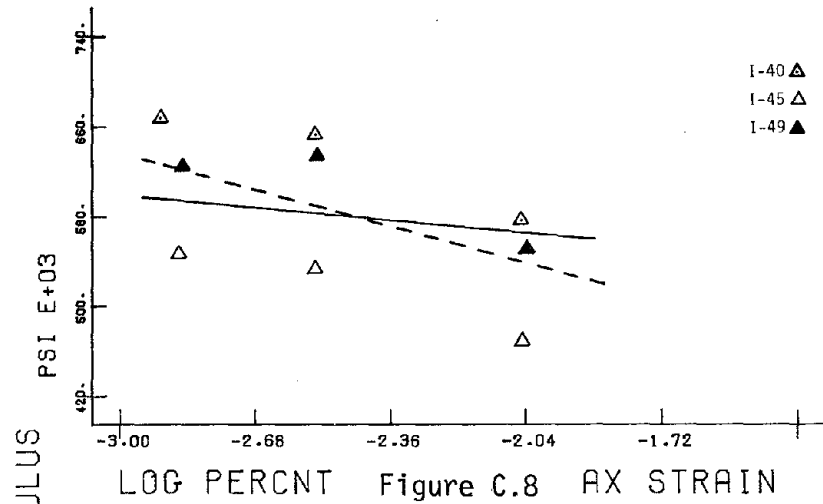
It is obvious that with the "screw and metal plate" coupling the effective length of the sample used to calculate dynamic properties would be slightly less than the total length of the sample. The effective length of the sample is extremely difficult to calculate because it is dependent on the dynamic elastic moduli of the specimens. Therefore, for practical purposes, the effective lengths were assumed to be 2.54 cm shorter than the full length, owing to a reduction of 1.27 cm from the top cap and 1.27 cm from the bottom cap. Even if the effective length is slightly in error it would result in only a small error in the evaluation of the dynamic modulus and axial strain. The lengths of the specimens were approximately 18 cm with corresponding effective lengths of about 15.5 cm. If the assumed effective length was ± 1 cm in error, the error in the dynamic modulus would be about 6.5% and the error in the strain would be about 7%.

APPENDIX C
CYCLIC TRIAXIAL TEST RESULTS: DYNAMIC
YOUNG'S MODULUS OF ICE

Test results of Dynamic Young's modulus for high density ice are shown in Figures C.1 to C.93, and those for low density ice are shown in Figures C.94 to C.126. The dashed lines in the figures represent the least squares best fit line of the data for a given test condition. The solid lines represent the average least squares best fit line for all the experimental data drawn through the "center" of the data set for a given test condition. (Refer to Section 4.4.1 and Figures 4.3 and 4.4 for further explanation.)

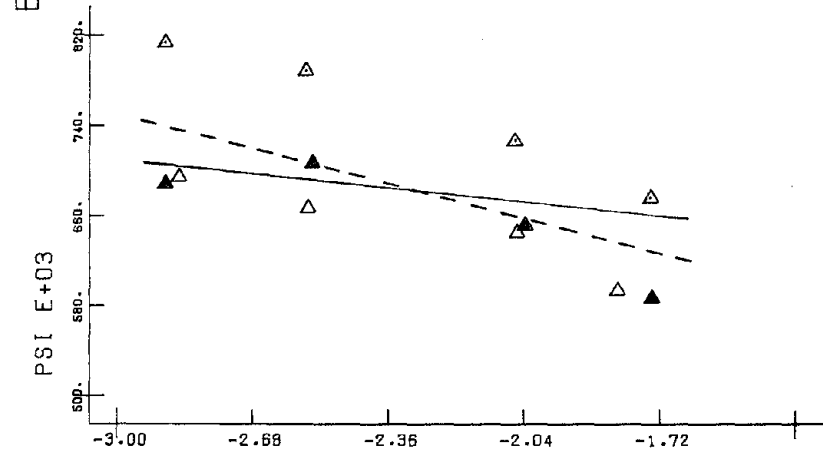






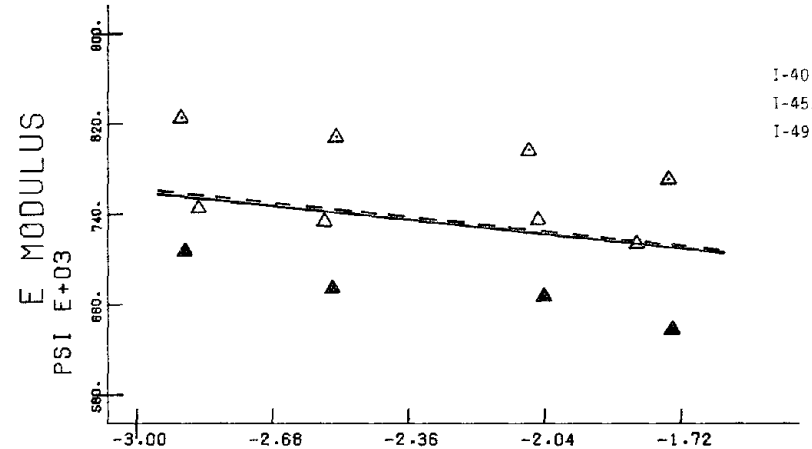
LOG PERCENT Figure C.8 AX STRAIN

ICE, T-1F.3CP50



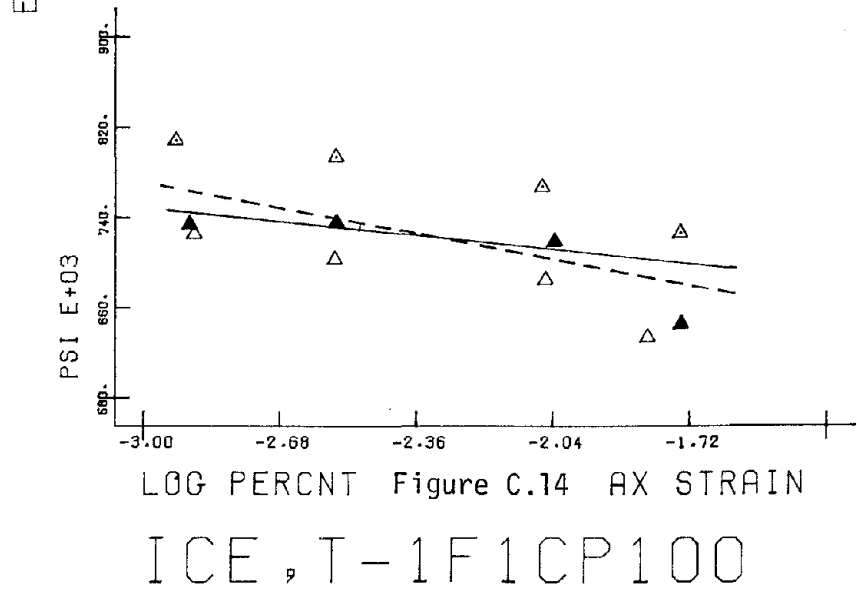
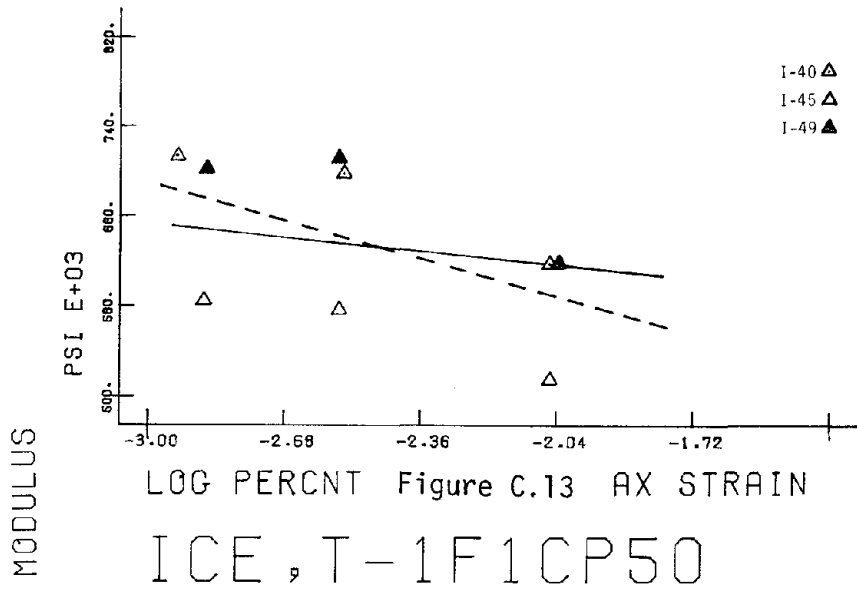
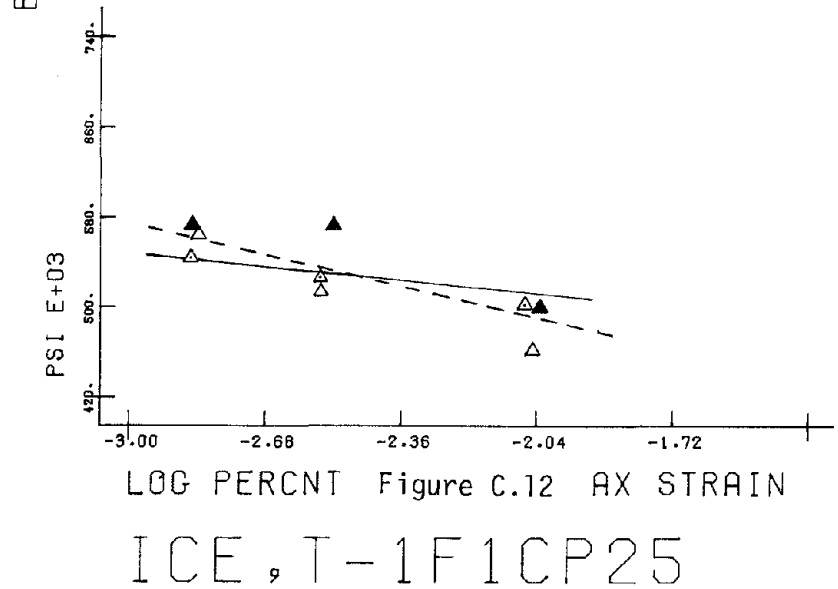
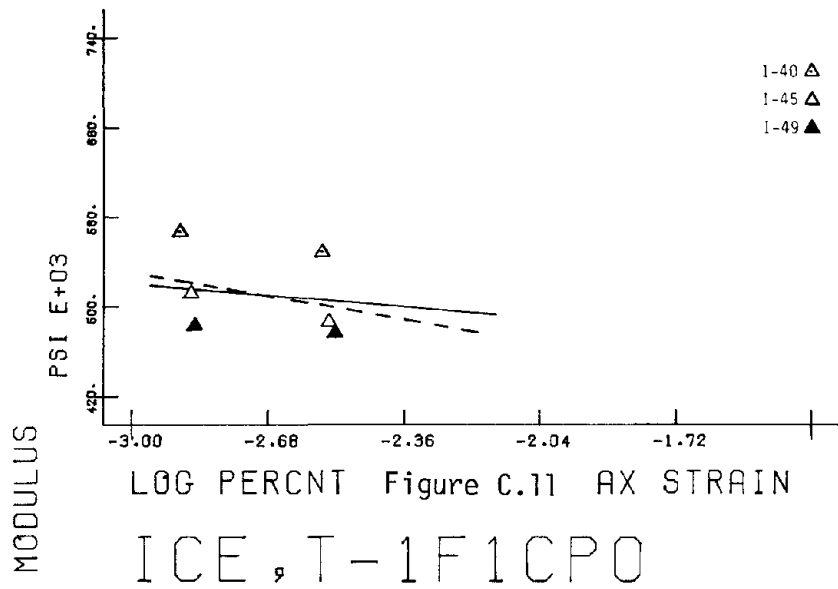
LOG PERCENT Figure C.9 AX STRAIN

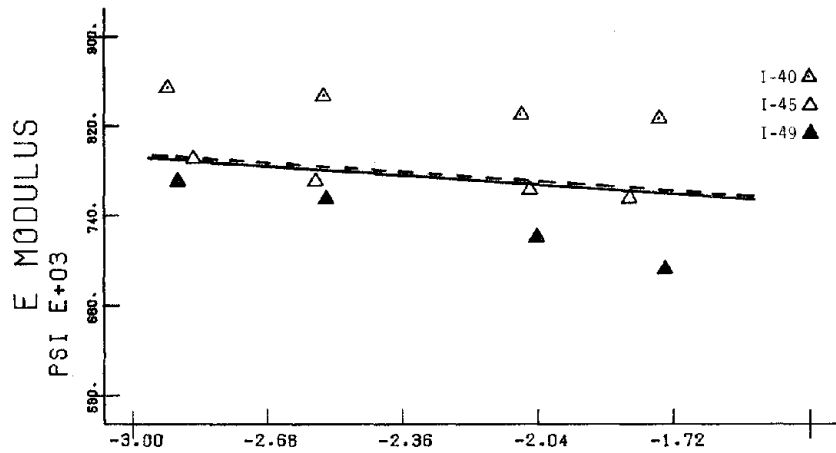
ICE, T-1F.3CP100



LOG PERCENT Figure C.10 AX STRAIN

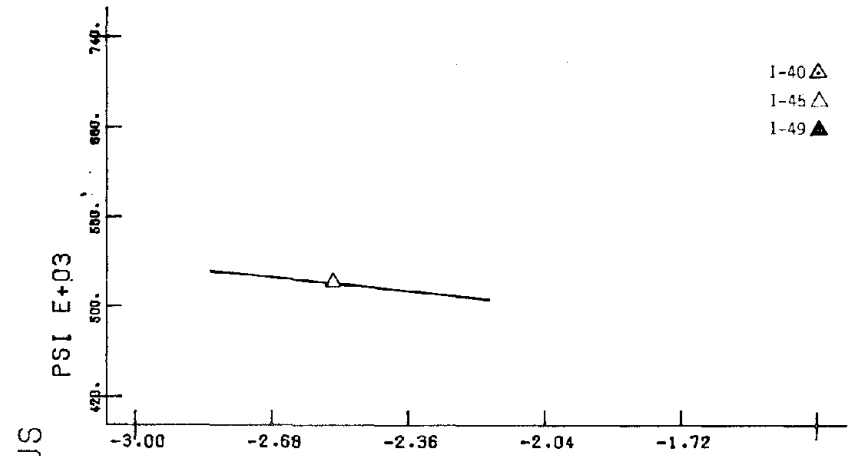
ICE, T-1F.3CP200





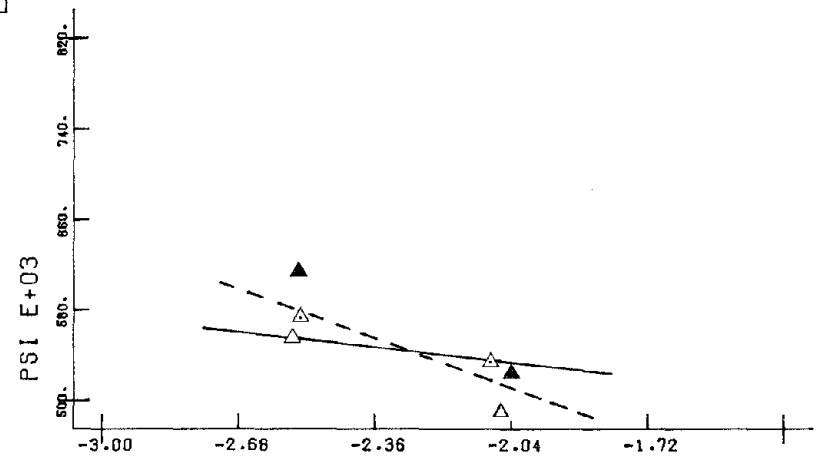
LOG PERCNT Figure C.15 AX STRAIN

ICE, T-1F1CP200



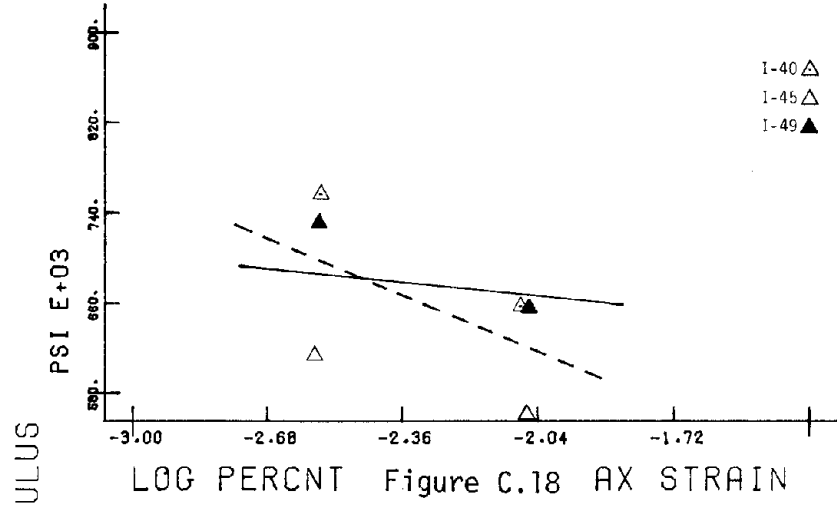
LOG PERCNT Figure C.16 AX STRAIN

ICE, T-1F5CP0

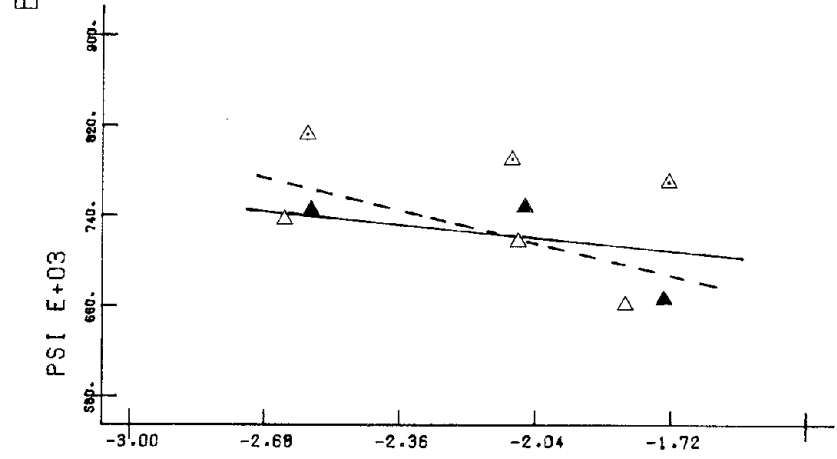


LOG PERCNT Figure C.17 AX STRAIN

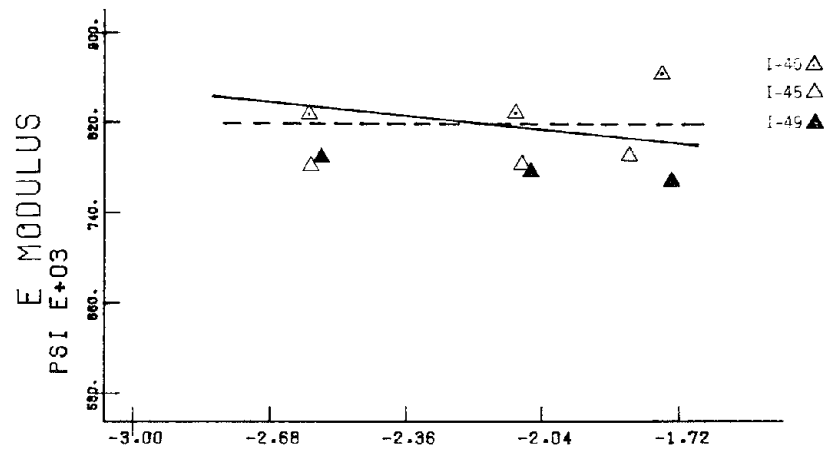
ICE, T-1F5CP25



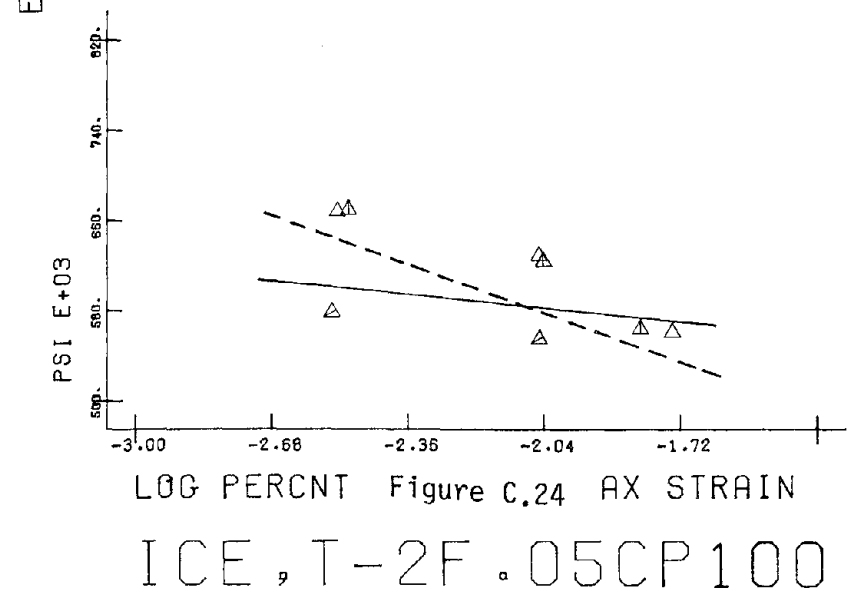
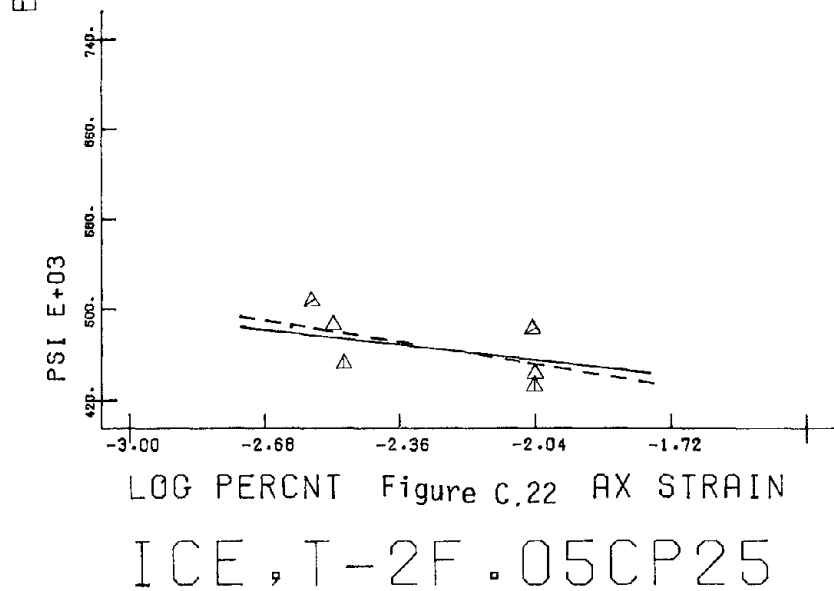
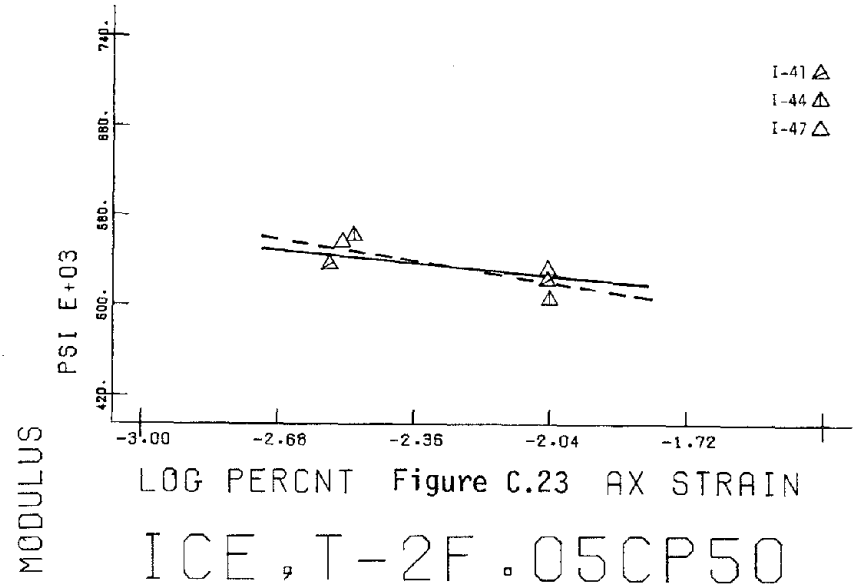
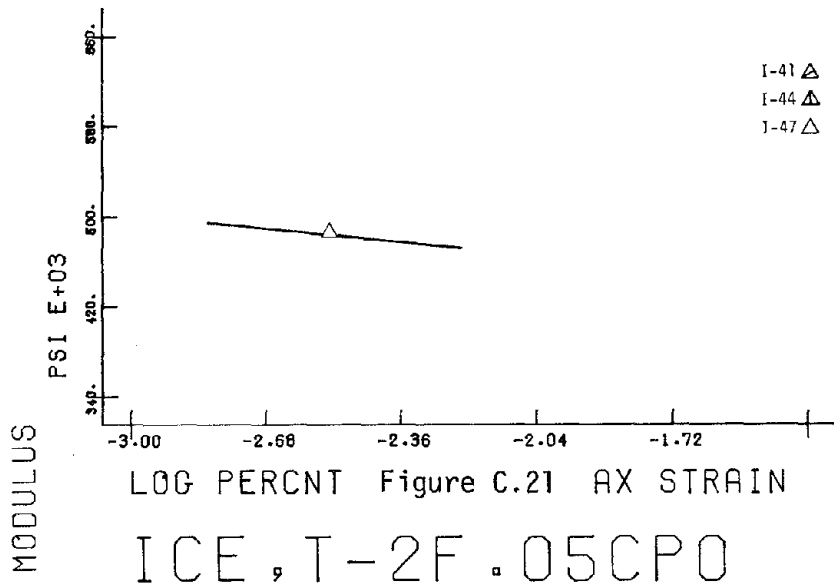
LOG PERCNT Figure C.18 AX STRAIN
 ICE, T-1F5CP50

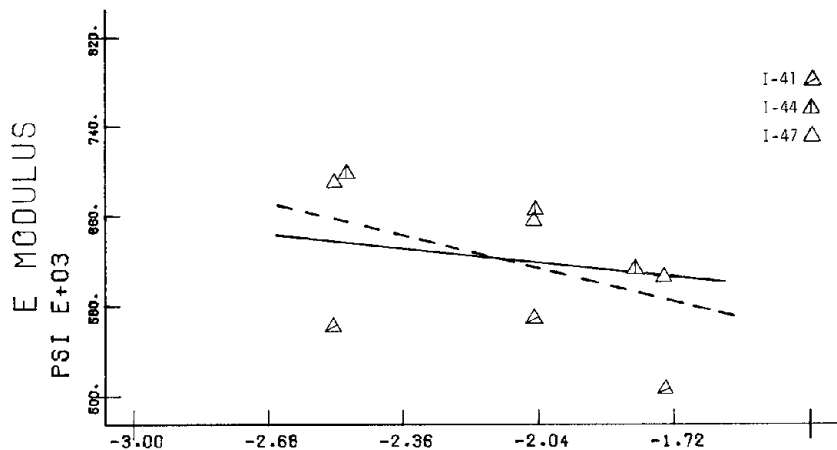


LOG PERCNT Figure C.19 AX STRAIN
 ICE, T-1F5CP100

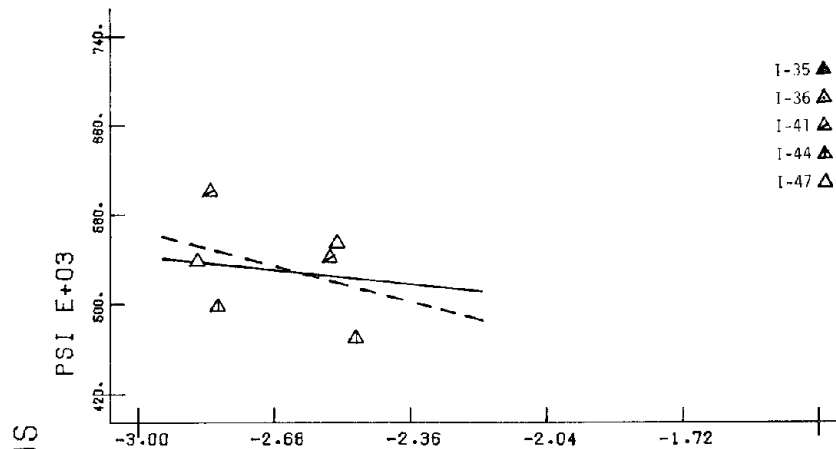


LOG PERCNT Figure C.20 AX STRAIN
 ICE, T-1F5CP200

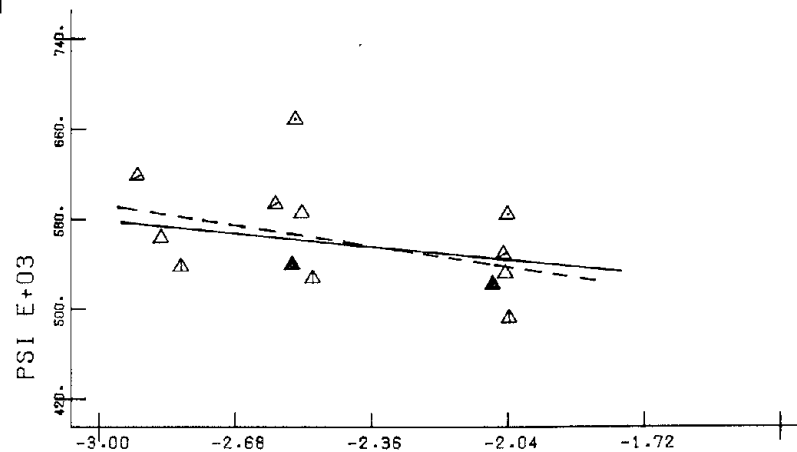




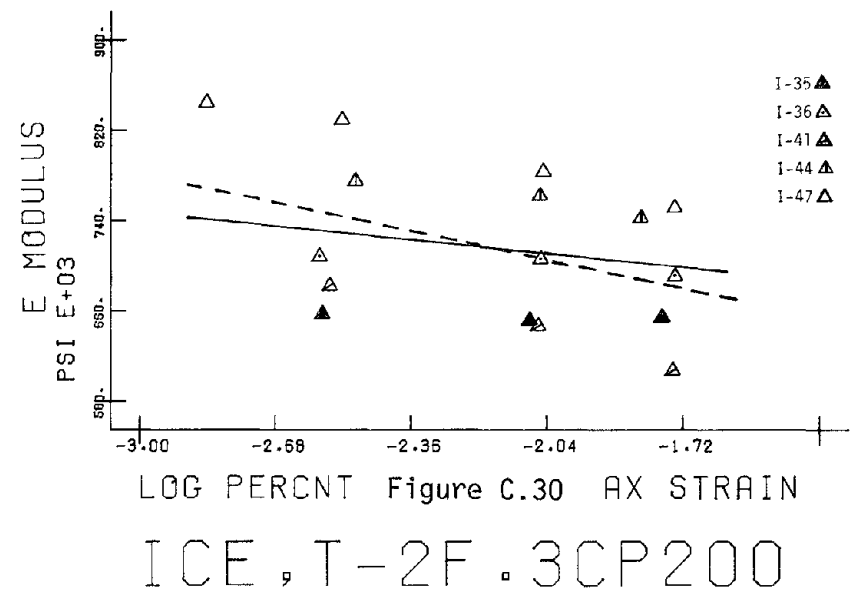
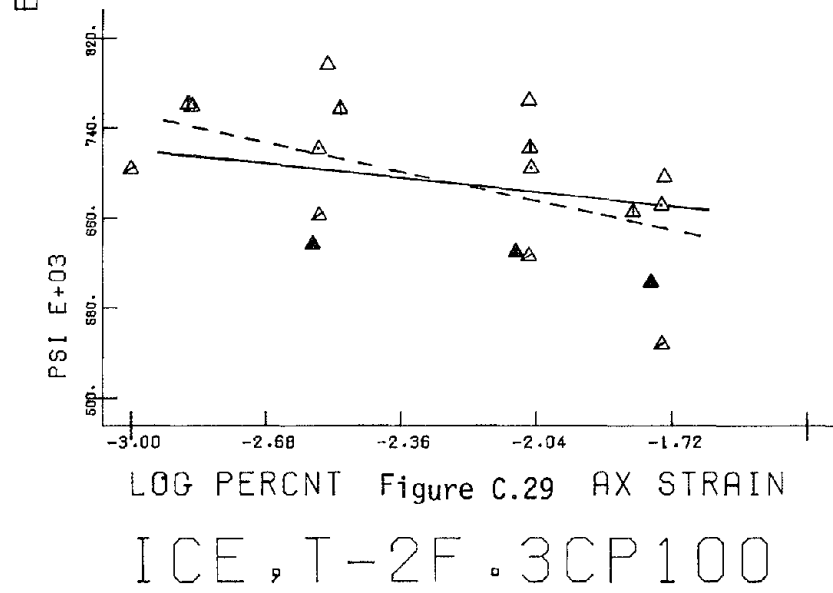
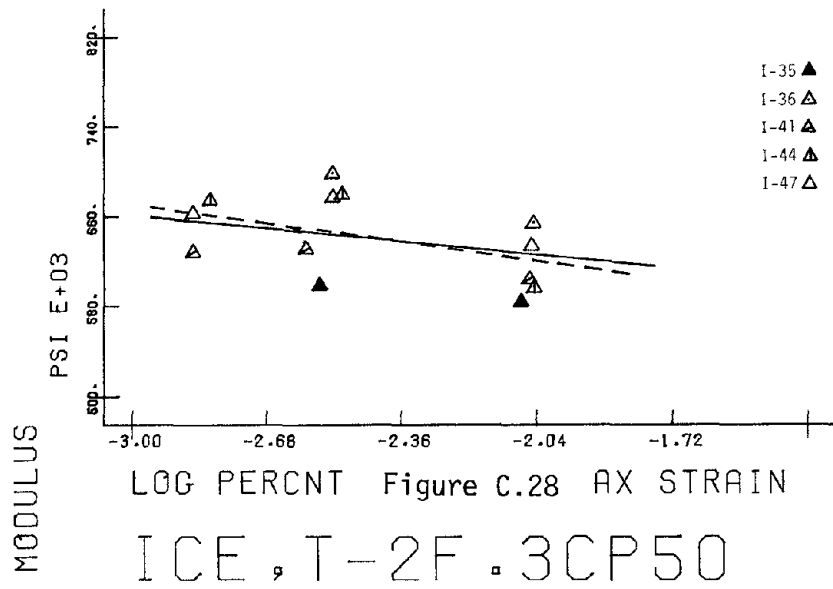
LOG PERCENT Figure C.25 AX STRAIN
 ICE, T-2F .05CP200

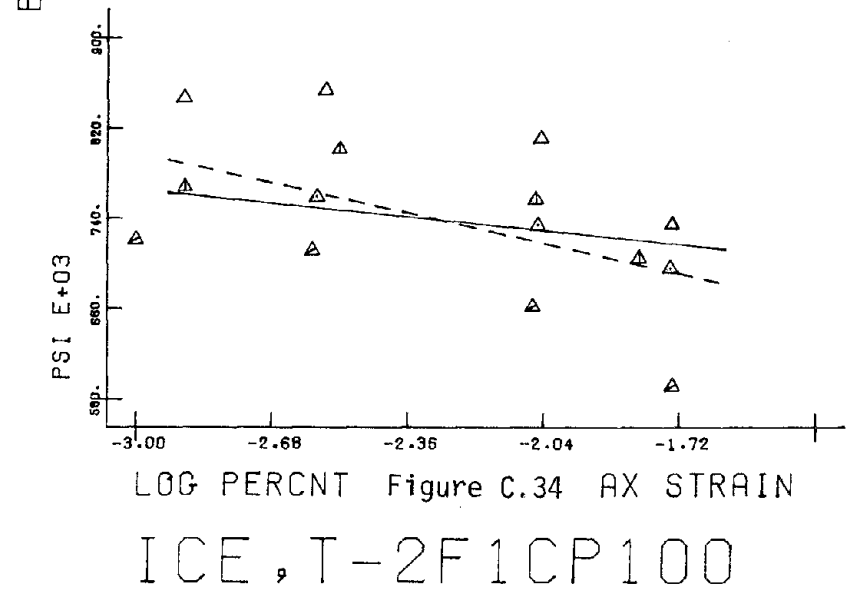
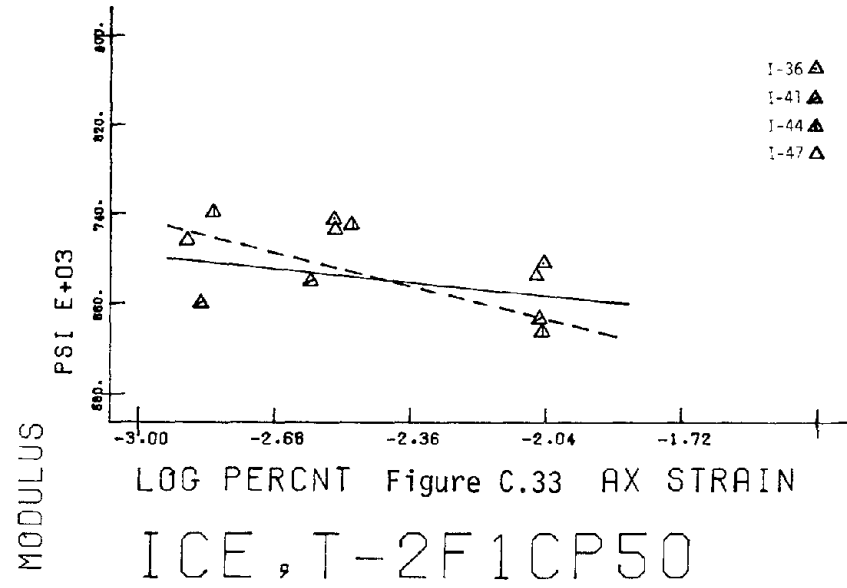
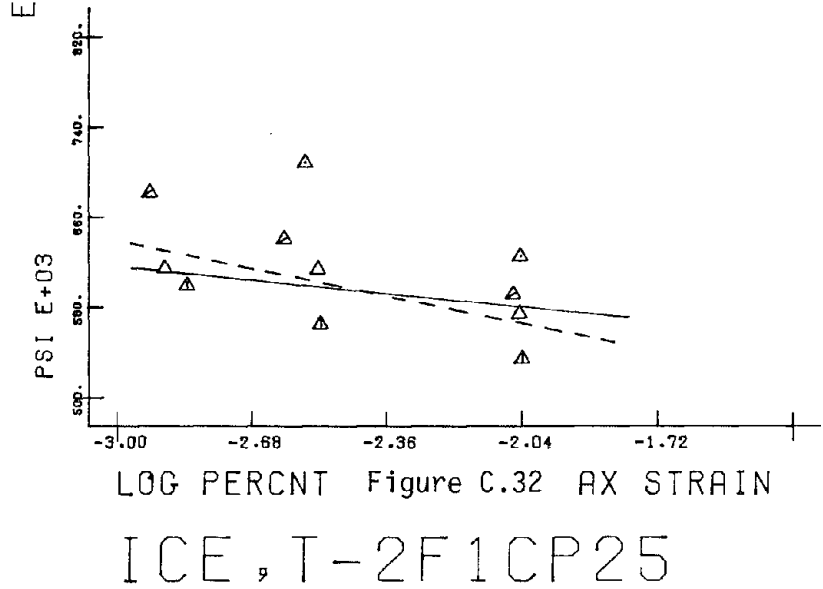
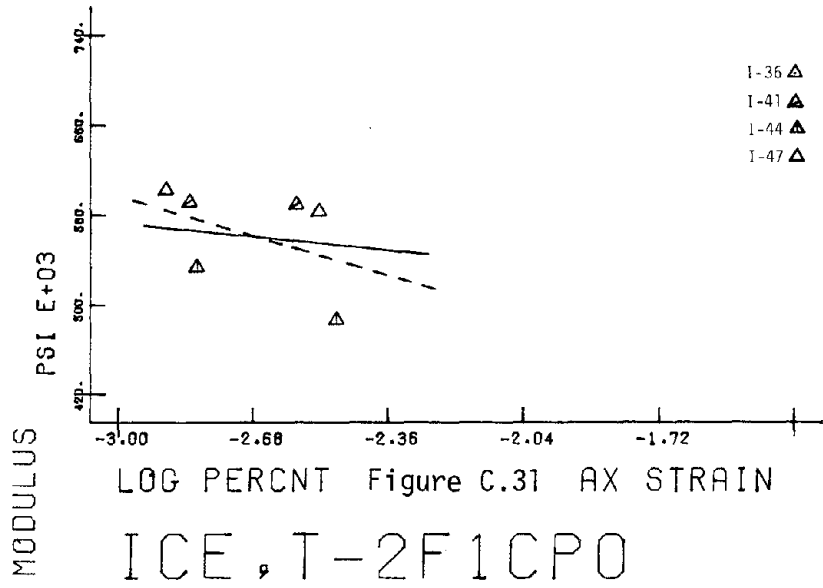


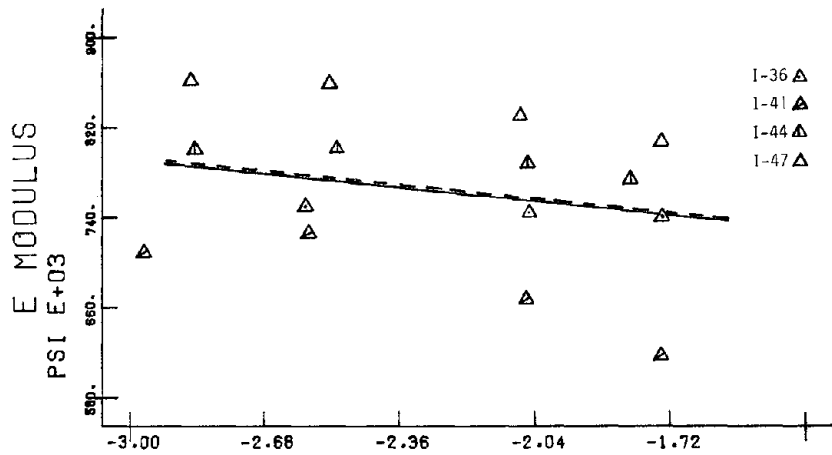
LOG PERCENT Figure C.26 AX STRAIN
 ICE, T-2F .3CP0



LOG PERCENT Figure C.27 AX STRAIN
 ICE, T-2F .3CP25

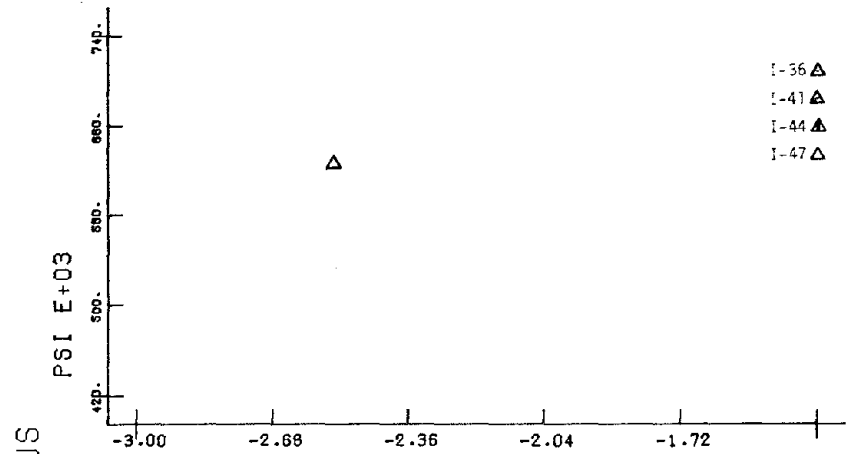






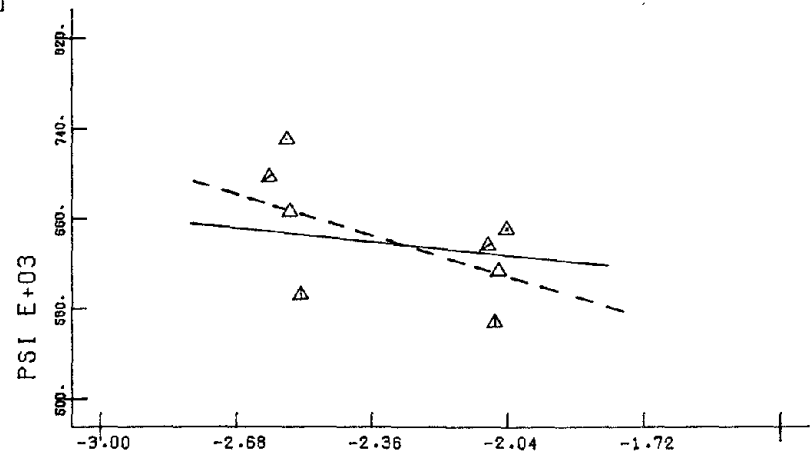
LOG PERCENT Figure C.35 AX STRAIN

ICE, T-2F1CP200



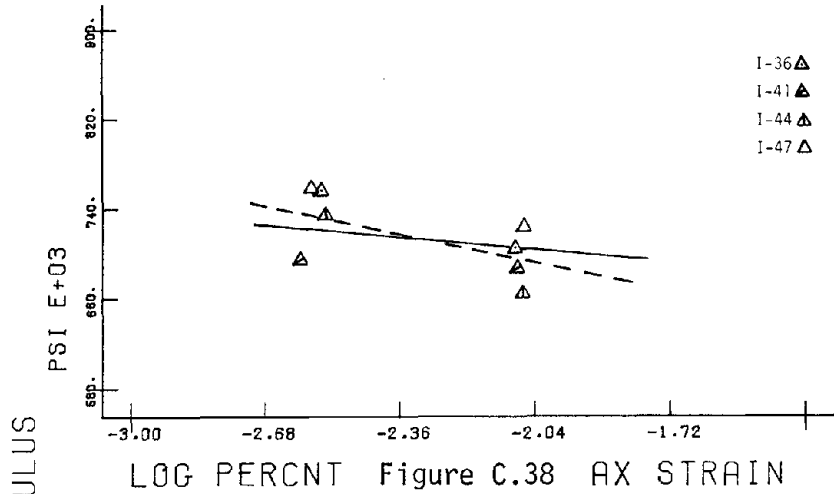
LOG PERCENT Figure C.36 AX STRAIN

ICE, T-2F5CPO



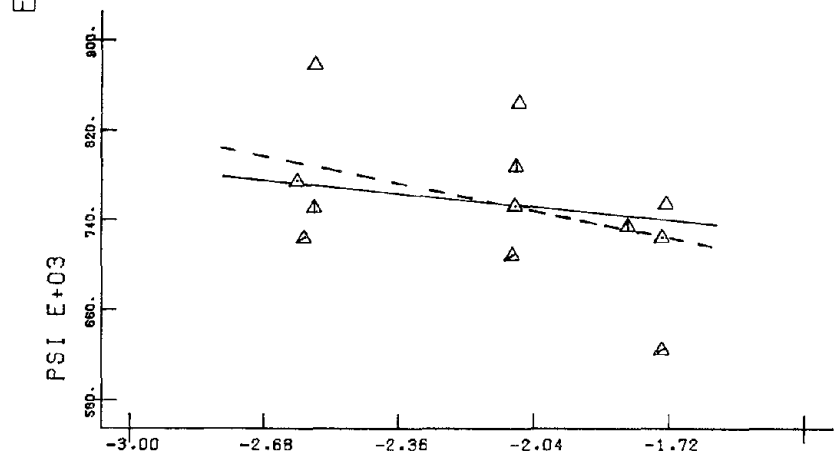
LOG PERCENT Figure C.37 AX STRAIN

ICE, T-2F5CP25



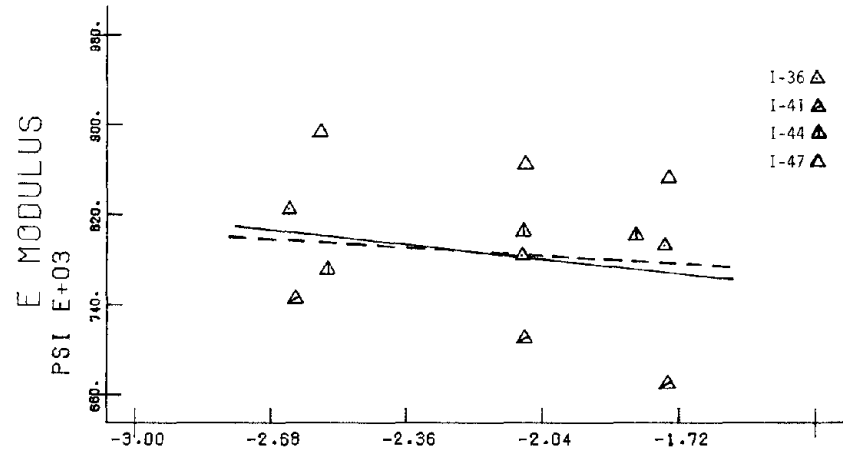
LOG PERCENT Figure C.38 AX STRAIN

ICE, T-2F5CP50



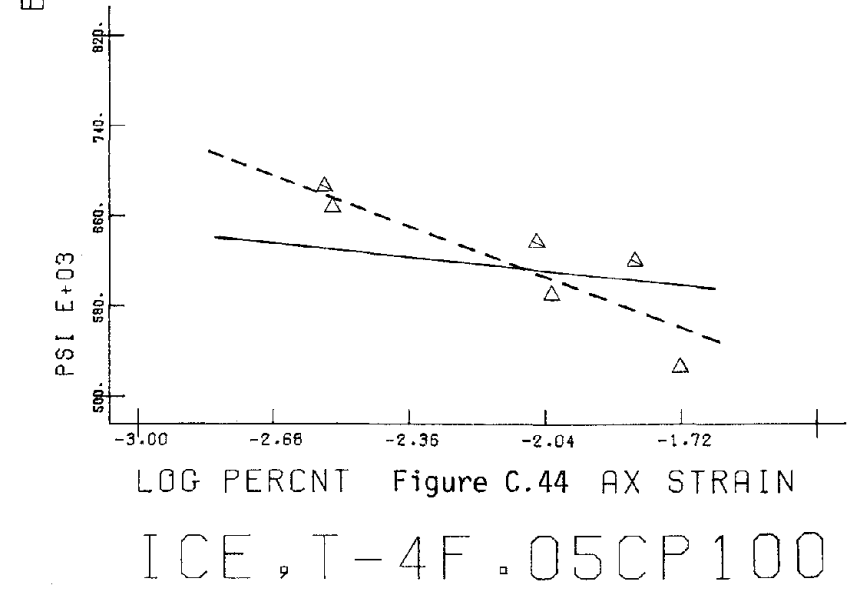
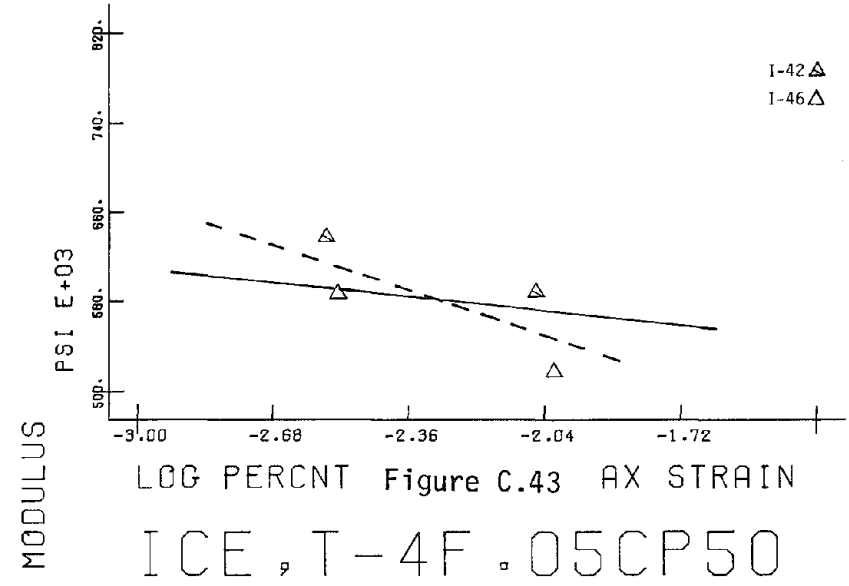
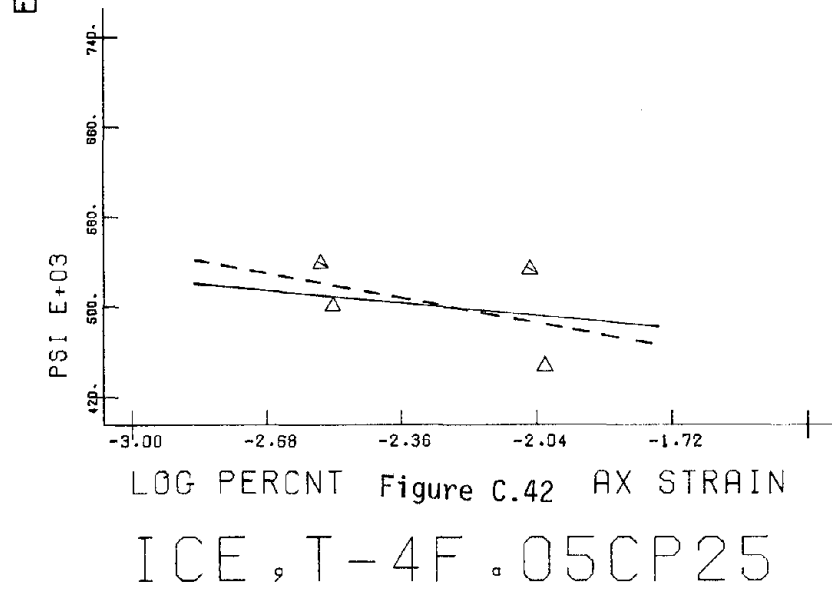
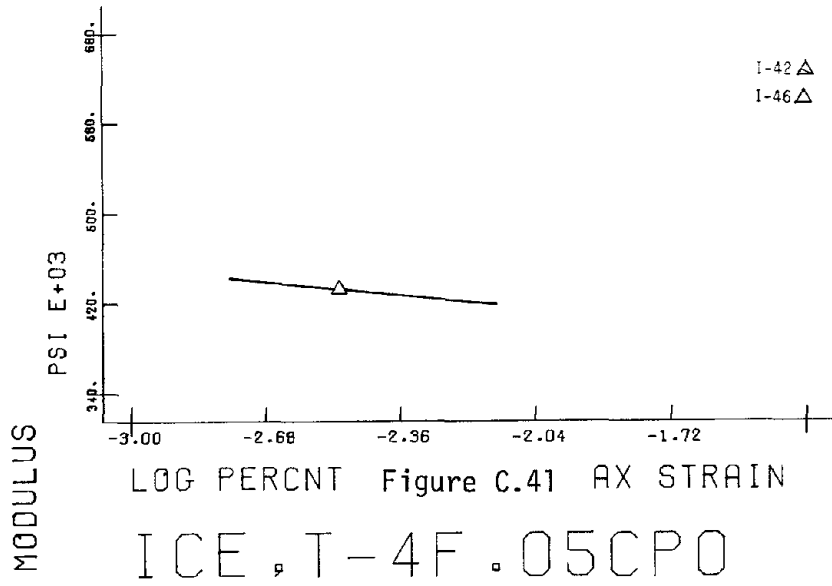
LOG PERCENT Figure C.39 AX STRAIN

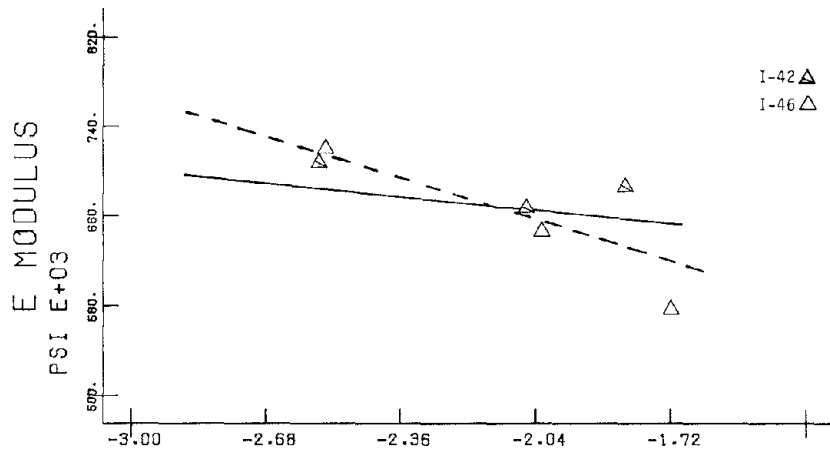
ICE, T-2F5CP100



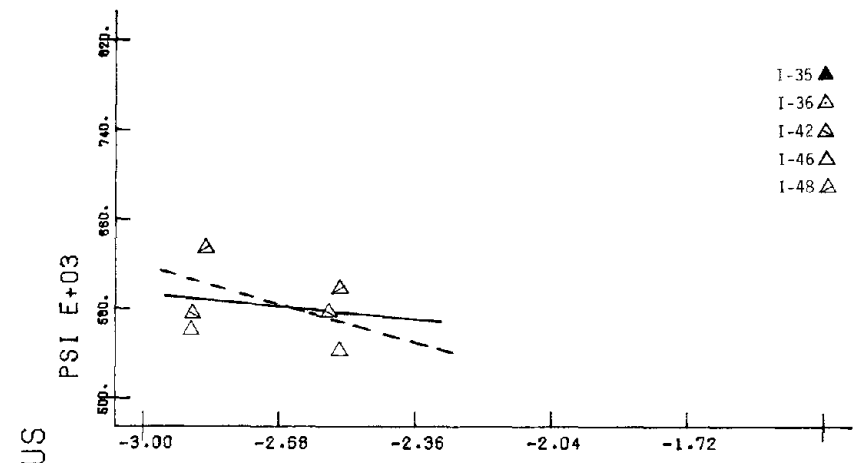
LOG PERCENT Figure C.40 AX STRAIN

ICE, T-2F5CP200

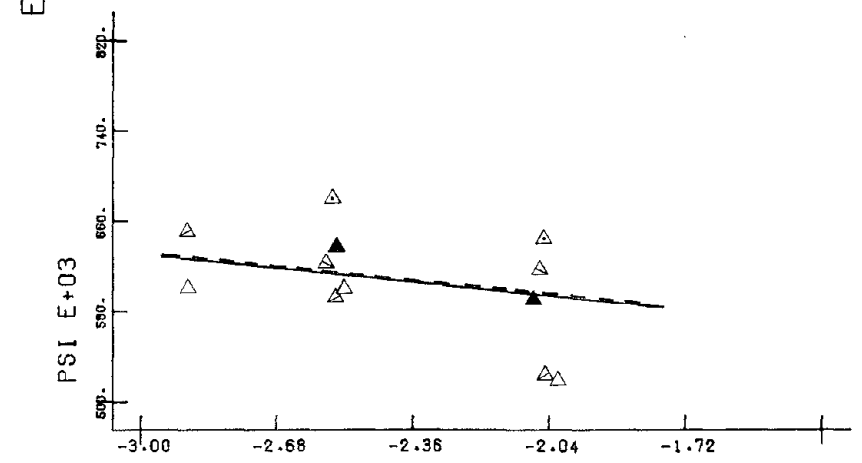




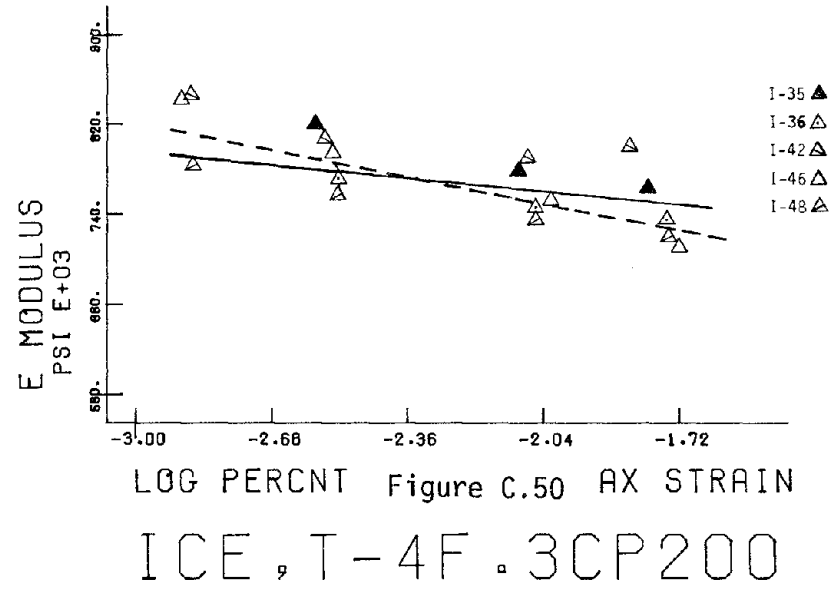
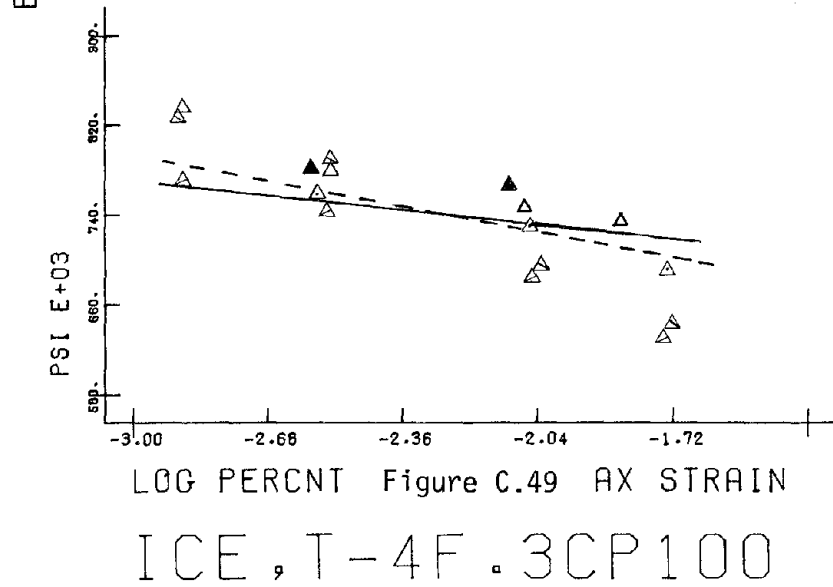
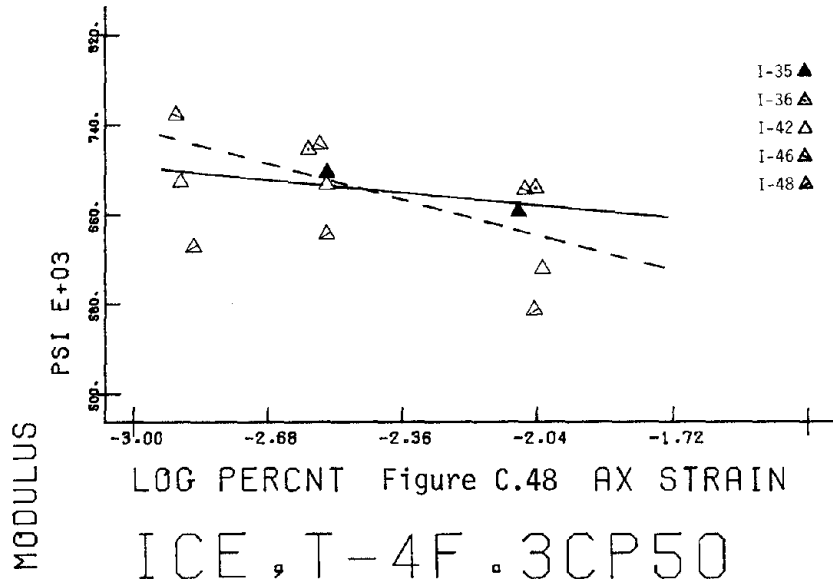
LOG PERCENT Figure C.45 AX STRAIN
 ICE, T-4F .05CP200

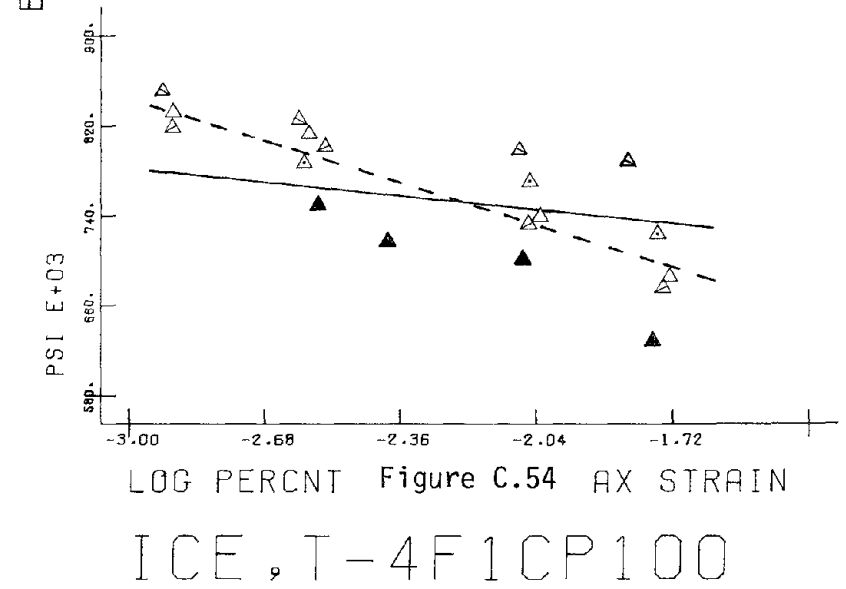
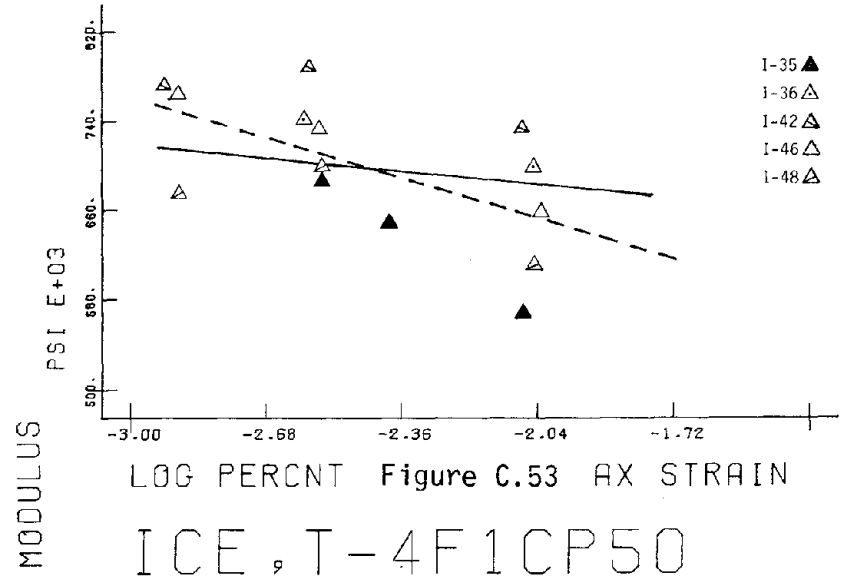
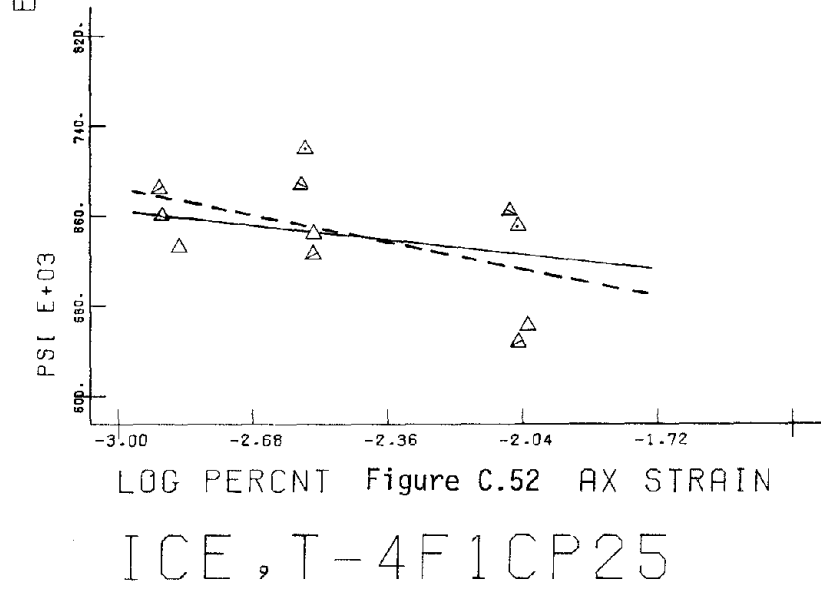
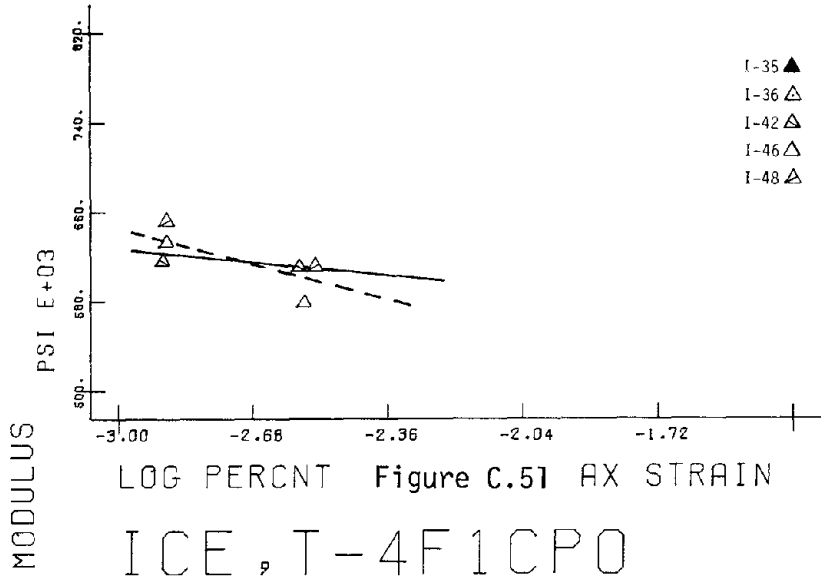


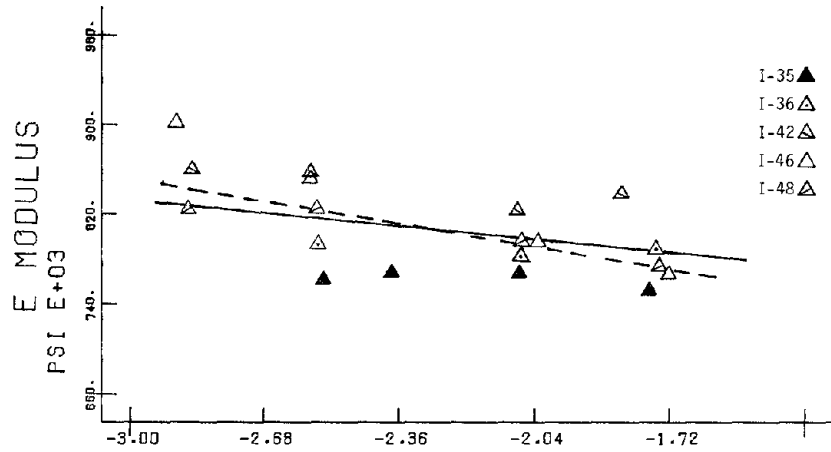
LOG PERCENT Figure C.46 AX STRAIN
 ICE, T-4F .3CP0



LOG PERCENT Figure C.47 AX STRAIN
 ICE, T-4F .3CP25

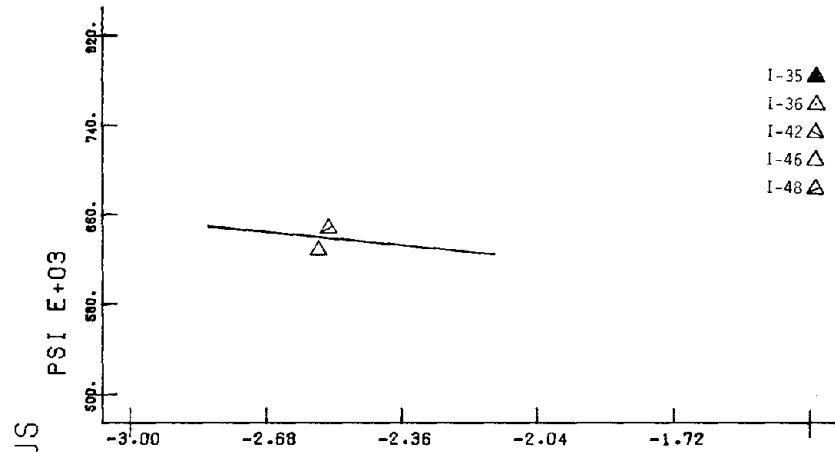






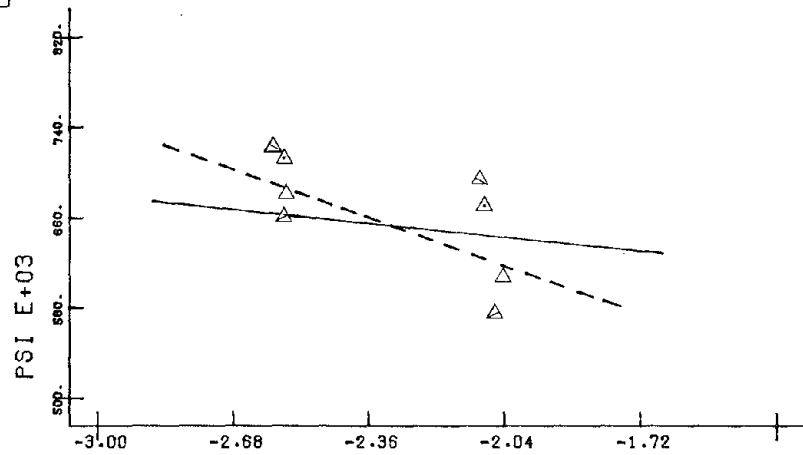
LOG PERCNT Figure C.55 AX STRAIN

ICE , T-4F1CP200



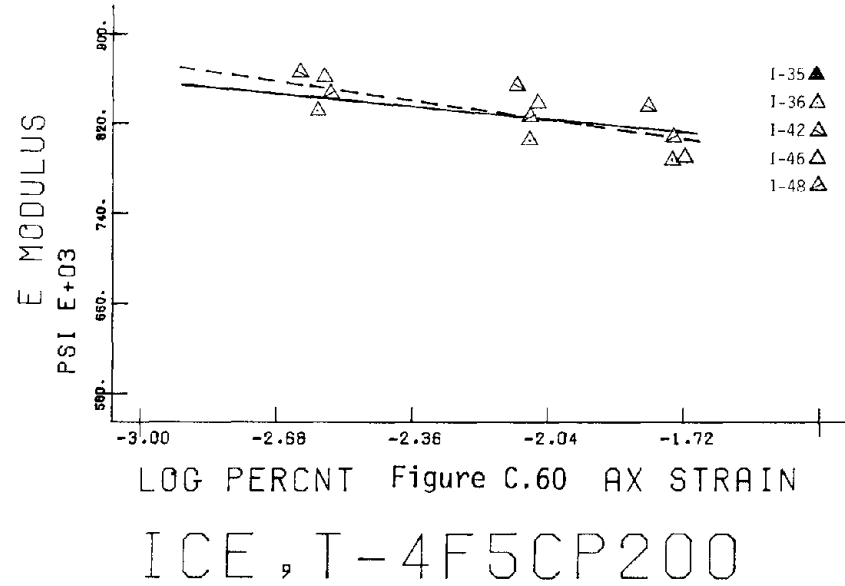
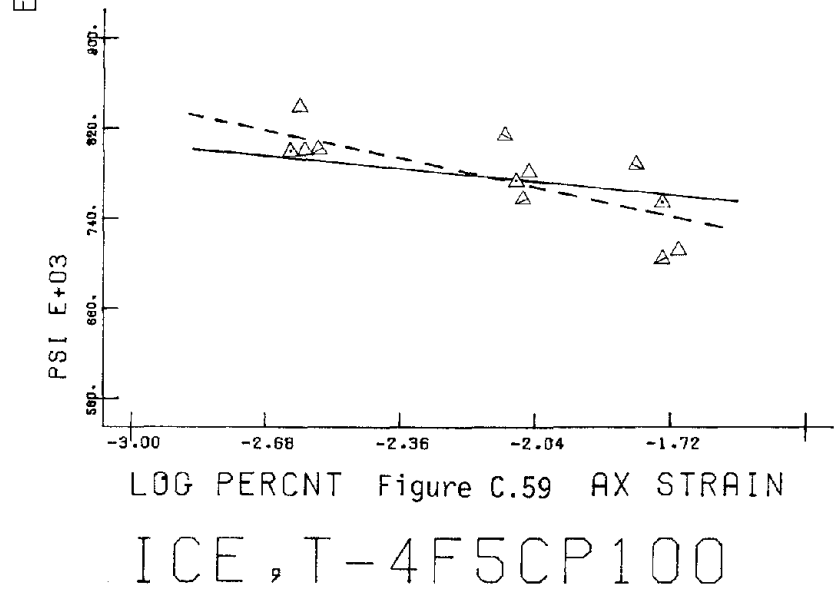
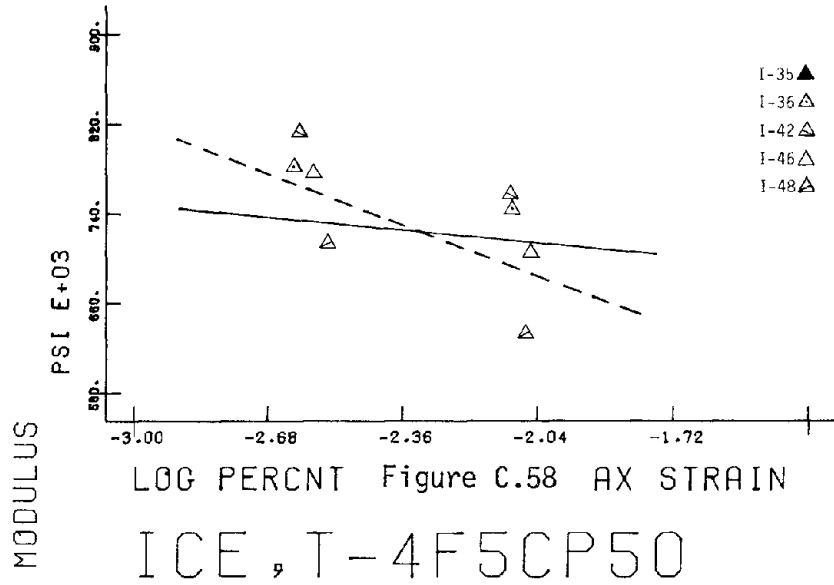
LOG PERCNT Figure C.56 AX STRAIN

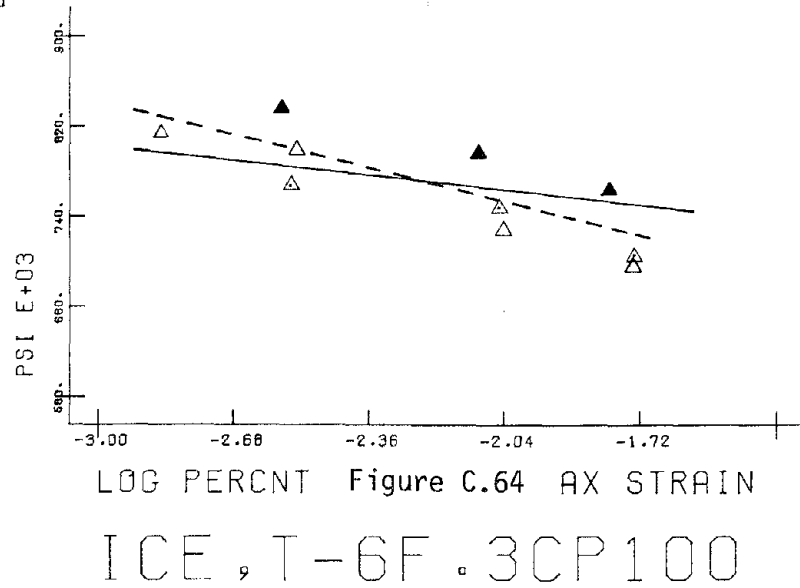
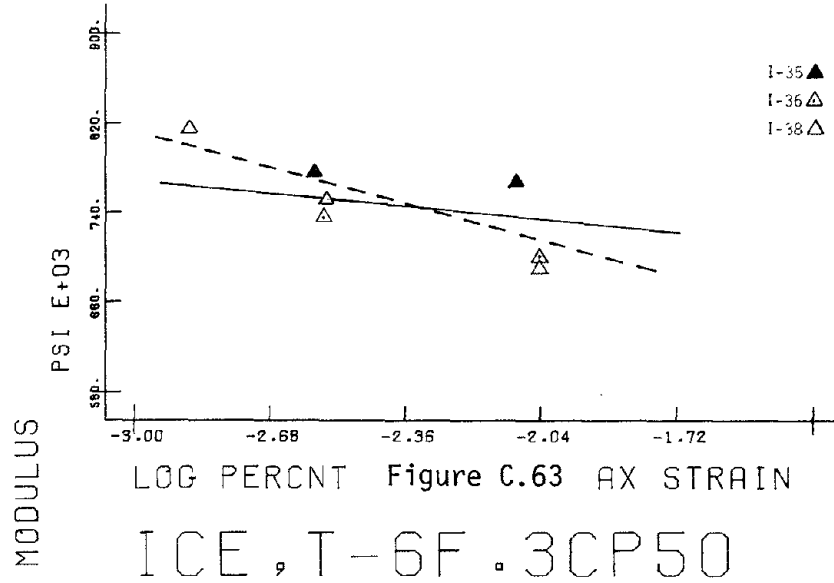
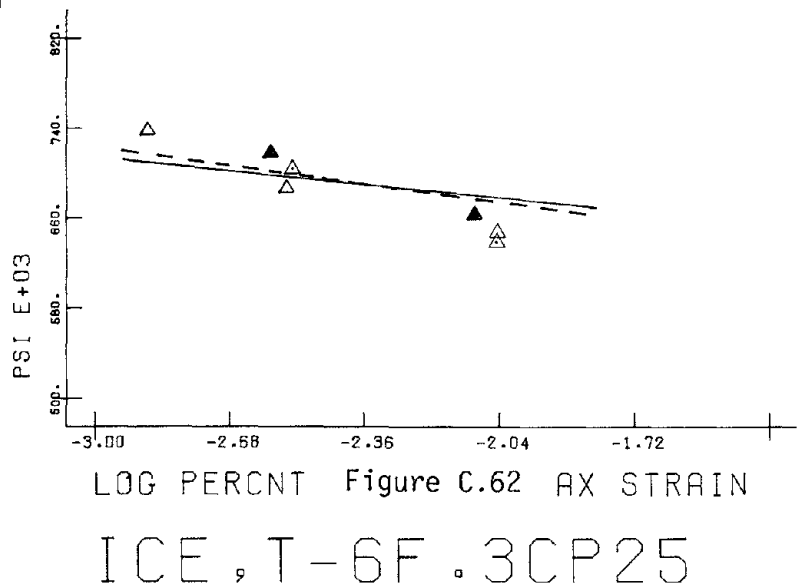
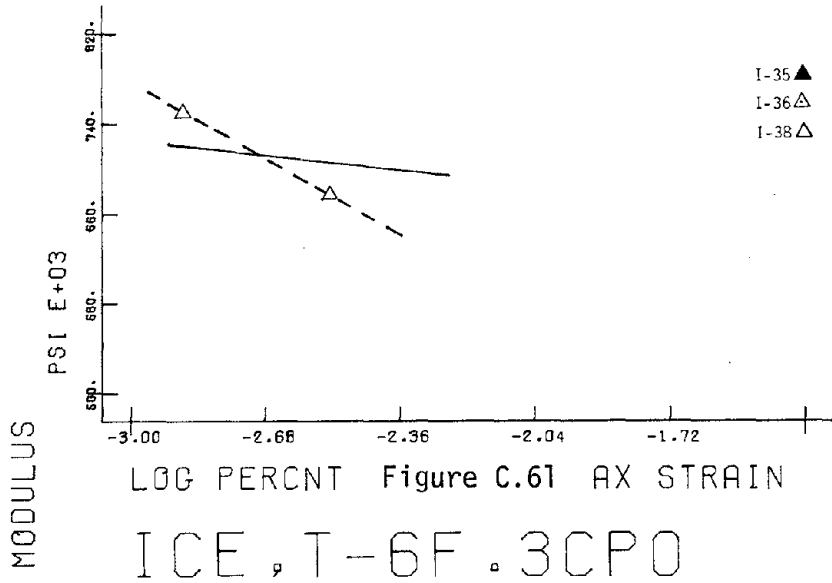
ICE , T-4F5CP0

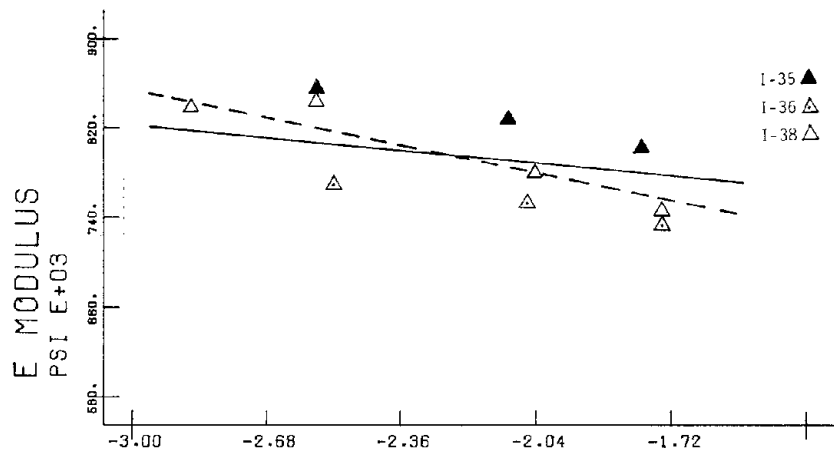


LOG PERCNT Figure C.57 AX STRAIN

ICE , T-4F5CP25

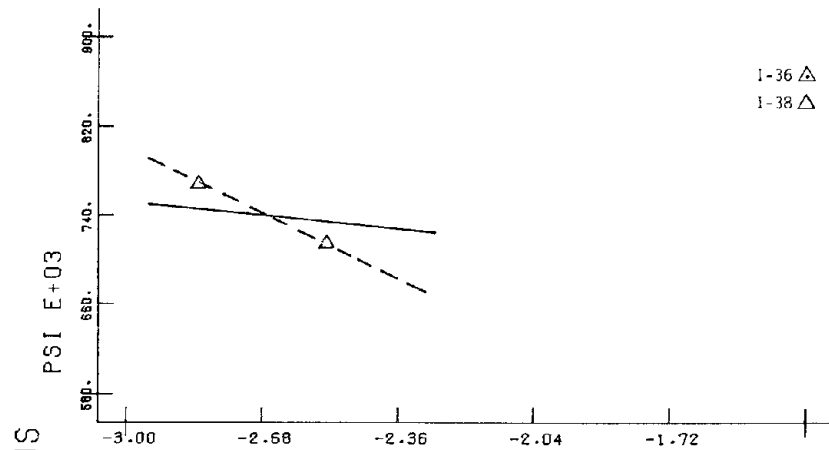






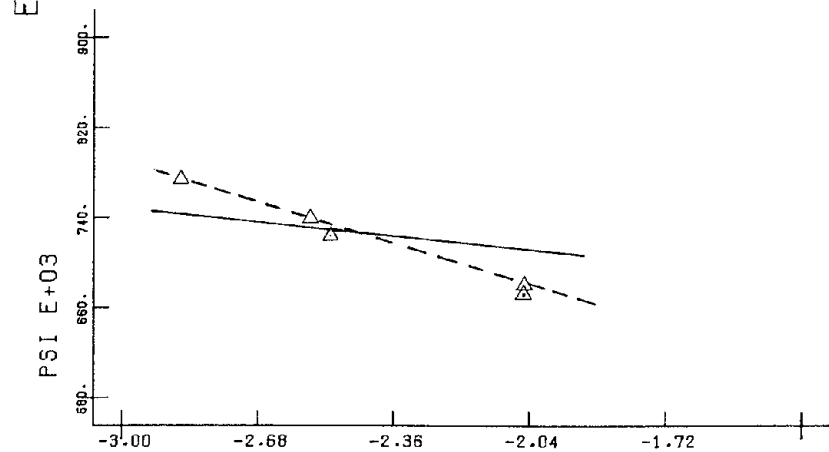
LOG PERCENT Figure C.65 AX STRAIN

ICE , T-6F .3CP200



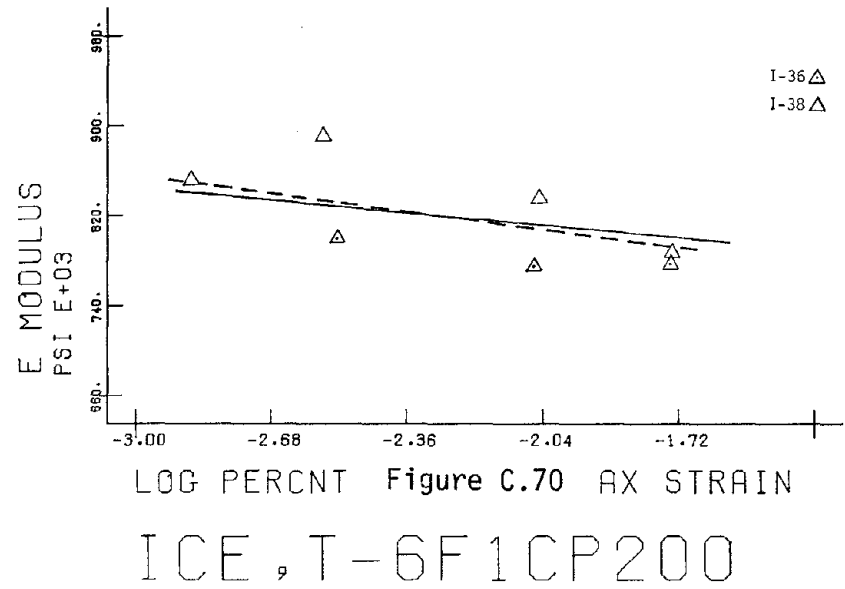
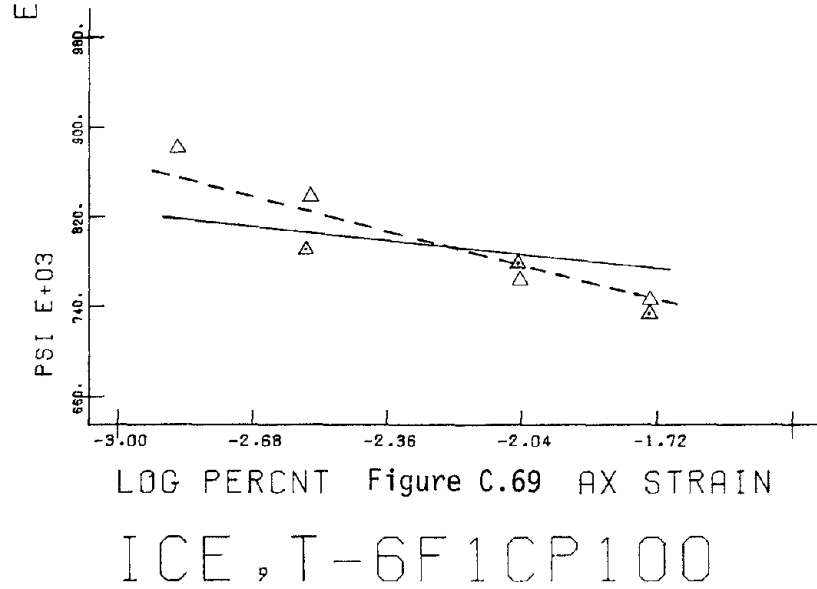
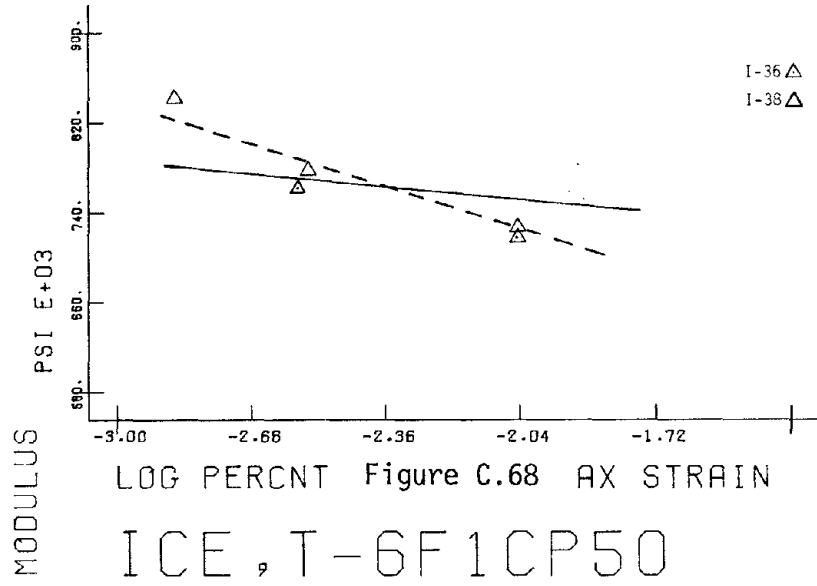
LOG PERCENT Figure C.66 AX STRAIN

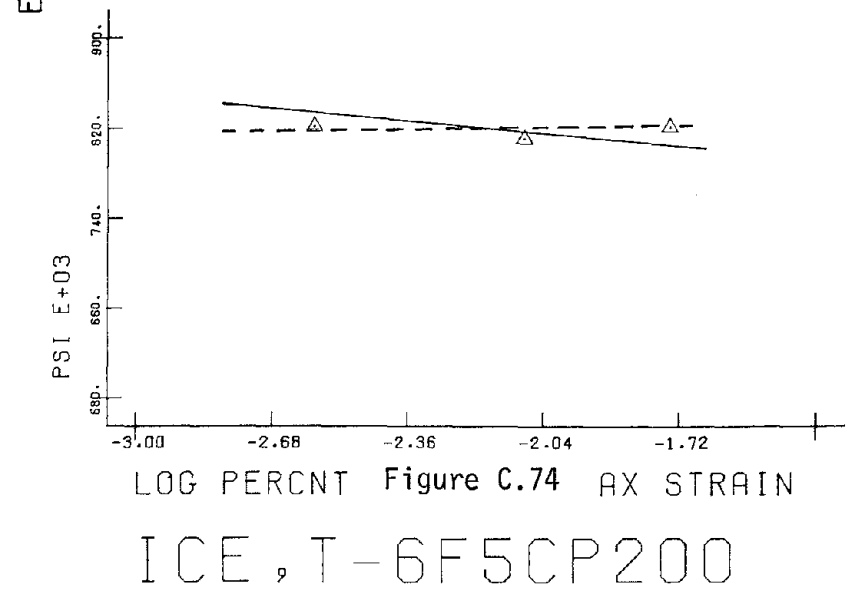
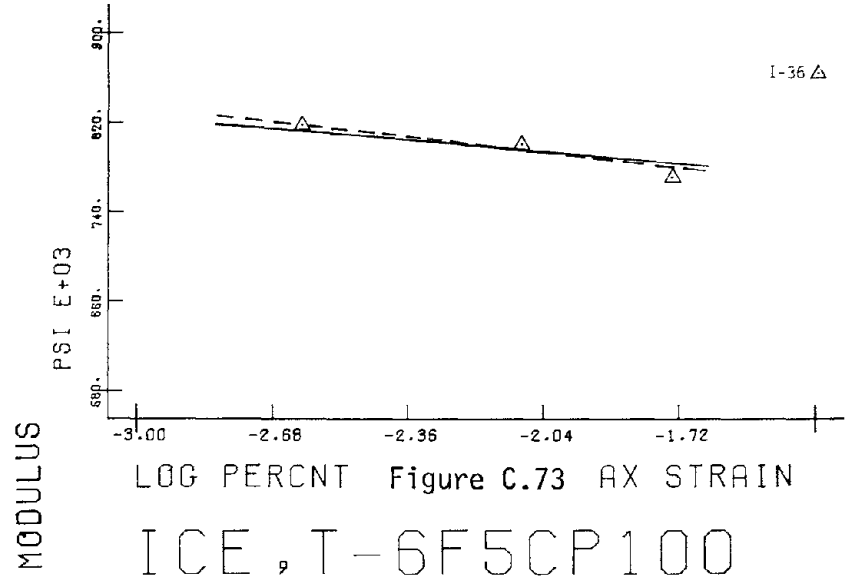
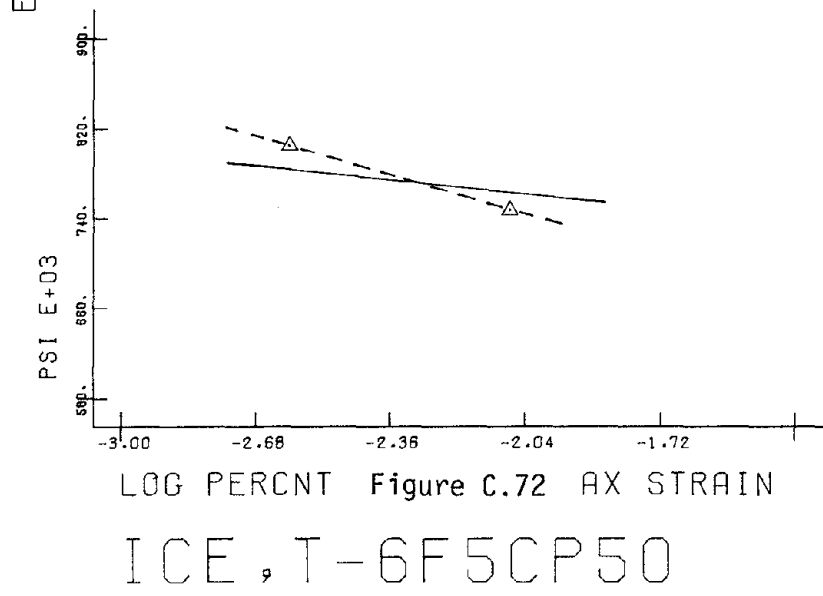
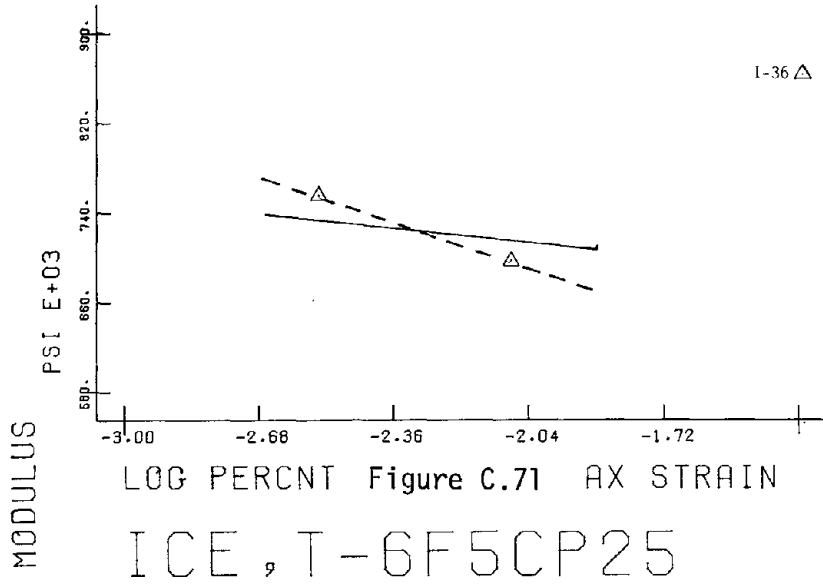
ICE , T-6F1CP0

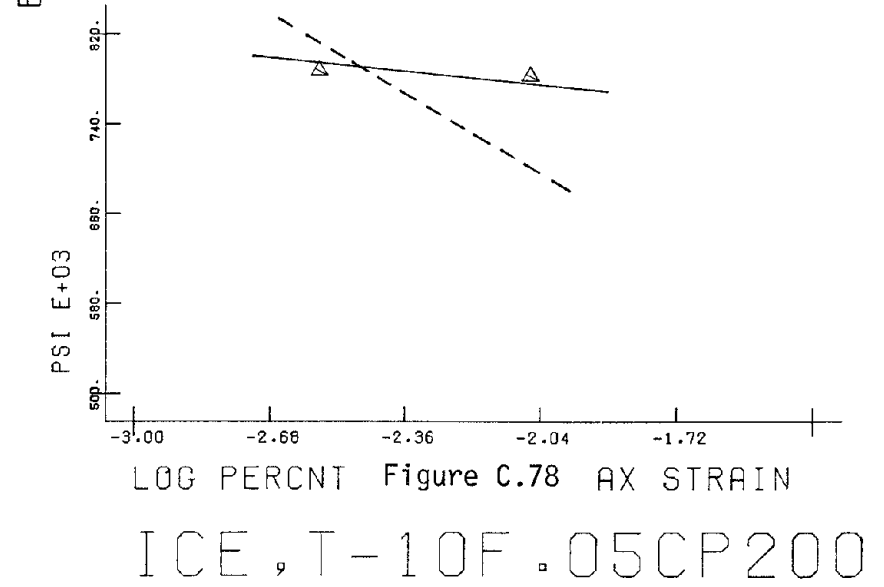
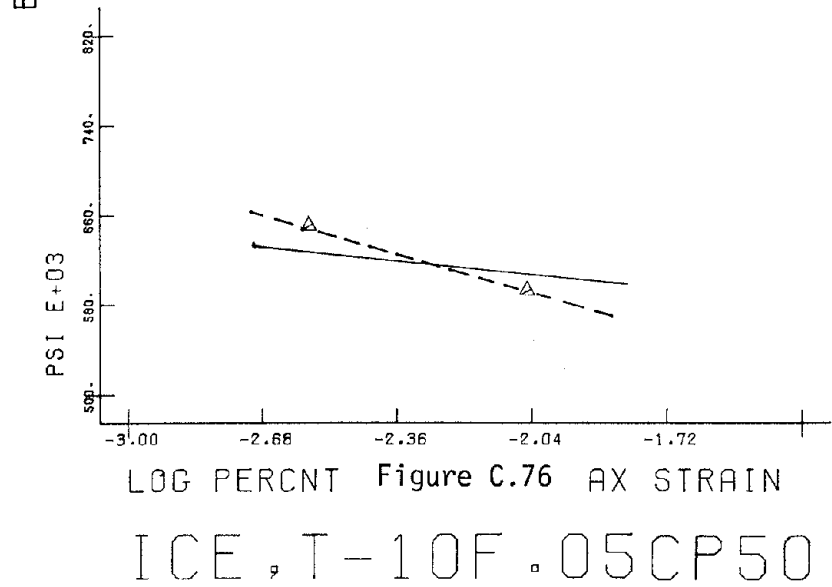
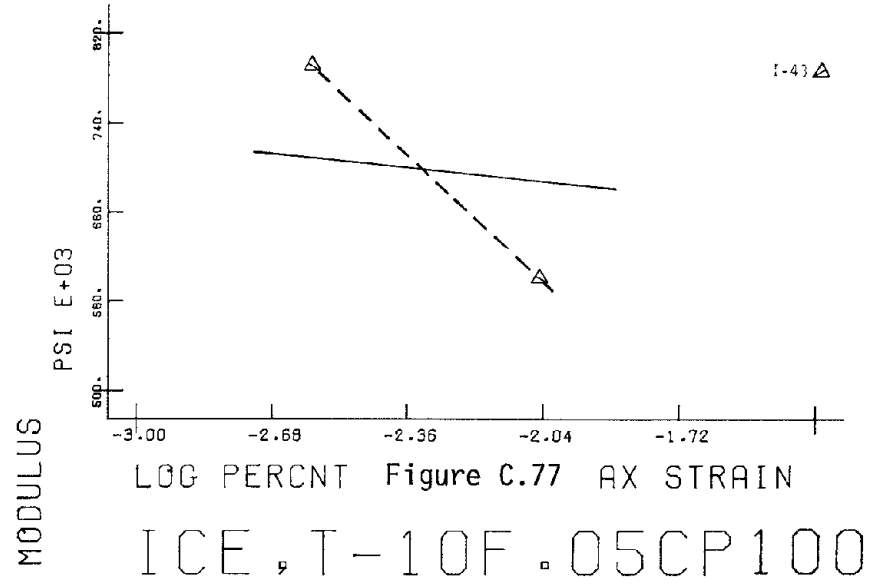
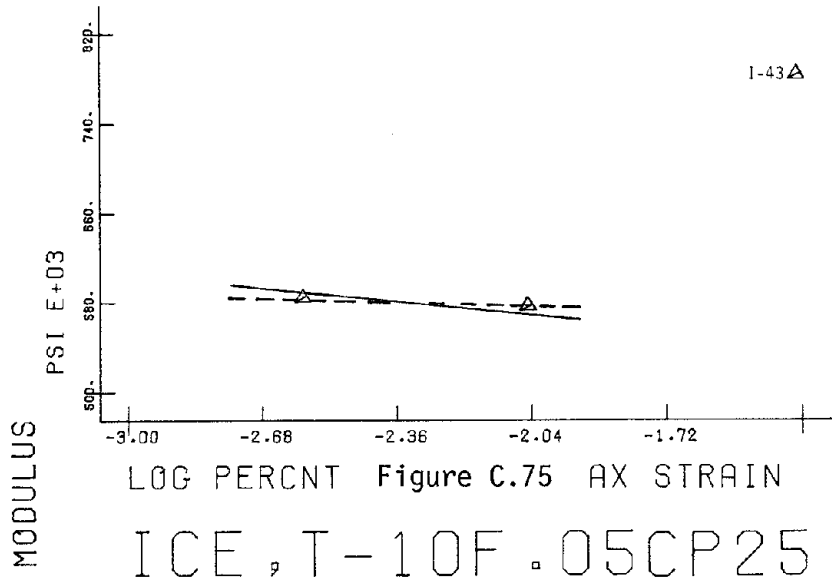


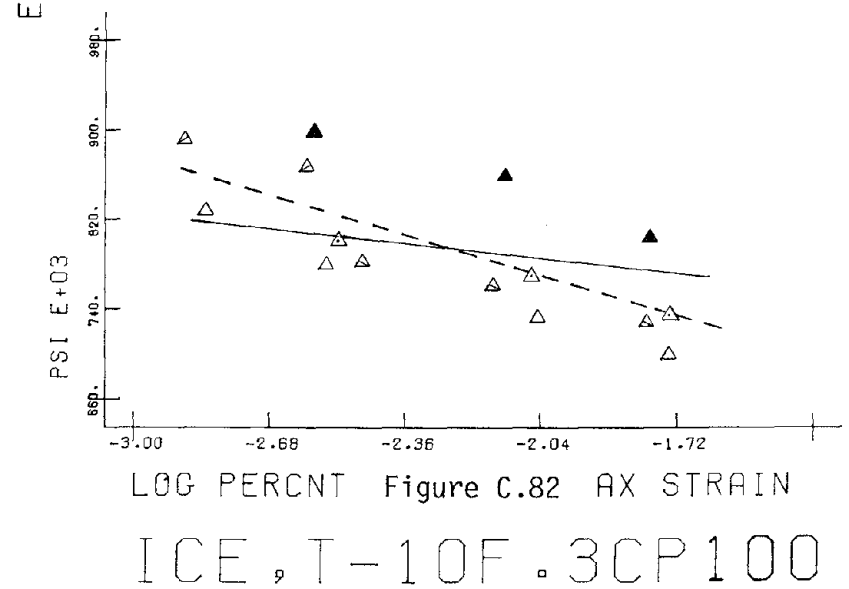
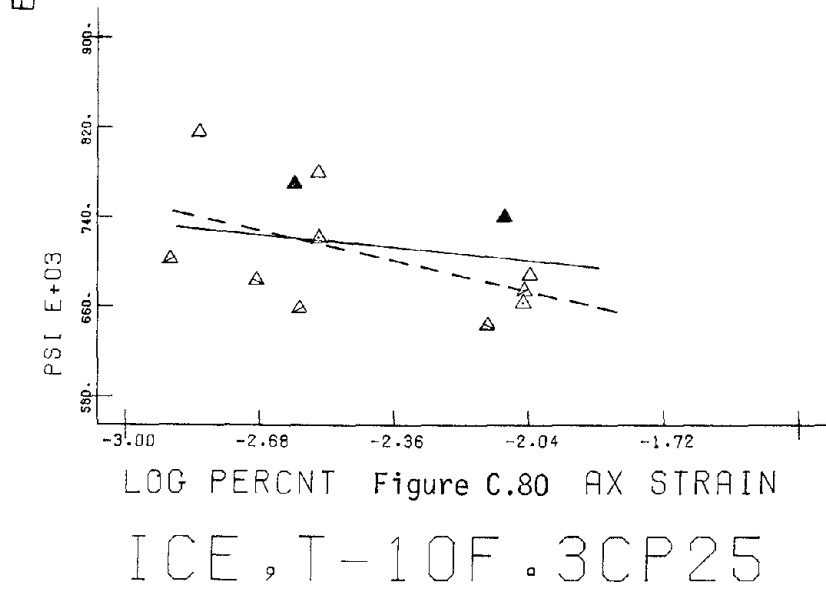
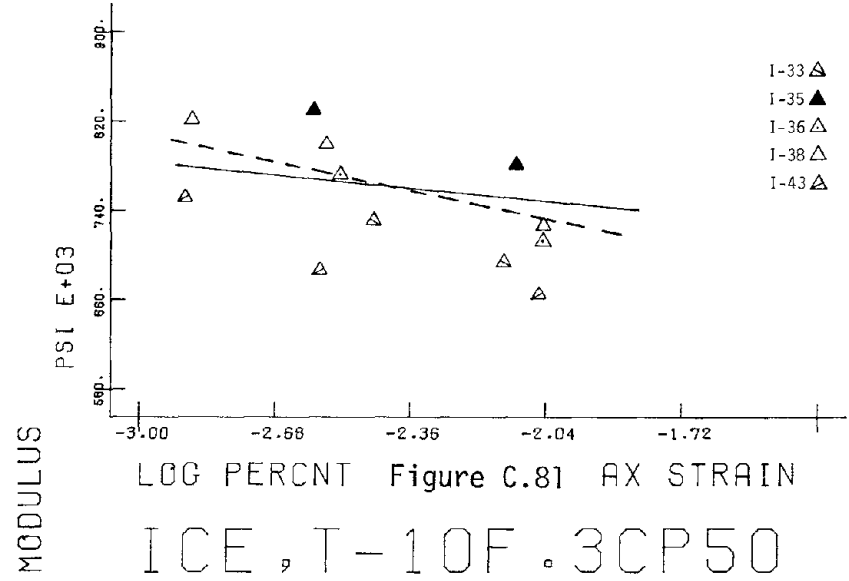
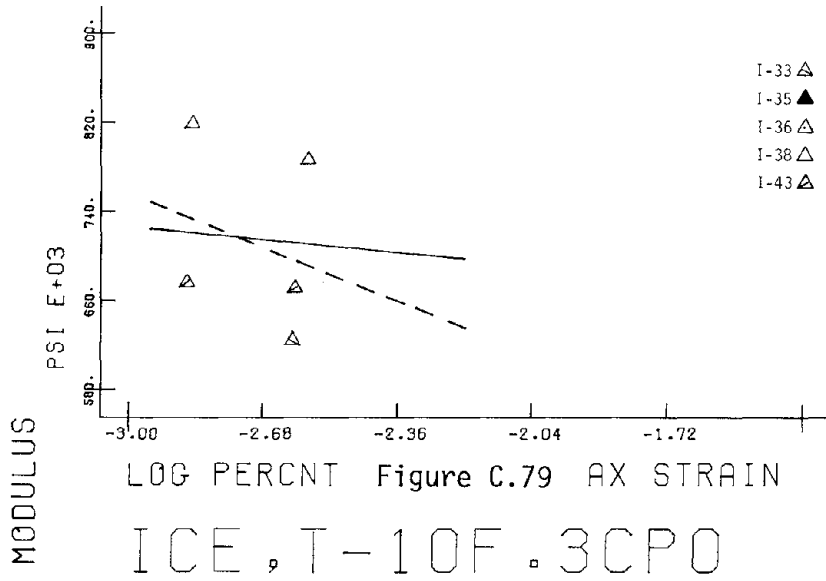
LOG PERCENT Figure C.67 AX STRAIN

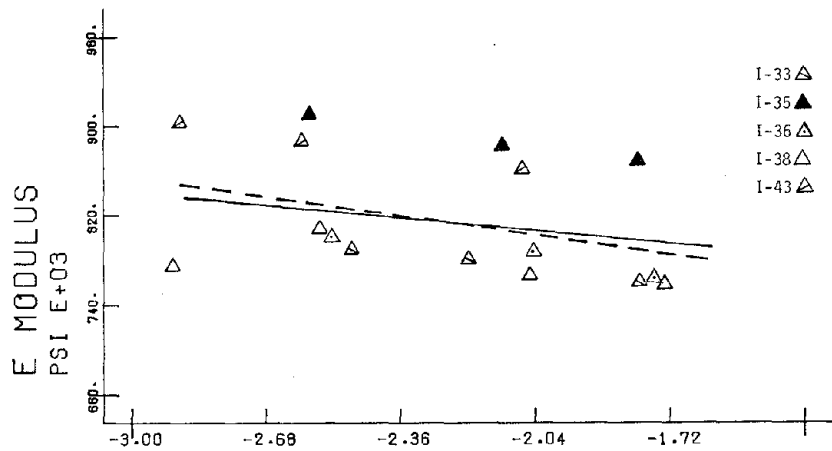
ICE , T-6F1CP25





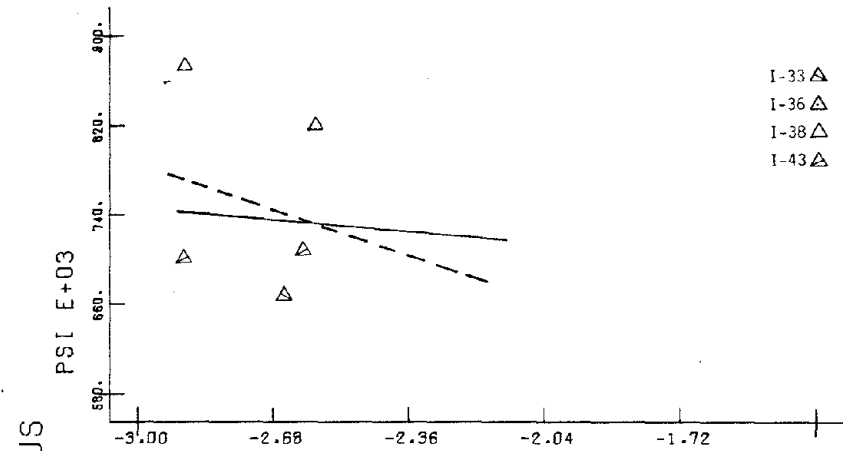






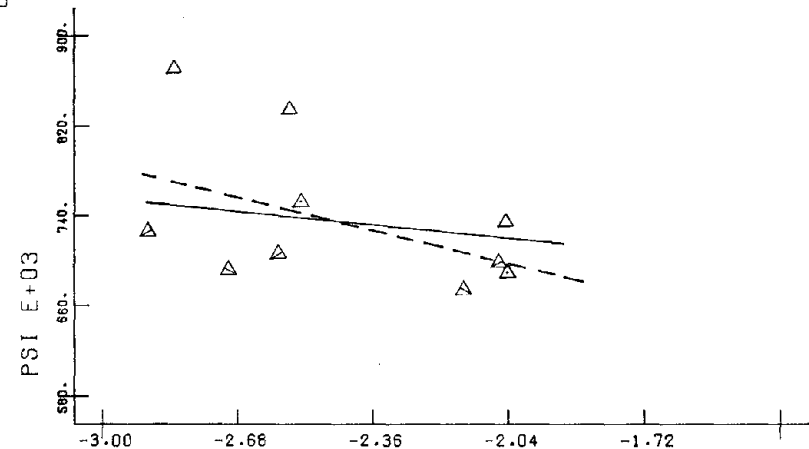
LOG PERCENT Figure C.83 AX STRAIN

ICE, T-10F.3CP200



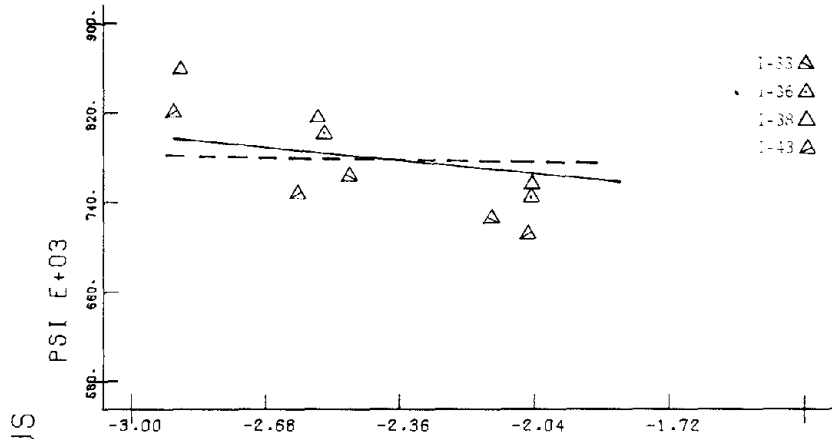
LOG PERCENT Figure C.84 AX STRAIN

ICE, T-10F1CP0



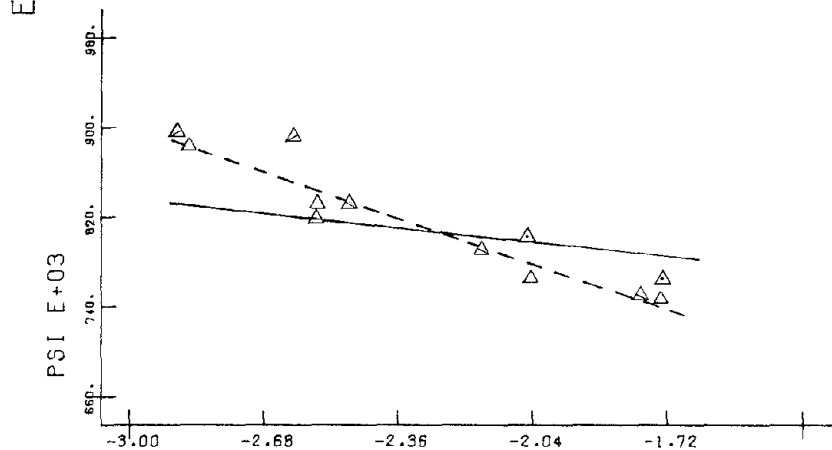
LOG PERCENT Figure C.85 AX STRAIN

ICE, T-10F1CP25



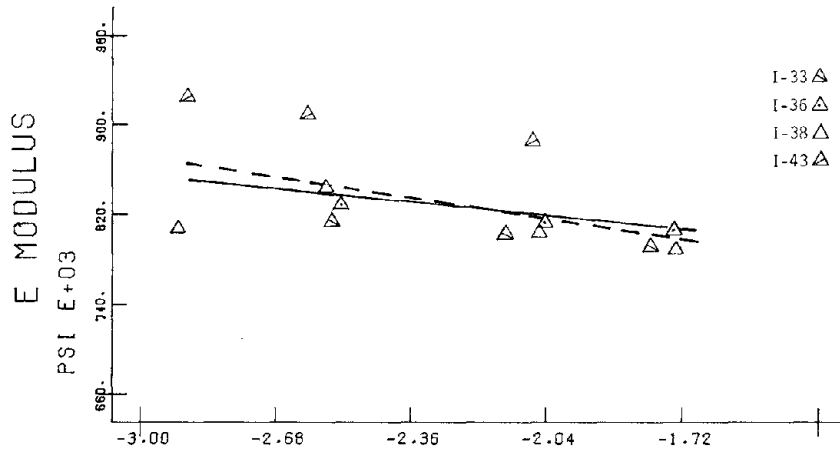
LOG PERCENT Figure C.86 AX STRAIN

ICE , T-10F1CP50



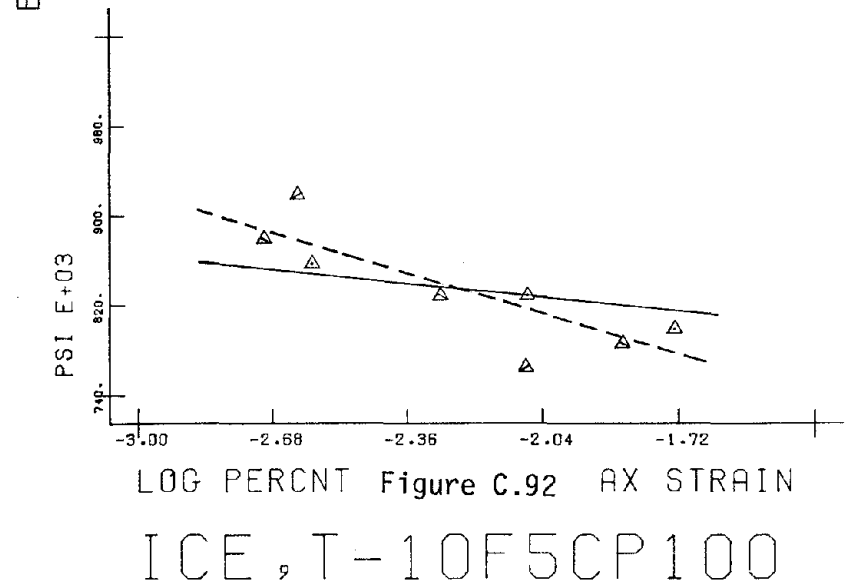
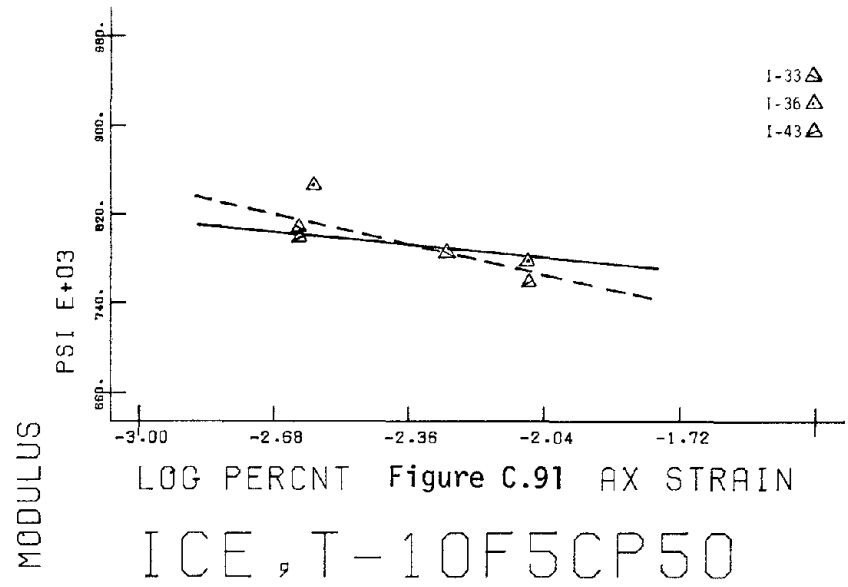
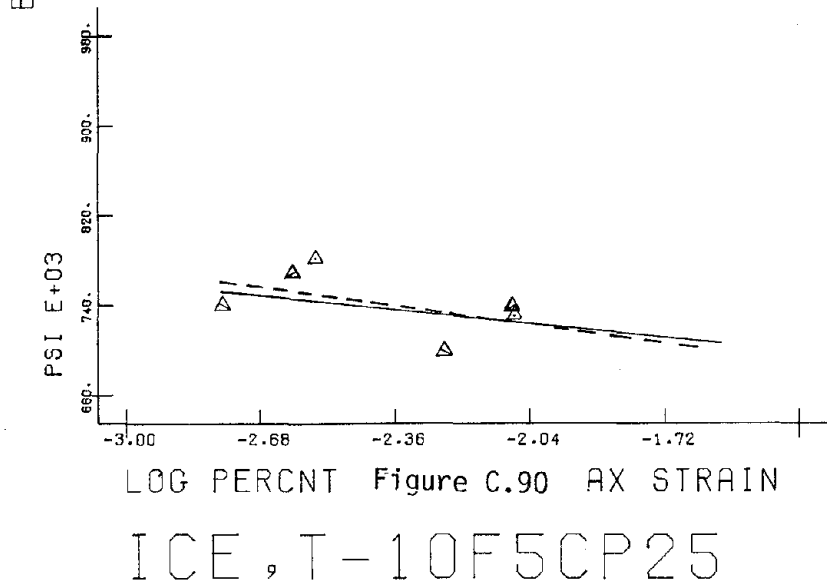
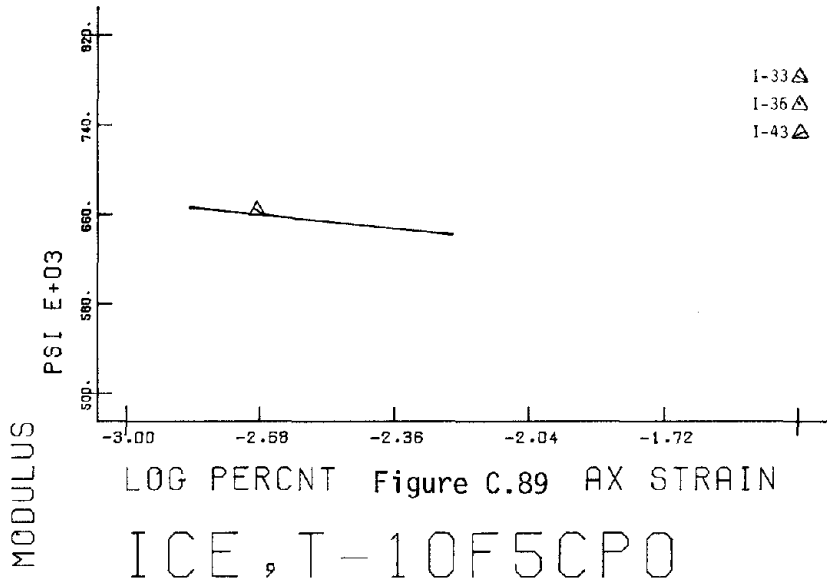
LOG PERCENT Figure C.87 AX STRAIN

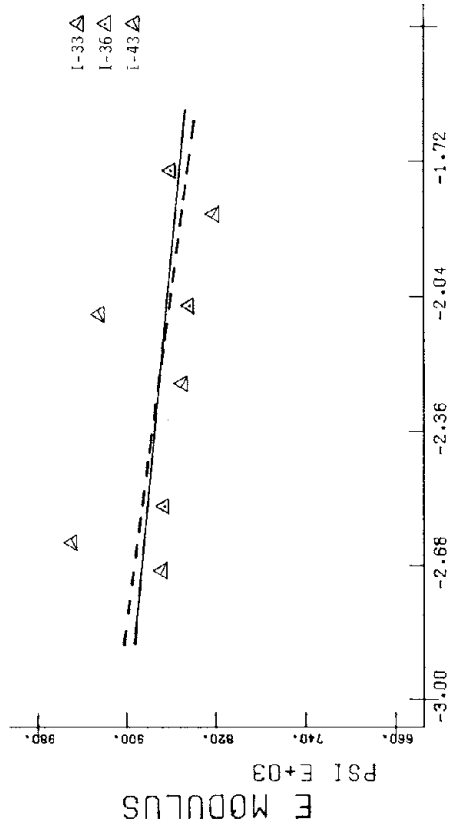
ICE , T-10F1CP100



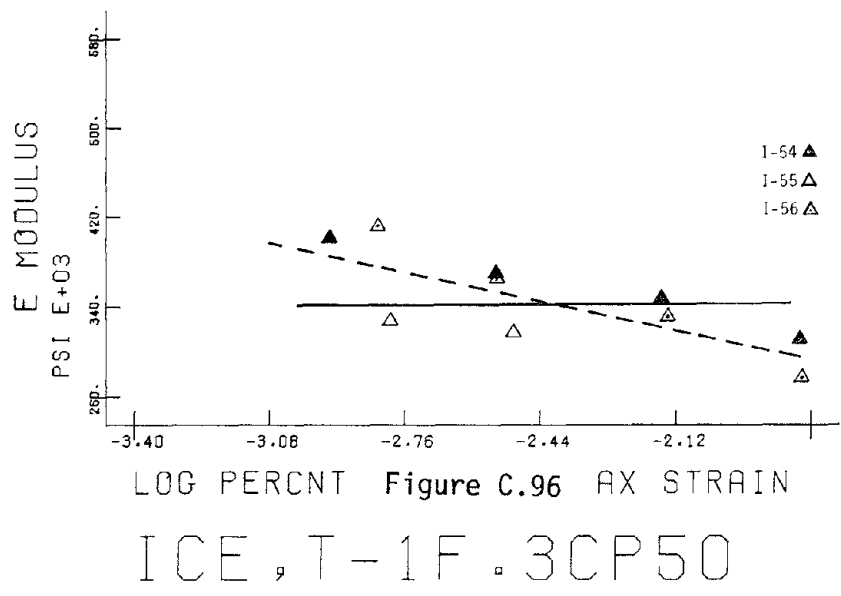
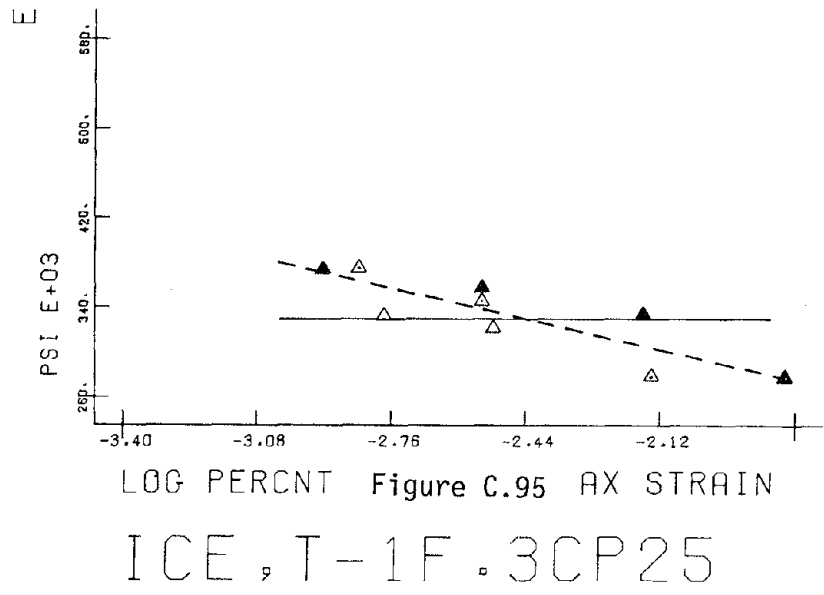
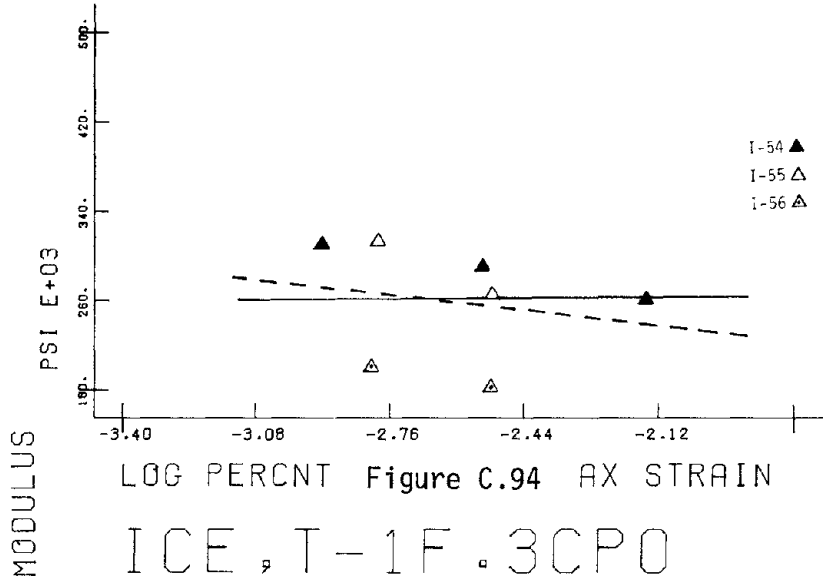
LOG PERCENT Figure C.88 AX STRAIN

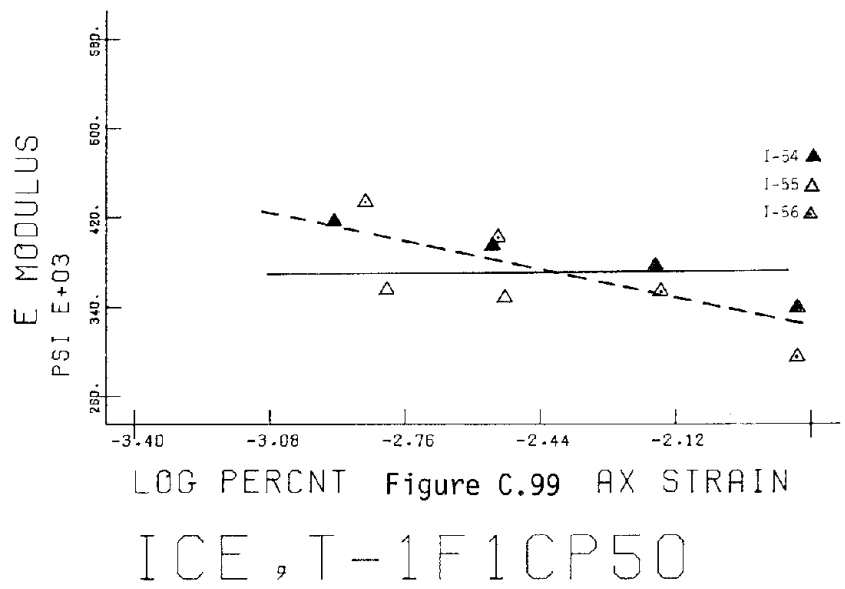
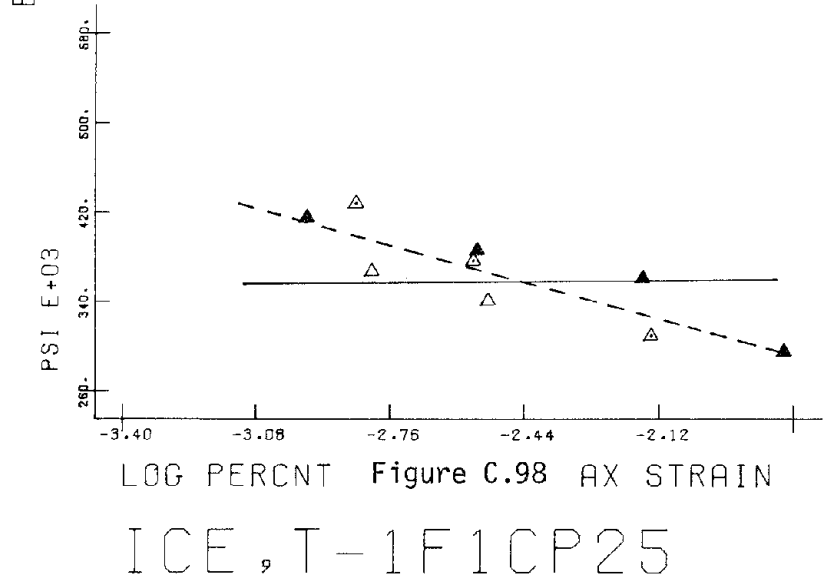
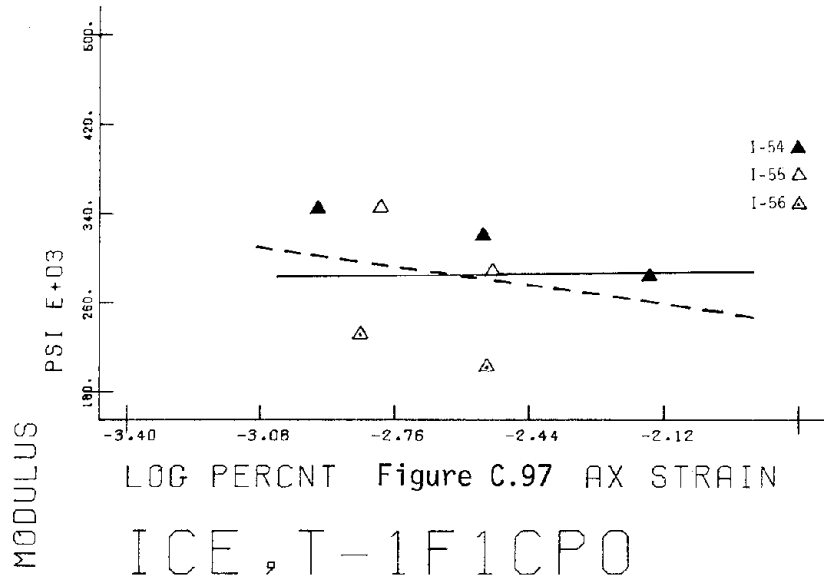
ICE , T-10F1CP200

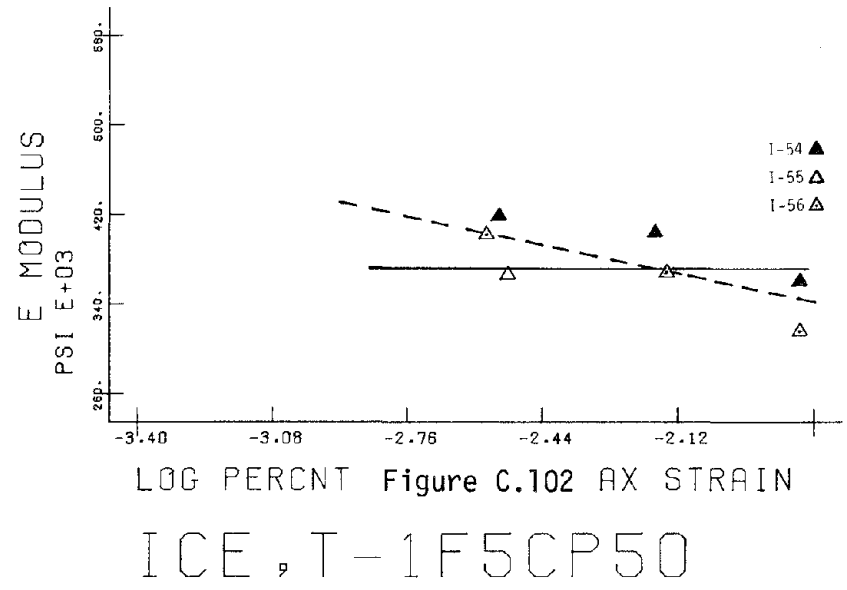
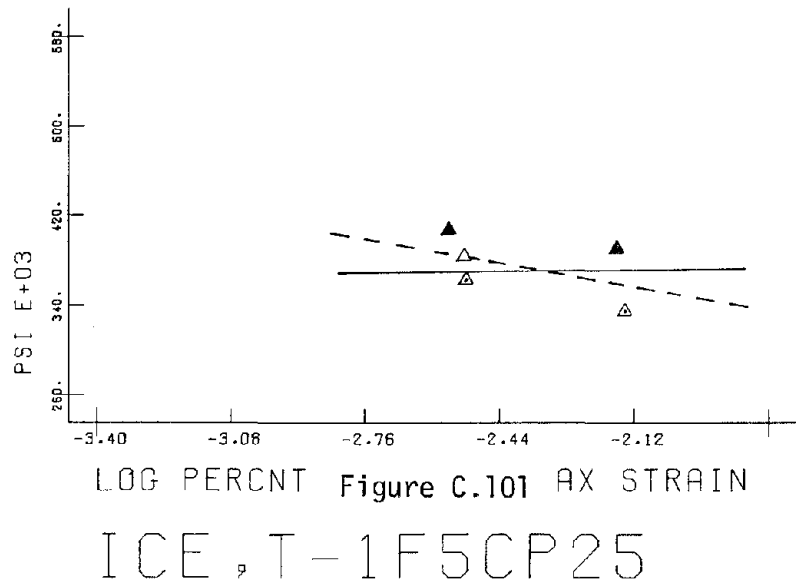
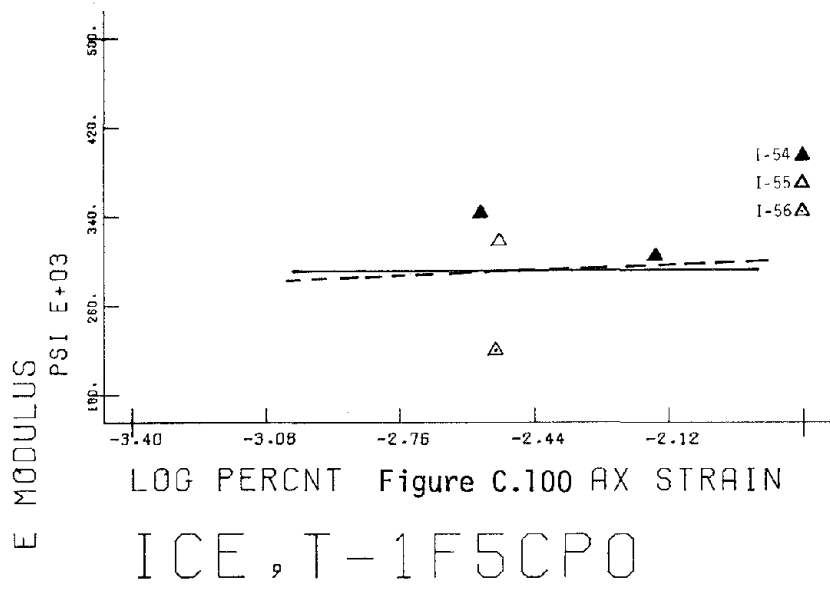


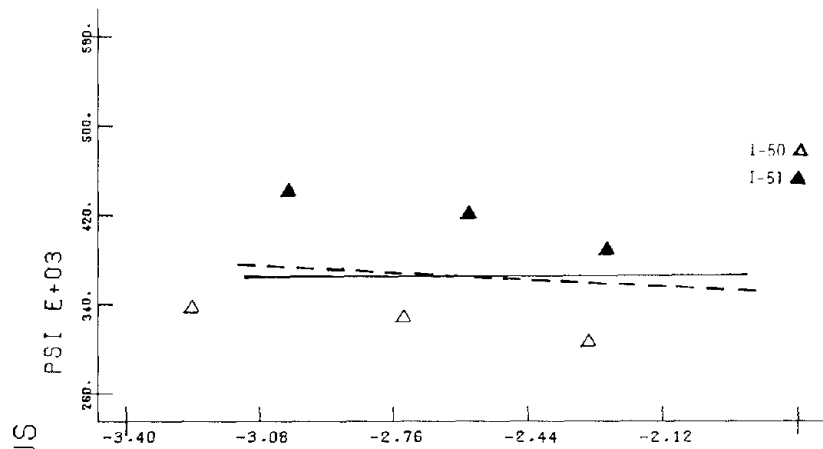


LOG PERCENT AX STRAIN
ICE, T-10F5CP200



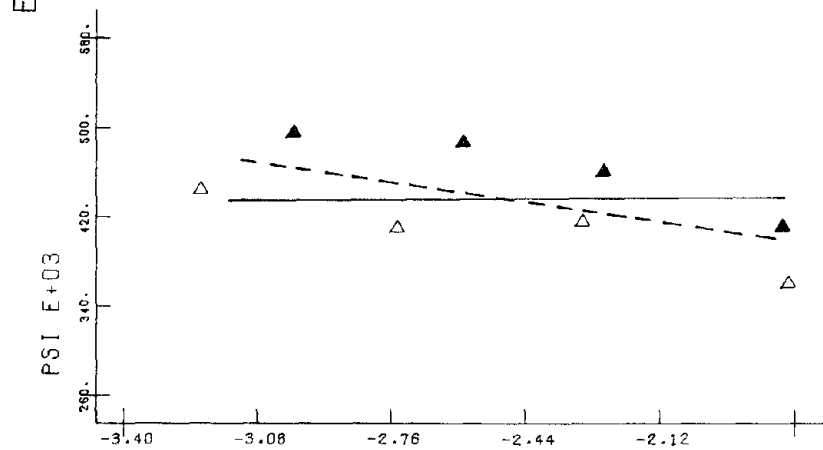






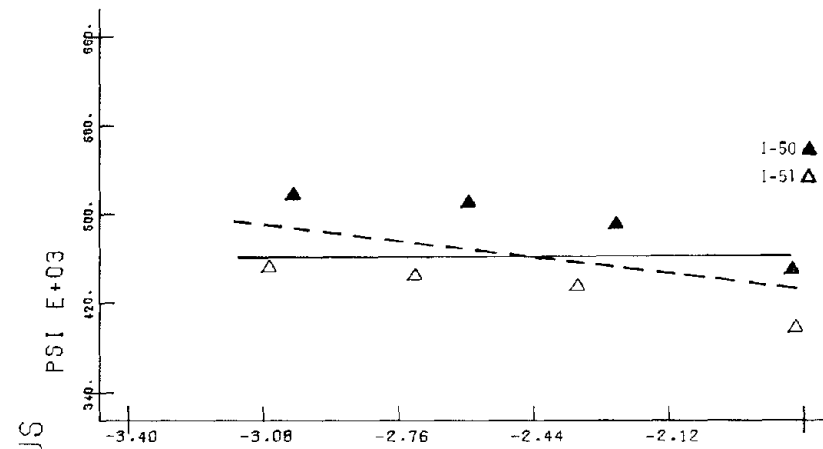
LOG PERCENT Figure C.103 AX STRAIN

ICE, T-4F.3CP0



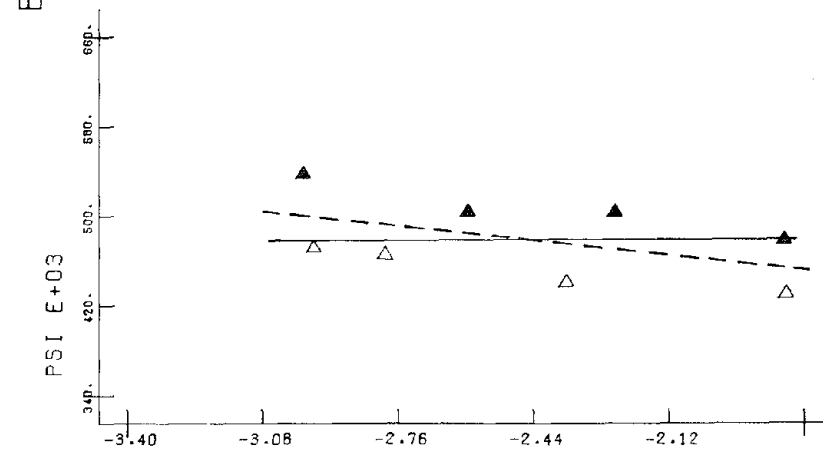
LOG PERCENT Figure C.104 AX STRAIN

ICE, T-4F.3CP25



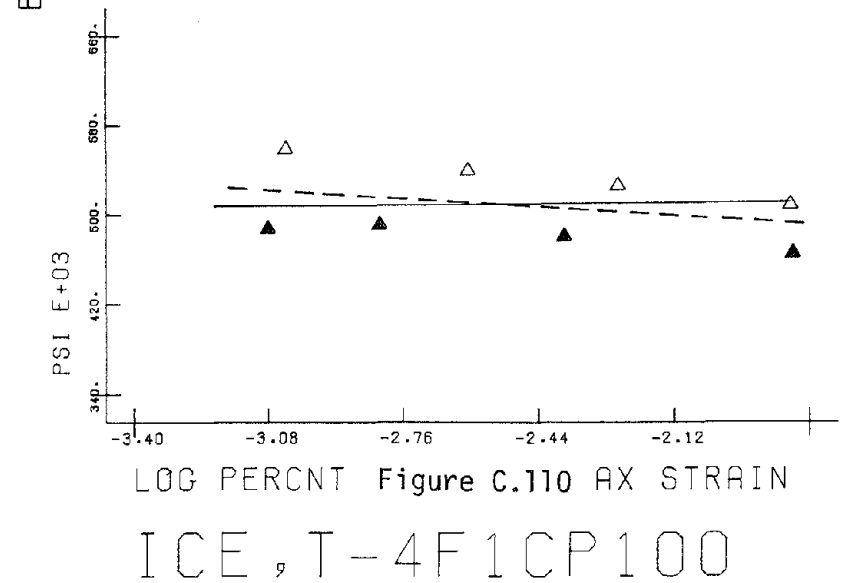
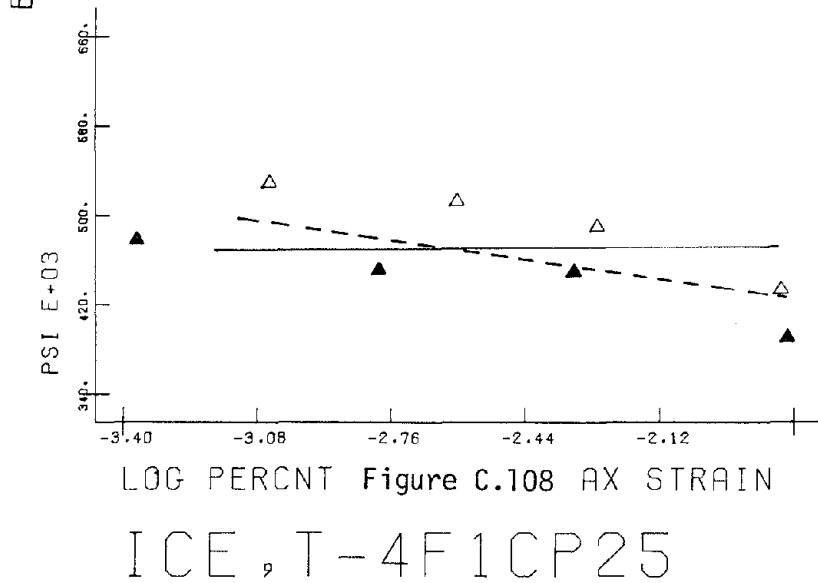
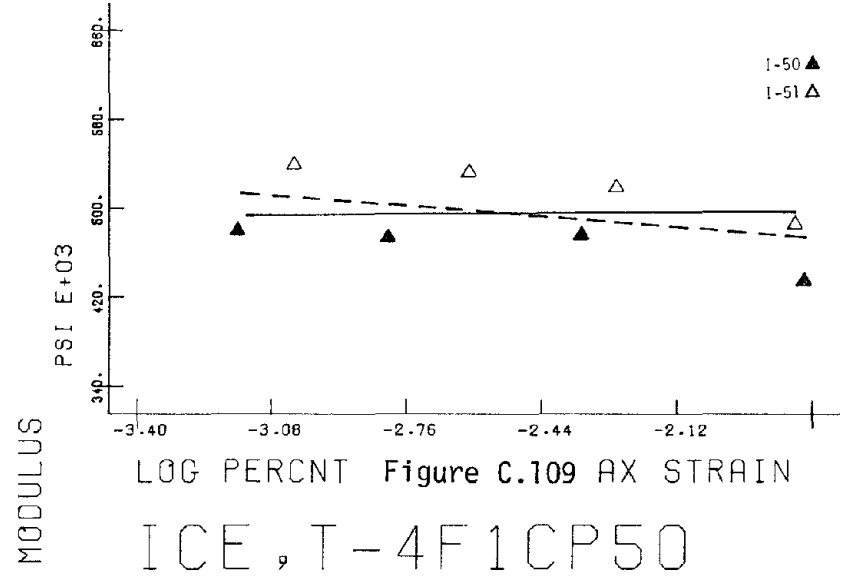
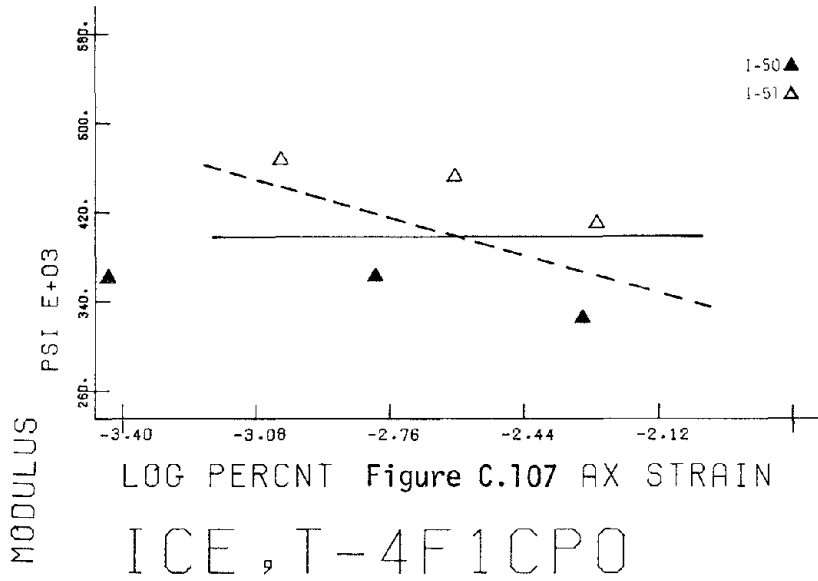
LOG PERCENT Figure C.105 AX STRAIN

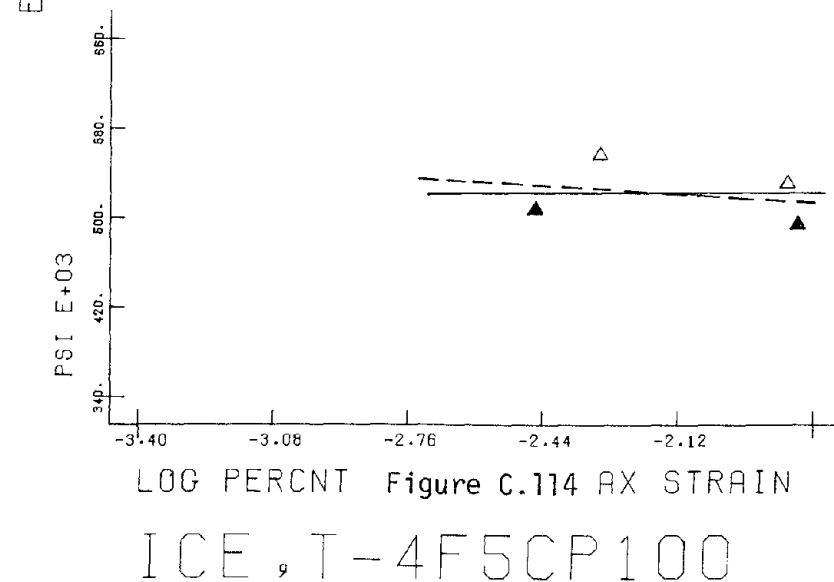
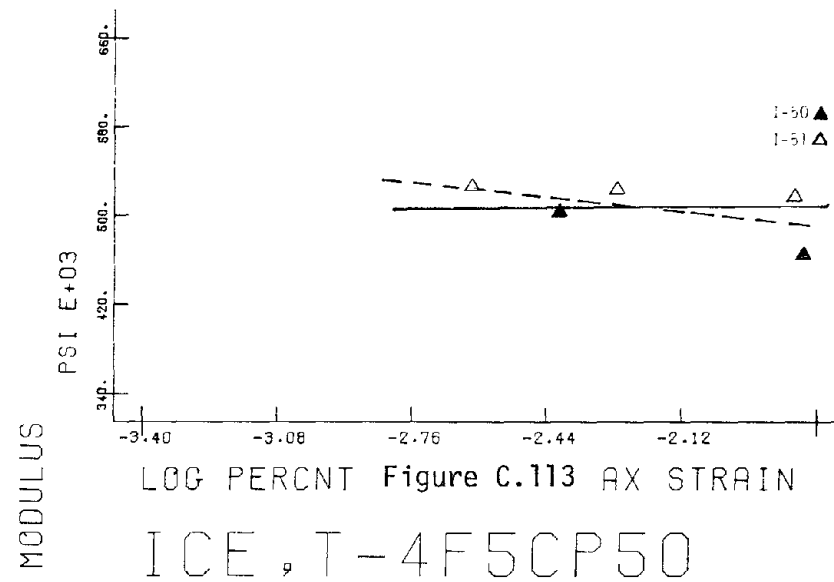
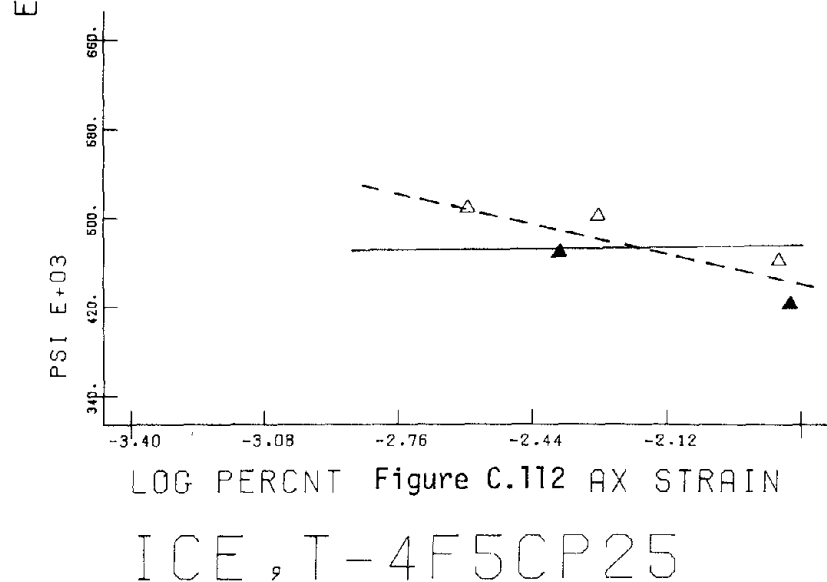
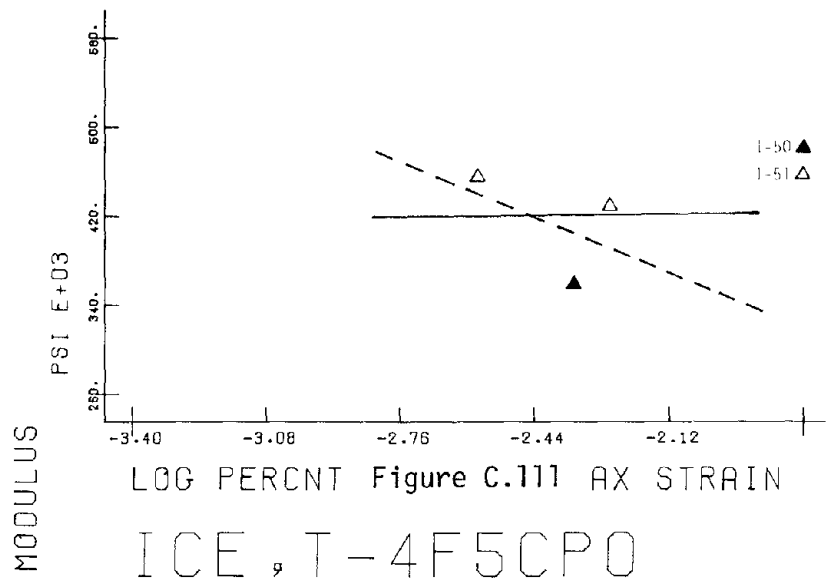
ICE, T-4F.3CP50

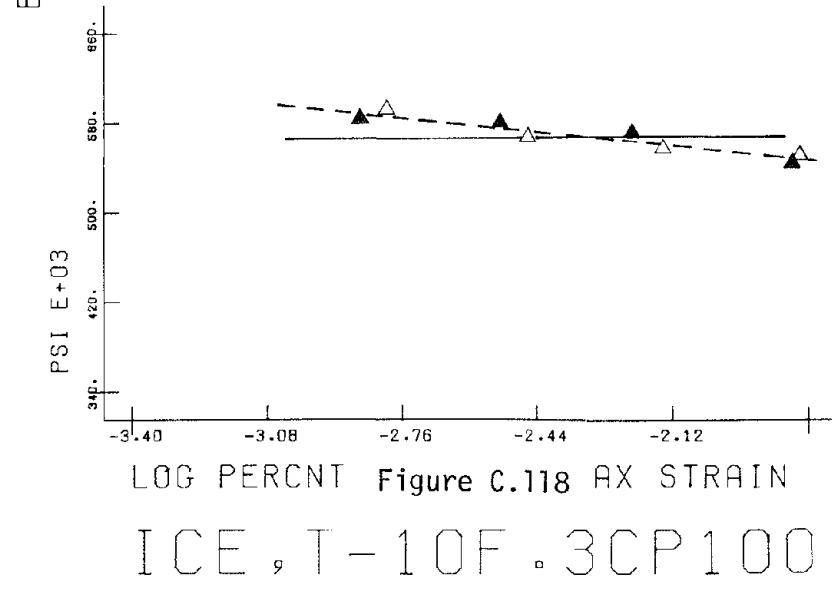
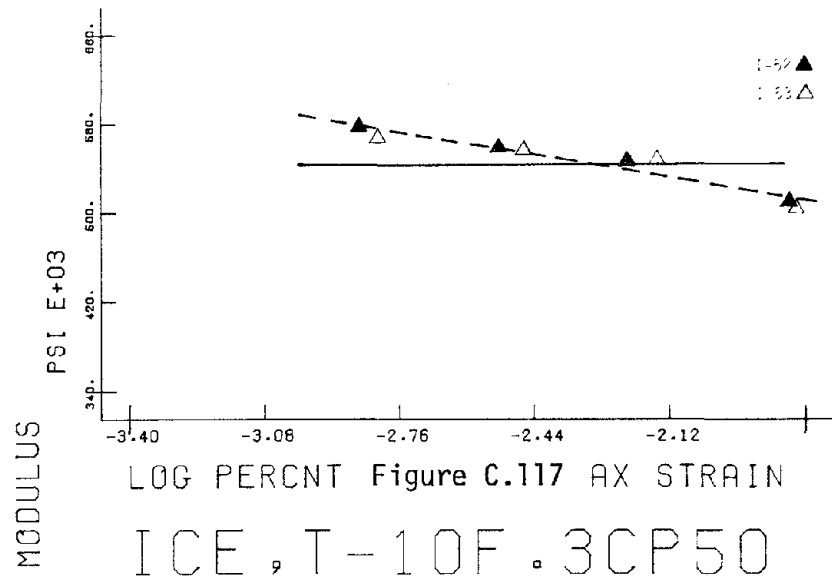
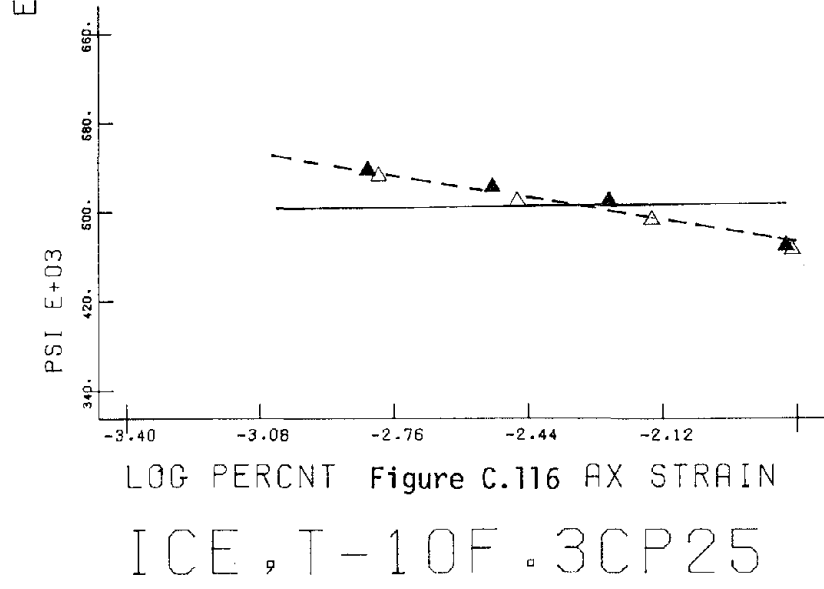
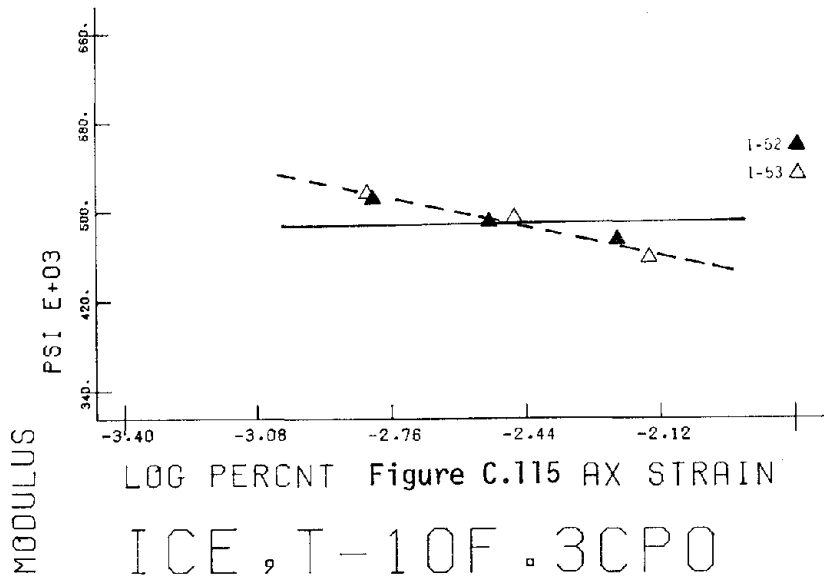


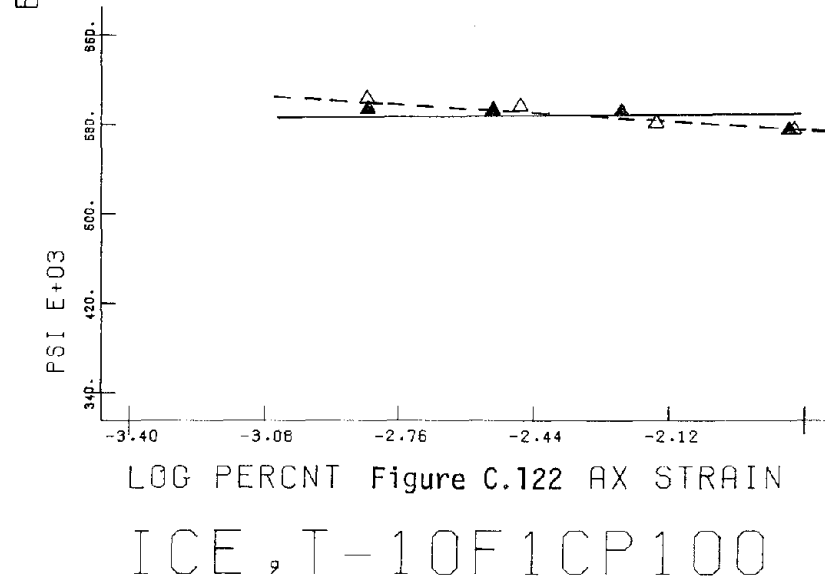
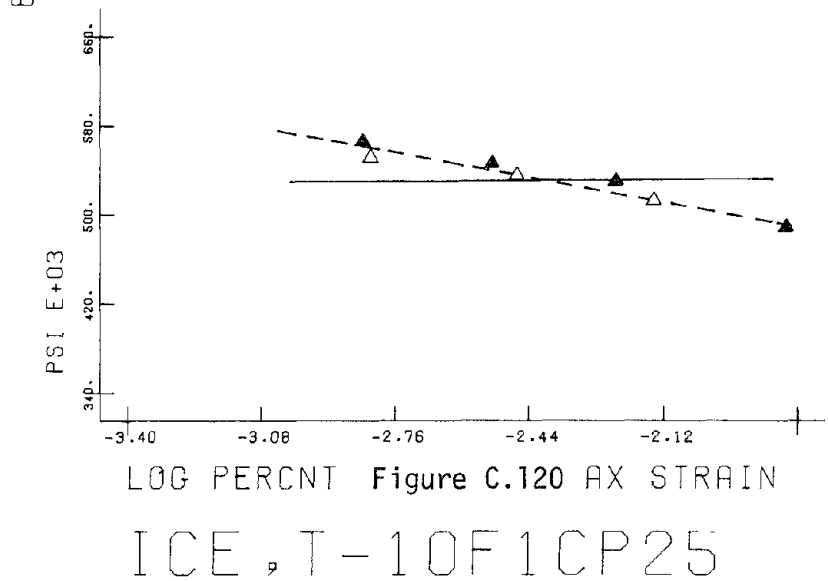
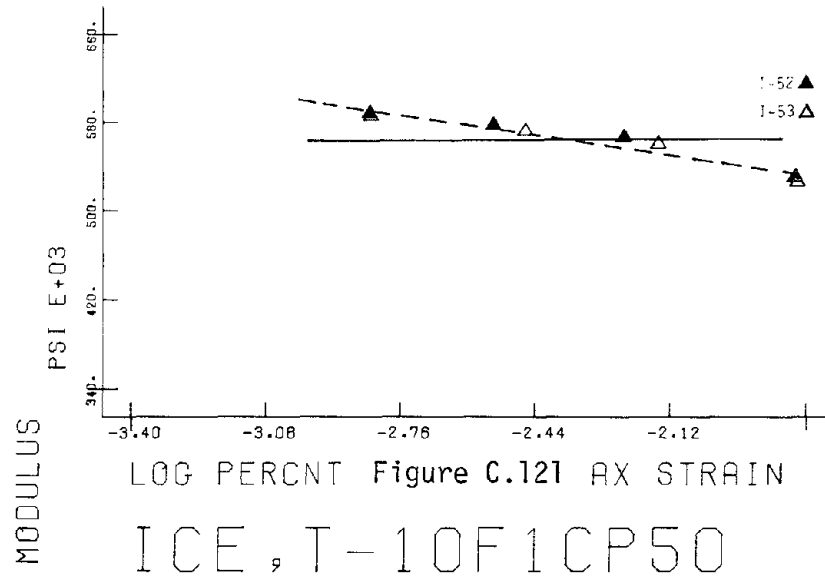
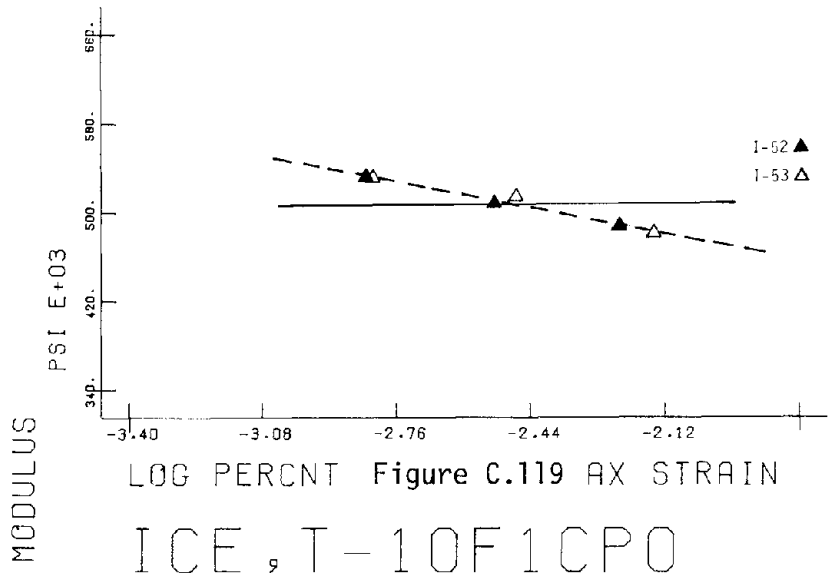
LOG PERCENT Figure C.106 AX STRAIN

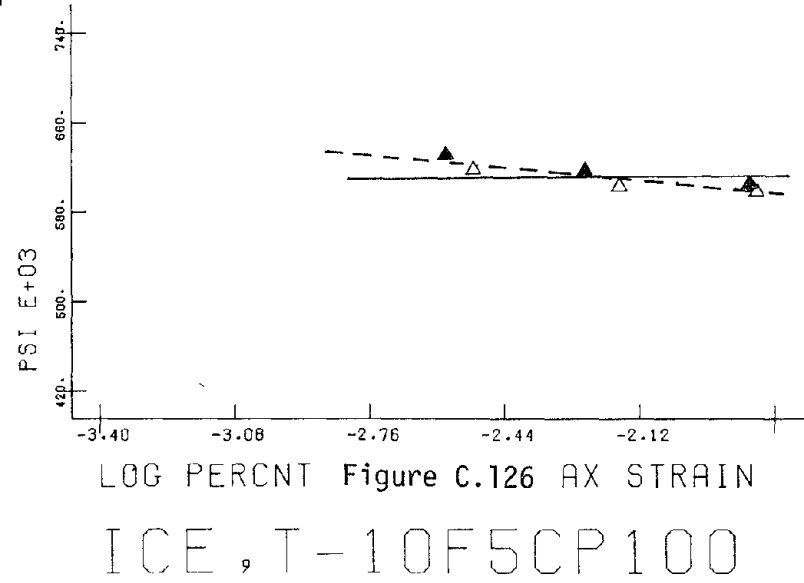
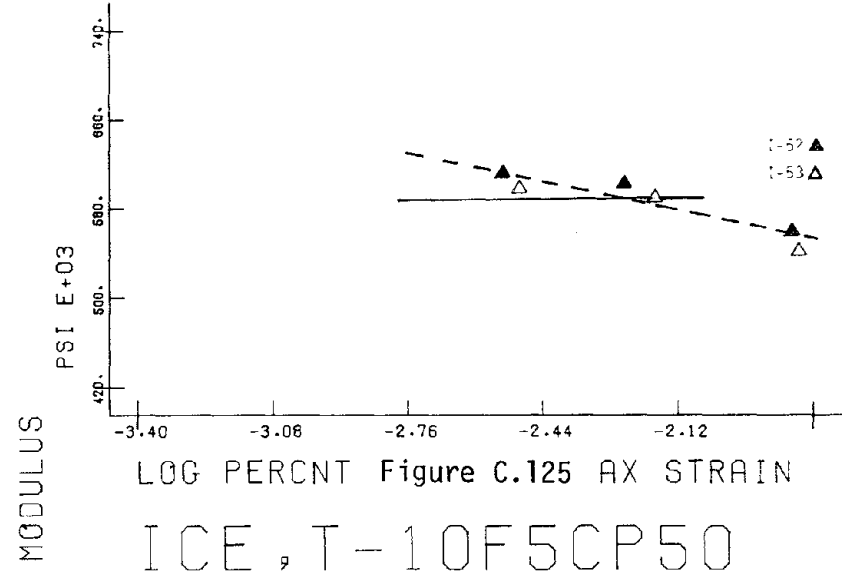
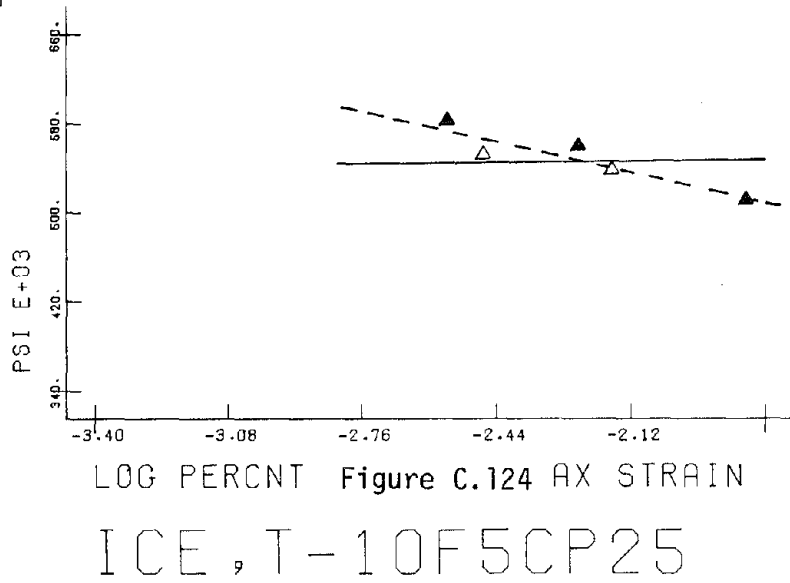
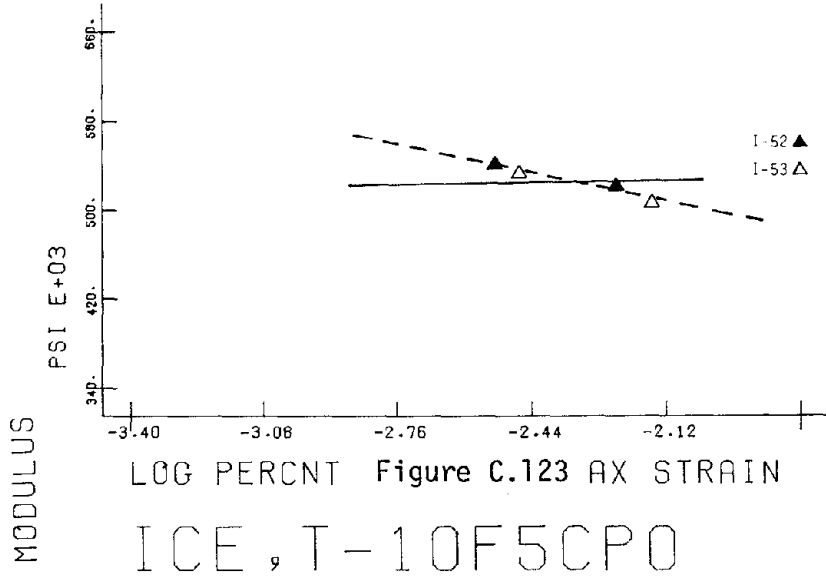
ICE, T-4F.3CP100







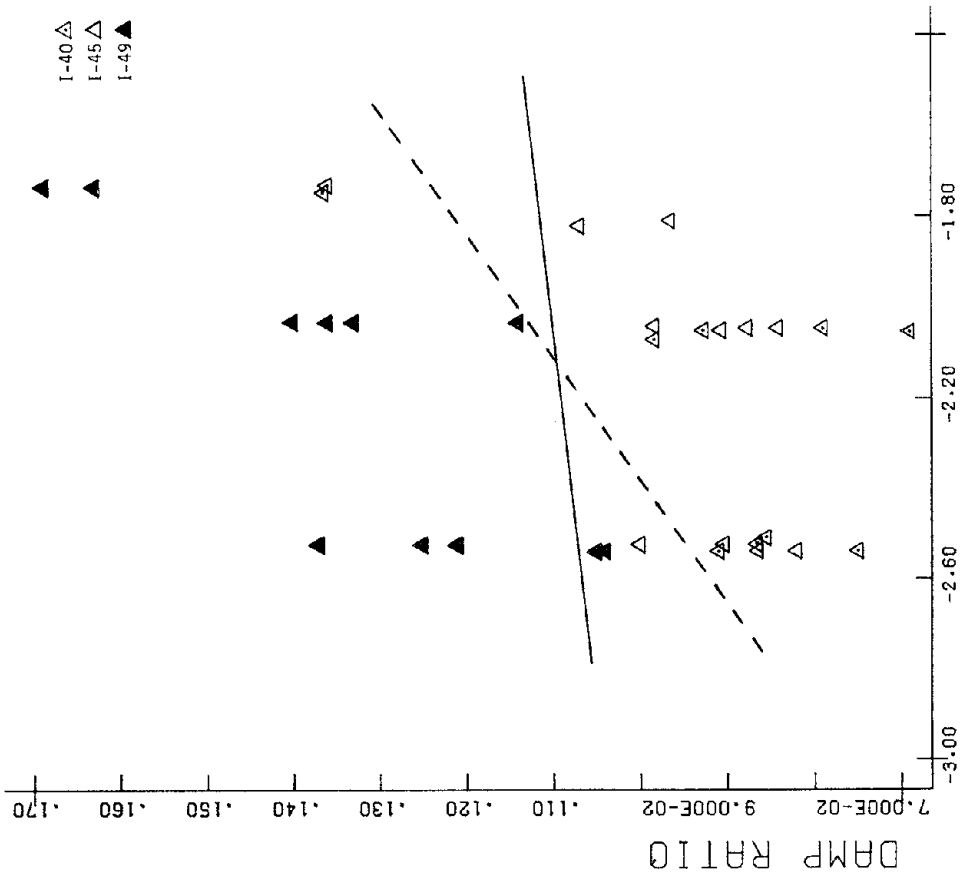




APPENDIX D

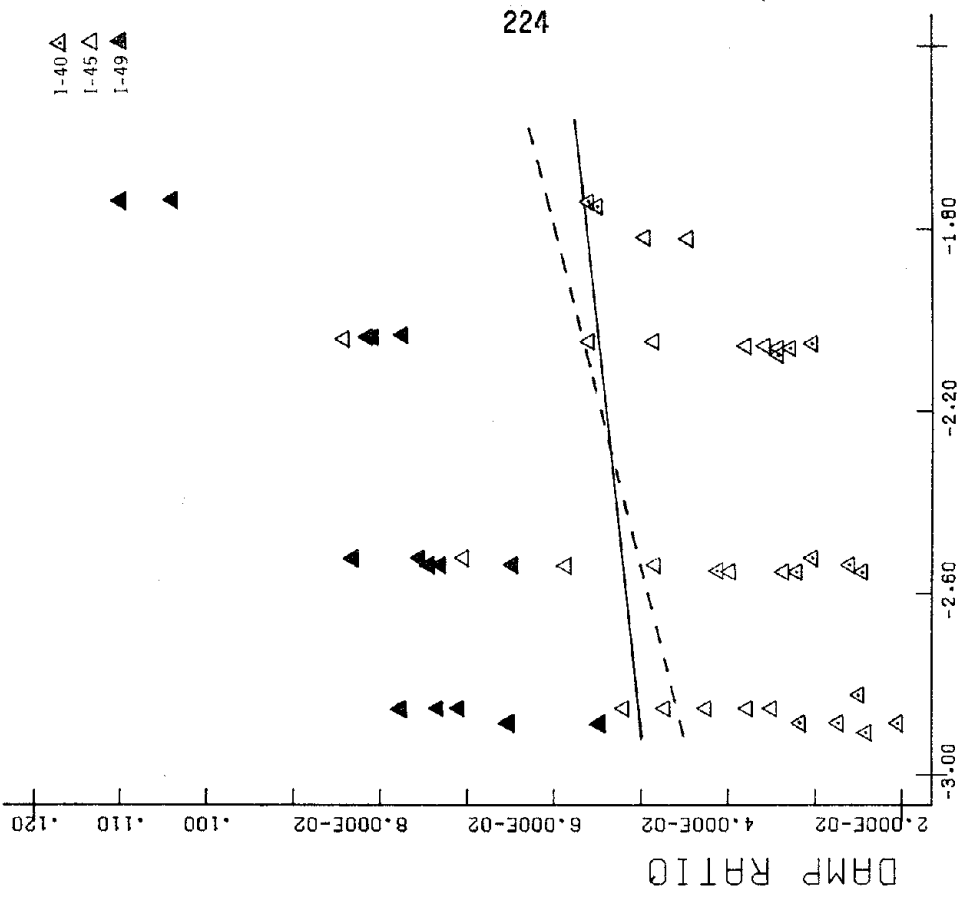
CYCLIC TRIAXIAL TEST RESULTS: DAMPING RATIO OF ICE

Figures D.1 to D.19 show test results of damping ratio for high density ice, and results for low density ice are shown in Figures D.20 to D.28. The dashed lines in the figures represent the least squares best fit line of the data for a given test condition. The solid lines represent the average least squares best fit line for all the experimental data drawn through the "center" of the data set for a given test condition. (Refer to Section 4.5.1 and Figures 4.63 and 4.64 for further explanation.)



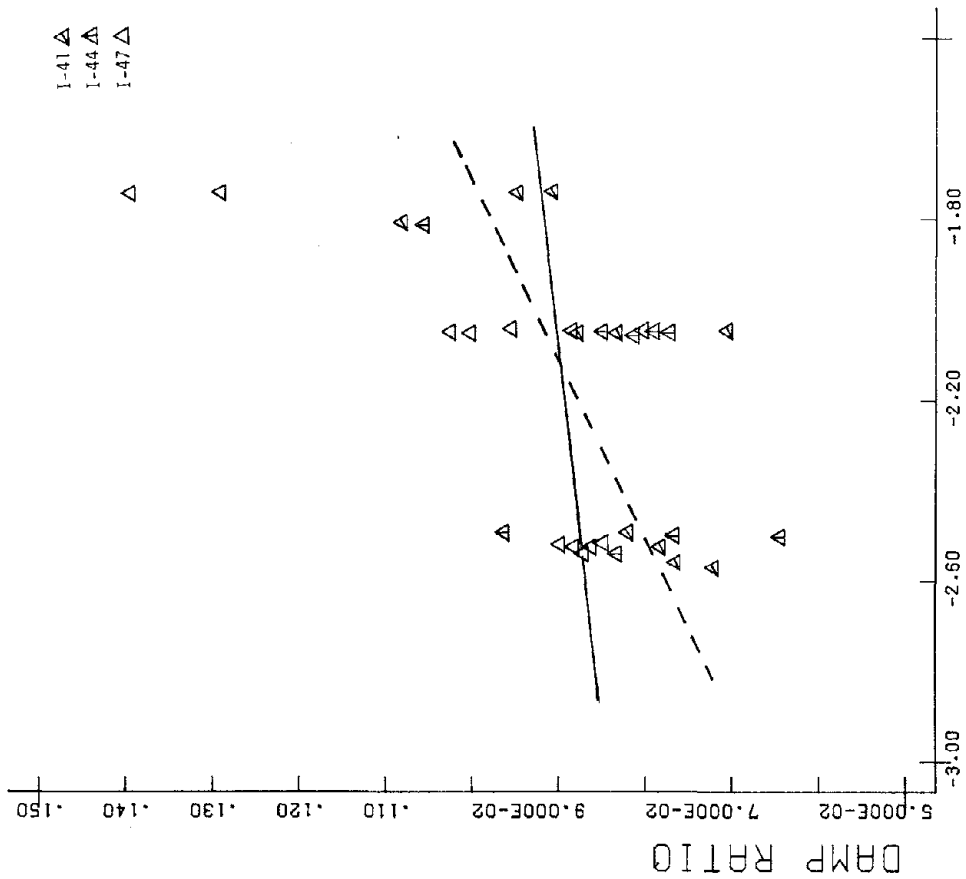
LOG PERCENT AX STRAIN

ICE, T-1F, 05ALLCP



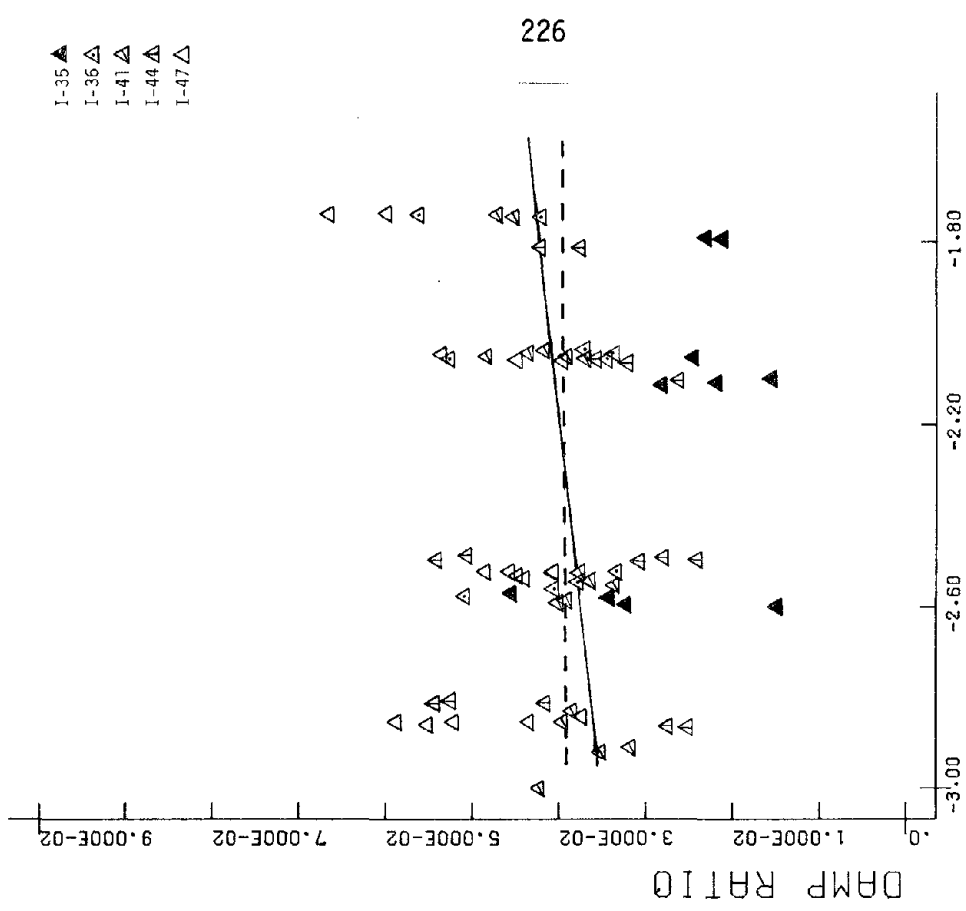
LOG PERCENT AX STRAIN

ICE, T-1F, 3ALLCP



LOG PERCENT AX STRAIN Figure D.5

ICE, T-2F, 05ALLCP



LOG PERCENT AX STRAIN Figure D.6

ICE, T-2F, 3ALLCP

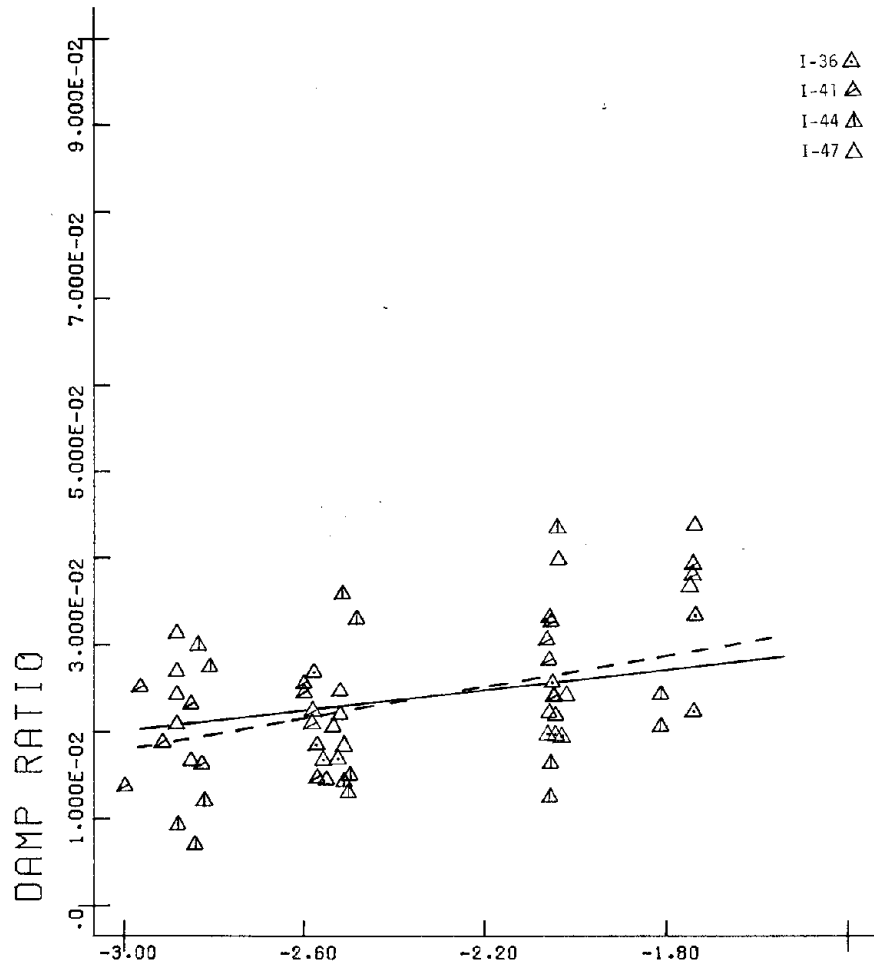


Figure D.7
ICE, T-2F1ALLCP

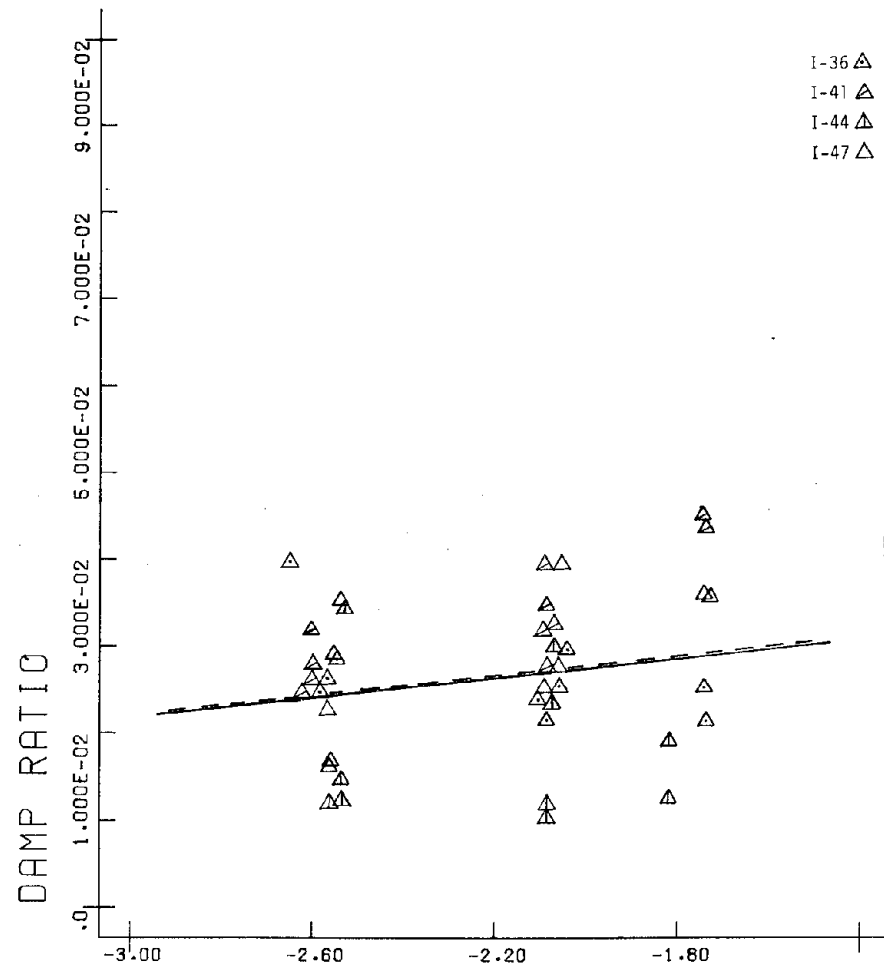
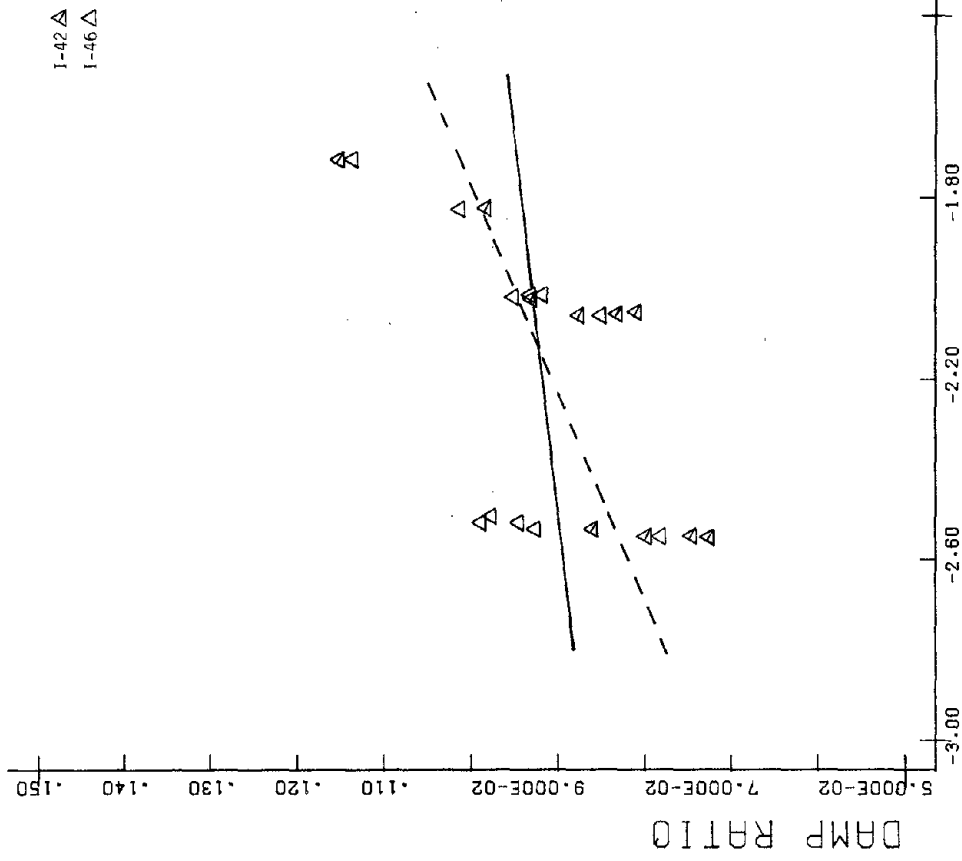
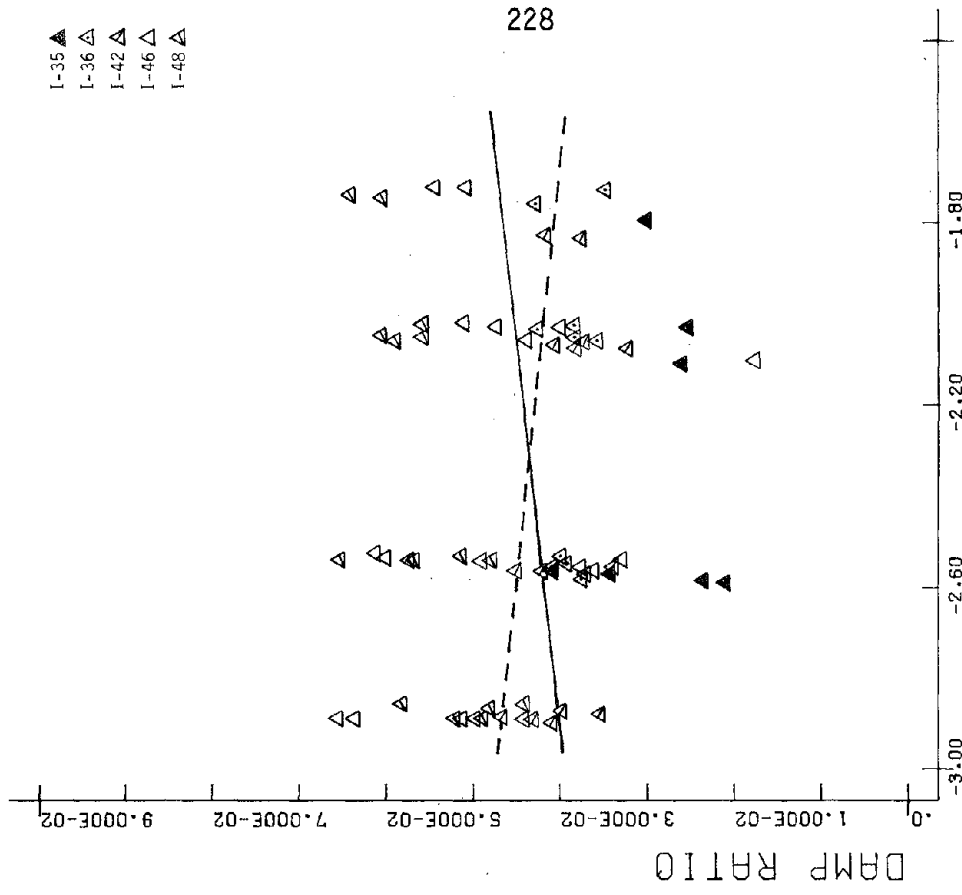


Figure D.8
ICE, T-2F5ALLCP



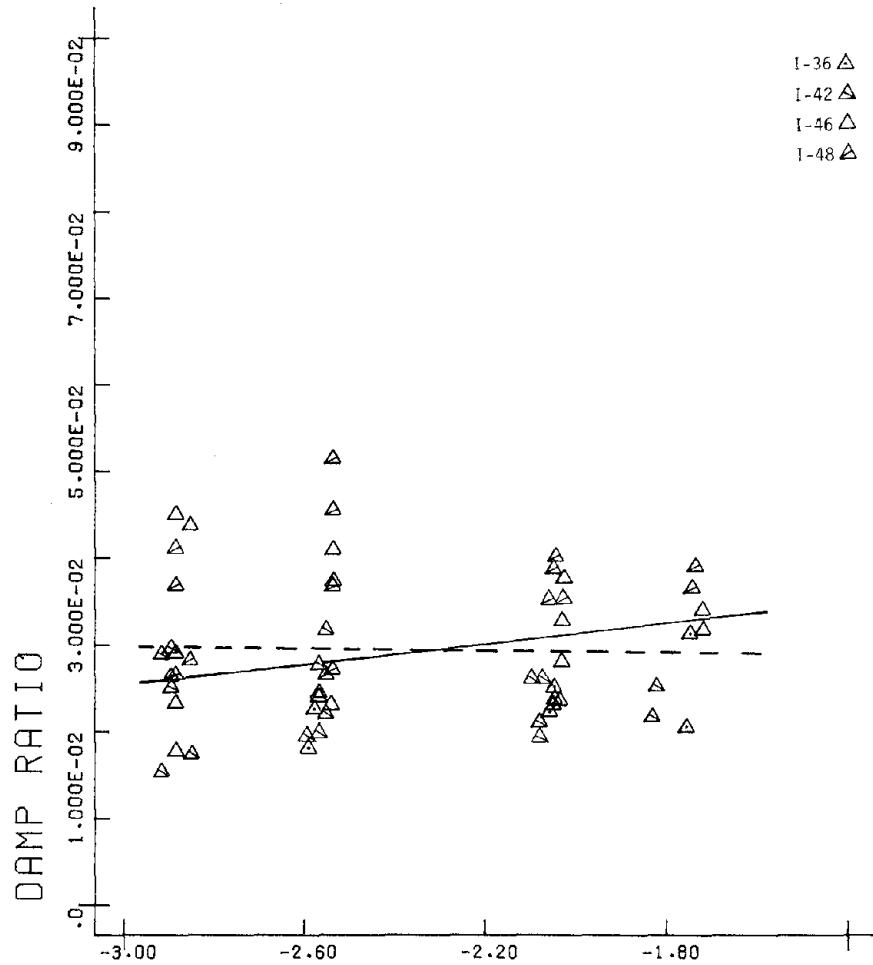
LOG PERCENT AX STRAIN

ICE, T-4F, 05ALLCP



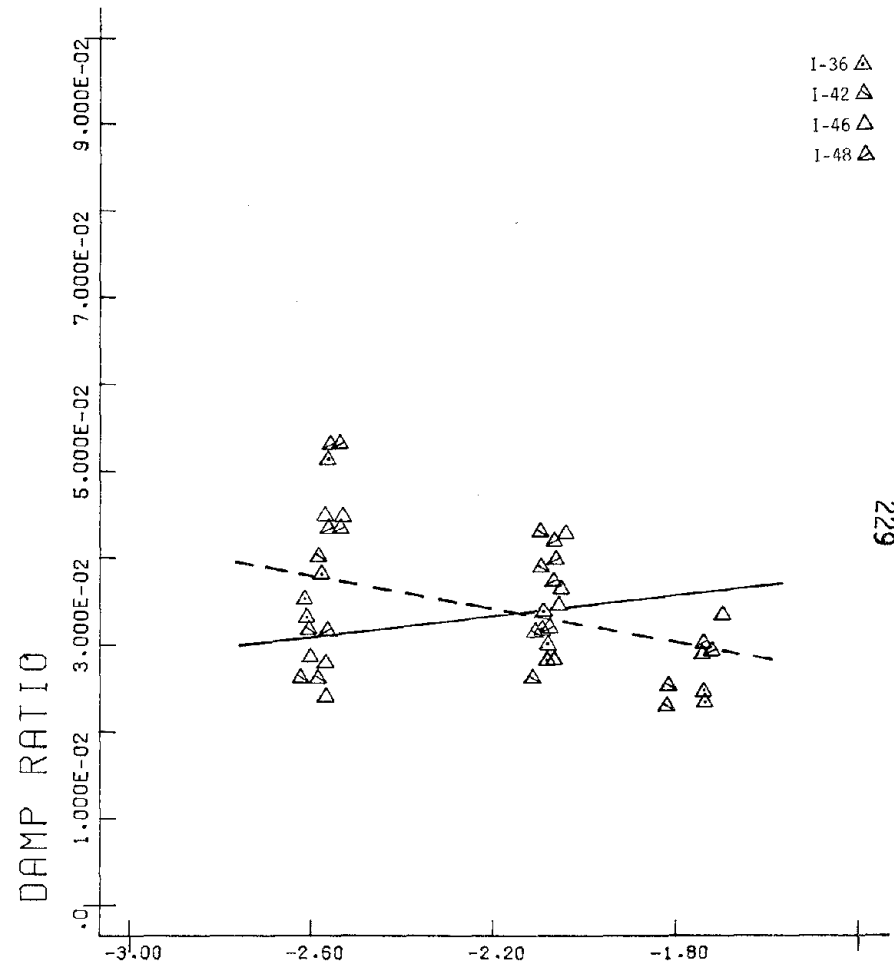
LOG PERCENT AX STRAIN

ICE, T-4F, 3ALLCP



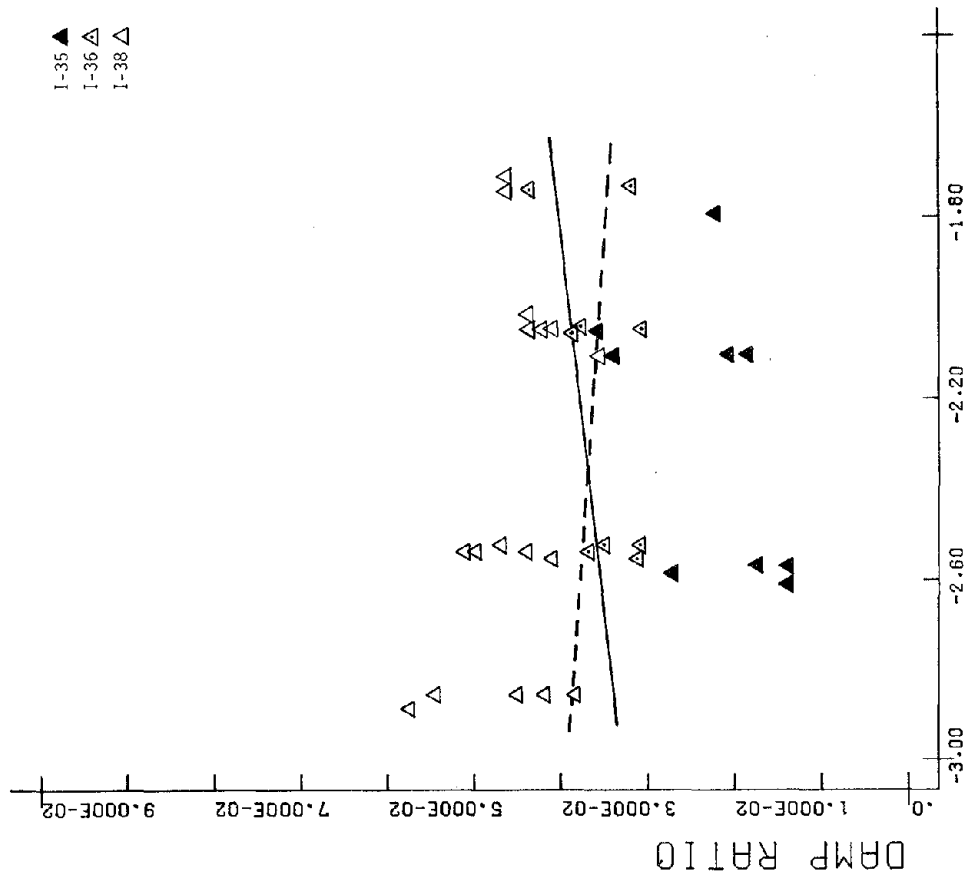
LOG PERCNT Figure D.11 AX STRAIN

ICE, T-4F1ALLCP



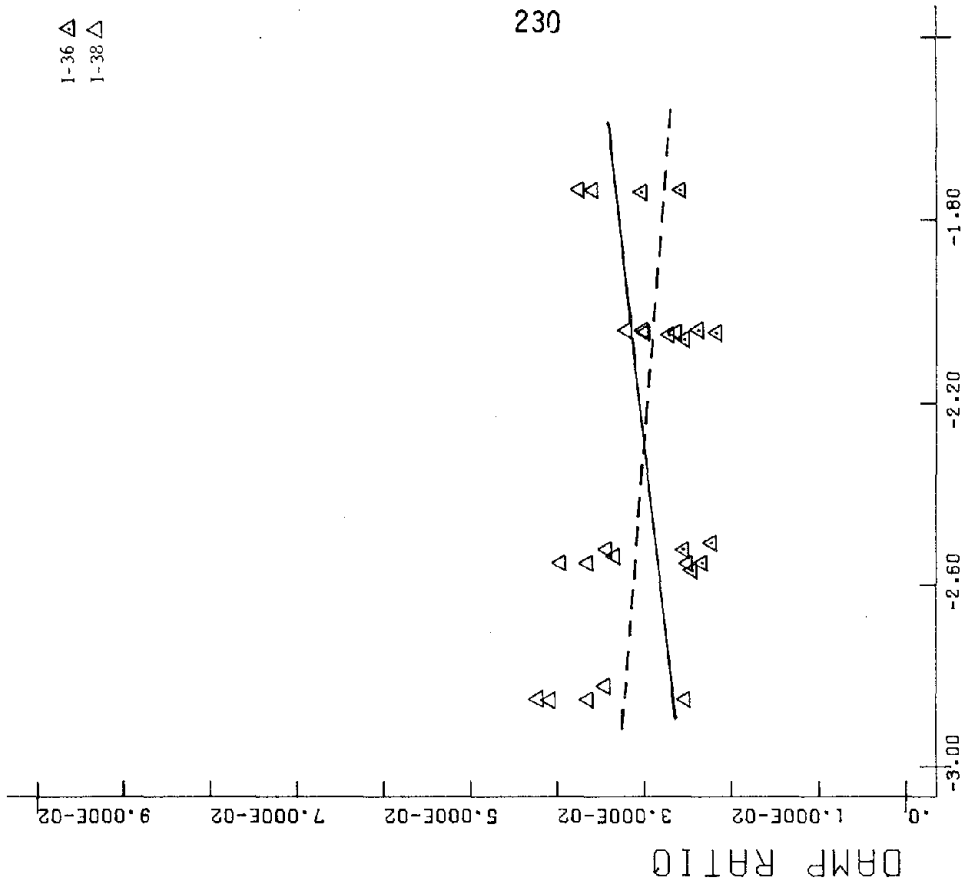
LOG PERCNT Figure D.12 AX STRAIN

ICE, T-4F5ALLCP



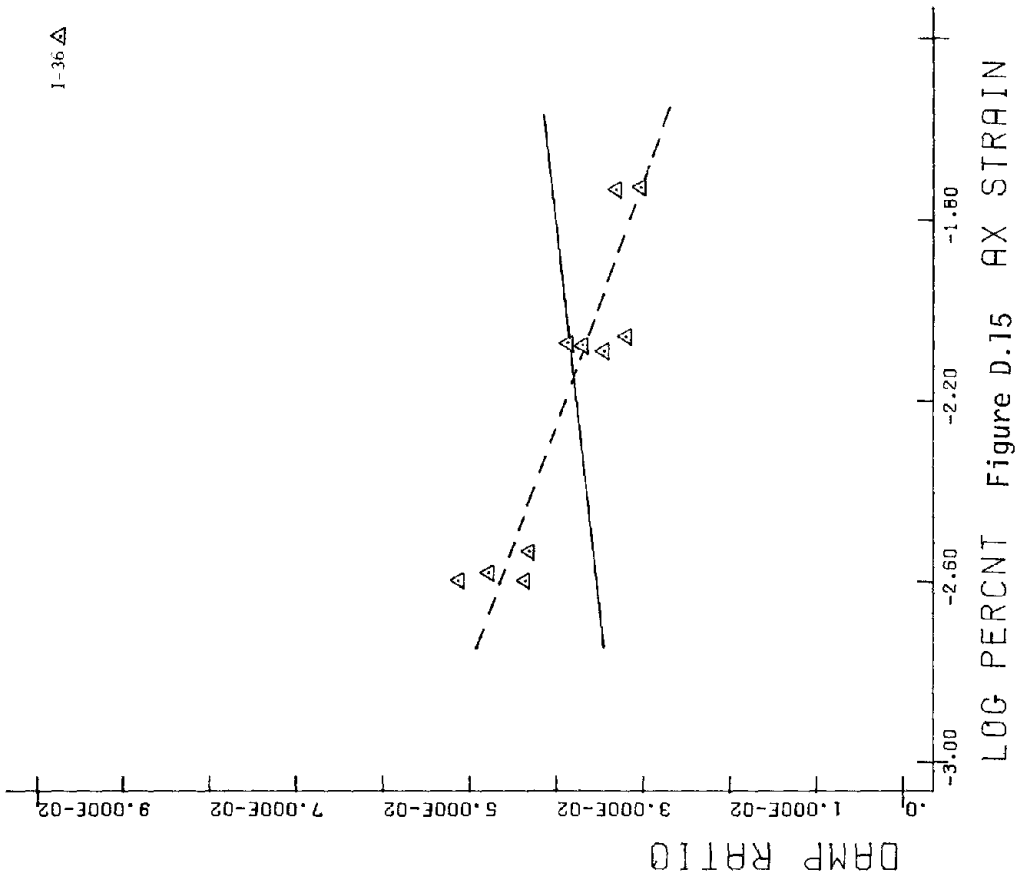
LOG PERCENT AX STRAIN Figure D.13

ICE, T-6F.3ALLCP



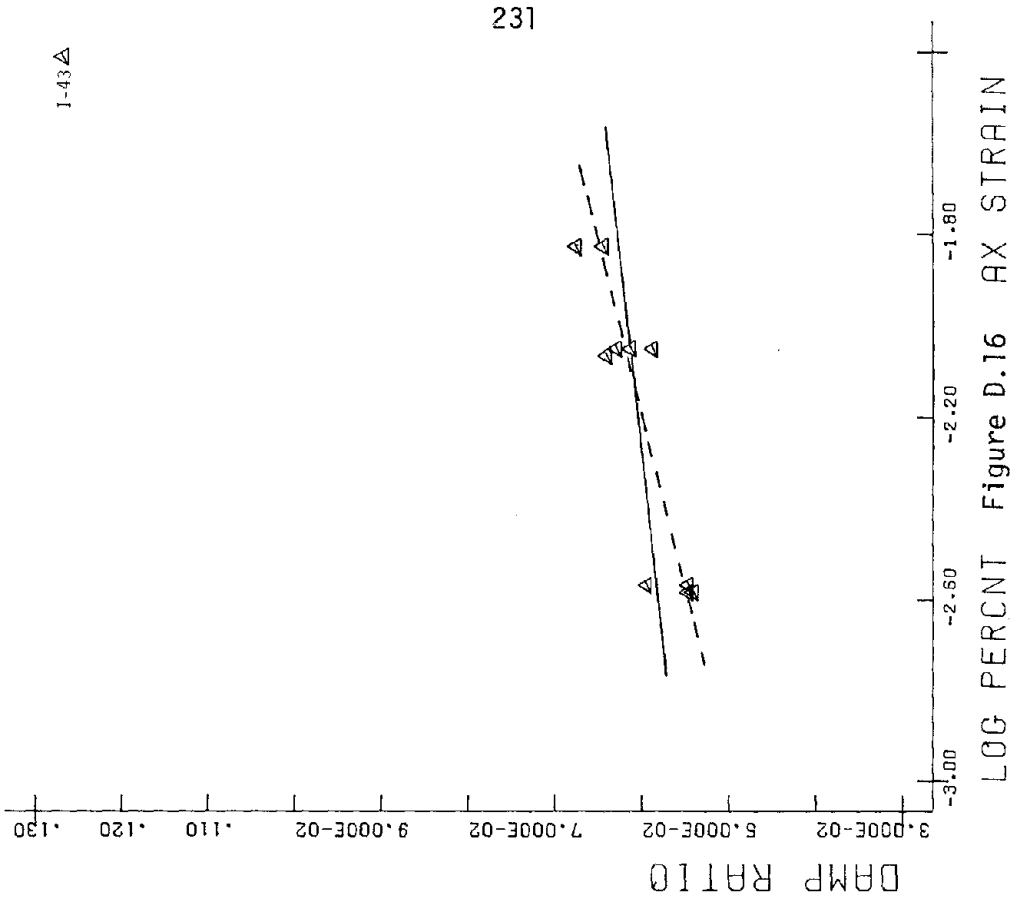
LOG PERCENT AX STRAIN Figure D.14

ICE, T-6F.1ALLCP



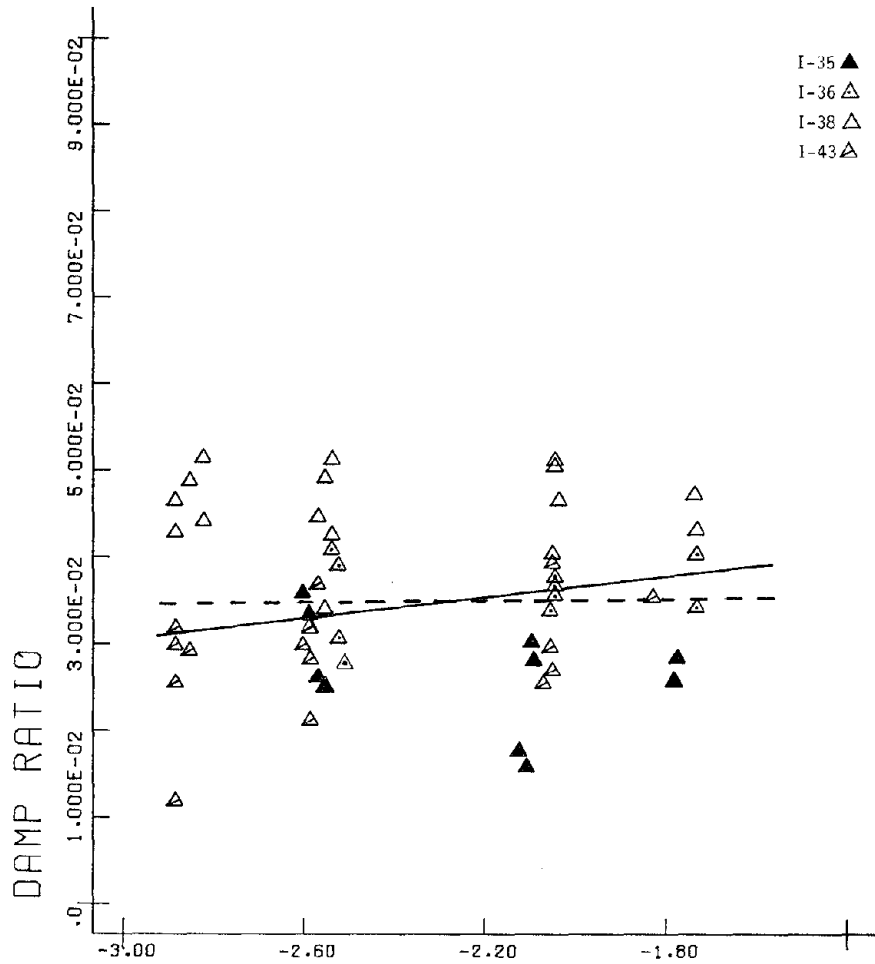
ICE, T-6F5ALLCP

Figure D.15



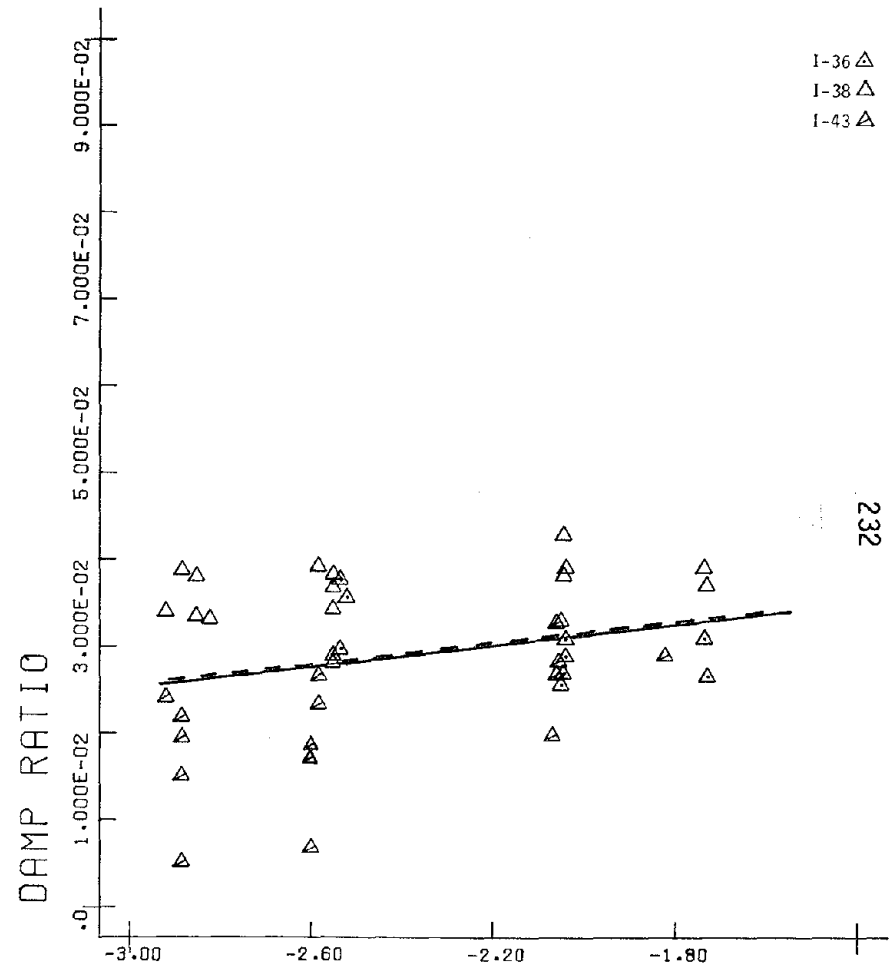
ICE, T-10F.05ALLCP

Figure D.16



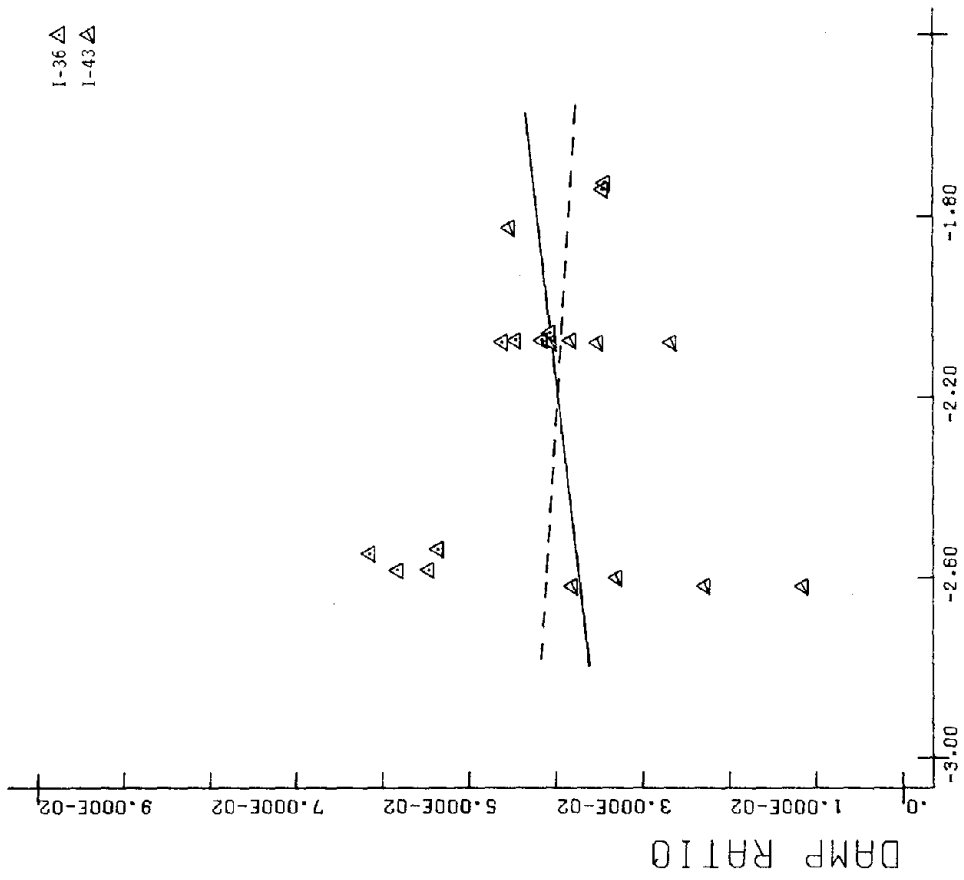
LOG PERCENT Figure D.17 AX STRAIN

ICE, T-10F.3ALLC



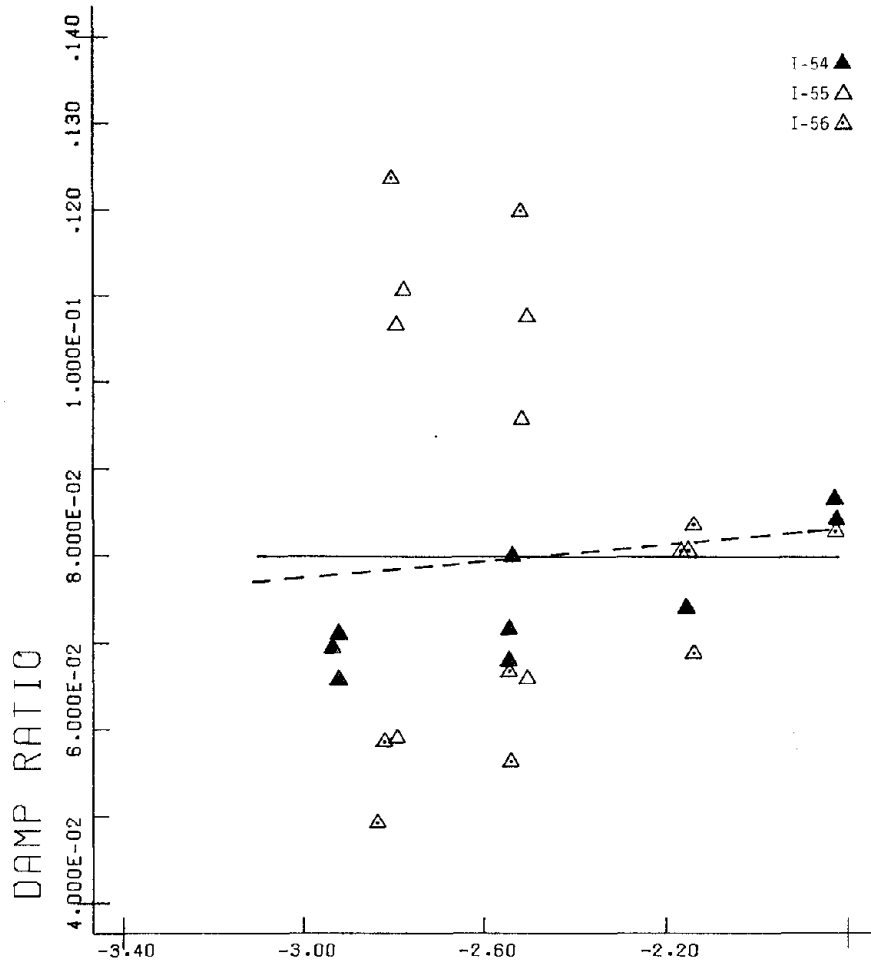
LOG PERCENT Figure D.18 AX STRAIN

ICE, T-10F1ALLCP



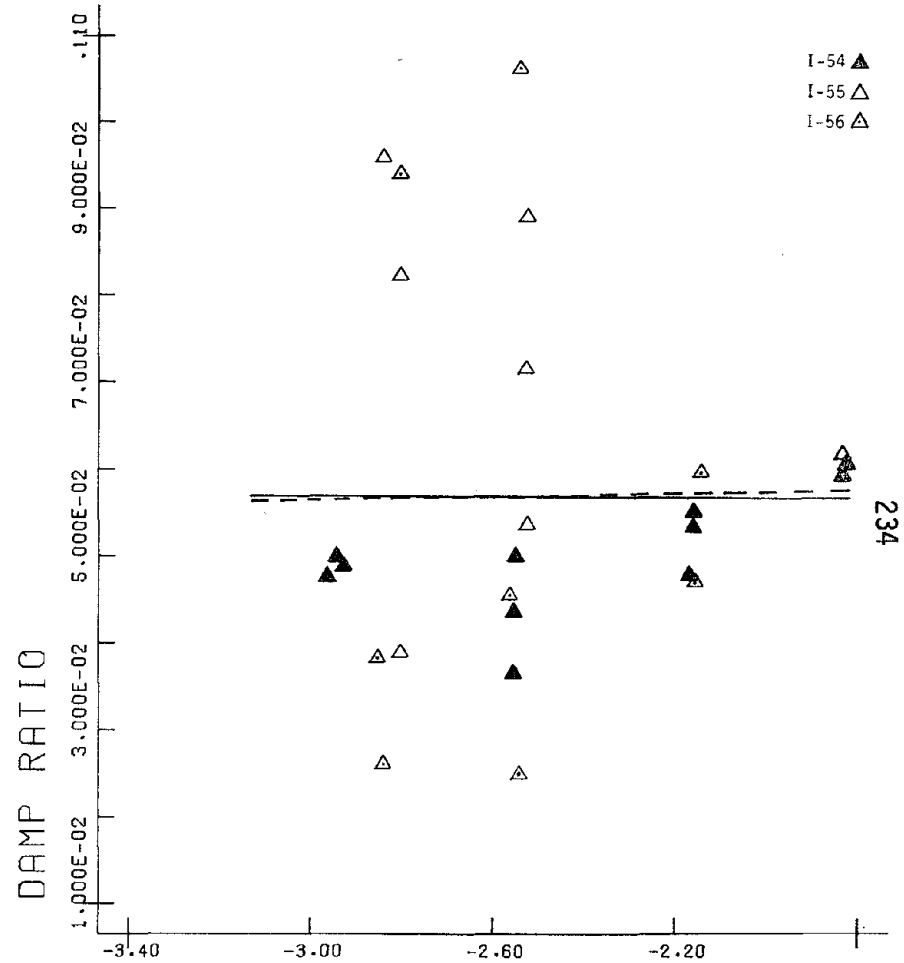
LOG PERCENT AX STRAIN Figure D.19

ICE, T-10F5ALLCP



LOG PERCENT Figure D.20 AX STRAIN

ICE, T-1F.3ALLCP



LOG PERCENT Figure D.21 AX STRAIN

ICE, T-1F1ALLCP

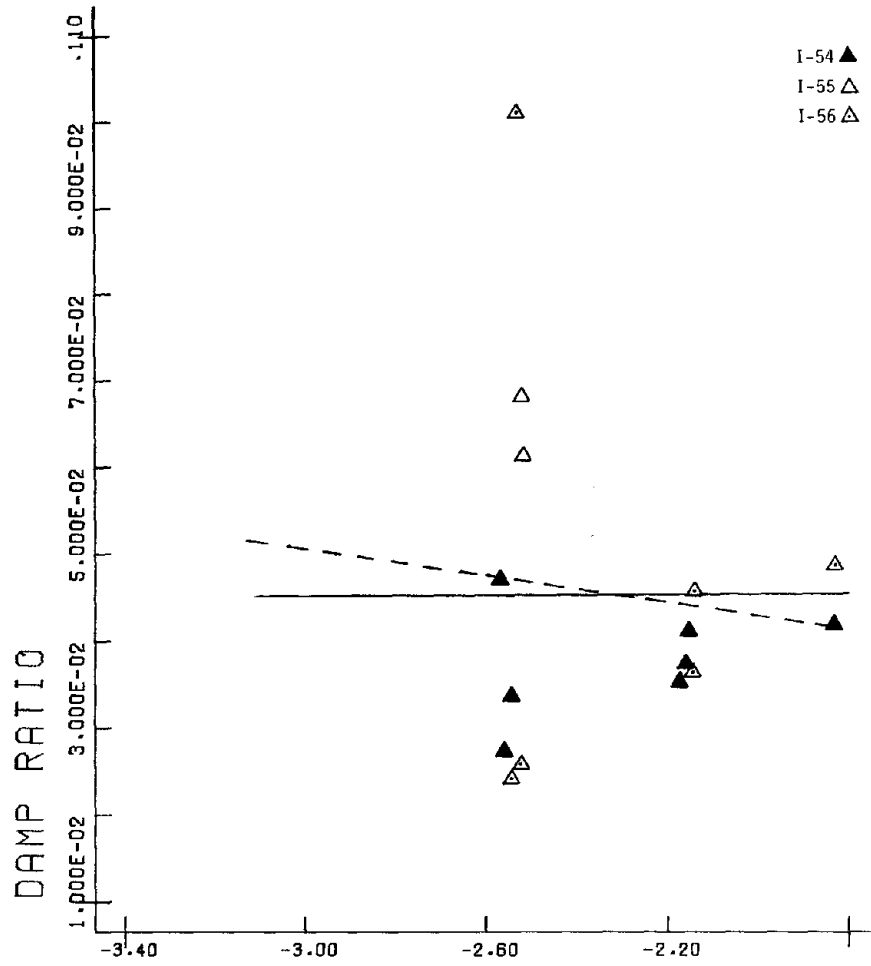
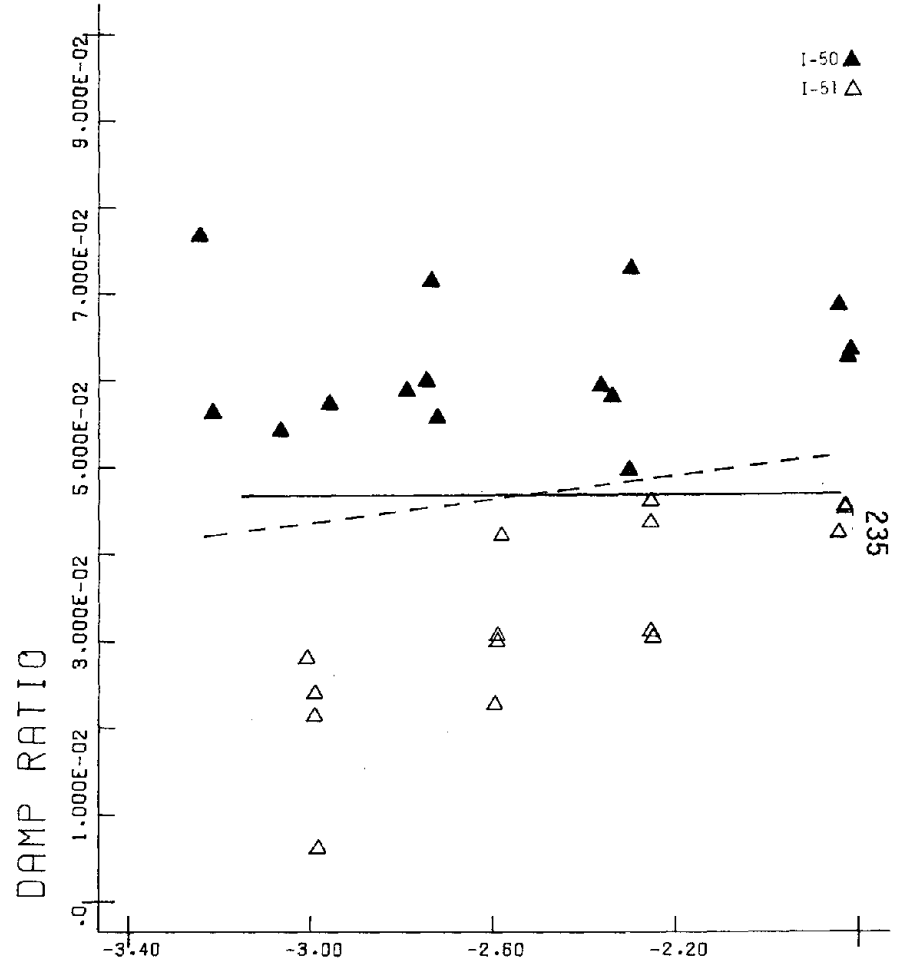
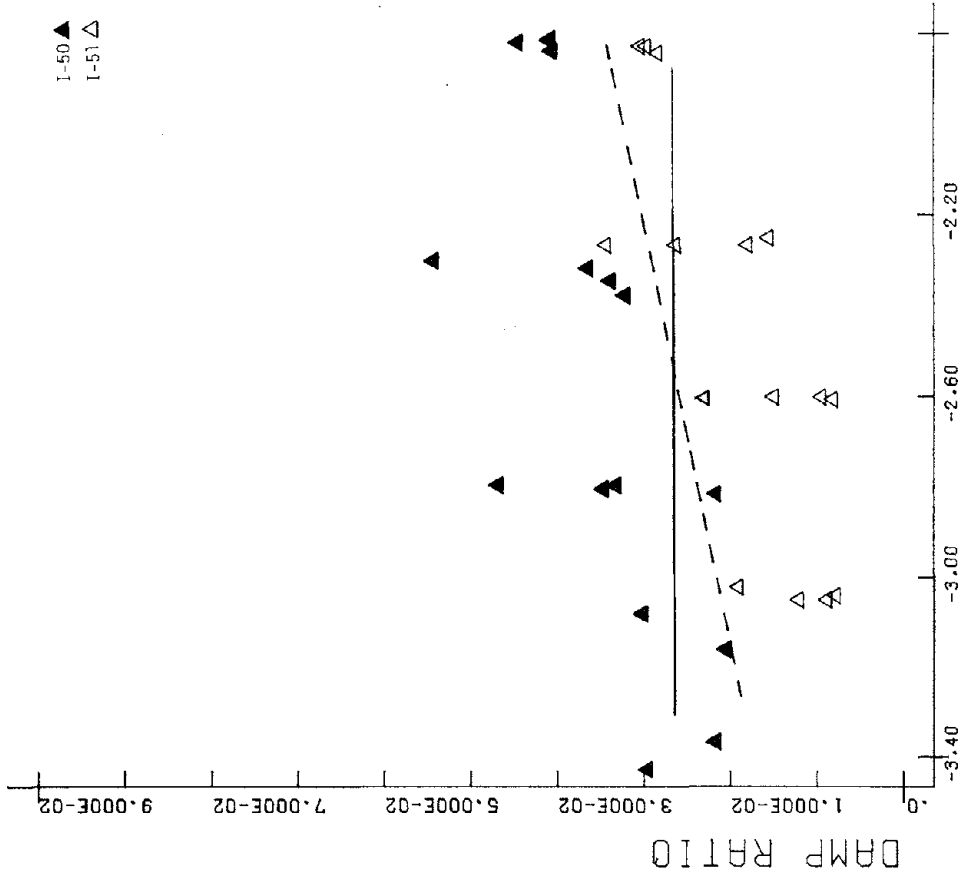


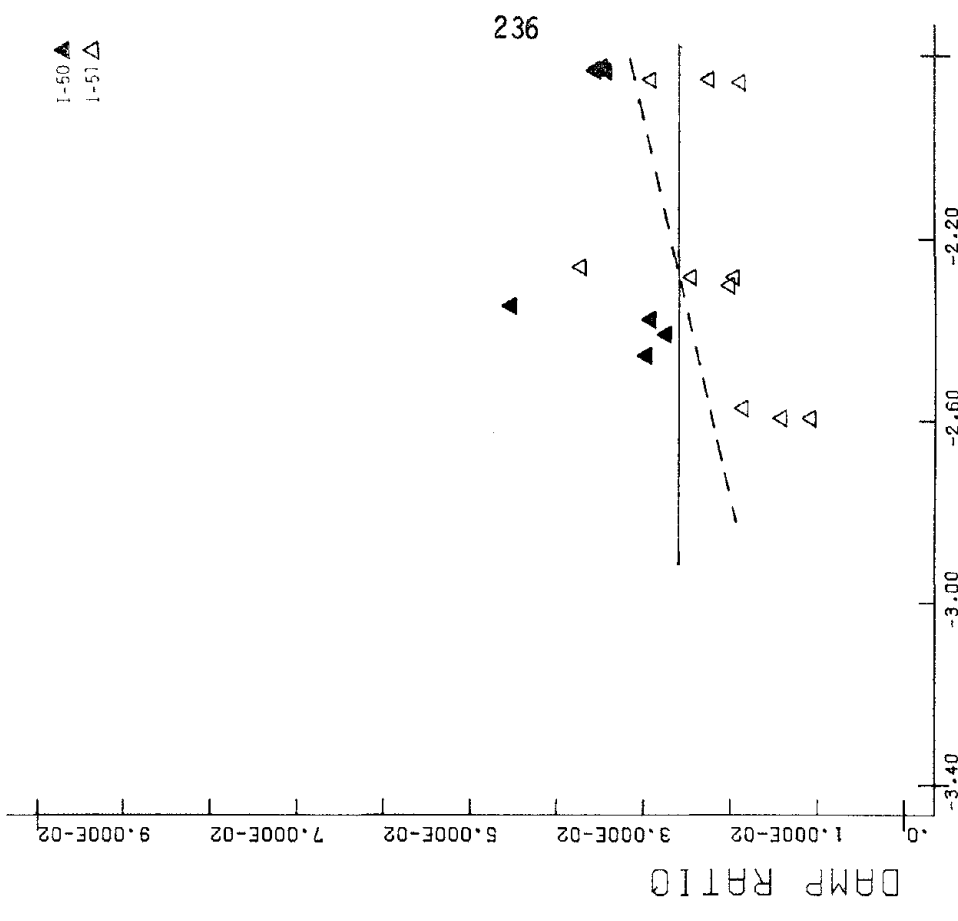
Figure D.22 AX STRAIN
ICE, T-1F5ALLCP





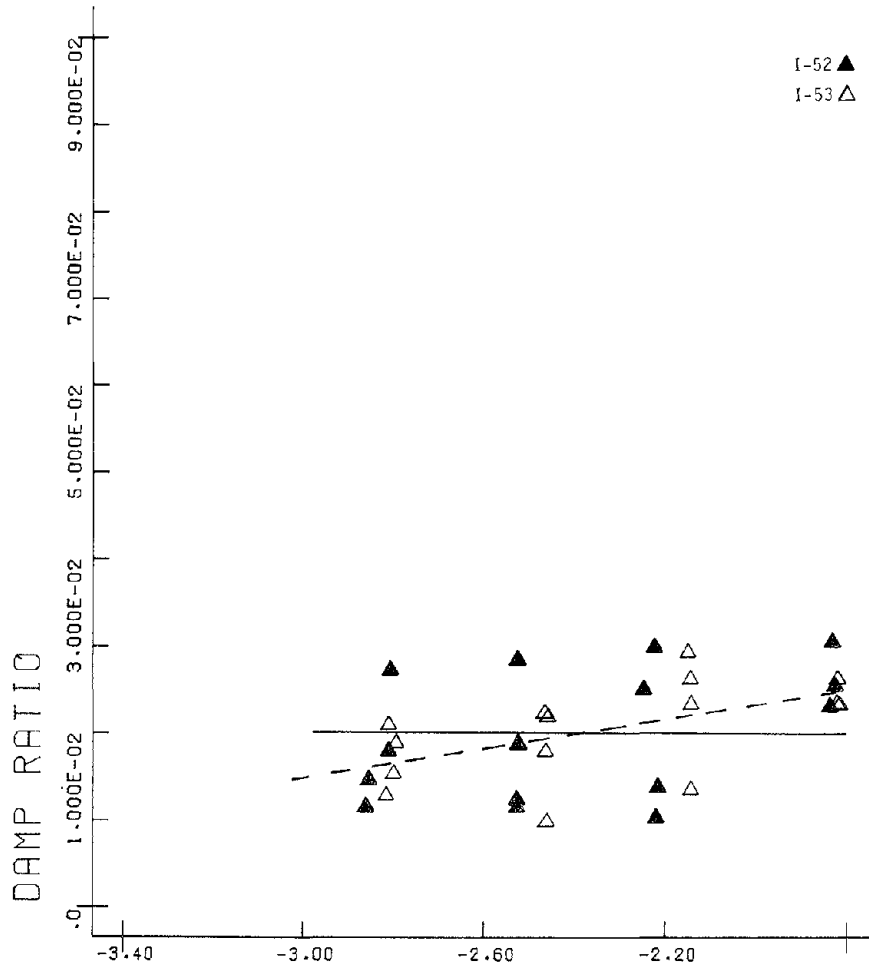
LOG PERCENT AX STRAIN Figure D.24

ICE,T-4F1ALLCP

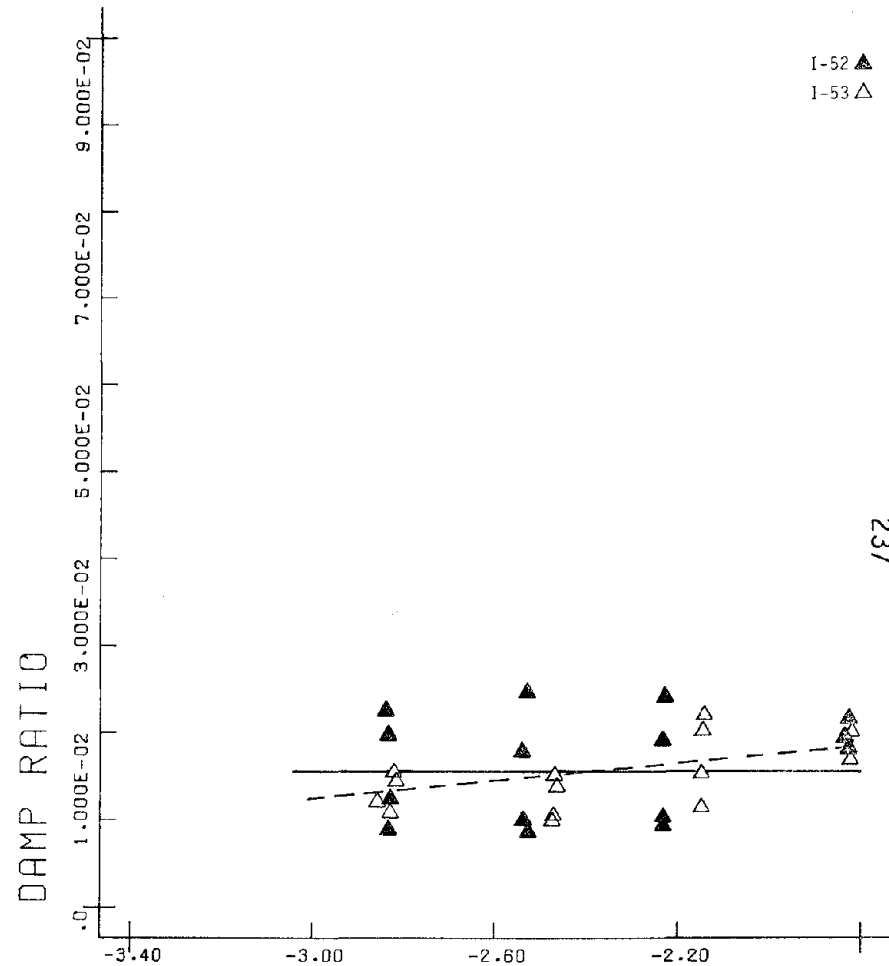


LOG PERCENT AX STRAIN Figure D.25

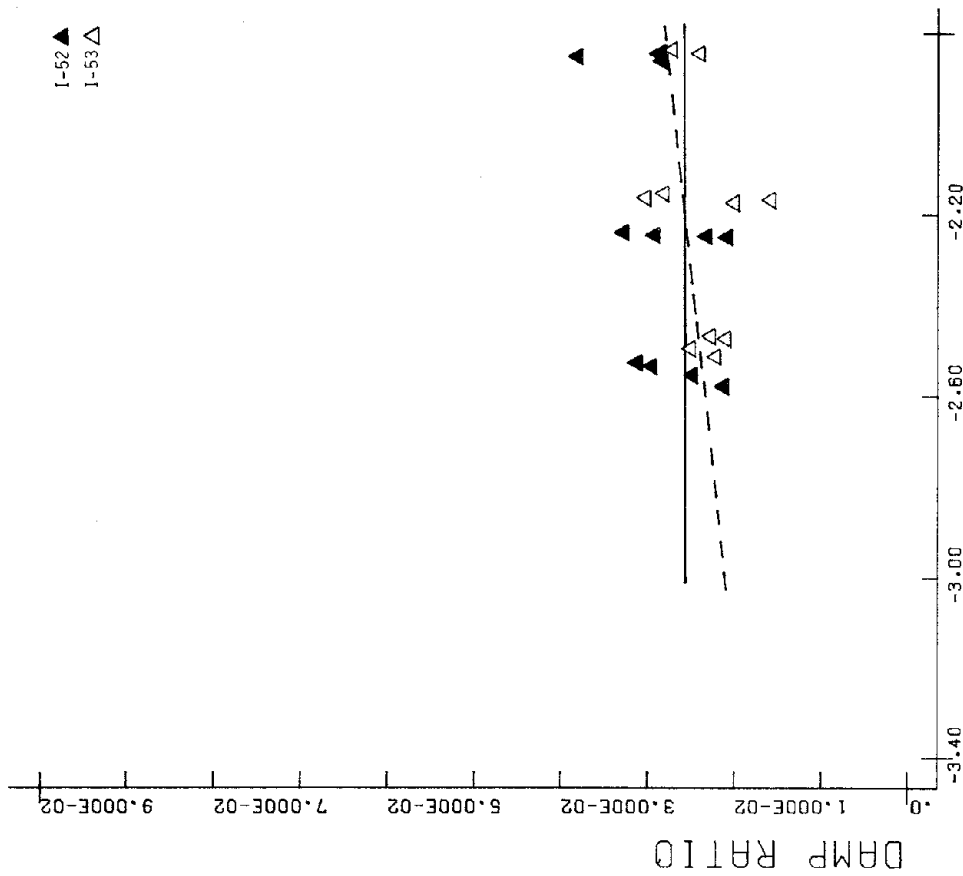
ICE,T-4F5ALLCP



LOG PERCENT AX STRAIN
 ICE, T-10F.3ALLCP



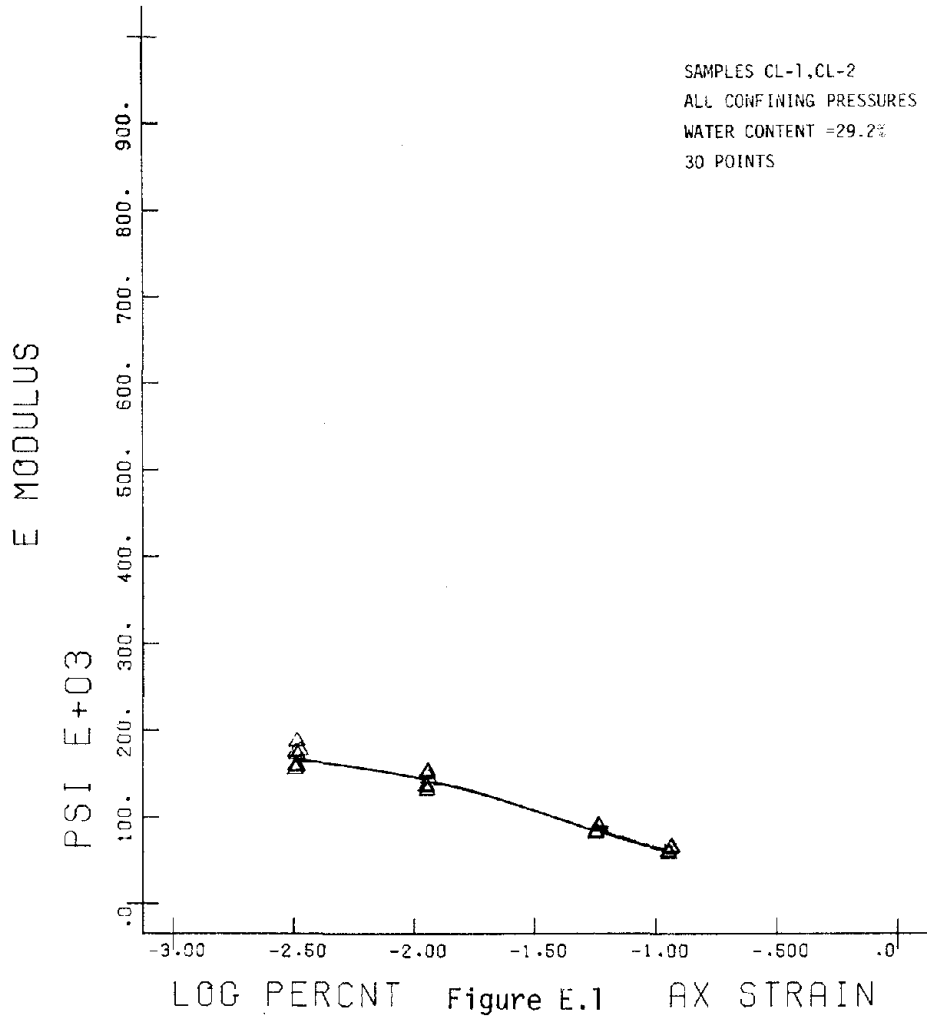
LOG PERCENT AX STRAIN
 ICE, T-10F1ALLCP



LOG PERCENT AX STRAIN Figure D.28

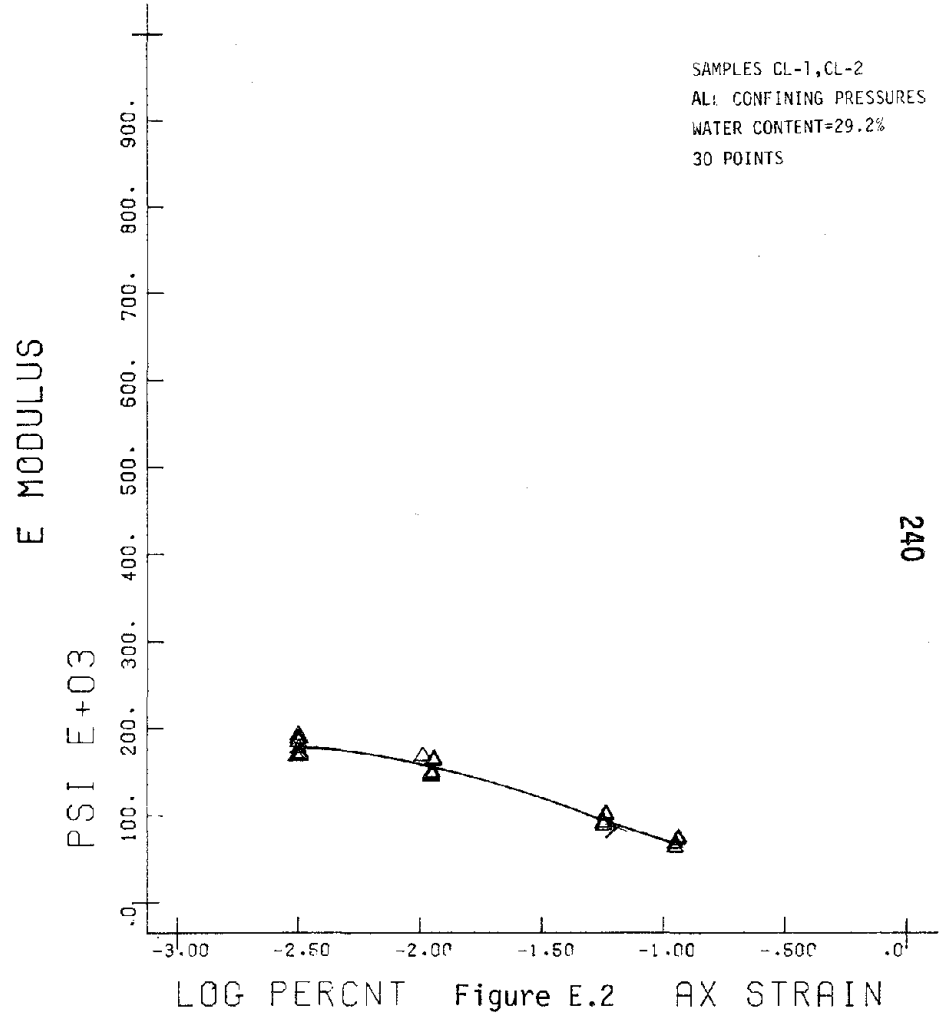
ICE, T-10F5ALLCP

APPENDIX E
CYCLIC TRIAXIAL TEST RESULTS: DYNAMIC
YOUNG'S MODULUS OF FROZEN CLAY



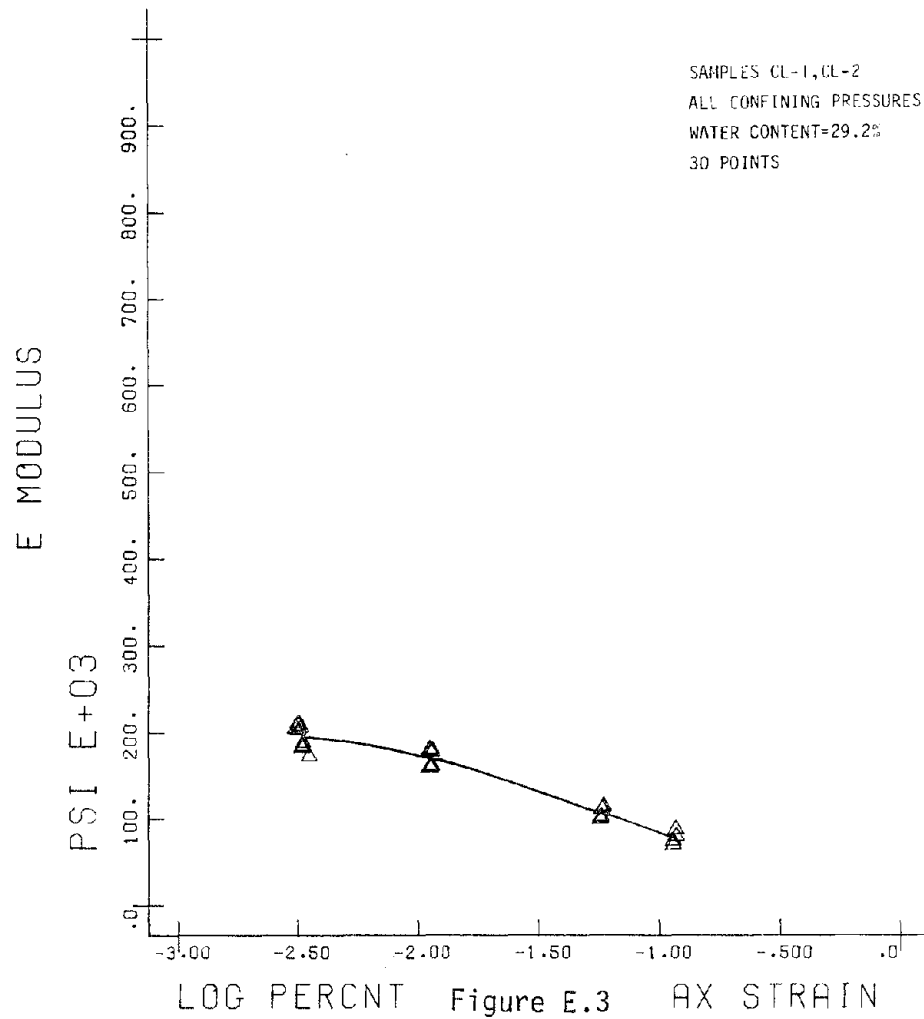
LOG PERCENT AX STRAIN Figure E.1

O-CLAYT-1F.3

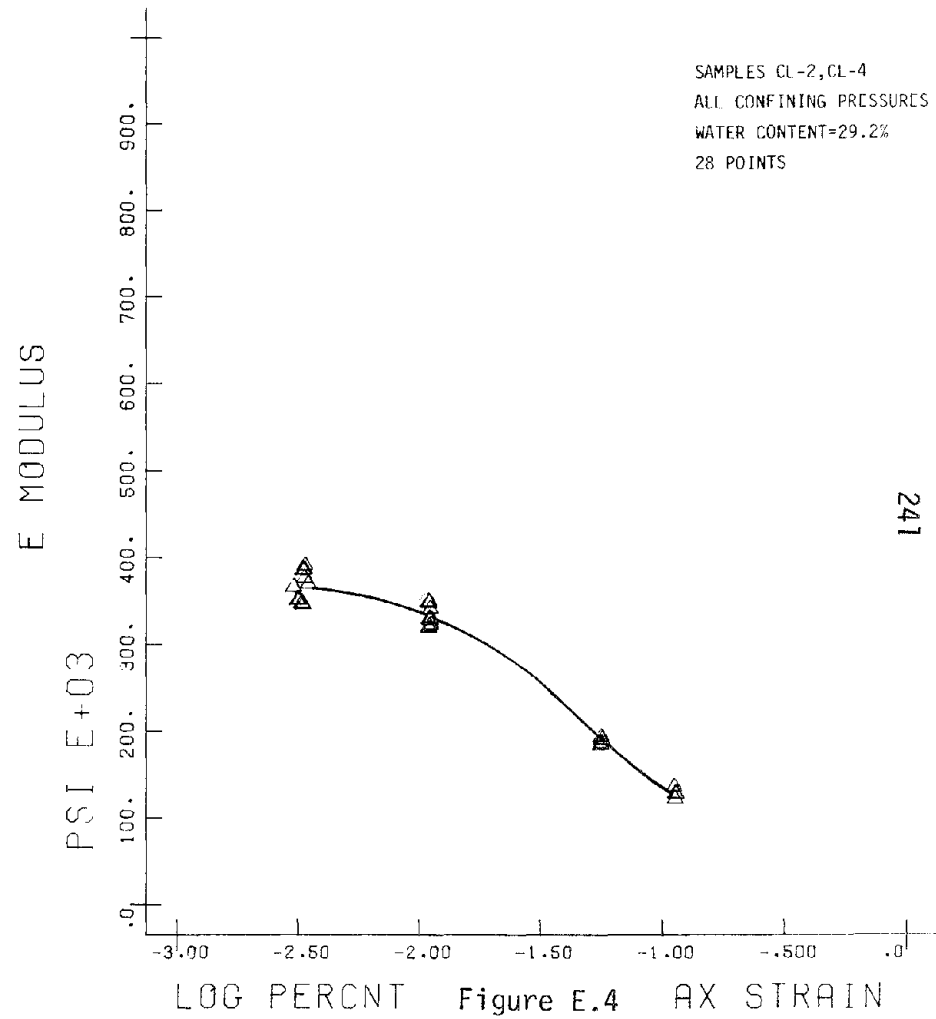


LOG PERCENT AX STRAIN Figure E.2

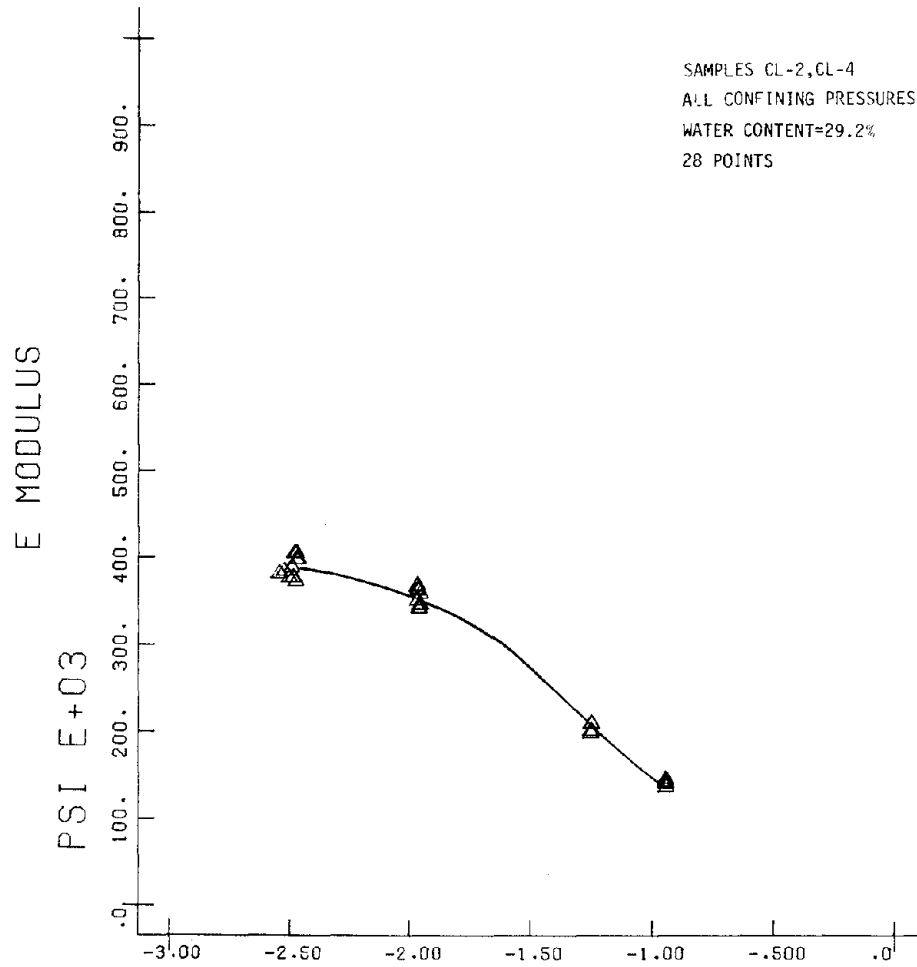
O-CLAYT-1F1



O-CLAYT-1F5

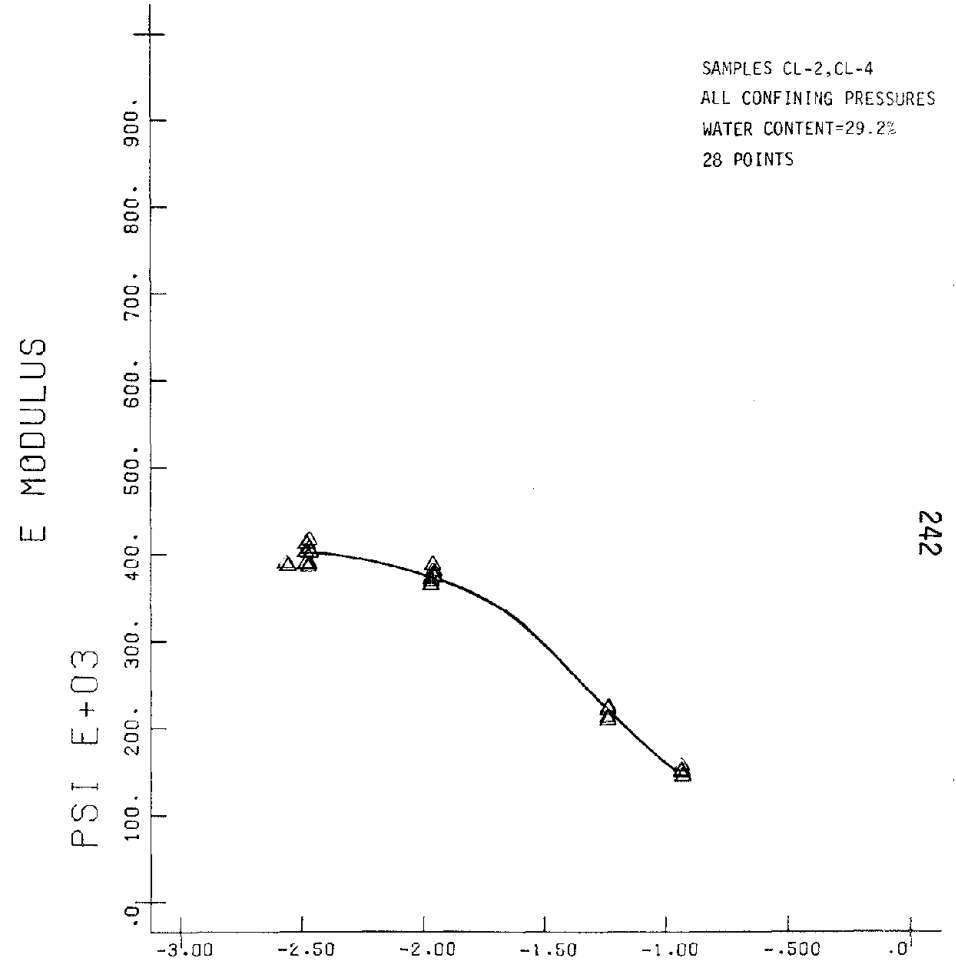


O-CLAYT-4F.3



LOG PERCENT Figure E.5 AX STRAIN

O-CLAYT-4F1



LOG PERCENT Figure E.6 AX STRAIN

O-CLAYT-4F5

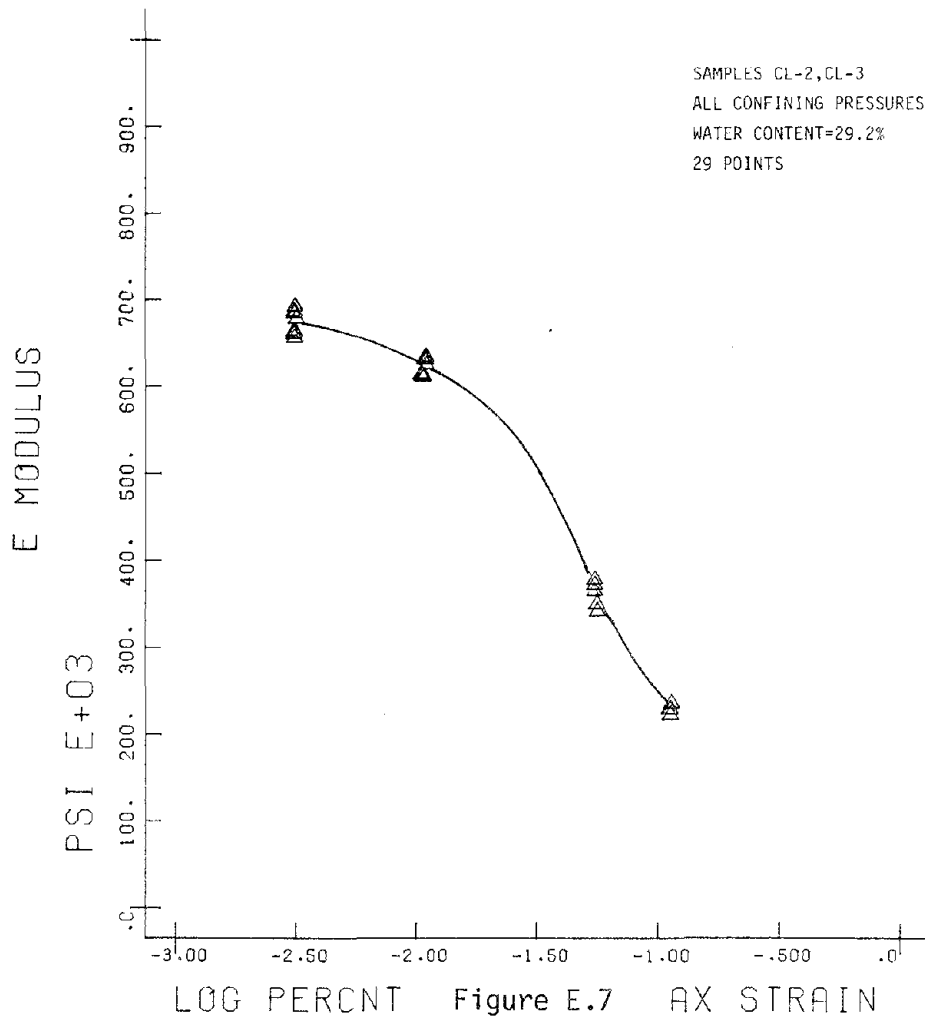


Figure E.7

O-CLAYT-10F.3

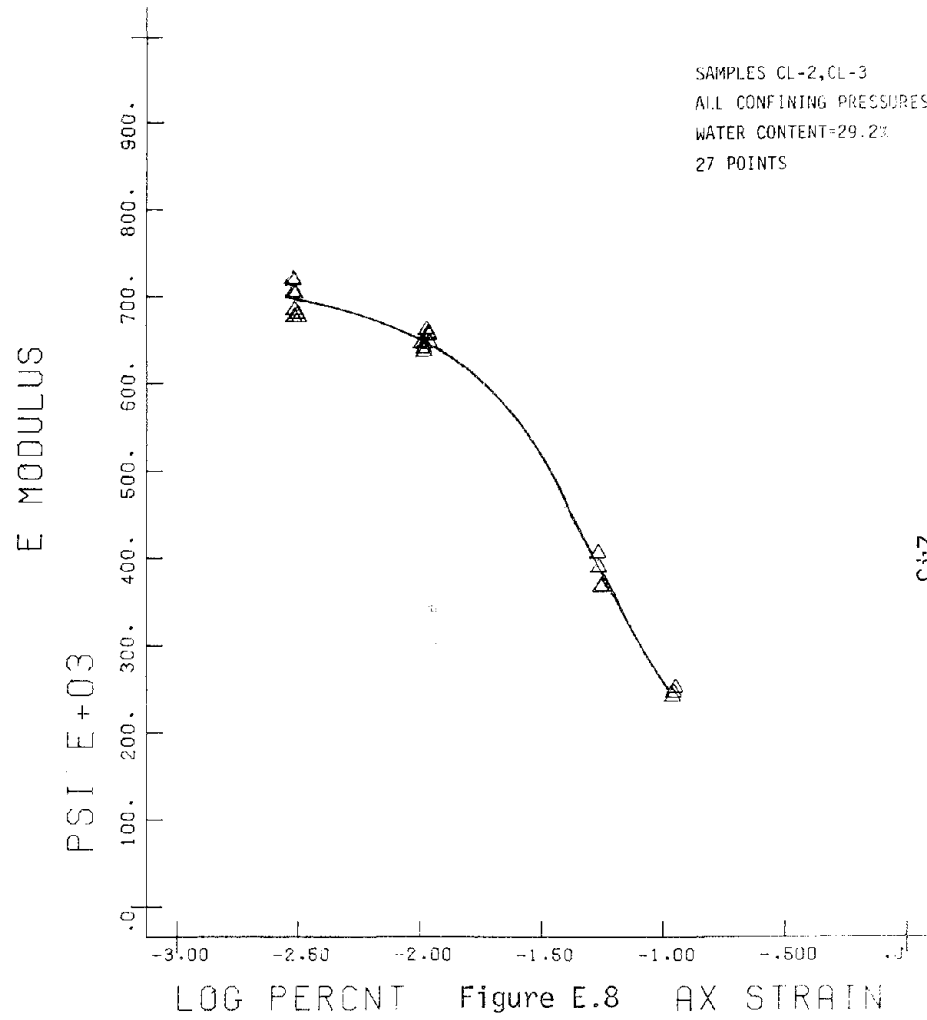
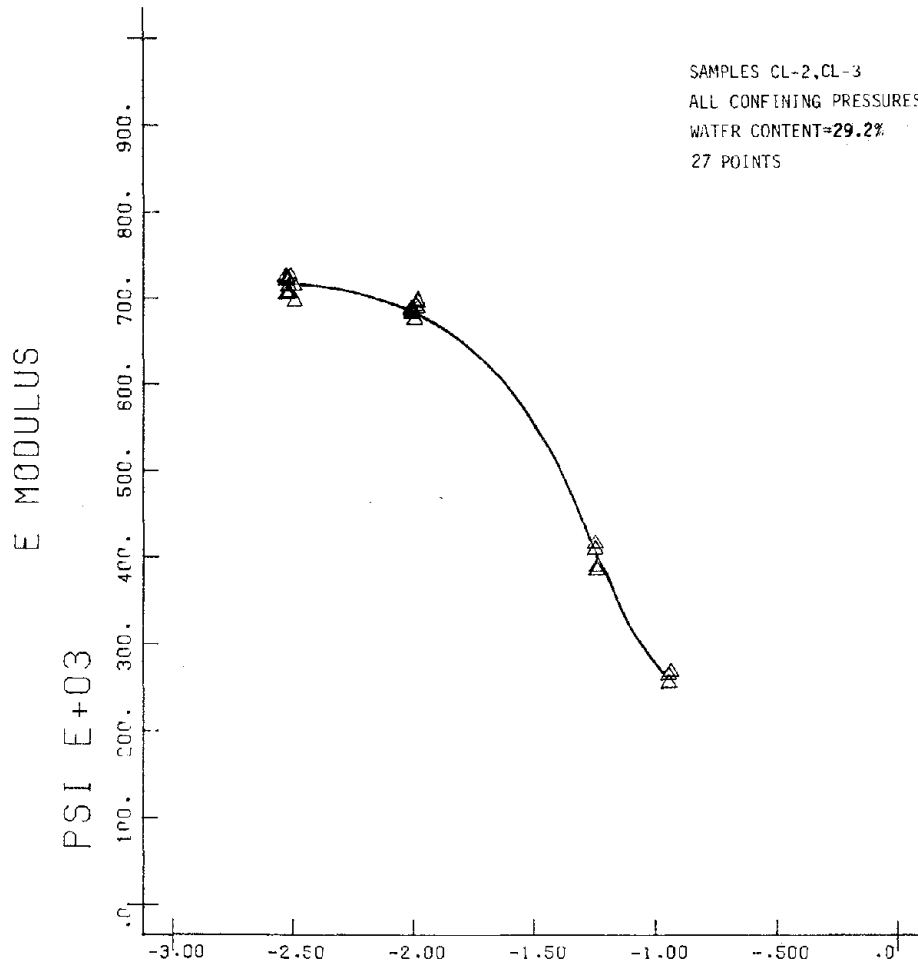


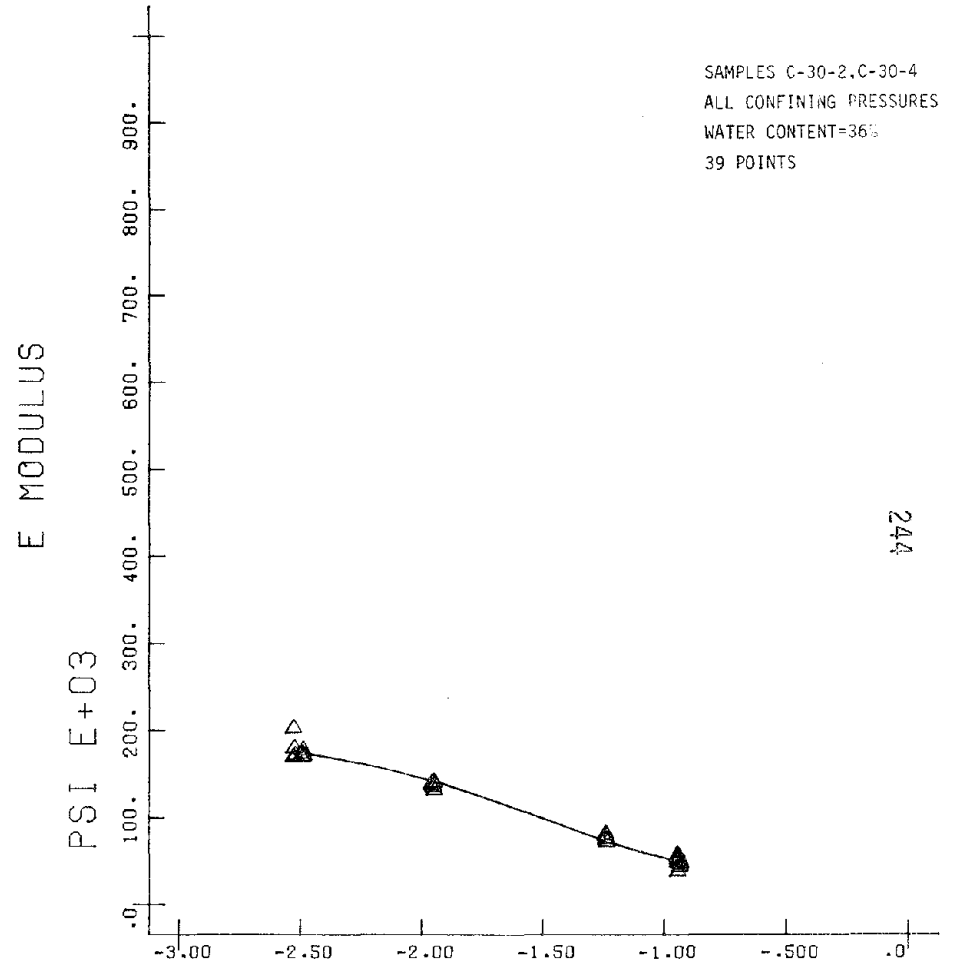
Figure E.8

O-CLAYT-10F.1



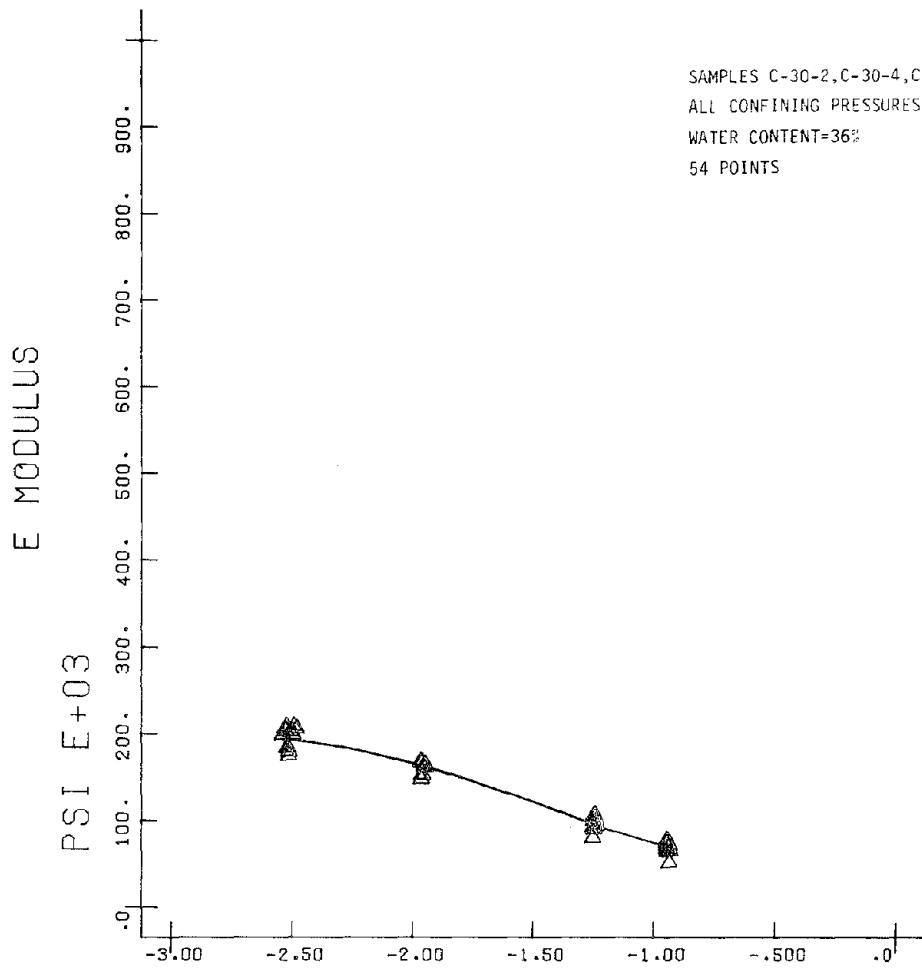
LOG PERCENT Figure E.9 AX STRAIN

O-CLAYT-10F5



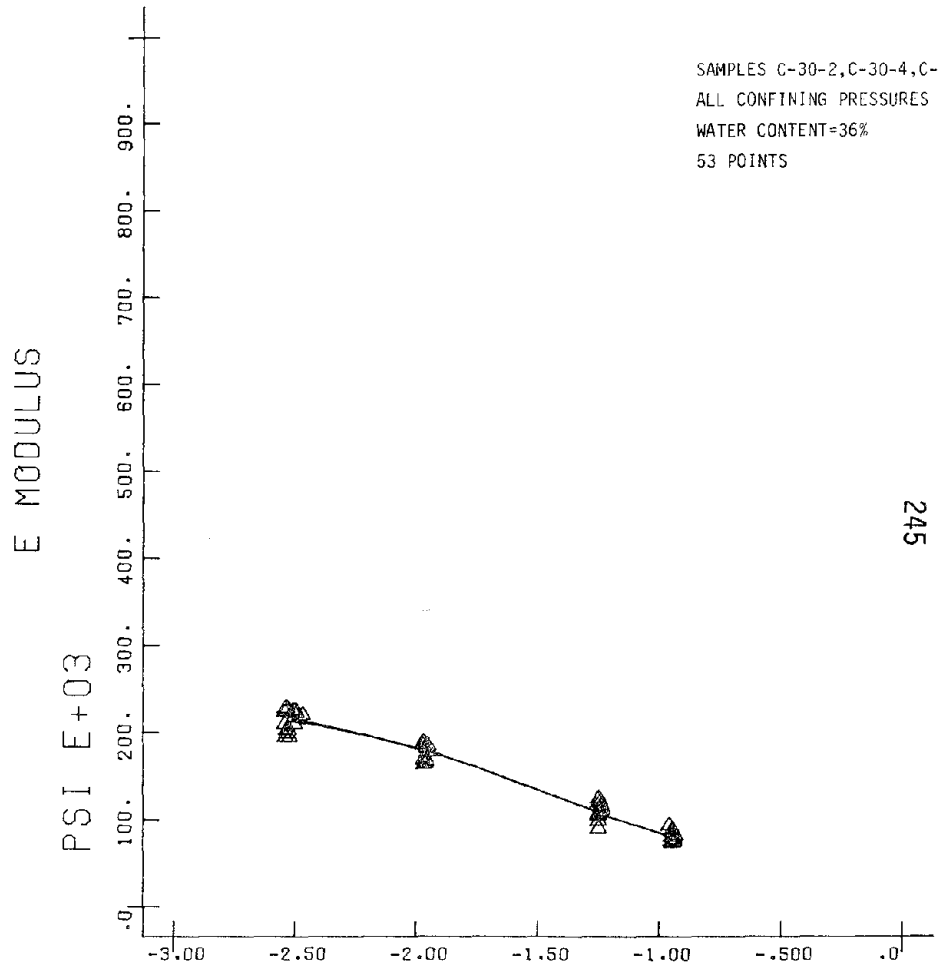
LOG PERCENT Figure E.10 AX STRAIN

O-CLAYT-1F.05



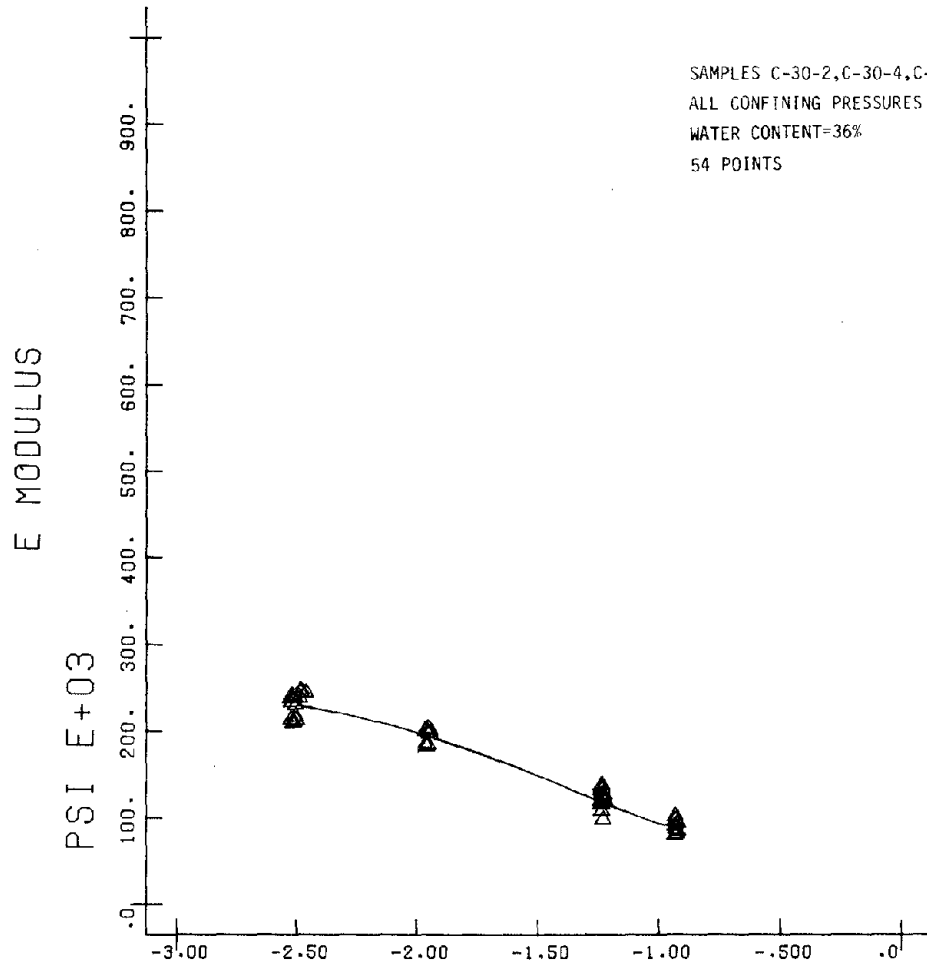
LOG PERCENT Figure E.11 AX STRAIN

O-CLAYT-1F.3



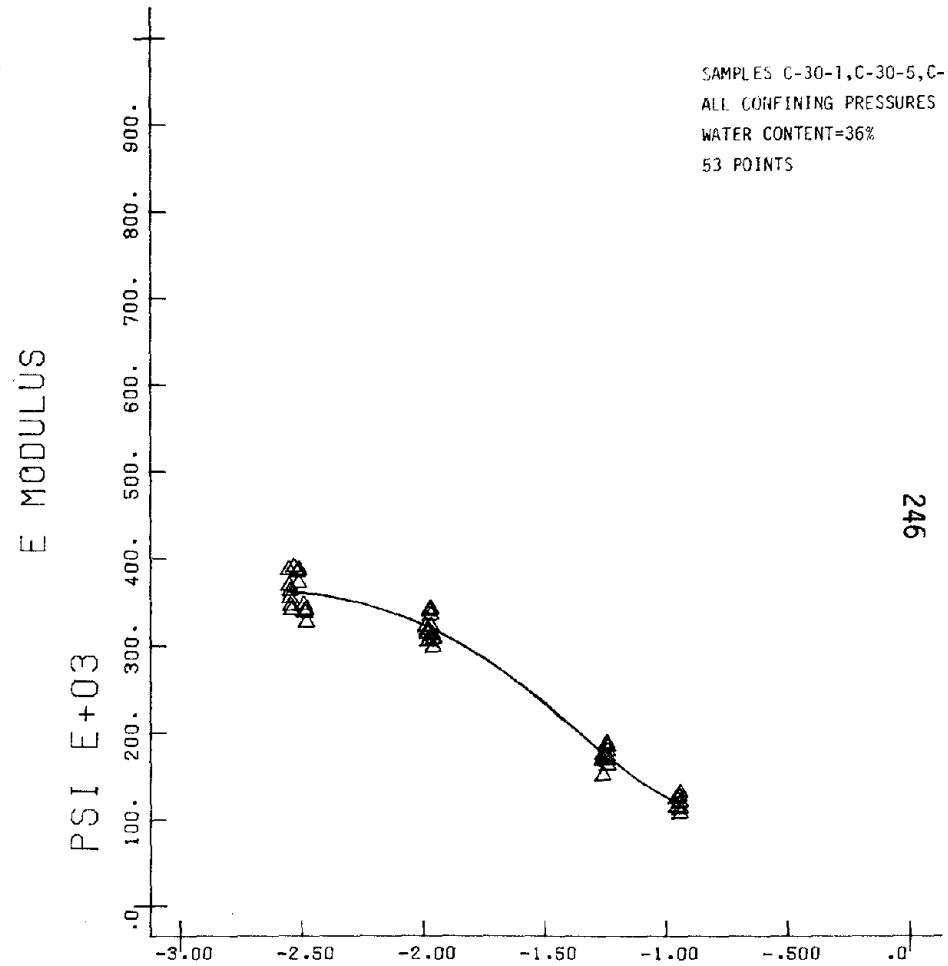
LOG PERCENT Figure E.12 AX STRAIN

O-CLAYT-1F1



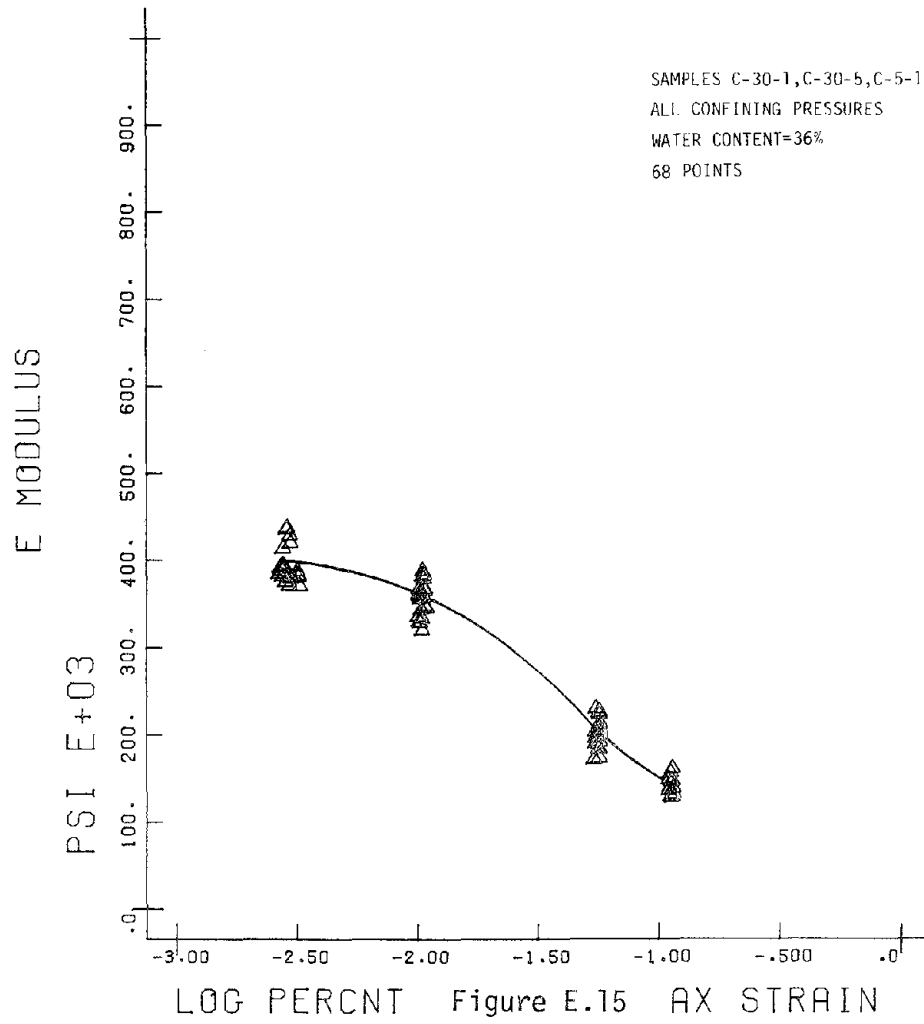
LOG PERCENT Figure E.13 AX STRAIN

0-CLAYT-1F5

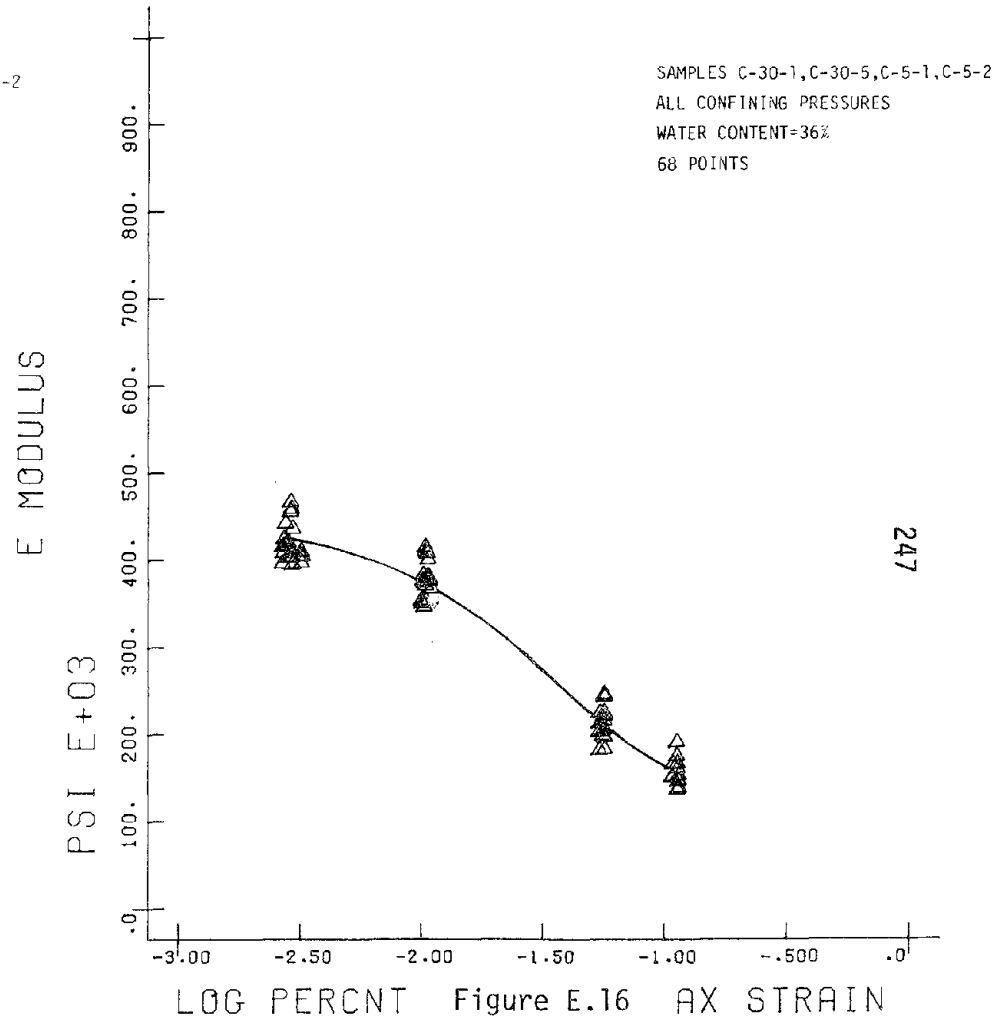


LOG PERCENT Figure E.14 AX STRAIN

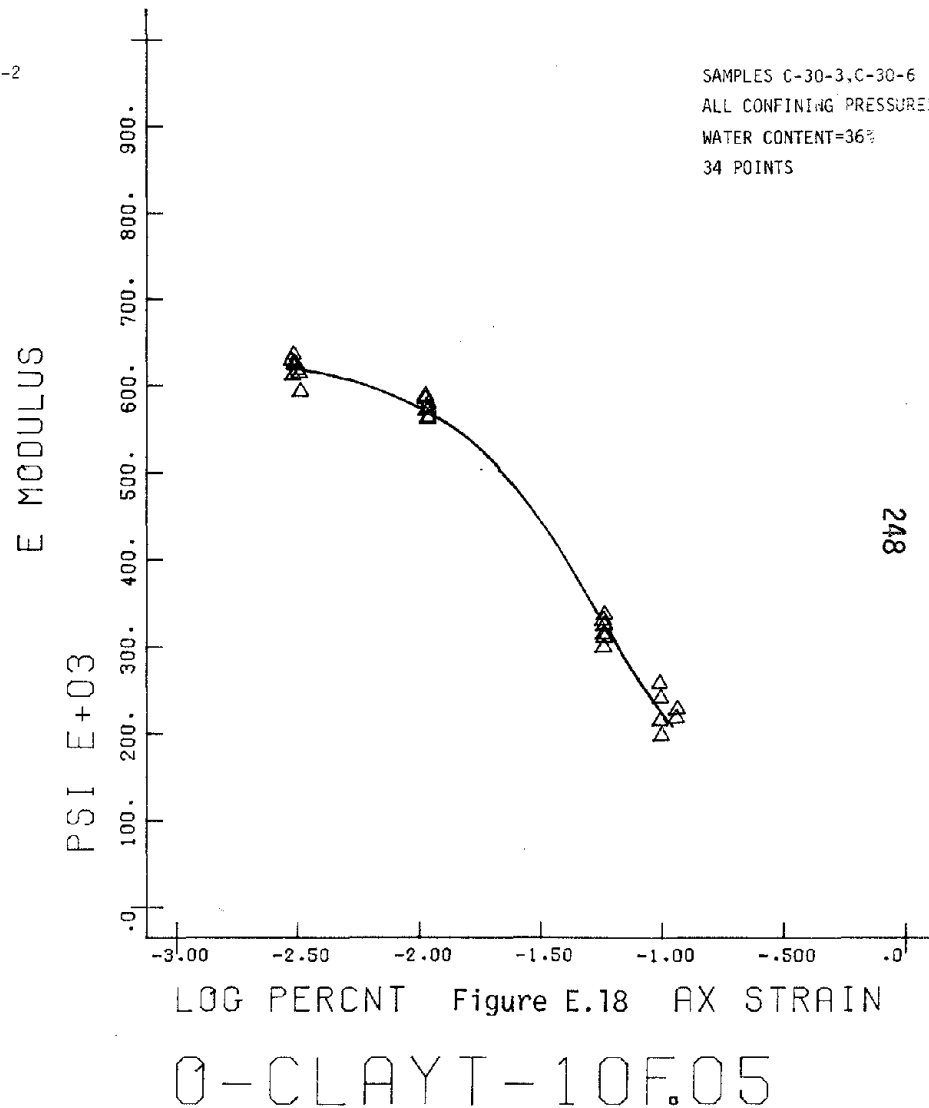
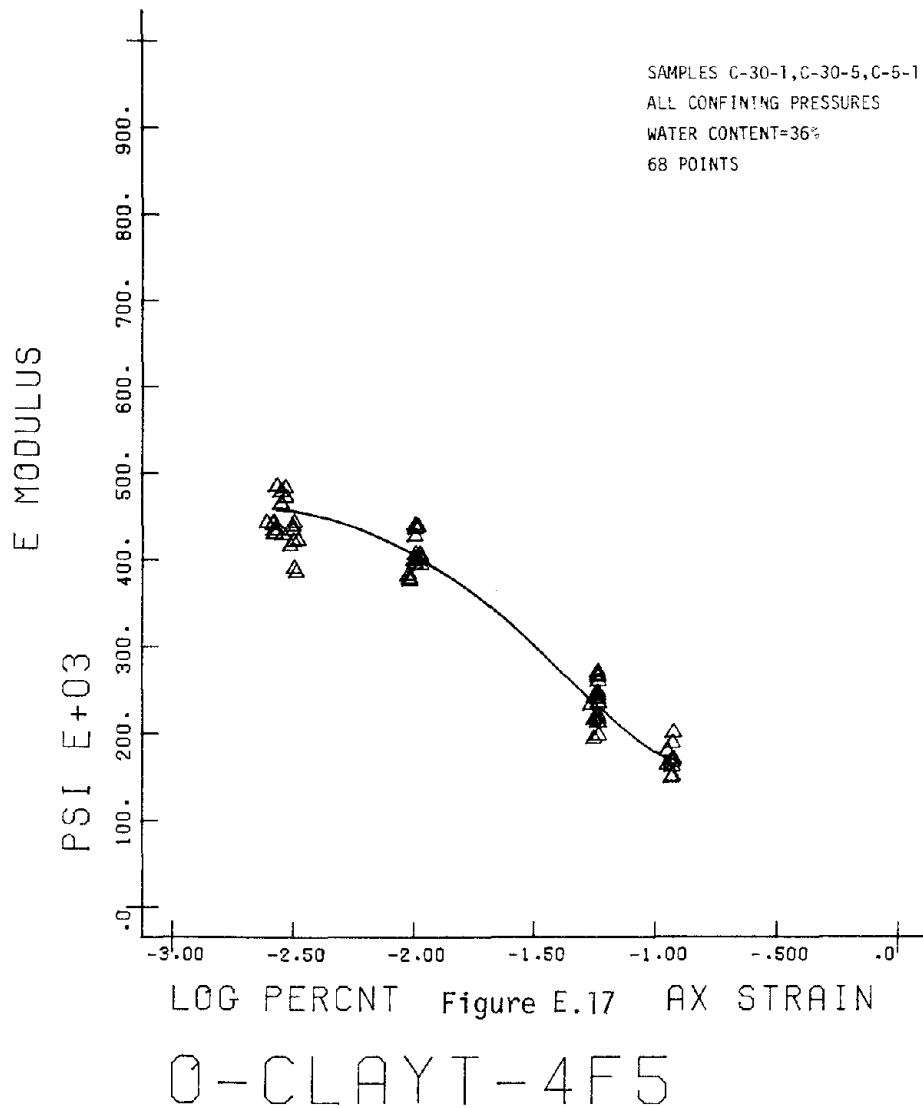
0-CLAYT-4F.05

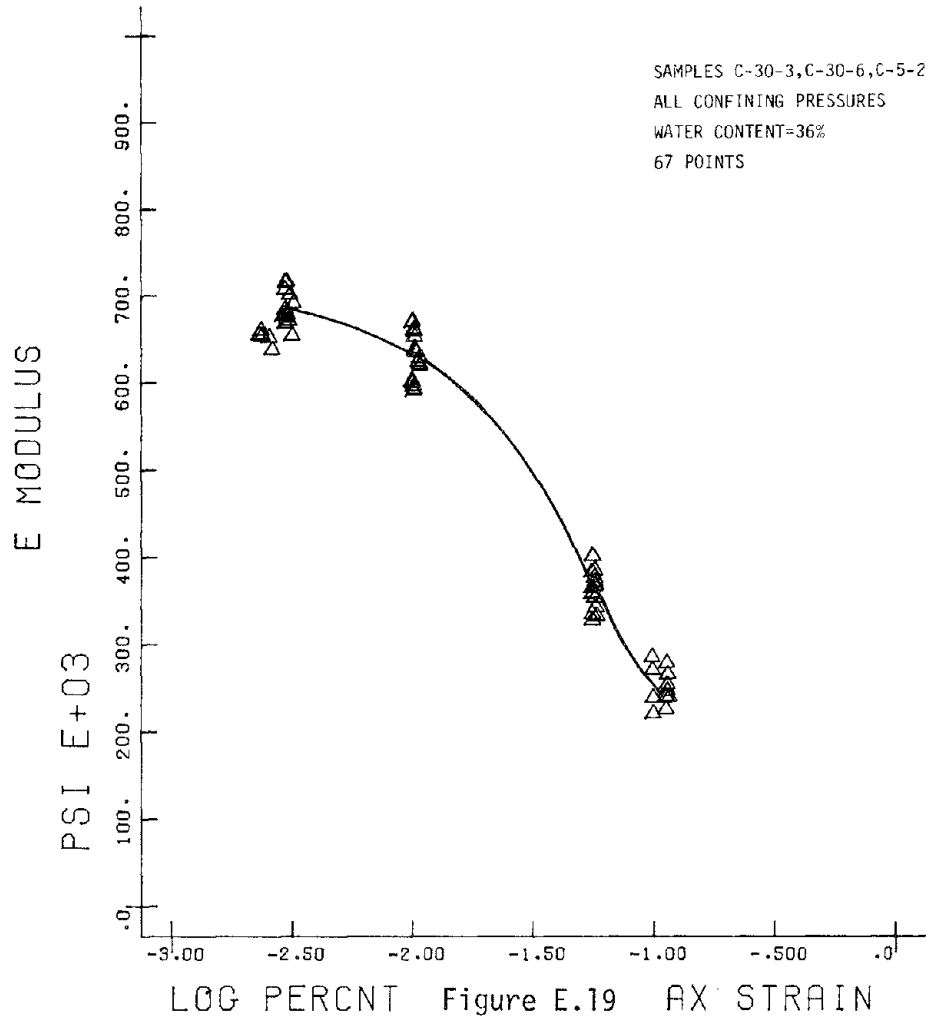


O-CLAYT-4F.3

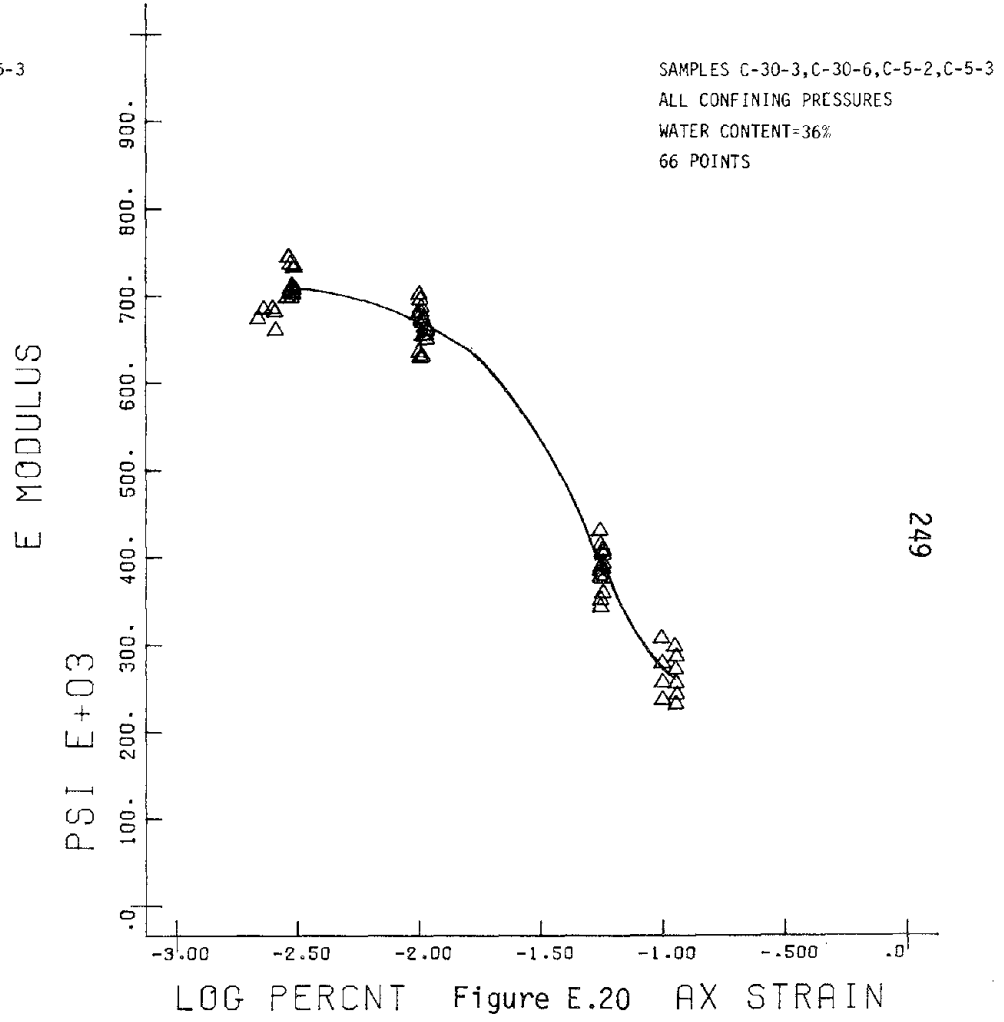


O-CLAYT-4F1

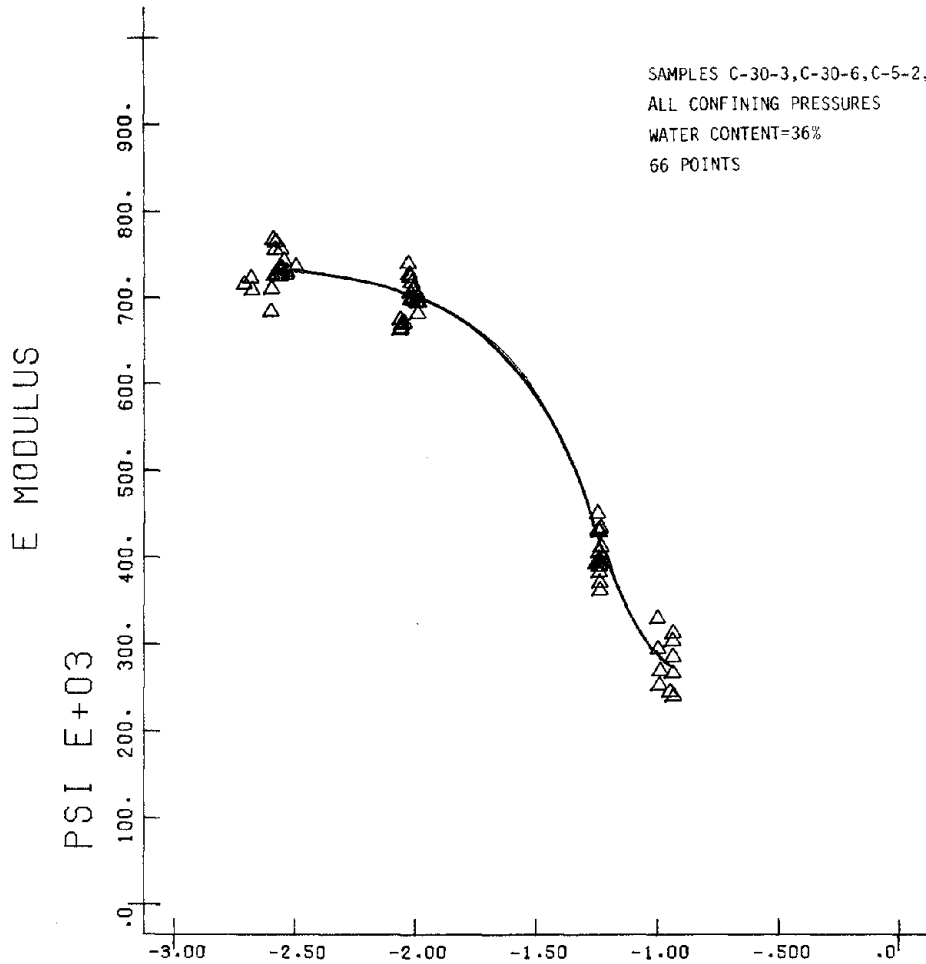




O-CLAYT-10F.3

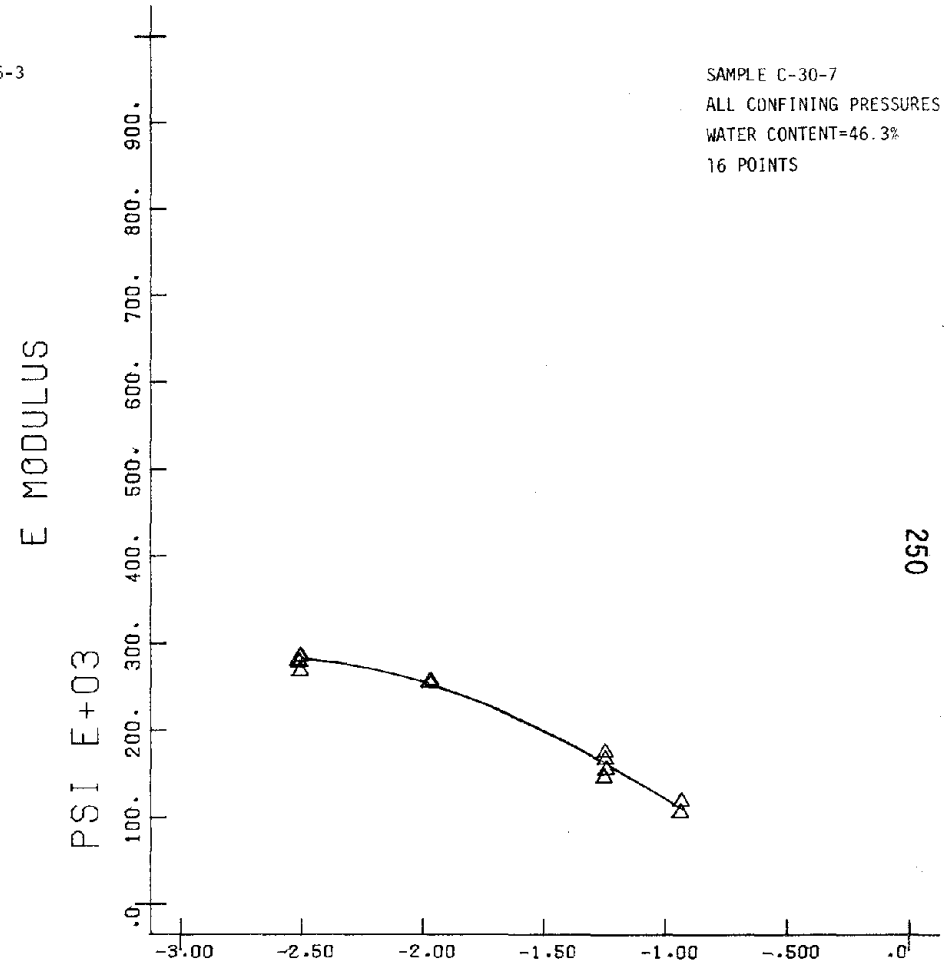


O-CLAYT-10F.1



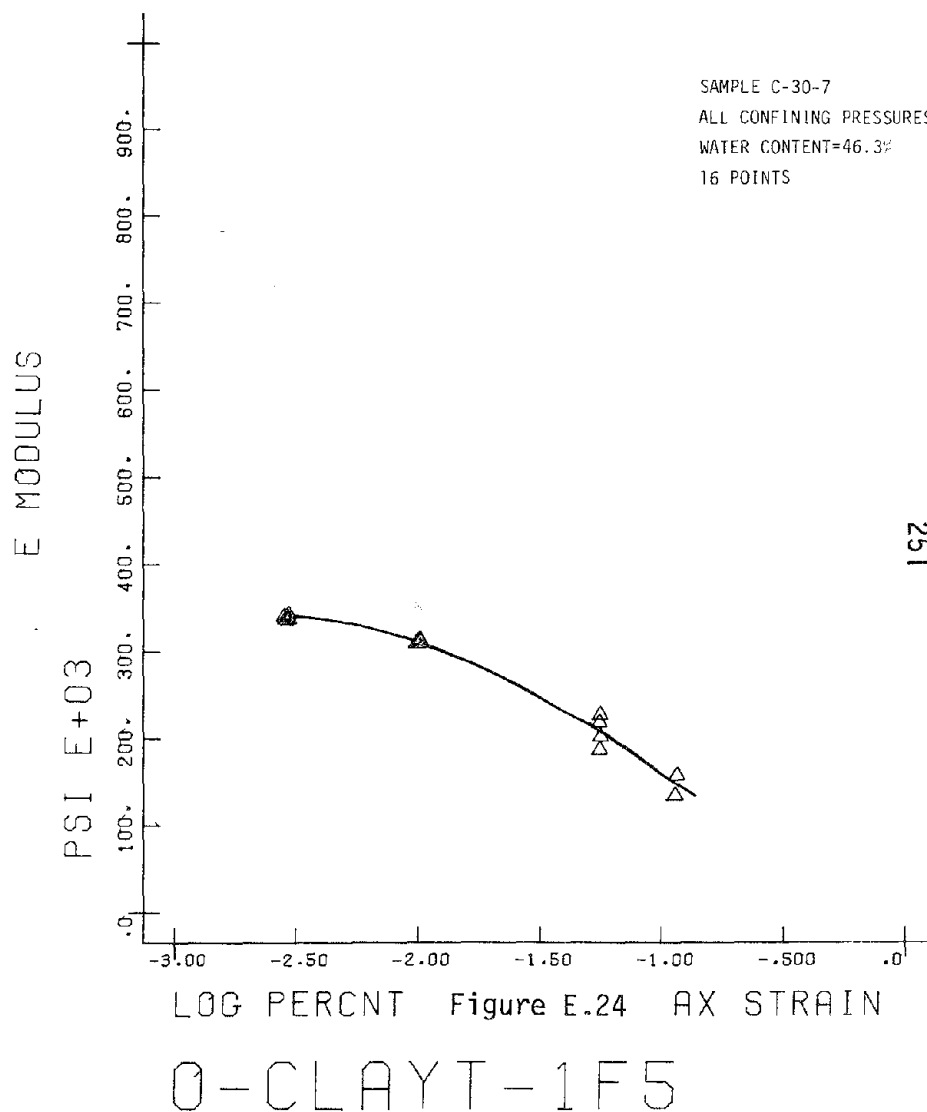
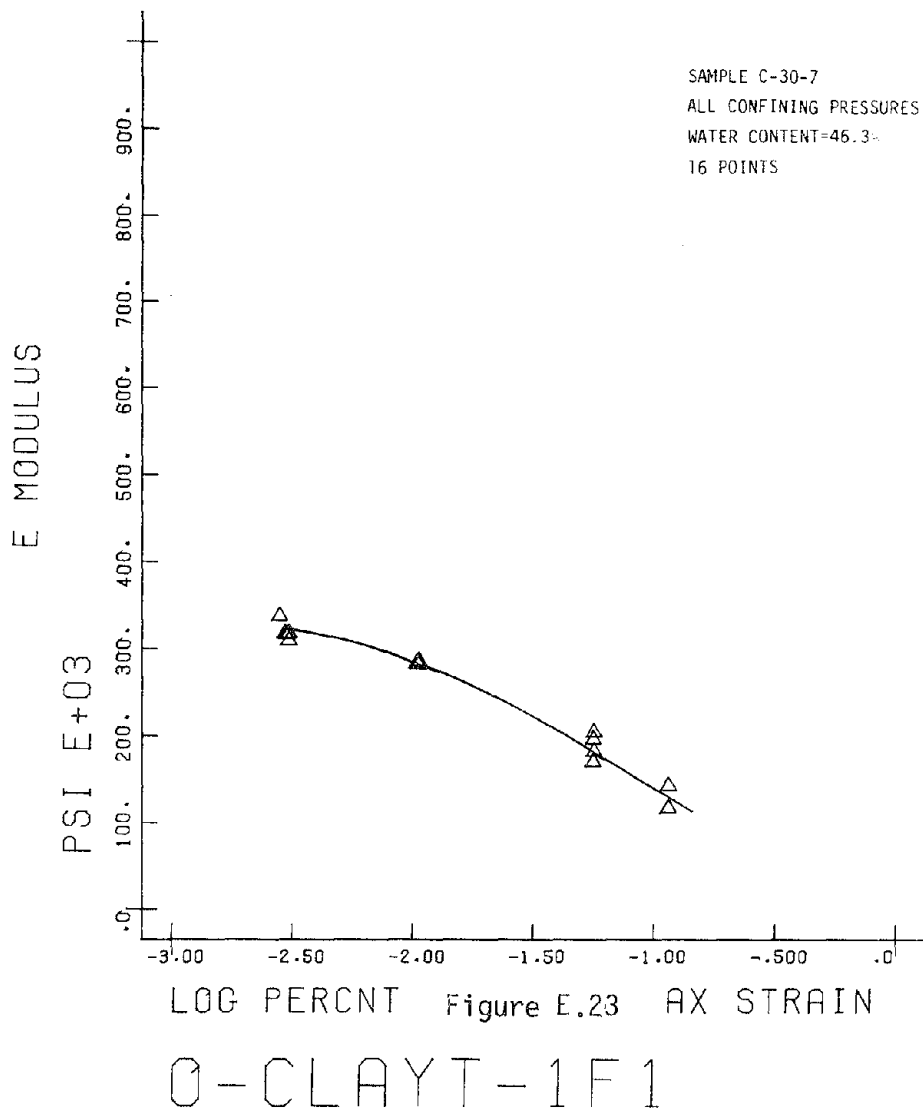
LOG PERCENT Figure E.21 AX STRAIN

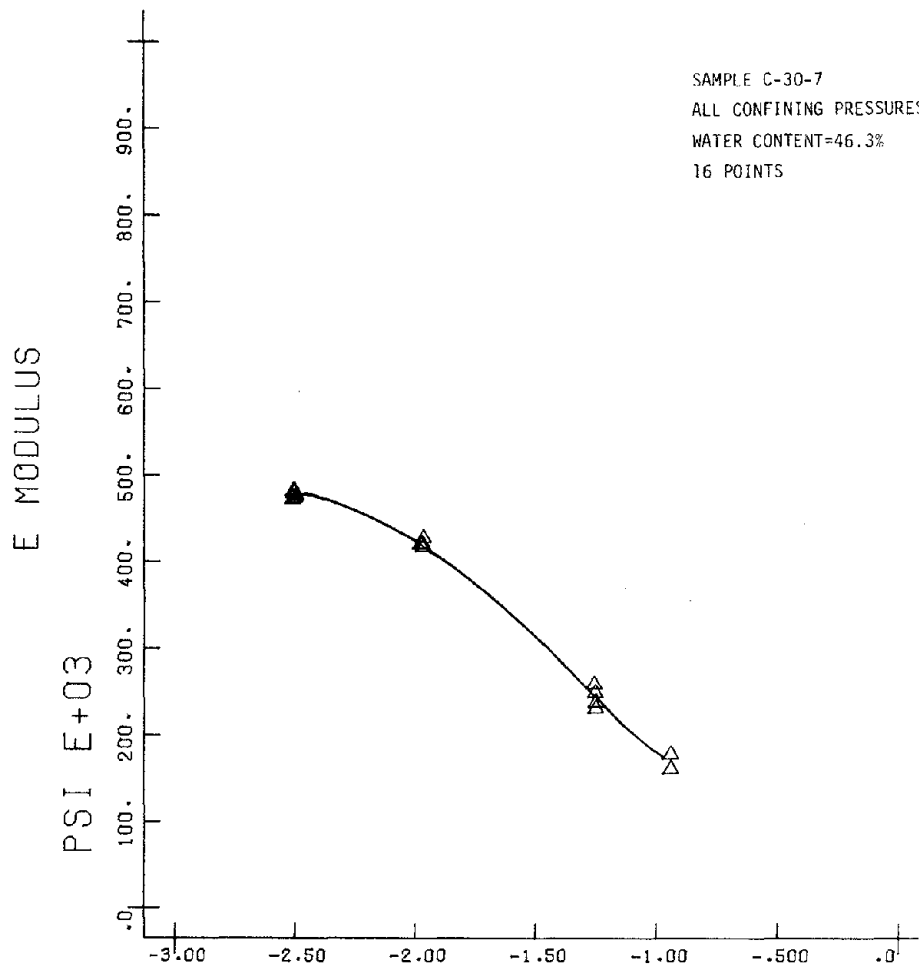
O-CLAYT-10F5



LOG PERCENT Figure E.22 AX STRAIN

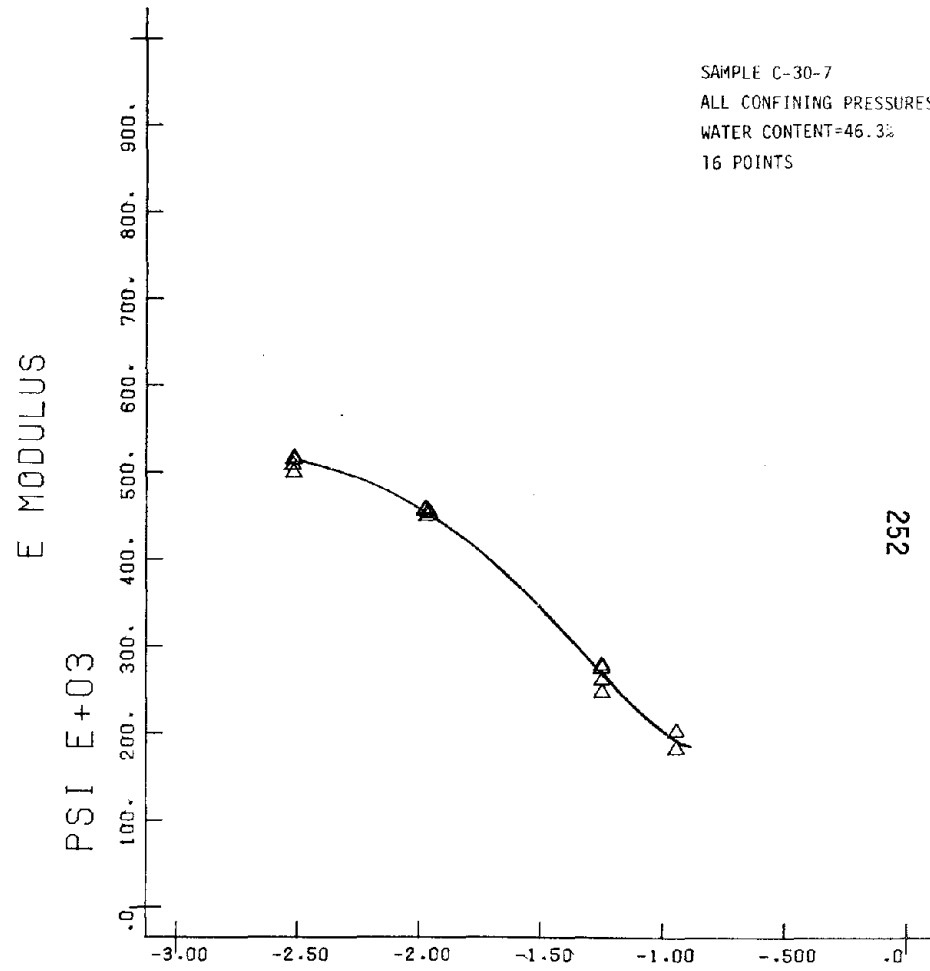
O-CLAYT-1F.3





LOG PERCENT Figure E.25 AX STRAIN

0-CLAYT-4F.3



LOG PERCENT Figure E.26 AX STRAIN

0-CLAYT-4F1

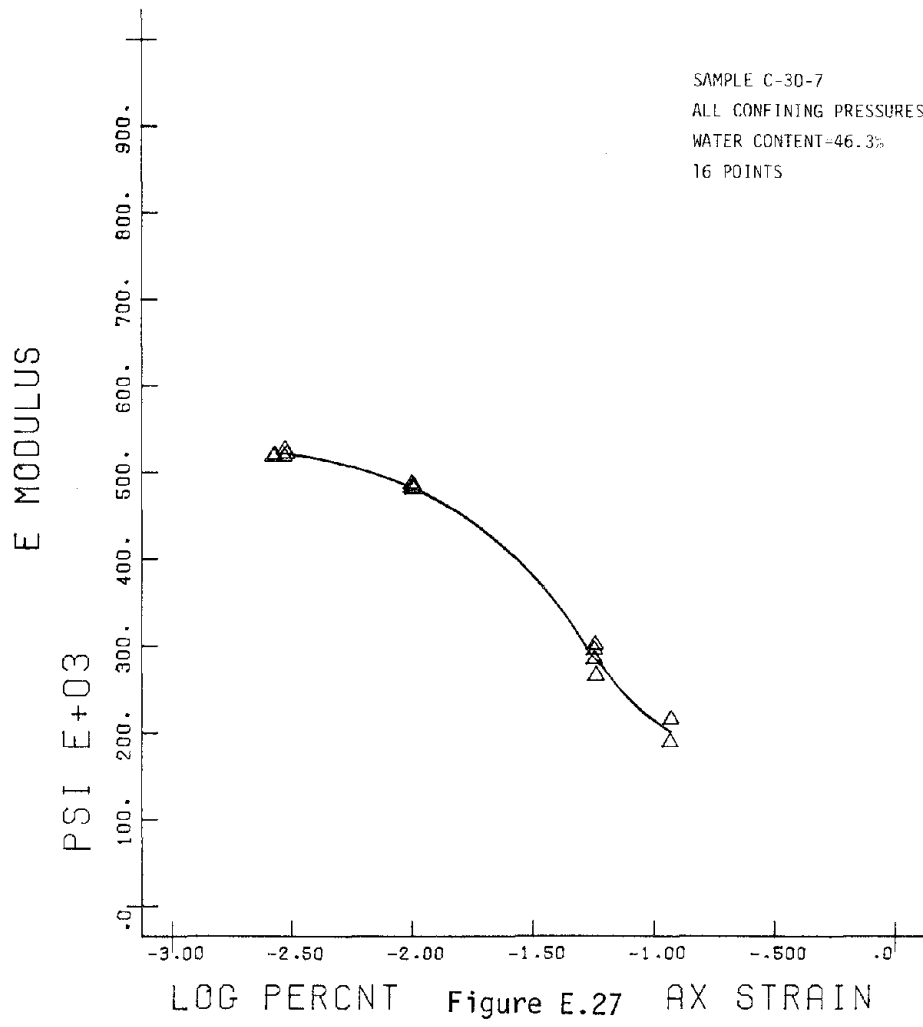


Figure E.27

0-CLAYT-4F5

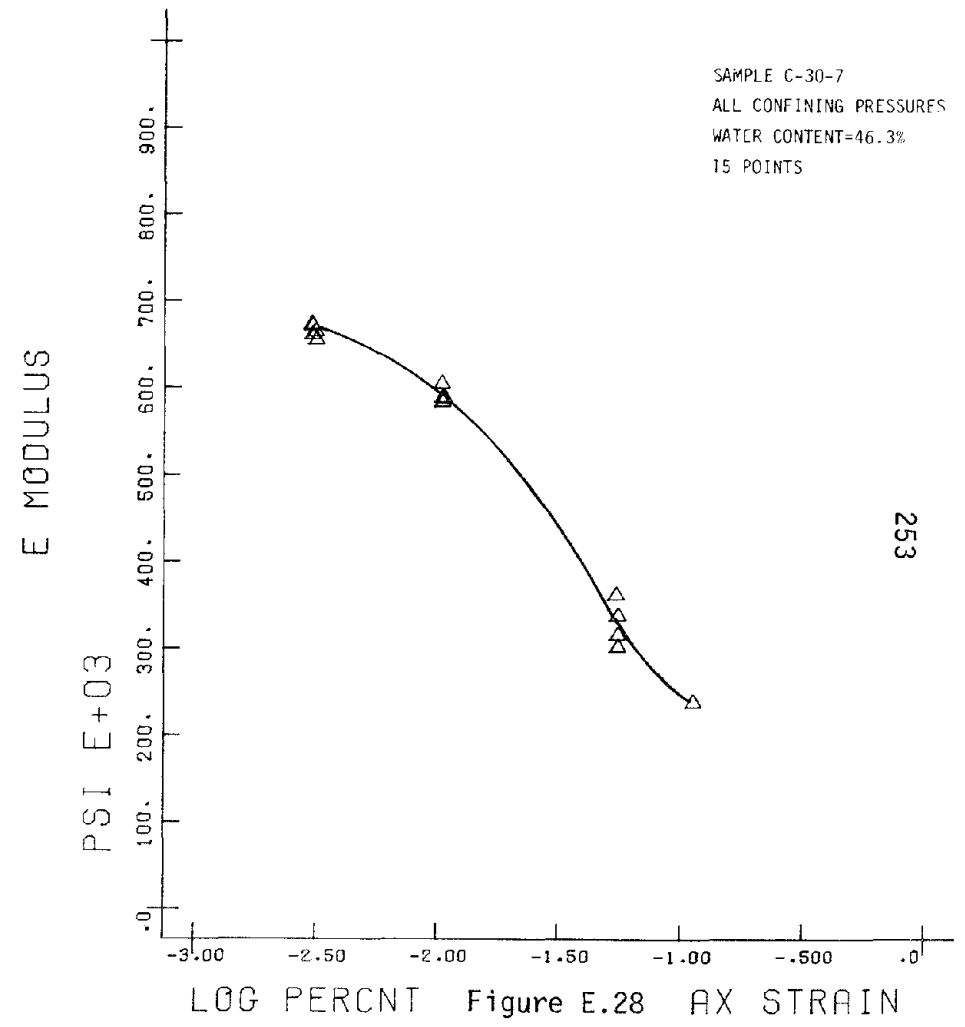
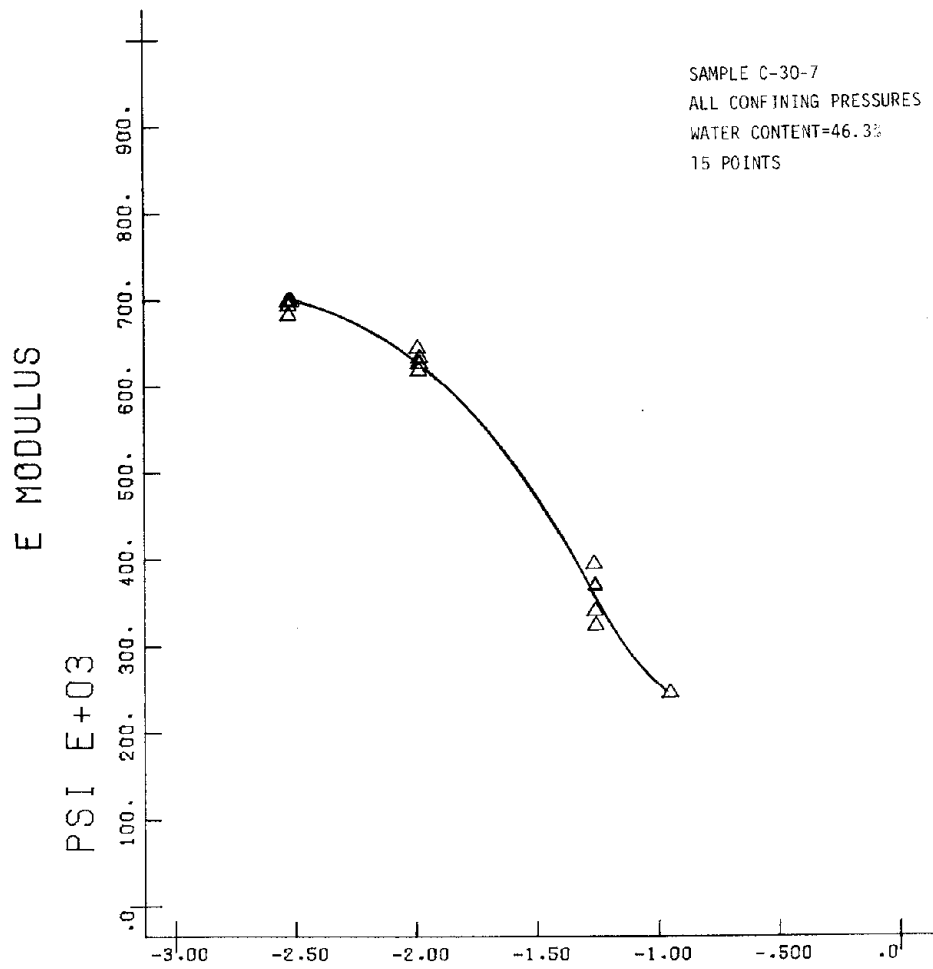


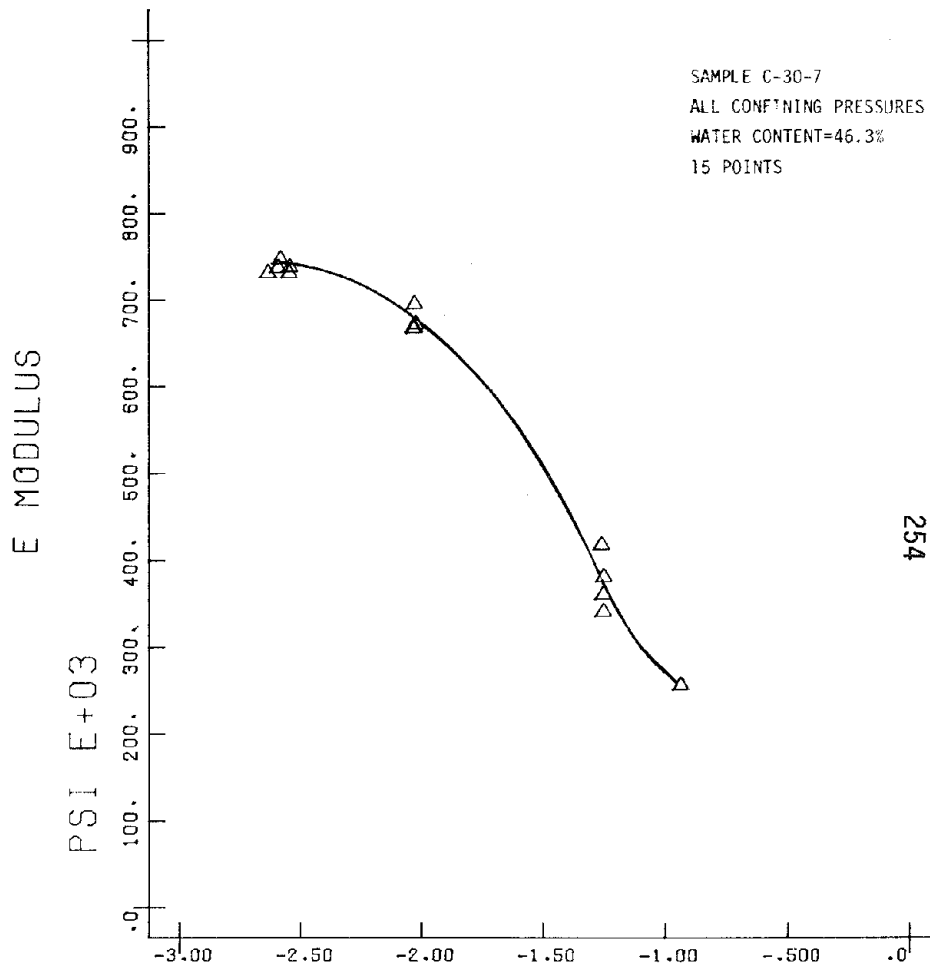
Figure E.28

0-CLAYT-10F.3



LOG PERCENT Figure E.29 AX STRAIN

0-CLAYT-10F1



LOG PERCENT Figure E.30 AX STRAIN

0-CLAYT-10F5

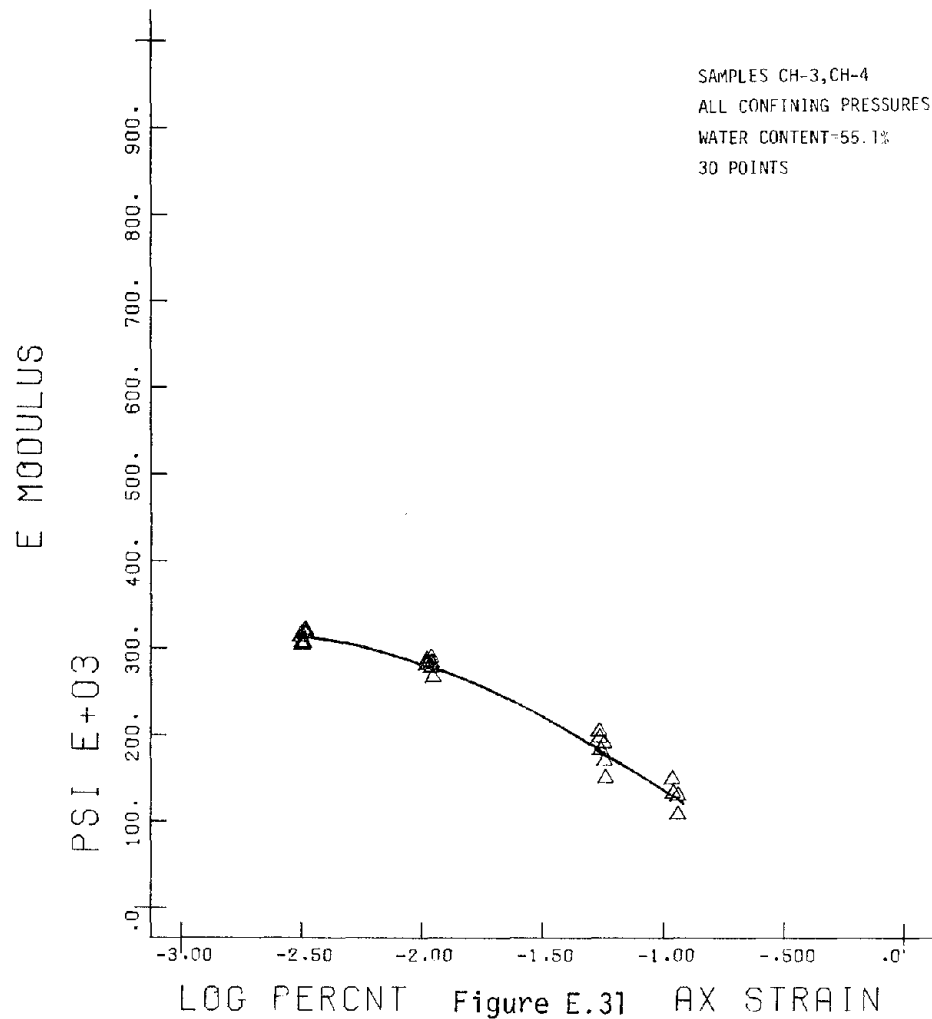


Figure E.31

O-CLAYT-1F.3

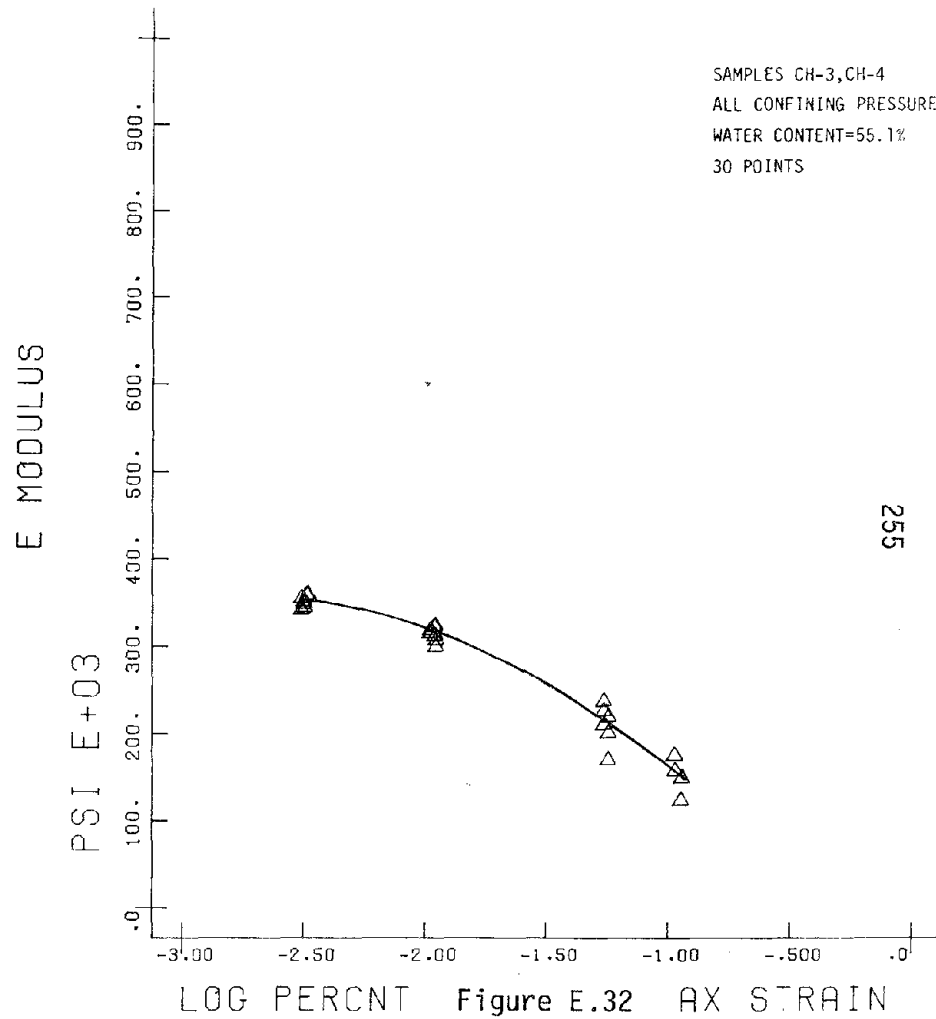
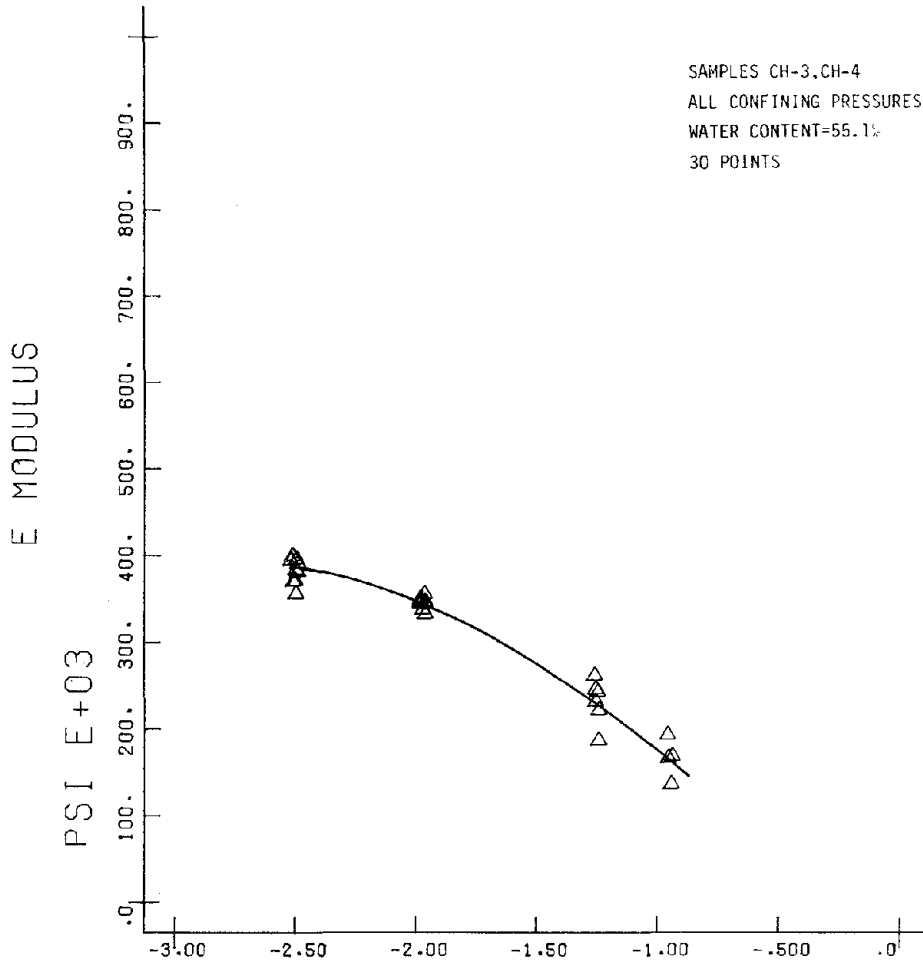


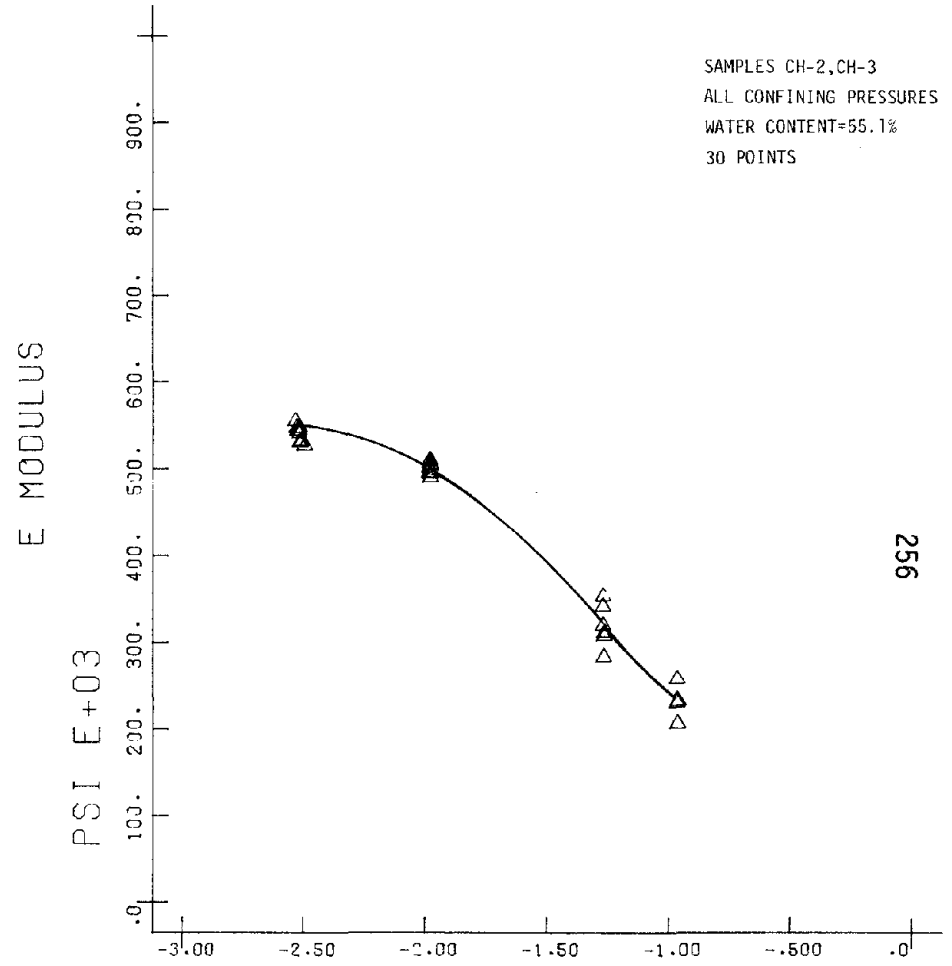
Figure E.32

O-CLAYT-1F1



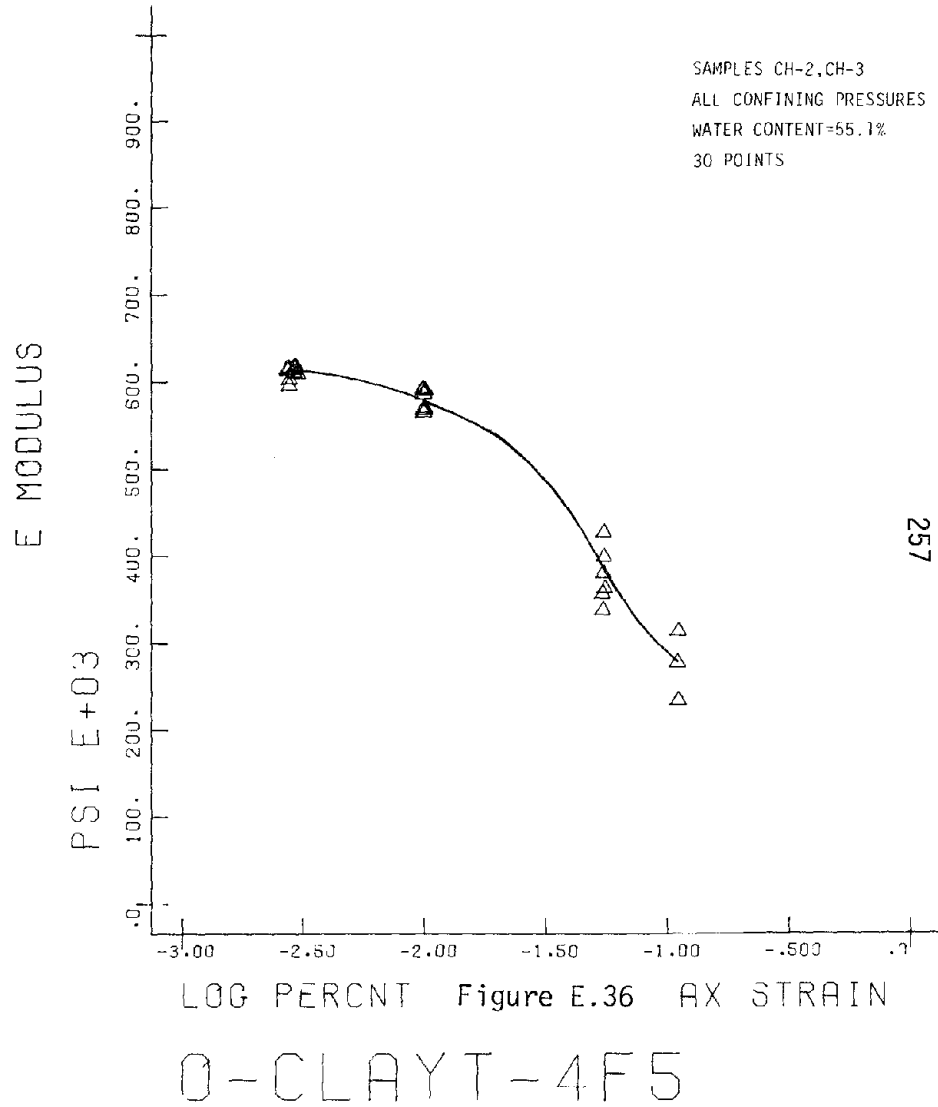
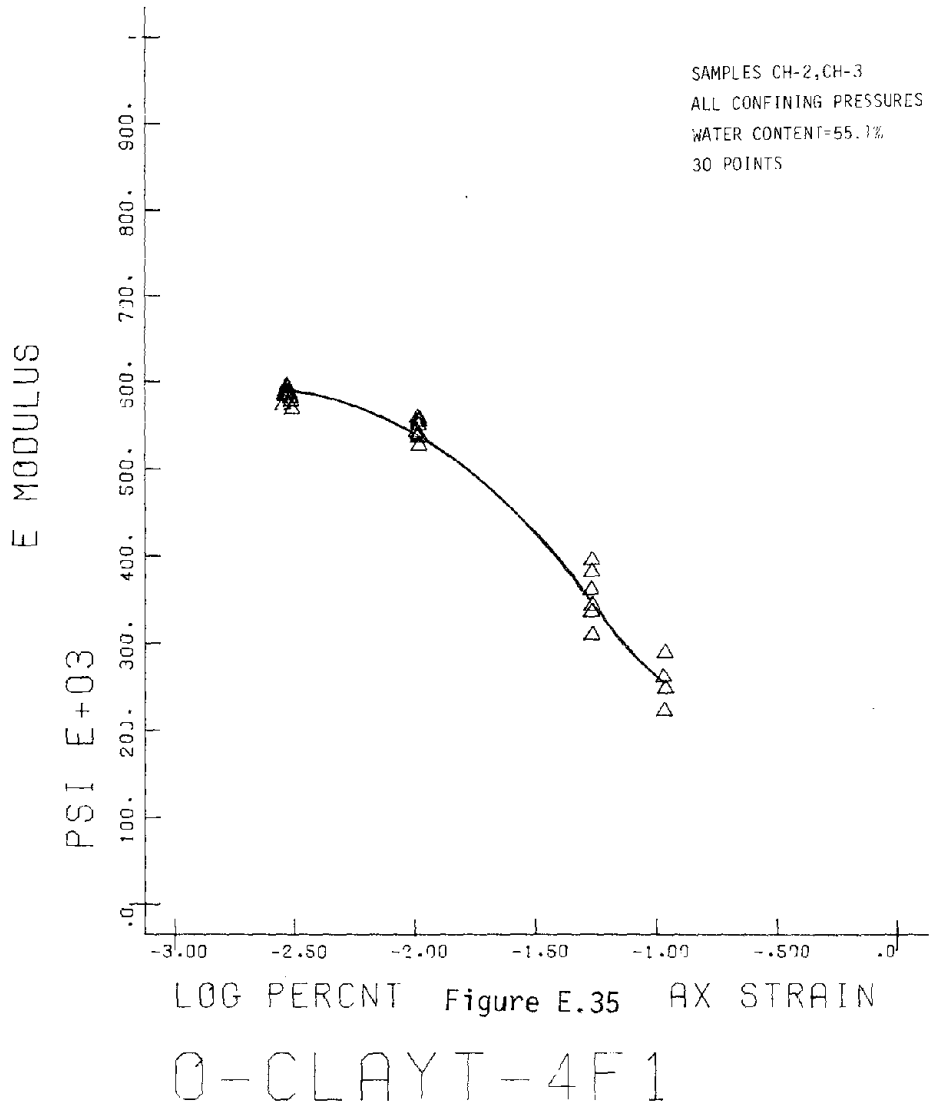
LOG PERCNT AX STRAIN Figure E.33

O-CLAYT-1F5



LOG PERCNT AX STRAIN Figure E.34

O-CLAYT-4F.3



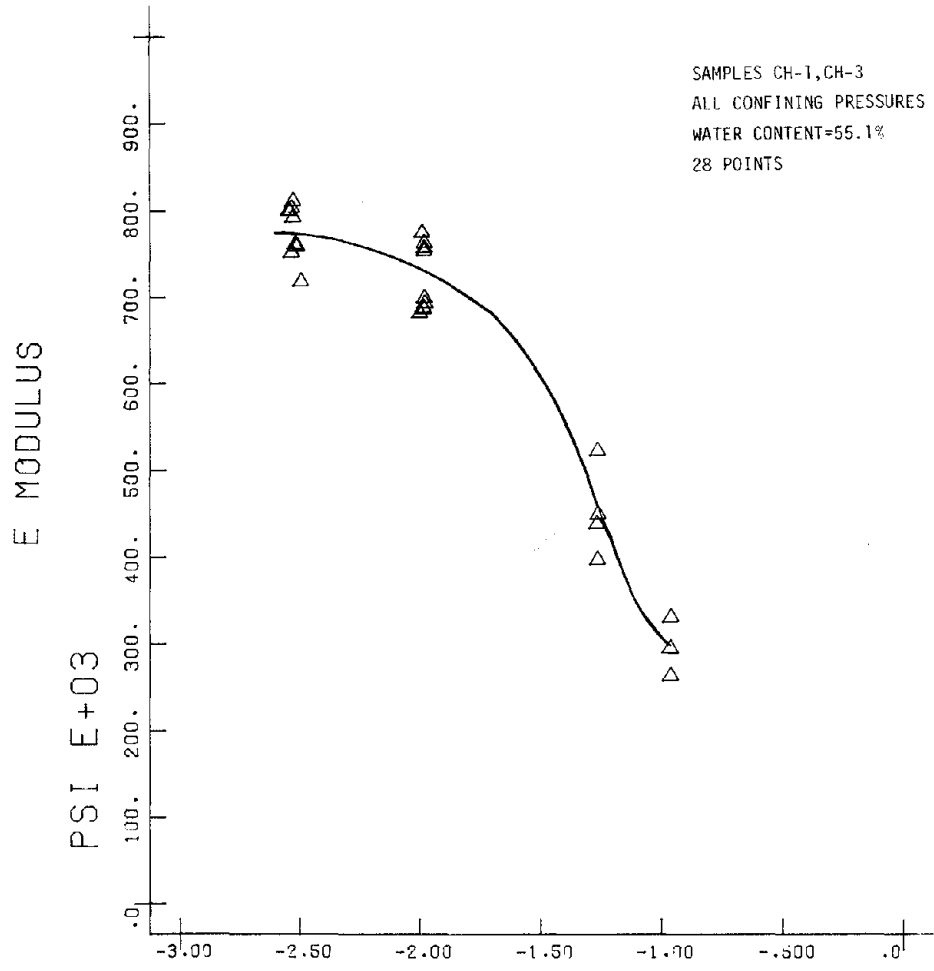


Figure E.37
O-CLAYT-10F.3

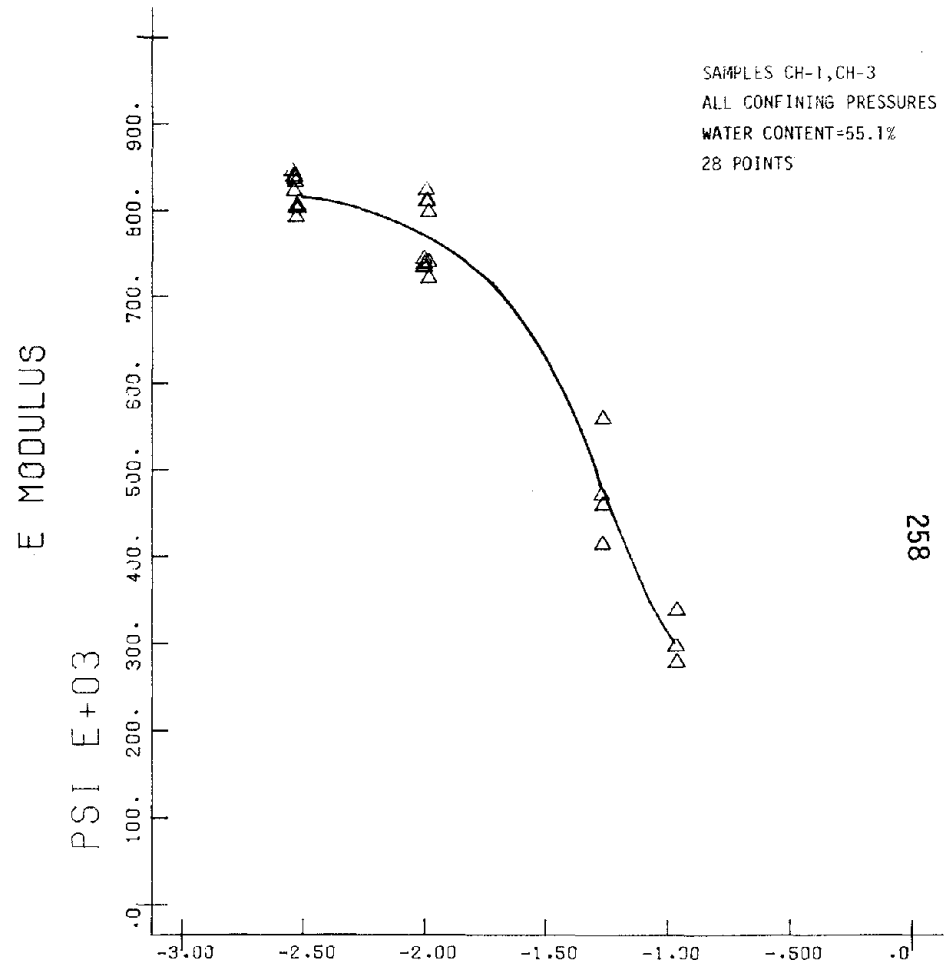
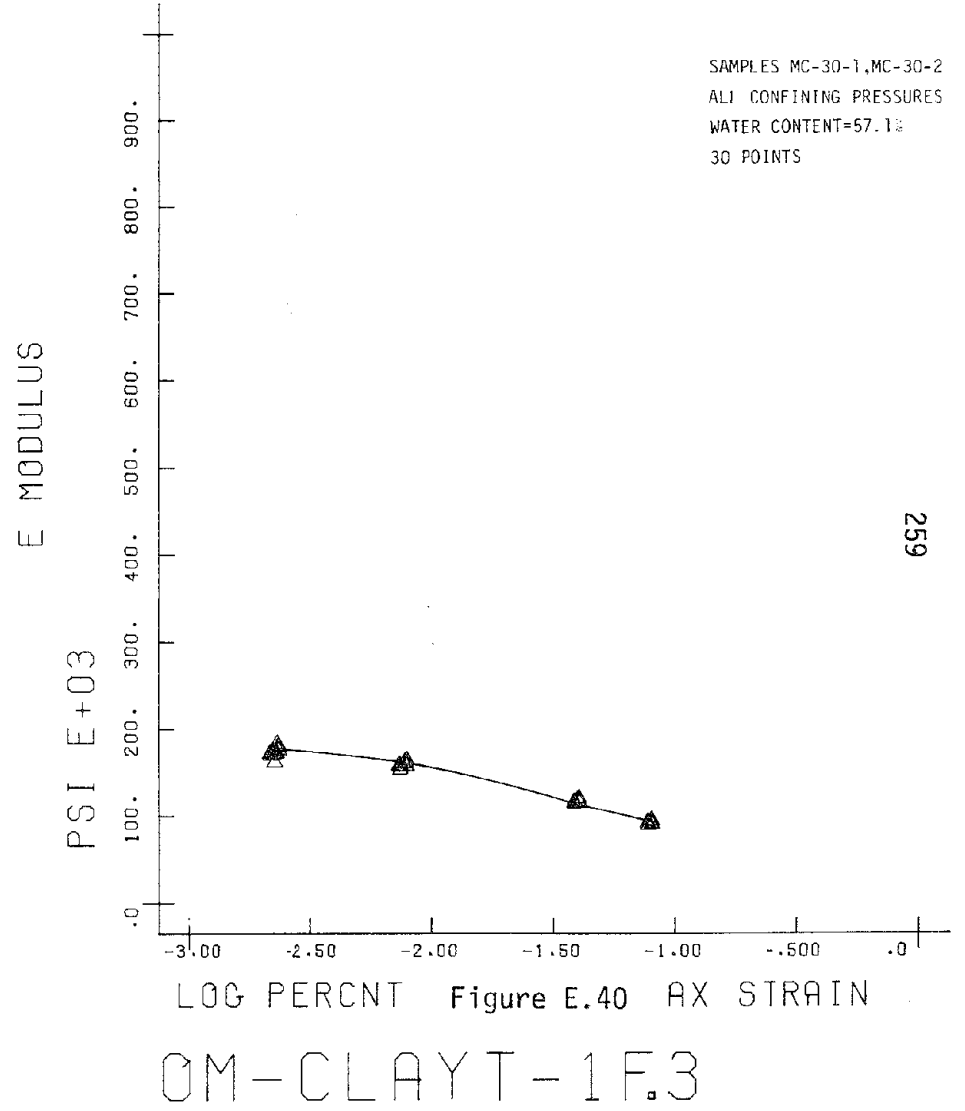
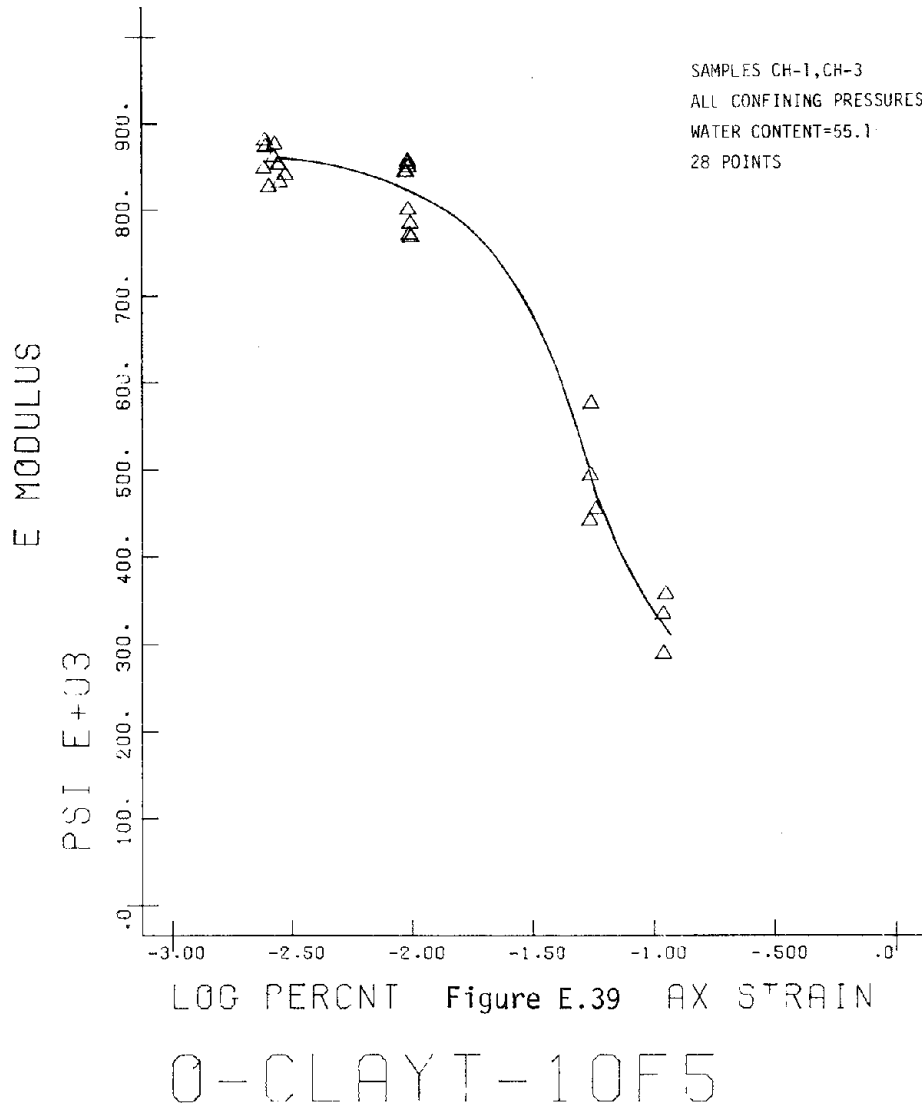
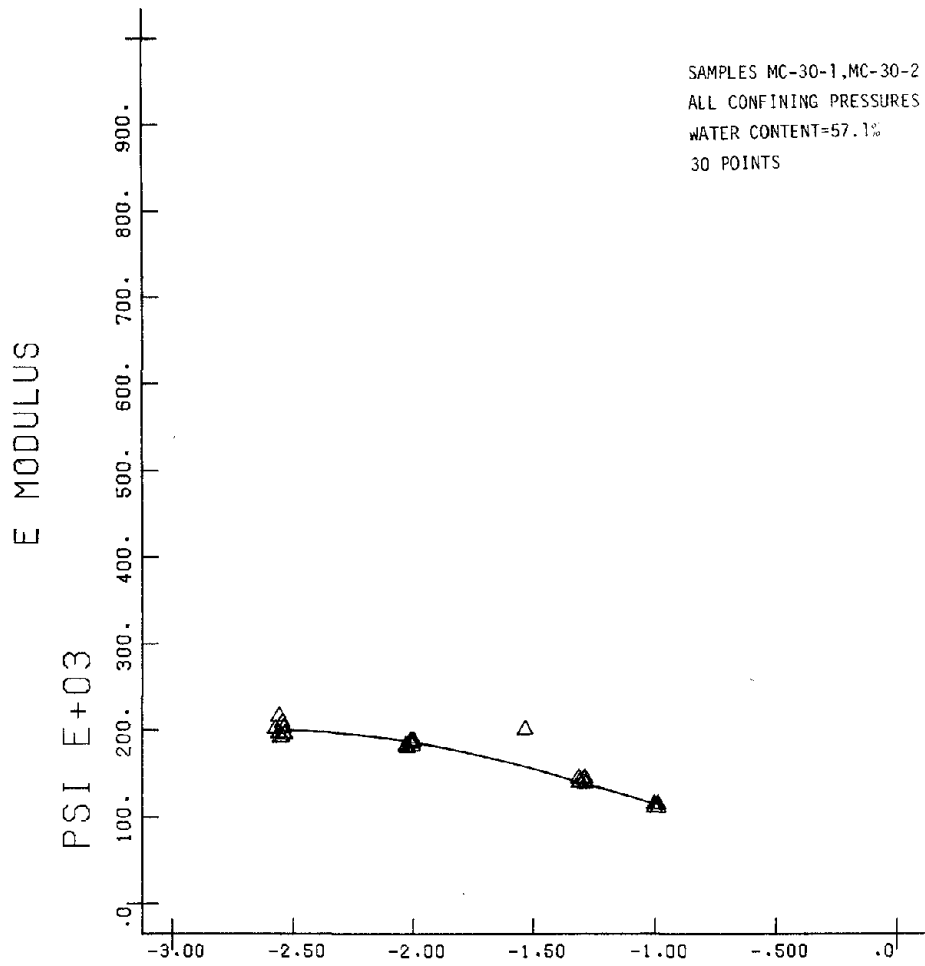


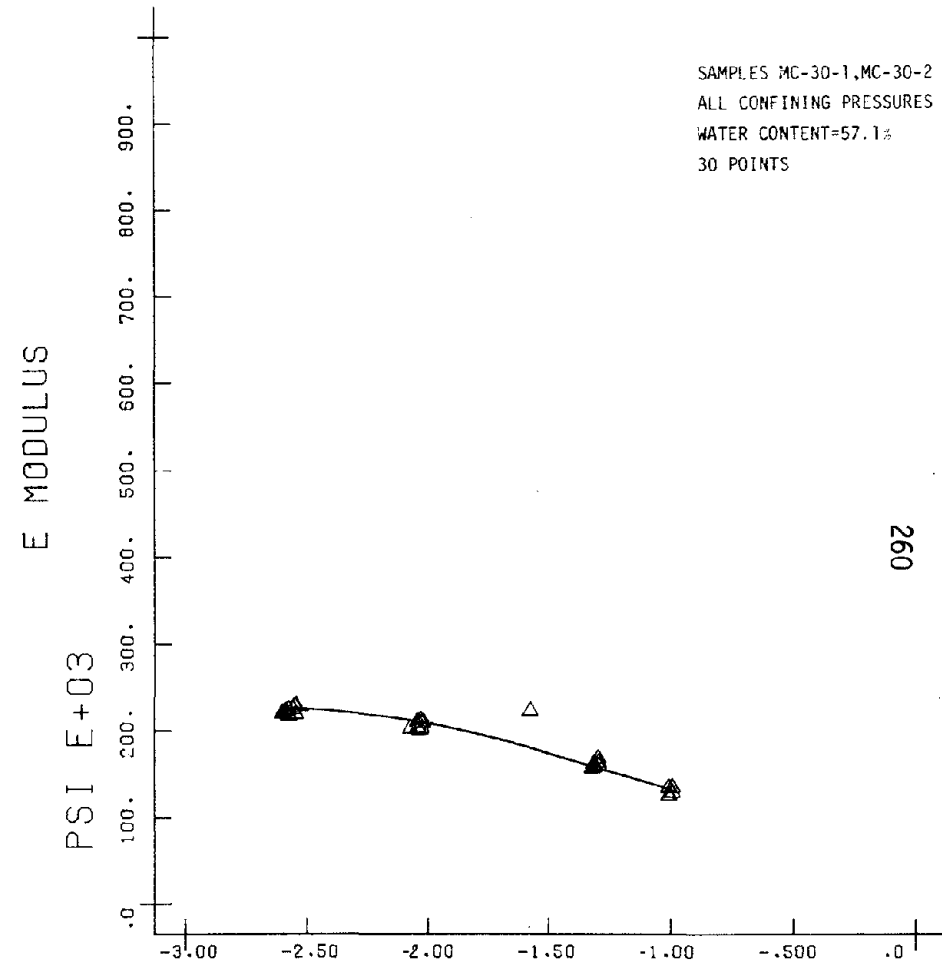
Figure E.38
O-CLAYT-10F1





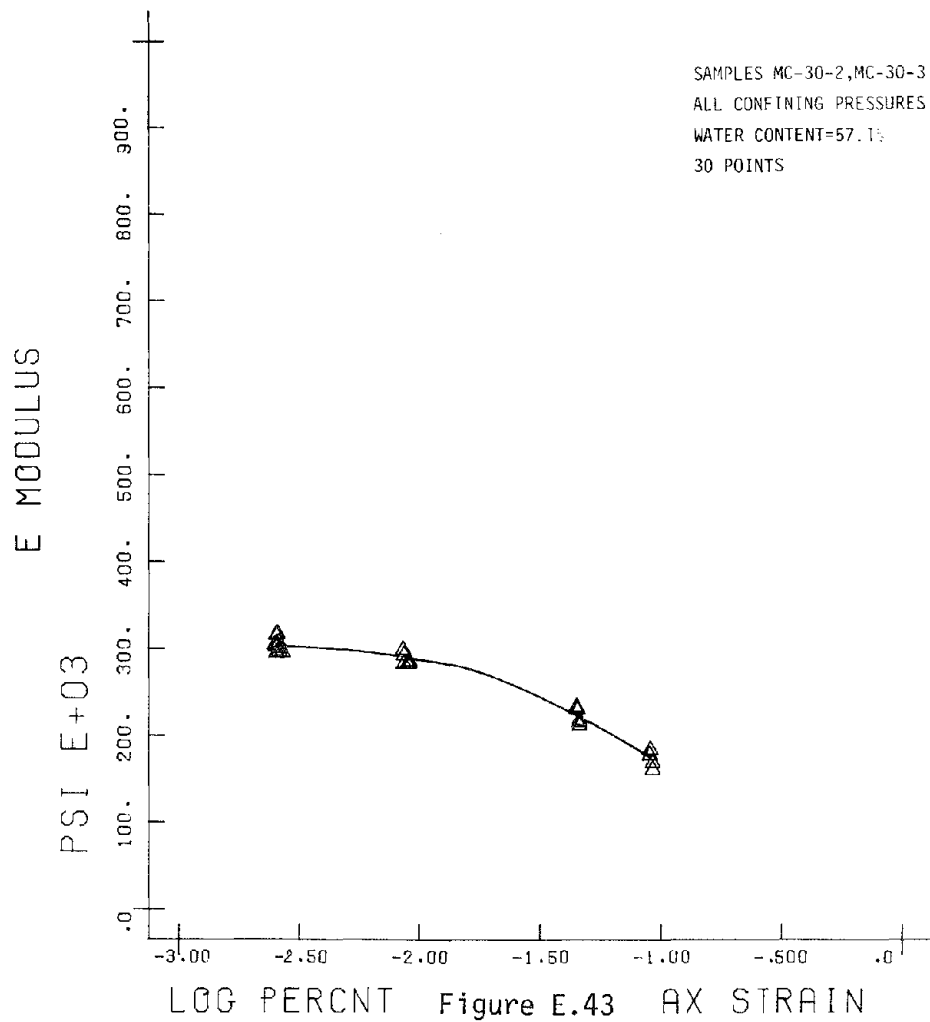
LOG PERCENT Figure E.41 AX STRAIN

OM-CLAYT-1F1

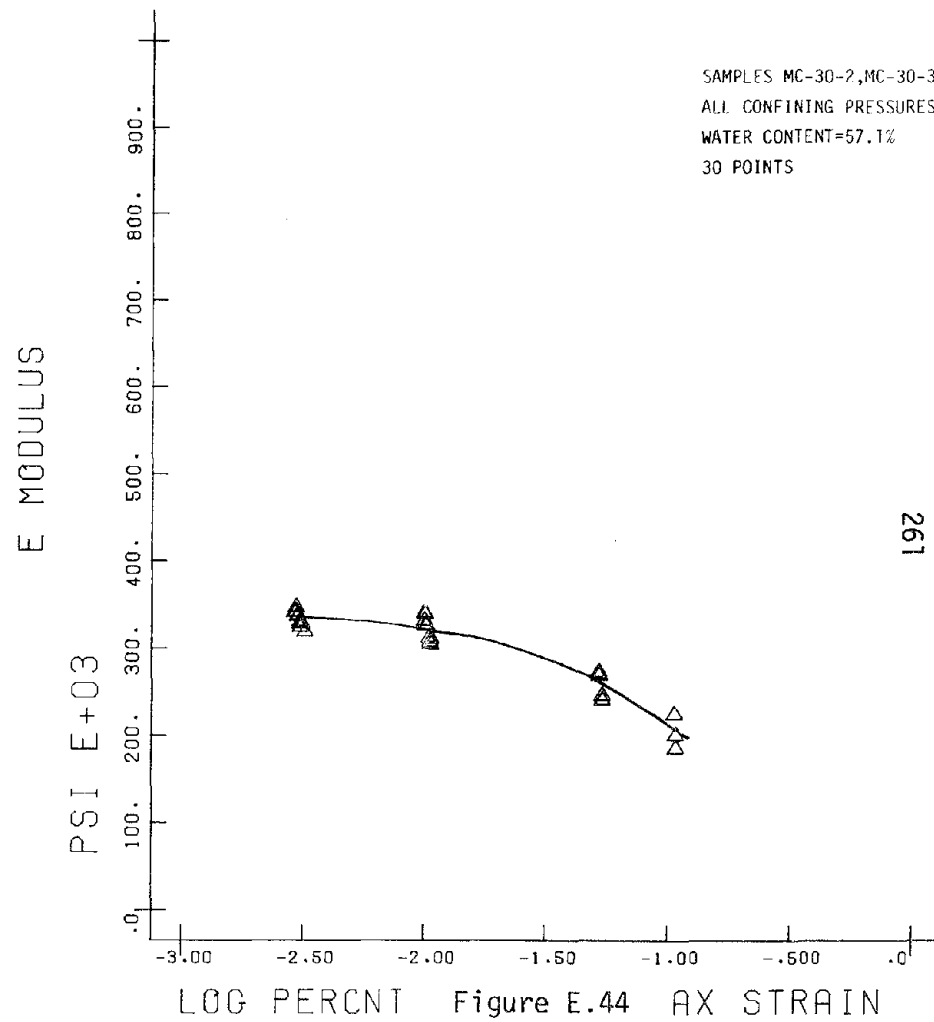


LOG PERCENT Figure E.42 AX STRAIN

OM-CLAYT-1F5



OM-CLAYT-4F.3



OM-CLAYT-4F.1

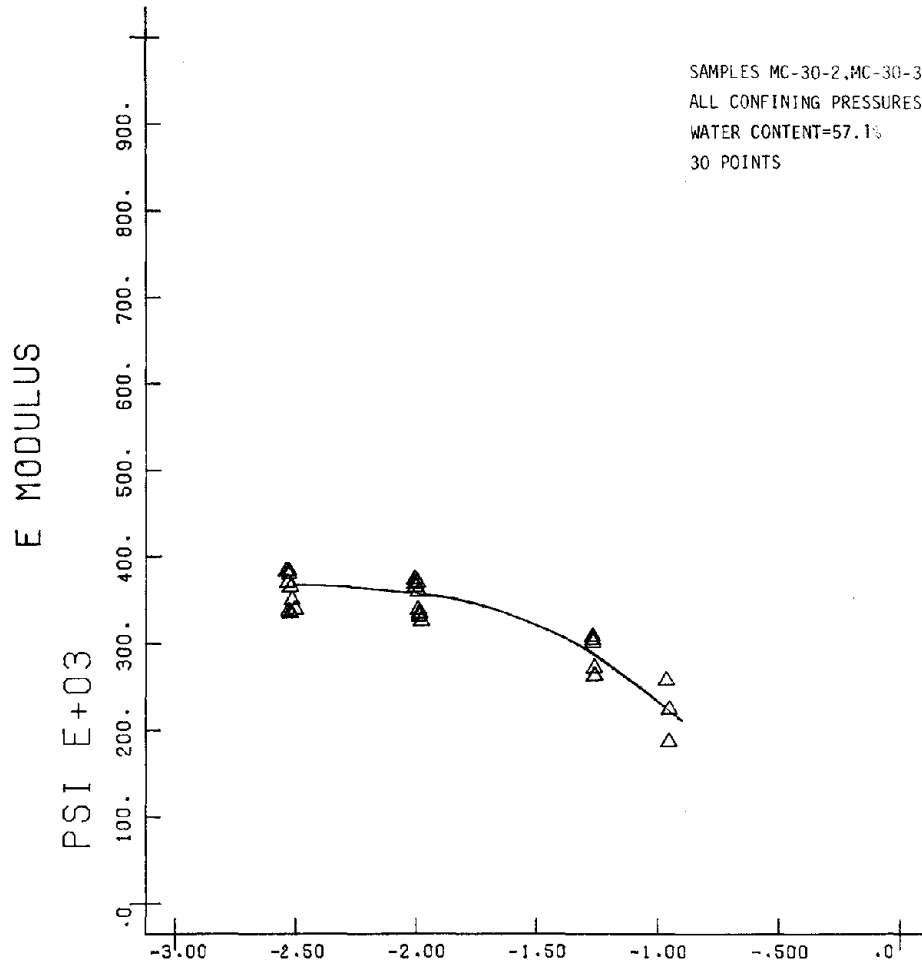


Figure E.45 AX STRAIN

OM-CLAYT-4F5

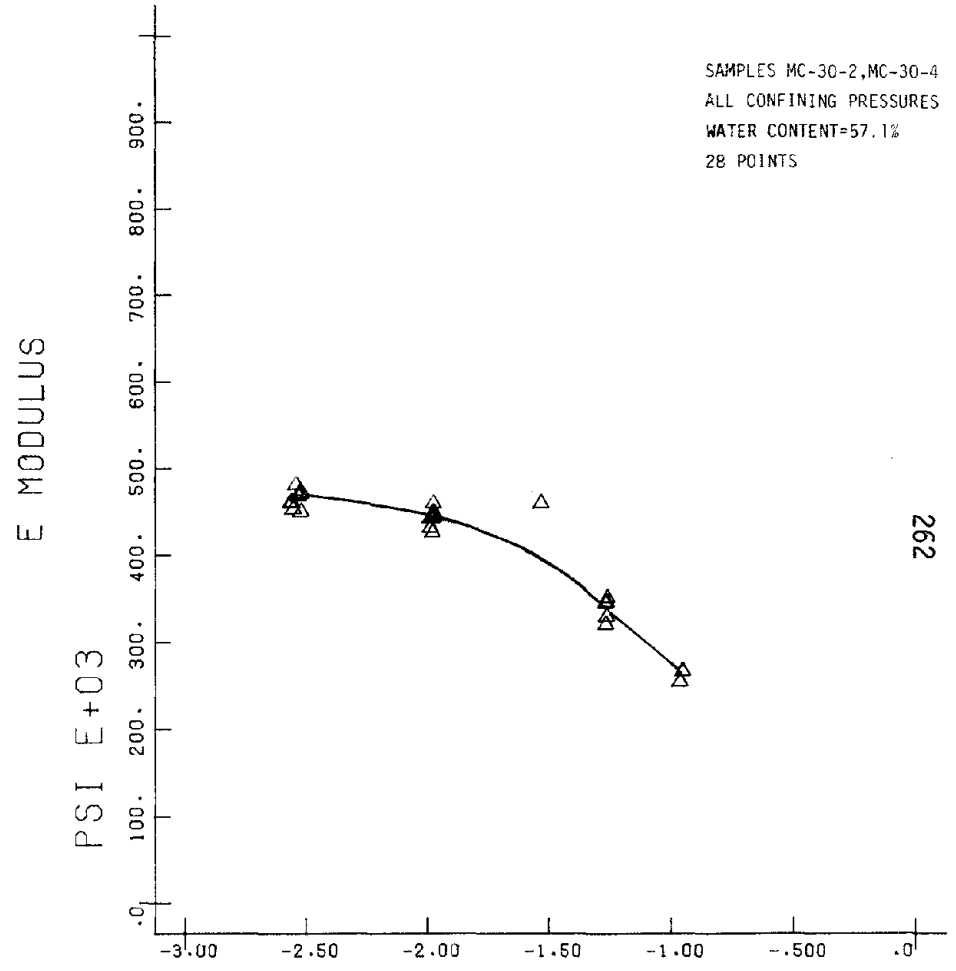
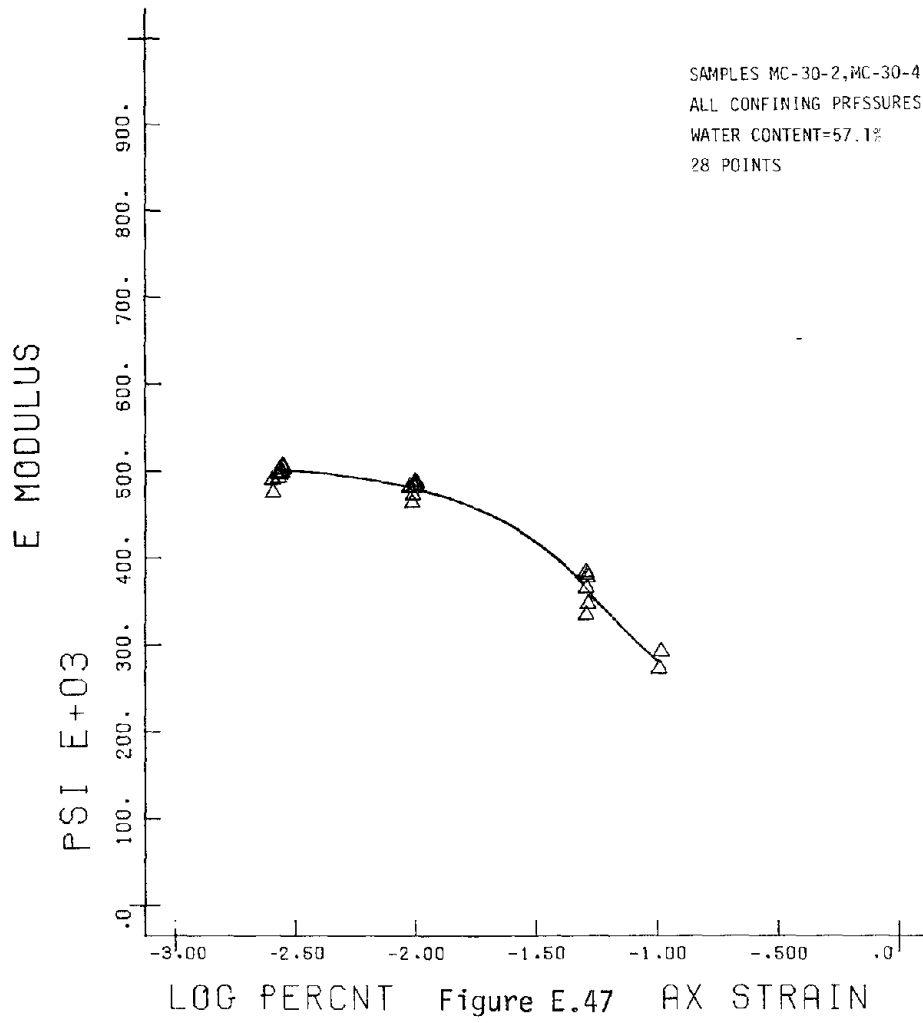
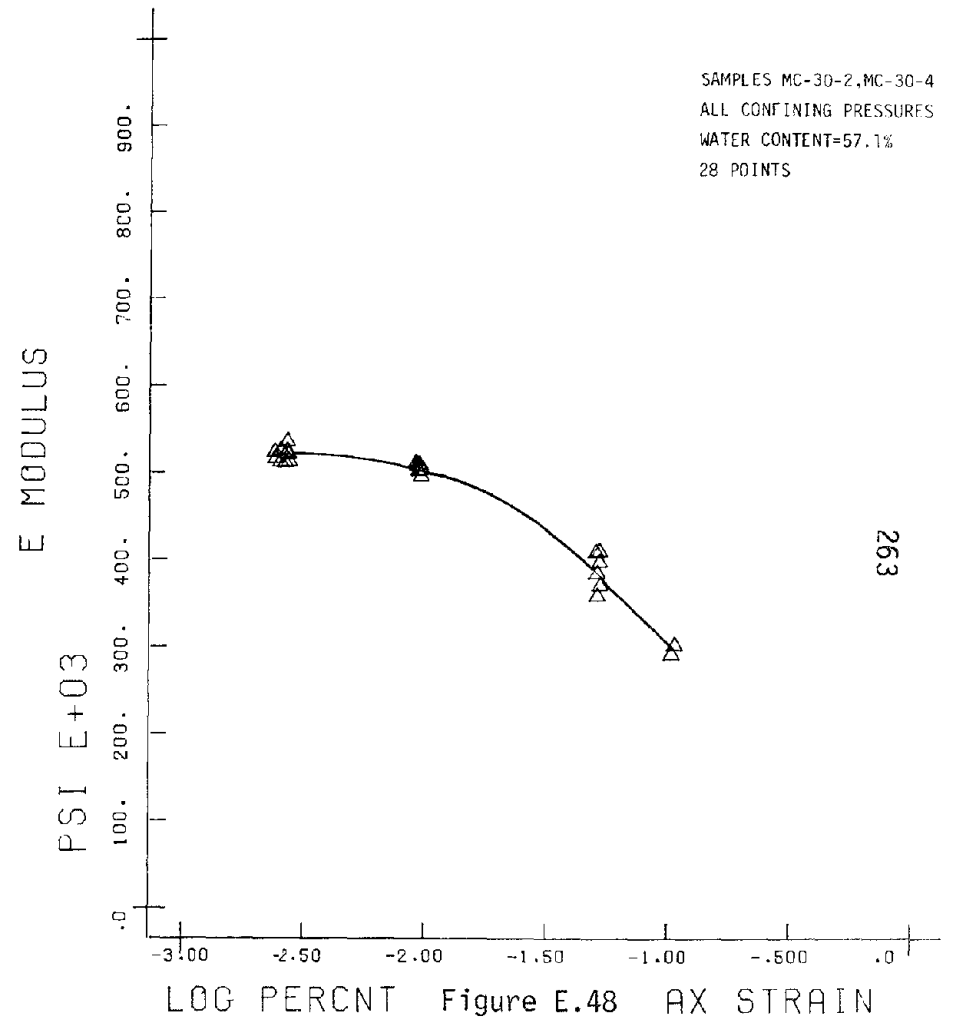


Figure E.46 AX STRAIN

OM-CLAYT-10F.3

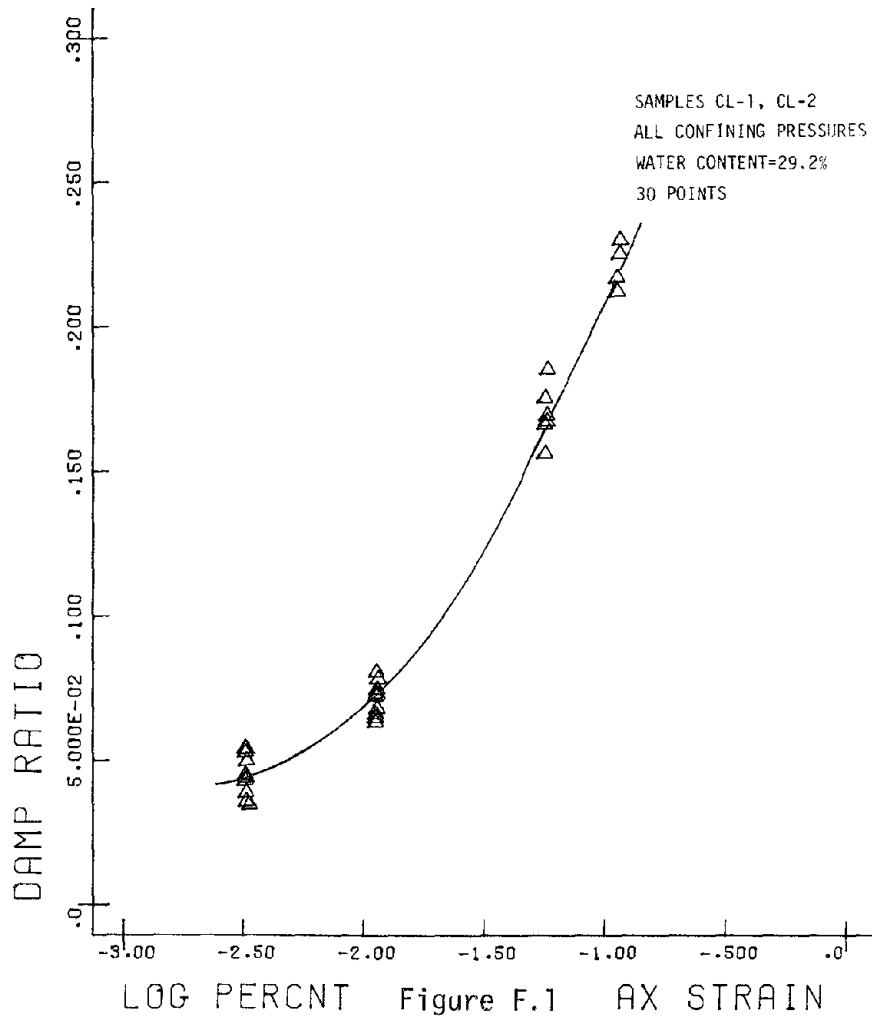


OM-CLAYT-10F1

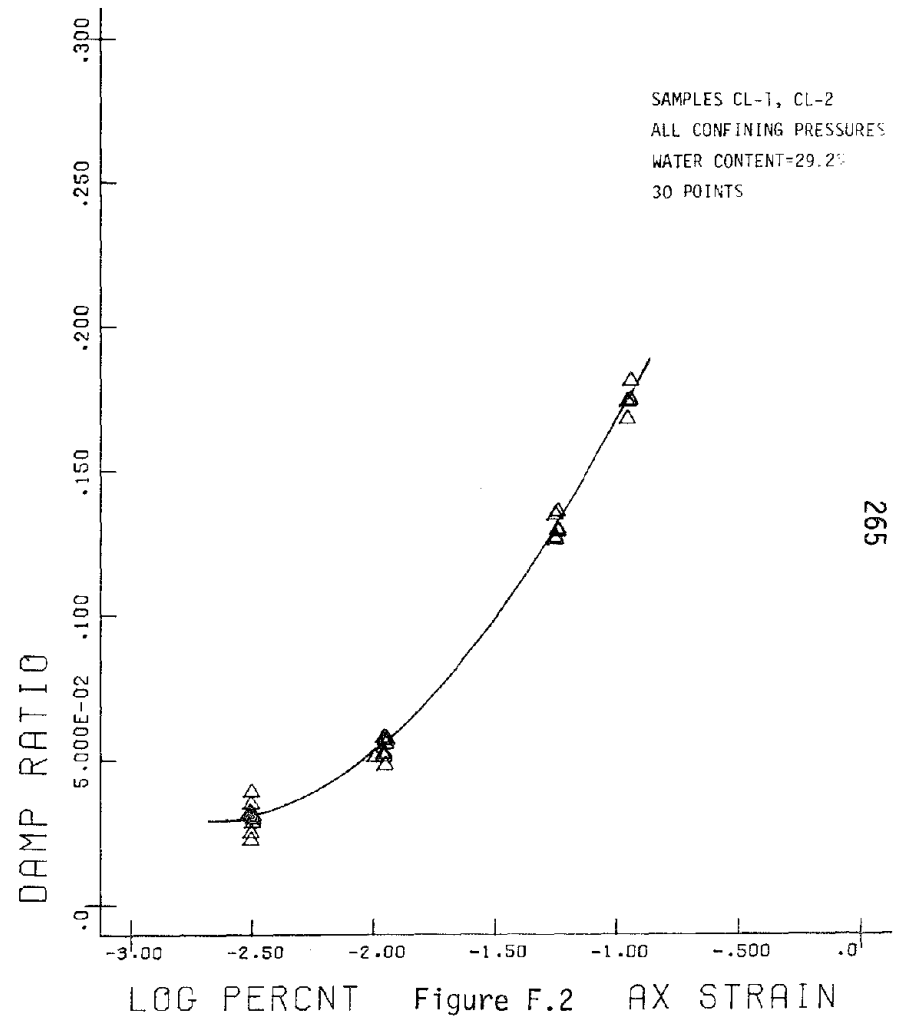


OM-CLAYT-10F5

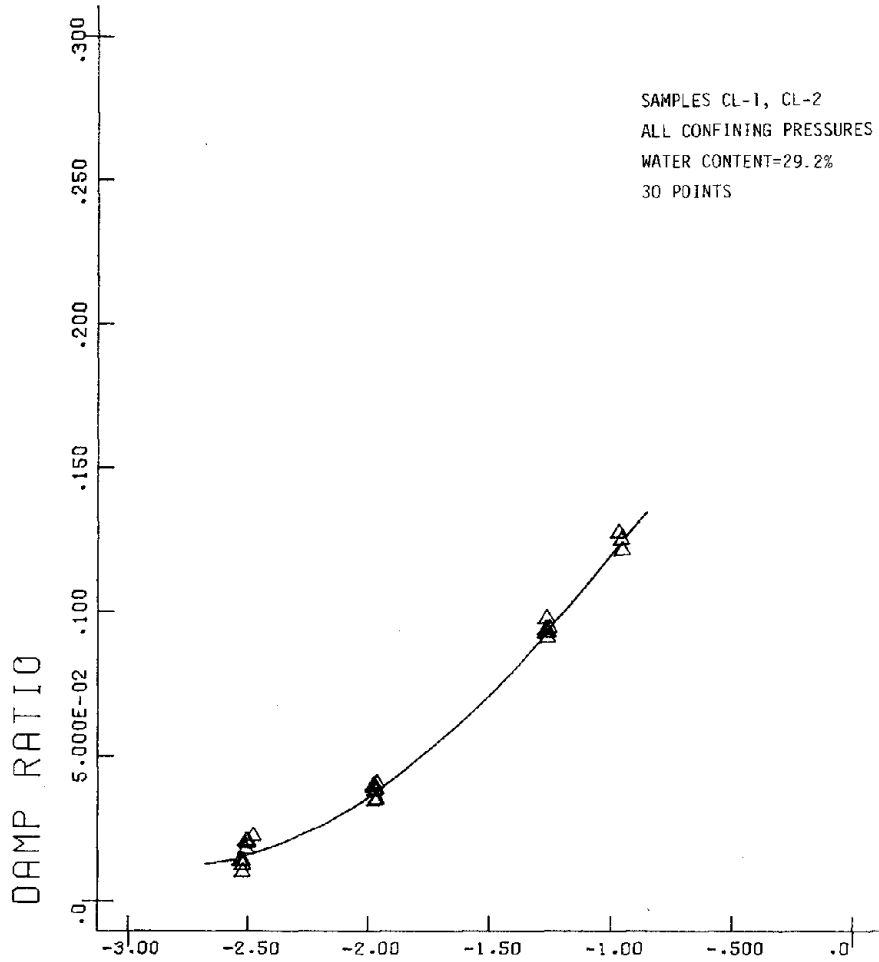
APPENDIX F
CYCLIC TRIAXIAL TEST RESULTS: DAMPING
RATIO OF FROZEN CLAY



0-CLAYT-1F.3

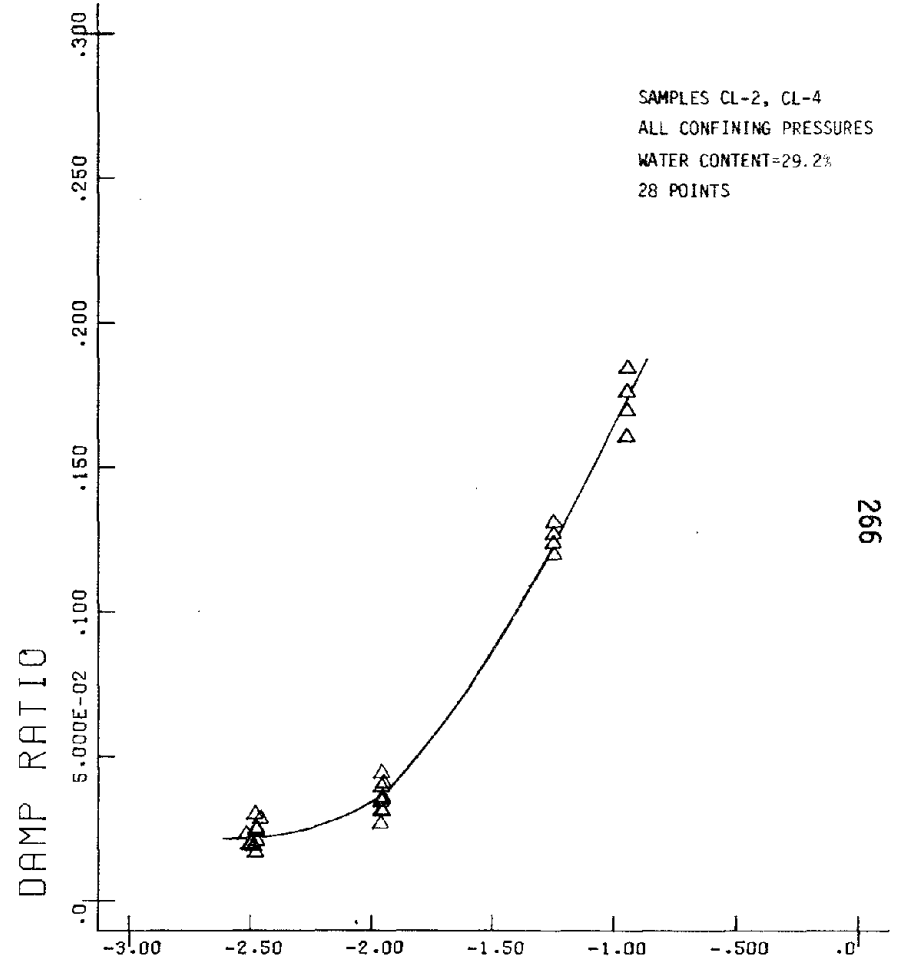


0-CLAYT-1F1



LOG PERCENT Figure F.3 AX STRAIN

O-CLAYT-1F5



LOG PERCENT Figure F.4 AX STRAIN

O-CLAYT-4F.3

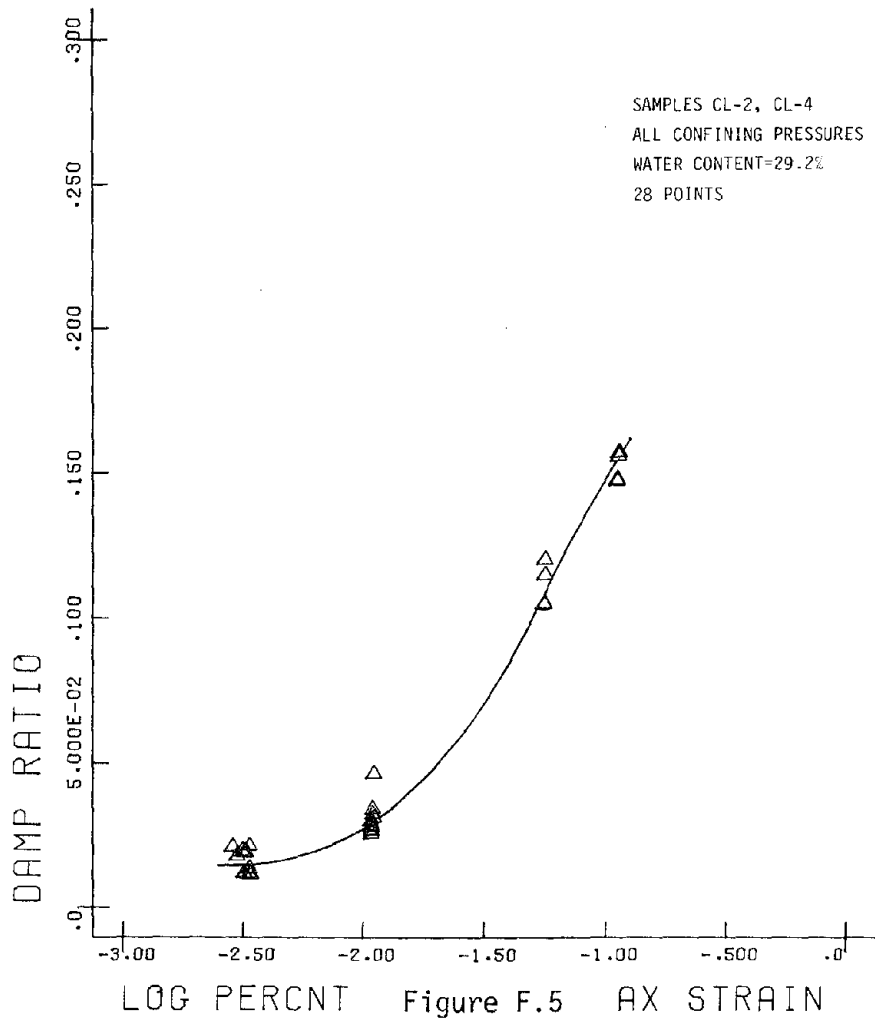


Figure F.5

O-CLAYT-4F1

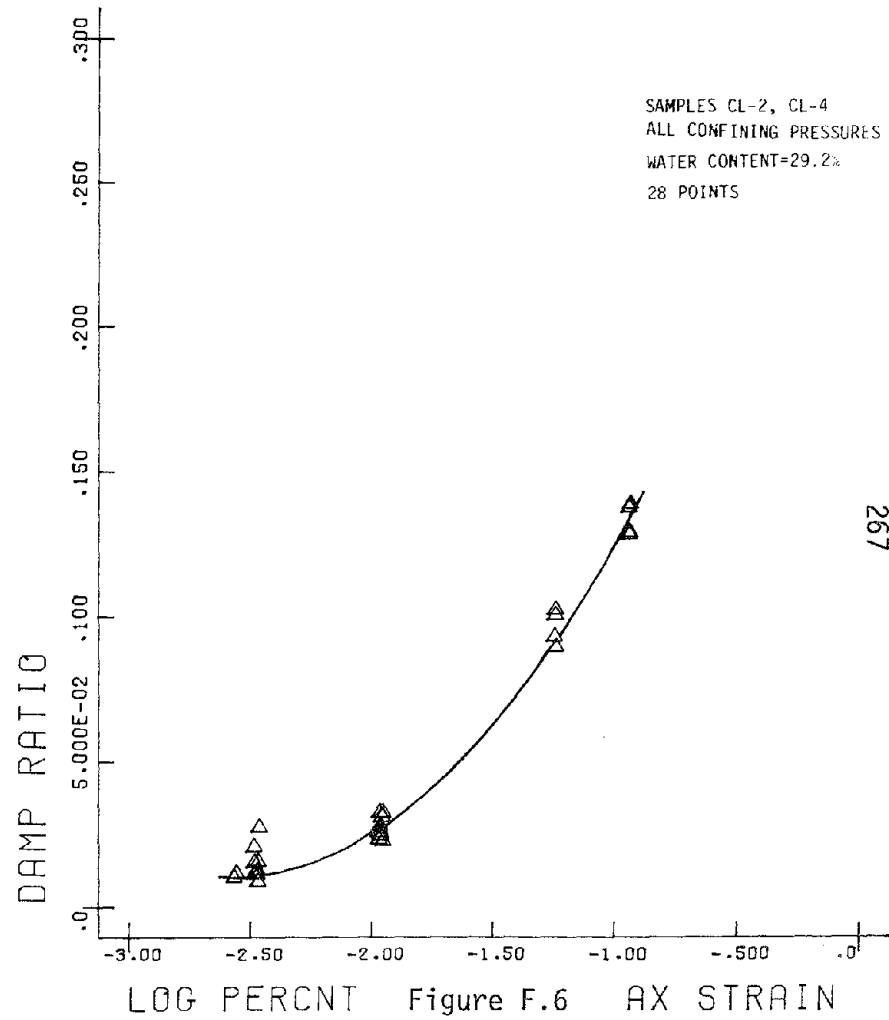
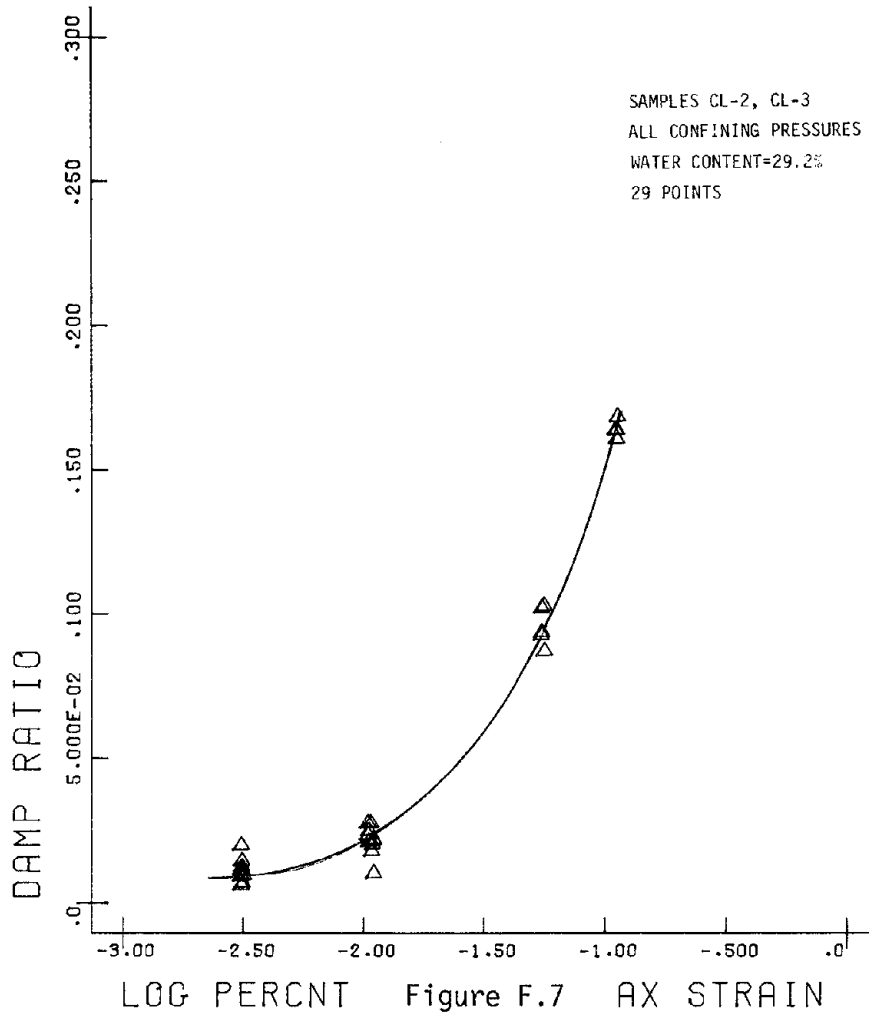
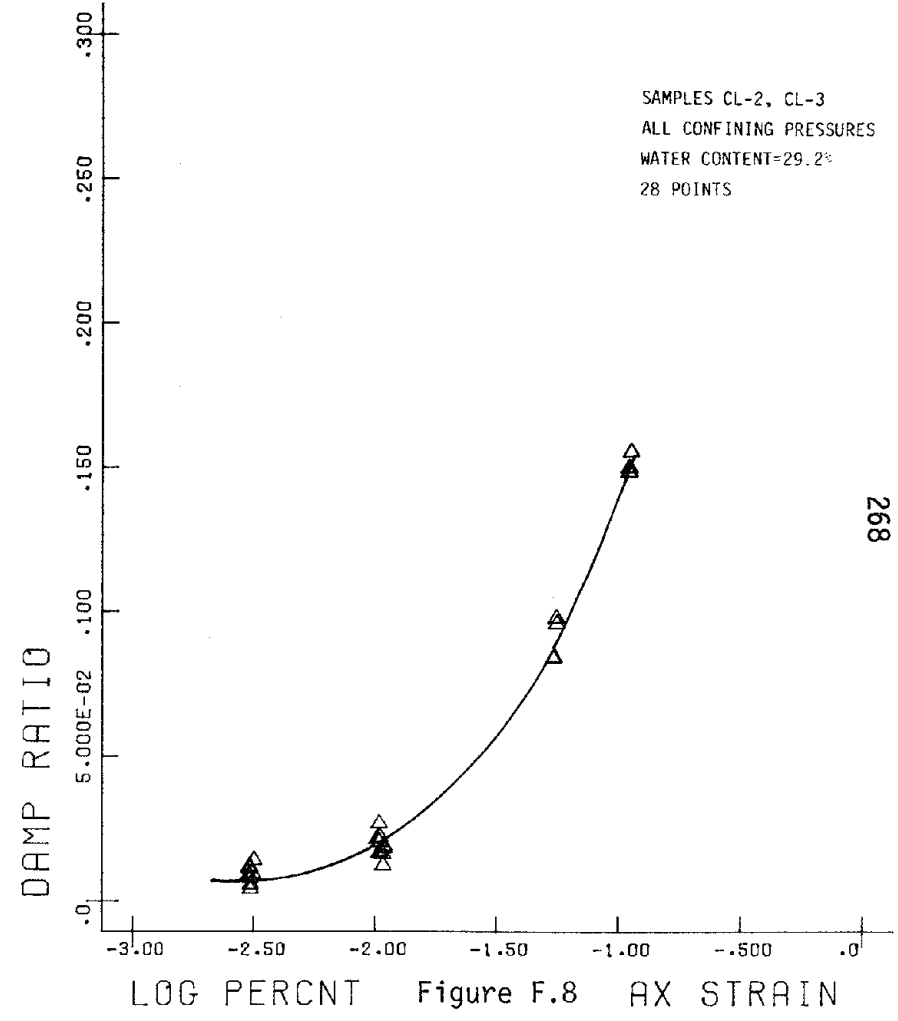


Figure F.6

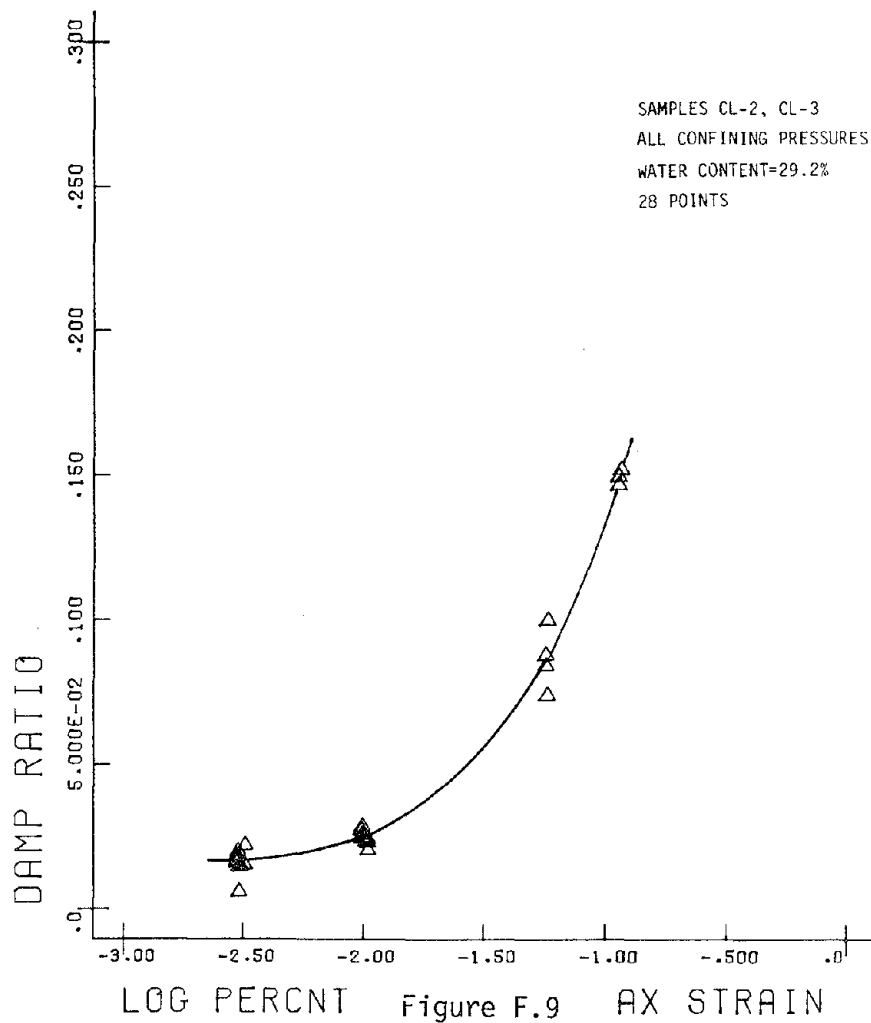
O-CLAYT-4F5



O-CLAYT-10F.3

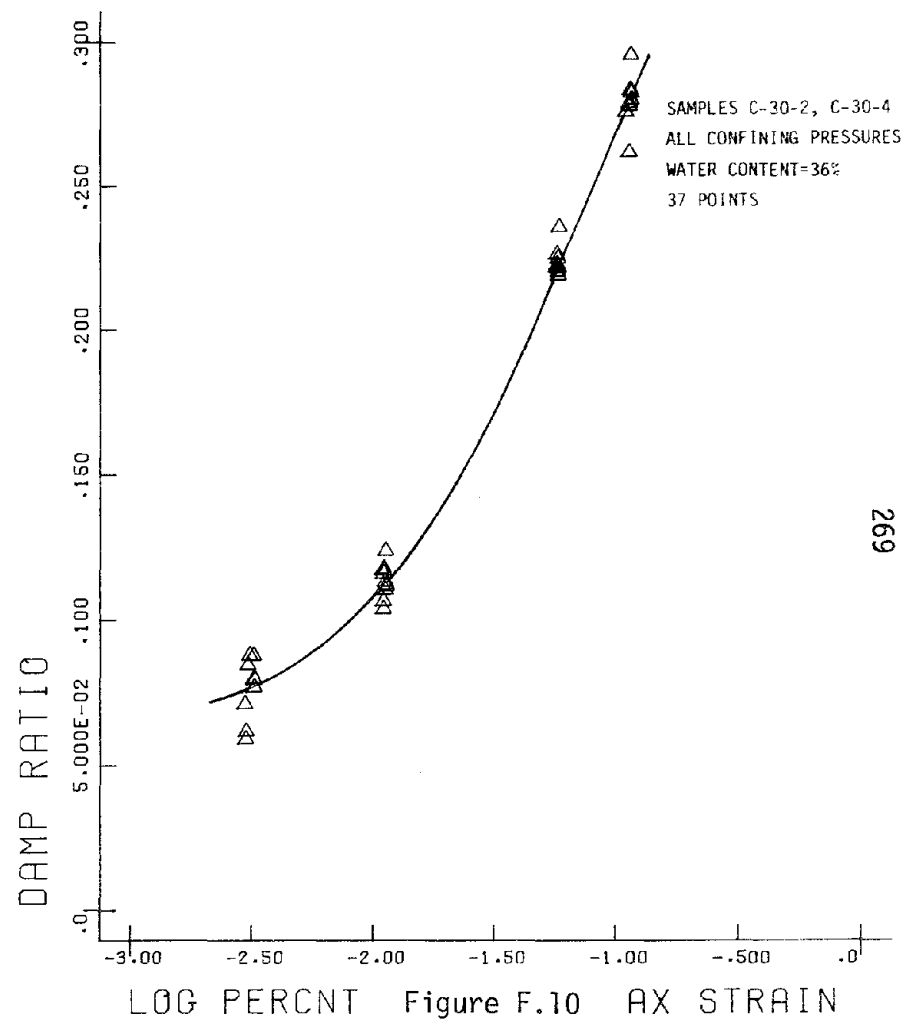


O-CLAYT-10F1



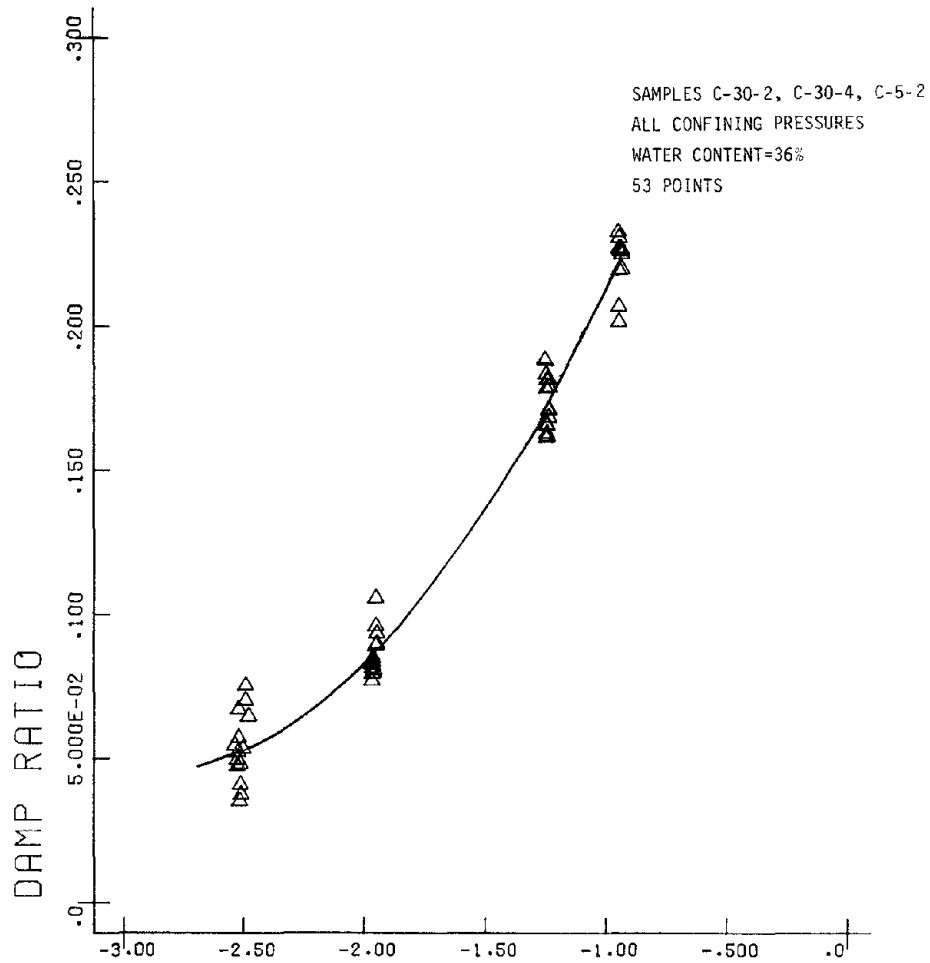
LOG PERCENT Figure F.9 AX STRAIN

O-CLAYT-10F5



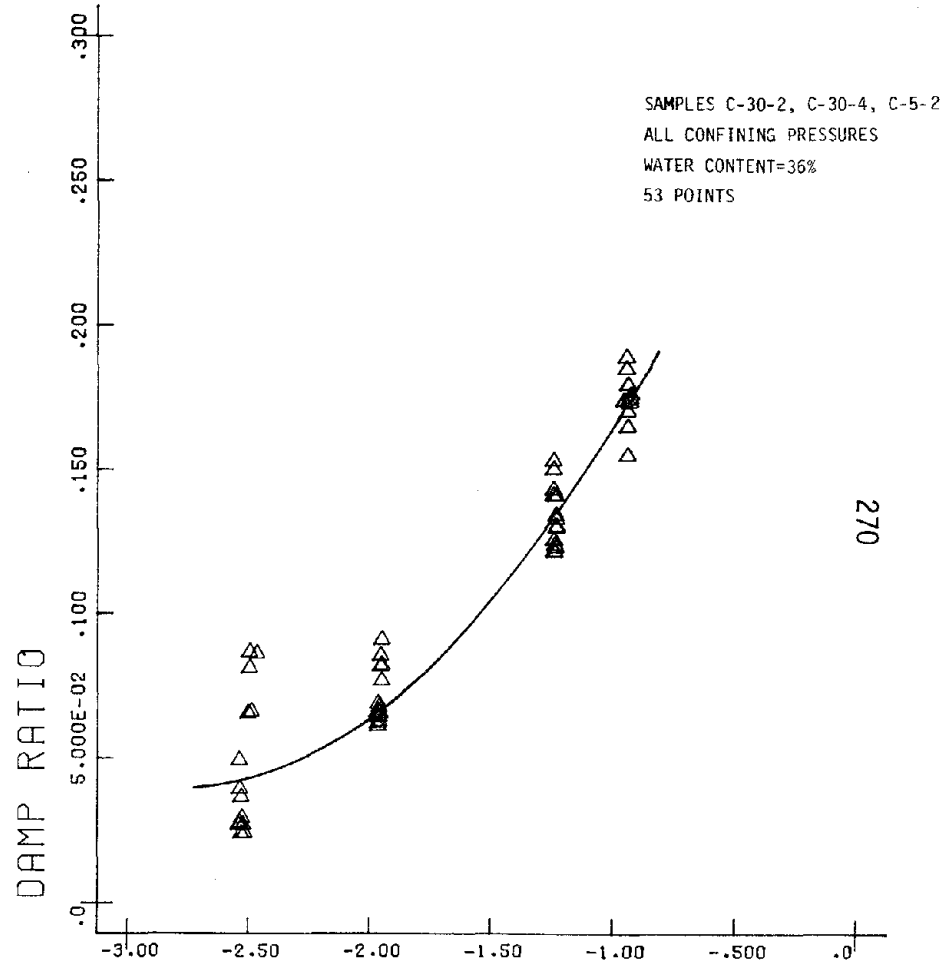
LOG PERCENT Figure F.10 AX STRAIN

O-CLAYT-1F.05



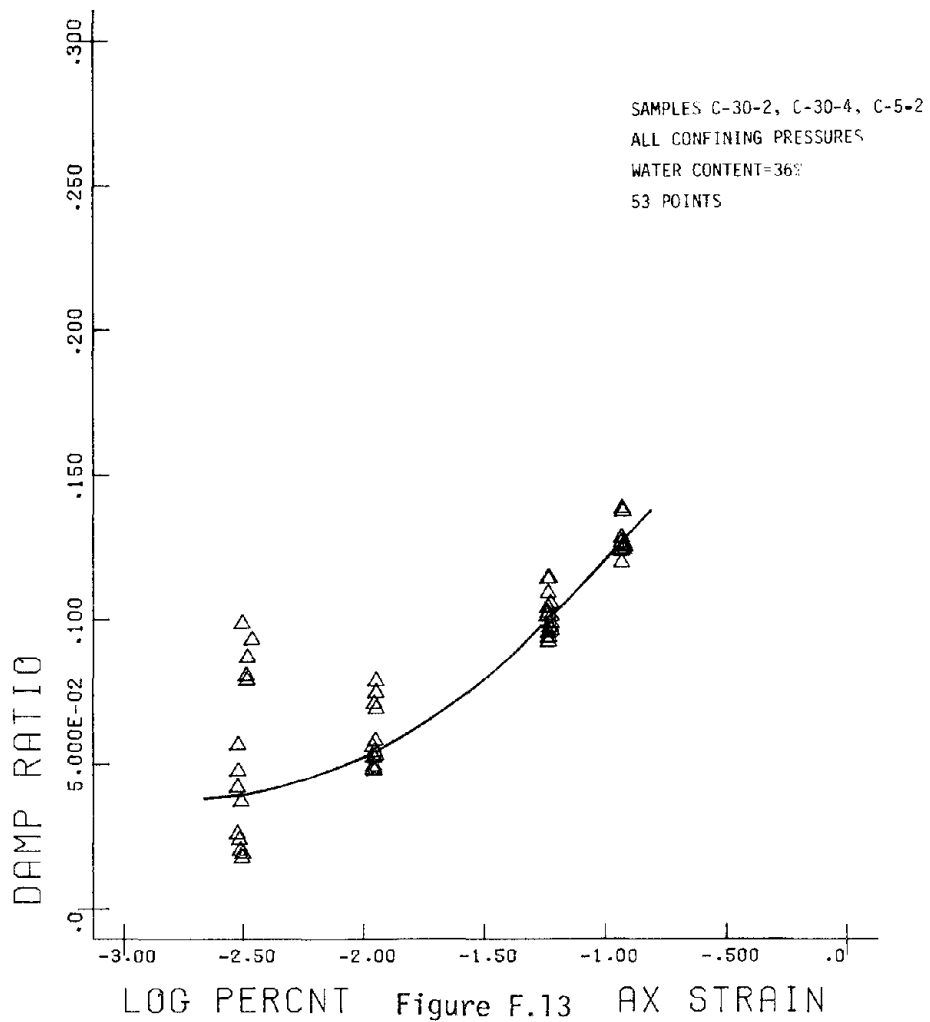
LOG PERCENT AX STRAIN Figure F.11

O-CLAYT-1F.3



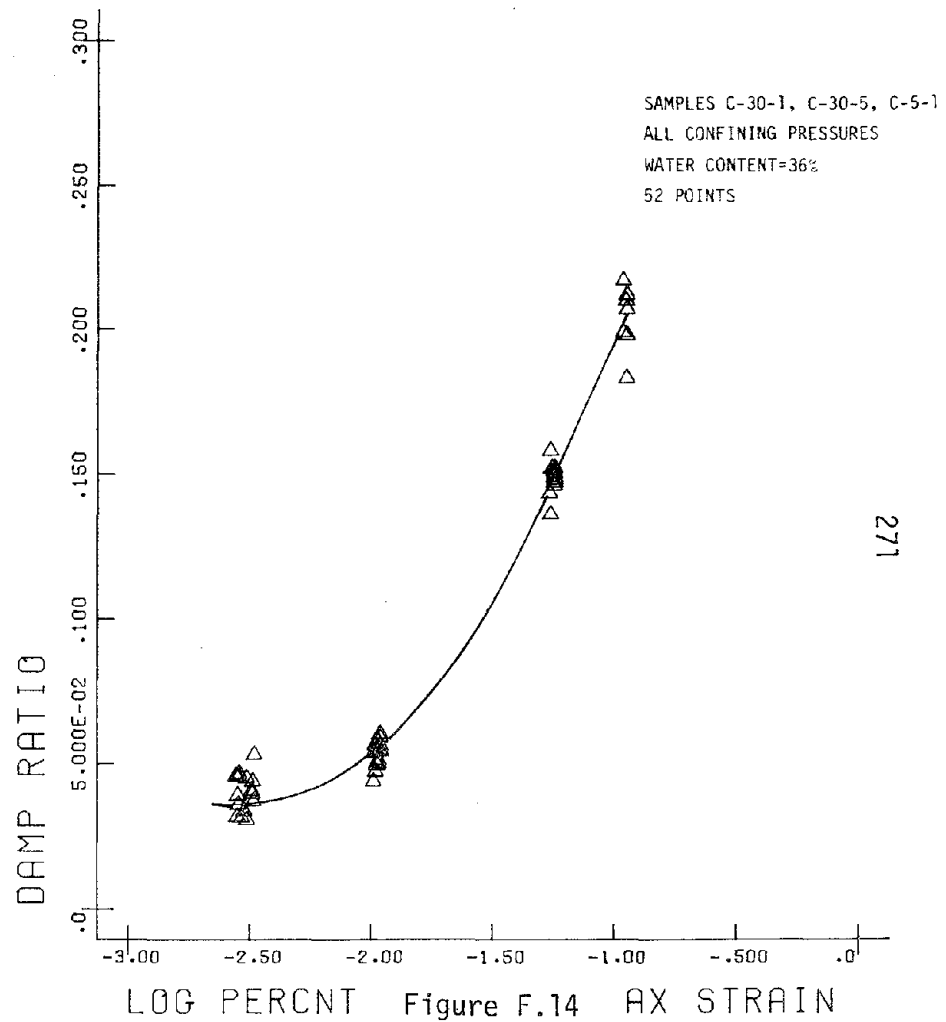
LOG PERCENT AX STRAIN Figure F.12

O-CLAYT-1F.1



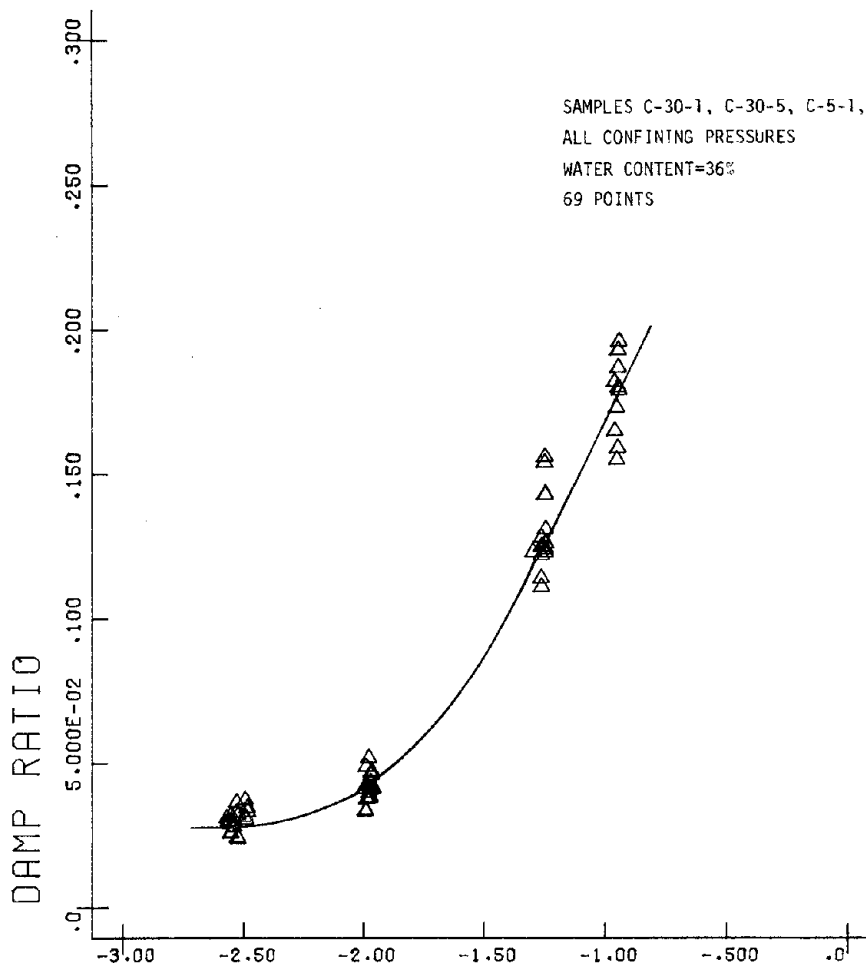
LOG PERCENT Figure F.13 AX STRAIN

O-CLAYT-1F5



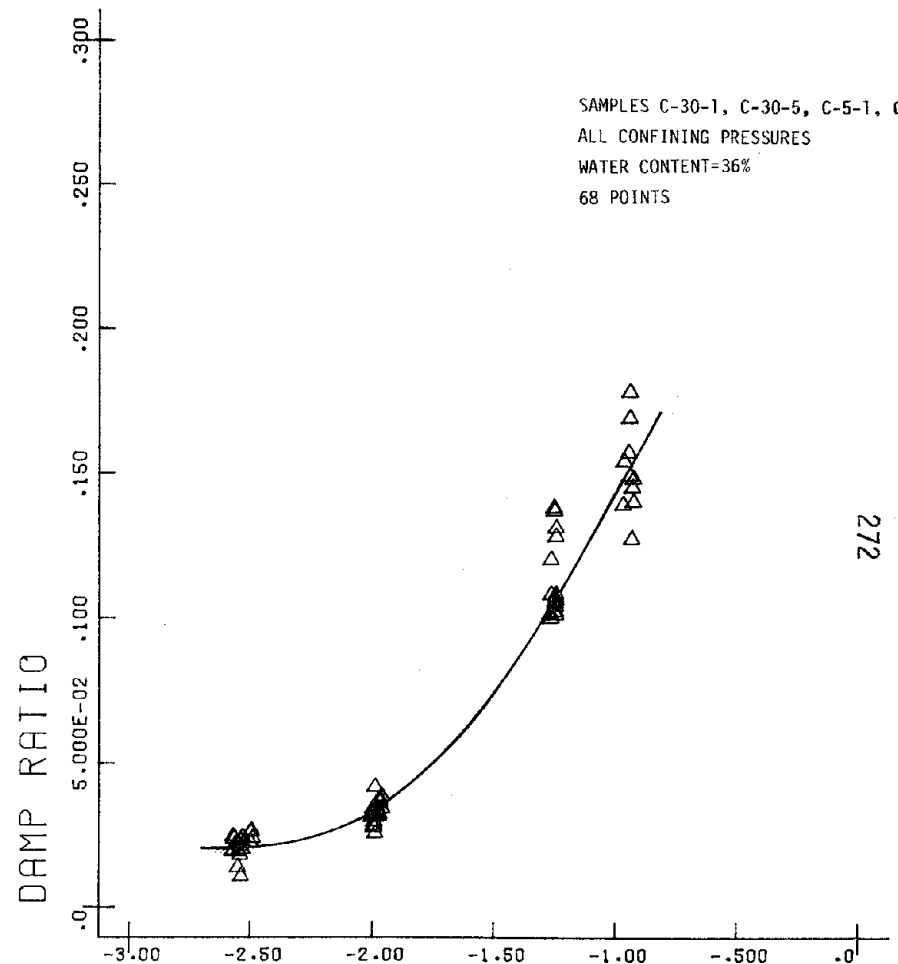
LOG PERCENT Figure F.14 AX STRAIN

O-CLAYT-4F.05



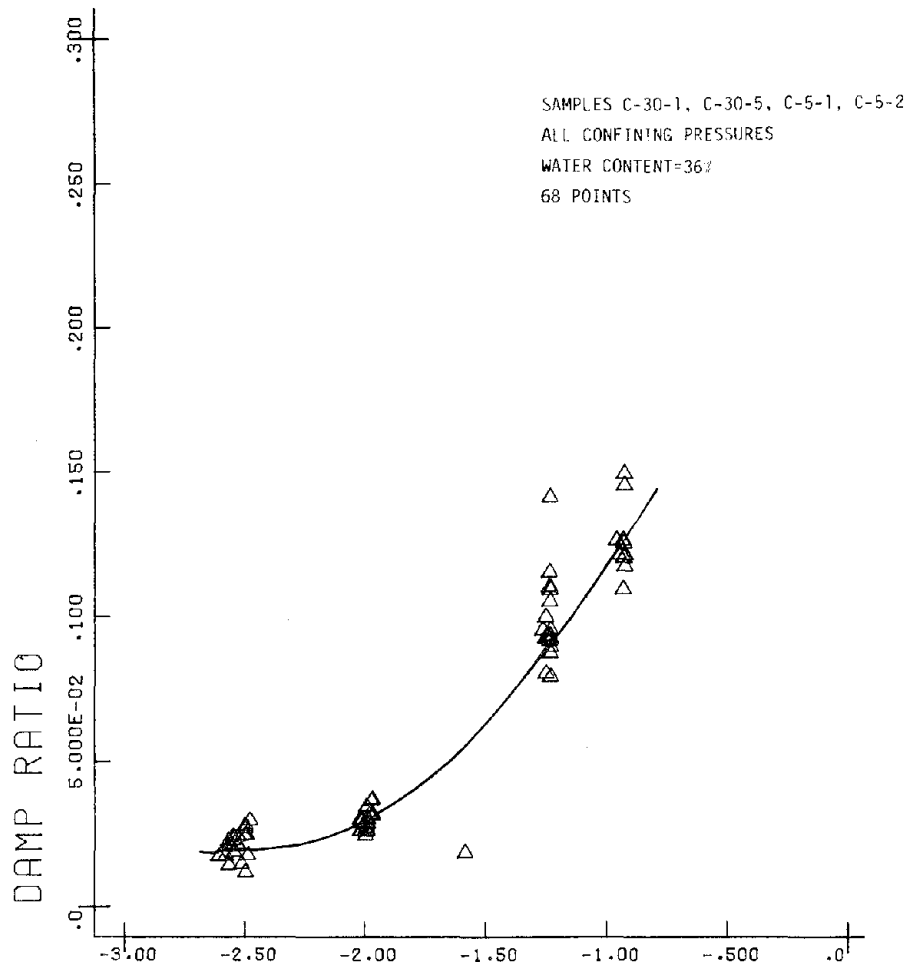
LOG PERCENT AX STRAIN Figure F.15

O-CLAYT-4F.3



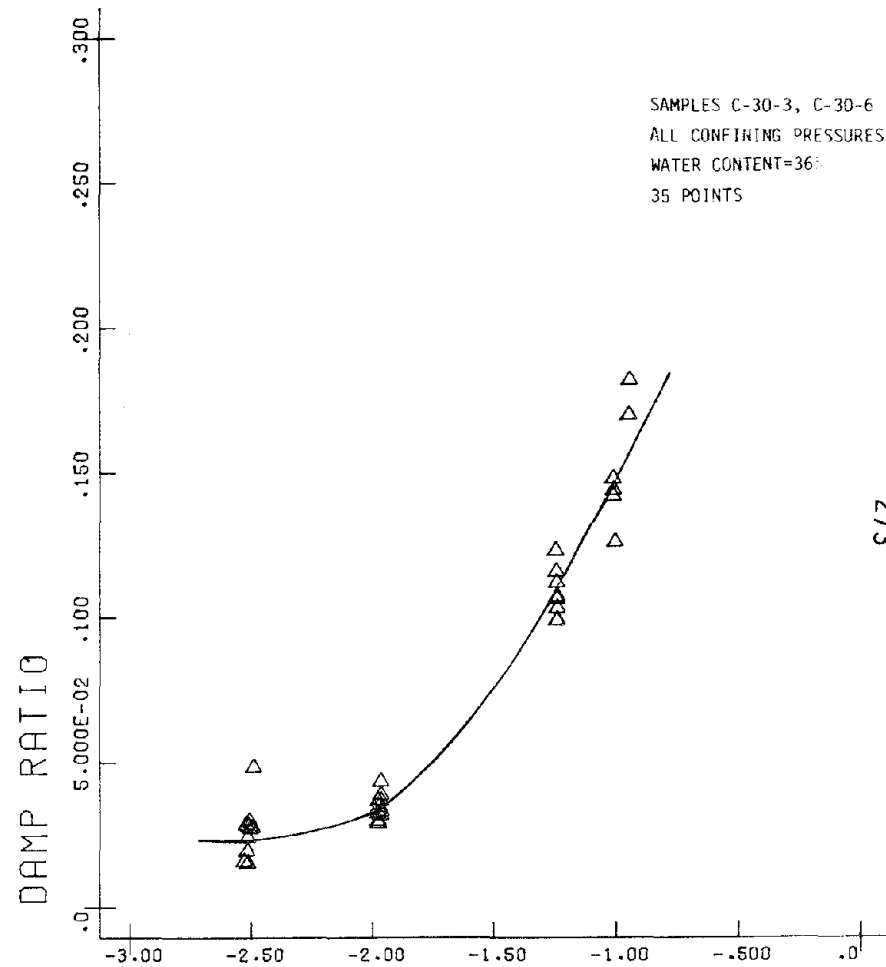
LOG PERCENT AX STRAIN Figure F.16

O-CLAYT-4F1



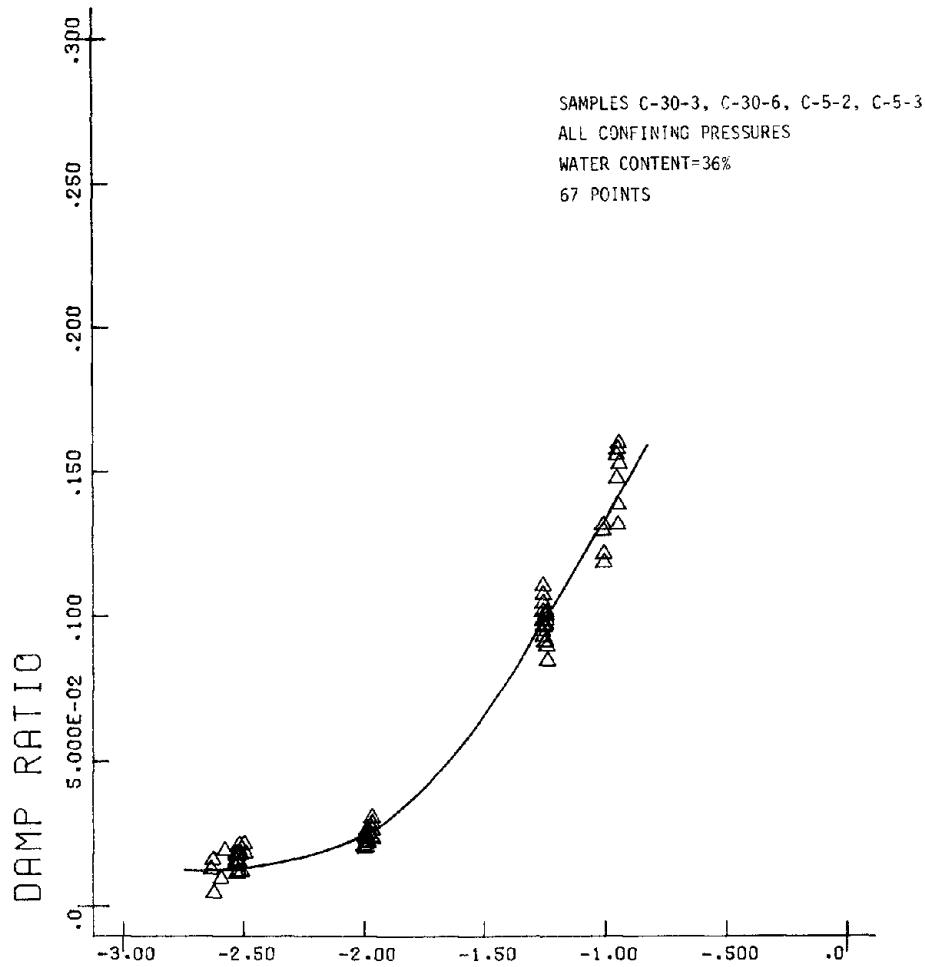
LOG PERCENT AX STRAIN Figure F.17

O-CLAYT-4F5



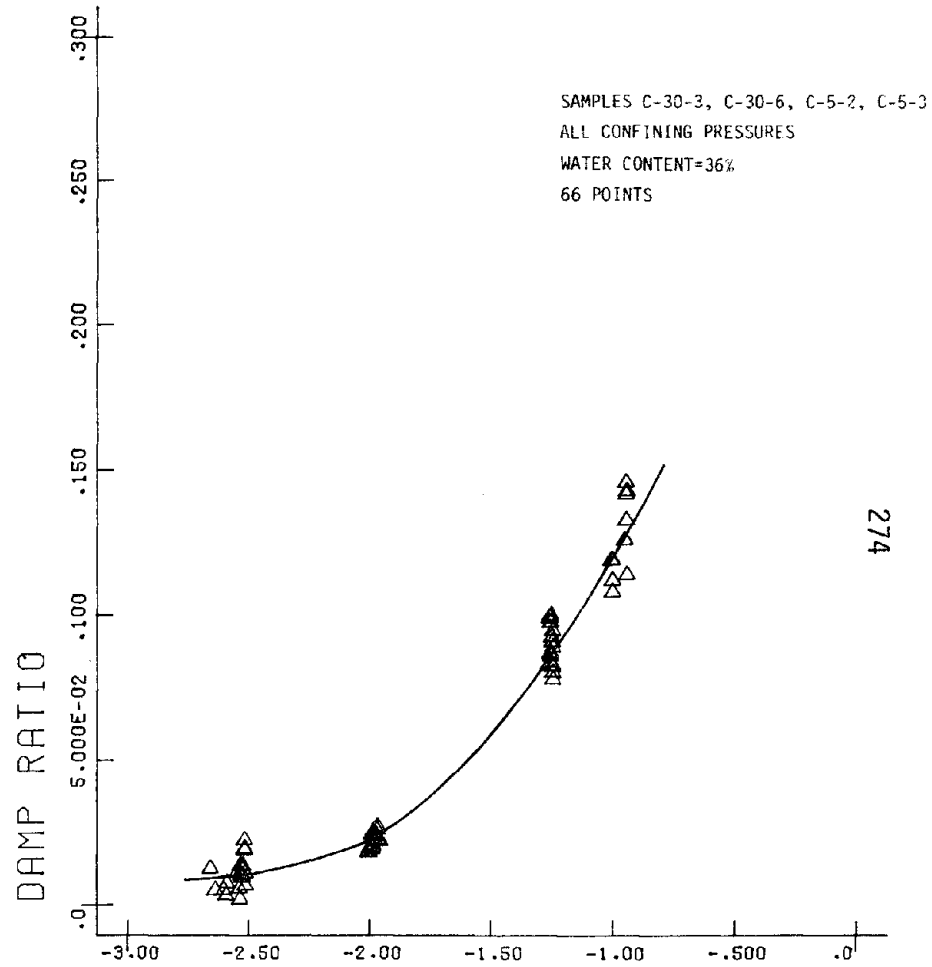
LOG PERCENT AX STRAIN Figure F.18

O-CLAYT-10F.05



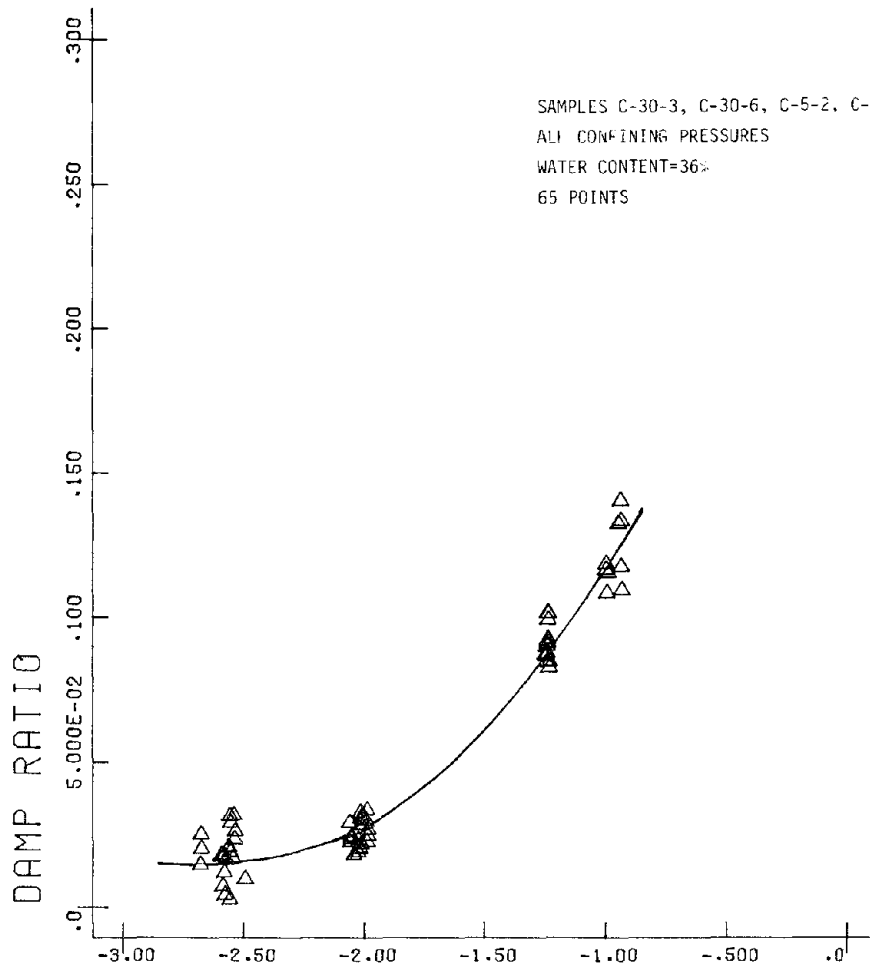
LOG PERCENT Figure F.19 AX STRAIN

O-CLAYT-10F.3



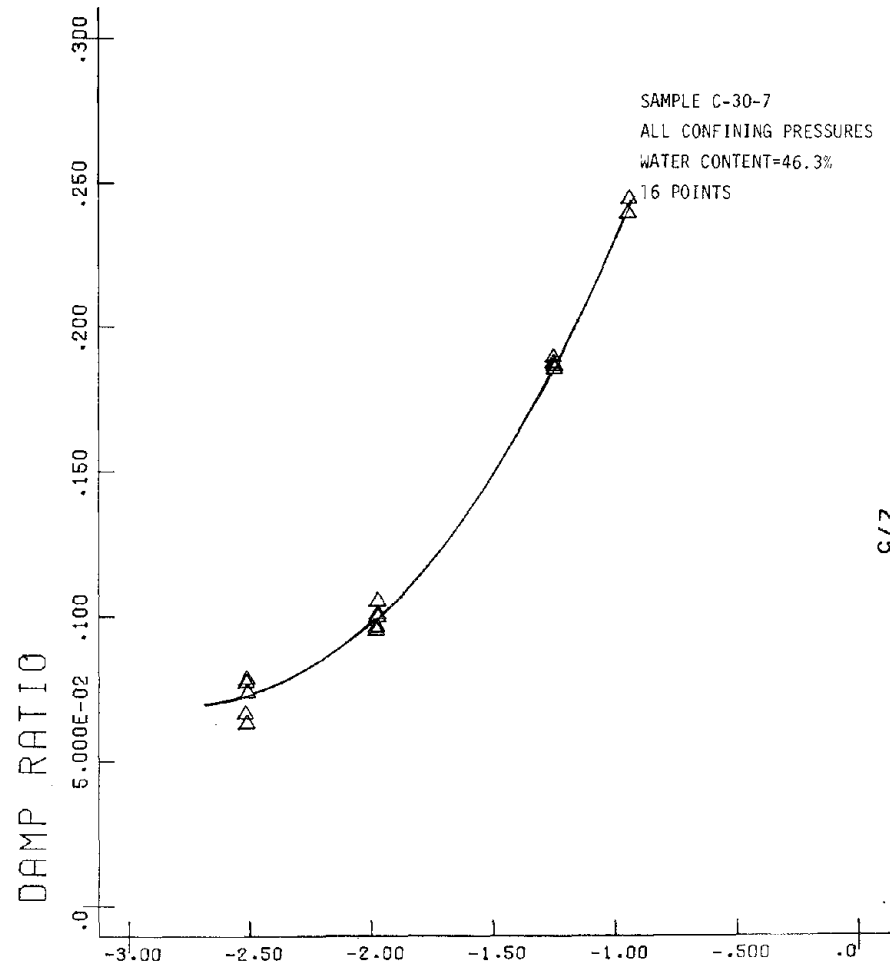
LOG PERCENT Figure F.20 AX STRAIN

O-CLAYT-10F.1



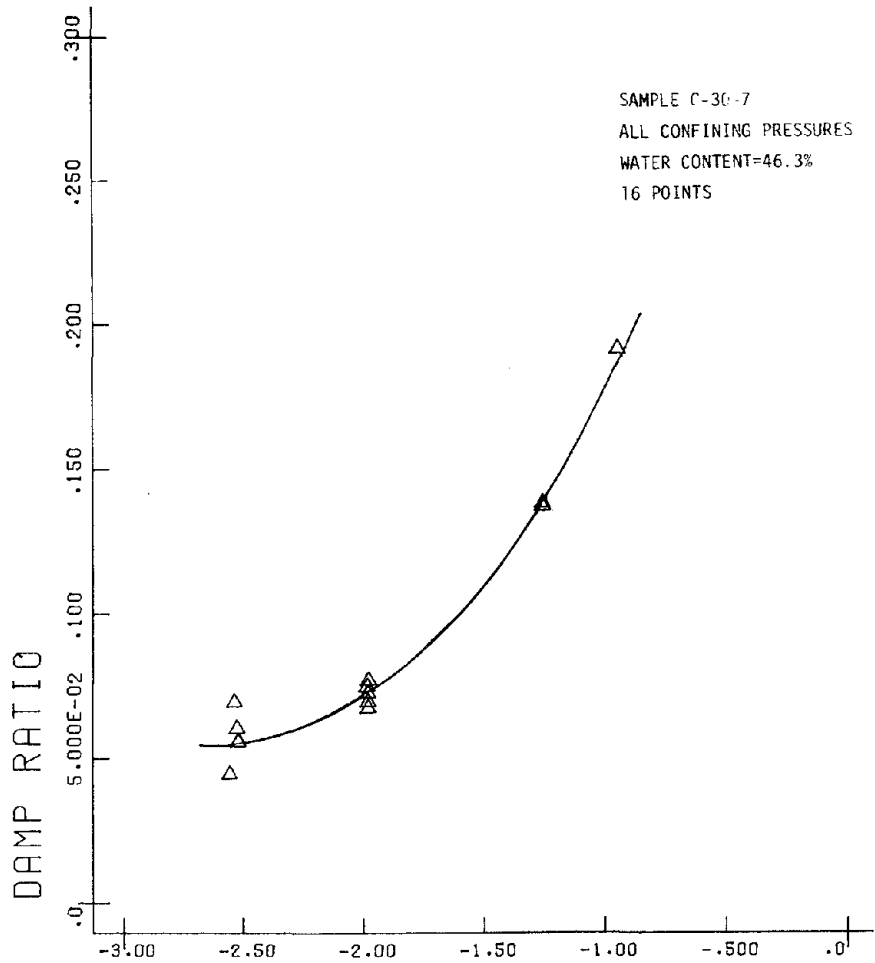
LOG PERCENT Figure F.21 AX STRAIN

O-CLAYT-10F5



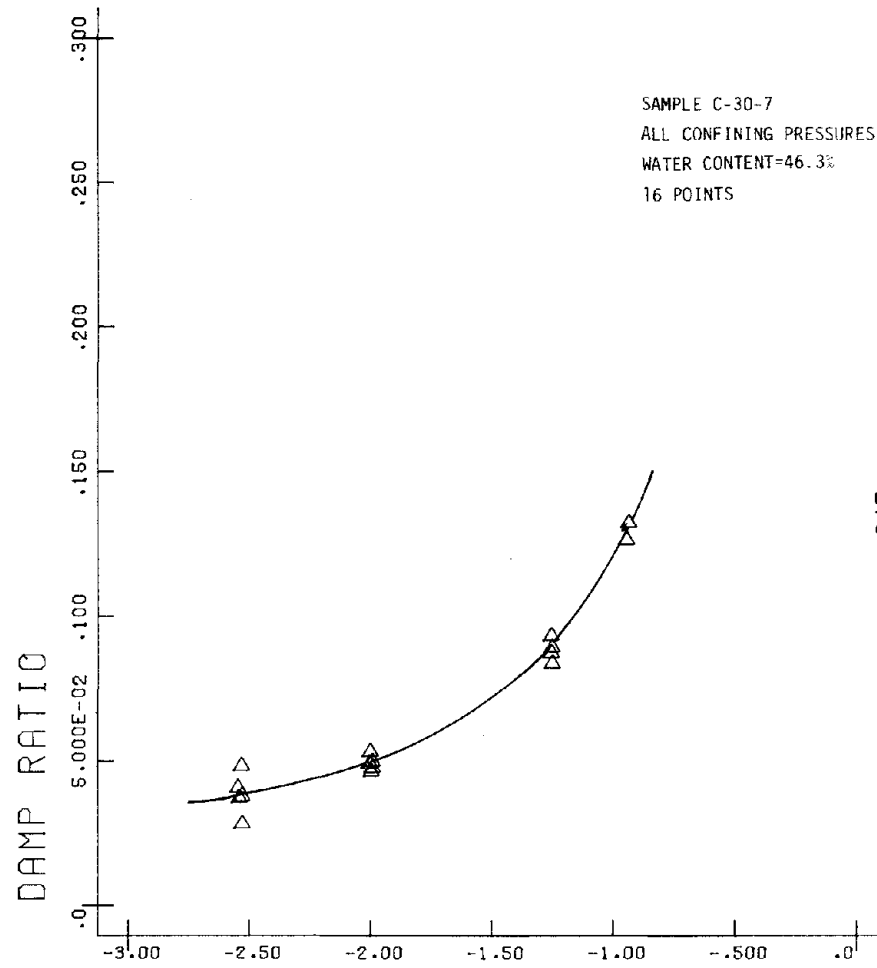
LOG PERCENT Figure F.22 AX STRAIN

O-CLAYT-1F.3



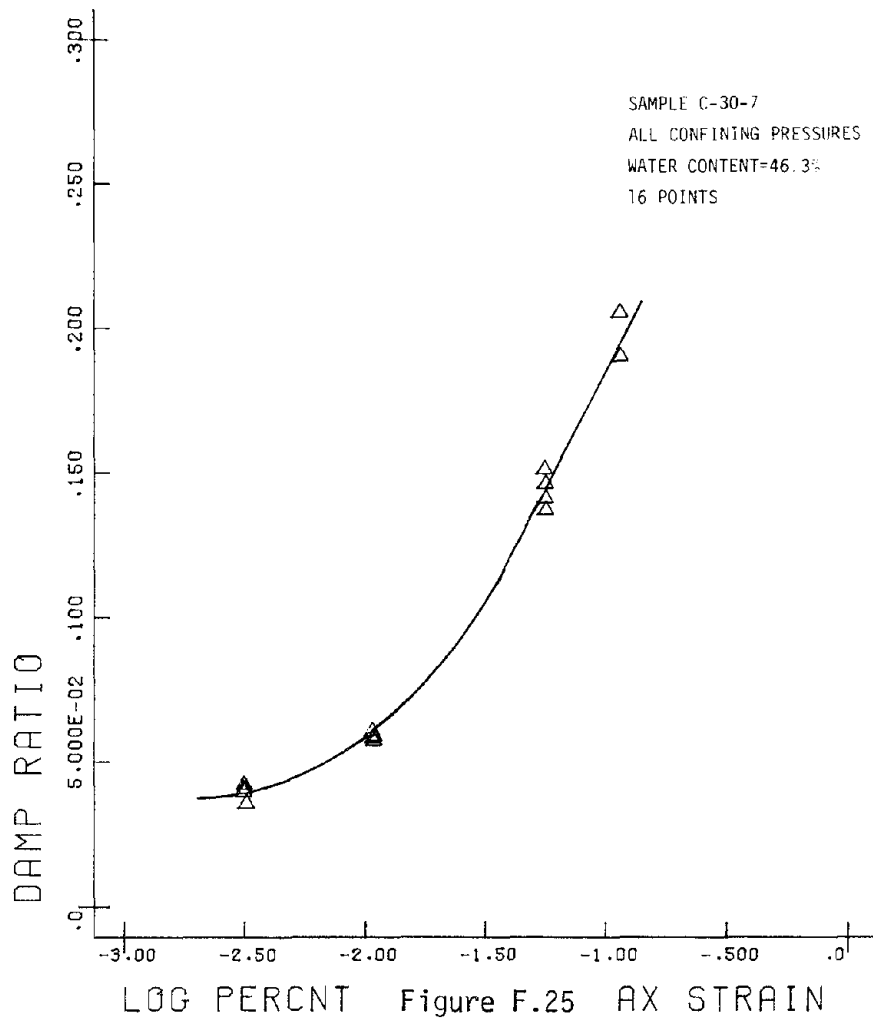
LOG PERCENT AX STRAIN Figure F.23

O-CLAYT-1F1



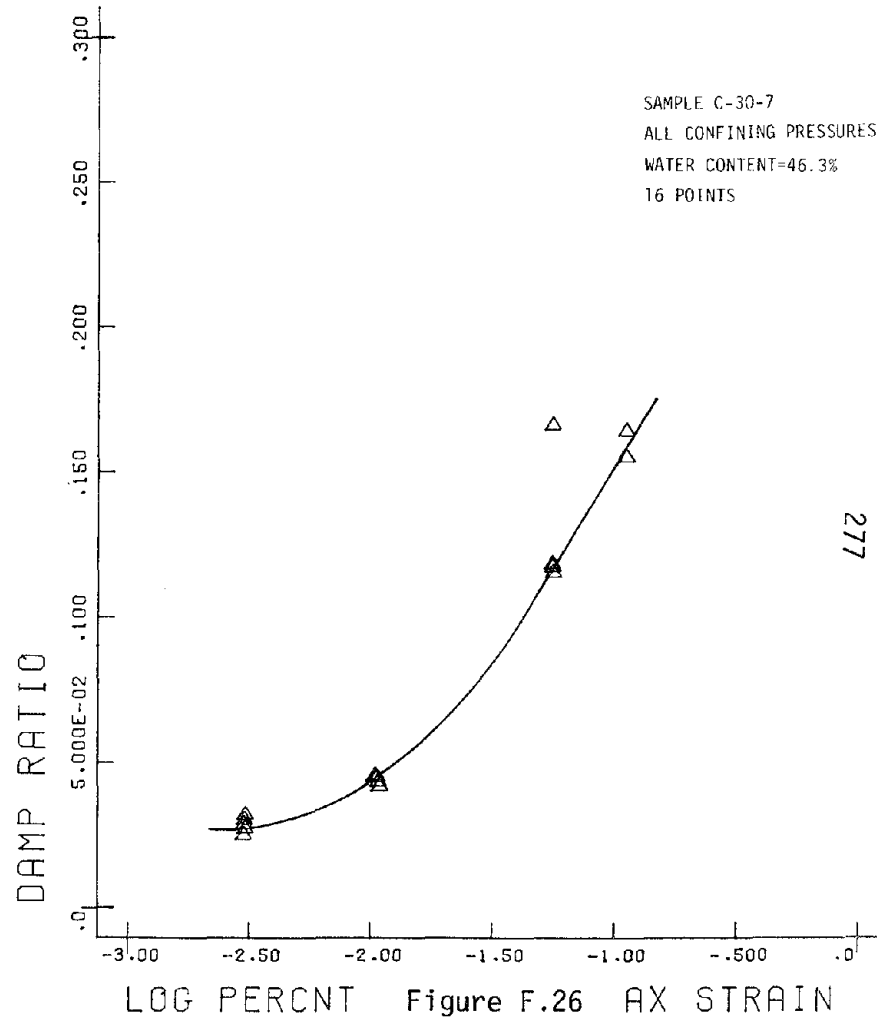
LOG PERCENT AX STRAIN Figure F.24

O-CLAYT-1F5



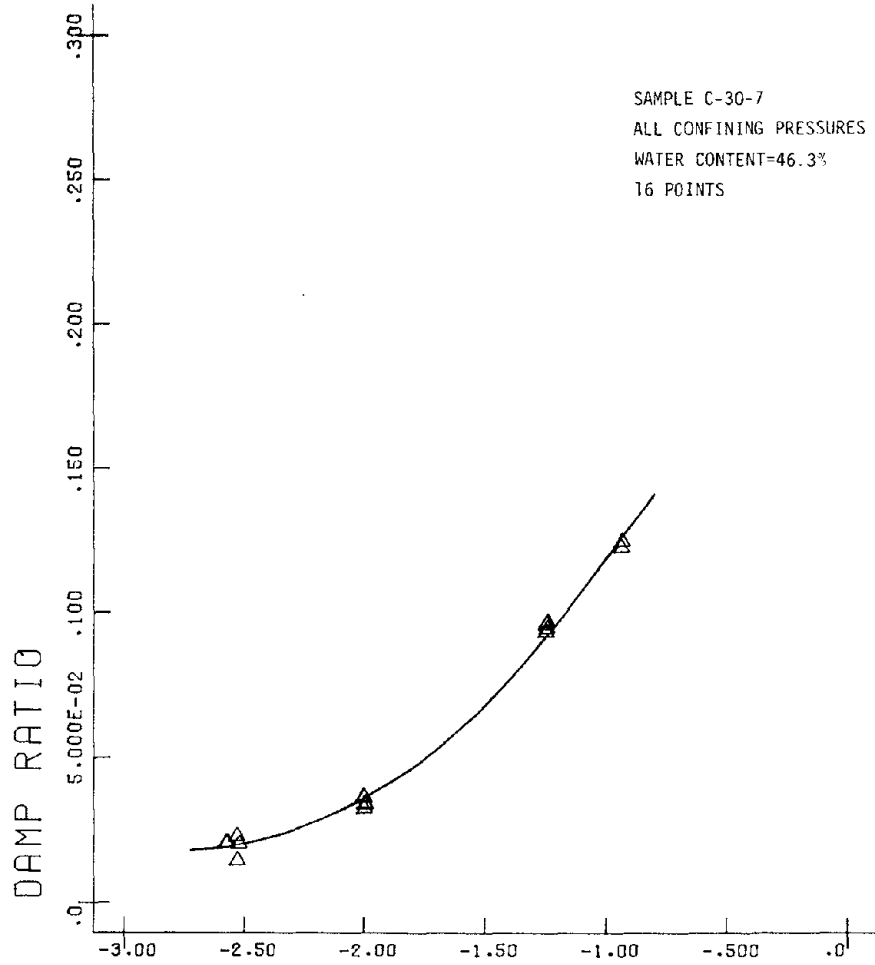
LOG PERCENT AX STRAIN Figure F.25

O-CLAYT-4F.3



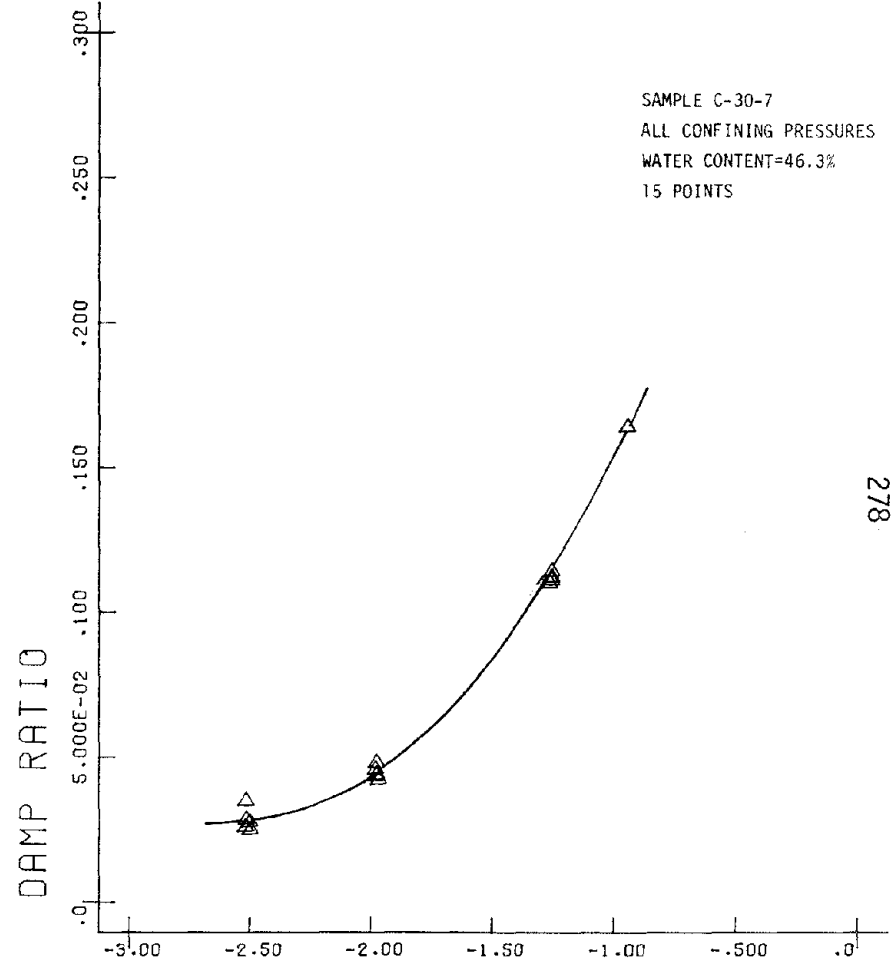
LOG PERCENT AX STRAIN Figure F.26

O-CLAYT-4F1



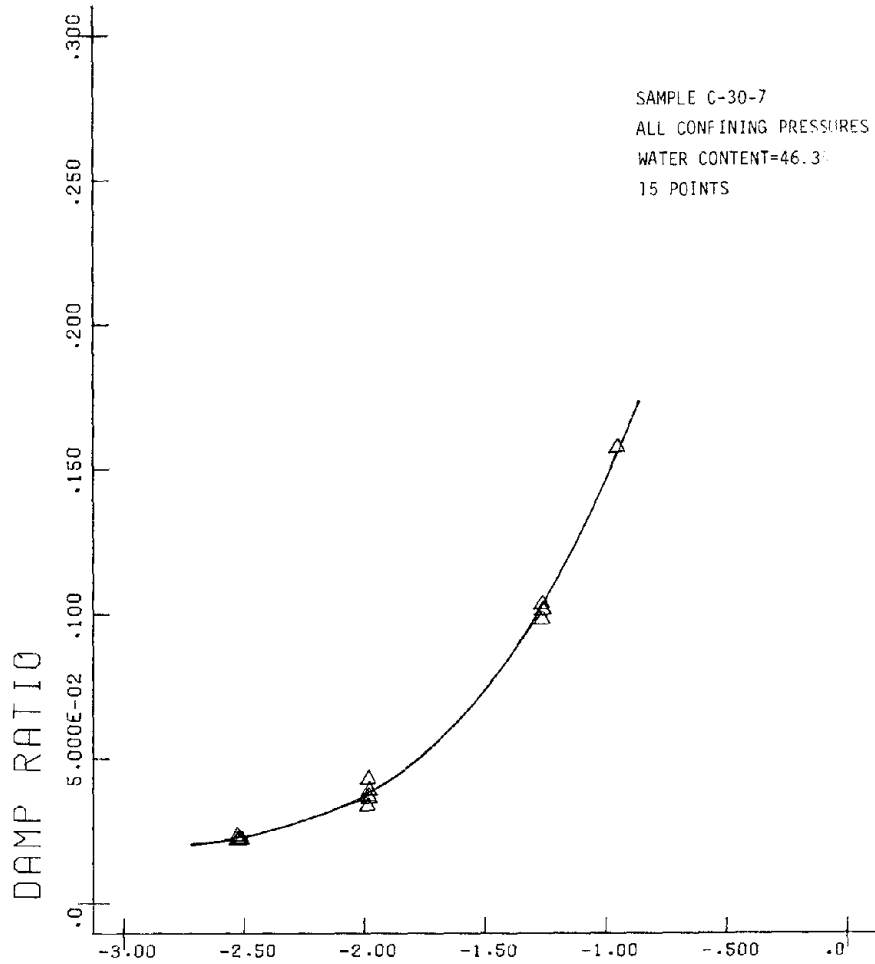
LOG PERCENT Figure F.27 AX STRAIN

O-CLAYT-4F5



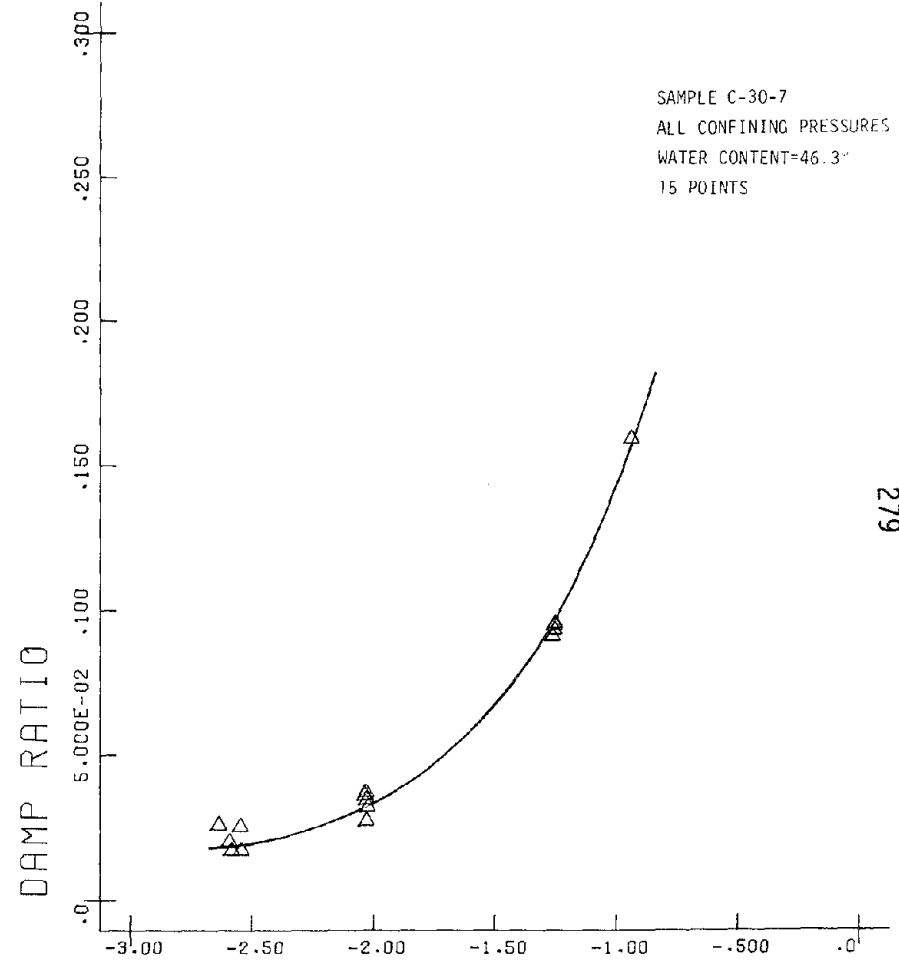
LOG PERCENT Figure F.28 AX STRAIN

O-CLAYT-10F.3



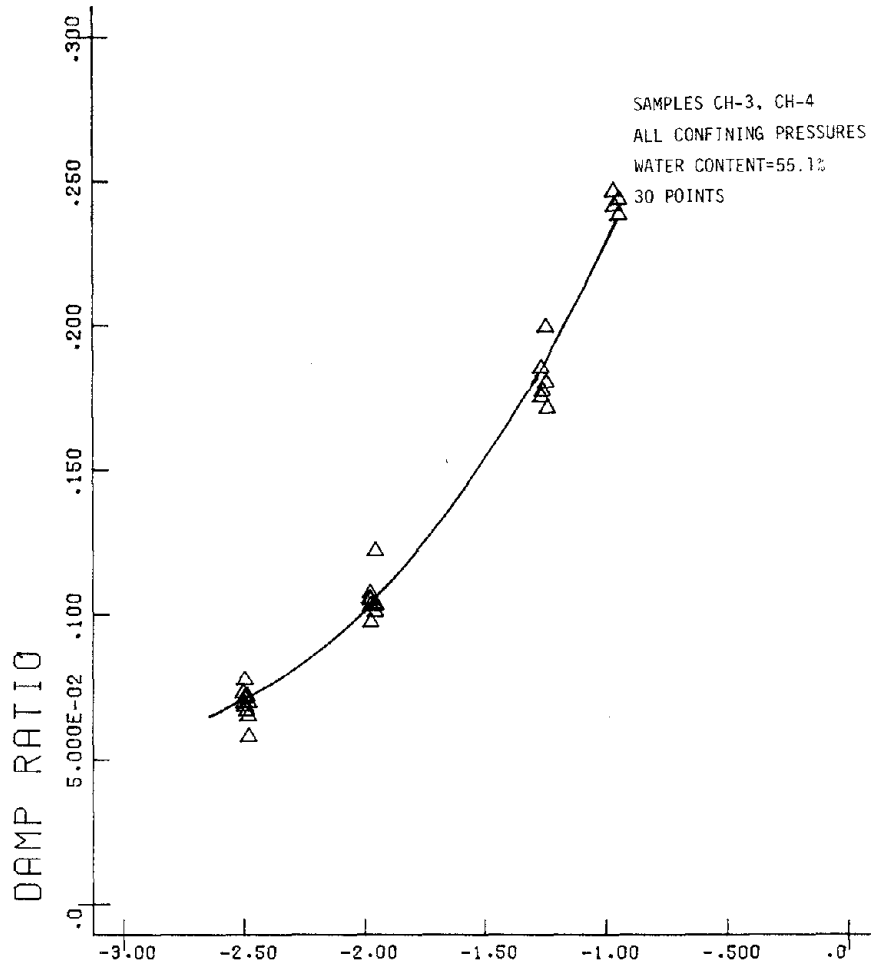
LOG PERCENT AX STRAIN Figure F.29

O-CLAYT-10F1



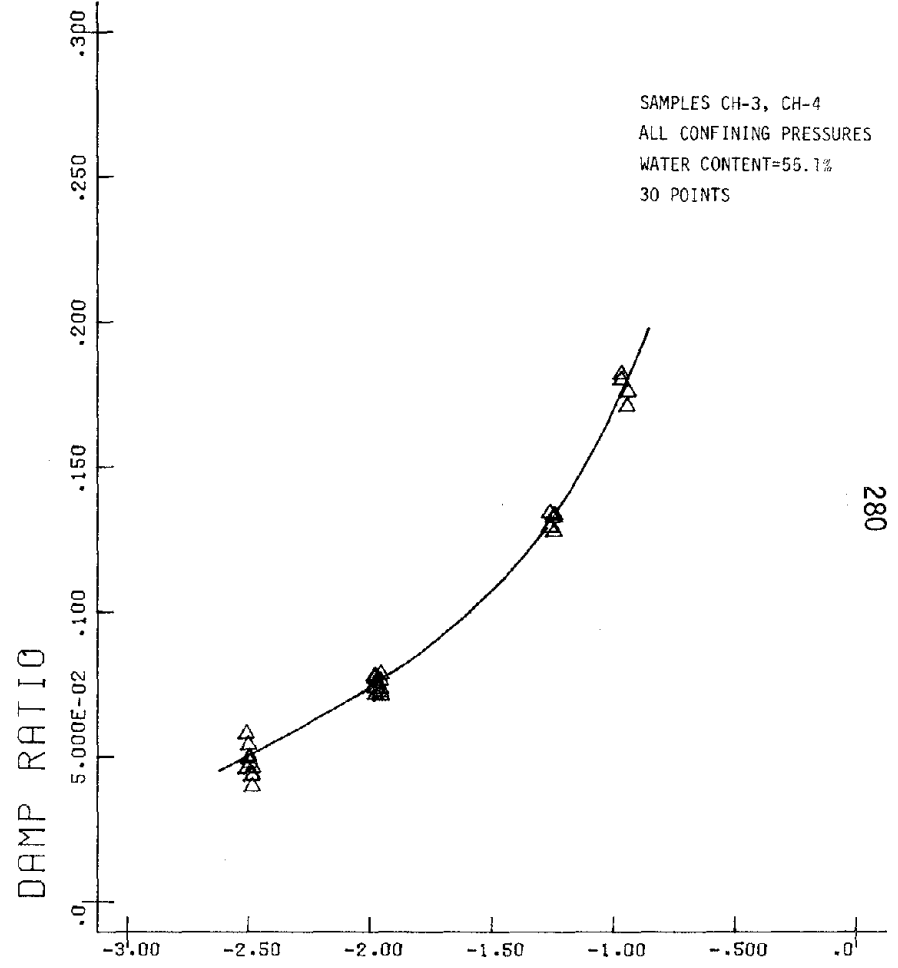
LOG PERCENT AX STRAIN Figure F.30

O-CLAYT-10F5



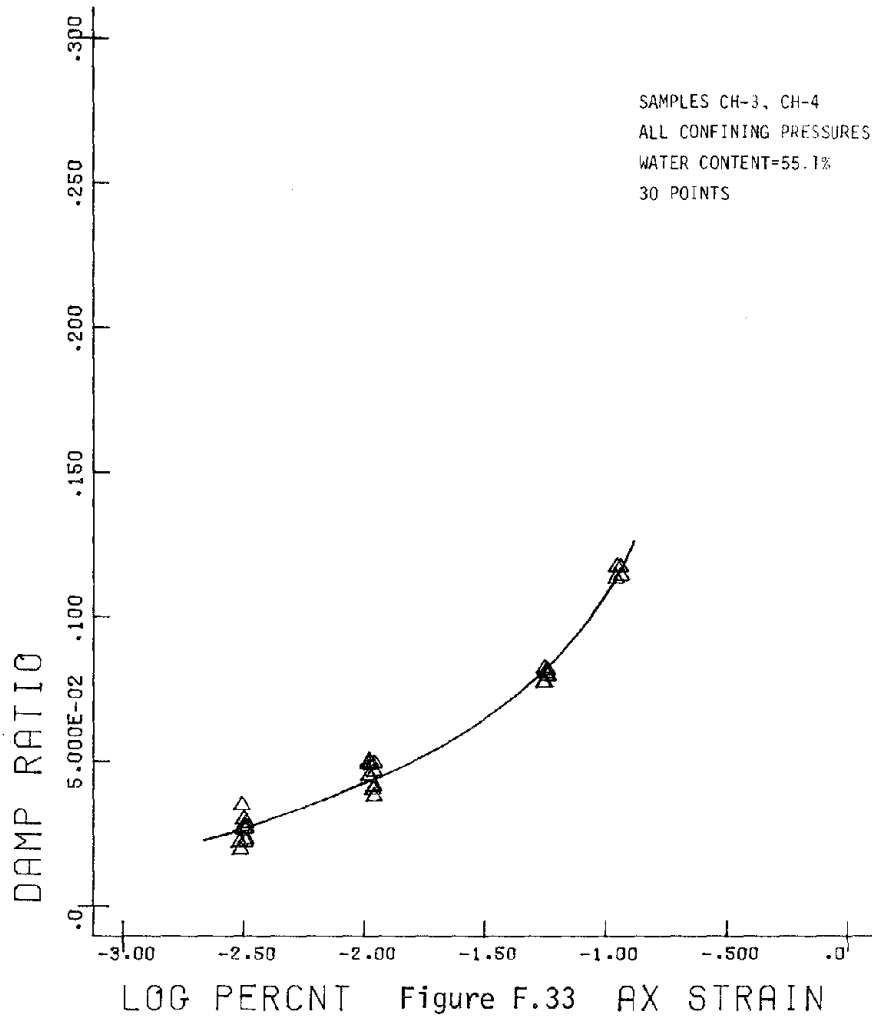
LOG PERCENT Figure F.31 AX STRAIN

O-CLAYT-1F.3

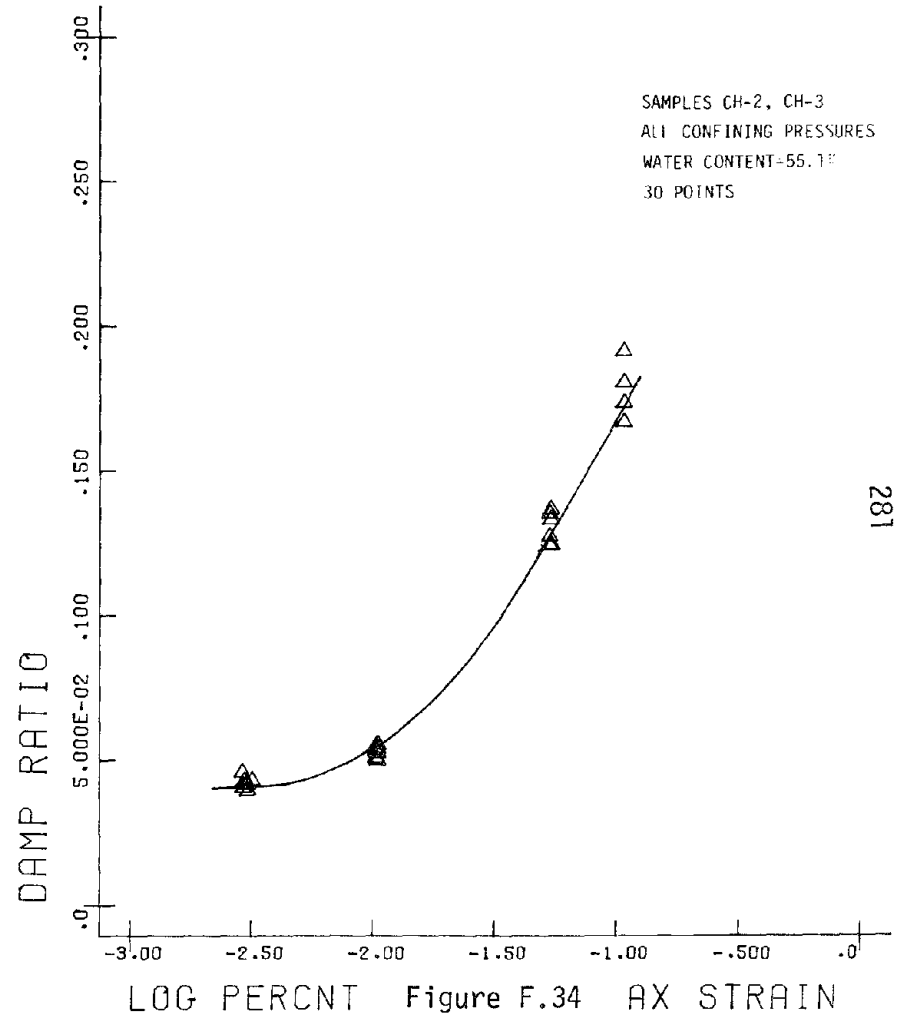


LOG PERCENT Figure F.32 AX STRAIN

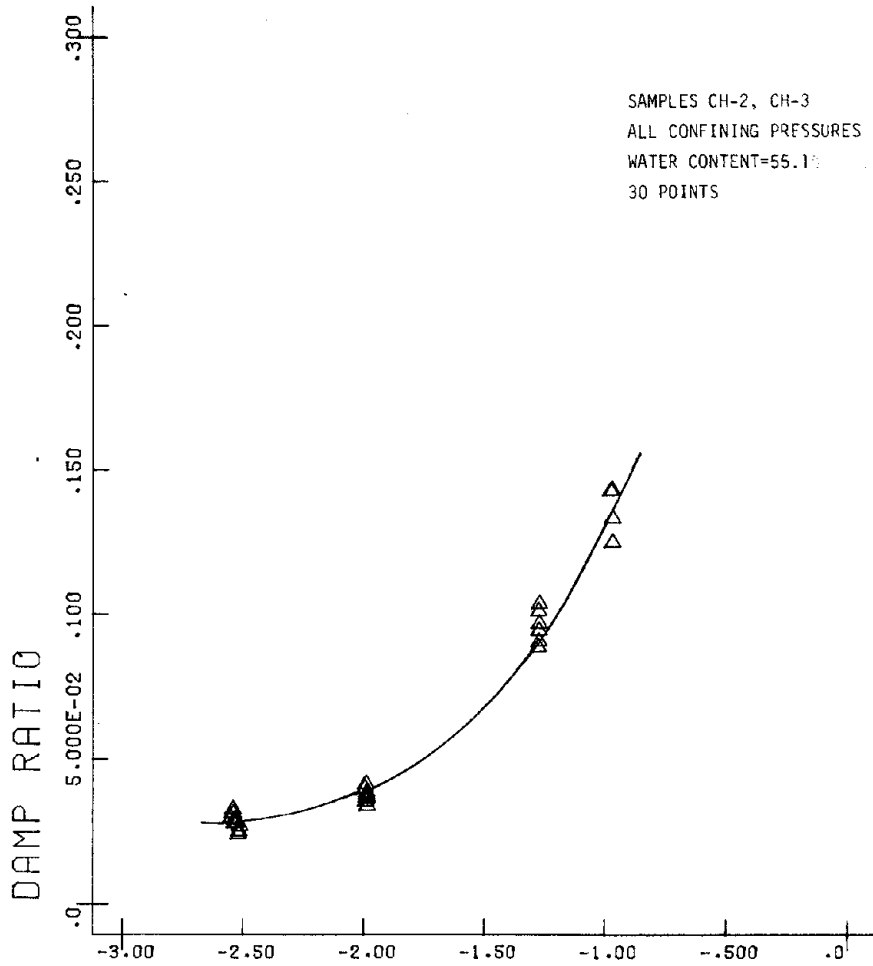
O-CLAYT-1F.1



0-CLAYT-1F5

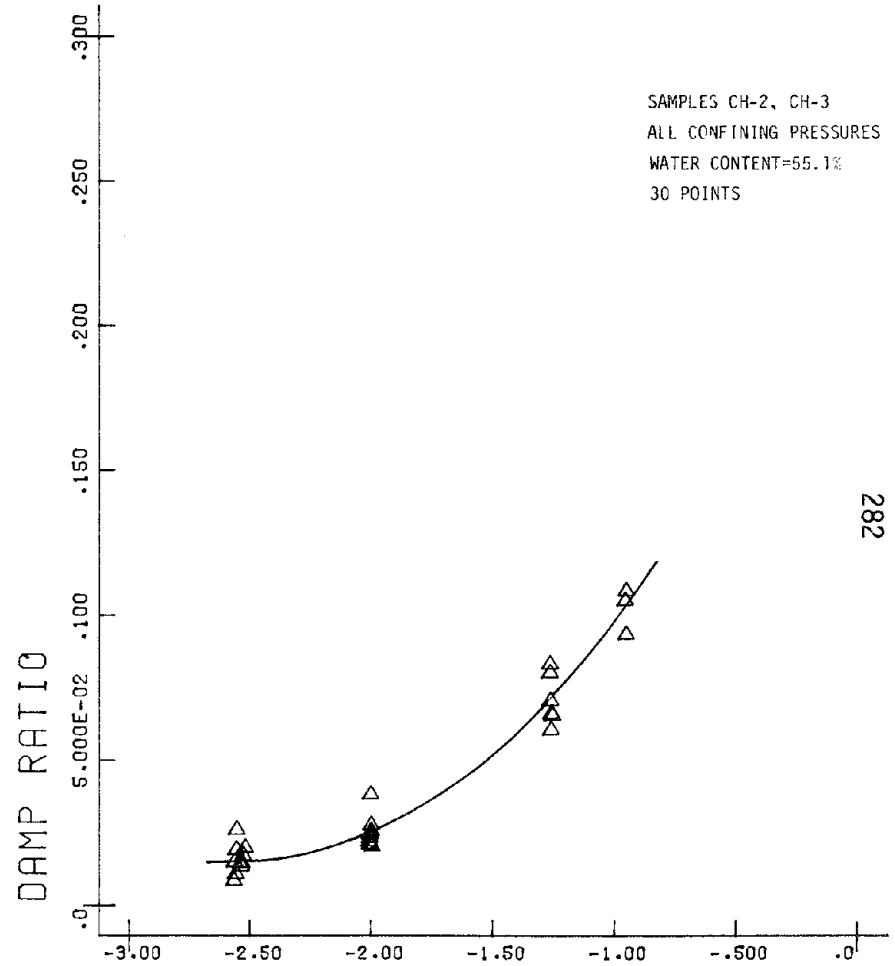


0-CLAYT-4F.3



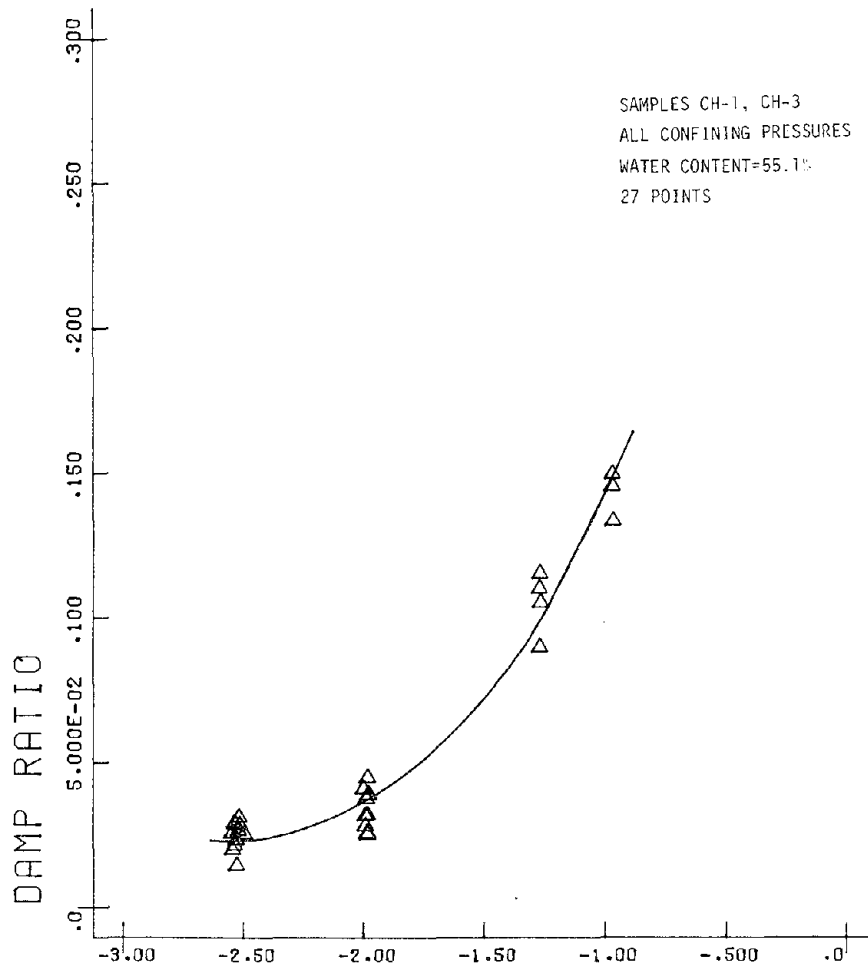
LOG PERCENT Figure F.35 AX STRAIN

O-CLAYT-4F1



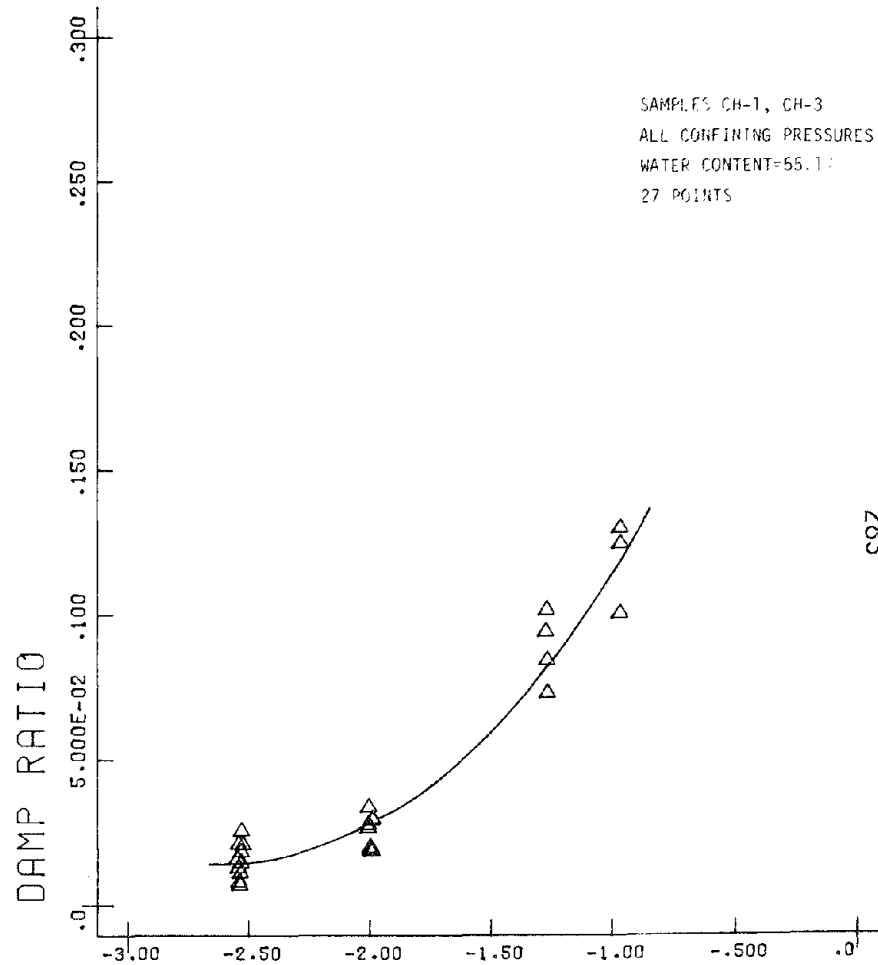
LOG PERCENT Figure F.36 AX STRAIN

O-CLAYT-4F5



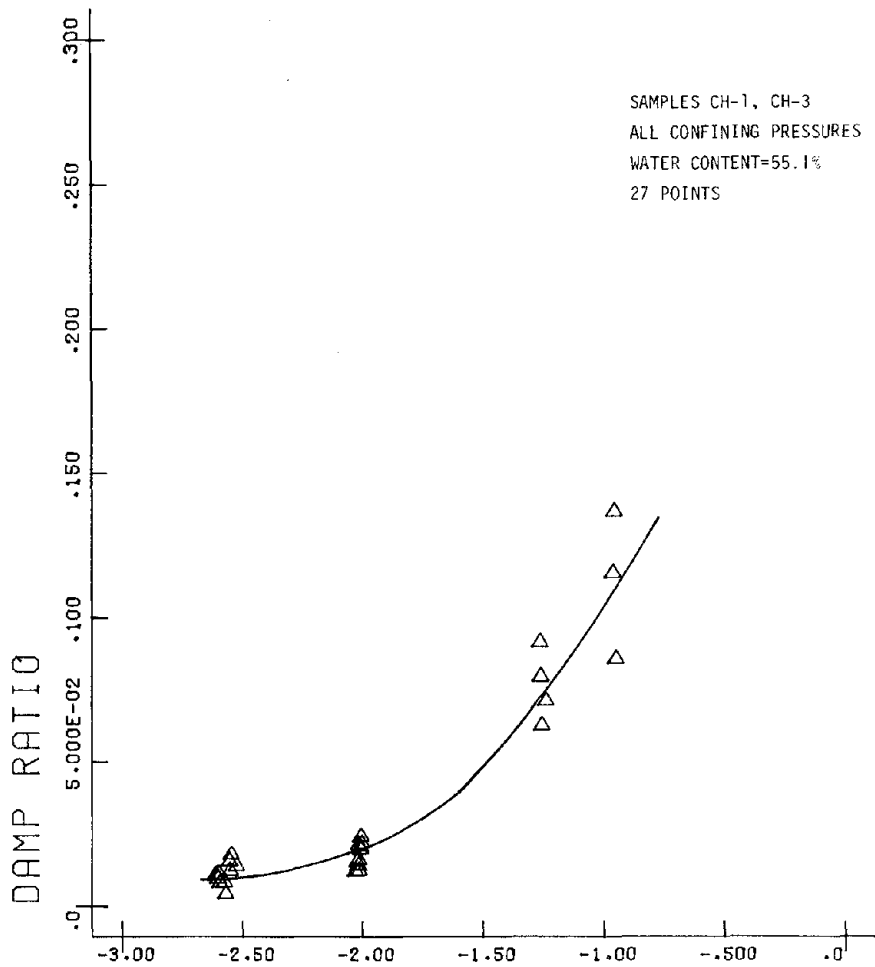
LOG PERCENT Figure F.37 AX STRAIN

O-CLAYT-10F.3



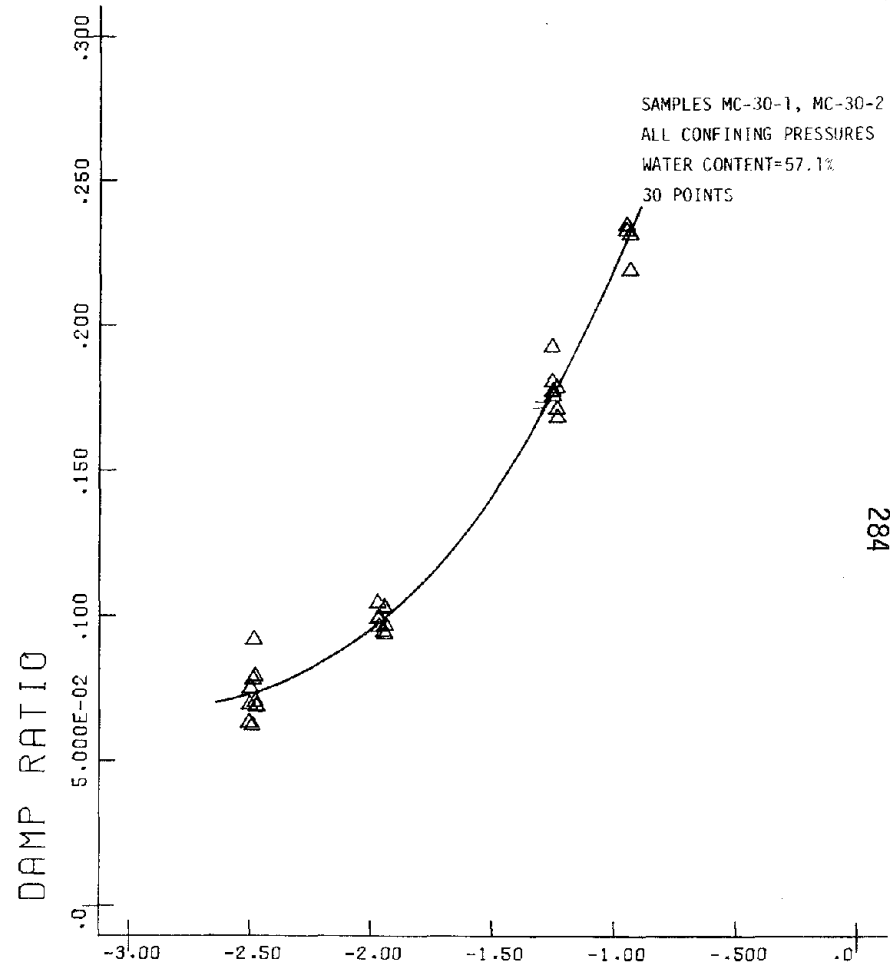
LOG PERCENT Figure F.38 AX STRAIN

O-CLAYT-10F1



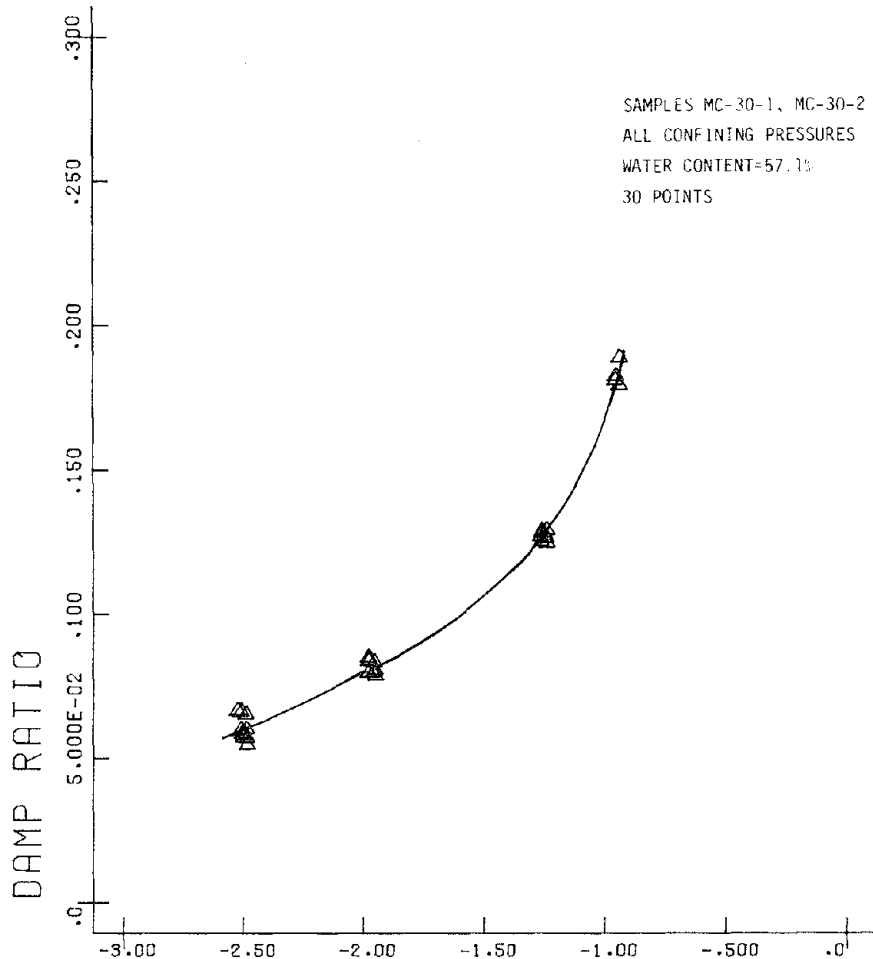
LOG PERCENT AX STRAIN Figure F.39

0-CLAYT-10F5



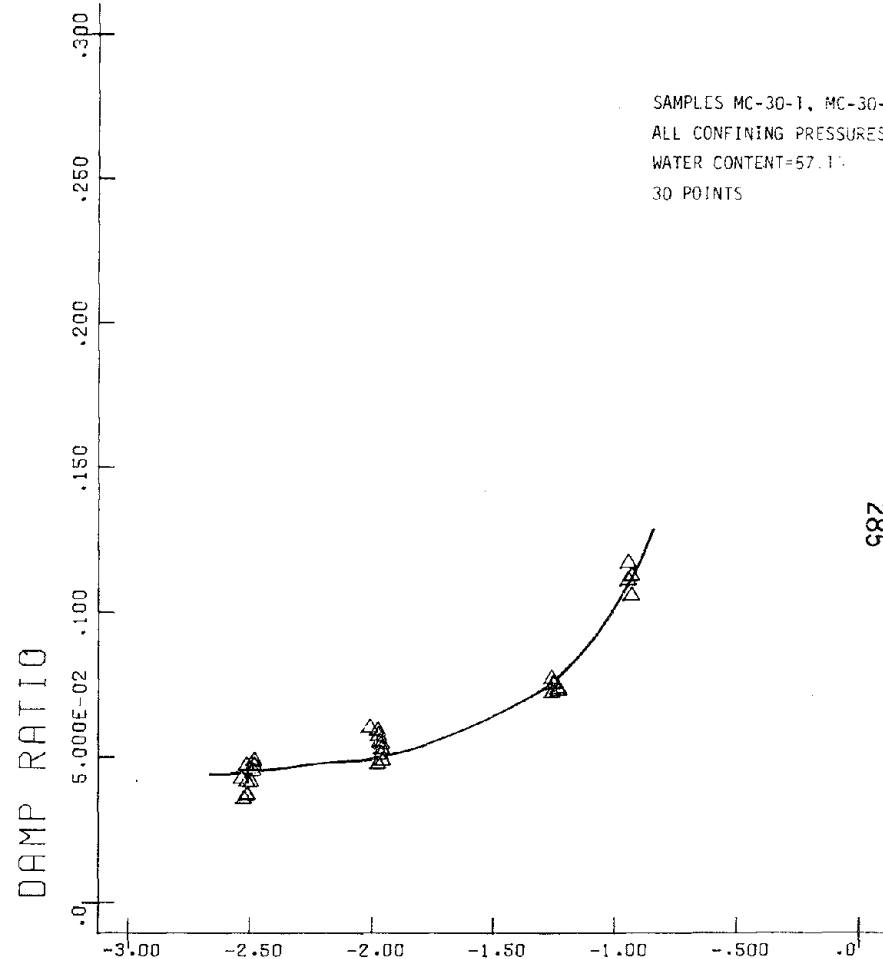
LOG PERCENT AX STRAIN Figure F.40

0M-CLAYT-1F.3



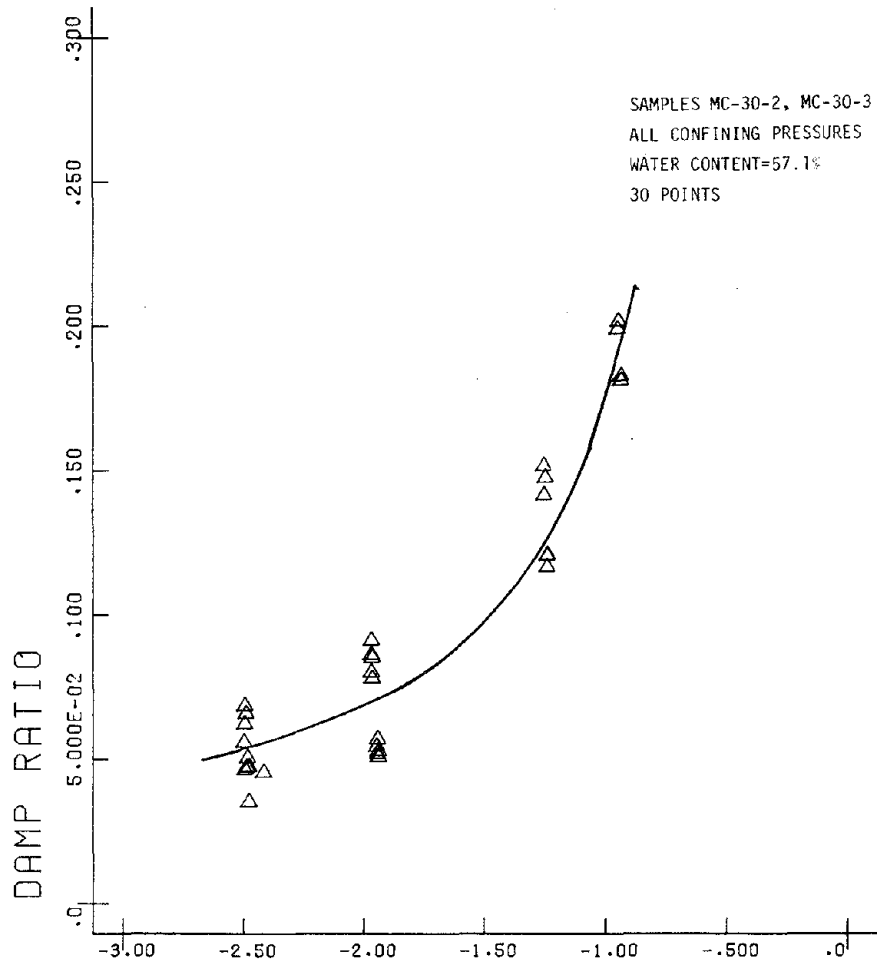
LOG PERCENT Figure F.41 AX STRAIN

OM-CLAYT-1F1



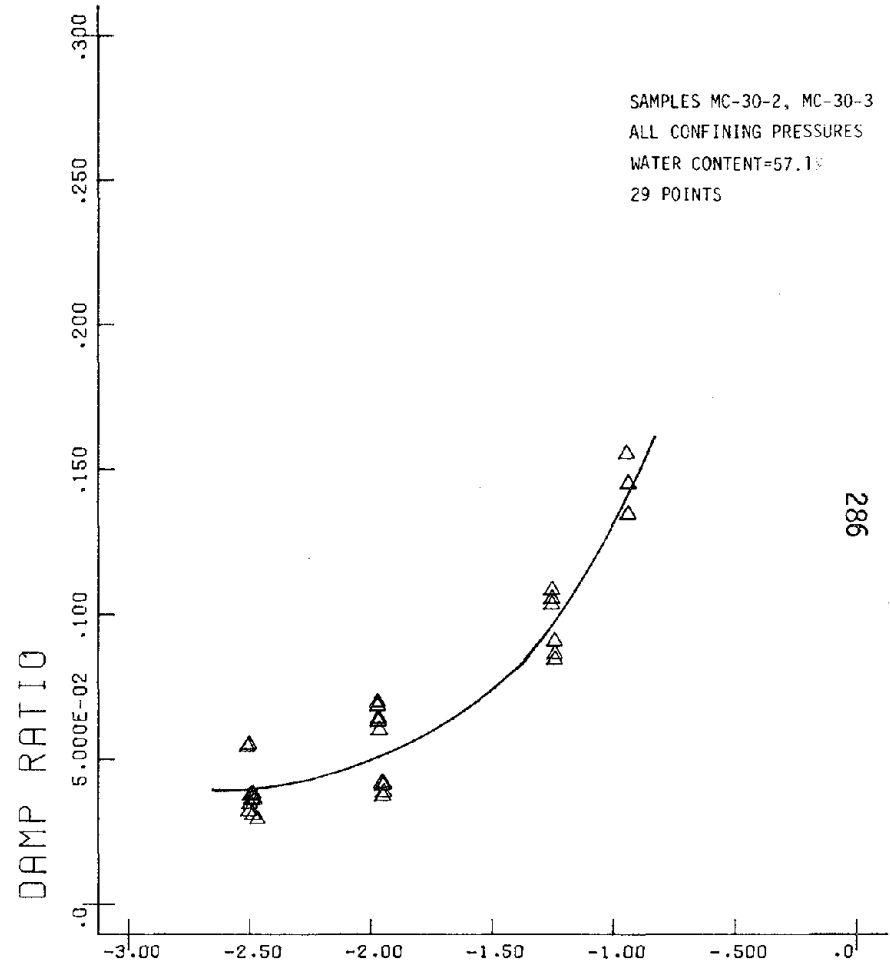
LOG PERCENT Figure F.42 AX STRAIN

OM-CLAYT-1F5



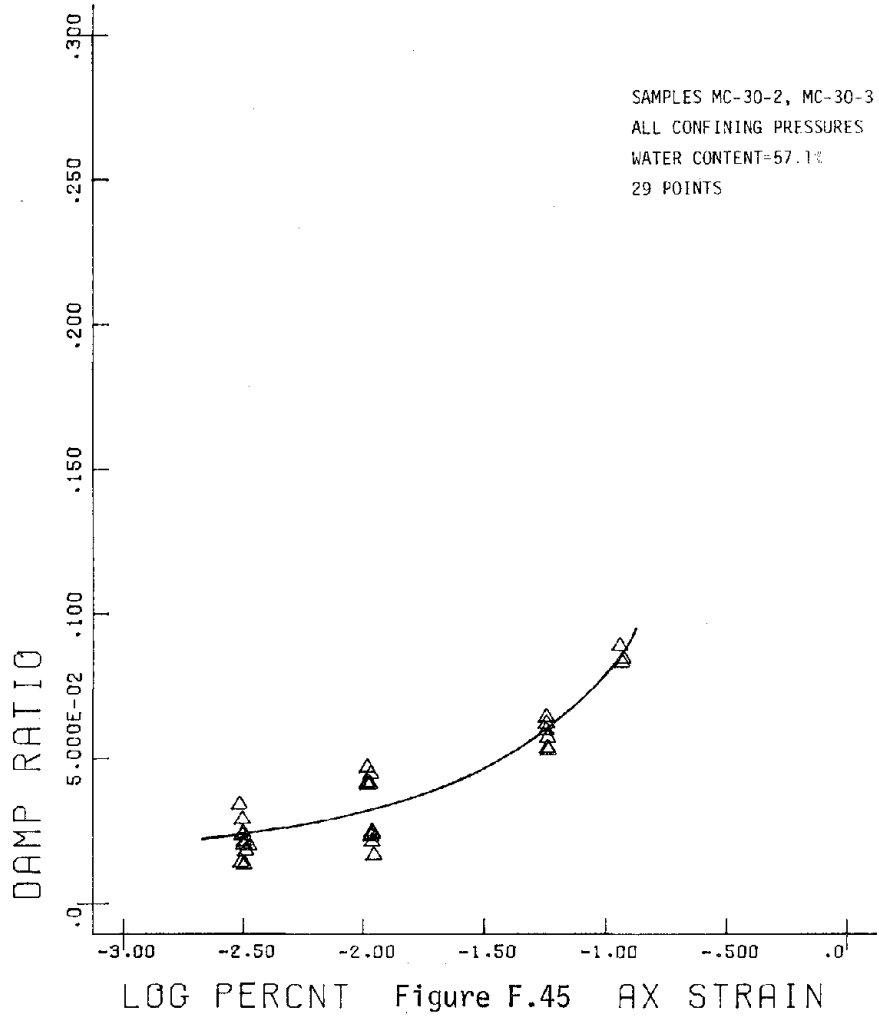
LOG PERCENT Figure F.43 AX STRAIN

OM-CLAYT-4F.3



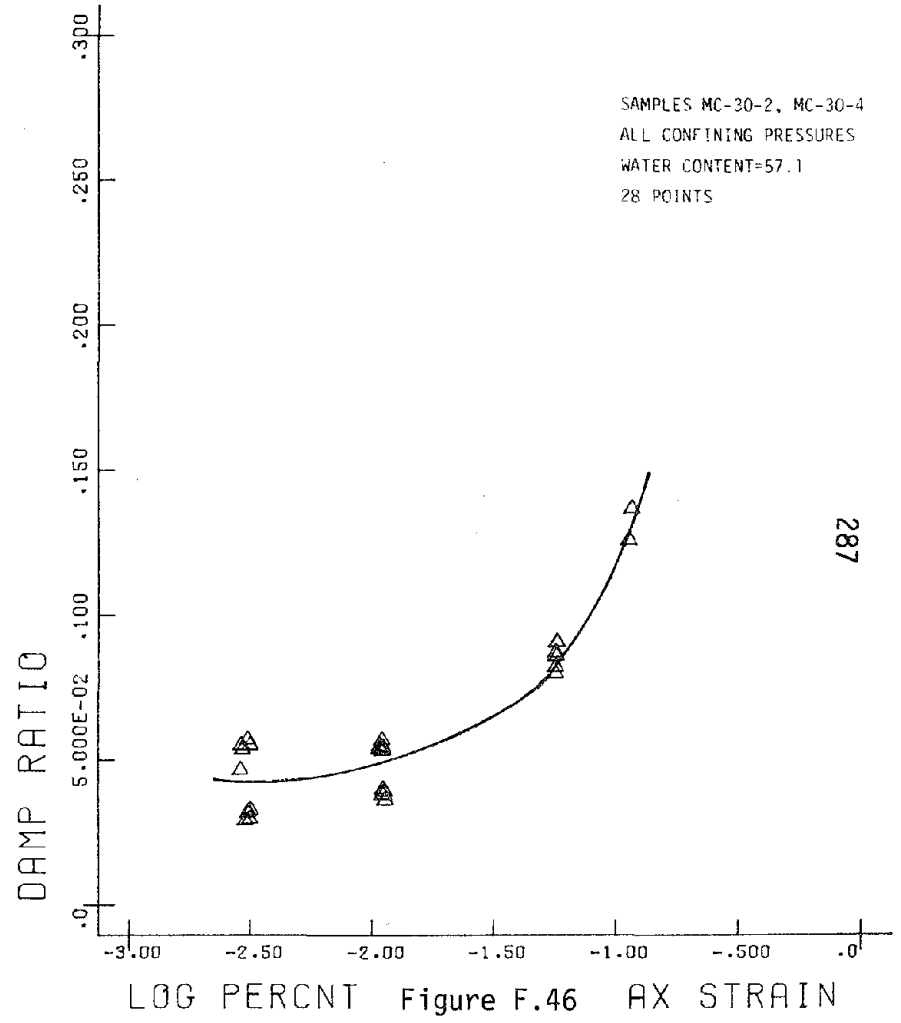
LOG PERCENT Figure F.44 AX STRAIN

OM-CLAYT-4F1



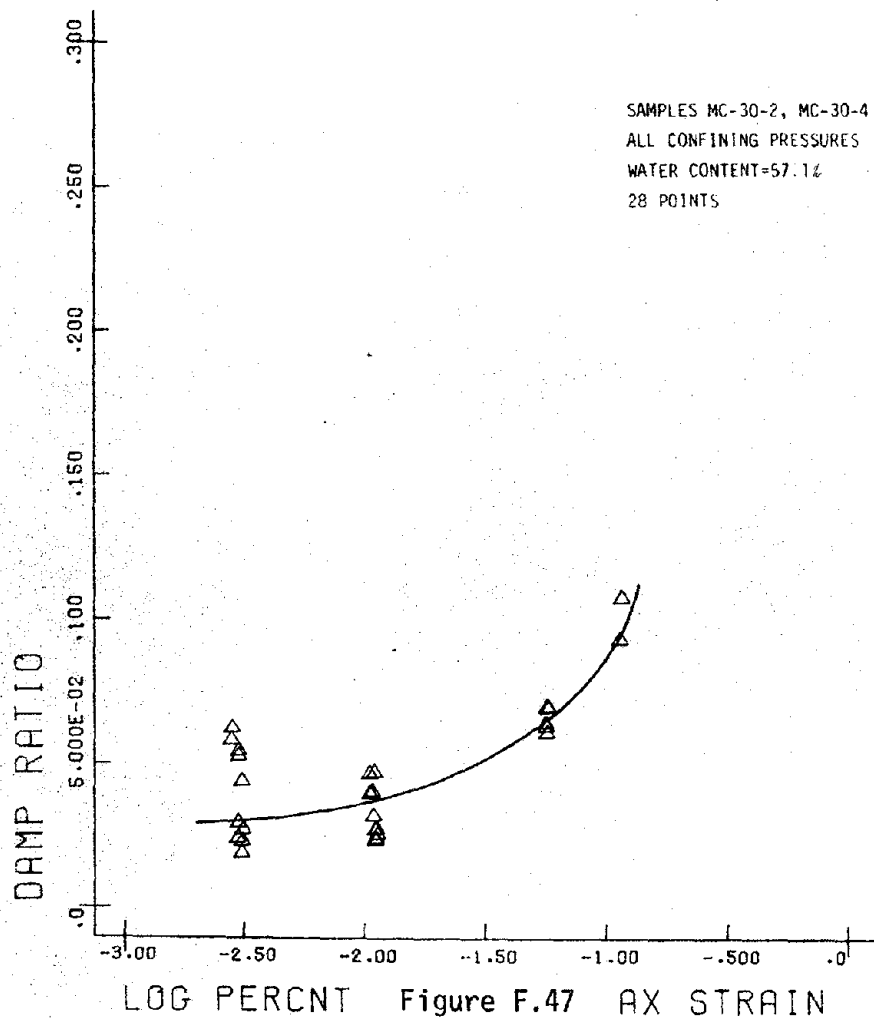
LOG PERCENT Figure F.45 AX STRAIN

OM-CLAYT-4F5



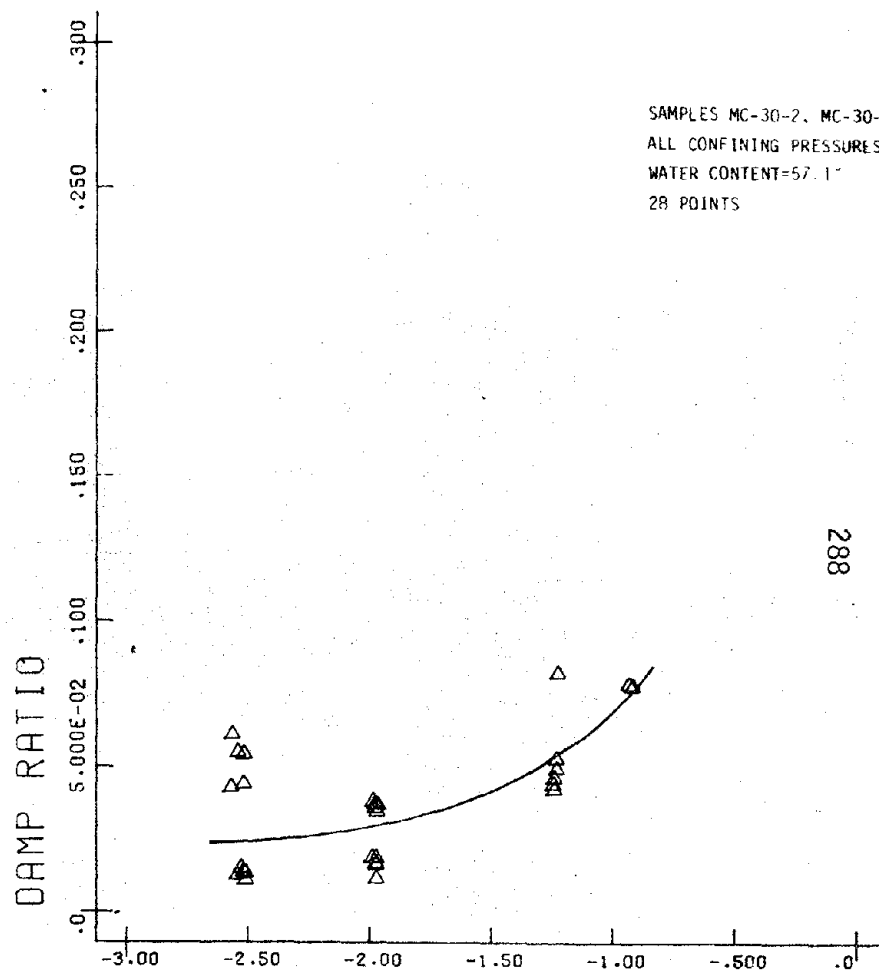
LOG PERCENT Figure F.46 AX STRAIN

OM-CLAYT-10F.3



LOG PERCENT Figure F.47 AX STRAIN

OM-CLAYT-10F1



LOG PERCENT Figure F.48 AX STRAIN

OM-CLAYT-10F5